PICES Scientific Report No. 36
2009

Proceedings of the Fourth Workshop on the Okhotsk Sea and Adjacent Areas

Edited by

Makoto Kashiwai and Gennady A. Kantakov

August 2009
Secretariat / Publisher
North Pacific Marine Science Organization (PICES)
P.O. Box 6000, Sidney, B.C., Canada V8L 4B2
E-mail: secretariat@pices.int Home Page: http://www.pices.int

Contents

Session B1

Biological processes/Disturbances by oil and gas development

Session B2

Walleye pollock

Preface

Being one of the most productive marginal seas in the world, the region where sea ice is formed at the lowest latitudes in the World's oceans, and the formation area of North Pacific Intermediate Water, the Okhotsk Sea has attracted attention of PICES scientists since the inception of the Organization. The very first Working Group established by PICES in 1992 was on *The Okhotsk Sea and Oyashio Region* (under the Physical Oceanography and Climate Committee). The final report of this Working Group 1, edited by Drs. Lynne Talley (U.S.A.) and Yutaka Nagata (Japan) was published as PICES Scientific Report No. 2 in 1995.

Built on this activity, the first PICES Workshop on "*The Okhotsk Sea and Adjacent Waters*" was held on June 19–24, 1995, in Vladivostok, Russia, and was co-convened by Drs. Yukata Nagata, Vyacheslav Lobanov (Russia) and Lynne Talley. Its purpose was twofold: to promote international cooperation in discussions of physical oceanography, fisheries and data exchange of the region and, in view of the importance of Russian contributions to the understanding of the area, to facilitate the incorporation of Russian information in the review of past work. A total of 144 scientists from 5 countries (Canada, Japan, Korea, Russia and U.S.A.) attended the workshop and presented 97 talks and 44 posters. The workshop proceedings were published as PICES Scientific Report No. 6 in 1996. In addition, the "*Multilingual Nomenclature of Place and Oceanographic Names in the Region of the Sea of Okhotsk*", prepared by Drs. Yutaka Nagata and Vyacheslav Lobanov, was published as PICES Scientific Report No. 8 in 1998.

The considerable interest generated from the first workshop led to a second one which took place from November 9–12, 1998, in Nemuro, Japan, and was co-convened again by Drs. Yukata Nagata, Vyacheslav Lobanov and Lynne Talley. The focus was mainly on physical oceanography, and the purpose was to exchange new findings and recent research results, and to review on-going and in-planning international and domestic projects in order to improve international cooperative research. There were 42 participants from 3 countries (Japan, Russia and U.S.A.) who presented 38 talks and 10 posters. The workshop outcome was published as PICES Scientific Report No. 12 in 1999.

A third workshop was held on June 4–6, 2003, again in Vladivostok, and was co-convened by Drs. Vyacheslav Lobanov, Yukata Nagata, Stephen Riser (U.S.A.) and Sei-Ichi Saitoh (Japan). The themes covered by this workshop were broadly based for the purpose of integrating physical, chemical and biological observations in the area. A novel element in the program was an attempt to synthesize the major findings in a discussion session at the end of the presentations. Almost 100 scientists from 3 countries (Japan, Russia and U.S.A.) attended the workshop and presented 38 talks and 45 posters. The workshop results were published in PICES Report No. 12 in 2004, and contributed significantly to the first PICES North Pacific Status Report (PICES Special Publication No. 1, 2004).

This report is the outcome of the fourth PICES Workshop on "*The Okhotsk Sea and Adjacent Waters*" held August 27–29, 2008, in Abashiri, Japan. The Co-convenors and participants of the workshop hope that these proceedings will contribute to future marine scientific research and stimulate international cooperation in the region.

1. Outline of the Workshop

The fourth PICES Workshop on "*The Okhotsk Sea and Adjacent Waters*" was held on August 27–29, 2008, at the campus of the Tokyo University of Agriculture (TUA) in Abashiri, the southernmost city and fisheries base in the rim of the Okhotsk Sea. The goal of the workshop was to develop an Okhotsk Sea component of the new PICES integrative science program, FUTURE (**F**orecasting and **U**nderstanding **T**rends, **U**ncertainty and

Responses of North Pacific Marine **E**cosystems). The intention was to bring together a team of international scientists interested in the Okhotsk Sea and adjacent areas, and their marine ecosystems, to better understand the increasing impacts of climate change in the region, to review and exchange "what is known", and to identify key scientific questions and necessary approaches to answer these questions. Co-convenors of the workshop were Prof. Makoto Kashiwai (TUA) and Dr. Gennady Kantakov (Sakhalin Fisheries and Oceanographic Research Institute). A total of 75 participants attended the workshop: 63 scientists (Japan 44; Russia 17; Canada 1; PICES 1), 1 journalist and 11 auditing students (Appendices 1 and 2).

The workshop began with welcome addresses by Prof. Michinari Yokohama (Dean of Faculty of Bioindustry, TUA) and Mr. Koji Kamada (Director of Abashiri Construction and Development Department Office, Hokkaido Regional Development Bureau, Ministry of Land, Infrastructure, Transport and Tourism). Then, the Co-convenors reviewed the workshop objectives, structure and expected outcome. Three plenary sessions (PS) were held on the first day and two concurrent sessions (A and B) on the second day as follows:

Plenary Sessions:
- PS1: Climate / Ocean dynamics
- PS2: Amur River / Geochemical cycle
- PS3: Primary production / Zooplankton / Marine mammals

Concurrent Session A:
- A1: Current dynamics
- A2: Sea ice, watermass and freshwater processes / Coastal lagoons
- A3: New technology

Concurrent Session B:
- B1: Biological processes / Marine ecosystem disturbances by oil and gas development
- B2: Walleye pollock

A total of 47 papers were presented at these sessions, including one by Dr. Skip McKinnell (Deputy Executive Secretary of PICES) on the status and trends of FUTURE Implementation planning. The schedule of presentations is provided in Appendix 3.

The third day was held in plenary to develop session reports and identify proposals for FUTURE. The reports by session Co-chairs, including a brief summary of presentations and future research plans, can be found in the next section of the Preface. After the announcements for the preparation of the workshop proceedings, the Co-convenors provided closing remarks.

Associated with the workshop, the fourth day was dedicated to the TUA program, the Okhotsk Practical Learning Open Seminar on "*How can we develop resilience of ecosystem and fishery of the Okhotsk Sea against global warming?*". This program was composed of (1) two keynote lectures based on the PICES workshop summaries, "*Possible changes in oceanographic conditions of the Okhotsk Sea with global warming*" by Dr. Vyacheslav Lobanov (Deputy Director, Pacific Oceanological Institute, Russia) and "*Impacts of changes of oceanographic conditions and ecosystems associated with global warming on fisheries in the Okhotsk Sea*" by Dr. Gennady Kantakov (Deputy Director, SakhNIRO, Russia); (2) two keynote reports on "*Effect of the rise in summertime water temperature associated with global warming on the survival of the scallop fishery*" by Dr. Yuji Nishihama (Visiting Professor, TUA) and "*Influence of global warming on northern fish populations*" by Prof. Michio J. Kishi (Hokkaido University); and (3) a panel discussion on "*In order for the fisheries of the Okhotsk Sea to be able to tolerate severe changes due to global warming, what subjects should be addressed by marine sciences?"* with problems posed by the leaders of fisheries cooperatives, students from a practical learning class on the Okhotsk Sea Rim Program, and young TUA scientists. The citizens and fisheries people of Abashiri, workshop participants and students were invited to participate in this program aided by Russian/Japanese sequential translations.

2. Session Reports

PS1: Climate/Ocean dynamics (Co-chairs: Andrey Andreev and Kay-Ichiro Ohshima)

Summary of presentations

In this session, results of the studies concerning long-term changes of the climatic regime (Glebova *et al.*), sea ice coverage (Tachibana and Ogi; Muktepavel and Shatilina), Dense Shelf Water formation (Sasajima *et al*.), seawater temperature, salinity and chemical parameters concentrations (Ohshima *et al.*; Andreev) in the Okhotsk Sea were discussed.

Future research should involve:

1. Monitoring of the long-term changes of heat and moisture fluxes, wind regime and Amur River discharge and its influence on the water temperature, salinity stratification, circulation and ice coverage in the Okhotsk Sea;
2. Organization of time-series observations and research vessel expeditions in the Okhotsk Sea to detect the climate change impact on physical and chemical parameters of the seawater, and a comparison with the results of numerical models;
3. Study (observations and ecological models simulation) of the impact of tides on the spatio-temporal variations of the nutrient fluxes, chlorophyll concentrations and primary production in the Okhotsk Sea and Kuril Straits area.

PS2: Amur River / Geochemical cycle (Co-chairs: M. Angelica Peña and Michio J. Kishi)

Summary of presentations

In this session, five presentations were made including a review of the Pacific Oceanological Institute program on the Amur River estuary and adjacent areas (Lobanov *et al.*), a study of the link between biogeochemical cycles in the Amur River and the western subarctic Pacific, in particular the transport of iron in Okhotsk Sea Intermediate Water (OSIW) to the western subarctic Pacific (Nakatsuka *et al.*), a study of factors controlling biogeochemical cycles in coastal waters using a biogeochemical model (Peña), and the two papers focused on the effect of sea ice on nutrient fluxes (Nomura *et al.*) and on material fluxes (Hiwatari *et al.*) in the Okhotsk Sea.

Future research should include:

1. A joint Japan-Russia-Canada project on the Okhotsk Sea to provide information on the role of iron/OSIW on biogeochemical cycles;
2. Development of a biogeochemical model embedded within a high resolution 3-D physical model to improve our understanding of the transport of iron and material cycles and to facilitate predictions of future ecosystem states, including higher trophic levels;
3. Extended field observations to cover the full annual cycle, especially variables measured under ice in winter;
4. Icebreaker expeditions focusing on biogeochemical studies and aiming to clarify wintertime processes.

PS3: Primary production / Zooplankton / Marine mammals (Co-chairs: Sei-Ichi Saitoh, Alexey M. Trukhin, Mari Kobayashi and Akihiro Shiomoto)

Summary of presentations

Presentations for this session were grouped into the following two classes:

Primary production

Prolonged high primary production in the scallop farming area (southern part of the Okhotsk Sea) was sustained after the spring bloom by the development of a frontal area (Cold Belt) along the Soya Warm Current (SWC) in summer and by forcing of the East Sakhalin Current (ESC) in autumn. The summer bloom occurs due to instability of the SWC, contributing >50% of annual total primary production in the area (Muzzneena and

Saitoh). In the offshore region of the southern Okhotsk Sea, the maximum concentration of chlorophyll *a* (Chl-*a*) was found in the surface layer in spring, but shifted to ~20 m depth in summer and autumn, forming the subsurface chlorophyll maximum (SMC). Seasonal variability of integrated primary production within the euphotic layer was low (Kasai *et al.*). Although no significant relationships were found in the Okhotsk Sea between photosynthetic parameters and temperature or nutrients, the surface primary production during August and September was significantly correlated with Chl-*a* concentrations. This suggests that primary production in summer basically depended on the biomass and not on their photosynthetic physiology or light intensity (Isada *et al.*).

Marine mammals

A remarkable increase in the abundance of spotted seals near northern Hokkaido has occurred, significantly expanding their range of inhabitation southward. With global warming, the ice area where seal pups are born and spend early stages of their lives is declining, which seems to have had a negative impact on the entire regional population (Kobayashi *et al.*). Seven species of pinnipeds inhabit the Okhotsk Sea, but the Steller sea lions and harbour seals are rare. Of the14 Steller sea lion rookeries, 11 are located in the Okhotsk Sea. The abundance of sea lions has stopped decreasing recently. During the last 10 years, increasing abundances of northern fur seals have been observed at Tuleny Island (Terpeniya Bay) near Sakhalin (Trukhin). Analysis of 19 mitochondrial DNA haplotypes found in harbour porpoises near Japan indicates that this population was established relatively recently (Taguchi *et al.*).

Future research should:

1. Summarize and evaluate the available information on the responses of marine organisms of the Okhotsk Sea (from phytoplankton to marine mammals and seabirds) to variability in physical attributes of the ocean, such as seasonal sea ice cover, ocean temperature, stratification, and circulation;
2. Clarify the contribution of ice-algae to the total primary production in the Okhotsk Sea;
3. Understand the physical mechanism responsible for maintaining high primary production in the Okhotsk Sea (Coastal Green Belt), especially the role of advection of the SWC (Cold Belt) and upwelling zones in the Kuril Straits and inside the Okhotsk Sea;
4. Improve a satellite ocean color algorithm of Chl-*a* and primary productivity in the Okhotsk Sea and develop an algorithm to determine integrated Chl-*a* concentration within the euphotic zone;
5. Develop an ice thickness algorithm through remote sensing to evaluate ice thickness changes in the Okhotsk Sea;
6. Examine contributions of oceanic heat on sea ice melting/freezing/motion analysis and ocean–atmosphere heat flux relating to ice variation in relation to marine habitat;
7. Collect *in situ* bio-optical measurements of the phytoplankton community in the Okhotsk Sea;
8. Understand detailed responses of phytoplankton to sea ice dynamics in conjunction with other physical/biochemical parameters (ocean circulation, mixed layer depth, light/nutrients) using a 3-D coupled Ice-Ocean-Ecosystem Model;
9. Develop a plan for the study of zooplankton dynamics and population structure in the Okhotsk Sea;
10. Promote joint Japan-Russia studies on pinnipeds and other marine mammal species in the Okhotsk Sea for sharing biological samples and data.

A1: Currents dynamics (Chair: Takuya Nakanowatari)

Summary of presentations

This session considered studies on currents dynamics in the Okhotsk Sea and North Pacific by numerical models and observations. One of the presentations (Uchimoto *et al.*) described a model of the circulation of the intermediate layer in the Okhotsk Sea. Their Ocean Global Climate Model (OGCM) reproduced features on the $26.8\sigma_\theta$ surface reasonably well, despite a relatively coarse resolution. Tracers injected at the model sea surface in the northwestern part of the Okhotsk Sea are transported to the Pacific *via* the Kuril Straits in the intermediate layer. In these experiments, the tidal mixing effect was essential for the realistic simulation of water mass property and circulation in the Okhotsk Sea. Using observational and hindcast data from an

OGCM experiment, a model was developed to successfully represent the observed multidecadal-scale cooling in the western North Pacific (Nakanowatari *et al.*). This cooling is related to increased cross-gyre transport of the western boundary current. Since the change in potential temperature originates from the western boundary, this indicates that the mechanism is different from the response of westward propagating Rossby waves from the central North Pacific, as has been previously reported by several studies On the other hand, a linear trend in the Okhotsk Sea Intermediate Water was not well simulated. Vertical movements of water masses in the western Okhotsk Sea are evident in observational data (Kantakov). Temperature inversions inside the dichothermal layer are located at convergence zones and/or close to the thermal fronts in the sea. There are at least two types of convection, one connected with salt transport by the SWC in the warm months and another with cooling and brine rejection during fall and winter. The characteristics of tidal and residual currents for the Shmidt Peninsula, Okhotsk Sea shelf of Urup and Kunashir islands were shown from observational mooring data (Shevchenko *et al.*). The energetic characteristics of tidal and residual sea level oscillations in the Okhotsk Sea were also examined from satellite altimetry data (Shevchenko and Romanov). In summary, OGCM experiments provide good representation of oceanic structure and currents in the Okhotsk Sea. However, the interannual variations and current mesoscale structure, including tidal currents, are not simulated well by models. The key components of realistic simulations of physical processes in the region involve tidal mixing and sea ice formation. Incorporating feedback from observational data to a numerical model is important to improve the simulation of the ocean circulation in the Okhotsk Sea.

Future research should focus on:

1. Estimation of the effect of the multi-decadal scale change in the Oyashio on material circulation and ecology in the North Pacific;
2. Realistic simulations of OSIW dynamics;
3. Variability of the vertical movements of water masses in the Okhotsk Sea (possibly a part of FUTURE due to obvious impacts of those phenomena on marine biota, especially at the early ontogenetic stages), climate oscillations and hydrography.

A2: Sea ice, watermass and freshwater processes / Coastal lagoons (Co-chairs: Yoshihiro Tachibana and Anastasiya Abrosimova)

Summary of presentations

A study of sea-ice flow from the Okhotsk Sea through Nemuro Strait in 2008 revealed that in addition to wind drift, the southwestward flow of the Coastal Oyashio and Oyashio currents are important factors controlling sea-ice drift along the southern coast of Hokkaido and result in ice blocking of some bays (Motoi *et al*.). Data obtained by the Hokkaido Kushiro Experimental Station indicated that outflow water from the Okhotsk Sea influences the eastern coastal ecosystem of Hokkaido (Nagata). Evidence of deep convection in the Okhotsk Sea was found (Kashiwai). This winter convection at the open ocean polynya can be an important process, along with the progress of global warming. A study of the influence of Amur River discharge on hydrological conditions of the estuary area indicated that a mesoscale lens of Amur River water is formed during a spring–summer flood (Abrosimova *et al*.). Re-analysis data were used to investigate the relationship of Amur River discharge with vertically-integrated atmospheric horizontal moisture flux (Oshima *et al*.). It was shown that variations in the Asian monsoon and Arctic circulation play an important role in the freshening of the Okhotsk Sea. A review of the coastal lagoons of the Okhotsk Sea found high biodiversity and important species for mariculture (Brovko).

Future research should concentrate on:

1. Paths of outflow of the Okhotsk Sea water;
2. Mechanisms and frequencies of deep convection;
3. Dynamics, conditions of formation, and evolution of the Amur River plume;
4. Oceanography and ecosystems of lagoons, as well as their influence on biochemical processes in adjacent marine areas.

A3: New technology (Co-chairs: Alexander Romanov and Naoto Ebuchi)

Summary of presentations

In this session, six reports were presented on topics ranging from HF radar (Ebuchi *et al.*), ionosphere monitoring (Romanov *et al.*), diagnostics for earthquakes (Romanov *et al.*), spectro-ellipsometry for ecological monitoring (Mkrtchyan *et al.*), radiometry for ecosystem bio-complexity assessment (Krapivin and Mkrtchyan), and airborne lidar for registration of fish schools and plankton (Chernook *et al.*).

Future research

1. Described technologies should be verified and improved by international cooperation under the umbrella of PICES, and new technologies should be developed to: (1) monitor ice-covered oceans in winter; (2) provide stable isotope analyses of sea water and biological samples; (3) assess biodiversity by DNA analyses; (4) improve remote sensing technology, and (5) create tools and methods for biological process studies, especially for monitoring the environment in the Okhotsk Sea.
2. Inviting technical specialists from various fields to future Okhotsk Sea workshops should be considered to enhance our monitoring technologies.

B1: Biological processes/ Disturbances by oil and gas development (Co-chairs: Atsushi Yamaguchi and Vyacheslav S. Labay)

Summary of presentations

This session dealt with presentation on phytoplankton (Shimada *et al.*), zooplankton (Asami *et al.*; Yamaguchi *et al.*), river fish communities (Kanaiwa *et al.*) and benthos (Kashiwai and Kantakov; Samatov and Labay).

Future research

The following points were included in a future research plan:

1. Remote sensing provides only the total amount of phytoplankton (pigment), but to understand spatial and temporal changes in phytoplankton community structure, detailed species composition is needed, especially for toxic species like *Alexandrium tamarense*;
2. The zooplankton community in the Okhotsk Sea is classified into a coastal community (dominated by *Pseudocalanus* spp.) and open sea community (dominated by *Metridia okhotensis*). Since *M. okhotensis* is the predominant component in the open part of the Okhotsk Sea, this copepod is considered a key species in this region. To evaluate its quantitative role in the biogeochemical cycle in this region, its ecology, especially its life cycle, should be studied;
3. Liquid natural gas (LNG), oil and gas activities on the east coast of Sakhalin Island, Magadan and western Kamchatka demand that the impact of such human development on marine ecosystem, especially benthos, should be addressed;
4. Since the characteristics of the Okhotsk Sea differ among locations (*e.g.*, depth, water masses, sea ice) affecting the spatial distribution of biota, cooperative research between Russia and Japan are needed in the future;
5. Since sampling and analytical procedures vary by country, making direct comparisons difficult, establishing standard sampling and analytical methods for biological processes should be considered.

B2: Walleye pollock (Co-chairs: Yasunori Sakurai, Alexander Varkentin and Vladimir Kulik)

Summary of presentations

This session showed that despite such a long period of walleye pollock study in the Okhotsk Sea, new information is still emerging about its biology. (Kulik; Ovsyannikov *et al.*; Yamamoto *et al.*). In particular, it has been established recently that Okhotsk Sea waters off the northern Kuril Islands and the southwestern Kamchatka area is the spawning region of walleye pollock of East Kamchatka origin (Buslov and Varkentin).

Future research should:

1. Summarize and evaluate available information on the responses of marine organisms of the Okhotsk Sea (from phytoplankton to marine mammals and seabirds) to variability in physical attributes of the ocean, such as seasonal sea ice cover, ocean temperature, stratification, and circulation;
2. Assemble existing biophysical datasets and time series from the Okhotsk Sea ecosystem to facilitate joint comparative studies of future climate change issues;
3. Conduct ecosystem studies of the Okhotsk Sea every year at the same time periods and at the same area polygons to ensure that statistical analysis of strong and significant multivariate, canonical and other analyses will not lead to unacceptable biological nonsense;
4. Improve ichthyoplankton survey methods in view of new knowledge about walleye pollock biology in the Okhotsk Sea waters off the northern Kuril Islands and in southwestern Kamchatka to clear up the rates and reasons of walleye pollock migrations to the Okhotsk Sea, and investigate in detail the hydrological conditions in this region;
5. Examine interannual walleye pollock reproductive strategy changes depending on climate and food conditions, stock level and other factors;
6. Explore how the extent of ice cover affects the fate of walleye pollock around the Okhotsk Sea.

3. Acknowledgements

All of the workshop achievements you find in these proceedings are due to the efforts of scientists who spared their precious time and traveled a long way to Abashiri to make valuable presentations and contribute to fruitful discussions. On behalf of all the participants, the workshop Co-convenors would like to acknowledge the Local Supporting Committee, consisting of young staff and students of the TUA campus in Abashiri, for their efforts in making the workshop a success. We thank TUA for providing the workshop venue and transportation not only for daily access to and from the campus but also between the campus and Wakkanai ferry terminal. We would also like to express our sincere gratitude to PICES, TUA, and the Abashiri Construction and Development Department Office for their financial support which made this workshop possible.

Makoto Kashiwai and Gennady Kantakov

Plenary Session 1

Climate/Ocean dynamics

Session Chairs

Andrey Andreev and Kay-Ichiro Ohshima

Long-term changes of atmospheric centers and climate regime of the Okhotsk Sea in the last three decades

Svetlana Glebova, Elena Ustinova and Yuri Sorokin

Pacific Fisheries Research Centre (TINRO-Centre), Vladivostok, Russia. E-mail: glebova@tinro.ru

Abstract

The thermal regime of the Okhotsk Sea is determined by the Aleutian Low and Siberian High interaction in winter but depends on the interaction of the Far Eastern Low and Hawaiian High in spring and summer. These large-scale cyclones and anticyclones are referred to as "centers of atmosphere action". In the last three decades (1974–2007), both winter centers shifted gradually southwestward and weakened. As a result, the quantity of the "cold" and "moderate–cold" types of atmospheric processes decreased, the duration of the local winter monsoon over the Okhotsk Sea shortened, and its activity lessened. Hence, the thermal regime of the Okhotsk Sea changed towards a decrease in ice cover and an increase in sea surface temperature in spring. The position of the summer centers also changed. The Far Eastern Low shifted southwestward, farther from the sea shore, and the Hawaiian High moved northwestward, moving nearer to the Okhotsk Sea. In particular, the intensity of both atmospheric centers has increased recently. These changes have caused a decrease in local summer monsoon activity, but its influence has been prolonged which means that autumn processes begin later. As the result, sea surface temperature in the Okhotsk Sea in summer is increasing. We conclude that the long-term reorganization of the barometric regime which occurred during the last several decades has caused a warming of the Okhotsk Sea climate.

Introduction

The Okhotsk Sea has unique hydro-meteorological conditions favorable for many commercial species. Therefore, these conditions should be revealed for the future estimation of Okhotsk Sea bio-productivity.

Thermal conditions in the Okhotsk Sea are closely connected with large-scale atmospheric processes, formed by the atmospheric actions centers (AAC), such as the Aleutian Low and Siberian High in winter and the Far Eastern Low and Hawaiian High in summer.

Data and Methods

The position of the AAC was determined by analysis of sea surface atmospheric pressure charts of 10-day averaging for the period 1974–2007. A total of 1188 averaged charts were prepared (36 charts per a year). Latitude, longitude and intensity of the seasonal AACs were determined and the atmospheric processes over the Okhotsk Sea were classified. The position and intensity of the AAC, in particular the Aleutian Low, and the direction of wind over the Okhotsk Sea were used as the main criteria for the definition of the synoptic types. A total of seven characteristic synoptic situations or types have been determined for the Okhotsk Sea (Glebova, 2004); Katz's meridional indices of atmospheric circulation (as the quantitative parameter of intensity and direction of local wind transfer over the Okhotsk Sea) (Katz, 1954) were calculated as a number of isobars crossing latitudes inside and on the boundaries of the area 40–60°N, 130–160°E (including the Okhotsk Sea), taking into account their orientation. Using the formula $Im = Is – In/N$, where Is is the number of isobars orientated from south to north, In is their number orientated from north to south, N is the number of the crossed latitudes, and $Im > 0$ characterizes southern wind (summer monsoon) while $Im < 0$ characterizes northern wind (winter monsoon).

Monsoon changes occur over the Okhotsk Sea in spring and autumn. (In spring northern winds usually cease by the third 10-day period of April, and in autumn they begin in the third 10-day period of September; in terms of real synoptic situations, a change of monsoon can occur earlier or later than these "average" terms.)

The values of all parameters were averaged for the cold season (October–March) and warm season (April–September) of each year. Thermal conditions of the Okhotsk Sea were characterized by ice cover and sea surface temperature in spring and summer (obtained from http://goos.kishou.go.jp/rrtdb/usr/pub/JMA/cobesst/). To determine long-term tendencies, and for the best comparability of results, all meteorological and oceanologic parameters were averaged using 5-year periods.

Results and Discussion

It is known that in winter the climatic regime and character of wind transfer in the Okhotsk Sea depend on the Aleutian Low and Siberian High. Their interaction usually forms the northern circulation over the entire region of the Okhotsk Sea.

The analysis of long-term changes in parameters of both atmospheric centers has shown that during the last three decades their condition has gradually varied. As can be seen, the Aleutian Low and Siberian High have constantly shifted to the south and west (Fig. 1A–D). In addition, pressure in the Aleutian Low has heightened (Fig. 1E) and the pressure in the Siberian High has slightly lowered (Fig. 1F).

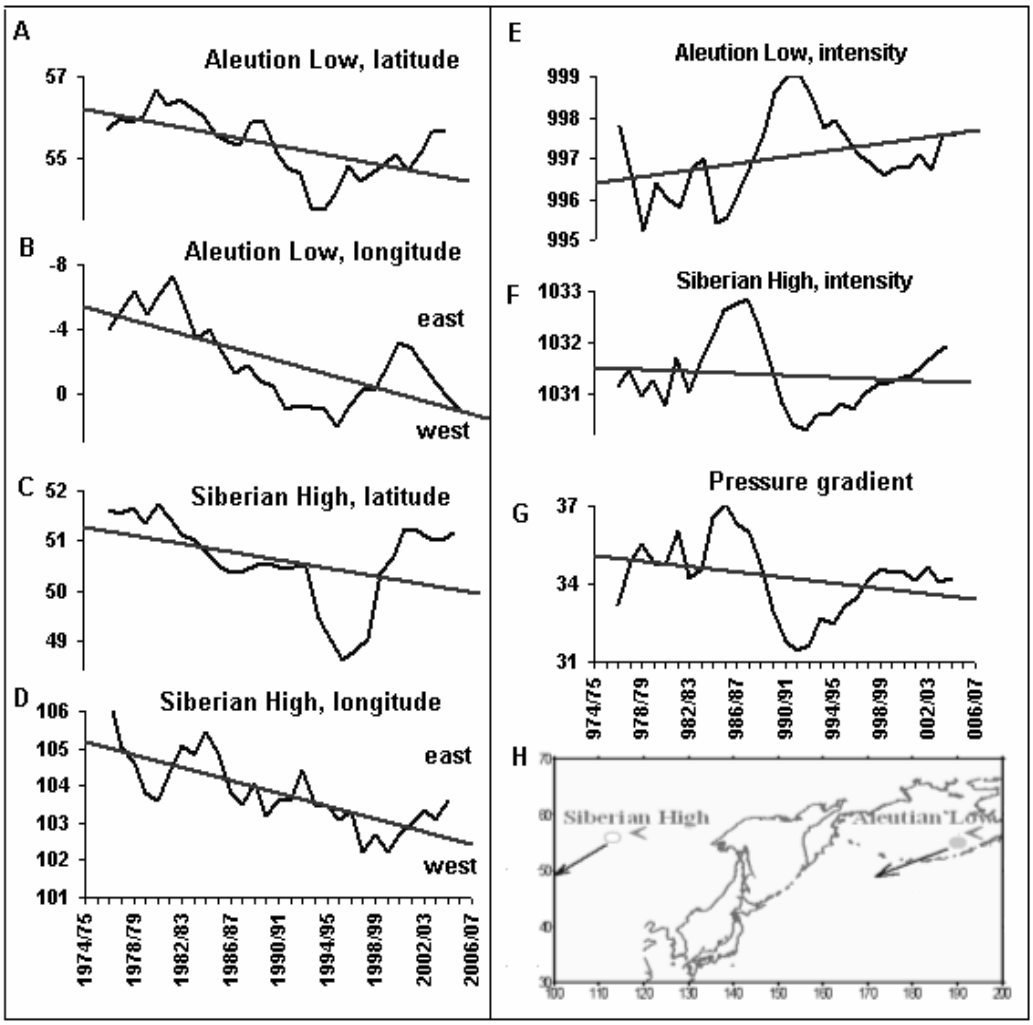

Fig. 1 Long-term changes in the parameters of the winter (October–March) atmosphere action centers (AACs) from 1974 to 2007. Pressure is in mbars.

The pressure gradient between these centers has also decreased (Fig. 1G). It is a parameter of general northern circulation over the region, and its weakening means that the intensity of cold air invading the sea area has decreased.

As a result of the southwestward shift (Fig. 1H), a wedge of the Siberian High has been removed from the Okhotsk Sea while a trough of the Aleutian Low, on the contrary, has moved closer to the sea where its influence has amplified in comparison with the Siberian High. Therefore, atmospheric processes directly over the Okhotsk Sea have also varied: the repeatability of "warm" and "moderate–warm" synoptic types with excessive cyclonic activity over the Kuriles and over the Okhotsk Sea has begun to increase (Fig. 2A). This implies that warm oceanic air masses have entered the Okhotsk Sea with cyclonic activity and that the quantity of the "cold" and "moderate-cold" atmospheric types with intensive northern wind transfer and intrusion of Arctic cold air masses have been reduced (Fig. 2B). The changes in the atmosphere are reflected in the thermal regime of the sea. The ice cover has been generally reduced in the last three decades (Fig. 2C). Although there have been interdecadal fluctuations, the last "wave" of heightened ice cover in the early 2000s was much lower than the previous one in the early 1980s when the quantity of the "cold" and "moderate–cold" types was maximal.

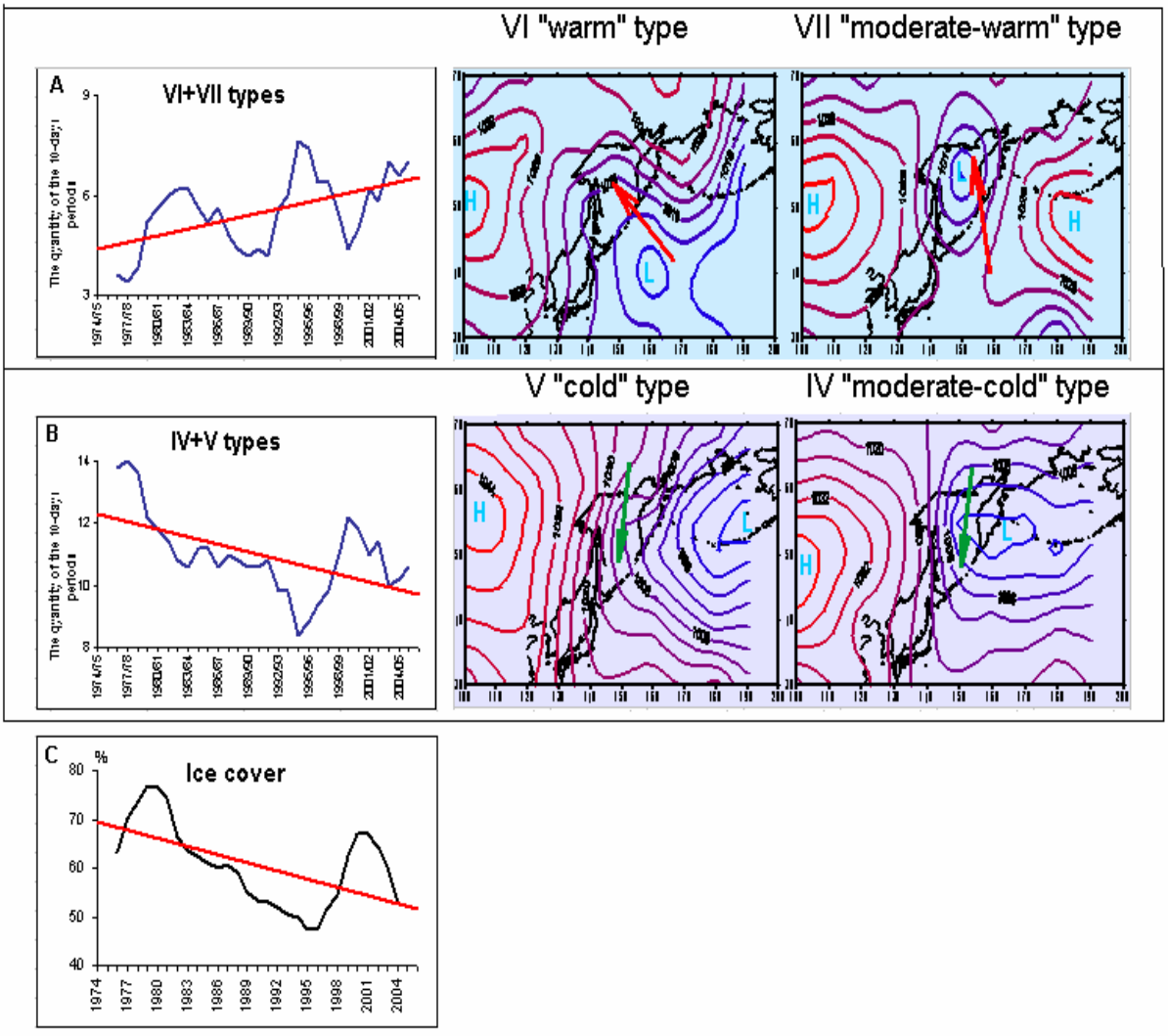

Fig. 2 Long-term trends in the change in repeatability of atmospheric processes over the Okhotsk Sea and ice cover in the cold season (October–March) from 1974 to 2007.

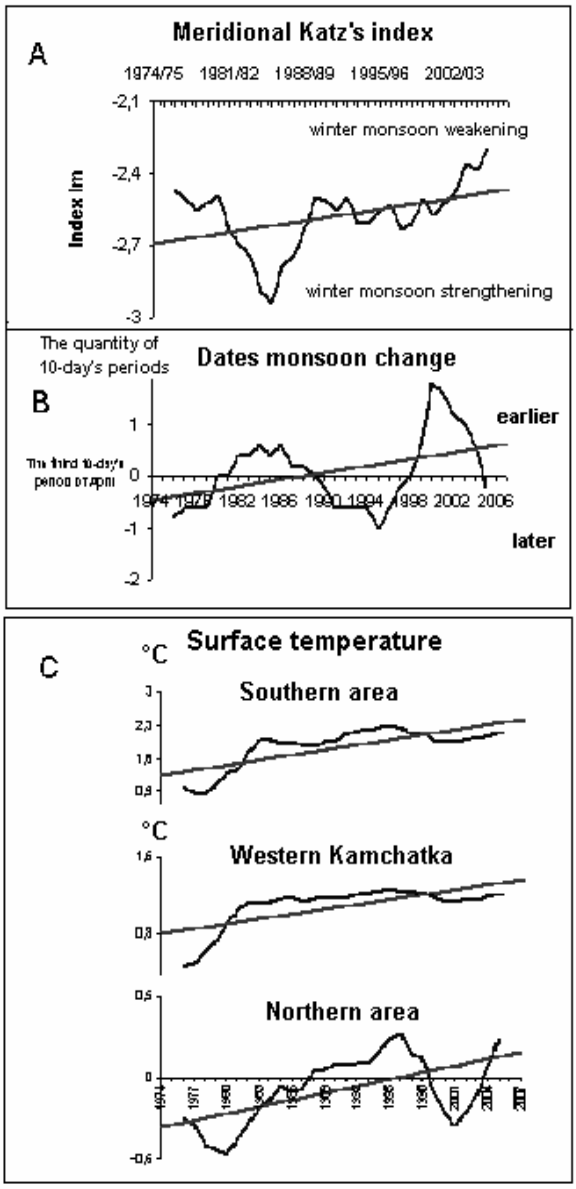

Fig. 3 Trends in variability of (A, B) winter monsoon parameters and (C) sea surface temperature in the Okhotsk Sea in spring.

Climate change in the Okhotsk Sea is also revealed in the character of wind transfer. As shown in Figure 1G, during last 30 years a relaxation of the general circulation (pressure gradient) has occurred over Pacific region in winter. Undoubtedly, this event should be reflected in the character of the local wind transfer in the Okhotsk Sea. The intensity of the northern wind (a winter monsoon) in the Okhotsk Sea has begun to decrease too, and in recent years it has happened especially quickly (Fig. 3A). It is curious that the duration of the winter monsoon has also varied, namely, the termination date of northern transfer (and beginning of formation of southern transfer) has gradually moved to earlier times (Fig. 3B). In other words, the duration of the northern monsoon has been reduced and the spring processes have started earlier in the Okhotsk Sea. It is quite possible that exactly these factors — the lessening of the winter monsoon activity and its shortened duration — have been the cause of the increase in sea surface temperature in spring in various areas of the Okhotsk Sea (Fig. 3C). The atmospheric regime during the warm seasons has also undergone considerable changes. As a general rule, the southern overall circulation is observed in spring and summer as a result of the interaction between the Far Eastern Low and Hawaiian High.

As can be seen in Fig. 4E–F, the intensity of both AACs have increased gradually (the pressure in the Far Eastern Low has lowered and the pressure in the Hawaiian High has heightened). Recently, the intensity of both centers has reached their highest values yet. The pressure gradient between them has also increased (Fig. 4G) so that the southern general circulation over the Pacific region has become more active. Both atmospheric centers have shifted westward (Fig. 4A and C) and simultaneously, the Far Eastern Low has also moved towards the south (Fig. 4D) and the Hawaiian High has moved toward the north (Fig. 4B), *i.e.*, the Far Eastern Low has moved from the coast deeper into the continent, and its influence on the Okhotsk Sea has lessened (Fig. 4H). However, the Hawaiian High has steadily come nearer to the Okhotsk Sea, and it has had important consequences. On the one hand, the field of high pressure, prevailing over the Okhotsk Sea, is responsible for a considerable weakening of the local southern wind transfer (summer monsoon) (Fig. 5A). On the other hand, it is accompanied by more frequent sunny days and, accordingly, increasing radiation warming. As a result, an increase in the sea surface temperature has been observed in different areas of the Okhotsk Sea (Fig. 5B).

One more important feature of a summer monsoon is noted — the gradual change of its end date to a later time (Fig. 6A) which means a delay in the formation of autumn processes in the Okhotsk Sea. As discussed above, the termination date of the northern transfer has shifted to an earlier time (Fig. 3B), *i.e.*, in general, the duration of the warm season in the Okhotsk Sea has become longer, and the cold season has shortened (Fig. 6B).

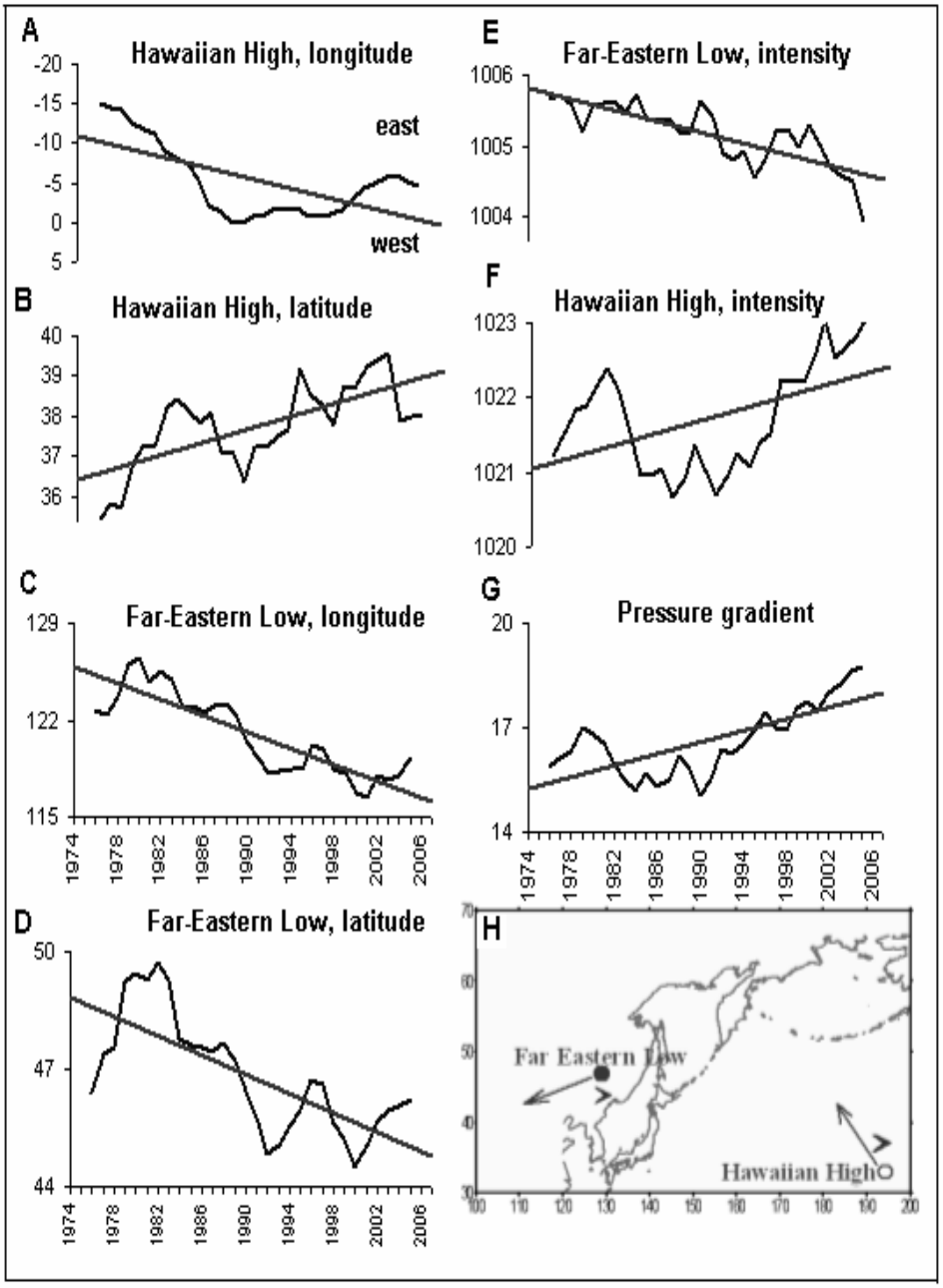

Fig. 4 Long-term changes in parameters of the summer atmosphere action centers (April–September).

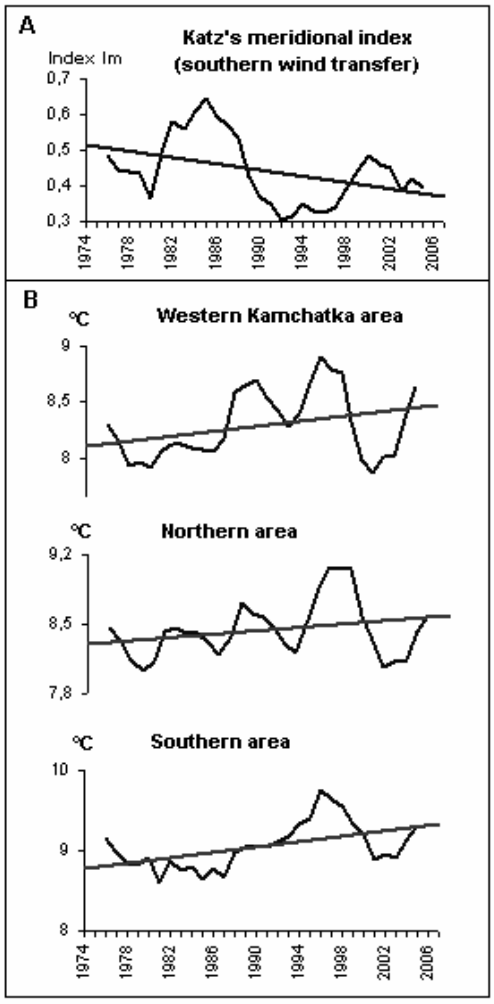

Fig. 5 Variability in intensity of local southern wind transfer (monsoon) and sea surface temperatures in the Okhotsk Sea in summer.

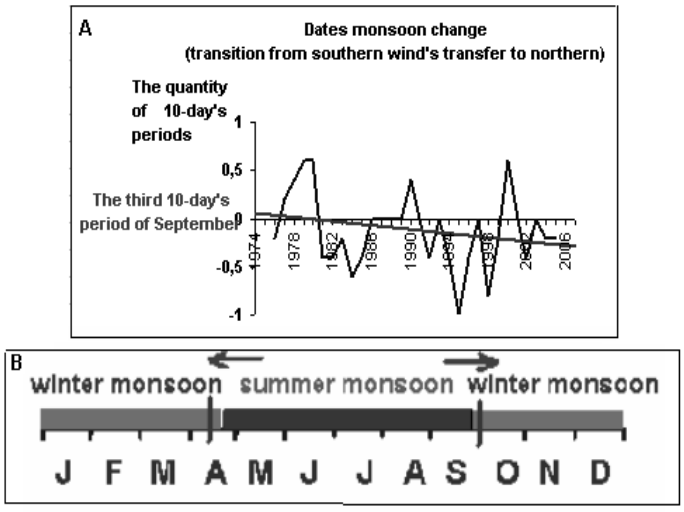

Fig. 6 Dates showing local monsoon changes in (A) autumn and (B) the period of formation of the winter and summer monsoon in the Okhotsk Sea.

Summary

Thus, the most important changes in the atmospheric regime have been during the last three decades in the Okhotsk Sea and adjacent regions.
In winter there has been:

- A relaxation and southwestward shift of the Aleutian Low and Siberian High;
- A weakening of the prevailing northern circulation over the Pacific region;
- A reduction of the "cold" and "moderate-cold" synoptic situations with an intrusion of Arctic air masses and more frequent "warm" and "moderate-warm" atmospheric processes with cyclonic activity, causing warm oceanic air masses to enter the Okhotsk Sea;
- A lessening in the intensity and duration of local winter monsoons;
- A reduction of ice cover and sea surface warming in spring.

In summer there has been:

- An activization of the Far Eastern Low and Hawaiian High, especially in recent years;
- A strengthening of the prevailing southern circulation over the Pacific region;
- A southwestward shift of the Far Eastern Low and a northwestward shift of the Hawaiian High;
- A weakening of the local summer monsoon over the Okhotsk Sea, but with an increased duration;
- An increase in radiation warming in the Okhotsk Sea as the result of the Hawaiian High's influence;
- An increase in sea surface temperature in the Okhotsk Sea in summer.

All the facts discussed above indicate a gradual warming of the Okhotsk Sea climate, which has occurred during last 3 decades on the background of large-scale changes of atmospheric circulation over the whole Pacific region.

References

Glebova, S.Yu. 2004. Influence of the atmospheric processes over the Okhotsk Sea on variability of its ice cover. Proceeding of the 19th International Symposium on Okhotsk Sea and Sea Ice, Mombetsu, Hokkaido, Japan. pp. 169–172.

Katz, A.L. 1954. On studying and estimation of the general circulation of atmosphere. *Meteorol. Hydrol.* **6**: 11–29.

Influence of the annual Arctic Oscillation on the negative correlation between Okhotsk Sea ice and Amur River discharge

Yoshihiro Tachibana[1,2] and Masayo Ogi[3,4]

[1] Institute of Observational Research for Global Change, Japan Agency for Marine-Earth Science and Technology, Yokosuka, Japan. E-mail: tachi@bio.mie-u.ac.jp
[2] Faculty of Bioresources, Mie University, Tsu, Japan
[3] The Joint Institute for the Study of the Atmosphere and Ocean, University of Washington, Seattle, WA, U.S.A.
[4] Frontier Research Center for Global Change, Japan Agency for Marine-Earth Science and Technology, Yokohama, Japan

Abstract

Newly obtained observational discharge data reveal the cause of a significant negative correlation between Amur River discharge and Okhotsk Sea ice at multiyear timescales. The annually integrated Arctic Oscillation (AO) influences both summer discharge and winter ice. Summer discharge is larger and winter ice is reduced during positive AO years. The annual AO also influences the annual horizontal moisture flux convergence in the river basin. When the annual AO is positive, the annual mean air temperatures are warm over Eurasia, particularly over the Amur River basin and the Okhotsk Sea. Consequently, autumn sea surface temperatures (SSTs) are warmer in the Okhotsk Sea. The warmer autumn SSTs suppress ice formation during the following winter. Freshwater from the river is not the main control of multiyear ice variability. Consideration of the annual AO provides a new look at climate system persistence at the multi-seasonal scale.

This work is partially based on a paper by Ogi and Tachibana (2006) in *Geophysical Research Letters*.

Introduction

Freshwater discharging from large rivers is an important factor controlling the formation of sea ice because it causes a large stratification that suppresses deep convection and promotes freezing. The Amur River is the fourth largest river in northern Eurasia and it supplies much of the freshwater to the Okhotsk Sea, one of the southernmost ice-covered oceans in the Northern Hemisphere. Atmospheric circulations are also important in the formation of sea ice in the Okhotsk Sea (*e.g.*, Fang and Wallace, 1994; Tachibana *et al.*, 1996). Yamazaki (2000) showed that the Okhotsk Sea ice formation is influenced by the winter North Atlantic Oscillation (NAO). Variations in Okhotsk Sea ice are therefore influenced by both large-scale atmospheric circulations and hydrological processes associated with the river. Ogi *et al.* (2001) used time series analyses from 1971 to 1993 to suggest that interannual variations in Okhotsk Sea ice were negatively correlated with discharge from the Amur River. Years with large river discharge are followed by suppressed sea ice formation in the Okhotsk Sea and *vice versa*. This negative correlation is counter to the expected influence of freshwater. Discharge data given by Ogi *et al.* (2001) ends in 1993, and this lack of data precludes a determination of whether the negative correlation is causal. In addition, the reason for the negative correlation is unclear.

Recently, we have obtained discharge data from the Far Eastern Regional Hydrometeorological Research Institute, Russia (FERHRI), extending the discharge data record to 2004. These extra data and additional recent data are consistent with a negative correlation. Figure 1 shows the annual mean Amur River discharge and the maximum sea ice coverage in the Okhotsk Sea from 1971 through 2004. Clearly, discharge is negatively correlated with sea ice coverage. A 3-year moving average highlights multiyear timescale changes and shows a clearer negative correlation than at interannual timescales.

This study will identify the cause of the negative correlation between discharge and sea ice with respect to long-term climate variations. The Amur River freezes in winter; discharge is largest in summer (Ogi *et al.*, 2001, Fig. 2). Thus, the summer atmosphere controls the discharge. However, the

Okhotsk Sea is ice-covered only in winter. The season-to-season connection suggests a persistence in the atmosphere that extends beyond one or two seasons. Ogi *et al.* (2003) showed an example of such seasonal atmospheric persistence by which summertime atmospheric circulations were influenced by the NAO/AO of the previous winter. The summer atmospheric pattern related to the winter NAO/AO was also characterized by a seesaw pattern, which is similar to the winter AO. The leading mode of an empirical orthogonal function (EOF) analysis for individual calendar months appears as a seesaw pattern between the Arctic and mid-latitudes in both summer and winter (Ogi *et al.*, 2004a). The winter-to-summer linkage described by Ogi *et al.* (2003) was interpreted as a preferred transition from one polarity of the winter AO to the same polarity of the summer AO. The negative correlation in Figure 1 may therefore be related to persistent atmospheric variations in winter and summer. The first step to solving the season-to-season connection must consider variations in annual mean atmospheric patterns and their connection to both discharge and sea ice. This paper will show that the annually integrated AO influences both summertime discharge and wintertime sea ice.

Data

We obtained Amur River discharge data recorded at Bogorodskoye from 1971 through 2004 from FERHRI. Data from 1979 were missing, and the climatological mean in the present analysis was substituted for that year. The annual mean (January–December) discharge data are used as the discharge index. Sea ice data for the Okhotsk Sea were derived from Japan Meteorological Agency (JMA) data from 1971 through 2004. The sea ice coverage index is the maximum sea ice extent in a year. Sea ice extent is normally largest in late February or March. Atmospheric data come from the NCEP/NCAR reanalysis data set covering 1971 to 2004 (Kistler *et al.*, 2001). The AO (Thompson and Wallace, 1998) index from 1971 to 2004 is available from the Climate Prediction Center. The annual mean value (January–December) of the AO index is used as the annual AO index. The monthly mean SST data set includes global sea ice coverage and SST data (HadISST) from 1971 to 2003.

The main seasons for discharge and sea ice are summer and winter, respectively (Tachibana *et al.*, 2008); thus, calendar years for comparing discharge and ice differ. Sea ice time series were therefore shifted 1 year earlier in all correlation analyses that consider the influence of the discharge on sea ice. In addition, a 3-year moving average filter was applied to all data analyzed in this study because the negative correlation in Figure 1 is more pronounced at multiyear timescales than at interannual timescales.

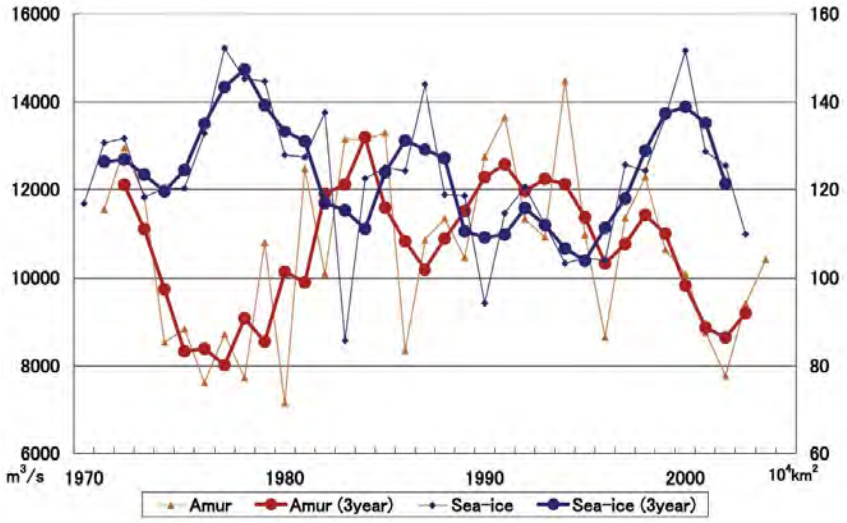

Fig. 1 Time series of the annual mean discharge from the Amur River to the Okhotsk Sea (blue lines). The thick lines are filtered with a 3-year moving average filter (red lines) and maximum sea ice area over the Okhotsk Sea 3-year moving average; the red and blue lines are discharge and sea ice, respectively. Note that the sea ice series is shifted to the left by 1 year.

Results

Annual mean large-scale atmospheric patterns that influence annual discharge and sea ice are presented. Figure 2a shows an annual mean sea level pressure (SLP) anomaly pattern regressed onto the annual discharge. A seesaw pattern occurs between a negative area over the Arctic Ocean and positive areas over the mid-latitudes. SLP patterns related to the sea ice variation (Fig. 2b) show a similar seesaw pattern but with the opposite sign. A negative correlation was found between the discharge and the sea ice, as shown in Figure 1; thus, the similar atmospheric large-scale patterns with opposite signs in Figures 2a and 2b are reasonable. Similarities in the atmospheric patterns indicate that the seesaw pattern between mid- and high latitudes influences both the discharge and the sea ice. The annual mean AO (Fig. 2c), also a seesaw pattern between mid- and high latitudes, is similar to the pattern in Figure 2a and is of the opposite sign to that in Figure 2b. Pattern correlation coefficients poleward of 30°N for the discharge (Fig. 2a) and the sea ice (Fig. 2b) with the AO (Fig. 2c) are 0.80 and –0.82, respectively. Negative anomalies near the pole and positive anomalies at mid-latitudes are characteristic of a positive AO pattern (Thompson and Wallace, 1998). Thus, present results show that during positive AO years, discharge is greater and sea ice is suppressed in the following winter. When the annual mean atmospheric patterns at upper levels were regressed onto the discharge, the sea ice and the annual mean AO index resembled the surface patterns shown in Figure 2.

The annual mean temperature anomaly at 850 hPa regressed onto the annual discharge shows negative values over the Arctic and positive values over mid-latitudes (Fig. 2d). The regression of the annual mean temperature at 850 hPa onto the sea ice in the following winter resembles the pattern of the discharge regression, but with the opposite sign (see Figs. 2d and 2e). A prominent warm temperature signal at 850 hPa related to the annual AO (Fig. 2f)

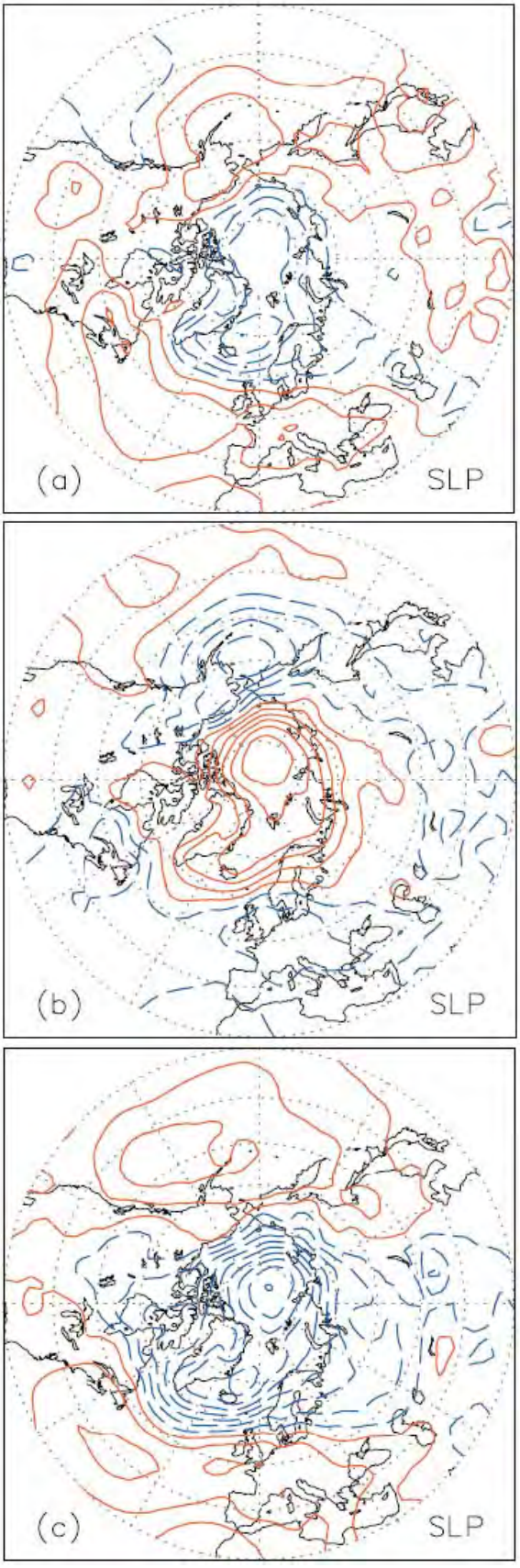

Fig. 2 (a–c) Horizontal maps of annual mean sea level pressure (SLP) and (d–f) temperature at 850 hPa regressed onto the annual mean Amur River discharge (Figs. 2a and 2d), the maximum sea ice in the Okhotsk Sea (Figs. 2b and 2e), and the annual mean AO index (Figs. 2c and 2f). Red solid contours denote positive values, and blue dashed contours indicate negative values. Contour intervals are 0.2m for SLP and 0.1 K for the temperature. All data were filtered with a 3-year moving average.

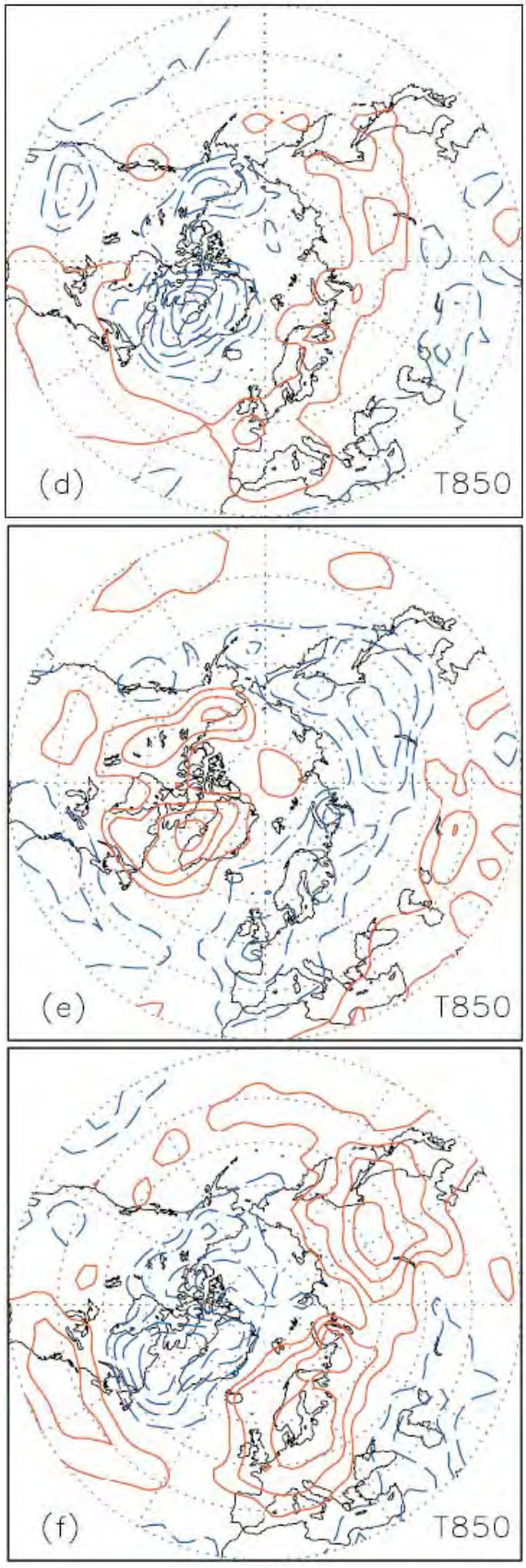

Fig. 2 Continued.

covers wide areas of Eurasia with centers in both northern Europe and the Far East; a cold temperature signature covers the Arctic. Annual mean atmospheric temperature patterns correlated with both discharge and sea ice therefore resemble AO signatures. Thompson and Wallace (1998) noted that the wintertime AO is strongly coupled with surface air temperature fluctuations over Eurasia. Ogi *et al.* (2004a) also demonstrated that the summer air temperature over Eurasia is related to the summer AO. The annual mean AO signal in Figure 2f reflects the surface temperature signals over Eurasia throughout the year. Therefore, a positive annual AO causes anomalous warmth over the Amur River basin and the Okhotsk Sea.

SSTs before the ice formation season are an important parameter influencing subsequent ice formation. The Okhotsk Sea usually starts to freeze in early December; thus, SST conditions during autumn (September–November) were considered. Figure 3 shows the correlation/regression coefficients of the autumn SST over the Okhotsk Sea with the discharge (a), the sea ice (b), and the annual AO index (c). Autumn SST anomalies show positive, negative and positive correlations with discharge, sea ice and annual AO, respectively, over the Okhotsk Sea. Autumn SSTs are warmer when the annual AO phase is positive. Such SST anomalies are consistent with the correlation of the annual AO with the sea ice because the positive annual AO causes anomalously warm air temperatures over the Okhotsk Sea (see Figure 2f). The warmer SSTs inhibit ice formation in the subsequent winter.

Discussion and Conclusions

This study investigated the negative correlation between Amur River discharge and Okhotsk Sea ice formation. The results show that the annual AO regulates the annual Amur River discharge. Positive annual AO causes anomalous horizontal moisture flux convergence over the Amur River basin, resulting in increased discharge. It should be noted that atmospheric patterns for the warmer half of the year that is correlated with the annual discharge and the ice are also similar to those of the AO. The warmer atmospheric temperatures accompanying the positive annual AO cause anomalously warm autumn SSTs in the Okhotsk Sea. The warm temperatures related to the annual AO are consistent with the warm summer temperatures given by Ogi *et al.* (2004a), which showed that anomalously warm

summer temperatures over Eurasia are closely related to the positive phase of the summer AO. The warm autumn SSTs inhibit subsequent sea ice formation. Yamazaki (2000) and Ogi *et al.* (2004b) have suggested that the winter NAO/AO influences Okhotsk Sea ice formation because of the warm atmospheric temperatures over Eurasia associated with the positive winter AO. Therefore, AO-related warm temperatures in autumn and winter over Eurasia and the Okhotsk Sea also inhibit sea ice formation. The presence of a strong control, that is, the annual AO, on both summer discharge and winter ice masks the influence of the freshwater supply on the sea ice variation at least at multiyear timescales. If the influence of freshwater discharge dominated, discharge and sea ice would be positively correlated. In practice, the negative correlation between the discharge and the sea ice arises mainly from variations in the annual AO.

This study investigated atmospheric correlations between individual months and annual river discharge and the sea ice. However, significant AO-like signatures, as exhibited in Figure 2, were not present in the maps of the individual months. It is the longtime integration of AO-related atmospheric circulations that influence both annual discharge and sea ice. Examinations from the perspective of the annual AO thus yield a new look at persistence in climate systems that extend beyond seasons, in particular for climate subsystems that have a longer memory than the atmosphere.

Better correlations using the three-year moving average than without the moving average may be due to the following reasons. In the winter half of the year, precipitation over the Amur basin is in the form of snow, which does not melt until the following spring. The snowfall thus plays a role in memory beyond the year. Because the AO is related to the air temperature, the ratio between the snowfall and the rainfall over the basin is also related to the AO. Warm summer air temperature brings about a large amount of snowmelt, which also influences the river discharge.

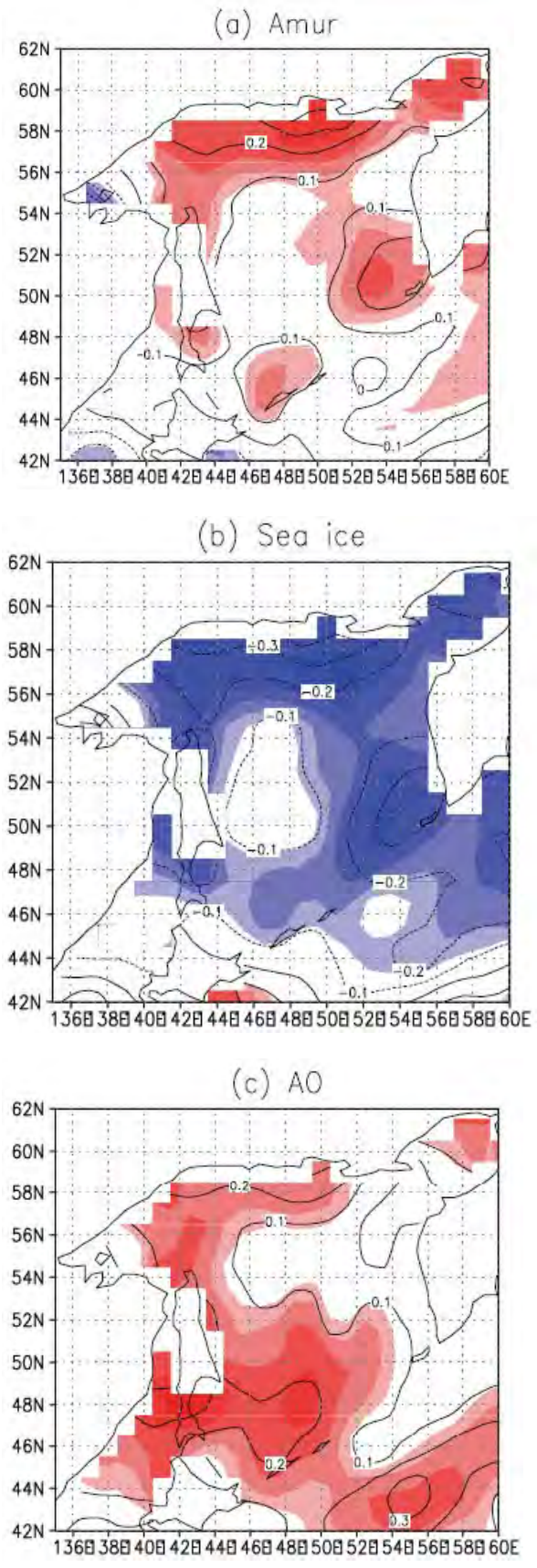

Fig. 3 As in Figure 2 except for the correlation/ regression maps of sea surface temperature (SST) in autumn (September–November) and (a) the annual mean Amur River discharge, (b) the maximum sea ice in the Okhotsk Sea, and (c) the annual mean AO index. Contours show regression values and shadings indicate the correlation coefficients. The correlation coefficients below 0.3 are not plotted.

This study demonstrated only the cause of the negative correlation. The next step is a detailed analysis of the large-scale hydrological processes related to the annual AO in the Amur River basin, and quantitative analyses of the relationship between autumn SST preconditioning and the winter sea ice formation. The present results suggest persistence in the AO from the previous summer to winter, which will be examined in future work.

Acknowledgements

The authors express their thanks to H. Kaneko, K. Oshima, and T. Yasunari. We deeply thank all the staff in Far Eastern Hydrometeorology and Environmental Monitoring, and FERHRI, Russia, in particular M.A. Danchenkov for his special collaboration on this research.

References

Fang, Z. and Wallace, J.M. 1994. Arctic sea ice variability on a timescale of weeks and its relation to atmospheric forcing. *J. Clim*. **7**: 1897– 1914.

Kistler, R., Kalnay, E., Collins, W., Saha, S., White, G., Woollen, J., Chelliah, M., Ebisuzaki, W., Kanamitsu, M., Kousky, V., van den Dool, H., Jenne, R. and Fiorino, M. 2001. The NCEP-NCAR 50-year reanalysis: Monthly means CD-ROM and documentation. *Bull. Am. Meteorol. Soc*. **82**: 247–267.

Ogi, M. and Tachibana, Y. 2006. Influence of the annual Arctic Oscillation on the negative correlation between Okhotsk Sea ice and Amur River discharge. *Geophys. Res. Lett.* **33**: L08709, doi:10.1029/2006 GL025838.

Ogi, M., Tachibana, Y., Nishio, F. and Danchenkov, M.A. 2001. Does the fresh water supply from the Amur River flowing into the Sea of Okhotsk affect sea ice formation? *J. Meteorol. Soc. Jpn*. **79**: 123–129.

Ogi, M., Tachibana, Y. and Yamazaki, K. 2003. Impact of the wintertime North Atlantic Oscillation (NAO) on the summertime atmospheric circulation. *Geophys. Res. Lett.* **30**: 1704, doi: 10.1029 /2003GL017280.

Ogi, M., Yamazaki, K. and Tachibana, Y. 2004a. The summertime annular mode in the Northern Hemisphere and its linkage to the winter mode. *J. Geophys. Res.* **109**: D20114, doi: 10.1029/2004 JD004514.

Ogi, M., Tachibana, Y. and Yamazaki, K. 2004b. The connectivity of the winter North Atlantic Oscillation (NAO) and the summer Okhotsk high. *J. Meteorol. Soc. Jpn.* **82**: 905–913.

Tachibana, Y., Honda, M. and Takeuchi, K. 1996. The abrupt decrease of the sea ice over the southern part of the Sea of Okhotsk in 1989 and its relation to the recent weakening of the Aleutian low. *J. Meteorol. Soc. Jpn*. **74**: 579– 584.

Thompson, D.W.J. and Wallace, J.M. 1998. The Arctic Oscillation signature in the wintertime geopotential height and temperature fields. *Geophys. Res. Lett*. **25**: 1297– 1300.

Yamazaki, K. 2000. Interaction between the wintertime atmospheric circulation and the variation in the sea ice extent of the Sea of Okhotsk. *Seppyo* **62**: 345–354 (in Japanese with English abstract).

Changes in the Sea of Okhotsk due to global warming – Weakening pump function to the North Pacific

Kay-Ichiro Ohshima, Takuya Nakanowatari, Takeshi Nakatsuka, Jun Nishioka and Masaaki Wakatsuchi

Institute of Low Temperature Science, Hokkaido University, Sapporo, Japan
E-mail: ohshima@lowtem.hokudai.ac.jp

Introduction

It is known that North Pacific Intermediate Water (NPIW), characterized by a salinity minimum at 26.8σ_θ, is a major water mass at the intermediate level of the North Pacific (*e.g.*, Reid, 1965). Figure 1 shows the distribution of potential temperature and oxygen content on the 27.0σ_θ isopycnal surface in the North Pacific. Cold, high oxygen water seems to originate from the Sea of Okhotsk. High chlorofluorocarbon concentrations (Warner *et al.*, 1996) also originate from the Sea of Okhotsk. These distributions suggest that the ventilation source of intermediate water in the North Pacific, including NPIW, is the Sea of Okhotsk. Since large amounts of sea ice are formed in the Sea of Okhotsk, the densest water in the North Pacific (or to be exact, the densest water on the surface of the North Pacific) is produced there. Sinking of this dense water creates an overturning down to the intermediate depths in the North Pacific. The Okhotsk thus plays a role as the pump of the North Pacific.

Figure 2 shows the annual mean cumulative sea ice production calculated from microwave ice information and heat budget (Ohshima *et al.*, 2003). The northwestern shelf is found to be the far highest ice production region in the Sea of Okhotsk. Over the northwestern shelf, a large amount of sea ice is produced due to severe winds from northeastern Eurasia in winter. The sea ice production leads to the formation of cold, oxygen-rich dense shelf water (DSW) with densities of up to 27.0σ_θ (Shcherbina *et al.*, 2003). The DSW is transported southward into the intermediate layer in the southern Okhotsk Sea, and is mixed with intermediate water coming from the North Pacific. This mixing forms the coldest, freshest and oxygen-richest water in the North Pacific in the density range of 26.8–27.4σ_θ (Talley, 1991), which is called Okhotsk Sea Mode Water (Yasuda, 1997) or Okhotsk Sea Intermediate Water (OSIW) (Itoh *et al.*, 2003). The signal of OSIW extends downward to 27.4σ_θ owing to diapycnal mixing caused by strong tidal currents around the Kuril Straits (Wong *et al.*, 1998). The OSIW outflows to the North Pacific through the Kuril Straits and then mixes with East Kamchatka Current Water to form the Oyashio water. The Oyashio water reaches the confluence of the subtropical and subarctic gyres, and then part of the Oyashio water flows northeastward as the Subarctic Current (SAC), bounding the subarctic gyre on the south.

Warming and Oxygen Decrease Trend

The results of the analyses in this section are based on Nakanowatari *et al.* (2007). For the trend analyses, we have used all available data for

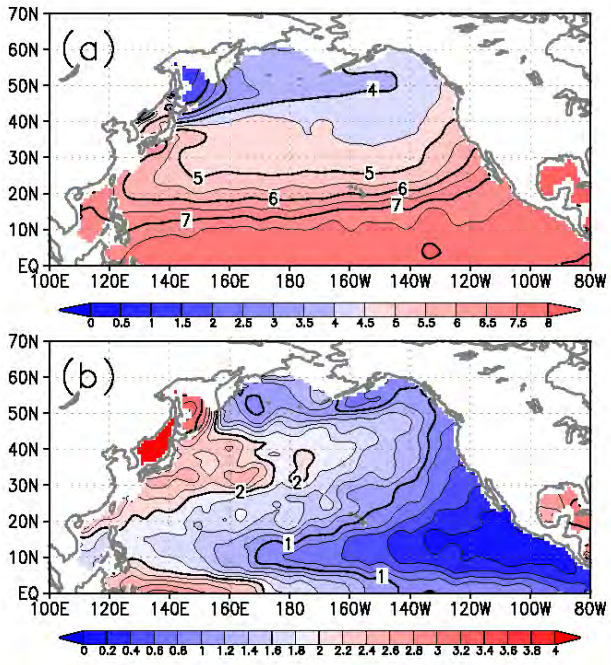

Fig. 1 Horizontal distribution of (a) potential temperature (°C) and (b) dissolved oxygen content (ml/l) on the 27.0σ_θ isopycnal surface in the North Pacific. These maps are based on World Ocean Atlas 1994 (Levitus *et al.*, 1994).

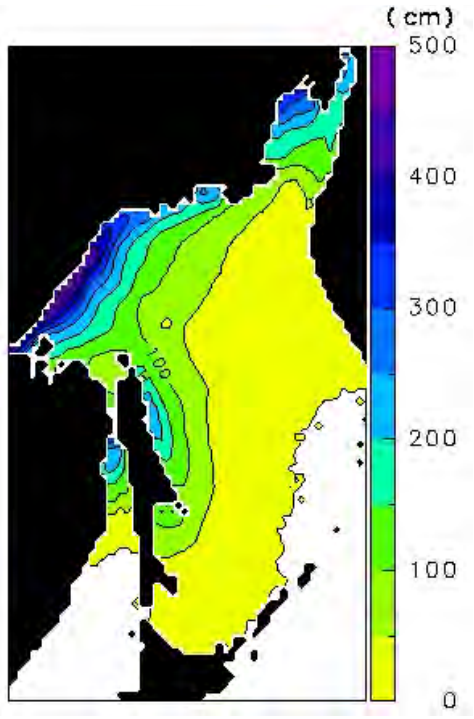

Fig. 2 Annual mean cumulative sea ice production, represented by the ice thickness (cm). Estimation is based on the sea ice information from the satellite microwave and heat budget calculation. After Ohshima *et al.* (2003).

temperature, salinity and dissolved oxygen, taken from the World Ocean Database (WOD01), observational data obtained by the Japan–Russia–United States international joint study of the Sea of Okhotsk from 1998 to 2004, data archived by the Japan Oceanographic Data Center, and profiling float data obtained by the international Argo program from 2000 to 2004. After the quality control, a gridded dataset of potential temperature anomalies on isopycnal surfaces was then prepared for the period 1955–2004, and one of dissolved oxygen for the period 1960–2004.

Figure 3 shows linear trend maps of intermediate water temperature on the $27.0\sigma_\theta$ isopycnal surface for the past 50 years. Significant warming trends are observed in the northwestern North Pacific and the Sea of Okhotsk. The warming trend in these regions is most prominent at density $27.0\sigma_\theta$, and the largest warming area exists in the western part (47.5°–55°N, 145°–147.5°E) of the Sea of Okhotsk with an average of 0.68°C/50-yr. The warming trend at $27.0\sigma_\theta$ seems to extend along the pathway of the OSIW (see the acceleration potential at $27.0\sigma_\theta$, indicated by green contours in Figure 3). A significant warming trend is observed in the Oyashio and SAC regions, but not in the East Kamchatka Current region, *i.e.*, upstream of the Sea of Okhotsk. Since the intermediate water masses in the Oyashio and SAC regions are largely affected by the OSIW (Yasuda, 1997), these results indicate that the warming trend in the northwestern North Pacific may be caused by advection of warmed OSIW.

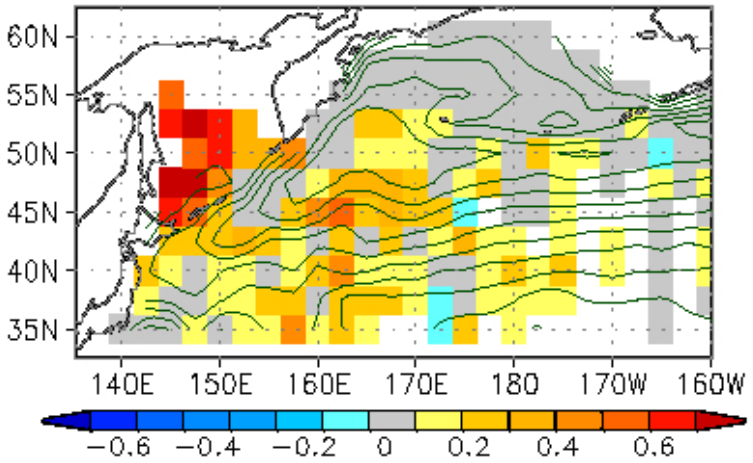

Fig. 3 Linear trends (colors in °C/50-yr) of potential temperature anomalies at density $27.0\sigma_\theta$ (approximately 300–500 m deep) from 1955 to 2004 in the North Pacific. Green contours indicate acceleration potential at $27.0\sigma_\theta$ relative to 2000 dbar, derived from our dataset. Modified from Nakanowatari *et al.* (2007).

Figure 4 shows the time series of temperature and oxygen content anomalies at 27.0σ_θ, averaged over the Sea of Okhotsk. A positive and negative linear trend is the most significant feature for temperature and oxygen content, respectively. The temperature has increased by 0.62 ± 0.18°C (significant at a 99% confidence interval) during the past 50 years from 1955 through 2004. A similar result is obtained by Itoh (2007). The oxygen has decreased by 0.58 ± 0.34 ml/l (significant at a 95% confidence interval) for the past 45 years. The Oyashio and SAC regions also show a warming trend with the magnitude being about half of that for the Okhotsk and a decreasing trend for oxygen with a value less than that for the Okhotsk. The decreasing trend for oxygen in the Oyashio is consistent with Ono *et al.* (2001).

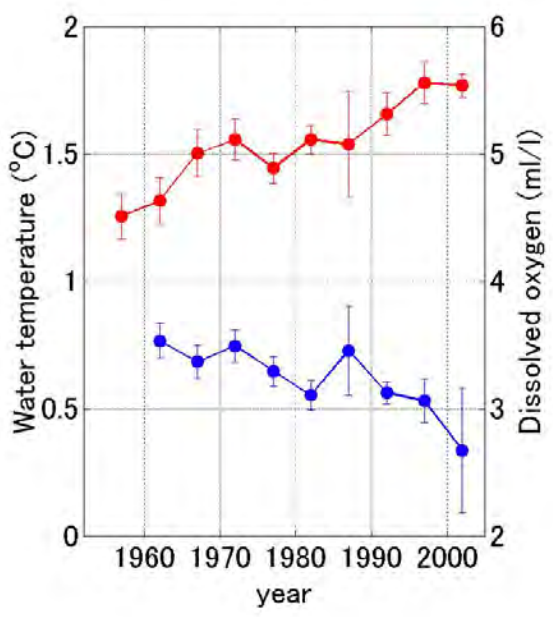

Fig. 4 Time series of potential temperature (red line) and dissolved oxygen content (blue line) of the intermediate water at 27.0σ_θ, averaged over the Sea of Okhotsk, during the past 50 years. Closed circles show a 5-yr average with errors at the 95% confidence interval for the averages.

It is shown that warming and oxygen-decreasing trends in the intermediate water are most prominent in the Sea of Okhotsk. Moreover, these trends appear to extend to the northwestern North Pacific along the pathway of the water mass originating from the Sea of Okhotsk. These facts suggest that the trends in the northwestern North Pacific are due to preceding changes of water-mass properties in the Sea of Okhotsk. Intermediate water in the Sea of Okhotsk retains its cold and oxygen-rich properties by mixing with dense shelf water (DSW) associated with sea ice production in the coastal polynya of the northwestern shelf. The largest warming trend occurs in the western part of the Sea of Okhotsk (Fig. 3), to which DSW is transported from the northwestern shelf (Fukamachi *et al.*, 2004). Therefore, we suppose that the main cause of the warming and oxygen-decreasing trends is the weakening of DSW production.

Global Warming and the Sea of Okhotsk

DSW formation is caused by sea ice production. Thus we examine the change of the sea ice extent or production in the Sea of Okhotsk. Over the last three decades since accurate observation by satellite became possible, sea ice extent in the Sea of Okhotsk has decreased by approximately 150,000 km^2, corresponding to about 10% of the entire area of the Sea of Okhotsk (blue line in Fig. 5). It has been also revealed that yearly variability of sea ice extent in the Sea of Okhotsk is highly correlated with that of surface air temperatures in the upwind region of the Okhotsk (red line in Fig. 5). Of particular note is that this temperature has risen by approximately 2.0°C over the past 50 years (2.0 ± 1.4°C/50-yr, significant at a 99% confidence level). This value far exceeds the rate of average temperature increase worldwide (0.74°C over the past 100 years), thereby clearly indicating that the region is significantly affected by global warming. The correlation between this temperature and the sea ice extent (r = –0.61, significant at a 95% confidence level) suggests that decreases in the sea ice preceded the beginning of satellite observations.

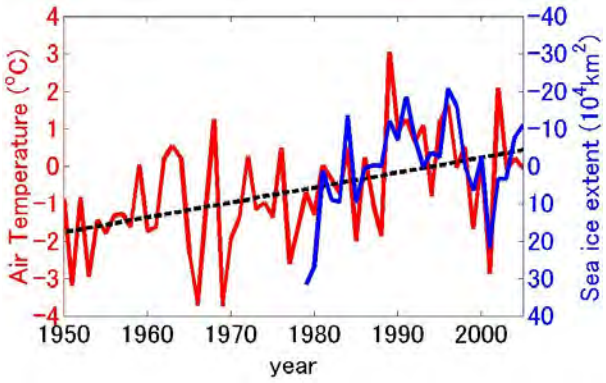

Fig. 5 Time series of sea ice extent anomaly in February (blue line) and surface air temperature anomaly in the upwind region (50°–65°N, 110°–140°E) (red line) for the Sea of Okhotsk. Note that the scale of the sea ice extent is inverted (the axis on the right). Surface air temperatures are the mean values between October and March. Modified from Nakanowatari *et al.* (2007).

Although satellite measurements have been available only since the 1970s, visual observations at the Hokkaido coast, located on the southern boundary of sea ice extent in the Sea of Okhotsk, show the decreasing trend in the length of the sea ice season during the past 100 years (Aota, 1999). These trends of air temperature and sea ice season suggest that sea ice extent, accordingly sea ice production, has likely decreased during the past 50 years. During the current global warming, the surface air temperature anomaly in autumn and winter is particularly large over northeastern Eurasia (Serreze *et al.*, 2000). The DSW production area of the northwestern shelf in the Sea of Okhotsk is located where the winter monsoon from northeastern Eurasia directly transports cold air masses. Therefore, intermediate water in the Sea of Okhotsk, which is ventilated through DSW, may be sensitive to the global warming.

Possible Scenario

In a nutshell, the Sea of Okhotsk is highly sensitive to global warming: over the past 50 years, the level of sea ice production has decreased and the amount of dense water sinking has thus declined, thereby weakening the overturning in the North Pacific scale. To put it simply, the recent global warming has weakened the Sea of Okhotsk's workings as a pump.

Recent studies suggest that OSIW has a significant role in material circulation of the intermediate layer in the North Pacific. Hansell *et al.* (2002) indicated that dissolved organic carbons in NPIW originate from the Sea of Okhotsk. Nakatsuka *et al.* (2004) showed that large amounts of dissolved and particulate organic carbons are exported from the highly productive northwestern shelf into the intermediate layer in the Sea of Okhotsk through the outflow of DSW. Moreover, recent observational data show that in the northwestern North Pacific, iron may come from the intermediate water of the Sea of Okhotsk (Nishioka *et al.*, 2007). Iron is an essential micronutrient for phytoplankton and is thus considered an important factor in determining biological productivity. It has been recently revealed that when dense shelf water sinks to the intermediate layer in the Sea of Okhotsk, iron is also brought to this layer. We hypothesize that this iron is also supplied to the western area of the North Pacific and supports high biological productivity there. If that is the case, it is also suggested that if global warming weakens sea ice production in the Sea of Okhotsk, iron supplies will decrease in the North Pacific as well as in the Sea of Okhotsk, thus reducing levels of biological productivity and fishery resources.

Figure 6 summarizes our proposal with schematics. Because the Sea of Okhotsk is an area sensitive to the current global warming, it has experienced a decrease in the production of sea ice and dense shelf water in the northwestern shelf during the past 50 years. This possibly causes a decrease in the supply of iron in the intermediate layer in the Sea of Okhotsk and further in the North Pacific. Finally, this might induce the decrease in primary biological production, fishery resources, and capacity of CO_2 absorption.

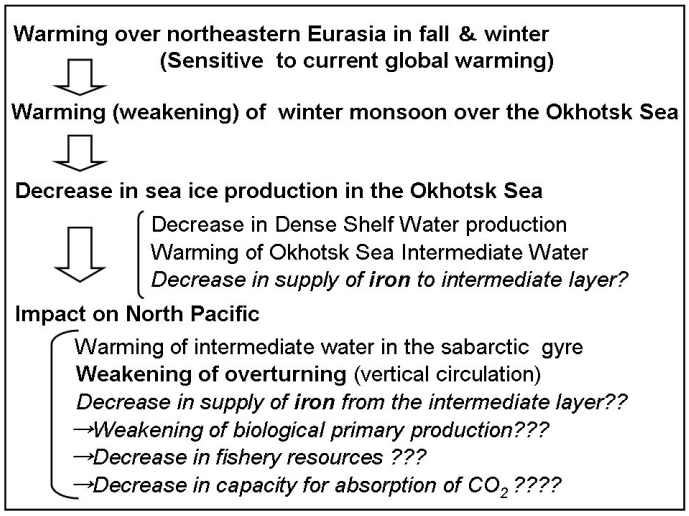

Fig. 6 Schematic showing the impact of the Sea of Okhotsk on the North Pacific through global warming. Bold letters indicate a fact evidenced by observations and analyses. Italic letters indicate a hypothesis. The larger the number of question marks indicates the larger the uncertainty.

Acknowledgements

This work has been carried out under the cooperation with the Far Eastern Regional Hydrometeorological Research Institute, Russia and S. C. Riser of the University of Washington. We would like to thank Kazuya Ono and Kyoko Kitagawa for their support in data processing.

References

Aota, M. 1999. Long-term tendencies of sea ice concentration and air temperature in the Okhotsk Sea coast of Hokkaido. PICES Sci. Rep. No 12, pp. 1–2.

Fukamachi, Y., Mizuta, G., Ohshima, K.I., Talley, L.D., Riser, S.C. and Wakatsuchi, M. 2004. Transport and modification processes of dense shelf water revealed by long-term moorings off Sakhalin in the Sea of Okhotsk. *J. Geophys. Res*. **109**: C09S10, doi:10.1029/2003/JC001906.

Hansell, D.A., Carlson, C.A. and Suzuki, Y. 2002. Dissolved organic carbon export with North Pacific Intermediate Water formation. *Global Biogeochem. Cycles* **16**: 1007, doi:10.1029/2000GB001361.

Itoh, M. 2007. Warming of intermediate water in the Sea of Okhotsk since the 1950. *J. Oceanogr*. **63**: 637–641.

Itoh, M., Ohshima, K.I. and Wakatsuchi, M. 2003. Distribution and formation of Okhotsk Sea Intermediate Water: an analysis of isopycnal climatology data. *J. Geophys. Res*. **108**: 3258, doi:10.1029/2002JC001590.

Levitus, S., Burget, R. and Boyer, T. 1994. World Ocean Atlas 1994. NOAA Atlas NESDIS 3 and 4, U.S. Department of Commerce, Washington, DC.

Nakanowatari, T., Ohshima, K.I. and Wakatsuchi, M. 2007. Warming and oxygen decrease of intermediate water in the northwestern North Pacific, originating from the Sea of Okhotsk, 1955–2004. *Geophys. Res. Lett.* **34**: L04602, doi:10.1029/2006GL028243.

Nakatsuka, T., Toda, T., Kawamura, K. and Wakatsuchi, M. 2004. Dissolved and particulate organic carbon in the Sea of Okhotsk: Transport from continental shelf to ocean interior. *J. Geophys. Res*. **109**: C09S14, doi:10.1029/2003JC001909.

Nishioka, J., Ono, T., Saito, H., Nakatsuka T., Takeda S., Yoshimura, T., Suzuki, K., Kuma, K., Nakabayashi, S., Tsumune, D., Mitsudera, H., Johnson, W.K. and Tsuda, A. 2007. Iron supply to the western subarctic Pacific: importance of iron export from the Sea of Okhotsk. *J. Geophys. Res.* **112**: C10012, doi:10.1029/2006JC004055.

Ohshima, K.I., Watanabe, T. and Nihashi, S. 2003. Surface heat budget of the Sea of Okhotsk during 1987–2001 and the role of sea ice on it. *J. Meteorol. Soc. Jpn.* **81**: 653-677.

Ono, T., Midorikawa, T., Watanabe, Y.W., Tadokoro, K. and Saino, T. 2001. Temporal increases of phosphate and apparent oxygen utilization in the surface waters of western subarctic Pacific from 1968 to 1998. *Geophys. Res. Lett*. **28**: 3285–3288.

Reid, J.L. 1965. Intermediate water of the Pacific Ocean. Johns Hopkins Oceanogr. Stud. 2, 85 pp.

Serreze, M.C., Walsh, J.E., Chapin, F.S., III, Osterkamp, T., Dyurgerov, M, Romanovsky, V., Oechel, W.C., Morison, J., Zhang, T. and Barry, R.G. 2000. Observational evidence of recent change in the northern high-latitude environment. *Climatic Change* **46**: 159–207.

Shcherbina, A.Y., Talley, L.D. and Rudnick, D.L. 2003. Direct observations of North Pacific ventilation: brine rejection in the Okhotsk Sea. *Science* **302**: 1952–1955.

Talley, L.D. 1991. An Okhotsk Sea water anomaly: implications for ventilation in the North Pacific. *Deep-Sea Res. Part A* **38**(suppl.): S171–S190.

Warner, M.J., Bullister, J.L., Wisegraver, D.P., Gammon, R.H. and Weiss, R.F. 1996. Basin-wide distributions of chlorofluorocarbons CFC-11 and CFC-12 in the North Pacific. *J. Geophys. Res*. **103**: 2849–2865.

Wong, C.S., Matear, R.J., Freeland, H.J., Whitney, F.A. and Bychkov, A.S. 1998. WOCE line P1W in the Sea of Okhotsk: 2. CFCs and the formation rate of intermediate water. *J. Geophys. Res.* **103**: 15625–15642.

Yasuda, I. 1997. The origin of the North Pacific Intermediate Water. *J. Geophys. Res*. **102**: 893–909.

Interannual variations of the East-Kamchatka and East-Sakhalin Currents volume transports and their impact on the temperature and chemical parameters in the Okhotsk Sea

Andrey G. Andreev

V.I. Il'ichev Pacific Oceanological Institute, FEB RAS, Vladivostok, Russia. E-mail: andreev@poi.dvo.ru

Introduction

The Okhotsk Sea is one of the marginal seas of the North Pacific Ocean, and is bounded by the Kamchatka Peninsula, Siberia, Sakhalin Island, Hokkaido and the Kuril Islands. It is connected with the Japan Sea through the La Perouse (Soya) and Tartar Straits and with the Pacific Ocean through the Kuril Island Chain. The physical and chemical parameters in the intermediate waters of the Okhotsk Sea are determined by the supply of the Dense Shelf Water (formed in the coastal polynyas as result of cooling and brine injection under ice), the inflow of dense transformed subtropical waters from the Japan Sea in spring through La Perouse Strait, and the water exchange between the Okhotsk Sea and the subarctic Pacific. The increase/decrease in water exchange between the subarctic Pacific and the Okhotsk Sea and the decrease/increase in the supply of Dense Shelf Water (DSW) result in the decrease/increase in dissolved oxygen (DO) and increase/decrease in temperature, dissolved inorganic carbon (DIC) and nutrients in intermediate waters of the Okhotsk Sea (Andreev and Zhabin, 2000; Andreev and Kusakabe, 2001; Andreev and Baturina, 2005).

Andreev and Baturina (2005) have shown that between 1948 and 2000 in the Kuril Basin of the Okhotsk Sea there is an average increase in isopycnal depth (H) of $26.8\sigma_\theta$ and $27.0\sigma_\theta$ with a rate of 2.0 ± 0.9 m yr^{-1} and 1.4 ± 1.0 m yr^{-1}, respectively. At σ_θ= 27.0 the increase in H coincides with an increased temperature (0.010 ± 0.004°C yr^{-1}). The interdecadal variations and trend in DO show a good correlation with the intensity of the Aleutian Low pressure cell, represented by the North Pacific Index in winter (Andreev and Kusakabe, 2001). In the intermediate water layer of the Kuril Basin (σ_θ = 26.8 and σ_θ = 27.0) there is an average decrease in the DO concentration at a rate of –0.9 ± 0.4 µmol kg^{-1} yr^{-1} (Andreev and Baturina, 2005). The interannual variations in the DO, DIC and temperature in the Kuril Basin area could be explained by the variations in the Alaska Gyre intermediate waters supply (by the Alaskan Stream and East-Kamchatka Currents) to the western subarctic Pacific (Andreev and Baturina, 2005). In addition to the water exchange between the subarctic Pacific and Okhotsk Sea, the variations in the formation and transport rates of the DSW (by the East-Sakhalin Current) probably can generate the interannual DO and temperature signals observed in the Kuril Basin region of the Okhotsk Sea.

In this study we investigate the interannual variations in the East-Kamchatka and Oyashio Currents (EKC/Oyashio) and East-Sakhalin Current (ESC) volume transports and their impact on temperature and chemical parameters in the Kuril Basin of the Okhotsk Sea (Fig. 1). We demonstrate that there is a strong correlation between the interannual changes of EKC/Oyashio and ESC transport rates computed by using the Sverdrup relation and the temporal variations in the sea level at coastal stations in winter. The variations in EKC/Oyashio volume transport are responsible for the observed temperature and DO interannual changes in the intermediate waters of the Okhotsk Sea.

Data and Methods

To analyze the temporal changes of temperature and chemical parameters in the intermediate waters of the Okhotsk Sea, the data sets of the NOAA Oceanographic Data Center, Japan Oceanographic Data Center, Institute of Ocean Sciences (Line P oceanographic data) and the Pacific Oceanological Institute were used. Sverdrup volume transports in the Okhotsk Sea and subarctic Pacific were calculated from the wind stress data provided by the NOAA-CIRES Climate Diagnostic Center NCEP/NCAR (National Centers for Environmental Prediction/National Center for Atmospheric Research) Reanalysis Project. The sea level measurements at the coastal stations of the Kamchatka Peninsula (Petropavlovsk-Kamchatsky),

Kuril (Severo-Kurilsk) and Sakhalin (Vzmorie) islands (Fig. 1) were provided by the Sakhalin Meteorological Agency. Sea level data were corrected for the variations in atmospheric pressure.

Results and Discussion

East-Kamchatka/Oyashio and East-Sakhalin currents volume transports

Positive wind stress curls over the northern North Pacific and Okhotsk Sea in winter, determined by the strength and position of the Aleutian Low and Siberian High, force the cyclonic circulations in these basins. The ESC and EKC/Oyashio currents are the western boundary currents of the wind-driven cyclonic gyres in the Okhotsk Sea and the northern North Pacific, respectively. Spin up/down of the cyclonic gyres in the Okhotsk Sea and subarctic Pacific driven by the wind stress curl results in the increased/decreased ESC and EKC/Oyashio volume transports and increase/decrease in sea level at the coastal stations of the Sakhalin and Kuril Islands and Kamchatka Peninsula.

The interannual variations in the volume transports of the EKC/Oyashio and ESC calculated by the Sverdrup relation show a good correlation with the change in sea level at the coastal stations of Kamchatka Peninsula, Kuril Islands and Sakhalin Island in winter (Fig. 2, Andreev and Shevchenko, 2008). The cross-correlation coefficients between the volume transport of the EKC/Oyashio and the sea level at Stns. Petropavlovsk-Kamchatsky (1965–2002) and Severo-Kurilsk (1968–1995) are equal to 0.69 and 0.60, respectively. The cross-correlation coefficient between the volume transport of the ESC and the sea level at Stn. Vzmorie (1952–1988) is 0.72.

The wide northern shelf can interrupt the Sverdrup balance in the Okhotsk Sea and significantly reduce the wind-driven volume transport of the ESC due to bottom friction (Simizu and Ohshima, 2006). In our study, the change in EKC Sverdrup transport driven by bottom friction over the shelf is not taken into consideration.

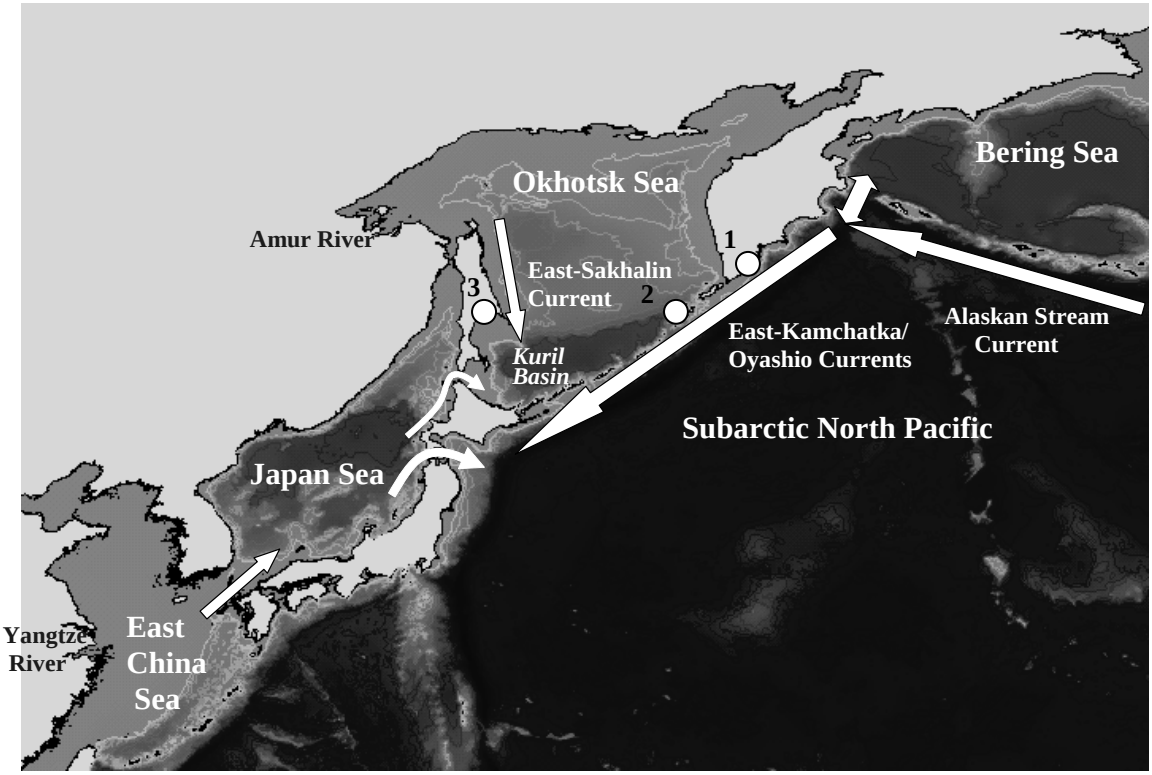

Fig. 1 Schematic representation of currents in the northwestern North Pacific and the location of coastal sea level observation stations. Number 1 refers to Petropavlovsk-Kamchatsky, 2 to Severo-Kurilsk, and 3 to Vzmorie.

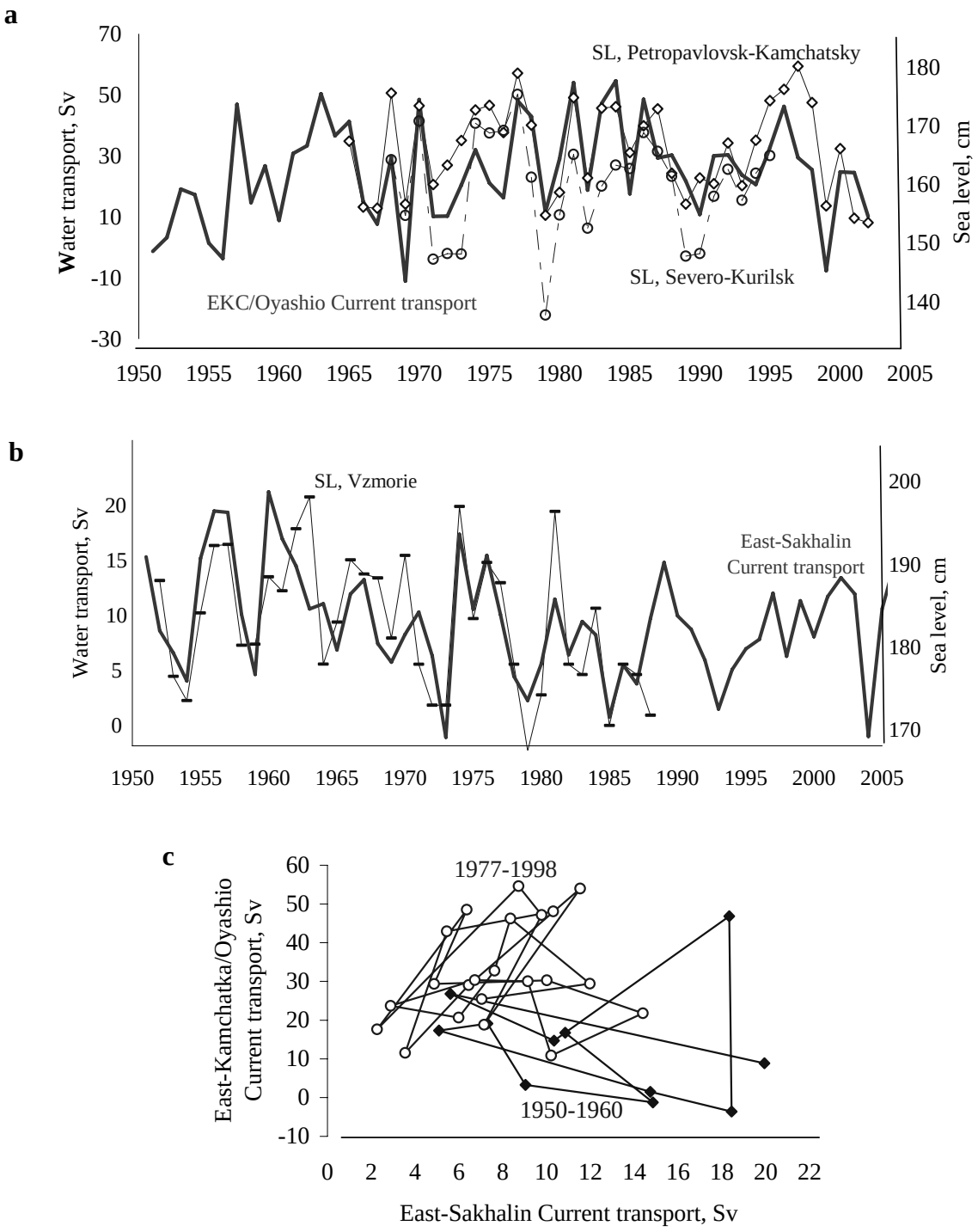

Fig. 2 (a) Temporal variations of the EKC/Oyashio volume transport and sea level (SL) at the Stns. Petropavlovsk-Kamchatsky and Severo-Kurilsk in winter, (b) temporal variations of the ESC volume transport and the sea level at the Stn. Vzmorie in winter, and (c) EKC/Oyashio volume transport versus ESC volume transport in winter.

There is no statistically significant correlation (r = –0.10) between the interannual variations in the EKC/Oyashio volume transport and the ESC volume transport for a 60-year period (1949–2008). Such a correlation was observed during brief (10–20 years) periods determined by the strength and position of the Aleutian Low and Siberian High in winter. Between 1950 and 1960 the spinup of the cyclonic circulation in the subarctic North Pacific (and an increased transport of the EKC/Oyashio) was accompanied by a slowdown of the ESC transport. Between 1977 and 1998 the increased/decreased ESC transport corresponded to the increased/ decreased EKC/Oyashio transport (Fig. 2c).

Impact of the EKC/Oyashio and ESC on temperature and dissolved oxygen

The interannual changes in the depth of the $26.8\sigma_\Theta$ isopycnal, the temperature on the $27.0\sigma_\Theta$ isopycnal and DO on the $26.8\sigma_\Theta$ and $27.0\sigma_\Theta$ isopycnals in the Kuril Basin of the Okhotsk Sea between 1950 and 1995 can be described by a linear combination of the EKC/Oyashio and ESC volume transports (Figs. 3a, b and c).

The cross-correlation coefficients between the volume transport of the EKC/Oyashio (filtered by a 3-yr running mean) and the depth of the $26.8\sigma_\Theta$ isopycnal, the temperature on the $27.0\sigma_\Theta$ isopycnal and DO on the $26.8\sigma_\Theta$ and $27.0\sigma_\Theta$ isopycnals are 0.71, 0.65, –0.54 and –0.66, respectively. An intensification of the subarctic cyclone gyre (and an increase of the EKC/Oyashio volume transport) decreases the residence time of the Alaskan waters at the northern boundary, and therefore, the intermediate and surface waters become less modified (by cooling and tidal mixing) while they move off the Aleutian Islands and Kamchatka coast. This leads to an increased temperature and decreased DO, and deepening of isopycnals in the Okhotsk Sea. The deepening of the isopycnals, driven by the increased EKC/Oyashio volume transport is probably related to an excess supply of eastern subarctic surface waters ($\sigma_t \sim 25.5$–26.0).

The cross-correlation coefficients between the interannual variations in the ESC volume transport (filtered by a 3-yr running mean) and the depth of $26.8\sigma_\Theta$, temperature on the $27.0\sigma_\Theta$ isopycnal and DO on the $26.8\sigma_\Theta$ and $27.0\sigma_\Theta$ isopycnals in the Kuril Basin area are –0.40, –0.42, 0.49 and 0.40, respectively. The enhanced ESC volume transport corresponds to increased DO, decreased temperature and the shallow depth of $26.8\sigma_\Theta$. The relationships between the Sverdrup transport of the ESC, computed by using wind stress curl and the temperature and DO on the $26.8\sigma_\Theta$ and $27.0\sigma_\Theta$ isopycnals in the Kuril Basin, can be due partly to changes of the DSW formation rate forced by northwest winds in winter.

There are significant discrepancies between the calculated (using the volume transports of ESC and EKC/Oyashio) and the observed temperature and DO in 2000, 2003 and 2004 years (Fig. 3). These discrepancies reflect the changes in DO and temperature of the upstream region (Alaska Gyre area) (Andreev and Baturina, 2006). The intermediate waters of the Alaska Gyre are impacted by a huge (low oxygen and high temperature) eastern subtropical pool (Andreev and Baturina, 2006). The eastern subtropical waters are transported northward by the California undercurrent and then by the Alaska Current and Alaskan Stream Current into the western subarctic Pacific and Okhotsk Sea. The temporal variations in DO and temperature in the Alaska Gyre area show a good correlation with the intensity of the Aleutian Low pressure cell, represented by the North Pacific Index (an averaged sea-level atmospheric pressure in the northern North Pacific in winter (Andreev and Baturina, 2006). Intensification of the Aleutian Low results in the increased northward meridional wind stress at its eastern boundary and enhanced transport of low oxygen eastern subtropical waters into the subarctic region. Figure 3d shows the interannual variations in the difference in DO concentration between the Okhotsk Sea and Alaska Gyre waters ($\Delta DO_{OS\text{-}AG}$). The intensification of the EKC/Oyashio decreases $\Delta DO_{OS\text{-}AG}$ while enhanced ESC volume transport leads to the increased $\Delta DO_{OS\text{-}AG}$.

In addition to the DO, the routine oceanographic observations include the measurements of nutrients and DIC. Comparison of the differences in chemical parameters between the Okhotsk Sea (Kuril Basin region) and Alaska Gyre and the accuracy of its measurements (Table 1) shows that the DO is the best parameter to study the impact of northeastern Pacific waters on the western subarctic Pacific and Okhotsk Sea.

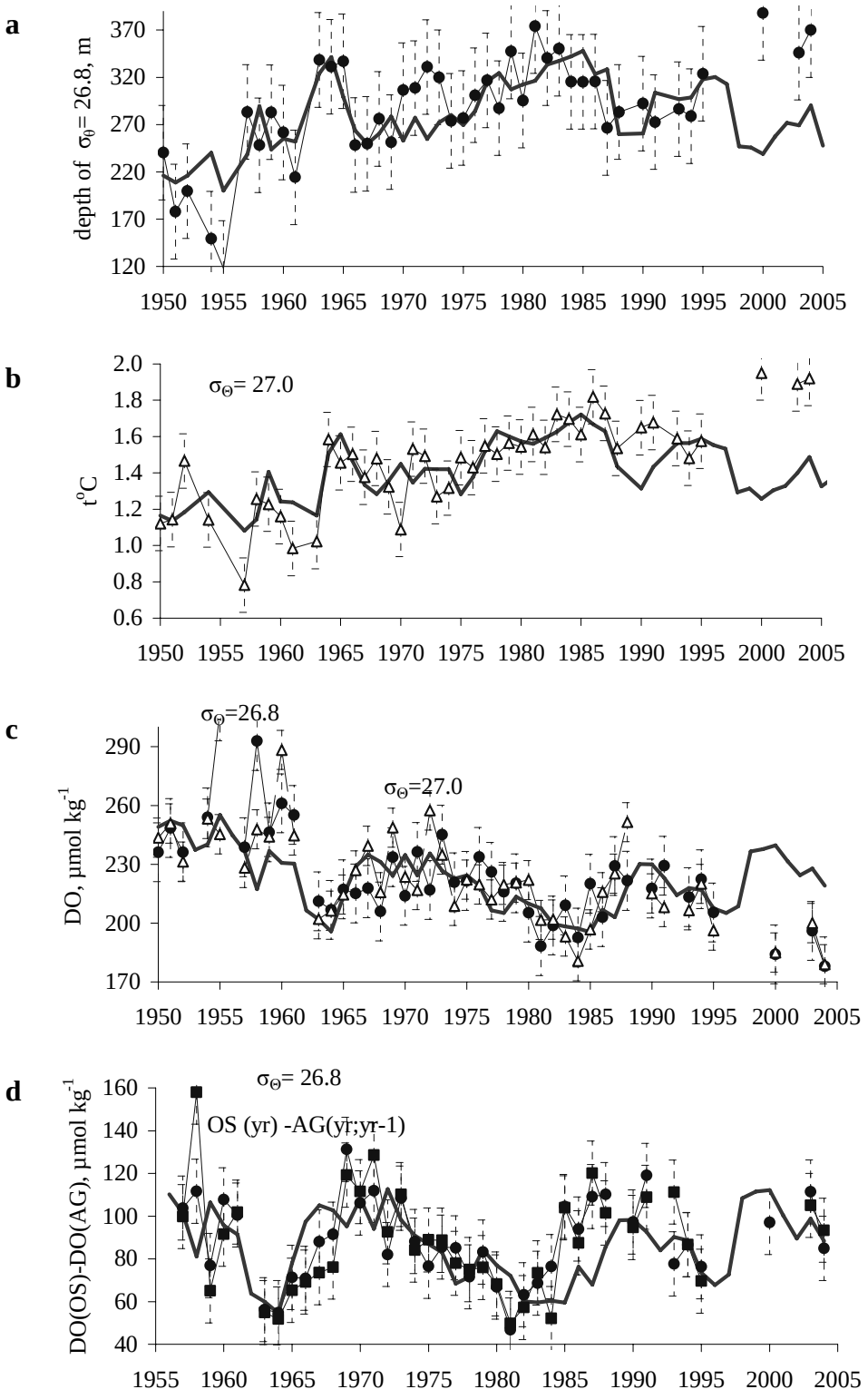

Fig. 3 Temporal variations in (a) the depth of the 26.8σ_θ isopycnal, (b) the temperature on the 27.0σ_θ isopycnal, (c) the DO on the 26.8σ_θ and 27.0σ_θ isopycnals, and (d) the difference in DO between the Okhotsk Sea (OS) and the Alaskan Gyre (AG) waters at σ_θ = 26.8. Solid lines (a–d) show the isopycnal depth, temperature, DO and the difference in DO between OS and AG computed by the linear combination of the EKC/Oyashio and ESC volume transports (filtered by a 3-yr running mean). The errors bars are 95% confidence intervals for isopycnal depth, temperature and DO values.

Table 1 Difference in temperature and chemical parameters between the eastern subarctic Pacific (Alaska Gyre) and the Okhotsk Sea (Kuril Basin region) on isopycnals of $26.8\sigma_\Theta$ and $27.0\sigma_\Theta$.

Parameter	Alaska Gyre–Okhotsk Sea	Accuracy of measurements
Temperature (°C)	3.0	± 0.001–0.005
Dissolved oxygen (μM)	–150	± 2–4
Dissolved inorganic carbon (μM)	50	± 2–3
Nitrate (μM)	6	± 0.2–0.6
Phosphate (μM)	0.4	± 0.02–0.06

Impact of the Bering Sea

The observed temperature and DO changes in the Okhotsk Sea waters can be related to Alaskan water modification in the Bering Sea (Andreev and Watanabe, 2002). Due to a strong halocline, the salt supply into the surface layer is the necessary component for subarctic North Pacific intermediate water ventilation. In the Bering Sea it can be added to seawater as brine during ice formation in the northern and western shelf areas. Interaction of the Bering Slope Current water with the DSW formed in the Bering Sea in winter can enhance the intermediate waters of the EKC with DO. Another source of salt for the surface layer of the Bering Sea is an advection of the more saline water from low latitude areas through the straits of the Aleutian Islands. Intensification of the Western Subarctic Gyre in the 1950s increased meridional transport of saline water from low to high latitudes in the central North Pacific, thereby triggering the formation of dense water and intermediate layer ventilation in the Bering Sea. During this period the EKC waters were a source of low temperature and high oxygen waters for the intermediate layer of the Okhotsk Sea (Andreev and Watanabe, 2002; Andreev and Baturina, 2006).

Impact of the Japan Sea

The Okhotsk Sea is connected to the Japan Sea through La Perouse (Soya) Strait. Warm saline water, originating from the Tsushima Warm Current in the Japan Sea, flows into the Okhotsk Sea and forms the Soya Current flowing southeastward along the coast of Hokkaido. Japan Sea surface and subsurface waters are significantly impacted by East China Sea (ECS) shelf waters. Our results suggest that the variations in the transport rate of the ECS subsurface (low oxygen and relatively high nutrients) waters in summer and fall are responsible for the interannual change of the DO in the intermediate waters of the Japan Sea (Andreev, 2008). Human impact on the Yangtze River waters leads to the increase of N* ($[NO_3^-] -16 \cdot [PO_4^{3-}]$) concentrations in the upper waters of the Tsushima Current (Andreev, 2009), and probably the Soya Current.

Future study should clarify how changes in the chemical parameters of the surface and subsurface waters in the Japan Sea (driven by changes in the water transport through the Tsushima Strait and the human impact on the East China Sea waters) affect the biology and chemistry of the Okhotsk Sea waters.

Summary

The impact of the interannual variations in East-Kamchatka and Oyashio Currents (EKC/Oyashio) and East-Sakhalin Current (ESC) volume transports on temperature and chemical parameters in the Kuril Basin of the Okhotsk Sea was analyzed. It is shown that there is a strong correlation between the interannual variations in EKC/Oyashio and ESC Sverdrup transport and the temporal changes of the sea level at the coastal stations of the Kamchatka Peninsula, and Kuril and Sakhalin islands in winter. The variations in EKC/Oyashio and ESC volume transports are responsible for the observed temperature and DO interannual changes in the intermediate waters of the Kuril Basin of the Okhotsk Sea.

References

Andreev, A.G. 2009. Interannual variations of the water transport through the Tsushima/Korea Strait and its impact on the dissolved oxygen in the Japan Sea. *Meteorol. Hydrol.* **34** (in Russian), in press.

Andreev, A.G. and Baturina, V.I. 2005. Interannual variability of the dissolved oxygen and inorganic carbon in the Kuril Basin of the Okhotsk Sea. Proc. of the 20th international symposium on Okhotsk Sea and Sea Ice, Japan, February 20–25, 2005. Mombetsu,

Hokkaido, Japan. The Okhotsk Sea and Cold Ocean Research Association, pp. 85–90.

Andreev, A.G. and Baturina, V.I. 2006. Impacts of the tides and atmospheric forcing variability on dissolved oxygen in the subarctic North Pacific *J. Geophys. Res.* **111**: C05007, doi: 10.1029/2005JC 003277.

Andreev, A. and Kusakabe, M. 2001. Interdecadal variability in DO in the intermediate water layer of the Western Subarctic Gyre and Kuril Basin (Okhotsk Sea). *Geophys. Res. Lett.* **28**: 2453–2456.

Andreev, A.G. and Shevchenko, G.V. 2008. Interannual variations of the East-Kamchatka and East-Sakhalin Currents and its impact on the dissolved oxygen in the Okhotsk Sea and subarctic Pacific. *Meteorol. Hydrol.* **33**: 657–664 (in Russian).

Andreev, A. and Watanabe, S. 2002. Temporal changes in dissolved oxygen of the intermediate water in the subarctic North Pacific. *Geophys. Res. Lett.* **29**: 1680, doi:10.1029/2002GL015021.

Andreev, A.G. and Zhabin, I.A. 2000. Distribution of freons and dissolved oxygen in the Okhotsk Sea intermediate water. *Meteorol. Hydrol.* **25**: 61–69 (in Russian).

Simizu, D. and Ohshima, K.I. 2006. A model simulation in the Sea of Okhotsk and the East Sakhalin Current. *J. Geophys. Res.* **111**: C05016, doi:10.1029/2005JC002980.

Some regularities in the formation of extremely low-ice winter seasons in the Okhotsk Sea

Larisa Muktepavel and Tatyana Shatilina

Pacific Research Institute of Fisheries and Oceanography (TINRO-Center), Vladivostok, Russia
E-mail: Larisamk@tinro.ru; Shatilina@tinro.ru

Introduction

Ice conditions are formed as a result of complex mechanisms taking place between the atmosphere and ocean. Research needs to continue in order to reveal the interdependencies between the atmosphere and ice, and to explore their causal relationships in order to make predictions. The evolution of ice cover in the Okhotsk Sea for the period of observations determined in this paper is divided into relatively low-ice and extreme ice periods. There is a certain cyclic recurrence in the distribution of interannual variability estimations of ice conditions. However, these regularities have a generalized character.

The prevalence of cold winter conditions in the Okhotsk Sea was noted until the mid-1980s. Later, a radical change occurred in the course of average annual ice conditions values. The prevalence of low-ice winter seasons was noted since 1984 (Muktepavel, 2001). In certain situations, low ice-cover distributions at separated years, or even at separated periods, has an untypical character and can interrupt the long-term averages. So, extremely low-ice winters in the Okhotsk Sea were noted in 1991, 1996, 1997 and 2006.

The baric fields above the central part of the Northern Hemisphere at 30°–70°N, 120°–160°E were analyzed to reveal the mechanism for the ice formation phenomena. It is shown in this paper that such ice condition extremes are formed as a result of anomalous 500 hPa geopotential growth above the Okhotsk Sea. The anomalous atmospheric circulation promotes the carrying of warm air masses to offshore water. These masses are localized above the central part of the Okhotsk Sea, where the temperature anomalies are about +8°.

In this paper we identify a mechanism for the formation the regularities of extremely low-ice winters in the Okhotsk Sea with a provision for large-scale processes above the second natural synoptical region in the North Hemisphere.

Data and Methods

The complete database of averaged 10-day ice cover in the Okhotsk Sea was obtained from satellite imagery. The anomalies of ice cover in February for extreme ice years in the Okhotsk Sea were chosen:

$L_M - Lcp > 1/2\ A$ for extremely high ice years,
$L_M - Lcp < 1/2\ A$ for extremely low ice years

where L_M is the monthly mean ice cover in February, Lcp is the mean annual ice cover in February, and A is the amplitude in the change of parameter.

Data of aerologic stations from 1950–2006 were used from the Far Eastern Regional Hydro-meteorological Research Institute's archives. The archives of average monthly data on H500 geopotential were obtained from the CD-ROM "NCER/NCAR reanalysis of monthly mean CD-ROM 1948–1998" and the average monthly data on above-earth pressure was taken from http://dss.ucar.edu/datasets/ds.010.1/data for 1948–2003.

Results and Discussion

Figure 1 shows the long-term distribution of average annual deviations of ice cover in the Okhotsk Sea on a background of ice cover anomaly distributions.

It demonstrates the presence and length of short and long cycles of the anomalous increase and decrease in ice cover from 1957 to 2007. Starting from 1984, there is an accumulation of negative anomalies that represent low-ice years. Years of extremely low-ice conditions in Okhotsk Sea, in which ice cover was more than 20% less than the annual mean average, were determined for 1984, 1991, 1996, 1997, and 2006.

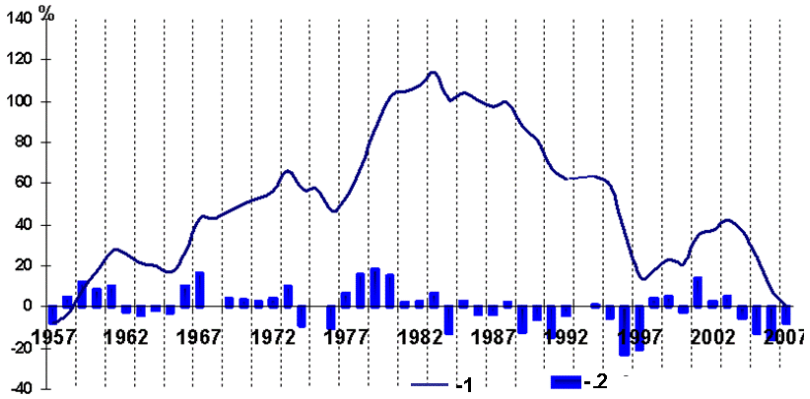

Fig. 1 (1) Long-term distribution of average annual deviation of ice cover in the Okhotsk Sea on (2) background of ice cover anomaly distributions.

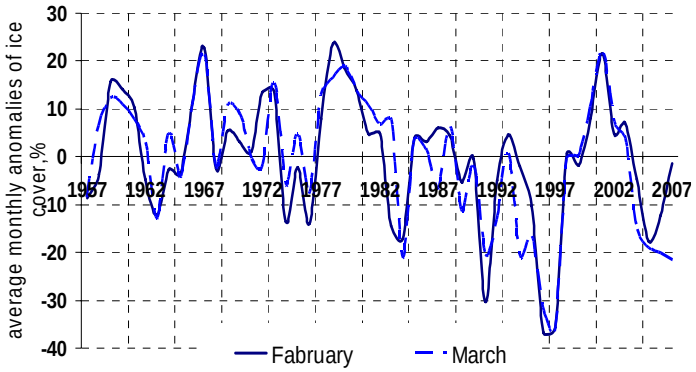

Fig. 2 Long-term distribution of ice cover anomaly in February (—) and in March (- -).

Figure 2 shows the long-term distribution of anomaly ice cover during months of maximum development of the ice area in the Okhotsk Sea. The anomalous low-ice years of 1984, 1991, 1996, 1997, 2006 were determined when ice cover was more than 20% less than the annual mean average.

Figure 3 shows the mean annual ice positions of the ice edges during extremely low-ice years. During these years, there is a characteristic absence of ice in the central part of the Okhotsk Sea and to northeast of the Sakhalin shelf. For comparison, the positions of the ice edge for the extremely high ice year (2001) is also shown.

The significant changes in the baric fields at AT 500 over the Asia-Pacific region existed during the 1990s (Shatilina, 1998). First, to explain the mechanism of extremely low ice formation, we analyzed the local atmospheric processes over the Okhotsk Sea using observed data of aerological stations, located on perimeter of the Okhotsk Sea.

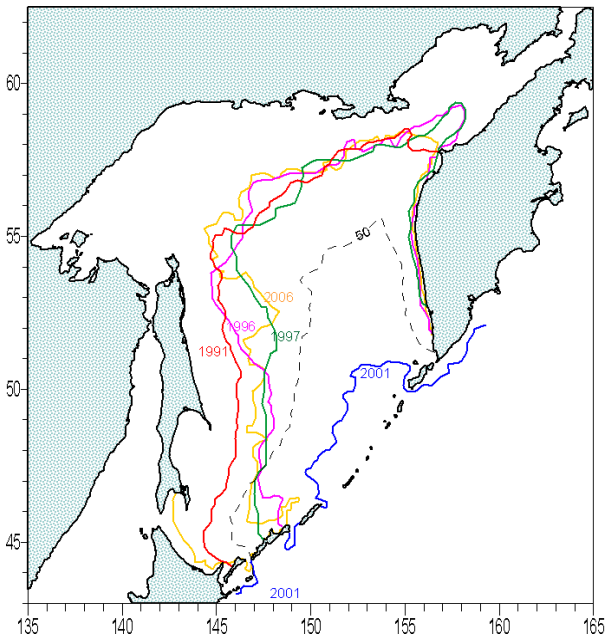

Fig. 3 The location of the ice edge in February of extreme ice years in the Okhotsk Sea (by remote sensing).

In Figure 4 we see the general regular pattern of atmospheric processes for extremely low-ice years. There is a high pressure system over Okhotsk Sea that causes a growing geopotential here. In 1984, the area of the low heights at a level of AT500 was displaced into the region of the south Kuril Islands while high-altitude Pacific atmospheric ridge intruded into the Okhotsk Sea (Fig. 4a). Anomalies of geopotential reached 6–9 dam over the sea (Fig. 4 b). In January 1996 the Okhotsk Sea was also under the influence of a high-altitude Pacific tropospheric ridge. The tropospheric whirl was displaced on continental regions adjacent to the northwestern part of the Okhotsk Sea (Fig. 4 d).

In 2006 there was the same regularity over the Okhotsk Sea as in 1984, 1996, 1997. We found a general regularity in the structure of the atmospheric baric field over the Okhotsk Sea in extremely low-ice years. Figure 5 shows the anomalous increasing geopotential heights over the sea.

Figure 6 shows the difference of the high-altitude baric field in extreme high-ice years in comparison with extreme low-ice years in the Okhotsk Sea. For example, in February of 1979 and 2001 historical maximum ice cover was situated in the area of the Okhotsk Sea having a very low pressure at a level of AT500 (502–504 hPa) (Fig. 6a and c). Its anomalies in the eastern part of the sea ranged from –10 to –16 dam (Fig. 6b and d).

The regularities in the change of atmospheric circulation forming extreme ice cover are a response to the large-scale processes existing in the North Pacific and near Arctic. Figure 7 presents such a large-scale process with the average annual of baric field at AT500. The position of the main climatic hollow (isobar 516 hPa) on the eastern side of the Okhotsk Sea can be seen. South of it is the High Altitude Frontal Zone of the Northern Hemisphere. The cold climatic hollow is located over the Okhotsk Sea.

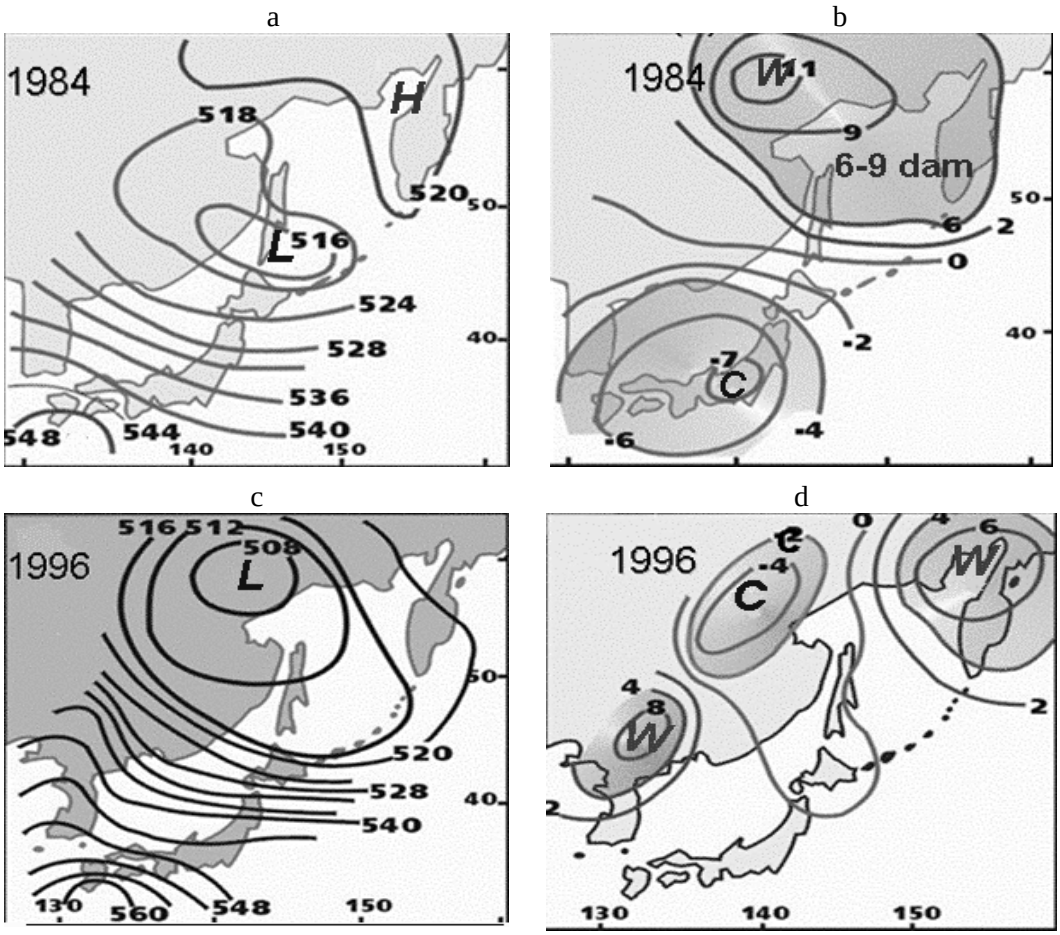

Fig. 4 Structure of high-altitude fields during the extremely low-ice period of January 1984 and 1996 (a and c) AT500 field; (b and d) anomalies of 500 hPa geopotential (data from aerologic stations).

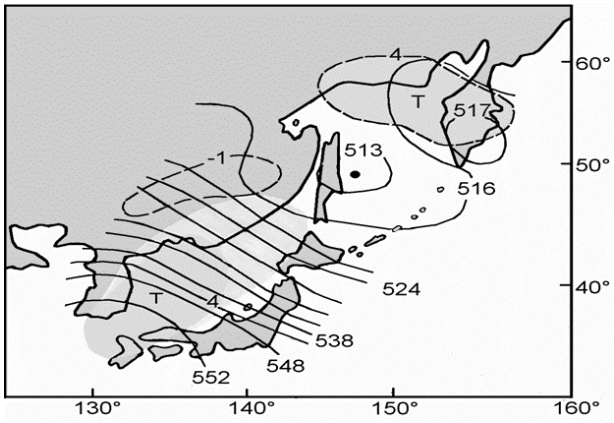

Fig. 5 Structure of the high-altitude (AT500) baric field during extremely low ice over the Okhotsk Sea, in January 2006.

Figure 8 shows the large-scale field AT500 in January 1991 and 1997 when extreme H500 values were registered over the Okhotsk Sea. These anomalies were shown by the position of a tropospheric hollow, which was practically absent in extreme warm winters (Shatilina, 1998). The Okhotsk tropospheric cyclone occupied the southern position over the north Kuril Islands. The hollow is not noted in extreme warm winters.

The increase of high-altitude pressure in January and February means a weakening of the high-altitude climatic hollow and Okhotsk minimum (the secondary arctic curl). This means a decrease in the intensity of incoming arctic cool air on the surface of the Okhotsk Sea.

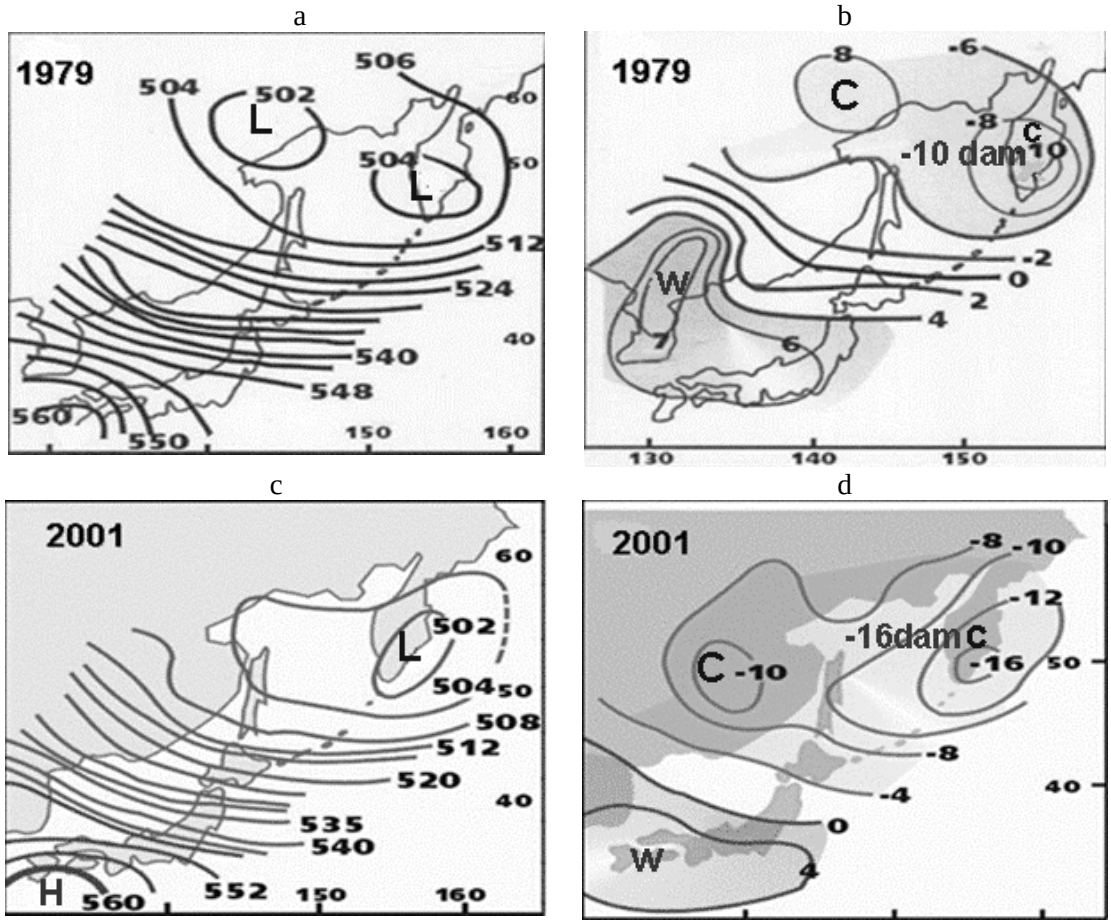

Fig. 6 High-altitude baric field distribution during an extreme high-ice winter 1979, 2001: (a and c) AT500 field, January; (b and d) anomalies of 500 hPa geopotential, January (data of aerological stations).

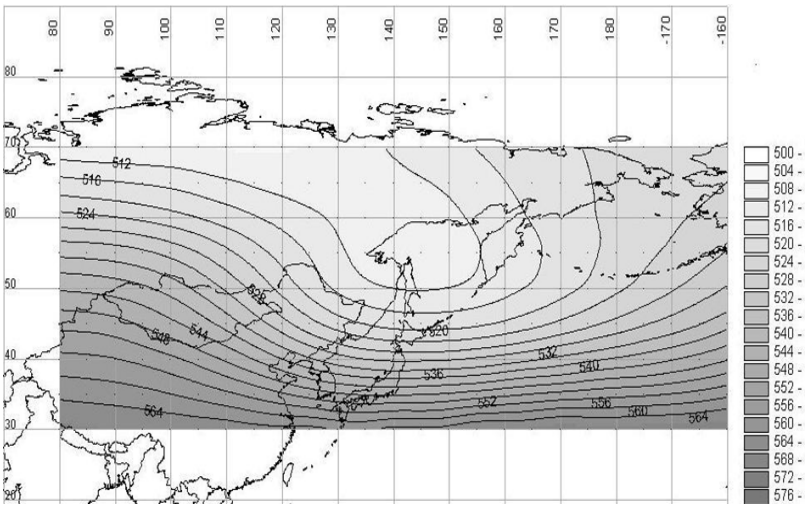

Fig. 7 Average annual of baric field at a level of AT500 in January (data from Reanalysis MONTHLY Mean CD-ROM 1948–1998).

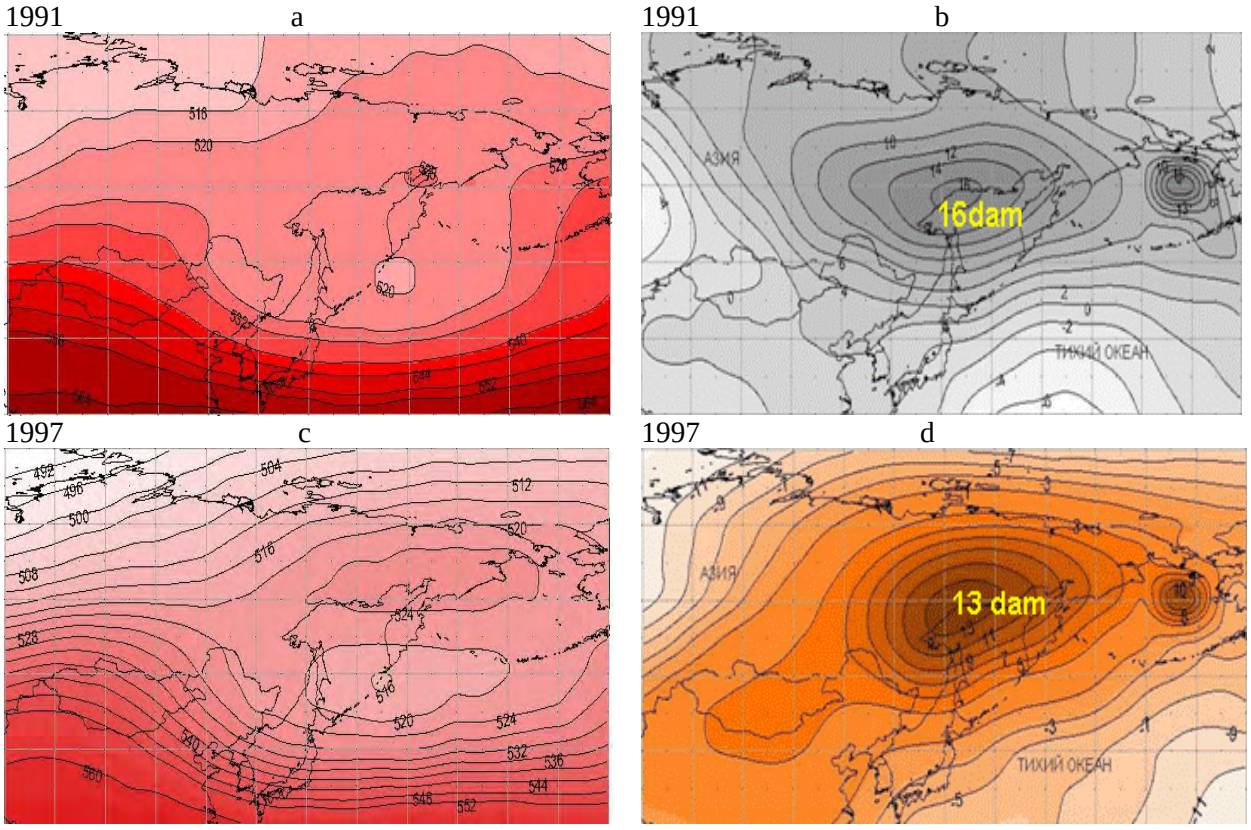

Fig. 8 (a and c) Spatial distribution large-scale baric fields at a level of AT500 and (b and d) distribution anomalies of 500 hPa geopotential for January 1991, and 1997 (Shatilina and Matyushenko, 2006).

In January 1996 (Fig. 9a and b) the northeastern part of the Okhotsk Sea was under the influence of a Pacific high-altitude ridge which means that there was an intensive intrusion of warm air over the Okhotsk Sea water (a high-altitude ridge is formed over the warm water of the Pacific Ocean).

The anomalous circulation in the troposphere prompted a change in the trajectory of surface cyclones forming a cyclogenesis over the Okhotsk Sea. The trailing part of the cyclones displaced over the Okhotsk Sea caused the transportation of warm air and increased warm ocean water advection through the Kuril Straits (Fig. 9) (Pavlichev and Muktepavel, 2000).

For comparison of the position of the climatic hollow and of the Okhotsk tropospheric cyclone, Figure 10 shows large-scale processes in January 1978 which was an extreme high-ice year. The position of large anomaly centers (marked with "Cold" and "C") in the H500 field can be seen, one of which lies over the northwestern part of the Okhotsk Sea. The results show that large-scale processes for extremely low-ice conditions in the Okhotsk Sea were due to a localization of warm air over the central part of the sea. Positive anomalies of the air temperature along 55°N were about 8°C (Fig. 11). Increased advection of warm ocean water inside the Okhotsk Sea through Bussol Strait is seen in Figure 12 for the noted years

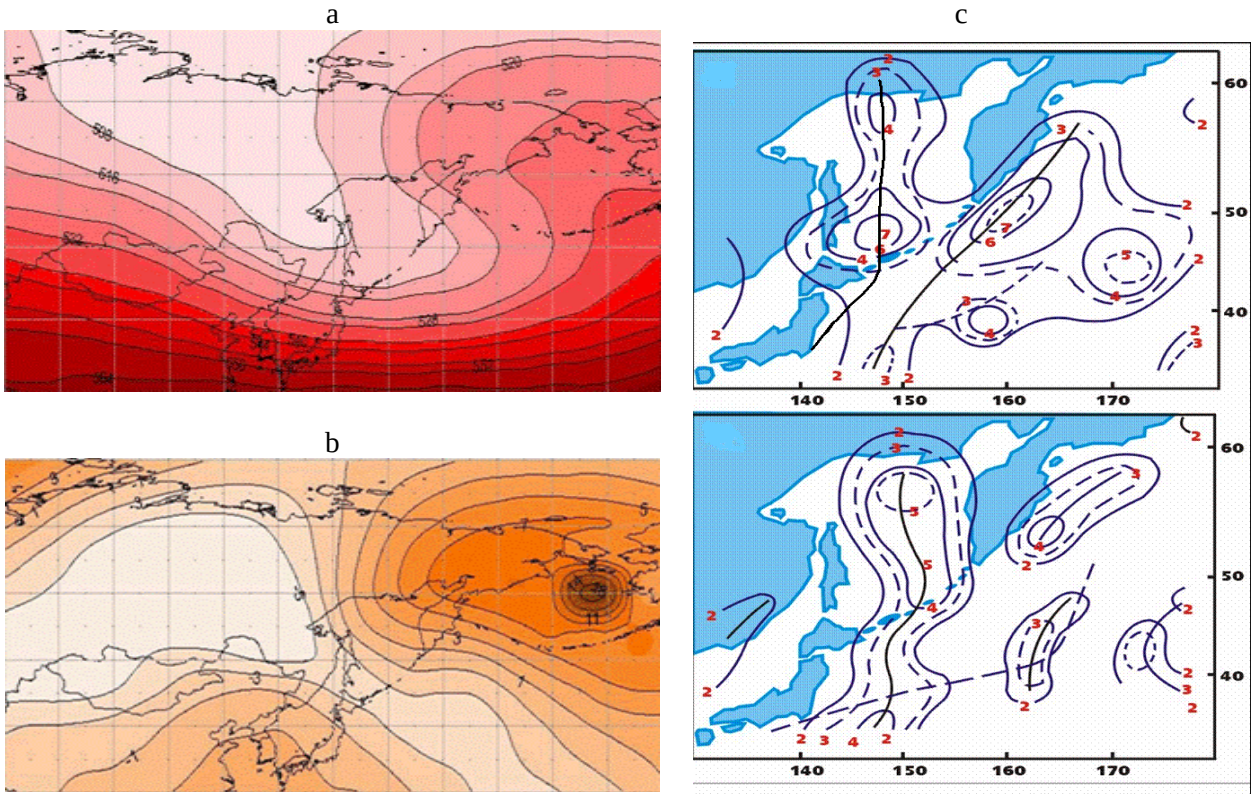

Fig. 9 (a) Spatial distribution of the baric field at a level of AT500; anomalies of 500 hPa geopotential (b) in January 1996. Paths and frequency of occurrence (days) of surface cyclones in (a) January and (b) February 1996, (c) Pavlychev and Muktepavel (2000).

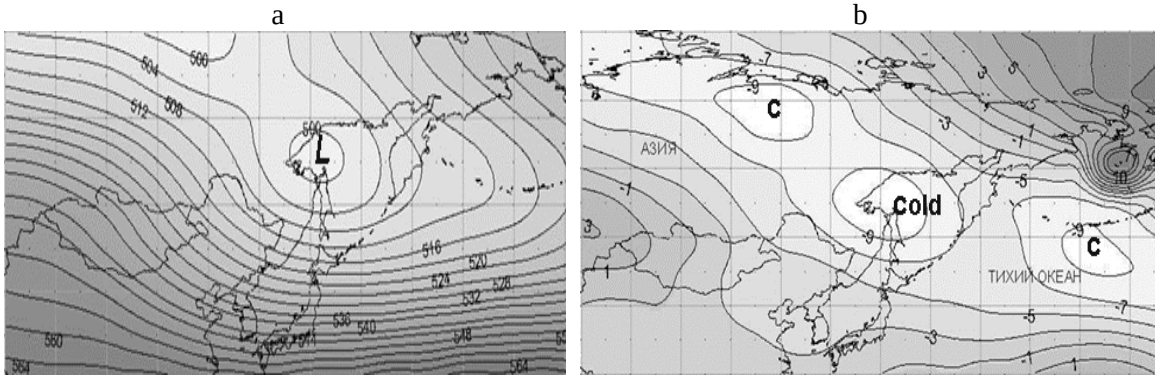

Fig. 10 (a) Spatial distribution baric field at a level of AT500 and (b) anomalies of 500 hPa geopotential, in January 1978.

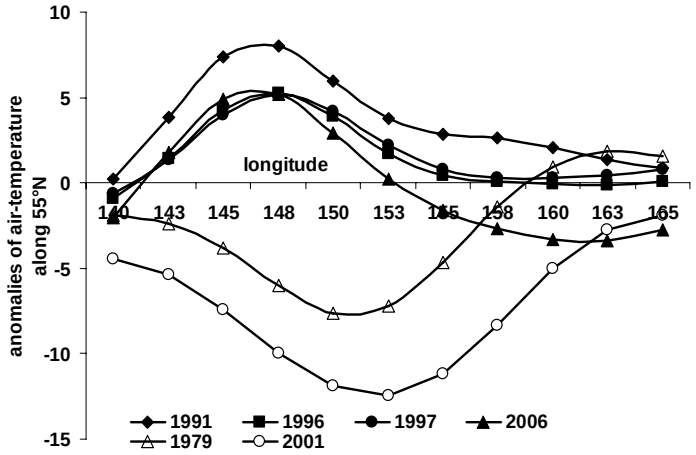

Fig. 11 Distribution anomalies of air temperature over the Okhotsk Sea along 55°N in February.

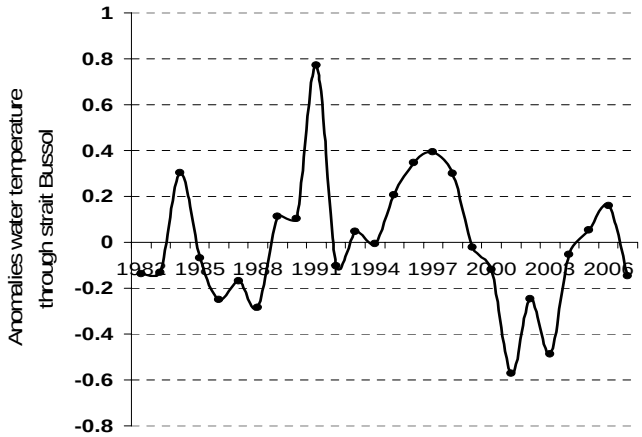

Fig. 12 Intra-annual run of water temperature anomalies in Bussol Strait in January–March from 1982 to 2007.

Conclusions

Figure 13 presents a general scheme of large-scale processes responsible for the formation of extreme low-ice in the Okhotsk Sea.

We conclude that:

- An Okhotsk Sea tropospheric cyclone (in January, February) weakens and is displaced on continental regions under extremely low-ice conditions;
- A cold centre in the troposphere over the Okhotsk Sea had large positive anomalies of 500 hPa geopotential (centres of the heat);
- Such a situation formed as a result of frequent intrusions of a Pacific tropospheric ridge over most areas of the Okhotsk Sea;
- The anomalous circulation in the troposphere of the research region prompted a change in the trajectory of surface cyclones forming a cyclogenesis over the Okhotsk Sea;
- The trailing part of the cyclones, displaced over the Okhotsk Sea, caused the transportation of warm air and increased the advection of relatively warm ocean water through the Kuril Straits;
- Localization of the warm air is observed above a central part of the Okhotsk Sea.

.

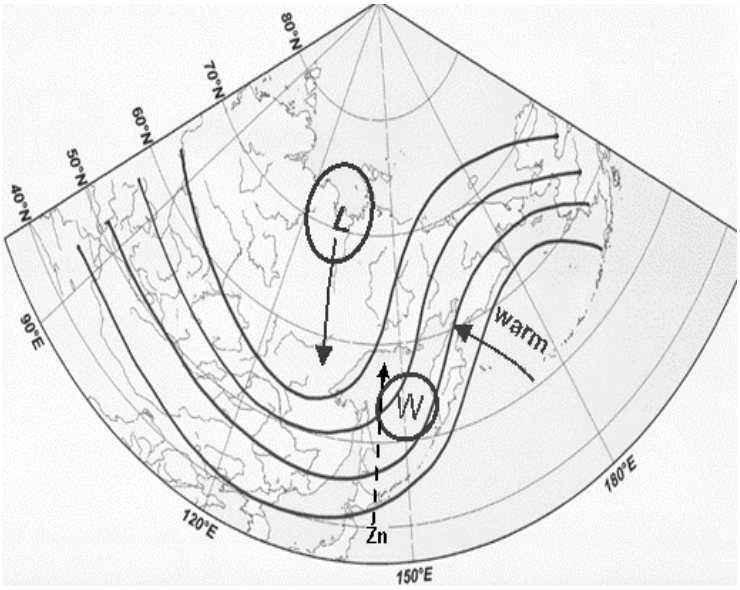

Fig. 13 Scheme of large-scale processes forcing the formation of extreme low-ice in the Okhotsk Sea.

References

Muktepavel, L.S., Plotnikov, V.V. and Colony, R.L. 2001. The causes of anomalous ice conditions in the Okhotsk and Bering Seas. Proceedings of the Arctic Regional Centre **3**: 29–39, Dalnauka, Vladivostok.

Shatilina, T.A. 1998. Long-term variability of atmospheric circulation over Far eastern region and its influence upon thermal mode and water dynamics. *Izv. TINRO* **124**: 681–707.

Pavlychev, V.P. and Muktepavel, L.S. 2000. To the influence of atmospheric processes on ice conditions of the Sea of Okhotsk. Global change studies in the Far East. pp. 31–32. Abstracts of Workshop, September 11–15, Vladivostok, Russia.

Shatilina, T.A. and Matyushenko, L.Yu. 2006. Modeling of baric fields in the research of the climate variability. *Izv. TINRO* **145**: 300–311.

A sensitivity study on the Dense Shelf Water formation in the Okhotsk Sea

You-ichiro Sasajima[1], Hiroyasu Hasumi[1] and Tomohiro Nakamura[2]

[1] Center for Climate System Research, University of Tokyo, Chiba, Japan
E-mail address: sasajima@ccsr.u-tokyo.ac.jp
[2] Institute of Low Temperature Science, Hokkaido University, Sapporo, Japan

Introduction

The Okhotsk Sea (Fig. 1) is believed to be the main source of North Pacific Intermediate Water (NPIW; *e.g.*, Talley, 1991; Yasuda *et al.*, 1997). The source water of the NPIW in the Okhotsk Sea is called the Okhotsk Sea Mode Water (OSMW) and is characterized by a minimum of potential vorticity whose density range is 26.6–27 σ_θ (Yasuda, 1997). The OSMW is formed by the mixing of the Dense Shelf Water (DSW), the Western Subarctic Water from the North Pacific through the Kuril Straits (Kitani, 1973), and the Forerunner of the Soya Warm Current Water from the Japan Sea through the Soya Strait (Takizawa, 1982; Watanabe and Wakatsuchi, 1998).

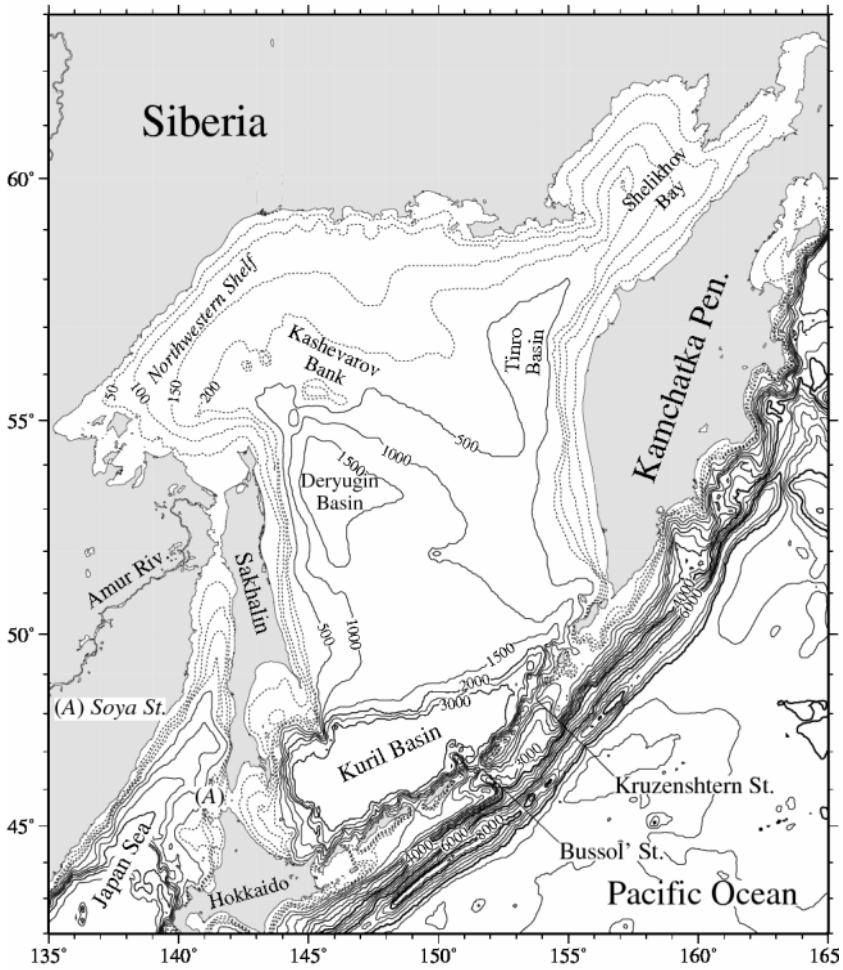

Fig. 1 Map of the Okhotsk Sea with bottom topography (in m).

The DSW is relatively cold and fresh water in the Okhotsk Sea. Its density range is within 26.6−27.05 σ_θ, although definitions of the range are slightly different among studies. Itoh *et al.* (2003) estimated the mixing ratio of the three types of water masses to form the OSMW from an isopycnal climatological dataset based on historical observations and suggested that nearly half of the OSMW consists of the DSW.

Kitani (1973) suggested that the DSW, with density up to 27.02 σ_θ, is formed by brine rejection through a high sea ice formation in the northwestern shelf region located northwest of Sakhalin (see Fig. 1). A high production of ice takes place in the coastal polynya along the northwestern coast of the Okhotsk Sea because of strong offshore winds and cold air temperature in winter, then it is considered that the brine rejection to form the DSW mainly occurs in that region (Alfultis and Martin, 1987; Martin *et al.*, 1998; Ohshima *et al.*, 2003; Shcherbina *et al.*, 2003). The formed DSW is transported to the south along the eastern coast of Sakhalin by the East Sakhalin Current (Ohshima *et al.*, 2002; Mizuta *et al.*, 2003) and contributes to the OSMW formation.

Impacts of factors leading to the DSW formation have been demonstrated by some numerical studies. Nakamura *et al.* (2006) investigated the effect of tidal mixing in the Kuril Straits for the DSW formation with a sea–ice coupled model. They simulated ocean circulations with and without the tidal mixing effect which is represented by setting a strong vertical diffusivity around the Kuril Islands and suggested that more DSW is formed by the tidal mixing effect through the following process. An upward salinity flux to the upper layer occurs due to the tidal mixing effect around the Kuril Islands and increases salinity in the upper layer. This positive anomaly of salinity by tidal mixing is transported from the Kuril Islands to the north through the eastern part of the Okhotsk Sea by a basin-scale cyclonic circulation which is mainly driven by wind stress (Ohshima *et al.*, 2004). As more saline (denser) brine is rejected in the northwestern shelf region because of the transported positive salinity anomaly, more DSW is formed.

Matsuda (2008) examined the impact of wind strength on the DSW formation with the tidal mixing effect, and showed that stronger winds also increase the DSW production. He explained that the wind-driven cyclonic circulation intensified by the amplified wind transports the more positive salinity anomaly originating with the tidal mixing effect to the northwestern shelf region. This transported salinity anomaly results in more saline (denser) brine and more DSW formation than those with the tidal mixing effect only. As mentioned later, it seems that the amplified wind has more effect on DSW formation.

However, the horizontal resolutions of the models are 1° in Nakamura *et al.* (2006) and a half degree in Matsuda (2008). These horizontal resolutions are too coarse to resolve well the northwestern coastal polynya which is several tens of kilometers in width (Martin *et al.*, 1998). Then, it is suggested that the DSW formation in the northwestern coastal polynya has not been well reproduced in former studies. In this study, the impacts of factors leading to the DSW formation are examined using a sea−ice coupled model with a horizontal resolution which is several kilometers in the northern part of the Okhotsk Sea. It is then expected that the model will resolve the coastal polynya along the northwestern coast.

Model Configuration

Numerical model

The Center for Climate System Research (CCSR) Ocean Component Model version 4.2 (COCO4.2; *e.g.*, Hasumi, 2006) is employed as the ice–ocean coupled model in this study. COCO4.2 solves primitive equations for three-dimensional ocean circulation and sea ice formation in the generalized curvilinear horizontal coordinate. By virtue of this coordinate system, one can arrange a computational grid pattern with locally high horizontal resolution and efficiently simulate phenomena on a small scale and their interaction with a circulation field in the relatively extensive surrounding area under a limitation of computational resources.

Figure 2a shows the model domain and the computational grid pattern in this study. The model domain covers the North Pacific. The horizontal resolution is up to 790 km in the South Pacific while it is less than 8 km in the northern part of the Okhotsk Sea to well resolve the northwestern coastal polynya and brine rejection (Fig. 2b).

The model topography is basically made from Earth Topography-5 Minute (ETOPO5; National Geophysical Data Center, 1988). The topography

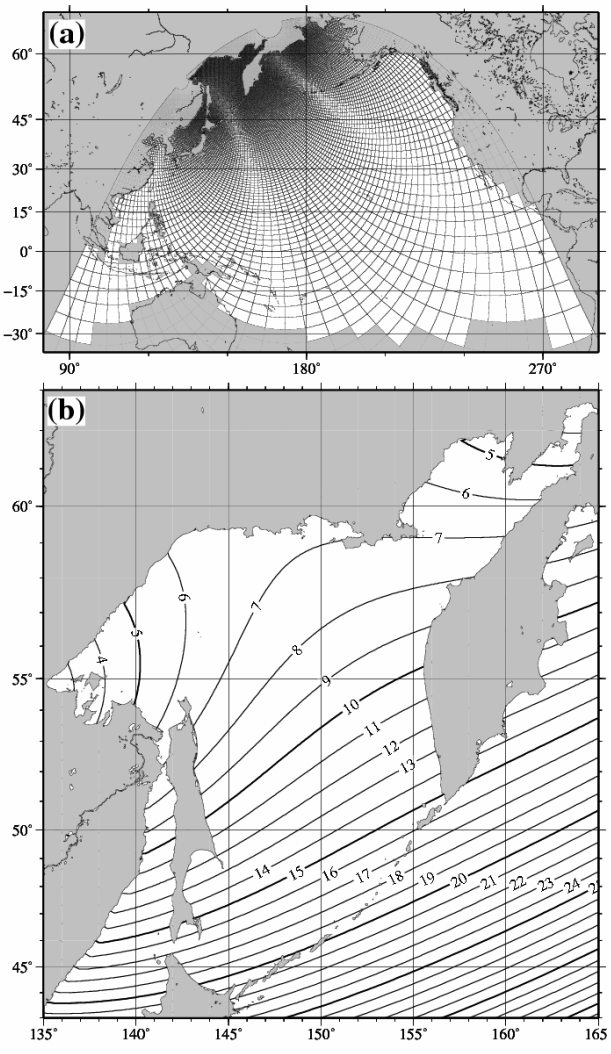

Fig. 2 (a) Computational grid pattern of the model in this study. The model calculates the ocean circulation and the sea ice formation in the white region. (b) Horizontal resolution of the model around the Okhotsk Sea (in km).

data made by Ono *et al.* (2006) is also used around the Kashevarov Bank because of inaccuracy of the ETOPO5 data in that region.

Boundary conditions

Simulated temperature and salinity are restored to the Polar Science Center Hydrographic Climatology (PHC; Steel *et al.*, 2001) from 15°S to the south. Sea surface salinity (SSS) is also restored to the PHC while it is not restored in the Okhotsk Sea in order to examine the salinity transport at the upper layer, as mentioned in Nakamura *et al.* (2006) and Matsuda (2008).

The experiments in this study are shown in Table 1. In all the experiments, the sea surface momentum and heat fluxes are calculated basically from the monthly climatological dataset of the Ocean Model Intercomparison Project (OMIP; Röske, 2001), which is based on European Centre for Medium-Range Weather Forecasts (ECMWF) 15-year reanalysis. The bulk formulae of Kara *et al.* (2000) are used for the flux calculation from the OMIP data. The OMIP dataset is directly applied in Run 1 and Run 2.

The vertical mixing effect by the tide in the Kuril Straits is implemented in Run 2, Run 3 and Run 4. The background vertical diffusivity coefficient is set to 200 $cm^2\ s^{-1}$ over the sill around the Kuril Islands in these experiments to represent the vertical mixing effect while it is less than 3 $cm^2\ s^{-1}$ (Tsujino *et al.*, 2000) in the other region. Nakamura *et al.* (2006) adopted the value of 200 $cm^2\ s^{-1}$ in their model, based on the results of former studies (Nakamura *et al.*, 2000; Nakamura and Awaji, 2004). Results of Matsuda (2008) also supported the validity of this value in terms of the DSW formation and its transport.

Ohshima *et al.* (2003) pointed out that the wind speed data reanalyzed by ECMWF are smaller than those of observed *in-situ* data, by about 25% in the Okhotsk Sea. Some numerical studies for the Okhotsk Sea have adopted the ECMWF wind stress amplified by factors of about 1.5 (*e.g.*, Simizu and Ohshima, 2002; Simizu and Ohshima, 2006). The wind stress of ECMWF is also used in Matsuda (2008), and he reported that a realistic circulation on the isopycnal surface of 26.8 σ_θ is reproduced with the amplified wind stress by a factor of 1.5. The wind stress of the OMIP data is also amplified by a factor of 1.5 in the Okhotsk Sea in Run 3 and Run 4.

Table 1 List of experiments.

Simulation	Description
Run 1	Directly driven by the OMIP data set.
Run 2	Run 1 with tidal mixing effect around the Kuril Islands.
Run 3	Run 2 with wind stress amplified by a factor of 1.5 in the Okhotsk Sea.
Run 4	Run 3 with removing river runoffs in the Okhotsk Sea, excluding the Amur river.

Figure 3 shows a comparison of river runoff in the Okhotsk Sea between the OMIP dataset and that from *in-situ* observation (Perry *et al.*, 1996). The river runoff of the OMIP is calculated by a land model using the ECMWF evaporation and precipitation data. The annual mean river runoff of the Amur River is about 10,000 $m^3 s^{-1}$ in the two datasets. On the other hand, the total amount of annual mean river runoffs in the Okhotsk Sea, excluding the Amur River, is 6,644 $m^3 s^{-1}$ in the OMIP data while it is 2,205 $m^3 s^{-1}$ in Perry *et al.* (1996). Results of SSS in Run 1, Run 2 and Run 3 (Figs. 4a, b and c), in which the OMIP river runoff data are directly used, show strong low-salinity fronts along the northwestern coast where the DSW is mainly formed. River runoffs in the Okhotsk Sea, except the Amur River, are removed in Run 4 in order to examine the impact of the uncertainty of river runoff among datasets to the DSW formation.

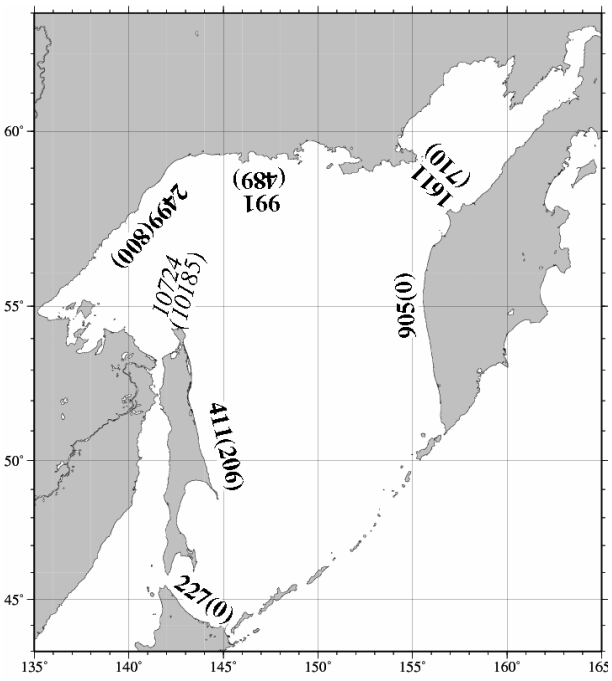

Fig. 3 Bracketed figures denote the annual mean runoffs from Perry *et al.* (1996) while those without brackets are values of the OMIP dataset along same coast (in $m^3 s^{-1}$). Figures in bold indicate, in clockwise order from the southwest, the runoffs along the northeastern coast of Hokkaido, the eastern coast of Sakhalin, the northwestern coast of the Okhotsk Sea, the northern coast of the Okhotsk Sea, the Shelikov Bay, and the western coast of the Kamchatka Peninsula while those in italics indicate the annual mean runoff of the Amur River.

In each experiment, the model is integrated for 16 model years from a static state with the temperature and salinity fields in January of the PHC. The sea ice formation, sea surface salinity and the DSW formation reach a steady state in the Okhotsk Sea. Results of the experiments in the 16th model year are compared in this study.

Results

Table 2 shows the production rate of the DSW in each experiment. Definition of the DSW production rate is based on Itoh *et al.* (2003). They defined the DSW as water on the northwestern shelf, with density within 26.75–27.05 σ_θ, temperature less than 0°C and its production rate as the total volume of DSW existing from spring to summer divided by a year. In this study, the DSW production rate is defined as the volume of the DSW existing from April to September in an area north of 54°N and west of 153°E, with the bottom depth shallower than 200 m divided by a year.

The DSW production rate by Run 1 is smaller than the range of estimates based on observations (Martin *et al.*, 1998; Gladyshev *et al.*, 2000; Itoh *et al.*, 2003). The DSW production increases on adding the effects of the tide around the Kuril Islands, the intensification of the wind stress and removing the runoffs in Run 2, Run 3 and Run 4, respectively, and is within the range of the observational estimates. DSW production rates in Run 2, Run 3 and Run 4 are clearly larger than those in the experiment with the vertical diffusion coefficient of 200 $cm^2 s^{-1}$ around the Kuril Islands in Nakamura *et al.* (2006). Even the production rate in Run 1, in which the tidal effect is not implemented, is slightly larger than that in the experiment in Nakamura *et al.* (2006). The annual sea ice production in the Okhotsk Sea in each experiment (Table 3) is much larger than that in the experiment in Nakamura *et al.* (2006) and close to that estimated from observed data (*e.g.*, Ohshima *et al.*, 2003). Figure 5 shows the horizontal distributions of annual sea ice production in the northwestern shelf region. The coastal polynya is clearly reproduced along the northwestern coast in each experiment because of the much higher resolution than that in Nakamura *et al.* (2006), as mentioned in the previous sections. The model in each experiment, then, also reproduced the high sea ice production in the coastal polynya mentioned in the observational studies (Alfultis and Martin, 1987;

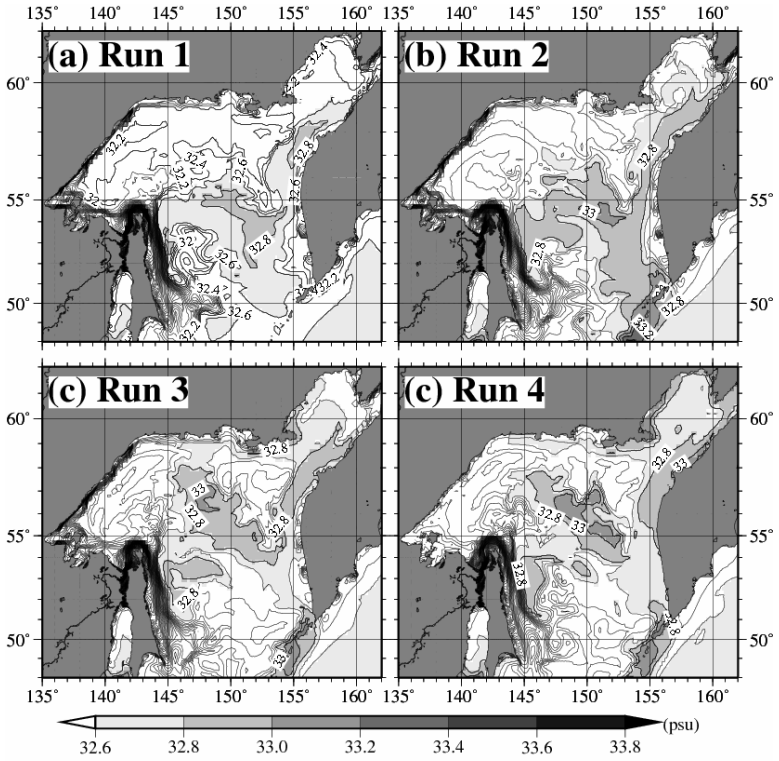

Fig. 4 Horizontal distributions of salinity in the top layer in September simulated in (a) Run 1, (b) Run 2, (c) Run 3 and (d) Run 4 (C.I. = 0.2 psu).

Martin *et al.*, 1998; Ohshima *et al.*, 2003). It can be considered that the more realistic the sea ice production results, the more brine rejection and DSW formation there is.

Abyssal density (Table 4) also increases by each effect. Horizontal distributions of abyssal density in September (Fig. 6) show that shaded regions where bottom water meets the criteria of the DSW in Itoh *et al.* (2003), increases by each effect. It corresponds to the increase of the DSW production rate. The observed distribution of abyssal density in September, 1999 around 56°N (thick solid line in Fig. 6a; Shcherbina *et al.*, 2003) shows a maximum near 140°E with density larger than 26.9 σ_θ. Such maxima of the abyssal density larger than 26.85 σ_θ are also shown on the same line in Run 3 and Run 4, in which the ECMWF wind stress is amplified by a factor of 1.5.

Annual mean SSS in the Okhotsk Sea (Table 5) mainly increases by adding the tidal effect (Run 2) and removing the river runoff (Run 4). SSS increases in all runs over the Okhotsk Sea by adding the tidal mixing effect (Fig. 4b). It seems that this increment is attributed to that of the northward salinity flux in the upper layer from the Kuril Islands originating with the upper salinity flux by the tidal mixing effect. The SSS intensification makes the brine in the northwestern shelf region more saline (denser) and results the more DSW formation, as mentioned in Nakamura *et al.* (2006). In Run 4 (Fig. 4d), the low-salinity front along the northwestern coast vanishes by removing the river runoffs in the Okhotsk Sea, except the Amur River. The increase of the abyssal density and the DSW formation may be attributed to the vanishing of the low-salinity front along the northwestern shelf region where the high production of sea ice and the brine rejection occurs.

Table 2 Annual mean DSW production rate (in Sv) in the northwestern shelf region.

Simulation	DSW prod. rate (Sv)
Run 1	0.14
Run 2	0.35
Run 3	0.48
Run 4	0.64
Nakamura *et al.* (2006)	0.13 (with the tidal effect)
Observational estimates	0.2–0.67

Note: The northwestern region is defined as the area north of 54°N and west of 153°E, with the bottom depth shallower than 200 m in this study.

Table 3 Annual sea ice production (in 10^{11} m^3) in the Okhotsk Sea.

Simulation	Ice production (10^{11} m^3)
Run 1	8.9
Run 2	9.4
Run 3	12.0
Run 4	12.2
Nakamura *et al.* (2006)	2.4 (With the tidal effect)
Ohshima *et al.* (2003)	13 (Observation)

Table 4 Annual mean abyssal density in the northwestern shelf region.

Simulation	Abyssal density (σ_θ)
Run 1	26.72
Run 2	26.80
Run 3	26.83
Run 4	26.88

Table 5 Annual mean sea surface salinity (SSS) in the Okhotsk Sea (in psu).

Simulation	SSS (psu)
Run 1	32.23
Run 2	32.37
Run 3	32.39
Run 4	32.60

SSS increases in the northern part of the Okhotsk Sea while it decreases in the southern part by the intensification of the wind stress in Run 3. The average SSS does not increase significantly in Run 3, (Table 5). It is considered that the wind-driven basin-scale circulation is intensified by the amplified wind in the Okhotsk Sea, and the salinity anomaly is transported farther north by the intensified circulation from the Kuril Islands, as mentioned in Matsuda (2008).

It seems there is one more effect of the amplified wind stress to the DSW formation. The annual sea ice production (Table 3) increases by intensification of the wind stress in Run 3 and Run 4. The northwestern coastal polynyas in Run 3 and Run 4 are wider and clearer than those in Run 1 and Run 2 because of intensification of the offshore wind along the northwestern coast. The horizontal distributions of annual sea ice production (Fig. 5) show a significant increment in sea ice production along the northwestern coast in Run 3 and Run 4. It is considered that the DSW formation is also intensified by the increase in brine rejection due to the intensification of the northwestern coastal polynya by the amplified wind.

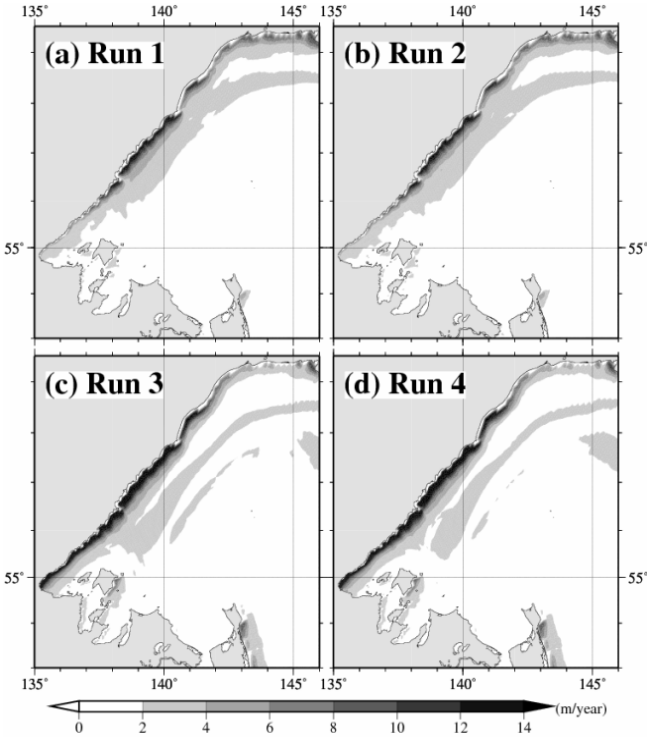

Fig. 5 Horizontal distributions of total annual sea ice production simulated in (a) Run 1, (b) Run 2, (c) Run 3 and (d) Run 4 (m $month^{-1}$).

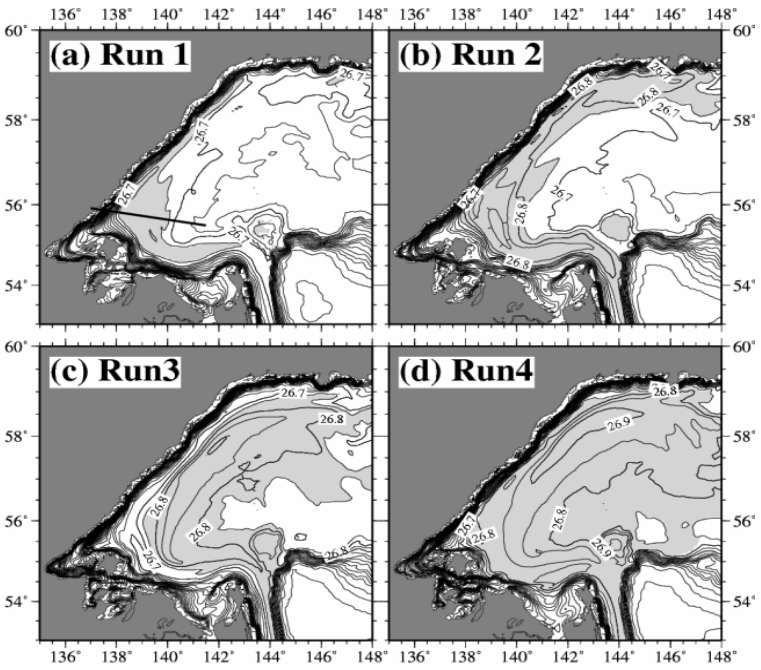

Fig. 6 Horizontal distributions of abyssal density around the northwestern shelf in September simulated in (a) Run 1, (b) Run 2, (c) Run 3 and (d) Run 4 (C.I. = 0.05 σ_θ). In shaded regions, abyssal density and temperature are larger than 26.75 σ_θ and colder than 0°C, respectively and match the DSW definition in Itoh *et al.* (2003). The solid line drawn at about 56°N in (a) indicates the observational line of Shcherbina *et al.* (2003).

Summary

In this study, the series of sensitivity experiments on the DSW formation in the Okhotsk Sea was performed with the sea–ice coupled model which well resolves the coastal polynya along the northwestern coast of the Okhotsk Sea.

The model reproduced more sea ice production and DSW formation than the former numerical studies because of the clearly reproduced northwestern coastal polynya. We confirmed the intensification of the DSW formation by the effects of tidal mixing in the Kuril Straits and the intensification of wind stress in the Okhotsk Sea, which makes the brine more saline in the northern shelf area, the same as in the former studies.

It was shown that the brine also becomes more saline by removing the unrealistically large amount of runoff in the Okhotsk Sea in the OMIP reanalysis dataset. On the other hand, Perry *et al.* (1996), which is used for validating the OMIP river runoff data, includes only runoffs of major rivers, and the accurate total amount of the river runoffs is currently not clear. Therefore, it cannot be said whether or not Run 4 reproduced more realistic DSW formation than Run 3 in the present study. We emphasize that there is a considerable amount of uncertainty in the river runoff datasets regarding DSW formation.

Sea ice production in the Okhotsk Sea increased because of the intensification of the wind stress in this study while it did not increase because of wind intensification in Matsuda (2008). This may be attributed to the reproduction of the clear coastal polynya because of the local high horizontal resolution of the model in this study. It is considered that the intensification of ice production due to wind intensification also contributes to the incremental amounts of brine and DSW production.

References

Alfultis, M.A. and Martin, S. 1987. Satellite passive microwave studies of the Sea of Okhotsk ice cover and its relation to oceanic processes, 1978−1982. *J. Geophys. Res.* **92**: 13,013−13,028.

Gladyshev, S., Martin, S., Riser, S. and Figurkin, A. 2000. Dense water production on the northern Okhotsk shelves – Comparison of ship-based spring-summer observations for 1996 and 1997 with satellite observations. *J. Geophys. Res.* **105**: 13,013−13,028.

Hasumi, H. 2006. CCSR Ocean Component Model (COCO) Version 4.0. CCSR report No. 25, 103 pp.

Itoh, M., Ohshima, K. and Wakatsuchi, M. 2003. Distribution and formation of Okhotsk Sea Intermediate Water: An analysis of isopycnal climatological data. *J. Geophys. Res.* **108**: doi:10.1029/2002JC001590.

Kara, A., Rochford, P. and Hurlburt, H. 2000. Efficient and accurate bulk parameterizations of air−sea fluxes for use in General Circulation Models. *J. Atmos. Ocean. Tech.* **17**: 1421−1438.

Kitani, K. 1973. An oceanographic study of the Okhotsk Sea. *Bull. Far Seas Fish. Res. Lab.* **9**: 45–77.

Martin, S., Drucker, R. and Yamashita, K. 1998, The production of ice and dense shelf water in the Okhotsk Sea polynyas. *J. Geophys. Res.* **103**: 27,771−27,782.

Matsuda, J. 2008. Numerical study of thermohaline circulation in the Sea of Okhotsk. M.Sc. thesis, 48 pp., Hokkaido Univ.

Mizuta, G., Fukamachi, Y., Ohshima, K.I. and Wakatsuchi, M. 2003. Structure and seasonal variability of the East Sakhalin Current. *J. Phys. Oceanogr.* **33**: 2430−2445.

Nakamura, T., Awaji, T., Hatayama, T., Akitomo, K., Takizawa, T., Kono, T., Kawasaki, Y. and Fukasawa, M. 2000. The generation of large-amplitude unsteady lee waves by subinertial K_1 tidal flow: a possible vertical mixing mechanism in the Kuril Straits. *J. Phys. Oceanogr.* **30**: 1601−1621.

Nakamura, T. and Awaji, T. 2004. Tidally induced diapycnal mixing in the Kuril Straits and its role in water transformation and transport: A three-dimensional nonhydrostatic model experiment. *J. Geophys. Res.* **109**: doi:10.1029/2003JC001850.

Nakamura, T., Toyoda, T., Ishikawa, Y. and Awaji, T. 2006. Enhanced ventilation in the Okhotsk Sea through tidal mixing at the Kuril Straits. *Deep-Sea Res. I* **53**: 425−448.

National Geophysical Data Center 1988. ETOPO−5 bathymetry/topography data. National Oceanic and Atmospheric Administration Data Announcement 88-MGG-02, U.S. Department of Commerce.

Ohshima, K.I., Wakatsuchi, M., Fukamachi, Y. and Mizuta, G. 2002. Near-surface circulation and tidal currents of the Okhotsk Sea observed with the satellite-tracked drifters. *J. Geophys. Res.* **107**: doi:10.1029/2001JC001005.

Ohshima, K., Watanabe, T. and Nihashi, S. 2003. Surface heat budget of the Sea of Okhotsk during 1987–2001 and the role of sea ice on it. *J. Meteorol. Soc. Jpn.* **81**: 653−677.

Ohshima, K.I., Simizu, D., Itoh, M., Mizuta, G., Fukamachi, Y., Riser, S.C. and Wakatsuchi, M. 2004. Sverdrup balance and the cyclonic gyre in the Sea of Okhotsk. *J. Phys. Oceanogr.* **34**: 513−525.

Ono, J., Ohshima, K.I., Mizuta, G., Fukamachi, Y. and Wakatsuchi, M. 2006. Amplification of diurnal tides over Kashevarov Bank in the Sea of Okhotsk and its impact on water mixing and sea ice. *Deep-Sea Res. I* **53**: 409–424.

Perry, G., Duffy, P. and Miller, N. 1996. An extended data set of river discharges for validation of general circulation models. *J. Geophys. Res.* **101**: 21,339−21,349.

Röske, F. 2001. An atlas of surface fluxes based on the ECMWF Re-analysis: A climatological dataset to force global ocean general circulation models. Max-Planck-Institut für Meteorologie Report 323, Max-Planck-Institute for Meteorology, p. 261.

Shcherbina, A., Talley, L. and Rudnick, D. 2003. Direct observations of North Pacific ventilation: Brine rejection in the Okhotsk Sea. *Science* **302**: 1952−1955.

Simizu, D. and Ohshima, K.I. 2002. Barotropic response of the Sea of Okhotsk to wind forcing. *J. Oceanogr.* **58**: 851−860.

Simizu, D. and Ohshima, K.I. 2006. A model simulation on the circulation in the Sea of Okhotsk and the East Sakhalin Current. *J. Geophys. Res.* **111**: doi:10.1029/2005JC002980.

Steele, M., Morley, R. and Ermold, W. 2001. PHC: A global ocean hydrography with a high-quality Arctic Ocean. *J. Climate* **14**: 2079−2087.

Takizawa, T. 1982. Characteristics of the Soya Warm Current in the Okhotsk Sea. *J. Oceanogr. Soc. Japan* **38**: 281−292.

Talley, L. 1991. An Okhotsk Sea water anomaly: implications for ventilation in the North Pacific. *Deep-Sea Res. A* **38**(Suppl. 1): S171−S190.

Tsujino, H., Hasumi, H. and Suginohara, N. 2000. Deep Pacific circulation controlled by vertical diffusivity at the lower thermocline depths. *J. Phys. Oceanogr.* **30**: 2853−2865.

Watanabe, T. and Wakatsuchi, M. 1998. Formation of 26. 8−26. 9 σ_θ water in the Kuril Basin of the Sea of Okhotsk as a possible origin of North Pacific Intermediate Water. *J. Geophys. Res.* **103**: 2849−2865.

Yasuda, I. 1997. The origin of the North Pacific Intermediate Water. *J. Geophys. Res.* **102**: 893−909.

Plenary Session 2

Amur River/Geochemical cycle

Session Chairs

M. Angelica Peña and Michio J. Kishi

Review of the Pacific Oceanological Institute program on the Amur River Estuary and adjacent marine areas

Vyacheslav Lobanov, O. Dudarev, P. Tishchenko, I. Zhabin, V. Zvalinksy, A. Charkin, A. Koltunova, A. Sagalaeva and M. Shvetsova

V.I. Il'ichev Pacific Oceanological Institute (POI), FEB RAS, Vladivostok, Russia. E-mail: lobanov@poi.dvo.ru

The Amur River is one of the largest rivers in the world and its influence on the Okhotsk Sea environment is significant. At the same time recent industrial development in the Maur River basin and its estuary suggests serious changes in the water characteristics, physical and biogeochemical processes, as well as structure of the ecosystem. However, our knowledge on the status of the environment and ecosystem of this region, as well as our understanding of the whole system functioning, are far from sufficient. Since 2003 POI, in collaboration with other institutes of the Far Eastern Branch of the Russian Academy of Sciences, has started a series of comprehensive surveys of the Amur River estuary and adjacent areas, including the lower part of the river, Sakhalin Bay of the Okhotsk Sea and northern part of the Tatar Strait in the Japan Sea. Six expeditions have been carried out to study summer, spring and winter conditions of the area, including high water and low water regimes and spring under the ice observations. The observations and sampling included CTD and current measurements, dissolved oxygen, nutrients, pH, total alkalinity, chlorophyll-*a*, humic substances, calcium, magnesium, suspended matter, microbiological activity in the water as well as structure, isotopic content and organic matter in the bottom sediments. Many of the observations and comprehensive surveys were never done here before. The results on the distribution of physical and chemical parameters, water exchange and mixing in the Amur Estuary, transport and transformation of river discharge on th natural barriers, production and destruction processes, distribution of the Amur waters into the Okhotsk and Japan seas, as well as the status of contamination, are discussed. Continuation of the field surveys is planned for the fall and winter periods.

Biogeochemical linkage between Amur River basin and western subarctic Pacific by iron transport through Okhotsk Sea Intermediate Water: A new paradigm to explain changes in ocean primary productivity

Takeshi Nakatsuka[1], Jun Nishioka[1], Takayuki Shiraiwa[2] and all members of the "Amur-Okhotsk" Project

[1] Institute of Low Temperature Science, Hokkaido University, Sapporo, Japan
E-mail: nakatuka@lowtem.hokudai.ac.jp
[2] Research Institute for Humanity and Nature, Kyoto, Japan

Most oceanographers believe that the indispensable element for phytoplankton growth, iron, is supplied to the open ocean as an atmospheric aerosol from arid regions. Here, we present a new hypothesis that the open ocean ecosystem is supported not only by atmospheric iron but also by intermediate water iron flowing from the coastal zone. The Amur River is the largest river in Russian Far East flowing into the Okhotsk Sea. Because of the broad wetlands in the watershed, dissolved iron concentrations in the Amur River water are about 1 mg/l, a million times higher than that in the open ocean surface. Most of the dissolved iron, in fact, precipitates by flocculation around the river mouth. However, part of the precipitated iron does not deposit on the shelf, but is re-suspended by strong tidal currents there and penetrates into the offshore intermediate layer (Okhotsk Sea Intermediate Water; OSIW) due to water ventilation induced by brine water rejection from sea ice formation. Part of the iron discharged into the OSIW is transported far into the western subarctic Pacific by strong ocean currents, without being scavenged owing to the scarce number of organisms in the intermediate layer, and finally re-entrained into the surface layer by tidal mixing near the Kuril archipelago, and winter convective mixing, supporting the huge phytoplankton bloom in western subarctic Pacific. Because this iron transport system can be easily damaged by global warming or land surface conversion through the reduction of sea ice formation or wetland areas, human activities may change the biological productivity in the western subarctic Pacific completely in the near future.

Modeling of biogeochemical cycles and climate change on the Continental Shelf: An example from the Pacific coast of Canada

M. Angelica Peña

Fisheries and Oceans Canada, Institute of Ocean Sciences, Sidney, British Columbia, Canada
E-mail: Angelica.Pena@dfo-mpo.gc.ca

Abstract

The development of a quantitative understanding of the interactions among physical, chemical and biological processes is critical for predicting the marine ecosystem response to climate change. This study presents results from a coupled plankton/circulation model (ROMS) developed to study factors influencing bloom dynamics on the continental shelf of southern Vancouver Island. Model results show the influence of the Juan de Fuca Eddy on the growth and retention of phytoplankton and the importance of different sources of nutrients (*i.e.*, wind-driven upwelling, topographically controlled upwelling, and the outflow from Juan de Fuca Strait) on primary production and biogeochemical cycles. The usefulness of this type of model to assess the potential responses of the marine ecosystem to climate change scenarios is discussed, as well as the limitations of present biogeochemical models, to predict future climate change.

Introduction

Ecosystem models are important tools to study biogeochemical cycles that are driven by complex interactions among physical, chemical and biological processes. In the open ocean, simple ecosystem models coupled to zero- or one-dimensional physical models have successfully contributed to the study of the importance of macro- and micronutrients on primary production, food-web interactions and physical–biological interactions (*e.g.*, Fasham *et al.*, 1990; Doney *et al.*, 1996). However, the high temporal and spatial variability of coastal regions makes it often necessary to couple ecosystem models to high resolution circulation models. Plankton ecosystem models coupled to circulation models are increasingly being applied to a variety of regions in the ocean to improve our understanding of ecosystem dynamics and to generalize discrete observations (*e.g.*, Gruber *et al.*, 2006; Powell *et al.*, 2006). These ecosystem models also have the potential to help us understand and quantify the interactions between marine ecosystems and climate change and to predict plausible ecosystem changes.

The southwestern coast of Vancouver Island (Fig.1) is one of the most productive fishing regions along the west coast of Canada (Ware and McFarlane, 1989). This region is at the northern end of the California Current System and is influenced by summer coastal upwelling. It is also influenced by freshwater inputs from the Fraser River, producing an estuarine circulation and strong tidal currents (Crawford, 1991). All these processes contribute to the dynamics of nutrient supply and phytoplankton and ultimately to the high primary productivity

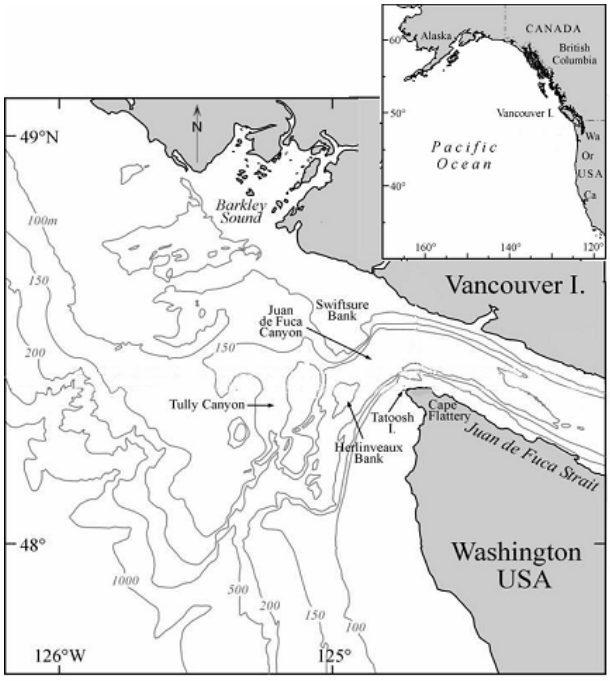

Fig. 1 Geography and bathymetry (m) of the southwestern coast of Vancouver Island in the Northeast Pacific.

observed in this region. In the summer, phytoplankton blooms are often found in this region associated with the Juan de Fuca Eddy, a seasonal cyclonic cold eddy located west of the entrance to Juan de Fuca Strait. This eddy is formed during periods of upwelling favorable winds, which in combination with the estuarine flow and tides, produce enhanced upwelling off Cape Flattery (Foreman *et al.*, 2008). Similarly, the Okhotsk Sea is one of the most biologically productive regions in the world with high fisheries production and high primary productivity, especially on the continental shelf (*e.g.*, Sorokin and Sorokin, 2002). In these dynamical regions, the coupling of an ecosystem model to a three-dimensional coastal ocean circulation model should yield new insight on the physical processes affecting the distribution of micronutrients in the region, and help understand the resulting impact on phytoplankton growth.

In this study, a simple plankton ecosystem model has been coupled to a circulation model (Regional Ocean Modeling System, ROMS) to study factors influencing summer bloom dynamics on the continental shelf off southwestern Vancouver Island. In the next section the model is described. Then, model results are presented and discussed, followed by a summary.

Model Description

Biological model

The model developed in this study is based upon the one-dimensional mixed layer/five-component NPZD (nutrient-phytoplankton-zooplankton-detritus) type model previously developed for the subarctic Pacific (Peña, 2003). The model was mainly modified to include the silicon cycle, separate compartments for NO_3 and NH_4, microzooplankton grazing on small and large phytoplankton, and differential re-mineralization of sinking silicon and nitrogen detritus. The increased complexity was necessary to represent conditions more characteristic of coastal regions. The modified ecosystem model has eight compartments: dissolved nutrients (NO_3, NH_4 and $Si(OH)_4$), diatoms that take up $Si(OH)_4$, a small size class of phytoplankton, microzooplankton, and two types of sinking detritus (nitrogen and silicon detritus). The food-web structure is shown schematically in Figure 2. All model compartments are expressed in terms of their nitrogen concentration (mmol-N m^{-3}). The processes incorporated in the model include growth of small phytoplankton and diatoms controlled by light, NO_3 and NH_4, and for diatoms also by $Si(OH)_4$. Uptake of nutrients by phytoplankton during the growth process is represented via a Michaelis-Menten formulation. Grazing by microzooplankton on small and large phytoplankton and nitrogen detritus is modeled by the Holling type-III formulation. Natural loss processes (*i.e.*, mortality and excretion) for both phytoplankton and zooplankton are linear. The differential remineralization of nitrogen and silicon detritus is linear as well. As in the previous model, the effect of top-down control by mesozooplankton in this model is formulated by imposing the grazing pressure of the observed biomass on diatoms and microzooplankton using a Holling type-III formulation. Also in the model, temperature affects all physiological parameters according to Q_{10} factors referenced to 10°C.

Biophysical model

The biological model is coupled to a three-dimensional coastal ocean circulation model. The circulation model is an implementation of the ROMS developed by Foreman *et al.* (2008). The model domain is bounded by approximately 45.5°N to 50.0°N and 123.5°W to 128.5°W, with 30 non-uniform vertical layers, with increased resolution near the surface and bottom boundary layers. A

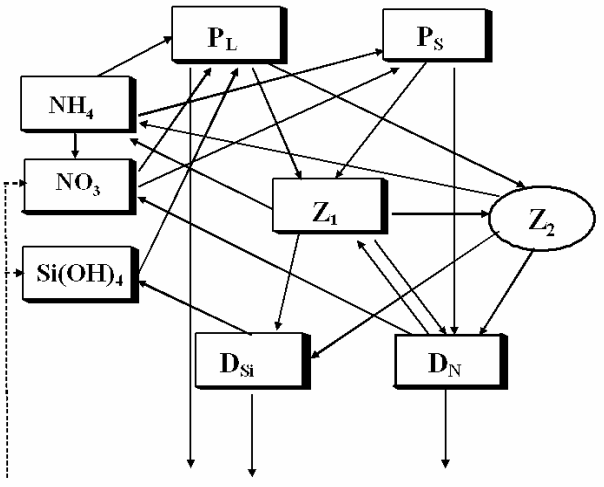

Fig. 2 Diagram of the food-web model: fluxes are shown with solid lines, external input of nutrients by dashed lines. Model compartments are represented by rectangles and the imposed biomass of mesozooplankton by an oval compartment. P_L represents diatoms, P_S small phyto-plankton, Z_1 microzooplankton, Z_2 mesozooplankton, D_N nitrogen detritus and D_{Si} silicon detritus.

stretched coordinate rectangular grid with horizontal resolution as coarse as 5 km adjacent to the western boundary and as fine as 1 km near the entrance of Juan de Fuca Strait is employed to obtain an accurate representation of topographic and coastal features of the region. The model is forced with tides, average summer upwelling-favorable winds, temperature and salinity monthly climatologies, and buoyancy boundary conditions that maintain an estuarine flow in Juan de Fuca Strait. The initial and boundary conditions of the model for nitrate and silicate are derived from three-dimensional summer climatology generated from a combination of data from the Institute of Ocean Sciences and the World Ocean Database 2001. For lack of better information, all other compartments are initialized with a constant value. Given the prescribed forcing, the model simulates summer conditions of temperature, salinity and currents that are in reasonable agreement with observations (Foreman *et al.*, 2008).

Results and Discussion

The model was run for 60 days and the results from the last 15 days are presented here. The modeled surface distribution of phytoplankton (diatoms and small phytoplankton) and nitrate concentration (Fig. 3) show the influence of the Juan de Fuca Eddy, located west of Juan de Fuca Strait, on the growth and retention of phytoplankton. Phytoplankton concentrations are higher around the eddy region and along the Washington upwelling coast. Similarly, nitrate is abundant (>15 mmol m^{-3}) nearshore and in the estuarine outflow from Juan de Fuca Strait that curls around the eddy in a counterclockwise manner. Nutrient concentrations decrease seaward such that no detectable nitrate was observed in the upper 10 m west of the continental shelf.

The modeled phytoplankton distribution patterns are in agreement with remotely-sensed observations of ocean color during the summer, as illustrated in Figure 4. In particular, the model captures the increased phytoplankton abundance in the continental shelf and eddy region, and lower concentrations offshore, but tends to over-predict phytoplankton biomass in Juan de Fuca Strait.

To determine the importance of different sources of nutrients (*i.e.*, wind-driven upwelling, topographically controlled upwelling, and the outflow from Juan de Fuca Strait) on phytoplankton biomass and primary production, the model was run with and without tidal forcing and wind forcing. Results from these experiments indicate that estuarine outflow from Juan de Fuca Strait is essential for nutrient enrichment and bloom generation. The strong influence of tidal mixing on nitrate fluxes from the estuarine outflow is illustrated in Figure 5, which shows that fluxes are significantly reduced in the simulation without tidal forcing compared to those from the simulation without winds but with tides. In the model, the eddy is formed

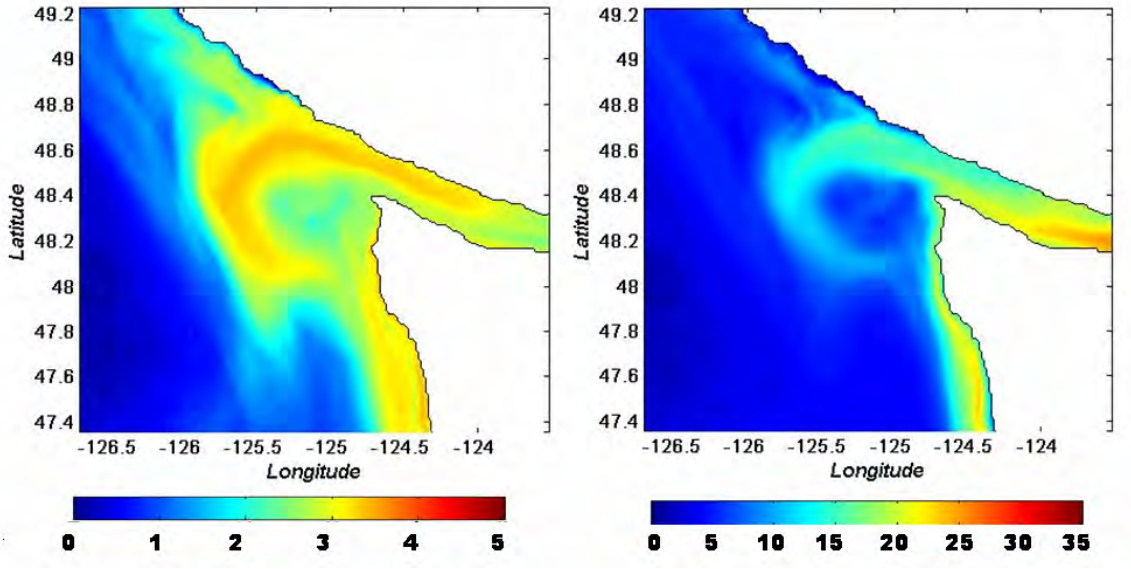

Fig. 3 Model surface phytoplankton (left panel, $P_S + P_L$) and nitrate concentration (right panel) average over days 46–60 of the 60-day simulation.

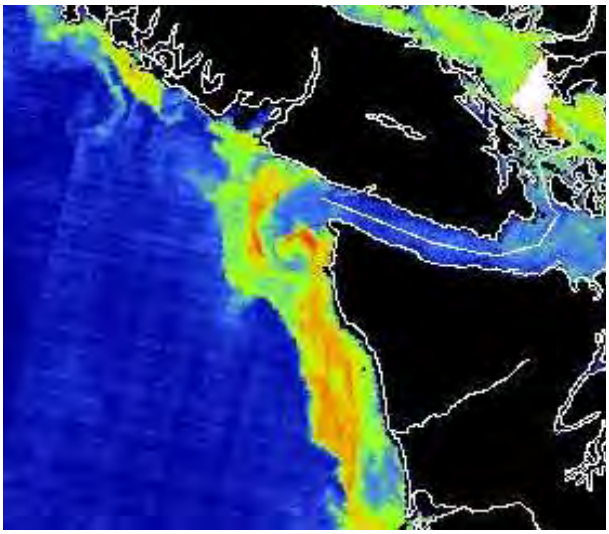

Fig. 4 MERIS satellite fluorescence for June 3, 2003 (courtesy of the European Space Agency and provided by J. Gower and S. King, IOS, Fisheries and Oceans Canada).

when either wind or tidal forcing is applied. A stronger bloom in the eddy region is obtained when the model is forced with estuarine flow and tides instead of with estuarine flow and winds.

In summary, our results indicate that phytoplankton production is influenced by nutrient fluxes, stratification, and temperature, all of which are likely to be affected by climate change. Impacts on phytoplankton will lead to cascading effects throughout the marine ecosystem. In coastal regions, the high temporal and spatial variability makes it challenging to detect ecosystem changes based on observations only. Thus, there is a need to develop three-dimensional circulation models that can point to plausible changes. To work towards this aim, the model was used to explore ecosystem responses to changes that might accompany climate change. Figure 6 shows preliminary results from a warming simulation where a constant offset of 3°C is applied to the initial temperature field. For the warming simulation, model phytoplankton biomass is of similar magnitude and distribution pattern to that of the standard run. In contrast, the model exhibits a more pronounced effect on primary production, resulting in higher productivity in the warming simulation. Since phytoplankton biomass is the result of growth and grazing, the results suggest that zooplankton grazing also increases with warming. It should be noted that in this simple warming simulation, the temperature offset applied to the model has no effect on the mixed-layer evolution and only explores the response of the ecosystem model to warming, separated from the response that might result from changes in the physical model.

Additional interpretation of these results is not warranted, since although the model can reproduce observations reasonably well, it has little 'predictive' power. The model currently lacks the complexity (species or functional groups, parameters that 'adapt/change' in response to changing ocean conditions/forcing, *etc.*) for the ecosystem to behave differently under different oceanic or climatic regimes. However, adding complexity (and realism) to models does not necessarily improve their predictive power, especially if the information

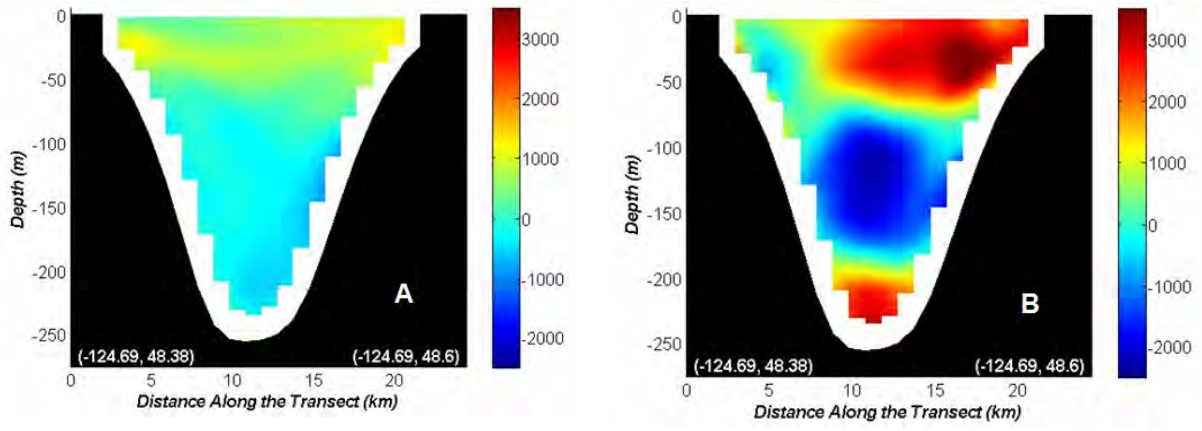

Fig. 5 Contours of the model fluxes of nitrate (mmol m^{-3} s^{-1}) along a transect at longitude 124.69°W across Juan de Fuca Strait, averaged over days 46–60 for (A) simulation with upwelling winds but no tides, and (B) simulation with tides but no wind.

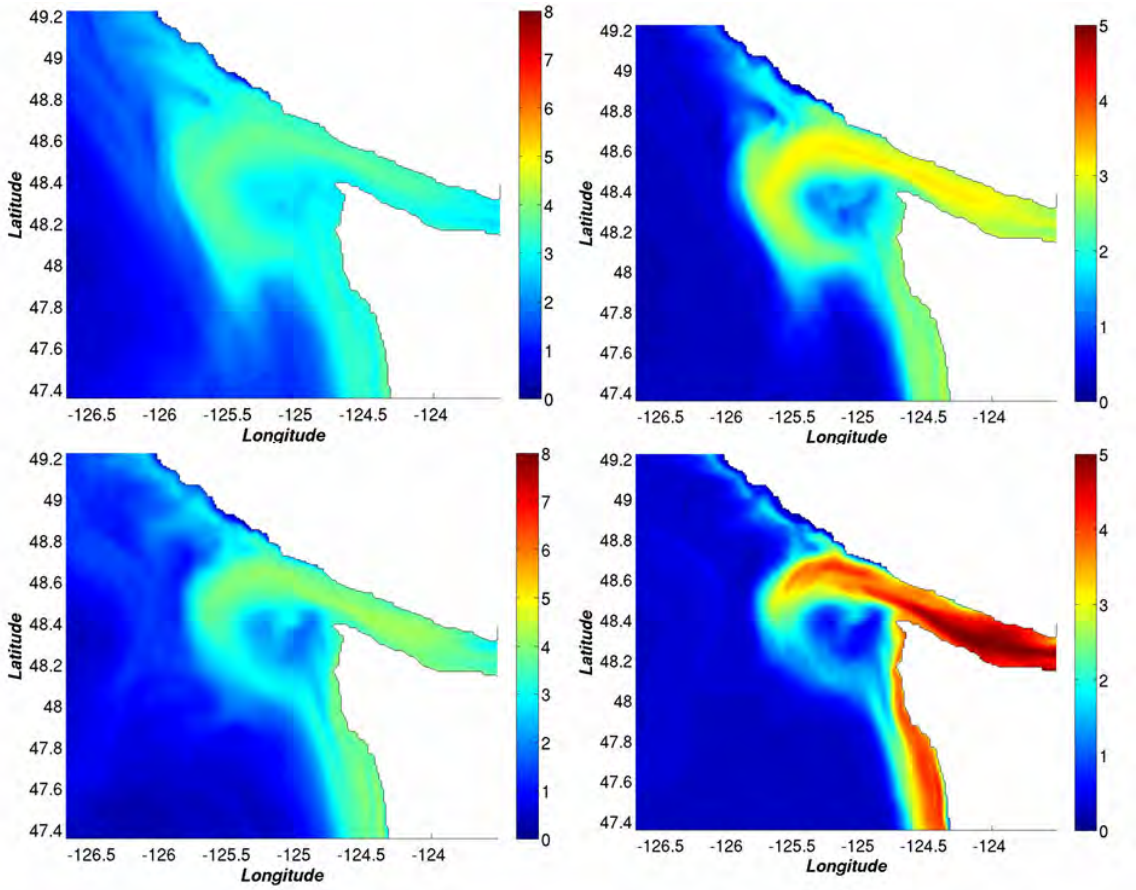

Fig. 6 Model surface phytoplankton (mmol-N m^{-3}, left panels) and primary production (mmol-N m^{-3} d^{-1}, right panels) average over days 46–60 of the 60-day simulation for the standard run (top panels) and for the warming simulation (bottom panels).

needed to construct and/or evaluate the more complex models is not available. Much work is necessary to improve confidence in climate-change prediction based on this type of ecosystem model.

Summary

Overall, this study provides an example of the utility of a coupled ecosystem/circulation model to the study of coastal ecosystems. In particular, the model was able to provide useful information on the importance of different sources of nutrients to phytoplankton growth and distribution, and to the transport of phytoplankton to the coast. The relatively simple ecosystem model developed here can be coupled to circulation models of other coastal regions, such as the Sea of Okhotsk, and can be used to address many ecosystem problems. In summary:

- The model is able to simulate the major biological features of the Vancouver Island shelf, higher surface nutrient and phytoplankton biomass in the Juan de Fuca Eddy, lower concentrations in Juan de Fuca Strait, and coastal upwelling off Washington State.
- The model indicates that the phytoplankton bloom in the Juan de Fuca Eddy region is the result of estuarine outflow from Juan de Fuca Strait and enhanced upwelling off Cape Flattery. The upwelling is generated by both the winds and the tides. A stronger bloom is generated in the eddy when the model is forced with estuarine flow and tides compared to the run forced by estuarine flow and winds.
- Preliminary results of the warming simulation suggest a strong response in the physiological rates of phytoplankton, with higher primary production and greater recycling rates but little change in concentrations.

References

Crawford, W.R. 1991. Tidal mixing and nutrient flux in the waters of southwest British Columbia. pp. 855–869 *in* Tidal Hydrodynamics *edited by* B.B. Parker, John Wiley and Sons, Inc.

Doney, S.C., Glover, D.M. and Najjar, R.G. 1996. A new coupled, one-dimensional biological-physical model for the upper ocean: Applications to the JGOFS Bermuda Atlantic Time-series Study (BATS) site *Deep-Sea Res. II* **43**: 591–624.

Fasham, M.J.R., Ducklow, H.W. and McKelvie, S.M. 1990. A nitrogen-based model of plankton dynamics in the oceanic mixed layer. *J. Mar. Res.* **48**: 591–639.

Foreman, M.G.G., Callendar, W., MacFadyen, A., Hickey, B.M., Thomson, R.E. and Di Lorenzo, E. 2008. Modeling the generation of the Juan de Fuca Eddy. *J. Geophys. Res.* **113**: doi:10.1029/2006JC 004082.

Gruber, N., Frenzel, H., Doney, S.C., Marchesiello, P., McWilliams, J.C., Moisan, J.R., Oram, J.J., Plattner, G.-K. and Stolzenbach, K.D. 2006. Eddy-resolving simulation of plankton ecosystem dynamics in the California Current System. *Deep-Sea Res. I* **53**: 1483–1516.

Peña, M.A. 2003. Modelling the response of the planktonic food web to iron fertilization and warming in the NE subarctic Pacific. *Progr. Oceanogr.* **57**: 453–479.

Powell, T.M., Lewis, C.V.W., Curchitser, E.N., Haidvogel, D.B., Hermann, A.J. and Dobbins, E.L. 2006. Results from a three-dimensional, nested biological-physical model of the California Current system and comparison with statistics from satellite imagery. *J. Geophys. Res.* **111**: doi:10.1029/2004JC 002506.

Sorokin, Y.I. and Sorokin, P.Y. 2002. Microplankton and primary production in the Sea of Okhotsk in summer 1994. *J. Plankton Res.* **24**: 453–470.

Ware, D.M. and McFarlane, G.A. 1989. Fisheries production domains in the Northeast Pacific Ocean. *In* Effects of ocean variability on recruitment and an evaluation of parameters used in stock assessment models *edited by* G.A. McFarlane, *Can. Spec. Publ. Fish. Aquat. Sci.* **108**: 359–379.

Nutrient status of snow cover and sea ice in the southern Sea of Okhotsk

Daiki Nomura[1,2], Kunio Shirasawa[1], Sumito Matoba[1], Jun Nishioka[1] and Takenobu Toyota[1]

[1] Institute of Low Temperature Science, Hokkaido University, Sapporo, Japan
E-mail address: daiki@lowtem.hokudai.ac.jp (D. Nomura)
[2] Japan Society for the Promotion of Science, Tokyo, Japan

Abstract

Samples of sea ice and snow cover on sea ice were collected with the icebreaker P/V *Soya* in early February 2007 in the southern Sea of Okhotsk in order to evaluate the amount of nutrients in the sea ice and snow. The concentration of nitrate + nitrite, phosphate and silicic acid in the samples was measured in conjunction with such physical parameters as temperature, salinity, oxygen isotopic ratio and ice texture. Sea ice was categorized into three types: snow-ice, granular ice and columnar ice, based on the oxygen isotopic ratio and ice texture. A higher nitrate + nitrite concentration up to 13.5 μmol L^{-1} was found in the snow and snow-ice, implying the deposition from the atmosphere, occurring as snowfall. Phosphate and silicic acid concentrations up to 14.3 μmol L^{-1} and 32.7 μmol L^{-1}, respectively, were highest in granular ice. These results indicate the incorporation of organisms and/or sediment from under-ice water and subsequent remineralization reactions in sea ice.

Introduction

In the Sea of Okhotsk, spring brooms were observed from satellite images after the ice melting season (*e.g.*, http://www.eorc.jaxa.jp/imgdata/topics/2004/tp040108.html). Despite the indications that sea ice melting has been considerd to play a role in the chemical budget and cycling in the Sea of Okhotsk, there is a distinct paucity of information on this aspect of sea ice.

During the ice formation process, sea ice contains a lot of particulate and dissolved materials (Masqué *et al.*, 2007). These materials are incorporated through atmospheric deposition (Granskog *et al.*, 2003; Granskog *et al.*, 2004) and suspension freezing in under-ice water (Masqué *et al.*, 2007). Therefore, sea ice acts as an effective transporter for particulate and dissolved materials. During the ice melting season, these materials are released and supplied to the under-ice water.

In this study, in order to examine the nutrient profiles in snow and sea ice, and mechanisms controlling the distribution of nutrients in snow and sea ice, samples of snow and sea ice were collected with the icebreaker P/V *Soya* during early February 2007 in the southern Sea of Okhotsk.

Materials and Methods

Sampling of snow, sea ice, and under-ice water

Field observations were carried out during the icebreaker P/V *Soya*'s cruise in the southern Sea of Okhotsk on February 12 and 13, 2007 (Fig. 1). Two different ice stations (A and B) were selected. Samples of sea ice cores, brine in sea ice and under-ice water were collected at each station. By using a basket suspended from the ship's crane, we could get access above the sea ice (Toyota *et al.*, 2007). Sea ice cores were collected with an ice core sampler of 9 cm diameter through a hole on the basket floor. Immediately after the ice core was collected, ice thickness and temperature of the ice core were measured by scale and by inserting a needle-like thermometer sensor into a drilled hole of the core, respectively. Thereafter, the ice cores were kept in a polythene bag in a deep freezer at –15°C during the cruise period, and transferred to the cold room at –16°C at the Institute of Low Temperature Science (ILTS) immediately after the cruise.

The under-ice water sample was collected through an ice core hole with a 500 mL Teflon water sampler (GL Science Inc., Japan) at depths of 1 m below the surface of sea ice. The sample was divided into a

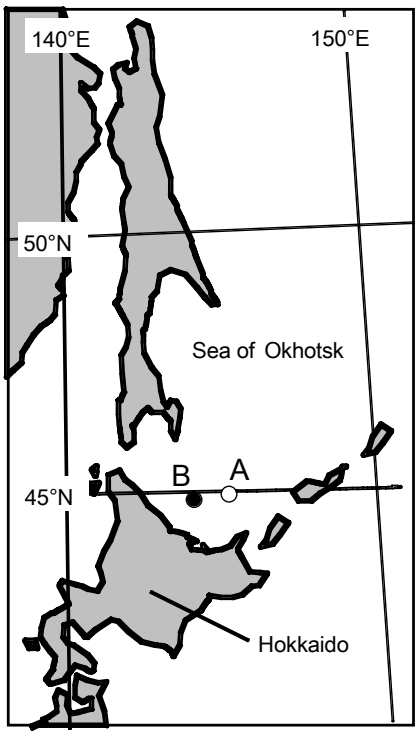

Fig. 1 Location map of Stn. A and B in the southern Sea of Okhotsk. Open circle indicates Stn. A (45°N 03′09.8″, 144°E 34′44.5″). Solid circle indicates Stn. B (45°N 01′23.0″, E143°E 47′14.0″).

10 mL glass vial as a sub-sample for measuring salinity and oxygen isotopic ratio ($\delta^{18}O$) and into a 10 mL polyethylene screw vial for measuring nutrients. Samples for nutrients were kept in the same manner as that for the sea ice core samples.

The snow sample deposited over sea ice was collected through the side of the basket directly into pre-cleaned polyethylene zip-lock bags. The depth and temperature of the snow were measured by scale and by inserting a needle-like thermometer sensor, respectively.

Sample analysis

In the cold room of the ILTS, the sea ice core was divided into two pieces longitudinally. One side of the ice core was used for the measurement of salinity, $\delta^{18}O$ and nutrients. The other was used for the analysis of physical properties.

The sea ice sample was cut to 4.5 cm × 2.5 cm in plane size by a band saw and then sliced into 3-cm thick sections to measure ice salinity, $\delta^{18}O$ and nutrients. In addition, the sea ice section was divided into two pieces longitudinally. One side of the section was kept in a Teflon container and then melted to measure salinity and $\delta^{18}O$. In order to avoid contamination, the other piece was trimmed with a knife previously washed by acid, and then put into pre-cleaned polyethylene bags and melted to measure nutrients.

Pictures of the sea ice section divided into two pieces were taken. Then, we analyzed the physical properties of sea ice using thin and thick sections in order to clarify the ice formation history. Details of this analysis were described by Granskog *et al.* (2004). In this study, sea ice was categorized into three types: snow-ice, granular ice and columnar ice, based on the oxygen isotopic ratio and ice texture.

Salinity of the under-ice water, melted snow and sea ice were measured using a salt analyzer (SAT-210, Toa Electronics Ltd., Japan). A standard deviation calculated from the 15 sub-samples taken from a single sample bottle gave a salinity of 0.03. Nutrients (Dissolved Inorganic Nitrogen: DIN-N, $Si(OH)_4$-Si and PO_4-P) were determined by an auto-analyzing system (AACS II, Bran+Luebbe, Germany) according to the JGOFS spectrophotometric method (JGOFS, 1994). DIN-N refers to the sum of the concentration of NO_3-N, NO_2-N and NH_4-N. $\delta^{18}O$ was determined with a mass spectrometer (DELTA plus, Finnigan MAT, USA). The $\delta^{18}O$ in per mil was defined as the deviation of $H_2{}^{18}O/H_2{}^{16}O$ ratio of the measured sample to that of the international standard water (SMOW). The precision of $\delta^{18}O$ analysis from duplicate determinations was within ± 0.02‰ (Toyota *et al.*, 2007).

Results and Discussion

Characteristics of snow, sea ice and under-ice water

Two ice cores with an ice thickness of 47 cm (Core 1) and 55 cm (Core 2) were collected at Stn. A on February 12, 2007. One ice core with an ice thickness of 84 cm (Core 3) was collected at Stn. B on February 13, 2007. Snow depth was 4 cm at Stn. A and 9 cm at Stn. B.

Vertical profiles of temperature, salinity and $\delta^{18}O$ in snow and sea ice are shown in Figure 2. Temperatures at the upper part of the sea ice were lower than that at the bottom of the sea ice. At the bottom of the sea ice, temperatures corresponded to the freezing point of –1.8°C. Snow temperature was

dependent on the atmospheric temperature of –3.1°C on February 12, 2007 and –5.5°C on February 13, 2007. Although the ice temperature increased linearly with increasing ice depth, the shape of the profile for ice salinity and $\delta^{18}O$ were irregular through the ice cores. These results suggest that the dynamic processes were dominated by ice growth in the southern Sea of Okhotsk (Toyota *et al.*, 2007).

Figure 3 shows the vertical profiles of the ice section, thick and thin section for Core 2. As seen in Figure 3(a), dirt layers were found at a depth of –30 cm, from –35 to –40 cm and from –40 to –50 cm. Because $\delta^{18}O$ was greater than 0‰ through the ice core for Core 2 (Fig. 2), sea ice was made from the seawater. Therefore, dirt layers were attributed to the incorporation of dissolved or particulate materials from under-ice water. Dirt layers were also observed at a depth of –10 cm in Core 1.

Based on the results obtained from the ice texture and $\delta^{18}O$ (Figs. 2(c) and 3), sea ice was categorized into three types: snow-ice, granular ice and columnar ice (Table 1). The average data shown in Table 1 indicate that granular ice was dominant in the total ice thickness. These relationships agreed well with the results obtained previously in same area (Toyota *et al.*, 2004).

Nutrient concentrations in snow, sea ice and under-ice water

Vertical profiles of nutrient concentrations in snow, sea ice and under-ice water are shown in Figure 4. A higher nitrate + nitrite concentration was found in the upper part of the sea ice and snow, while phosphate and silicic acid concentrations were low. Although phosphate and silicic acid concentrations were very small in Cores 1 and 3, extremely high concentrations were observed in Core 2, where the dirt layers were found. This suggests that high phosphate and silicic acid concentrations were due to the incorporation of the materials from under-ice water.

Table 2 shows the nutrient concentrations for snow and each ice type. High nitrate + nitrite concentrations were found in the snow and snow-ice, implying the deposition was from the atmosphere, occurring as snowfall. In the Baltic Sea, high dissolved inorganic nitrogen (DIN) concentrations in snow and snow-ice were observed (Granskog *et al.*, 2003). DIN deposited from the atmosphere with snowfall can accumulate on sea ice, and can also become incorporated into the ice due to snow-ice formation. Because our study area is located off the east coast of Asia, it is possible that polluted snow

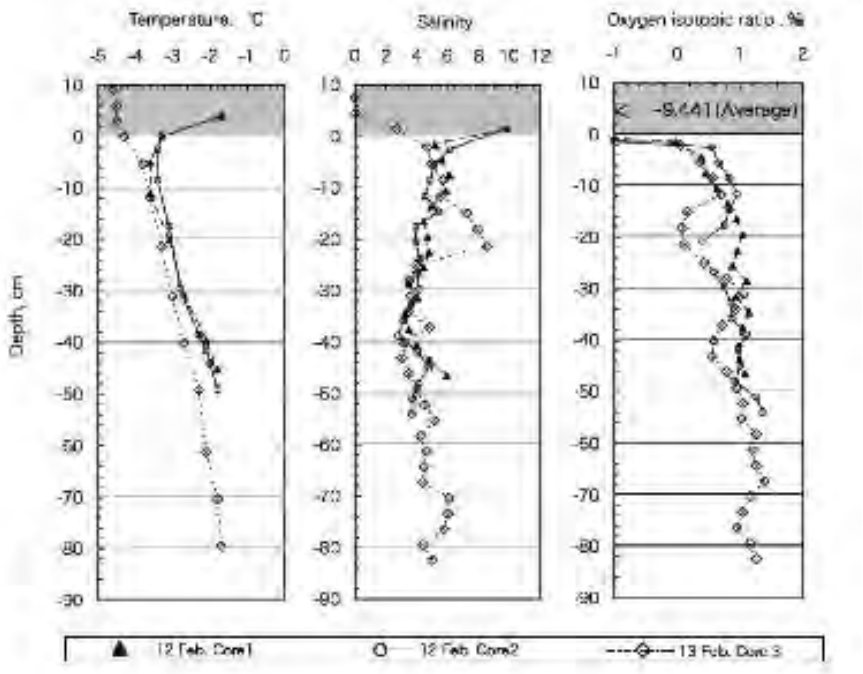

Fig. 2 Vertical profiles of temperature, salinity and $\delta^{18}O$ in sea ice and snow. Shaded areas indicate the part of the snow deposited over sea ice.

Table 1 Statistics of ice types and layer thicknesses.

Sample type	Core 1, Feb. 12, 2007		Core 2, Feb. 12, 2007		Core 3, Feb. 13, 2007		Average	
	Thickness (cm)	Fraction (%)	Thickness (cm)	Fraction (%)	Thickness (cm)	Fraction (%)	Thickness (cm)	Fraction (%)
Snow	4.0	7.8	4.0	6.8	9.0	9.7	17.0	8.4
Snow-ice	6.0	11.8	0.0	0.0	10.0	10.8	16.0	7.9
Granular	22.0	43.1	47.5	80.5	54.5	58.6	124.0	61.1
Columnar	19.0	37.3	7.5	12.7	19.5	21.0	46.0	22.7
Total	51.0	100.0	59.0	100.0	93.0	100.0	203.0	100.0

Table 2 Average nutrient concentration (μmol L^{-1}) for snow and each ice type (average ± standard deviation (number of samples)).

Sample type	Average		
	NO_2 +NO_3	Si	P
Snow	8.05 ± 4.68 (3)	0.47 ± 0.12 (3)	0.0 ± 0.0 (3)
Snow-ice	1.77 ± 0.96 (5)	2.25 ± 0.52 (5)	0.57 ± 0.71 (5)
Granular	1.04 ± 0.62 (40)	4.87 ± 6.61 (40)	1.86 ± 3.19 (40)
Columnar	1.10 ± 0.90 (16)	1.62 ± 1.06 (16)	0.07 ± 0.16 (16)

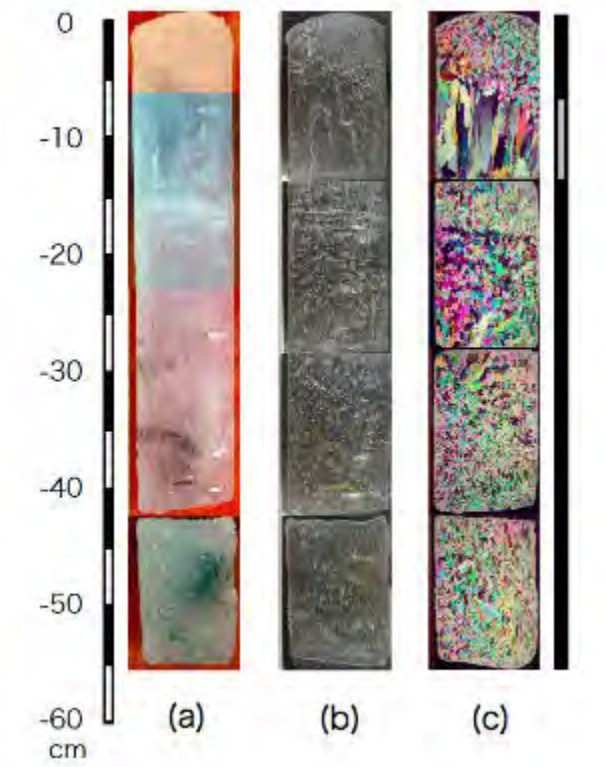

Fig. 3 Vertical profiles of (a) a picture of the section, (b) thick and (c) thin sections for Core 2. The black and gray bars indicate granular ice and columnar ice, respectively.

(high nitrate + nitrite concentration) was deposited over the sea ice. Therefore, in the Sea of Okhotsk, the atmospheric supply of DIN plays an important role in biological productivity within the sea ice and under-ice water, as in the Baltic Sea.

Phosphate and silicic acid concentrations were highest in granular ice, up to 14.3 μmol L^{-1} and 32.7 μmol L^{-1}, respectively. This probably results from the selective incorporation of phosphate and silicic acid from seawater to sea ice. During granular ice formation, suspended and planktonic organisms were scavenged by frazil ice crystals (Lisitzin, 2002). In shallow areas, sediments are incorporated into sea ice when sea ice rests on the seafloor. In addition, the aerobic remineralization and denitrification occurred in sea ice (Thomas *et al.*, 1995; Rysgaard and Glud, 2004). Therefore, nitrate + nitrite concentrations were low in granular ice. On the other hand, phosphate and silicic acid concentrations were high in granular ice.

Conclusions

In order to examine the nutrient profiles in snow and sea ice, and mechanisms controlling the distribution of nutrients in snow and sea ice, samples of snow and sea ice were collected with the icebreaker P/V

Soya in early February of 2007 in the southern Sea of Okhotsk. A higher nitrate + nitrite concentration up to 13.5 μmol L^{-1} was found in the snow and snow-ice, implying the deposition was from the atmosphere, occurring as snowfall. Phosphate and silicic acid concentrations were highest in granular ice up to 14.3 μmol L^{-1} and 32.7 μmol L^{-1}, respectively. This probably results from the incorporation of organisms and/or sediment from under-ice water and subsequent remineralization reactions in sea ice.

Acknowledgements

We would like to express heartfelt thanks to Dr. H. Y. Inoue and the crew of the Japan Coast Guard's P/V *Soya* for sampling assistance, providing measurement devices and their useful comments. This work is partly supported by the Research Fellowship of the Japan Society for the Promotion of Science (#195968).

References

Granskog, M.A. and Kaartokallio, H. 2004. An estimation of the potential fluxes of nitrogen, phosphorus, cadmium and lead from sea ice and snow in the Northern Baltic Sea. *Water Air Soil Pollut.* **154**: 331–347.

Granskog, M.A., Kaartokallio, H. and Shirasawa, K., 2003. Nutrient status of Baltic Sea ice: Evidence for control by snow-ice formation, ice permeability, and ice algae. *J. Geophys. Res.* **108**: doi:10.1029/2002JC001386.

Lisitzin, A.P. 2002. Sea-ice and Iceberg Sedimentation in the Ocean – Recent and Past. Springer-Verlag, Berlin.

Masqué, P., Cochran, J.K., Hirschberg, D.J., Dethleff, D., Hebbeln, D., Winkler, A. and Pfirman, S. 2007. Radionuclides in Arctic sea ice: Tracers of sources, fates and ice transit time scales. *Deep-Sea Res. I* **54**: 1289–1310.

Rysgaard, S. and Glud, R.N. 2004. Anaerobic N_2 production in Arctic sea ice. *Limnol. Oceanogr.* **49**: 86–94.

Thomas, D.N., Lara, R.J., Eicken, H., Kattner, G. and Skoog, A. 1995. Dissolved organic matter in Arctic multi-year sea ice during winter: major components and relationships to ice characteristics. *Polar Biol.* **15**: 477–483.

Toyota, T., Kawamura, T. and Ohshima, K.I. 2004. Thickness distribution, texture and stratigraphy, and a simple probabilistic model for dynamical thickening of sea ice in the southern Sea of Okhotsk. *J. Geophys. Res.* **109**: doi:10.1029/2003JC002090.

Toyota, T., Takatsuji, S., Tateyama, K., Naoki, K. and Ohshima, K.I. 2007. Properties of sea ice and overlying snow in the southern Sea of Okhotsk. *J. Oceanogr.* **63**: 393–411.

Interannual variation of material flux under seasonal sea ice in the Okhotsk Sea north of Hokkaido, Japan

Takehiko Hiwatari[1], Hiroshi Koshikawa[1], Kunio Kohata[1] and R. Nagata[2]

[1] National Institute for Environmental Studies, Tsukuba, Japan. E-mail: hiwatari.takehiko@nies.go.jp
[2] Okhotsk Garinko Tower, Mombetsu, Japan

Introduction

The offshore waters along the Okhotsk Sea coast of Hokkaido, Japan are the southernmost area of seasonal sea ice distribution in the Northern Hemisphere. Seasonal sea ice generally drifts ashore along the Okhotsk Sea coast of Hokkaido during January, reaching a maximum extent during February. The ice then moves offshore to the northeast under the influence of southwesterly winds and begins to melt during March, retreating progressively northward during April.

In the Arctic and Antarctic waters, vertical material flux – particularly that of ice algae and the fecal pellets of zooplankton – in regions of sea ice plays an important role in the pelagic–benthic coupling of material cycling and trophic linkages (Hoshiai *et al.*, 1987; Hobson *et al.*, 1995; Schnack-Schiel, 2003). However, a limited number of data on the downward material flux under the seasonal sea ice along the Okhotsk Sea coast of Hokkaido have been reported.

The present study was undertaken to document the spatial and temporal patterns of lithogenic and biogenic fluxes, particularly fluxes of opal and organic material, in relation to sea ice behavior during the pack-ice season at an offshore site in the Okhotsk Sea north of Hokkaido (about 14 km off the Mombetsu coast, water depth of 60 m) from January to March 2005 and 2006.

Materials and Methods

Sea ice coverage in the study area

The first-year ice off the Okhotsk Sea coast of Hokkaido from January to March 2005 behaved in an ordinary pattern; it drifted ashore along the coast late in January, developed to its widest area late in February, and retreated late in March (Hiwatari *et al.*, 2008). On the contrary, the sea ice in 2006 retreated one month earlier than the corresponding period of 2005 (ice data were provided by satellite images 'MODIS' of Japan Aerospace Exploration Agency).

Sediment trap mooring

We measured the material flux under seasonal sea ice using a time-series sediment trap at a site offshore of Mombetsu in the Okhotsk Sea (Fig.1; 44°28.691´N, 143°25.217´E, water depth 60 m). The sediment trap, comprising seven time-series collecting bottles (500 ml each), was situated at 40 m depth (20 m above the sea floor), and the collecting periods were 7 or 14 days in duration for each of the seven collecting bottles over the period from January 13 to March 24, 2005 and 2006 (Table 1).

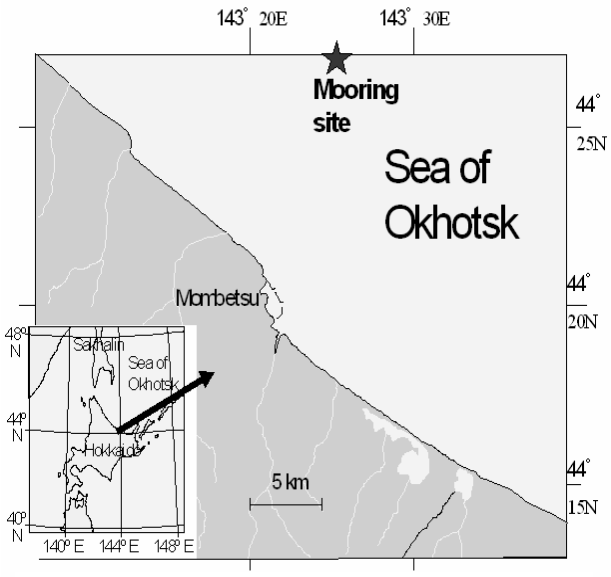

Fig. 1 Map of a portion of the central Okhotsk coast of Hokkaido, showing the location of the sediment trap mooring site.

Table 1 Sampling periods in 2005 and 2006 for the sediment trap.

Sampling bottle	Sampling period	Period (days)
1	January 13–27, 2005	14
	January 13–20, 2006	7
2	January 27–February 10, 2005	14
	January 20–27, 2006	7
3	February 10–24, 2005	14
	January 27–February 2, 2006	7
4	February 24–March 3, 2005	7
	February 3–10, 2006	7
5	March 3–10, 2005	7
	February 10–24, 2006	14
6	March 10–17, 2005	7
	February 24–March 10, 2006	14
7	March 17–24, 2005	7
	March 10–24, 2006	14

Chemical analyses

The sediment trap samples were analyzed for the following items: total mass as dry weight, particulate organic carbon (POC), $CaCO_3$, chlorophyll *a* (Chl-*a*), pheopigment, biosilica (BioSi), fecal pellet carbon of zooplankton, and cell identification and enumeration of phytoplankton.

The vertical material flux is expressed as the total mass flux, which consists of the lithogenic and biogenic component fluxes (Fischer and Wefer, 1996; Khim *et al.*, 2007) : total mass flux = lithogenic particle flux + biogenic particle flux, the latter of which is expressed as a total of opal flux, organic matter flux and calcium carbonate ($CaCO_3$) flux. The opal component was calculated by multiplying the BioSi content by 2.4 (Khim *et al.*, 2007). The organic matter was determined by multiplying the POC contents by 1/0.35 (Honda *et al.*, 1997). The lithogenic particle flux was obtained by subtracting the biogenic flux from the total mass flux. The organic matter flux in the study consisted of detritus, fecal pellets, and phytoplankton. In calculating the POC of the phytoplankton in 2005, we used POC = Chl-*a* × 20 (Taguchi *et al.*, 1997). For that of the phytoplankton in 2006, we used POC = cell number × 91.28 × 10–12 g C/cell (Strathmann, 1967). The organic matter fluxes of the phytoplankton and fecal pellets were then calculated by multiplying those POC contents by 1/0.35 (Honda *et al.*, 1997). The detritus flux was obtained by subtracting the organic matter fluxes of phytoplankton and fecal pellets from the total organic matter flux.

Results and Discussion

The total mass fluxes consisting of the lithogenic and biogenic component fluxes in 2005 and 2006 are shown in Figure 2. The total mass fluxes, particularly that of lithogenic particles, were greatest during the early sampling periods in both years. The occurrence of high fluxes of the lithogenic and biogenic (particularly organic material) particle components relative to the total mass recorded during the early sampling periods is consistent with the finding of Noriki and Matsubara (2002).

The particulate materials on early first-year ice were released into the water column as the sea ice melted in seawater temperatures of > 0°C. Oshima *et al.* (2001) observed ice melt around the margins of the sea ice on February 9, 1997, about 140 km northeast of Mombetsu. In this area, first-year ice floes had been advected from the north via the main stream of the southward current.

The organic matter fluxes consisting of detritus, fecal pellets and phytoplankton component fluxes in 2005 and 2006 are shown in Figure 3. The organic matter fluxes, particularly that of detritus in both years, were high during the early sampling periods. The fact that organic matter was found in the early first-year ice offshore from the Okhotsk coast in early February (Granskog, 1999) indicates that decomposition of the

organic matter to detritus via the processes of heterotrophic organisms would have occurred in the early first-year ice prior to melting.

During the period from early February to early March 2005, when persistent ice cover was recorded, the fecal pellets of zooplankton were the dominant component of sinking particles. In particular, organic matter comprising fecal pellets contributed more than 70% of the total organic matter flux. We also observed a large number of diatom frustules in the fecal pellets. The present data demonstrate the occurrence of fresh phytoplankton in the form of ice algae beneath the sea ice and the active grazing and egestion of zooplankton during the season of ice cover. On the other hand, fecal pellet flux in 2006 was very little. This suggests that the disappearance of fresh ice algae beneath the sea ice could not induce active grazing and egestion of zooplankton because of the rapid retreat of the sea ice.

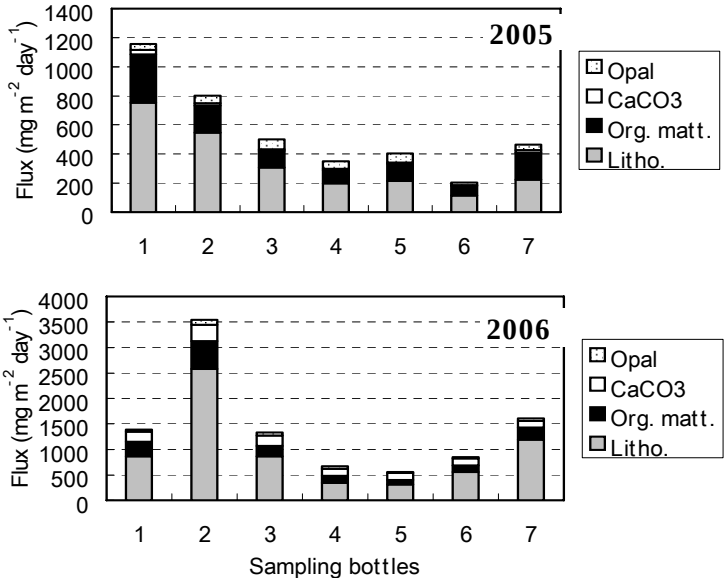

Fig. 2 Temporal variations of lithogenic and biogenic (organic matter, opal, and $CaCO_3$) fluxes consisted of the total mass flux in 2005 and 2006.

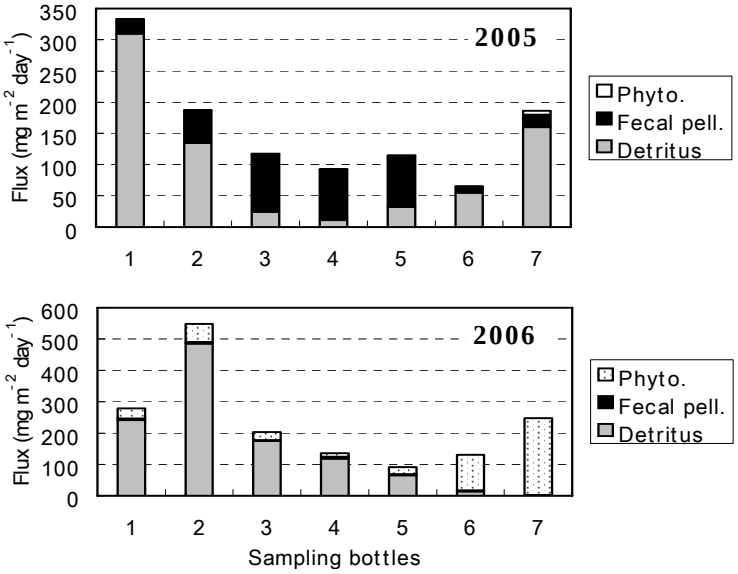

Fig. 3 Temporal variations of organic matter components (detritus, fecal pellets, and phytoplankton) fluxes in 2005 and 2006.

The phytoplankton component flux in 2006 was high during the late sampling periods which indicates that the phytoplankton bloom occurred (not ice algae species) because the sea ice retreated a month earlier than in the corresponding period of 2005.

Conclusions

- The sea ice in 2006 retreated one month earlier than in the corresponding period of 2005.
- Total mass fluxes during January to early February in both years were greater than those in other years. In those periods, lithogenic material occupied more than 60% of the total mass fluxes, much of which would be derived from the sea ice as ice-rafted debris.
- Fecal pellets of zooplankton in 2005 were the dominant components of sinking particles from February to early March, the periods corresponding to a persistent ice cover.

References

Fischer, G. and Wefer, G. 1996. Seasonal and interannual particle fluxes in the Eastern Equatorial Atlantic from 1989 to 1991: ITCZ migration and upwelling. pp. 199–214 *in* Particle Flux in the Ocean *edited by* V. Ittekkot, P. Schafer, S. Honjo and P.J. Depetris, Wiley and Sons, Chichester.

Granskog, M. 1999. Observation of particulate matter in the ice of the Sea of Okhotsk and Saroma-ko Lagoon. Low Temp. Sci. Ser. A 58, Hokkaido Univ., pp. 63–71.

Hiwatari, T., Shirasawa, K., Fukamachi, Y., Nagata R., Koizumi, T., Koshikawa, H. and Kohata, K. 2008. Verticla material flux under seasonal sea ice in the Okhotsk Sea north of Hokkaido, Japan. *Polar Sci.* **2**: 41–54.

Hobson, K.A., Ambrose, W.G. and Renaud, P.E. 1995. Sources of primary production, benthic-pelagic coupling, and trophic relationships within the Northeast Water Polynya: insights from $\delta^{13}C$ and $\delta^{15}N$ analysis. *Mar. Ecol. Prog. Ser.* **128**: 1–10.

Honda, M., Kusakabe, M., Nakabayashi, S., Manganini, S.J. and Honjo, S. 1997. Change in pCO_2 through biological activity in the marginal seas of the western North Pacific: the efficiency of the biological pump estimated by a sediment trap experiment. *J. Oceanogr.* **53**: 645–662.

Hoshiai, T., Tanimura, A. and Watanabe, K. 1987. Ice algae as food of Antarctic ice-associated copepod, *Paralabidocera antarctica* (I.C. Thompson). *Proc. NIPR Symp. Polar Biol.* **1**: 105–111.

Khim, B.K., Shim, J., Yoon, H.I., Kang, Y.C. and Jang, Y.H. 2007. Lithogenic and biogenic particle deposition in an Antarctic coastal environment (Marian Cove, King George Island): seasonal patterns from a sediment trap study. *Estuar. Coast. Shelf Sci.* **73**: 111–122.

Noriki, S. and Matsubara, N. 2002. Evaluation of the sea ice effects and diatom bloom in the Sea of Okhotsk based on the chemical analysis of the sinking particles. *Kiyo Mon.* **30**: 152–157. Special Edition (in Japanese).

Ohshima, K.I., Mizuta, G., Itoh, M., Fukamachi, Y., Watanabe, T., Nabae, Y., Suehiro, K. and Wakatsuchi, M. 2001. Winter oceanographic conditions in the southwestern part of the Okhotsk Sea and their relation to sea ice. *J. Oceanogr.* **57**: 451–460.

Schnack-Schiel, S.B. 2003. The macrobiology fo sea ice. pp. 211–239 *in* Sea Ice, An Introduction to its Physics, Chemistry, Biology and Geology *edited by* D.N. Thomas and G.S. Dieckmann, Blackwell Science, Oxford.

Strathmann, R.R. 1967. Estimating the organic carbon content of phytoplankton from cell volume or plasma volume. *Limnol. Oceanogr.* **12**: 411–418.

Taguchi, S., Saito, H., Hattori, H. and Shirasawa, K. 1997. Vertical flux of ice algal cells during the ice melting and breaking periods in Saroma Ko Lagoon, Hokkaido, Japan. *Proc. NIPR Symp. Polar Biol.* **10**: 56–65.

Plenary Session 3

Primary production/Zooplankton/Marine mammals

Session Chairs

Sei-Ichi Saitoh, Alexey M. Trukhin, Mari Kobayashi and Akihiro Shiomoto

Satellite measured seasonal and interannual variability of primary production at the scallop farming area in the Okhotsk Sea

Muzzneena Ahmad Mustapha[1,2] and Sei-Ichi Saitoh[1]

[1] Laboratory of Marine Bioresource and Environment Sensing, Graduate School of Fisheries Sciences, Hokkaido University, Hakodate, Hokkaido, Japan. E-mail: ssaitoh@salmon.fish.hokudai.ac.jp
[2] Universiti Kebangsaan Malaysia, Selangor, Malaysia

Abstract

Seasonal and interannual variation of primary production after the retreat of sea ice at the scallop farming area along the Hokkaido coast off Okhotsk Sea (1998–2004) was determined using satellite images. Interannual variability of primary production occurred from the variability in occurrences of physical processes associated with the advection of the Soya Warm Current (SWC) and intrusion of the East Sakhalin Current (ESC). Variability in primary production resulted in variability of Chl-*a* concentration that was also demonstrated by EOF analysis. Enhancement of Chl-*a* in the frontal area in late spring was shown by the second EOF mode of Chl-*a* (14.2% of variance) in parallel with the generation of a well developed frontal area resulting from the advection of warm waters of the SWC along coast in late spring indicated by the second EOF mode of SST (1.8% of variance). Elevated Chl-*a* and occurrence of cold waters of the ESC in late autumn were also highlighted by the third EOF mode of Chl-*a* (9.0 % of variance) and SST (1.5% of variance). Prolonged high primary production in the scallop farming area after spring is supported by the development of a frontal area in summer and enforcement of the ESC in autumn.

Seasonal variability of primary production off Abashiri, the southern Okhotsk Sea[1]

Hiromi Kasai, Tsuneo Ono and Kazumasa Hirakawa

Hokkaido National Fisheries Research Institute, Fisheries Research Agency, Hokkaido, Japan
E-mail: kasaih@fra.affrc.go.jp

Introduction

The Okhotsk Sea is the southernmost marginal sea that is ice-covered during winter; therefore, it is considered to be an area having sensitive environmental characteristics due to the influence of global warming. In order to detect such environmental changes, monitoring of oceanographic conditions is considered important. However, few monitoring studies have been made in the offshore area of the Okhotsk Sea due to difficulties making observations in the ice-cover season.

The Hokkaido National Fisheries Research Institute of the Fisheries Research Agency has been conducting monitoring surveys in the southern Okhotsk Sea since 2000. In this study, we report some results about oceanographic conditions on primary production from monitoring observations in the southern Okhotsk Sea.

Observations

Two observation lines (N-line and S-line) were set up in the area off Abashiri, in the southern Okhotsk Sea (Fig. 1). The oceanographic surveys along these lines were conducted in the non-ice seasons (generally April–October) 4–5 times a year. The routine surveys were CTD casts, vertical profiles of chlorophyll *a* and nutrients (nitrate, phosphate and silicate), and netplankton biomass collected with a NORPAC net. For detailed methods, see Saito *et al.* (1998) and Kasai *et al.* (2001). At some of the stations, daily primary production was measured with a simulated *in situ* incubation method using ^{13}C as tracer (Yokouchi *et al.*, 2006).

Results and Discussion

During the survey periods, the observation area could be classified into two water masses. For example, the T-S diagrams obtained in April, May, July and October of 2005 are shown in Figure 2. As the season progressed, two coastal stations showed characteristics of high temperature and high salinity corresponding to the characteristics of the Soya Warm Current. Therefore, the coastal stations should be considered under the influence of the Soya Warm Current. On the other hand, stations in the offshore area showed characteristics of low salinity in the surface layer, and a temperature minimum at around a salinity of 33 at about 200 m depth.

In this paper, we classify the study area according to two water masses: the Coastal Area and the Offshore Area. Because the oceanography of the Coastal Area has been well investigated for environmental conditions related to scallop culturing (Nishihama, 1994; Horii *et al.*, 1992; Shinada, 2006), we will report mainly on oceanographic conditions of the Offshore Area.

Seasonal changes in the vertical profiles of temperature and salinity in the Offshore Area are

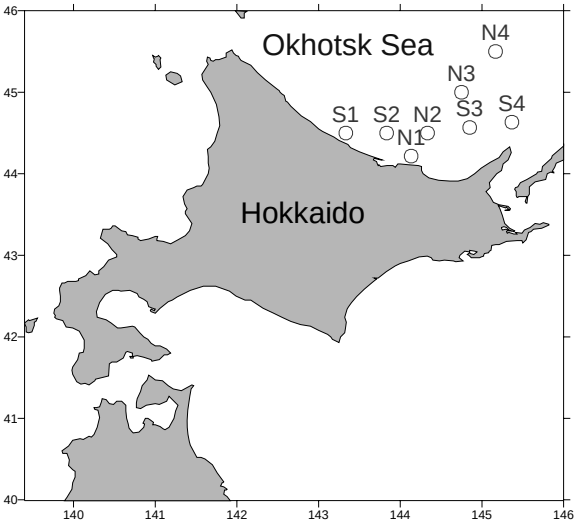

Fig. 1 Location of the N-line and the S-line.

[1] Some results from this study have also been submitted to the *Journal of Oceanography*.

shown in Figure 3. In April, the temperature profile remains constant vertically, but the water column becomes stratified by the salinity gradient. After May, the temperature in the surface layer increases through solar heating, and stratification of the water column progresses with the season. Because T-S characteristics in the deeper water hardly changed, a pycnocline developed remarkably around 20 m depth in summer and autumn.

Figure 4 shows the seasonal changes in vertical profiles of chlorophyll *a* mean concentration in the Offshore Area. In spring (April), a phytoplankton bloom was observed at the surface. In the summer and autumn, the maximum layer of chlorophyll *a* moved to the subsurface layer at around 20 m depth, forming a subsurface chlorophyll *a* maximum (SCM). The depth of the observed formation of SCM corresponds to the pycnocline (Fig. 3).

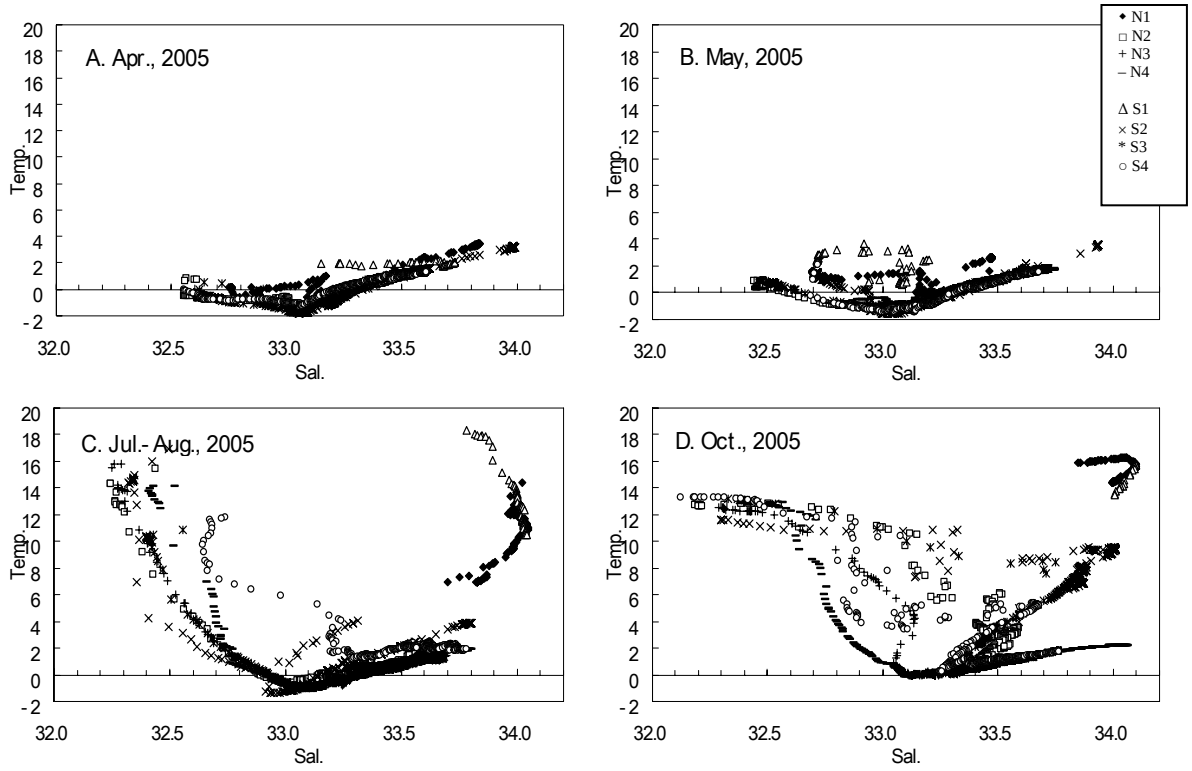

Fig. 2 T-S diagrams from 4 cruises conducted in 2005. (A) April, (B) May, (C) July–August, and (D) October. Temperature is in °C.

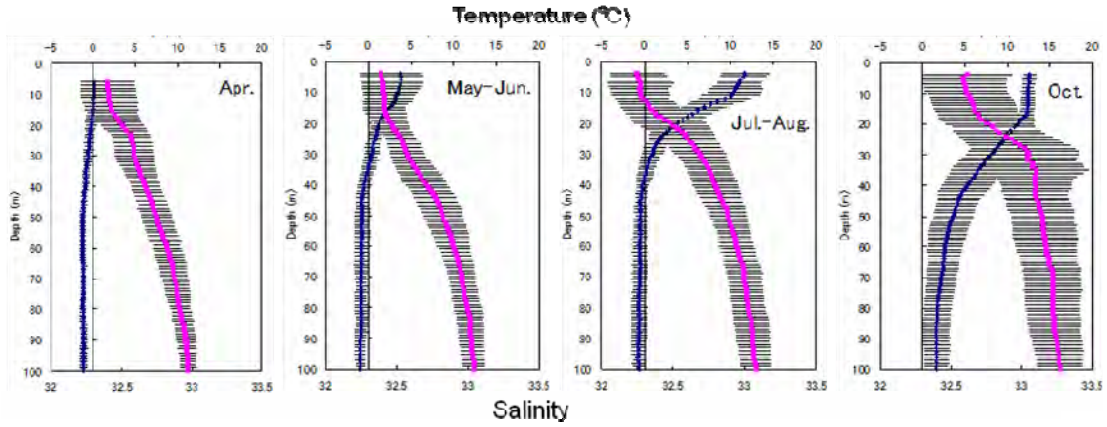

Fig. 3 Temporal changes in the vertical profiles of temperature (blue) and salinity (red) in the Offshore Area. Each value is the mean obtained from the observations between 2000–2006. Horizontal bars show the standard deviation obtained at each depth.

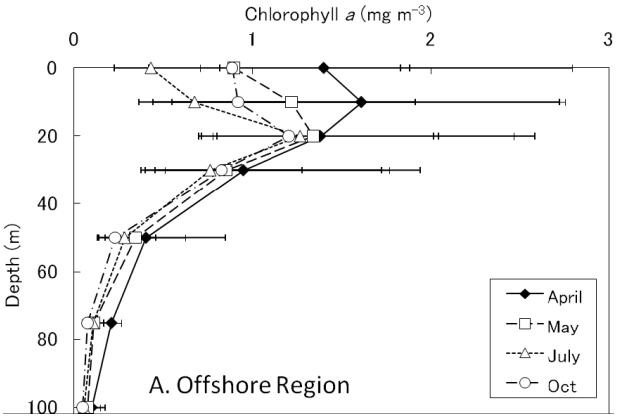

Fig. 4 Temporal change in the vertical profiles of chlorophyll *a* concentration. Each value is the mean obtained from the observations between 2000–2006. Horizontal bars show the standard deviation obtained at each depth.

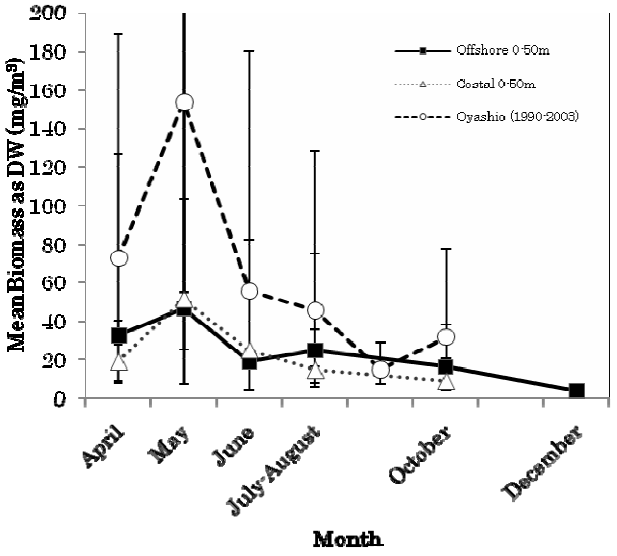

Fig. 5 Seasonal change of netplankton biomass as the mean dry weight (DW) concentration within the layer of 0–50 m depth. Vertical bars show the standard deviation obtained at each month.

Seasonal changes in the vertical profiles of nutrient concentrations (nitrate, phosphate and silicate) showed a similar trend. After April, the nutrient concentration in the surface layer decreased with season due to feeding by phytoplankton. The consumption of nutrients was observed in the layer shallower than 20 m depth, corresponding to the SCM. In summer and autumn, nitrate was at low level in the surface layer, limiting primary productivity. This suggests that the SCM was maintained using the nutrients supplied from the deeper layer through the pycnocline.

Netplankton biomass was highest in May in both the Offshore and Coastal areas (Fig. 5). A similar trend in seasonal variation of netplankton biomass was also observed in the Oyashio region; however, variability was much larger in the Oyashio region, compared to the small seasonal variation in the southern Okhotsk Sea. The seasonal change in species composition of netplankton samples is presently unknown. For future study, the temporal succession of species composition of not only zooplankton, but also phytoplankton, associated with movement between water masses, should be examined.

Using obtained data from this study, we can generally describe the seasonal change of daily primary production in the Offshore Area of the southern Okhotsk Sea (Fig. 6). Variability in primary production was seasonally small from spring to autumn; monthly mean production was about 500 mgC m^{-2} day^{-1}. However, it is notable that we cannot capture data on primary productivity in the early spring; phytoplankton blooms have occurred in the ice-edge area accompanied by ice-melting (Mustapha and Saitoh, 2008). Primary production in summer was comparable to that in spring. Primary production in spring occurred mainly in the surface layer; on the other hand, production in summer was mainly in the SCM layer. This suggests that primary production during summer in the offshore Okhotsk Sea is just as important as that during spring in order to supply particulate organic matter to higher trophic levels in the offshore area.

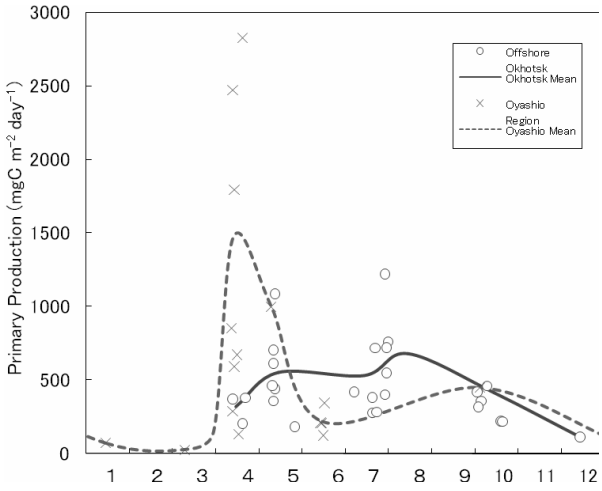

Fig. 6 Seasonal changes in daily primary production in the offshore area of the southern Okhotsk Sea and Oyashio region. Horizontal axis denotes months. Data in the Oyashio region was modified from Kasai (2000).

In this study, we have generally described the seasonal change of water column stability, nutrients, chlorophyll *a*, and primary production in the offshore area of the southern Okhotsk Sea. The importance of primary production at the SCM layer during summer and autumn can be indicated. In order to evaluate more precisely the primary productivity in the studied area, yearly monitoring of oceanographic conditions affecting primary productivity needs to be conducted. In the future, we can expect that a collaborative monitoring system with other laboratories and institutes will be established for evaluating and predicting the coastal ecosystem of the southern Okhotsk Sea in relation to global warming.

References

Horii, T., Tamura, M. and Ohtsuki, T. 1992. Oceanographic condition and diatoms distribution in the Okhotsk Sea coast of Hokkaido in March, 1989. Sci. Rep. Hokkaido Fish. Exp. Stn. 39, pp. 11–19 (in Japanese with English abstract).

Kasai, H. 2000. Seasonal variation of nutrients and primary production in the Oyashio region. *Bull. Plankton Soc. Japan* **47**: 116-118 (in Japanese).

Kasai, H., Saito, H., Kashiwai, M., Taneda, T., Kusaka, A., Kawasaki, Y., Kono, T., Taguchi, S. and Tsuda, A. 2001. Seasonal and interannual variations in nutrients and plankton in the Oyashio region: A summary of a 10-years observation along the *A-line*. *Bull. Hokkaido Natl. Fish. Res. Inst.* **65**: 55–134.

Mustapha, M.A. and Saitoh, S. 2008. Observations of sea ice interannual variations and spring bloom occurrences at the Japanese scallop farming area in the Okhotsk Sea using satellite imageries. *Estuar. Coast. Shelf Sci.* **77**: 577–588.

Nishihama, Y. 1994. Fishery of Japanese Scallop in the Okhotsk Sea. Hokkaido University Press, Sapporo (in Japanese).

Saito, H., Kasai, H., Kashiwai, M., Kawasaki Y., Kono, T., Taguchi, T. and Tsuda, A. 1998. General description of seasonal variations in nutrients, chlorophyll *a*, and netplankton biomass along the *A-line* transect, western subarctic Pacific, from 1990 to 1994. *Bull. Hokkaido Natl. Fish. Res. Inst.* **62**: 1–62.

Shinada, A. 2006. Effect of water temperature and food concentration on the growth of bottom cultured Japanese scallop *Mizuhopecten yessoensis*, in the coastal area of northeastern part of Hokkaido, Japan. *Bull. Japan Assoc. Benthol.* **61**: 41–44 (in Japanese with English abstract).

Yokouchi, K., Tsuda, A., Kuwata, A., Kasai, H., Ichikawa, T., Hirota, Y., Adachi, K., Asanuma, I. and Ishida, H. 2006. Simulated *in situ* measurements of primary production in Japanese waters. pp. 65–88 *in* Global Climate Change and Response of Carbon Cycle in the Equatorial Pacific and Indian Oceans and Adjacent Landmasses *edited by* K. Kawahata and Y. Awaya, Elsevier, Amsterdam.

Primary productivity and photosynthetic features of phytoplankton in the Sea of Okhotsk during late summer

Tomonori Isada[1], Koji Suzuki[1], Hongbin Liu[2], Jun Nishioka[3] and Takeshi Nakatsuka[3]

[1] Graduate School of Environmental Science and Faculty of Environmental Earth Science, Hokkaido University, Sapporo, Japan. E-mail: t-isada@ees.hokudai.ac.jp
[2] Department of Biology Atmospheric, Marine and Coastal Environment (AMCE) Program, Hong Kong University of Science and Technology, Clear Water Bay, Kowloon, Hong Kong
[3] Institute of Low Temperature Science, Hokkaido University, Sapporo, Japan

Introduction

The Sea of Okhotsk is considered to be one of the most biologically productive regions in the world's oceans, especially on the continental shelf (Saitoh *et al*., 1996; Sorokin and Sorokin, 1999), and that supports high fisheries production. The Sea of Okhotsk, which is located in the northwestern Pacific rim, is one of the largest marginal seas in the world and is also characterized as a region where seasonal sea ice reaches the lowest latitudes (Kimura and Wakatsuchi, 2000). When sea ice is formed on the northwestern continental shelf in winter, a large amount of cold brine water is rejected. The brine water sinks to the bottom of the shelf and forms dense shelf water (DSW). Since the DSW has a large amount of resuspended particles due to strong tidal mixing on the shelf (Kowakik and Polyakov, 1998), the outflow of DSW results in a large flux of particles from the shelf to the open ocean (Nakatsuka *et al*., 2002). Furthermore, time-series sediment trap experiments in the western region of the Sea of Okhotsk revealed that biogenic and lithogenic particles are exported to the open ocean interior by an intermediate water flow (Nakatsuka *et al*., 2004). These previous studies suggested that DSW containing these particles contributes to lateral material transport and biological productivity. The Amur River, which is one of the largest rivers of eastern Eurasia, is also thought to play an important role as the major source of terrestrial organic matter to the Sea of Okhotsk, and of nutrients for phytoplankton growth (Nakatsuka *et al*., 2004). Strong tidal currents also affect nutrient distributions in the Sea of Okhotsk (Andreev and Pavlova, 2009). However, little is known about primary productivity and its controlling factors, especially after the spring blooms. Therefore, we examined primary productivity and photosynthetic features of phytoplankton in the Sea of Okhotsk during August and September 2006.

Methods

Seawater samples were collected from 17 stations on board the Russian R/V *Prof. Khromov* (Kh06 cruise) from August 13 to September 14, 2006 (Fig. 1). Samples for chlorophyll (Chl) *a* concentration and primary productivity using simulated *in situ* incubation over a day were obtained from the surface (1 m depth), and relative 60, 30, 10, 5 and 1% light depths (where relative light intensity in the sea surface was defined as 100%). Similarly, samples for the photosynthesis–irradiance (*P* – *E*) experiment, Chl-specific absorption coefficient of phytoplankton

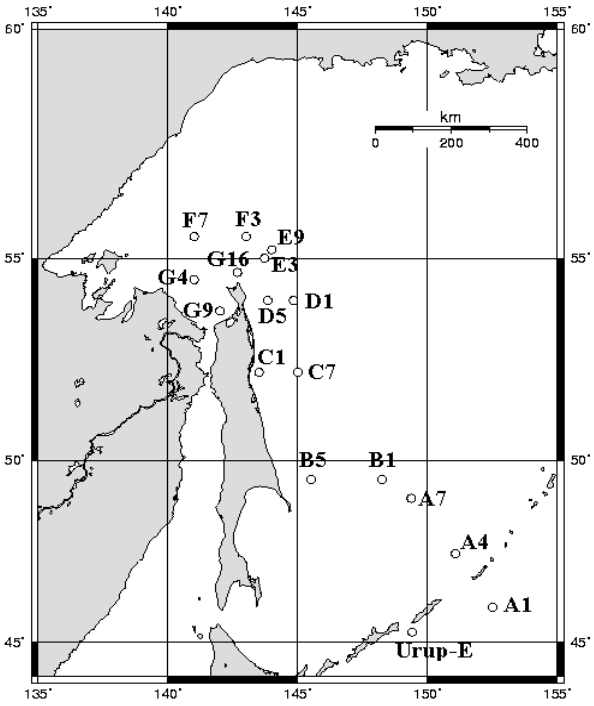

Fig. 1 Sampling stations in the Sea of Okhotsk during the cruise from August 13 to September 14, 2006 (open circles).

and size-fractionated Chl-*a* (microplankton: > 10 µm, nanoplankton: 2–10 µm and picoplankton: < 2 µm) were obtained from the surface and relative 5% light depth. Chl-*a* concentration was estimated by using a Tuner Designs 10-AU fluorometer. Photosynthetic rate was estimated with a ^{13}C tracer technique (Hama *et al*., 1983).

Results and Discussion

Chlorophyll *a* concentration

Chl-*a* concentrations were generally high in coastal waters near Sakhalin Island (Fig. 2). In particular, high Chl-*a* concentrations were observed in the continental shelf of Sakhalin (Station (Stn) C1) and Sakhalin Bay (Stn G9), and were 9.7 and 13 mg m^{-3}, respectively. Higher Chl-*a* concentrations were also found near Stns C1 and G9 in the previous study of Sorokin and Sorokin (1999). Similar temporal–spatial patterns were found in the composition of large-sized (> 10 µm) phytoplankton to the total. On the other hand, Chl-*a* concentrations in open waters were relatively low (< 1 mg m^{-3}).

Primary productivity

During our cruise, surface primary productivity and depth-integrated daily primary production within the euphotic layer ranged from 7 to 753 mg C m^{-3} d^{-1} and from 74 to 1,986 mg C m^{-2} d^{-1}, respectively. Higher surface primary productivity, as well as the Chl-*a* distribution, was observed at Stns C1 and G9 (Fig. 3). These values were within the ranges reported previously in the study area during early summer (Sorokin and Sorokin, 1999). The surface primary productivity correlated significantly with Chl-*a* concentration (R = 0.84, n = 17, P < 0.001), but not sea surface temperature, solar light intensity (photosynthetic available radiation; PAR) or nutrient concentrations. These results indicate that surface primary productivity in this study period largely depended on the phytoplankton biomass.

Photosynthetic parameters

We also estimated maximum quantum yield of carbon fixation in photosynthesis ($\Phi_{c\ max}$; mol C mol photon^{-1}) from the initial slope of the $P - E$ curve and the mean specific absorption coefficient of phytoplankton. $\Phi_{c\ max}$ is an index of light utilization efficiency in photosynthesis. Higher values of surface $\Phi_{c\ max}$ were found in the continental shelf of Sakhalin and Sakhalin Bay (0.061 and 0.086 mol C mol photon^{-1}, respectively), as well as the Chl-*a* concentration and primary productivity. On the other hand, surface $\Phi_{c\ max}$ was relatively low in the pelagic region. According to Bannister (1974) and Babin *et al*. (1996), $\Phi_{c\ max}$ for natural algal communities in optimum physiological conditions was about 0.06

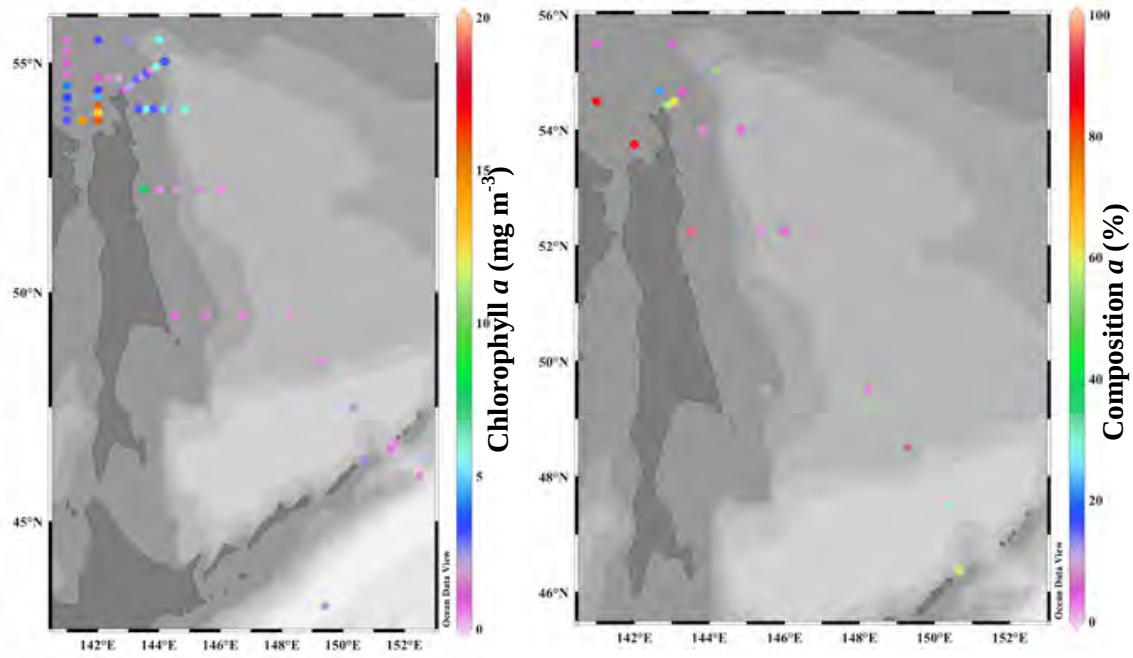

Fig. 2 Results of chlorophyll *a* concentration (left-side figure) and composition of micro-sized (> 10 µm) phytoplankton to the total (right-side figure).

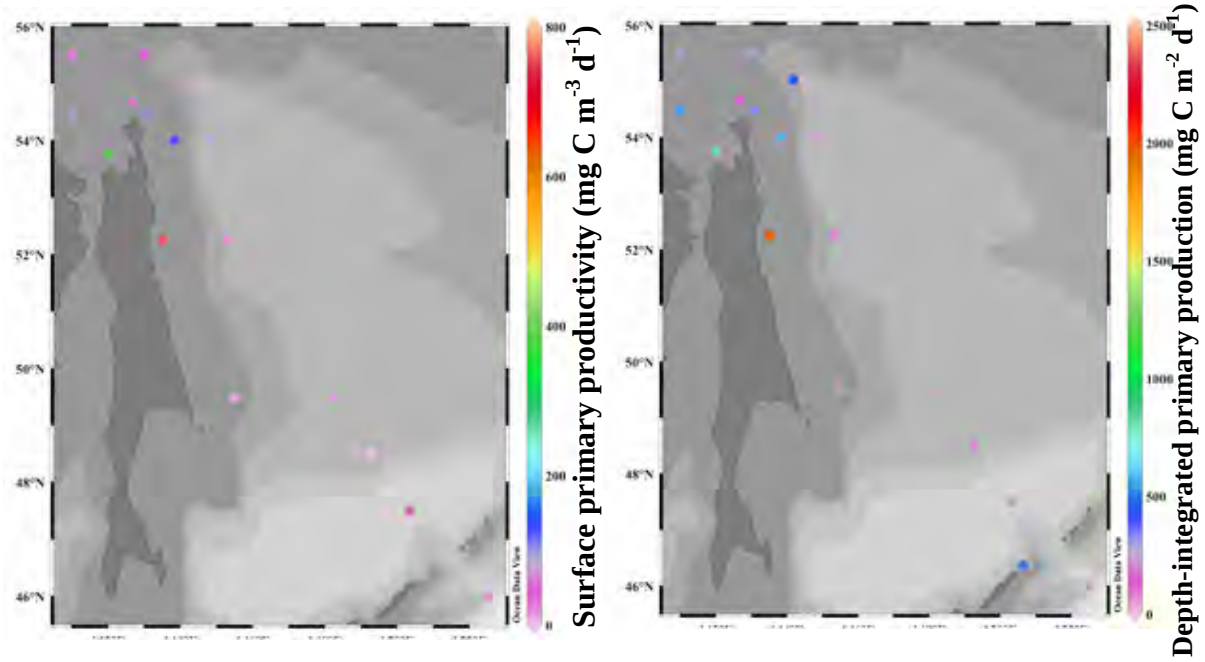

Fig. 3 Results of surface primary productivity (left-side figure) and depth-integrated primary production within the euphotic layer (right-side figure).

to 0.08 mol C (mol photon)$^{-1}$. Therefore, the data obtained at Stns C1 and G9 show that phytoplankton groups had higher light utilization efficiency in photosynthesis and that lower values in open waters might be caused by nutrient limitation. In fact, the F_v/F_m, which is the photochemical quantum efficiency of algal photosystem II (PSII) and is an index of nutrient (nitrate or Fe) limitations (Green *et al*., 1992), was lower in the pelagic region, as measured with pulse amplitude modulated (PAM) fluorometry, but increased after the addition of nutrients (Liu *et al*., 2009). Although no significant relationships were found between photosynthetic parameters, including $\Phi_{c\ max}$ at the surface and both sea surface temperature and macronutrient levels, surface $\Phi_{c\ max}$ correlated with Chl-*a* concentration (R = 0.94, n = 17, P < 0.001). These results indicate that the phytoplankton groups with high abundance possessed high $\Phi_{c\ max}$ in the study area.

References

Andreev, A.G and Pavlova, G.Y. 2009. Okhotsk Sea. *In* Carbon and Nutrient Fluxes in Continental Margins: A Global Synthesis *edited by* K.-K. Liu, L. Atkinson, L.R Quiñones, and L. Talaue-McManus, The IGBP Series, Springer, Berlin.

Babin, M., Morel, A., Claustre, H., Bricaud, A., Kolber, Z. and Falkowski, P.G. 1996. Nitrogen- and irradiance-dependent variations of the maximum quantum yield of carbon fixation in eutrophic, mesotrophic and oligotrophic marine systems. *Deep-Sea Res. I* **43**: 1241–1272.

Bannister, T.T. 1974. Production equations in terms of chlorophyll concentration, quantum yield and upper limit to production. *Limnol. Oceanogr.* **19**: 1–12.

Greene, R.M., Geider, R.J., Kolber, Z.S. and Falkowski, P.G. 1992. Iron-induced changes in light harvesting and photochemical energy conversion processes in eukaryotic algae. *Plant Physiol.* **100**: 565–575.

Hama, T., Miyazaki, Y., Ogawa, T., Iwakuma, M. Takahashi., Otsuki, A. and Ichimura, S. 1983. Measurement of photosynthetic production a marine phytoplankton population using a stable ^{13}C isotope. *Mar. Biol.* **73**: 31–36.

Liu, H., Suzuki, K., Nishioka, J., Sohrin, R. and Nakatsuka, T. 2009. Phytoplankton growth and microzooplankton grazing in the Sea of Okhotsk during late summer of 2006. *Deep-Sea Res. I* **56**: 561–570.

Kimura, N. and Wakatsuchi, M. 2000. Relationship between sea-ice motion and geostrophic wind in the Northern Hemisphere. *Geophys. Res. Lett.* **27**: 2738–3735.

Kowalik, K. and Polyakov, I., 1998. Tides in the Sea of Okhotsk. *J. Phys. Oceanogr.* **28**: 1389–1409.

Nakatsuka, T., Yoshikawa, C., Toda, M., Kawamura, K. and Wakatsuchi, M. 2002. An extremely turbid intermediate water in the Sea of Okhotsk: implication for the transport of particulate organic matter in a seasonally ice-bound sea. *Geophys. Res. Lett.* **29**: 88–95.

Nakatsuka, T., Fujimune, T., Yoshikawa, C., Noriki, S., Kawamura, K., Fukamachi, Y., Genta, M., Ohshima, K.I. and Wakatsuchi, M. 2004. Biogenic and lithogenic particle flux in the western region of the Sea of Okhotsk. *J. Geophys. Res.* **109**: C09S13, doi:10.1029/2003JC001908.

Saitoh, S., Kishino, M., Kiyofuji, H., Taguchi, S. and Takahashi, M. 1996. Seasonal variability of phytoplankton pigment concentration in the Okhotsk Sea. *J. Remote Sens. Soc. Japan* **16**: 172–178.

Sorokin, Y. and Sorokin, P. 1999. Production in the Sea of Okhotsk. *J. Plankton Res.* **21**: 201–230.

Seasonal change in number and movement pattern of spotted seals (*Phoca largha*) migrating around the Sea of Japan

Mari Kobayashi1[5], Yasuo Kouno[2], Miyuki Ito[3], Mio Nishina[1], Yasuhiro Fujimoto[4] and Kikuo Kato[5]

[1] Laboratory of Aquatic Management, Department of Aqua-Bioscience and Industry Faculty of Bioindustry, Tokyo University of Agriculture, Japan. E:mail: m3kobaya@bioindustry.nodai.ac.jp
[2] Free investigator, Yagishiri Island, Hokkaido, Japan
[3] Free investigator, Bakkai Bay, Hokkaido, Japan
[4] Laboratory of Ecology, Department of Environmental Veterinary Sciences, Hokkaido University, Sapporo, Hokkaido, Japan
[5] Marine Wildlife Center of Japan, Abashiri, Hokkaido, Japan

Abstract

Recently, a large number of spotted seals (*Phoca largha*) have been observed migrating to the Sea of Japan from November to May. Local fishermen and residents, except Rishiri Island, have said they rarely observed these seals 20~30 years ago. In addition, the distribution area has spread and the number of spotted seals has tended to increase year after year. Spotted seals from the Okhotsk Sea area are contributing to the increase in the number of individuals recently because of reduced human impacts. The movement patterns of these seals have changed recently, too. On one hand, it is said that drift ice is decreasing rapidly due to the influence of global warming. The decrease in drift ice means that those seals will find it hard to seek adequate drift ice for birth and care of their pups. This may prevent some individuals from finishing the care of their pups due to the melting of the ice floes, and other individuals may have to birth their pups in the water because they cannot find adequate ice floes. On the other hand, seal pups will become easy prey for their predators. Such a situation is based on use of the same ice by many pups because of shrinking ice floes. If these assumptions are correct and there is an increase in initial deaths of spotted seals, then population dynamics will change in the future. Spotted seals depend heavily on ice floes, both physically and biologically, so we must extend the time to monitor both this species and ice floes.

Spotted Seals

General

Spotted seals are mid-sized seals indigenous to the northern Pacific Ocean; their northern limit is the Bering Sea and their southern limit is the East China Sea. They have their particular breeding habitat in winter and feeding habitat in summer, so their movement or migration area is quite wide. This species has characteristics which allow them to inhabit not only salty water, but also fresh water, such as rivers and lakes.

Life history

Spotted seals move to the coasts of Hokkaido starting in November, and they birth and nurse their pups on ice floes in the southernmost part of the Sea of Okhotsk starting mid-March. Pups are born with white lanugo. The nursing period takes about 2 weeks, and pups spend most of their time on the ice floes. At the end of the lactation period, their white lanugo starts to molt. The mating season comes after the nursing period, so male individuals can be seen near the nursing females and their pups on the ice floes. After mating, the seals follow the receding ice floes and go back to their summer feeding habitat farther north of Hokkaido.

Breeding areas

The breeding habitats of spotted seals are classified into 8 areas. Listing from the west, they are: the Bohai Sea, Peter the Great Gulf and Tatar Strait in the Sea of Japan, Sakhalin and Shelekhov Bay in the Okhotsk Sea, Karaginski Bay and the Gulf of Anadyr in the Bering Sea, and the eastern Bering Sea. Groups in the Kuril Islands, Kamchatka and Kommandor Islands have not been classified yet because investigations did not go far enough. It is supposed that the individuals moving to the coast of

Hokkaido and breeding on the ice floes in the southernmost region of the Okhotsk Sea are a part of the Sakhalin group.

Summer habitats

There are many haul-out sites where there are groups comprised of hundreds or thousands of individuals on the eastern coast of Sakhalin and in the northern areas of Hokkaido. If we compare the distribution of harbor seals that are a closely related to spotted seals in the Kuril Islands, harbor seals have their habitats and haul-out sites mostly on the mid and southern Kuril Islands, while spotted seals are mostly located on the northern and southern Kuril Islands (Sakhalinrybvod, 1991; Kobayashi, 2008). According to the research we did in the 4 northern islands, that is, the 4 southernmost Kuril Islands, spotted seals are found in waters north of Nemuro Strait and harbor seals are found on the Pacific Ocean side.

Changes in Biology

Present distribution of spotted seals

The distribution of spotted seals in Hokkaido in recent years is shown in Figure 1. There are generally 3 patterns. The first one shows the individuals migrating to the Sea of Japan or the Sea of Okhotsk sides, shown by dark grey circles. The dark grey circles that have place names signify where we can observe their haul-out sites every year; the ones without names are where we observed the swimming individuals or their occasional haul-out sites. The regular haul-out sites are found on Rebun, Rishiri, and Bakkai Bay, Teuri, Yagishiri, Soya, Shakotan, and Otaru on the Sea of Japan. On the Okhotsk Sea, they are found at Lake Saroma, Abashiri Lake, Cape Notoro and Lake Notoro. These individuals come to migrate around November, and they stay there until May of the next year.

The second pattern is composed of individuals on the Pacific Ocean side, shown by medium grey circles. Every year the seals are distributed on Cape Erimo and Daikoku Island, and also on the freezing Tokachi River or Akkeshi Lake, from February until May.

The third is pattern is made up of only two feeding habitats in the summer on Hokkaido, Notsuke and Lake Furen, shown by light grey circles. Seals stay there from June until February. The number of individuals in both habitats total roughly 100 (Kobayashi, unpublished data).

Changes in biology of spotted seals

The distribution of spotted seals in Table 1 is for these recent years (about the last 20 years), so we can observe the change in their ecology compared with the past.

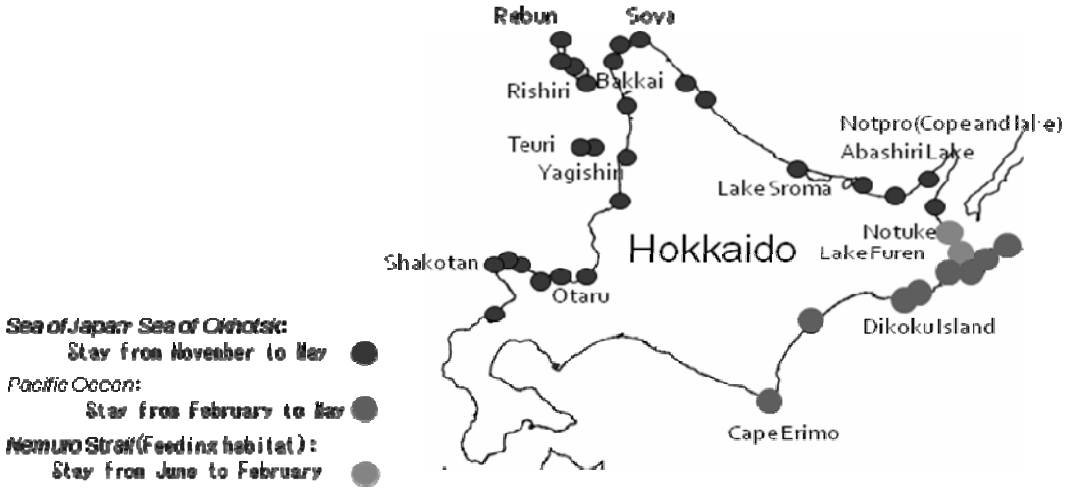

Fig. 1 Present distribution of spotted seals on Hokkaido.

Table 1 Changes of biology on spotted seals.

	Past*	Present
Migration area	Todo Island of Rebun	• More southern areas down to Shakotan and Otaru • More haul-out sites
Migration period	From December to March of next year	• From November to May of next year (more individuals are staying longer) • Rebun throughout the year
Individual's characteristics	Subadults	• Also pregnant individuals • Pups born on Todo Island (?)
Number of Individuals	Several hundred	• Several thousand • Increase year by year

* about 20 years ago.

About 20 to 30 years ago, they used to migrate only to Todo Island of Rebun. Nowadays, they migrate to more southern areas, down to Shakotan and Otaru which have more haul-out sites. Also, the migration period is getting longer, for example, they now stay at Rebun throughout the year. Originally, individuals used to migrate to Todo Island from November to May, so we supposed that they were subadults not taking part in breeding because adults are found at the southernmost area of the ice floes in the Okhotsk Sea during this period. Nowadays, however, we can observe pregnant individuals in each haul-out site on the Sea of Japan, too. It has even been reported that they birth pups on Todo Island. The migrating population used to amount only to several hundred before, but now it is several thousand in the Sea of Japan with the number of the migrating individuals increasing year by year. We surmise the following reasons for the expansion in distribution to the Sea of Japan. The use of seals by humans decreased and large-scale sealing disappeared around the 1970s; spotted seals grew in number in the Okhotsk Sea and they needed to find a new habitat. Also, as ice floes have decreased, it becomes possible to migrate from the Sea of Japan to the southernmost ice floes in the Okhotsk Sea before the breeding period starts. So, subadults and adults have been able to use the habitat of the Sea of Japan, recently (Table1).

Seasonal change of migrating individuals

We performed investigations on Yagishiri and Bakkai Bay from November 2003 to May 2004 when there was regularity in the seasonal changes and we were able to obtain the most complete records. The outcome is presented in Figure 2. The results show that the visiting period of the spotted seals started a half month earlier in Bakkai Bay than on Yagishiri, and the leaving period was a half month later in Bakkai Bay than on Yagishiri. The water temperature during the visiting period on Yagishiri was about 14°C, and was 8°C during the leaving period. We have no analysis for Bakkai because we could not get water temperature data. We observed two peaks, one at the beginning of January and one at the beginning of May on Yagishiri. However, the number of migrating individuals suddenly decreased from the peak in January and continued gradually until the leaving period in Bakkai Bay. In Yagishiri, the peaks come at the beginning of January and May, and the same number of migrating individuals were observed every year. Just before the second peak in May, there was a sudden increase at the end of April, resulting in a different pattern of seasonal change between Yagishiri (Kouno, unpublished data) and Bakkai Bay (Itou, unpublished data).

To summarize the seasonal change, the difference in patterns between the two regions is a lag of half a month in the visiting and leaving periods. Both feeding habitats in the summer and, in Yagishiri, the water temperature, was the same every year at the visiting and leaving periods, so it could possibly depend on the water temperature. Also, the two-peak characteristic was observed only in Yagishiri, and the number of individuals were the same in each peak. Therefore, we can inquire why such a seasonal change can be observed by making clear which individuals are migrating during the second peak, and how spotted seals move to each haul-out site in the Sea of Japan. Several common points were observed: the decrease in the number of individuals during the breeding period, a tendency of earlier visiting and later leaving, and an annual increase in the number of migrating individuals.

Movement pattern of spotted seals

In Yagishiri, we caught an immature male spotted seal on May 23, 2008, and we put Argos telemetry on it. Results show that after this individual stayed a couple of days in Yagishiri, it moved to Aniva Bay in Sakhalin, and at one time, it travelled 100 km within a day (Fig. 3). Though most of the haul-out sites are found on the east coast of Sakhalin, and as this individual was staying in Aniva Bay, it is probable that the individuals migrating to the Sea of Japan are found in feeding habitats relatively closer to haul-out sites in winter. Since the tracked individual was able to travel such a distance at one

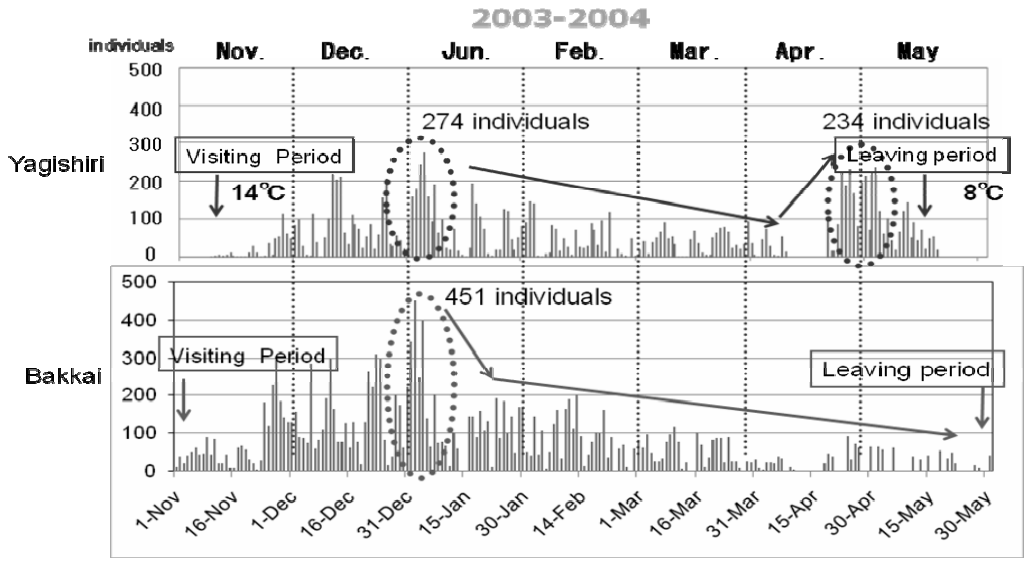

Fig. 2 Seasonal change of migrating individuals around Hokkaido.

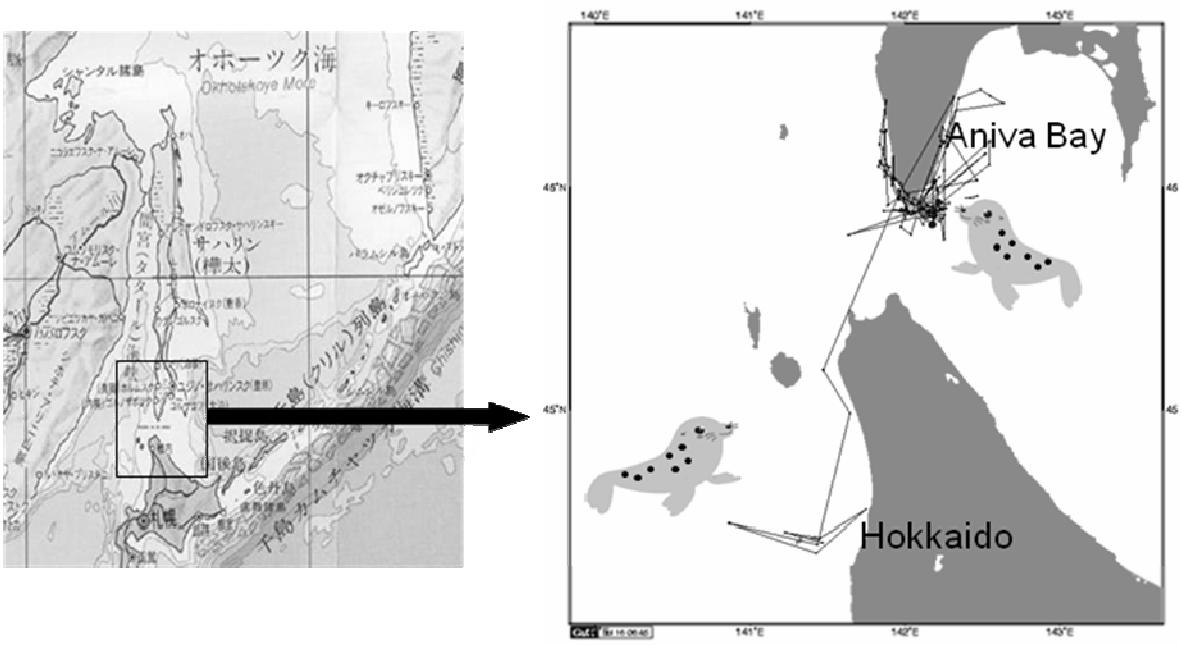

Fig. 3 Movement pattern of spotted seals from Yagishiri Island in the Sea of Japan.

time, we suppose that the seal had a definite destination. It would be important to know for future studies that if seals change their habitat, what are the factors that determine their feeding habitat? The internal telemetry sensor revealed that spotted seals can dive down to a maximum depth of 90 m, but usually no deeper than 50 m. It also showed that they often dive from the evening until nighttime, and stay mostly on the haul-out starting at dawn. However, they dive and haul-out much less frequently from the latter half of July (Fig. 4), so there is a different pattern of behavior in the water according to the season (Kobayashi, unpublished data). In the future, by analyzing data in detail and accumulating information about their predators, we hope to understand what their prey is and how frequently they prey on it.

Future Issues

Problems to be solved in the future

In the future, by making clear the feeding habitat of the individuals migrating to the Sea of Japan of Hokkaido, it will be possible to know the relationship between these individuals and the group of Tartar Strait or Sakhalin. Also, as there are different seasonal patterns regarding the number of individuals in Yagishiri and Bakkai Bay, by knowing how frequently the movements occur at each haul-out site in the Sea of Japan or what characteristics they have, that is, the difference between males and females, or age classes, will help us to understand the importance of each haul-out site on the Sea of Japan. Moreover, knowing that Todo Island of Rebun used to be a haul-out site only during the winter period in past years, but now is the site of year-round habitation where even pup births are reported, it is considered that Rebun is a principal haul-out site in the Sea of Japan. So, although we keep monitoring other haul-out sites for long terms, it is important to know the significance and role of Rebun in the Sea of Japan.

Change in quality and distribution of ice floes

From information obtained from the Japan Meteorological Agency, this author found that drift ice reached the coast of Hokkaido and remained late into 2008 in the Okhotsk Sea. When I made a survey by plane at the end of March, which is the breeding period for spotted seals, I saw that the ice of the floes were so thin that I could see through them. The ice would not be thick enough for seals to haul-out. Seals usually haul-out the edge of ice floes filled with canals; there were hardly such ice floes. I contacted the Meteorological Agency to find out the movements of the ice floes in March and April, 2007, the breeding period for seals, when it revealed that the ice floes were suddenly disappearing from the Okhotsk Sea in the middle of breeding period. It means that the ice was so thin and light that it melted fast and moved quickly and dramatically. In this sense, the quality of ice floes recently may be getting worse.

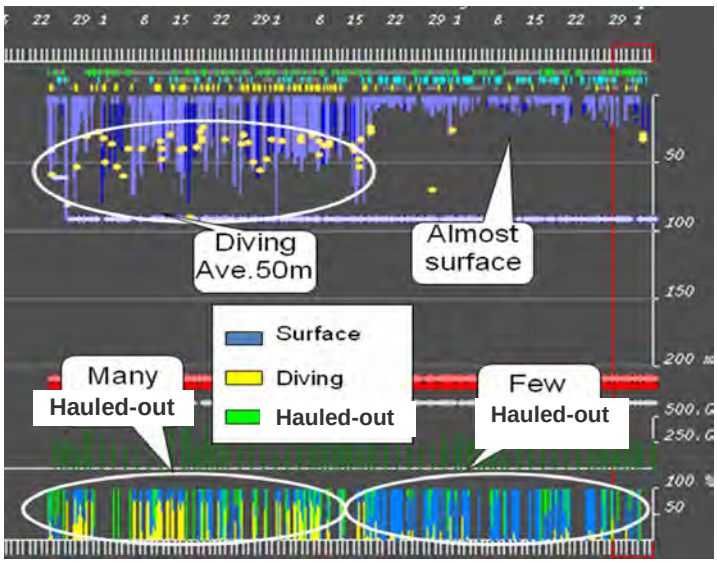

Fig. 4 Diving pattern of the spotted seal.

Effects of biology on seals

First, as a direct effect, pups can be lost or drowned because the ice floes of bad quality can melt while they are being born or nursed on the ice. If the parent cannot find an adequate ice floe for birthing, pups may be born in the water. Of course, a newborn pup can swim, but not enough to survive. If there is only a small amount of good ice, the breeding site will become too crowded due to competition, and if a natural enemy comes to prey, the risk must be considerable. It can be assumed that as infant mortality increases, aging may occur, and may affect the population dynamics.

Indirect effects may be much more serious. If ice floes decrease or disappear in the Okhotsk Sea, the productivity may decline, and accordingly, the fish and their prey will decrease. As the sea level rises because of the deterioration or decrease of the ice floes, the haul-out sites of the spotted seal may become scarce leading to the struggle for haul-outs and food. Finally, a large-scale extinction could occur. In the end, it is assumed that the decrease of ice floes could affect, directly or indirectly, all seals, not only spotted seals dependent on ice floes physically and biologically, but also harbor seals in the Pacific Ocean.

References

Kobayashi, M. 2008. Marine mammals in world heritage Shiretoko peninsula – Current state of seals-mammals in Japan. pp. 75–98 *in* The Third Marine Mammals *edited by* H. Kato, University of Tokyo Press.

Sakhalinrybvod. 1991. A report on the distribution and number of marine mammals in the Kuril Island 1991. Sakhalinrybvod, Sakhalin, Russia.

Current status of pinnipeds in the Sea of Okhotsk

Alexey M. Trukhin

V.I. Il'ichev Pacific Oceanological Institute, FEB RAS, Vladivostok, Russia. E-mail: trukhin@poi.dvo.ru

The Sea of Okhotsk is one of the main regions of pinniped distribution in the Russian Far East. There are 7 species of the pinnipeds living: 2 species (Steller sea lion and northern fur seal) are represented by the Otariidae family and 5 species (bearded seal, ringed seal, spotted seal, harbor seal and ribbon seal) are members of the Phocidae family.

In the second part of the last century, all species of true seals, except harbor seals, were the objects of harvest, and were caught year round. Consequently, these species were studied as well. However, in 1994 ship-based harvests of ice seals in the Sea of Okhotsk ended, resulting in a reduced level of study.

The main species for harvest in the Sea of Okhotsk was ringed seal, annual catches of which reached almost 100,000 individuals in certain years. The catch quantity of other pinnipeds was also impressive (Table 1). The most intensive harvest began in 1955, when the Far East fishing fleet flotilla was developed. The strength of the harvest led to a rapid decline in the number of seals. For example, the number of ringed seals in the Sea of Okhotsk dropped from 1 million to 600,000 from the mid-1950s to the mid-1960s. In 1969, some limitations on the seal harvest were enacted.

The last census of true seal populations in the Sea of Okhotsk was conducted in 1990 (Table 2). It can be seen from the table that the decrease in the number of seals stopped for nearly all species, and that the number of ringed seals has yet to fully rebound.

Table 1 Statistics of the commercial harvest of true seals in the Sea of Okhotsk (individuals).

Year	Ringed seal	Spotted seal	Ribbon seal	Bearded seal	Total
1955	72517	1987	9384	6562	90450
1960	98310	9264	3444	5202	116220
1965	83448	3996	5152	4737	97333
1970	30386	4618	5213	3127	43344
1975	19188	3937	3500	1435	28060
1980	5898	1689	3451	1616	12654
1985	17248	6846	10000	2959	37053
1990	22372	7352	14695	4639	49058
1995	284	132	0	101	517
2000	196	976	18	190	1380

Table 2 Data of aerial surveys of seal numbers (thousands) in the Sea of Okhotsk.

Year	Ringed seal	Ribbon seal	Spotted seal	Bearded seal
1968	780	116	67	233
1969	855	208	177	253
1974	876	173	172	110
1976	539	201	268	125
1979	706	449	246	187
1981	777	410	234	104
1986	833	508	174	143
1988	565	630	156	143
1989	709	445	96	105
1990	710	562	178	95

Eared seals, compared to the situation nowadays, have been better studied in recent years. Because the fur seal is regarded as a harvestable species, constant studies were focused on identifying the maximum sustainable yield. The Steller sea lion is a threatened species, particularly in the western Aleutian region, and this has motivated special attention devoted to research.

Steller Sea Lions

At the present time there are 14 major Steller sea lion (*Eumetopias jubatus*) rookeries in Russia, where annual reproduction of this species takes place (Fig. 1). Only 3 rookeries are located outside of the Sea of Okhotsk. Of the remaining 11, 7 are located on the Kuril Islands. In the 1970s, populations decreased rapidly, especially on the Kuril Islands. In the 1980s the numbers stablized at the lowest level ever seen during the whole period of research. The reasons for the population decline are still unknown, but the numbers have yet to recover. At the same time, during the several last years, there has been a trend of slow increase in pups born on the Kuril Islands.

Compared to the depressed condition of sea lion conditions in the Sea of Okhotsk, the rapidly growing population of sea lions on Robben (Tyuleny) Island on the eastern end of Sakhalin (Fig. 1) seems rather unusual. Sea lions were regularly observed on this island at least from the end of the 19th century, but the rookery only became reproductive in the 1970s, when about one to two pups started to appear almost annually. In 1980 six pups were born; since then, the number of newborn pups has begun to increase rapidly (Fig. 2). Currently, the Robben Island sea lion rookery can be described as flourishing. In 2006 the number of pups there exceeded 600 individuals.

Nearly half of the Sea of Okhotsk Steller sea lions reproduce on the Kuril Islands, where 7 reproductive rookeries are located, among them there are 5 rookeries, on which the number of pups born annually ranges from 200 to 800 (Fig. 3).

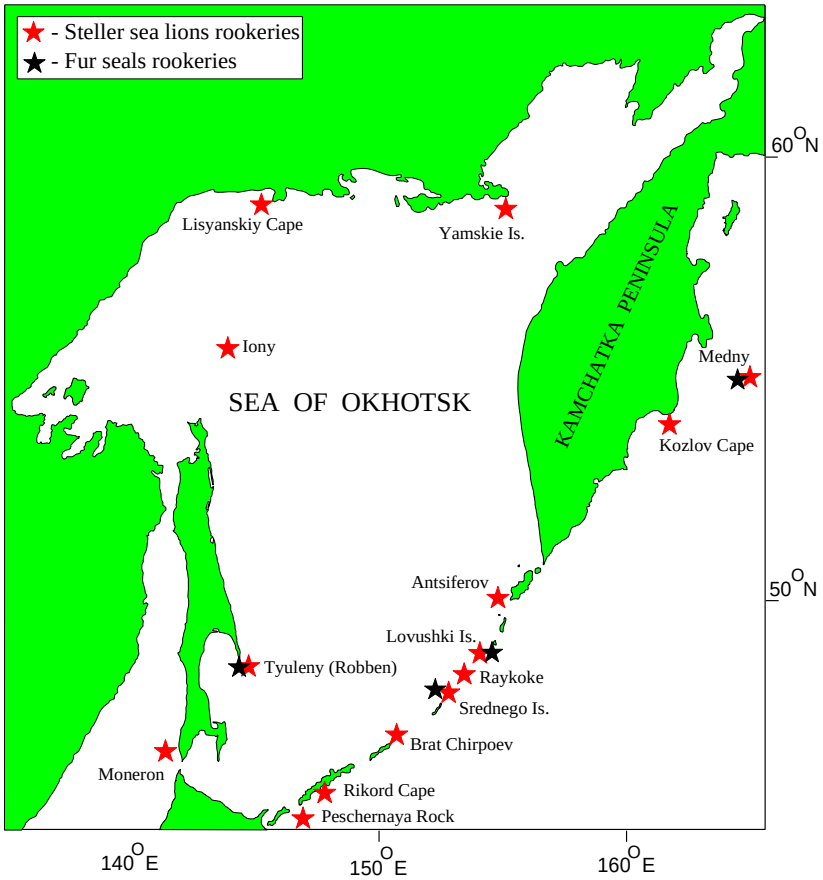

Fig. 1 Distribution of eared seal rookeries in Russia.

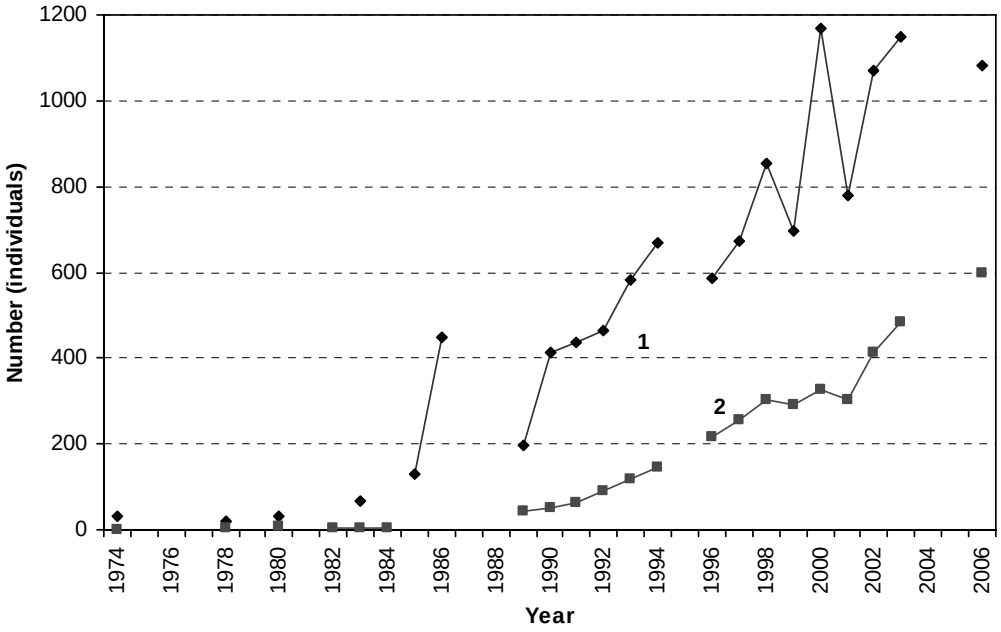

Fig. 2 Dynamics of the sea lions populations on Robben (Tyuleny) Island. 1 = +1 year old, 2 = pups.

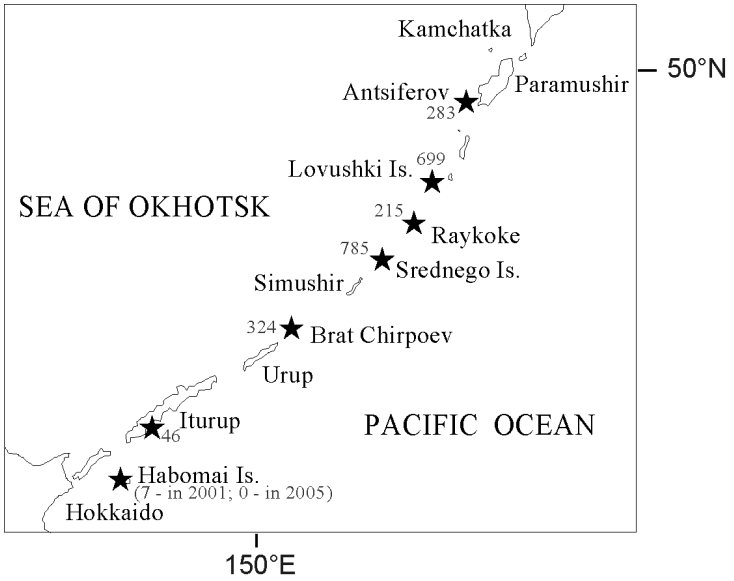

Fig. 3 Number (grey figures) of newborn sea lions on the Kuril Islands in 2005.

Northern Fur Seals

In total, there are 4 reproductive northern fur seal (*Callorhinus ursinus*) rookeries in Russian waters: the Kommandor Islands, Lovushki and Srednego Islands (both part of the Kuril Islands) and Robben Island. On the Kuril Islands, fur seal rookeries are in excellent condition; the number of pups born annually is about 20,000. The wintering grounds of fur seals, which reproduce on the islands, are generally situated on the Yamato Bank, in the central part of the Sea of Japan. Part of the population winters in the waters to the west of Japan.

Recently, an increase in the number of individuals was registered on Robben Island. From 1987–1994

about 16,000–20,000 calves were born annually on the island (Fig. 4). In 2006, the number of pups was calculated at 33,000. Nevertheless, this figure is still far from the 55,000 pups that were born here annually in the middle of the 1960s. The Kuril Islands population is not affected by harvest. On Robben Island, on the other hand, about 1,000 fur seals are harvested for fur every year; 2- to 5-year-old males are the ideal target for commercial catches on this island.

Bearded Seals

In the sealing years, this species (*Erignathus barbatus*) was mostly "ignored" and its numbers were not significantly impacted by the fisheries. Nowadays, this species is being caught in small numbers in the coastal areas of the northern part of the Sea of Okhotsk. In winter and spring, bearded seals are found on ice cover in relatively shallow waters (Fig. 5). In the late summer and autumn periods, bearded seals also keep near the shelf areas, and typically occur in waters less than 200 m depth. During this season, they form haul-outs on Sakhalin, the Shantar Islands and the northern coast of the Sea of Okhotsk.

Ringed Seals

The ringed seal (*Phoca hispida*) is the most numerous seal in the Sea of Okhotsk, and is widely distributed. The largest number of ringed seals can be found in the western part of the sea. In the area of the Shantar Islands, where in the beginning of summer the ice remains for a long time, ringed seals form mass molted gatherings in June. After the ice recedes, the ringed seals disperse widely in the coastal areas of the sea, where they accumulate fat before wintering by intensive feeding on different crustacean and schooling fish species.

Spotted Seals

Currently, spotted seals (also known as largha seals, *Phoca largha*) in the Sea of Okhotsk number about 200,000. The spotted seal is widely distributed in the waters of the whole sea, forming two separate populations, which are spatially well-segregated during the reproductive season. During the reproductive period, one population center is situated in the northern part of the sea in Shelikhov Bay; the center of the other is situated along the eastern coast of Sakhalin.

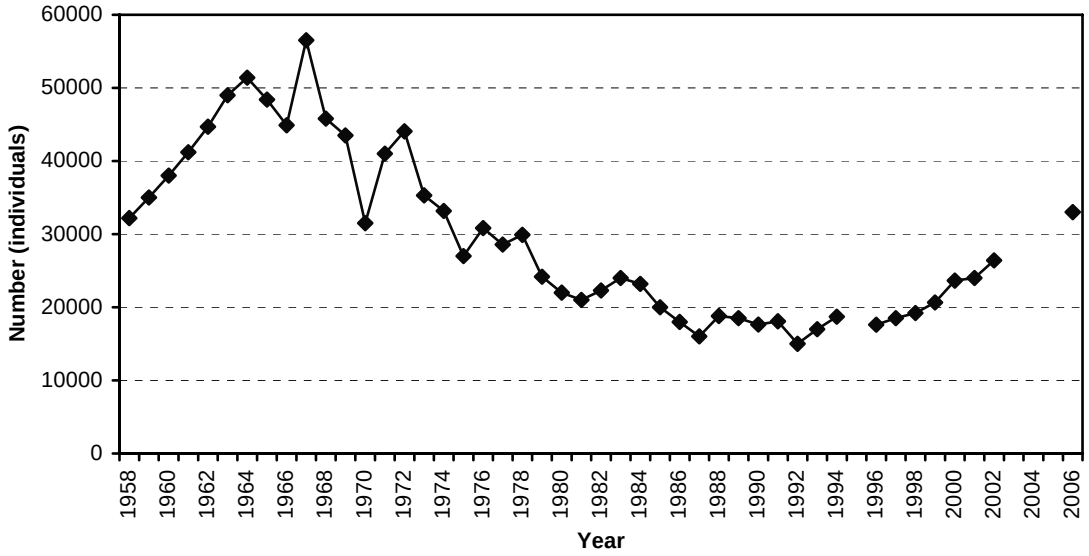

Fig. 4 Dynamics of the fur seals pups population on Robben (Tyuleny) Island.

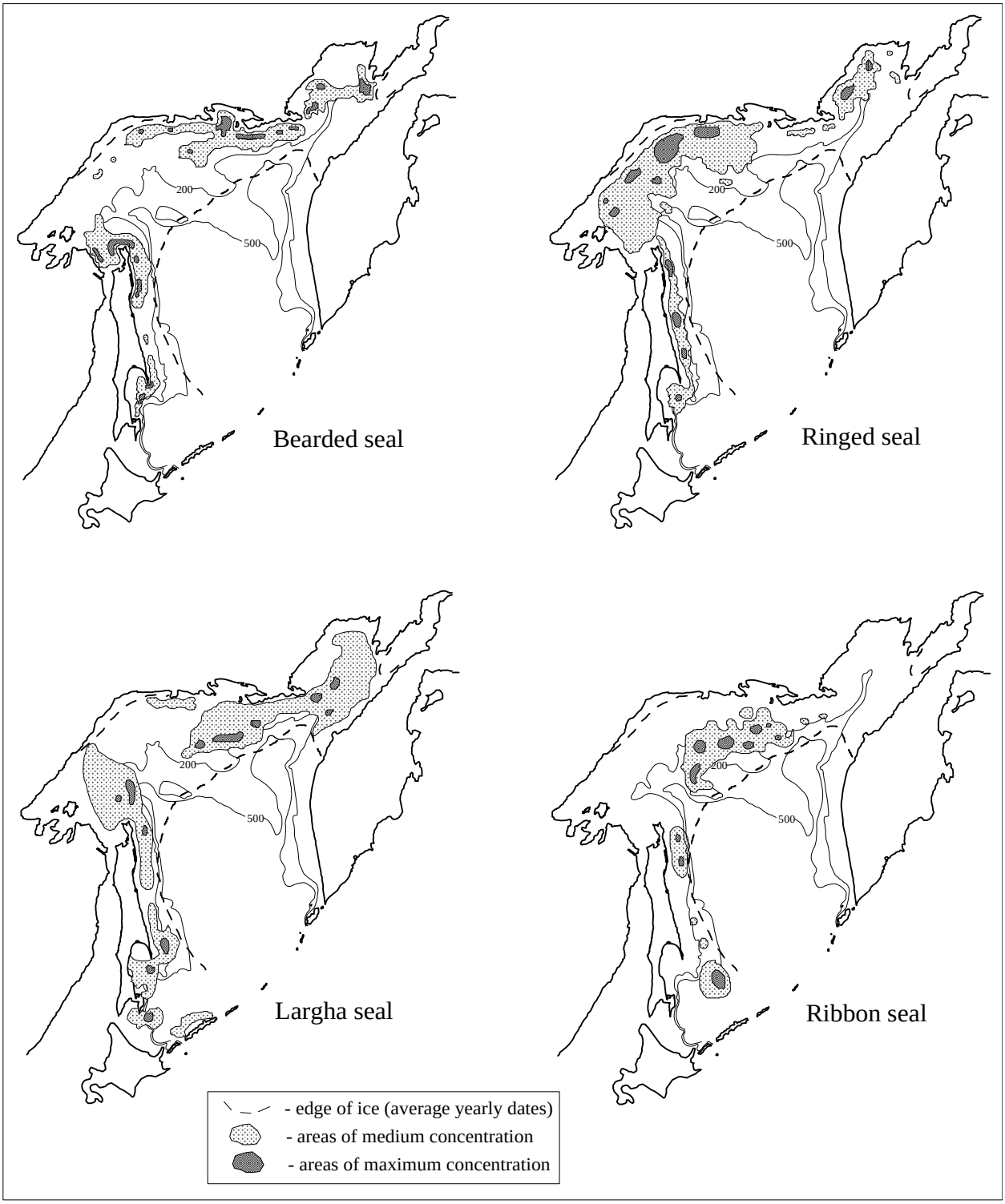

Fig. 5 Regions of maximum seal density in winter.

After the retreat of the ice cover, the spotted seal disperses along the coasts, forming large haul-outs, which can reach up to several thousand seals. The largest haul-outs are on the western coast of the Kamchatka Peninsula, and on Sakhalin (Fig. 6).

Currently, the spotted seal is the only representative of the true seals which is still harvested on the coastal haul-outs at the end of summer–early autumn on South Sakhalin and in the northren part of the Sea of Okhotsk.

Harbor Seals

Within the Sea of Okhotsk, harbor seals (*Phoca vitulina*) are found only on the Kuril Islands. Their population is not large and the species is registered in the Red Data Book of Russia. On the Kuril Islands, harbor seals are unevenly distributed. The largest number can be found on the Iturup, Shikotan and Habomai islands. In 2000 the whole territory of the Kuril Islands was carefully monitored, and about 3,000 individuals were counted. The inter-annual dynamics of harbor seal numbers indicate that the number of the seals on the Kuril Islands is roughly constant and that there is no danger to harbor seal survival in this region. The harbor seal is generally a non-migratory species, but it regularly travels locally between adjacent islands.

Ribbon Seals

This species of seal (*Phoca fasciata*) is the least studied in the Sea of Okhotsk. The reason for this is that during the ice period of the year life cycle, this seal is not connected to the land, and its summer-time habitat is situated in the pelagic area. This species is the earliest to mature, which explains the rapid growth of its population. Some females become mature at the age of 1 year, and at the age of 2 years most seals are ready to reproduce.

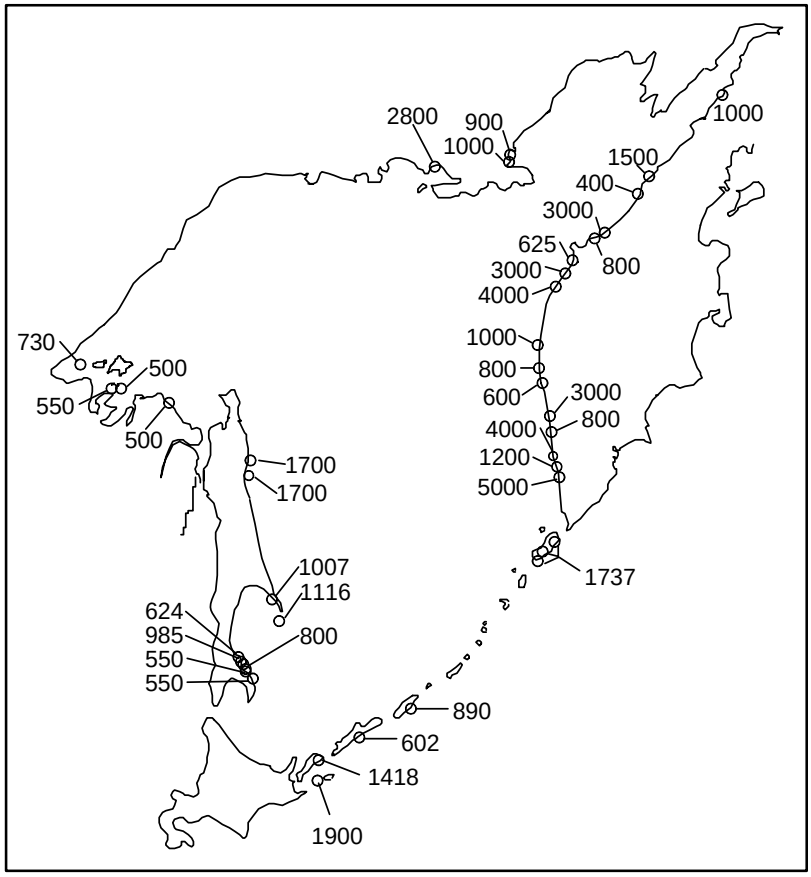

Fig. 6 The largest spotted (largha) seal haul-outs on the coast of Sea of Okhotsk and maximum number seals at each haul-out (Kuzin *et al.*, 1984; Kosygin *et al.*, 1986; Lagerev, 1988; Burkanov, 1991; Chupakhina and Panteleeva, 1991; Trukhin, 1998; Kornev *et al.*, 2001).

During the ice period, the highest density of ribbon seals is found in two areas of the Sea of Okhotsk: on the Kashevarov Bank, in the northern part of the sea, and along the east Sakhalin coastline. Reproduction for the majority of these populations takes place in these areas. Ribbon seals, after their departure from the ice, move into the open sea areas; some part of the population migrates towards the Pacific Ocean in summer.

Each species of seal is characterized by specific diets. In all areas of the Sea of Okhotsk the most frequently encountered types of prey of Steller sea lions are Atka mackerel (*Pleurogrammus monopterigius*), walleye pollock (*Theragra chalcogramma*), salmon (*Onchorynchus* sp.), sculpins (Cottidae), and cephalopods. Fur seals mainly feed on different types of fishes and squids. The feeding base of the bearded seal is represented by benthic invertebrates. The diet of the ribbon seal consists mostly of walleye pollock and squids. The ringed seal feeds on crustaceans and small fishes. The spotted seal diet includes different types of fish, cephalopods and crustaceans. In autumn the spotted seal concentrates in river mouths where they feed largely on stream-bound salmon. The ringed seal and the spotted seal can be described as having regional-specific feeding, and the structure of their diets in the northern and southern part of the sea varies considerably. The harbor seal eats different types of fishes and invertebrates which live in the shallow coastal waters of the Kuril Islands. All species display seasonal changes of the feeding structure.

In recent years, research on true seals in the Sea of Okhotsk carried out by Russian zoologists were, to the great extent, devoted to studying the potential impact of oil and gas development on the shelf of northeastern Sakhalin. The drilling platforms here are close to the coast, where seals form large beach rookeries. One of the rookeries is functioning in Piltun Bay, 25 km from an oil rig. There are 3 species of the seals located on this rookery: spotted seal, ringed seal and bearded seal, of which the first 2 are the most abundant. It is worth mentioning that the ringed seal haul-out here is the largest one known for this species. The number of the true seals on the haul-outs increases from summer to autumn (Fig. 7).

Intensive research performed on the rookery in Piltun Bay in 1999 did not indicate any negative influence of oil and gas development on the seal haul-out. Still, some potential risk for the haul-out exists. A severe accident occurring in the area could seriously threaten the adjacent haul-outs.

In recent years there has been a low level of ice coverage in the Sea of Okhotsk due to warming of the climate. It is, as yet, unclear what effect this has on the ice-bound seal populations. However, seasonal migrations and distributions of seals in the northern parts of the Sea of Okhotsk have been affected by late ice formation in the autumn and early breakup in spring. It is also possible that a shortage of ice cover and its comparatively short presence can affect the reproductive success and pup survival of seals. Investigation of this question requires further research.

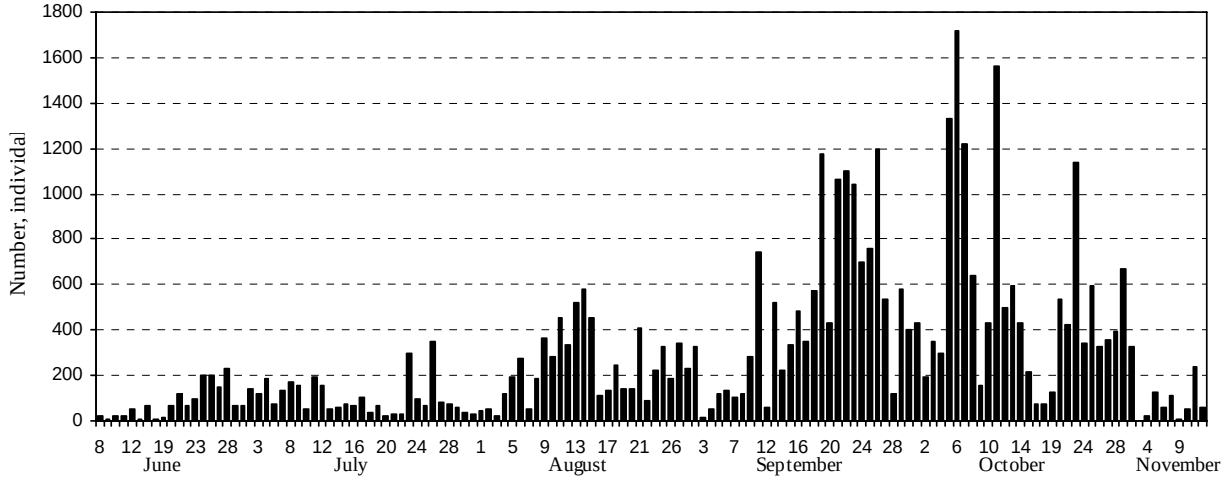

Fig. 7 Change of the number of true seals on the rookery in Piltun Bay.

References

Burkanov, V.N. 1991. Spotted seal of the Kamchatka's waters and seals influence to resources of salmons. Ph.D. thesis, Moscow, 22 pp.

Chupakhina, T.I. and Panteleeva, O.I. 1991. Results of the marine mammal's survey in the Kuril Islands in summer 1991 during cruise on the SRTM "Diana". Yuzhno-Sakhalinsk, 20 pp.

Kornev, S.I., Trukhin, A.M. Artyukhin, Yu.B. and Purtov, S.Yu. 2001. Results of marine mammal survey in the South Kamchatka and the Kuril Islands, June–August, 2000. pp. 191–204 *in* Results of the Far East Marine Mammal researches in 1991–2000: Materials of the 16th Working Group Meeting under project 02.05-61 "Marine Mammals" within the framework of the U.S.–Russia Agreement on Cooperation in the Field of Environmental Protection, *edited by* V.A. Vladimirov, VNIRO, Moscow.

Kosygin G.M., Trukhin, A.M., Burkanov, V.N. and Makhnyr, A.I. 1986. Haulouts of the spotted seal on the shores of the Sea of Okhotsk. pp. 60–70 *in* Nauch.-issled. raboty po mor. mlek. v sev. chasti Tikhogo okeana v 1984/1985 *edited by* E.P. Yakovleva, VNIRO, Moscow.

Kuzin, A.E., Maminov, M.K. and Perlov, A.S. 1984. The number of pinnipeds and sea otters in the Kuril Islands. Morskie mlekopitayushchie Dal'nego Vostoka, Vladivostok, pp. 54–72.

Lagerev, S.I. 1988. Results of an aerial survey of seal haulouts in the Sea of Okhotsk in 1986. pp. 80-89 *in* Nauch.-issled. raboty po mor. mlek. v sev. chasti Tikhogo okeana v 1986/1987 *edited by* L.A. Popov, VNIRO, Moscow.

Trukhin, A.M. 1998. Prospects of a craft of the spotted seals in the Far East. *Rybnoe Khozyaistvo* **2**: 48–49.

Mitochondrial DNA variation in the Japanese harbour porpoise (*Phocoena phocoena*)

Mioko Taguchi, S. Abe and T. Matsuishi

Graduate School of Fisheries Sciences, Hokkaido University, 3-1-1 Minato-cho, Hakodate, Hokkaido, Japan
E-mail: taguchi@fish.hokudai.ac.jp

Introduction

The harbour porpoise (*Phocoena phocoena*) is a small cetacean distributed in temperate and subarctic waters of the Northern Hemisphere. They have three major distribution areas, the North Atlantic, North Pacific and Black Sea to Sea of Azof (Fig.1, Gaskin, 1984).

They are top predators in coastal ecosystems, but today, are exposed to environmental pollutants and fisheries pressures (Jefferson and Curry, 1994; Beineke *et al.*, 2005; Jepson *et al.*, 2005). Especially, population reduction due to incidental catch has been a growing serious problem in a part of the North Atlantic (Woodley and Read, 1991; Trippel *et al*., 1996). It is important to understand their intraspecific genetic structure for appropriate management of harbour porpoises in such an environment.

In the North Pacific, two major local populations are known in the north and south coasts of North America, in the area designating the Northeast Pacific (Rosel *et al*., 1995). Moreover, some subpopulations in these two regions have been reported (Chivers *et al*., 2002). However, it is difficult to understand the genetic structure across the North Pacific because no population genetics study has been conducted in the Northwest Pacific, including Japan.

The Japanese harbour porpoise is distributed around Hokkaido to the northern mainland of Honshu in winter and east of Hokkaido to the Sea of Okhotsk in summer (Gaskin *et al*., 1993). Given the breeding season of the Japanese harbour porpoise, the Sea of Okhotsk is likely to be important as their breeding area. Thus, the present study is aiming to estimate the mitochondrial DNA variation of harbour porpoises in Japanese waters as a first step to understanding their genetic structure in the Northwest Pacific.

Materials and Methods

Samples and DNA extraction

A total of 56 tissue samples were obtained from stranded, incidentally caught or captive porpoises in Japan (Fig. 2). Tissues of muscle or skin were preserved in 95% ethanol or stored at –30°C. Total genomic DNA was extracted using Gentra Puregene kits (QIAGEN) following the manufacturer's protocol.

In addition, all nucleotide sequences in the Northeast Pacific of 40 individuals from Alaska and Strait of Georgia (NEP5), 52 individuals from San Juan Island and Vancouver Island (NEP4), 62 individuals from Washington and Columbia River (NEP3), 17 individuals from Oregon (NEP2), and 52 individuals from San Francisco and Monterey Bay (NEP1) (accession numbers AF461818 – AF461891, Chivers *et al.*, 2002) were collected from GenBank.

Mitochondrial control-region sequences

The 462 base pairs (bps) of the hypervariable portion from the 5' end of the mitochondrial (mt) DNA control region were amplified using polymerase chain reaction with primer L15824 (5'-CCTCACTCCTCCCTAAGACT-3') and H16265 (5'-GCCCGGTGCGAGAAGAGG-3') (Rosel *et al*., 1999). A reaction mixture at 20 μL contained 2 μL of 10x buffer, 0.25 μL of each primer, 0.15 mM dNTP and 0.02 U/μL *Taq* DNA polymerase. Amplification was carried out on an ASTEC PC320, 708 or 816 thermal cycler with a thermal profile consisting of an initial denaturation at 95°C for 30 s, followed by 30 cycles of 50 s at 94°C, 50 s at 55°C and 50 s at 72°C, and a final extension at 72°C for 5 min. The amplified products were purified using a DNA purification kit, and cycle-sequenced using an ABI BigDye® Terminator v3.1 cycle sequencing kit,

following the manufacturer's protocol. All samples were sequenced in both DNA strands with the primers used in the amplification, and sequence alignment was corrected by eye.

Analysis of mitochondrial DNA variation

Nucleotide and haplotype diversities (Nei, 1987) were estimated for all populations. An analysis of molecular variance (AMOVA) was conducted to measure the hierarchical genetic differentiation among populations using the program ARLEQUIN ver.3.1 (Excoffier and Schneider, 2005). The AMOVA calculates ϕ_{ST}, an index of population subdivision. The significance of ϕ_{ST} was tested by multiple permutations of the original data sets. A phylogenetic relationship among mtDNA haplotypes was performed with the neighbor-joining (NJ) method on a matrix of the pairwise distance, based on Kimura's two-parameter model (Saitou and Nei, 1987), using the finless porpoise (*Neophocoena phocaenoides*) as out group, with the program MEGA ver.4 (Tamura *et al.*, 2007). The reliability of internal tree branches was assessed by 1,000 bootstrap resamplings. A minimum spanning network of mtDNA haplotypes was constructed using the program TCS ver.1.21 (Clement *et al.*, 2000). Isolation by distance, known as the population genetic pattern, was estimated by regression analysis between ϕ_{ST} and the geographic distance among all pairwise populations, using Isolation by Distance Web Service (Jensen *et al*., 2005).

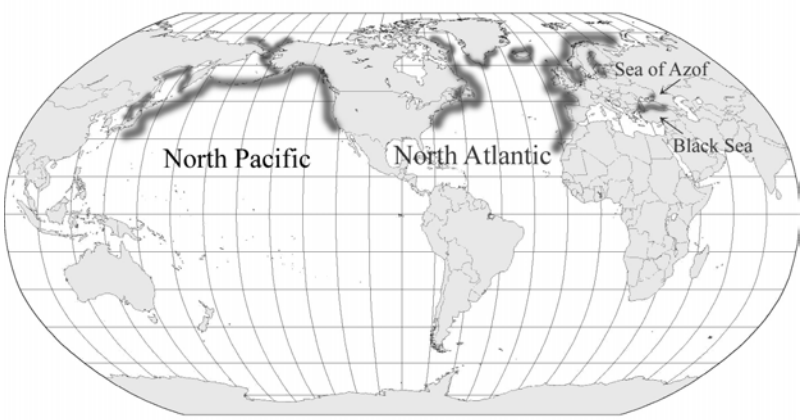

Fig. 1 Three distribution areas of the harbour porpoise.

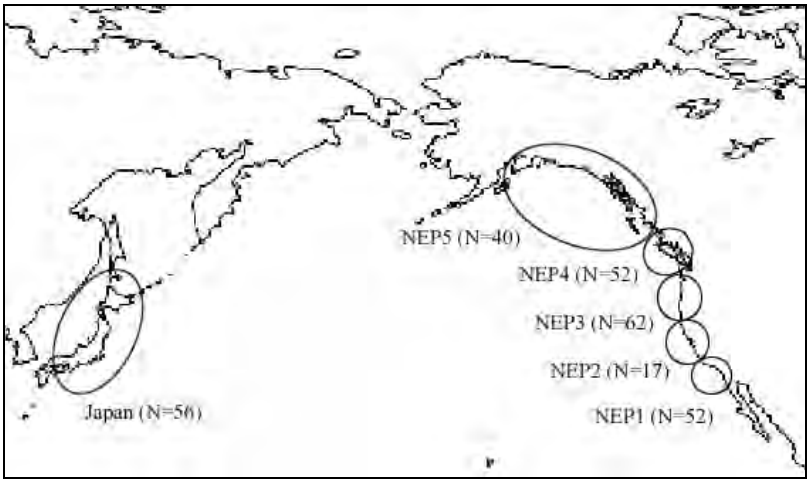

Fig. 2 Geographic locations and number of harbour porpoise specimens or sequences used in this study.

Results

Sequence analysis of 358 bps in the 5' 462 bps sequenced portion of the mtDNA control region revealed 23 variable sites, which defined 19 haplotypes among Japanese porpoises (Table 1).

Haplotype and nucleotide diversities were 0.78 and 0.006, respectively, in Japan. The haplotype diversity ranged from 0.64 to 0.91 and nucleotide diversity ranged from 0.006 to 0.016. Both diversities were lower in Japan and NEP5 than the other populations, and became higher toward south of the Pacific Rim. The reduced value in NEP2 might be caused by small sample size.

In the NJ tree for a total of 67 haplotypes, two geographic clusters, groups I and II, were confirmed, but not divided completely (Fig. 3). Although some haplotypes were endemic to the Japanese population, many other haplotypes were distributed across a broad geographic range and the reliability values of the tree were low.

A minimum spanning network resolved two main haplotype groups (groups I and II, Fig. 4), and these two groups were compatible with those of the NJ tree (Fig. 3). The Northeast Pacific populations had both haplotype groups, but the Japanese population had only group I. The most common haplotype, haplotype 49, was found in all sampling locations and was focal in a star-like group I genealogy. The second most common haplotype, haplotype3, was focal in the group II.

Table 1 Genetic diversity indices in 6 locations.

	Japan	NEP5	NEP4	NEP3	NEP2	NEP1
No. of samples	56	40	52	62	17	52
No. of polym. sites	23	25	35	33	17	30
No. of haplotypes	19	14	19	23	8	18
Haplotype diversity	0.78	0.64	0.88	0.91	0.73	0.90
Nucleotide diversity	0.006	0.007	0.015	0.015	0.011	0.016

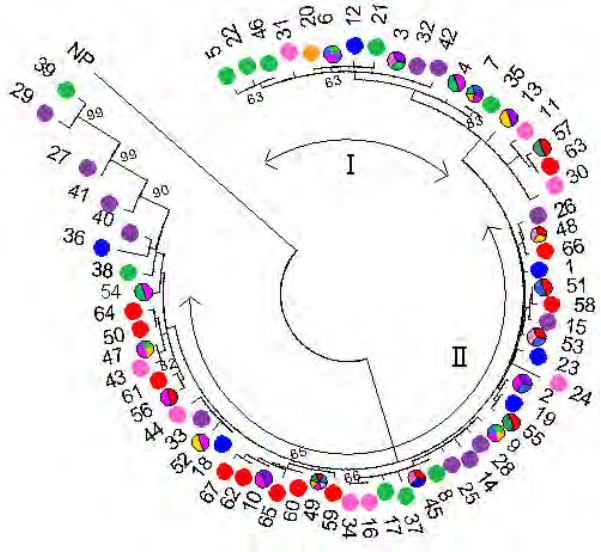

Fig. 3 Neighbor-joining tree for 76 haplotypes of harbour porpoises in the North Pacific. The nodal numbers indicate bootstrap support over 60% in 1000 replications. The circle colors show those haplotypes found in the following regions: red (Japan); blue (NEP5); violet (NEP4); pink (NEP3); orange (NEP2); green (NEP1).

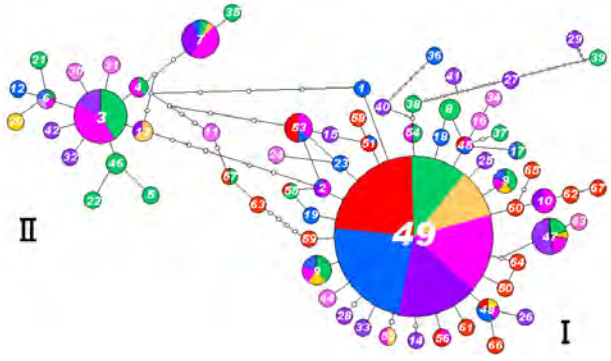

Fig. 4 The parsimony network for a total of 67 haplotypes of the harbour porpoise in the North Pacific. The numbers in the circles indicate haplotype ID. Circle size reflects the haplotype abundance and the color of the sampling locales referred to Figure 3. Small open circles are intermediate haplotypes.

The AMOVA showed a significant difference for ϕ_{ST} between Japan and the Northeast Pacific, except for NEP5, which was significantly differentiated from the other populations, except for Japan and NEP2 (Table 2). An insignificant value between NEP5 and NEP2 may be due to the small sample size in NEP2. Overall, differentiation increased southward in the Pacific Rim.

There was significant correlation between genetic distance for ϕ_{ST} and geographic distance among all pairwise populations (Fig. 5). This relationship suggests a restricted gene flow by distance in the North Pacific.

Discussion

Although two main geographic clusters were confirmed on the NJ tree of haplotypes in the harbour porpoise, its branching reliability was not high with weak to moderate bootstrap support. In addition, most of the observed haplotypes were distributed across a broad geographic range, although some were endemic to Japan. These results suggest the occurrence of a certain level of gene flow over the distribution range in the North Pacific.

A minimum spanning network also resolved two haplotype groups. A star-like genealogy of both haplotype groups suggests recent population expansion of the harbour porpoise in the North Pacific, as a whole. Most populations in the Northeast Pacific had these two groups. Although the Japanese population had only group I haplotypes, AMOVA did not show significant differentiation between Japan and NEP5, Alaska to Strait of Georgia. Moreover, there was a significantly positive relationship between genetic and geographic distances, suggesting a restricted gene flow with isolation by distance.

Both the genetic differentiation and haplotype diversity data obtained may indicate a contiguous expansion of their range from south to north along the North Pacific Rim, and the occurrence of the Japanese population in the Northeast Pacific populations after bottleneck. This also is supported by lower genetic diversities north of the Pacific Rim. Rosel *et al*. (1995) also reported lower genetic diversity of the harbour porpoise in the northern location of the Northeast Pacific, and they inferred that this phenomenon reflected historical colonization by a small group having a part of their lineage in an ancestral population.

No difference between the Japan and Alaska to the Strait of Georgia population despite the very long distance is puzzling. The Sea of Okhotsk may become a key area to resolving this problem. However, the role of the Sea of Okhotsk on gene flow of the harbour porpoise in the Northwest Pacific remains unknown because there are no population genetic data in the Bering Sea, around the Aleutian Islands and coastal Russia. In the future, studies using the data from these areas will help in appropriate management of the harbour porpoise in the Northwest Pacific.

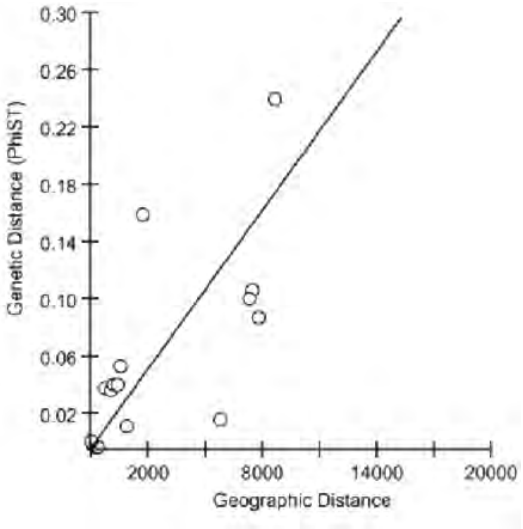

Fig. 5 Correlation between ϕ_{ST} and geographic distance among populations in the North Pacific.

Table 2 Pairwise population ϕ_{ST} with statistical significance ($p < 0.05$, below diagonal).

	Japan	NEP5	NEP4	NEP3	NEP2	NEP1
Japan		0.019	0.104	0.153	0.083	0.247
NEP5	–		0.048	0.097	0.016	0.175
NEP4	+	+		0.005	–0.0022	0.0147
NEP3	+	+	–		–0.005	0.013
NEP2	+	–	–	–		0.047
NEP1	+	+	+	–	–	

Acknowledgements

We are grateful to all the people who contributed to the collection of samples used in this study. We also would like to thank N. Azuma for her help in laboratory work.

References

Beineke, A., Siebert, U., Mclachlan, M., Bruhn, R., Thron, K., Failing, K., Muller, G. and Baumgartner, W. 2005. Investigations of the potential influence of environmental contaminants on the thymus and spleen of harbour porpoises (*Phocoena phocoena*). *Environ. Sci. Tech*. **39**: 3933–3938.

Chivers, S.J., Dizon, A.E., Gearin, P.J. and Robertson, K.M. 2002. Small-scale population structure of eastern North Pacific harbour porpoise (*Phocoena phocoena*) indicated by molecular genetic analyses. *J. Cetacean Res. Mgmt.* **4**: 111–122.

Clement, M., Posada, D. and Crandall, K. 2000. TCS: a computer program to estimate gene genealogies. *Mol. Ecol*. **9**: 1657–1660.

Excoffier, L., Laval, G. and Schneider, S. 2005. Arlequin ver. 3.0: An integrated software package for population genetics data analysis. *Evol. Bioinform*. **1**: 47–50. Online.

Gaskin, D.E. 1984. The harbour porpoise *Phocoena phocoena* (L.): regional populations, status, and information on direct and indirect catches. *Rep. Int. Whaling Comm.* **34**: 569–586.

Gaskin, D.E., Yamamoto, S. and Kawamura, A. 1993. Harbor Porpoise, *Phocoena phocoena* (L), in the Coastal Waters of Northern Japan. *Fish. Bull*. **91**: 440–454.

Jefferson, T.A. and Curry, B.E. 1994. A global review of porpoise (cetacean, phocoenidae) mortality in gillnets. *Biol. Conserv*. **67**: 167–183.

Jensen, J.L., Bohonak, A.J. and Kelley, S.T. 2005. Isolation by distance, web service. *BMC Genet.* **6**: 13. v.3.15 http://ibdws.sdsu.edu/

Jepson, P.D., Bennett, P.M., Deaville, R., Allchin, C.R., Baker, J.R. and Law, R.J. 2005. Relationships between polychlorinated biphenyls and health status in harbour porpoises (*Phocoena phocoena*) stranded in the the United Kingdom. *Environ. Sci. Technol*. **24**: 238–248.

Nei, M. 1987. Molecular Evolutionary Genetics. Columbia University Press, New York.

Rosel, P.E., Dizon, A.E. and Haygood, M.G. 1995. Variability of the mitochondrial control region in populations of the harbor porpoise, *Phocoena phocoena*, on interoceanic and regional scales. *Can. J. Fish. Aquat. Sci*. **52**: 1210–1219.

Rosel, P.E., Tiedemann, R. and Walton, M. 1999. Genetic evidence for limited trans-Atlantic movements of the harbor porpoise *Phocoena phocoena*. *Mar. Biol.* **133**: 583–591.

Saitou, N. and Nei, M. 1987. The Neighbor-joining method: a new method for reconstructing phylogenetic trees. *Mol. Biol. Evol*. **4**: 406–425.

Tamura, K., Dudley, J., Nei, M. and Kumar, S. 2007. MEGA4: Molecular Evolutionary Genetics Analysis (MEGA) software version 4.0. *Mol. Biol. Evol.* **24**: 1596–1599.

Trippel, E.A., Wang, J.Y., Strong, M.B., Carter, L.S. and Conway, J.D. 1996. Incidental mortality of harbour porpoise (*Phocoena phocoena*) by the gill-net fishery in the lower Bay of Fundy. *Can. J. Fish. Aquat. Sci*. **53**: 1294–1300.

Woodley, T.H. and Read, A.J. 1991. Potential rates of increase of a harbour porpoise (*Phocoena phocoena*) population subjected to incidental mortality in commercial fisheries. *Can. J. Fish. Aquat. Sci*. **48**: 2429–2435.

Session A1

Current dynamics

Session Chair

Takuya Nakanowatari

Modeling the circulation of the intermediate layer in the Sea of Okhotsk

Keisuke Uchimoto, Tomohiro Nakamura, Jun Nishioka and Humio Mitsudera

Institute of Low Temperature Science, Hokkaido University, Sapporo, Japan
E-mail: uchimoto@lowtem.hokudai.ac.jp

Introduction

Recently, the Sea of Okhotsk has been recognized as a primary iron source region to the northwestern Pacific (Nishioka *et al.*, 2007). Cold and dense water, which is referred to as Dense Shelf Water (DSW), is formed as a result of brine rejection from sea ice on the northwestern shelf in the Sea of Okhotsk. Iron, together with other chemical particles, is considered to be incorporated into DSW through, for example, tidal mixing (Nakatsuka *et al.*, 2004). DSW, including iron, is transported southward by the East Sakhalin Current in the intermediate layer off Sakhalin, and flows out into the Pacific through the Kuril straits. Thus iron is supplied to the northwestern Pacific.

We intend to model the iron circulation and distribution from the Sea of Okhotsk to the northeastern Pacific in the near future. We have constructed an Ocean General Circulation Model (OGCM) on which we will overlay an iron model. In this paper, we describe the OGCM and show some results of the OGCM, with the above picture of iron circulation in mind. Then, we show tracer experiments in which a tracer is injected in winter at the sea surface in the northwestern part of the Sea of Okhotsk to trace DSW in the model.

OGCM

The model used is Iced COCO ver. 3.4 (Hasumi *et al.*, 2004). It is the ice–ocean coupled model developed at the center for Climate System Research, University of Tokyo. In the ocean model, the vertical coordinate system is a hybrid of sigma (between the sea surface and a depth of 31 m) and z level coordinate (below 31 m). The partial step formulation is adopted for bottom topography (Adcroft *et al.*, 1997). For the tracer equations, the advection schemes are the Quadratic Upstream Interpolation for Convective Kinematics with Estimate Streaming Terms (Leonard, 1979) and the Uniformly Third-Order Polynominal Interpolation Algorithm (Leonard *et al.*, 1993), and isopycnal diffusion (Cox, 1987), thickness diffusion (Gent *et al.*, 1995), and the turbulence closure of Noh and Kim (1999) are used. The isopycnal and the thickness diffusion coefficients are 1.0×10^6 cm^2/s and 3.0×10^6 cm^2/s, respectively, and the background vertical viscosity and diffusion coefficients are 1.0 cm^2/s and 0.1 cm^2/s, respectively. In the ice model, the thermodynamic part is the zero layer model (Semtner, 1976), and the dynamic part is the elastic-viscous-plastic formulation of Hunke and Dukowicz (1997) with two-category thickness representation.

The model domain spans from 136°E to 179.5°W and from 39°N to 63.5°N. The horizontal resolution is 0.5° both in zonal and meridional directions. There are 51 levels in the vertical direction with thickness increasing from 1 m at the sea surface to 1000 m in the deepest layer.

The OGCM is forced at the sea surface by the daily mean climatology data set (wind stress, freshwater flux, radiation, wind speed, temperature, and humidity) from the Ocean Model Intercomparison Project. The freshwater flux data consist of evaporation, precipitation, and river runoff. While the freshwater flux is much larger at the northern mouth of the Mamiya (Tartar) Strait than its vicinities throughout the year, probably owing to the runoff from the Amur River, the runoff ought to drop or stop in winter because of freezing of the river. Therefore, we subtract the annual mean (which we regard as approximate river runoff) from the data at each grid the north of 53°N and the west of 142°E in winter (from December 15 to April 15) and the amount of the subtraction is evenly distributed to the rest of the days.

Temperature and salinity are restored to the World Ocean Atlas data (WOA) on the 6 grids from the boundaries, and the sea surface height is restored to

the basin-wide model outputs on the 3 grids from the boundaries. Temperature and salinity are also restored to the WOA at grids deeper than 2000 m. The sea surface salinity (SSS) is restored to the WOA. From December to April, the SSS is not restored to the WOA in the northern half of the Sea of Okhotsk, as the SSS around the northwestern part of the Sea of Okhotsk in the WOA is too low in winter probably owing to the spurious effects of the Amur River runoff.

Although circulations in and around the Sea of Okhotsk are strongly affected by tidal mixing along the Kuril Islands, this OGCM does not include tidal effects. Therefore, we increased the vertical diffusion coefficients as tidal effects along the Kuril Islands, where the coefficients are set at 500 cm^2/s at the bottom and decrease upward.

The OGCM is integrated for 116 years from the rest with the climatological temperature and salinity (WOA). The next section describes monthly means of the results in the last 1 year.

Results

Figure 1 shows barotropic streamlines in winter and summer. There is a cyclonic gyre in the center of the Sea of Okhotsk, which is strong in winter and weak in summer. In summer, in the southern part of the Sea near the Kuril Islands, the values are positive and some anticyclonic circulations are seen. These circulations and their seasonal variations are consistent with previous studies (*e.g.*, Ohshima *et al.*, 2004; Uchimoto *et al.*, 2007).

Figure 2 shows an ice concentration map in February. This shape of ice distribution is very similar to satellite observations (*e.g.*, Ohshima *et al.*, 2006). We should note that the concentration is somewhat low (less than 0.95) along the northern and northwestern coast. This low concentration is thought to be due to coastal polynyas, where sea ice is mainly produced and therefore much brine is rejected. This implies that DSW is produced in the OGCM.

Next, some features on and about the $26.8\sigma_\theta$ surface are shown. The $26.8\sigma_\theta$ surface is a typical surface in the intermediate layer. Figure 3 shows the depth. Although the model result is somewhat shallower than the climatology (Itoh *et al.*, 2003) almost everywhere in the Sea of Okhotsk, the model result has a general resemblance to the climatology. One of the salient features in the climatology is a deep zone (~300 m) in the Kuril Basin. In the OGCM, the deep zone is marginally represented; the area is smaller and the depth is shallower (~200 m). Another salient feature in the climatology is a deep region in the southeastern part of the Sea of Okhotsk. The deep region is represented in the OGCM, and it extends toward the northwest, the same as in the climatology.

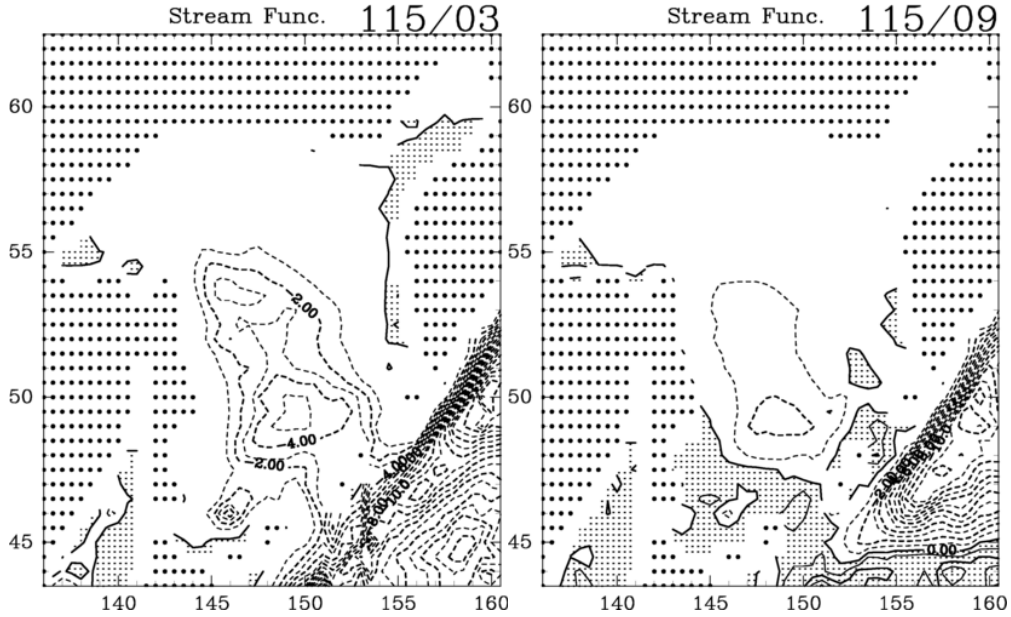

Fig. 1 Barotropic streamlines in March (left) and September (right). Shaded region denotes positive values of streamlines. Contour interval is 1 Sv.

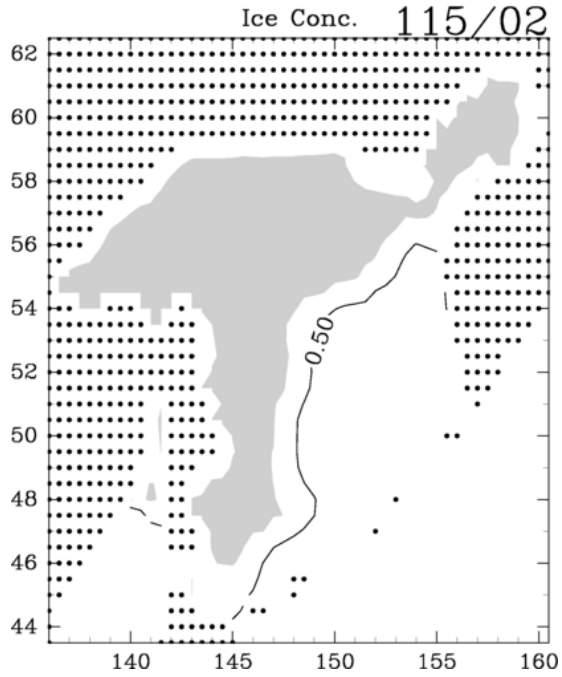

Fig. 2 Ice concentration map in February. Shaded region is where the concentration is larger than 0.95. The contour denotes concentration of 0.5.

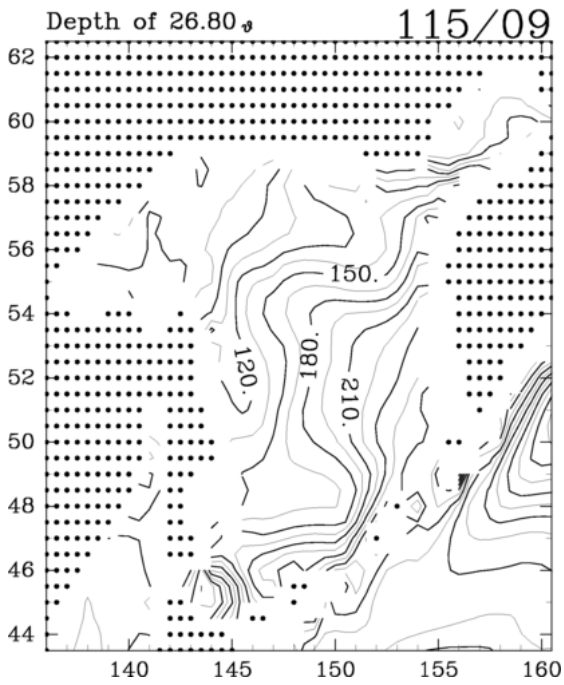

Fig. 3 Depth of the 26.8 σ_θ surface in September. Contour interval is 15 m.

The 26.8σ_θ surface in the OGCM outcrops in winter around the northwestern shelf (not shown). Cold water extends southward from the shelf along Sakhalin Island (Fig. 4). In the center and eastern part of the Sea, potential temperature is relatively high because warm water from the Pacific enters the Sea of Okhotsk. Temperature there is slightly higher, by about 0.8°C, in the OGCM than in the climatology.

The thickness of the 26.8σ_θ layer that is defined as the distance between the two surfaces of 26.75σ_θ and 26.85σ_θ is shown in Figure 5. The thick layer in the eastern part of the Sea is represented in the OGCM, but the thick layer in the southern part is, unfortunately, not represented.

In summary, the OGCM represents circulations and features of the 26.8σ_θ in the Sea of Okhotsk, of course not perfectly, but acceptably well, considering its coarse resolution. The area most poorly represented in the OGCM is the Kuril Basin. While the cause for it is not apparent at present, a possible cause is the parameterization of tidal mixing effects along the Kuril Islands. We should investigate more appropriate values and/or vertical profiles of the vertical diffusion coefficients using tidal mixing effects.

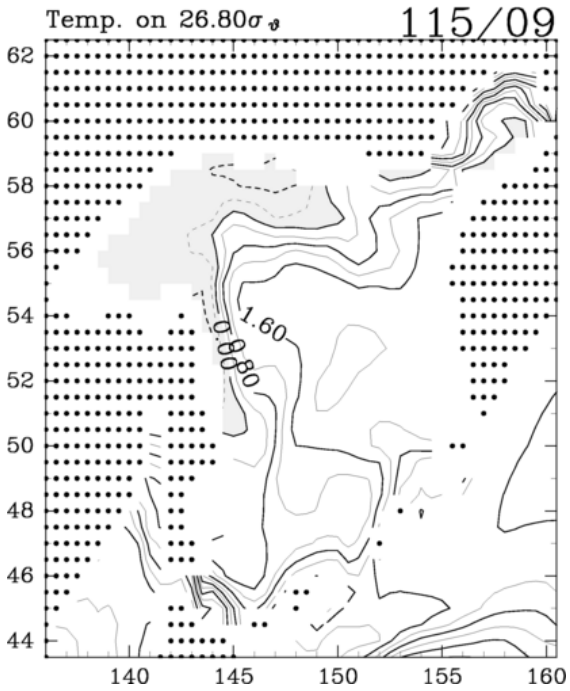

Fig. 4 Temperature on the 26.8σ_θ surface in September. Contour interval is 0.4°C. Regions where temperature is less than 0°C are shaded.

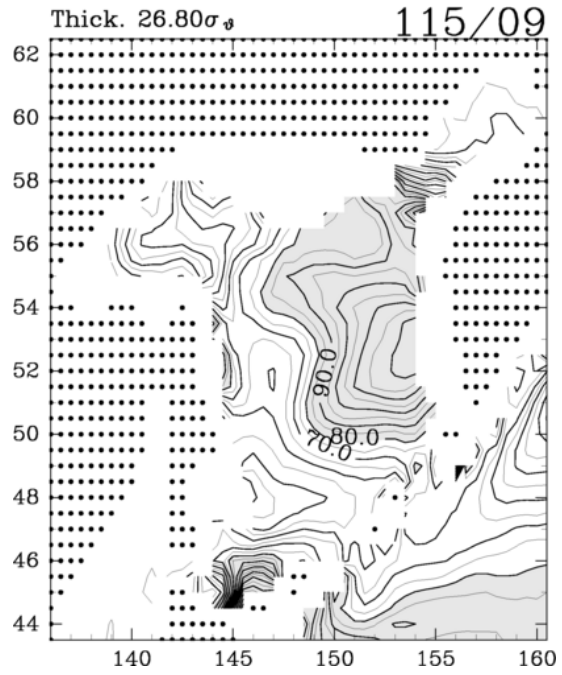

Fig. 5 Thickness of the 26.8σ_θ surface in September. Contour interval is 5 m. Regions where the thickness is larger than 80 m are shaded.

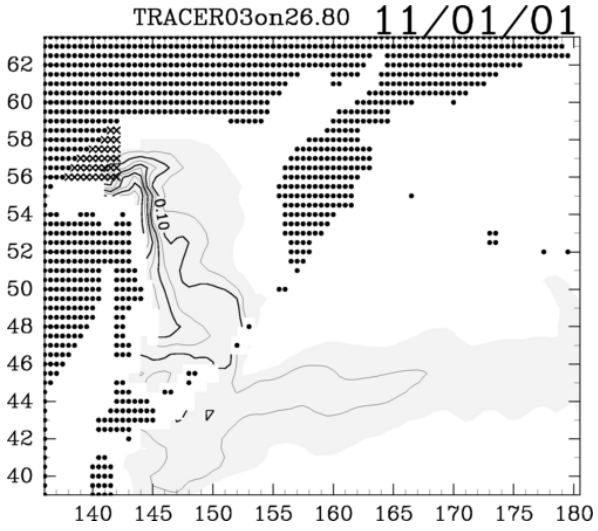

Fig. 6 Tracer concentration on the 26.8σ_θ surface 11 years after the start. The tracer injected from January to April at the sea surface in the northwestern shelf is denoted by crosses. Contour interval is 0.05. Regions where tracer concentration is larger than 0.1 are shaded.

Tracer experiments

To trace dense water that is produced as a result of cooling and brine rejection around the northwestern shelf, we conducted tracer experiments, where a passive tracer is restored to unity at the sea surface in the northwestern shelf (Fig. 6) from January to April.

Figure 6 displays tracer distribution on the 26.8σ_θ surface 11 years after the start. The tracer injected near the northwestern corner of the Sea moves southward along the western coast on the shelf and then eastward around 55°N. It moves southward along Sakhalin Island and goes toward the Kuril Islands. Some part of the tracer recirculates within the Sea of Okhotsk, and the other parts move into the Pacific through the Kuril Straits where they are transported eastward in the North Pacific.

Along 55°N the tracer leaves the shelf and proceeds on the slope. At first, the tracer appears in the vertical section along 55°N, with a stronger concentration near the bottom in the western part, creeps eastward, and then goes down the slope. However, it does not reach the bottom on the slope, but remains in the intermediate layer. This picture is consistent with observed DSW which is produced on the northwestern shelf and is transported in the intermediate layer, in a depth of a few hundreds meters.

We also conducted the same experiment but with *no* tidal mixing effects along the Kuril Islands. In the no mixing case, the tracer does not sink to the intermediate layer on the slope, but remains at almost the same depth as the shelf bottom (not shown). The difference between the two cases indicates that tidal mixing along the Kuril Islands indirectly pushes DSW to a depth of a few hundred meters, *i.e.*, the intermediate layer.

Concluding Remarks

We have shown some results of our OGCM which covers the Sea of Okhotsk and the northwestern Pacific. Considering its coarse resolution, we think that the OGCM can represent circulations and active tracer distributions in the intermediate layer well. Tracer experiments show that dense and cold water (DSW) produced on the northwestern shelf in the Sea of Okhotsk flows southward along Sakhalin in the intermediate layer.

We will overlay an iron model on the OGCM and investigate the iron circulation. Since iron is thought to be transported with DSW, the results suggest that the OGCM is likely to be useful for iron circulation modeling.

References

Adcroft, A., Hill, C. and Marshall, J. 1997. Representation of topography by shaved cells in a height coordinate ocean model. *Mon. Wea. Rev.* **125**: 2293–2315.

Cox, M.D. 1987. Isopycnal diffusion in a z-coordinate ocean model. *Ocean Modelling* **74**: 1–5.

Gent, P.R., Willebrand, J., McDougall, T.J. and McWilliams, J.C. 1995. Parameterizing eddy induced tracer transports in ocean circulation models. *J. Phys. Oceanogr*. **25**: 463–474.

Hasumi, H., Oka, A. and Komuro, Y. 2004. A study on the polar ocean freshwater budget and the global thermohaline circulation using the CCSR sea ice-ocean model (Iced-COCO). CGER's Supercomputure Activity Report, 11-2002, pp. 11–20.

Hunke, E.C. and Dukowicz, J.K. 1997. An elastic-viscous-plastic model for sea ice dynamics. *J. Phys. Oceanogr*. **27**: 1849–1867

Itoh, M., Ohshima, K.I. and Wakatsuchi, M. 2003. Distribution and formation of Okhotsk Sea Intermediate Water: An analysis of isopycnal climatological data. *J. Geophys. Res*. **108**: doi:10.1029/2002JC001590

Leonard, B.P. 1979. A stable and accurate convective modelling procedure based on quadratic upstream interpolation. *Comput. Method Appl. Mech. Eng*. **19**: 59–98.

Leonard, B.P., MacVean, M.K. and Lock, A.P. 1993. Positivity-preserving numerical schemes for multidimensional advection. NASA Tech. Memo. 106055, ICOMP-93-05.

Nakatsuka, T., Fujimune, T., Yoshikawa, C., Noriki, S., Kawamura, K., Fukamachi, Y., Mizuta, G. and Wakatsuchi, M. 2004. Biogenic and lithogenic particle fluxes in the western region of the Sea of Okhotsk: Implications for lateral material transport and biological productibity. *J. Geophys. Res*. **109**: C09S13: doi:10.1029/2003JC001908

Nishioka, J., Ono, T., Saito, H., Nakatsuka, T., Takeda, S., Yoshimura, T. Suzuki, K., Kuma, K., Nakabayashi, S., Tsumune, D., Mitsudera, H., Johnson, W.K. and Tsuda, A. 2007. Iron supply to the western subarctic Pacific: Importance of iron export from the Sea of Okhotsk. *J. Geophys. Res.* **112**: C10012: doi:10.1029/2006JC04055

Noh, Y. and Kim, J. 1999. Simulations of temperature and turbulence structure of the oceanic boundary layer with the improved near-surface process. *J. Geophy. Res.* **104**: 15,621–15,634.

Ohshima, K.I., Simizu, D., Itoh, M., Mizuta G., Fukamachi, Y., Riser, S.C. and Wakatsuchi, M. 2004. Sverdrup balance and the cyclonic gyre in the Sea of Okhotsk. *J. Phys. Oceanogr*. **34**: 513–525.

Ohshima, K.I., Nihashi, S., Hashiya, E. and Watanabe, T. 2006. Interannual variability of sea ice area in the Sea of Okhotsk: Importance of surface heat flux in fall. *J. Meteor. Soc. Japan* **84**: 907–919.

Semtner, A.J., Jr. 1976. A model for the thermo-dynamic growth of sea ice in numerical investigations of climate. *J. Phys. Oceanogr*. **6**: 379–389

Uchimoto, K., Mitsudera, H., Ebuchi, N. and Miyazawa, Y. 2007. Anticyclonic eddy caused by the Soya Warm Current in an Okhotsk OGCM. *J. Oceanogr*. **63**: 379–391.

50-yr scale change in the intermediate water temperature in the western North Pacific simulated by an eddy resolving sea ice coupled OGCM

Takuya Nakanowatari[1], Humio Mitsudera[1], Tatsuo Motoi[2], Kay-Ichiro Ohshima[1] and I. Ishikawa[3]

[1] Institute of Low Temperature Science, Hokkaido University, Sapporo, Japan
E-mail: nakano@lowtem.hokudai.ac.jp
[2] Meteolorogical Research Institute, Tsukuba, Japan
[3] Japan Meteorological Agency, Tokyo, Japan

Introduction

The global ocean dataset shows that water temperature has significantly increased during the past 50 years (Levitus *et al.*, 2005). Since the increase in ocean temperature is prominent at upper levels, the cause of the warming seems to be related to global warming.

Recently, it was reported that a warming trend is found in the western North Pacific, including the Sea of Okhotsk at the intermediate layer, which is not affected by local surface heat flux (Nakanowatari *et al.*, 2007). Since the warming trend originates from the Sea of Okhotsk, which is known to be the ventilation source of North Pacific Intermediate Water (NPIW) (*e.g.*, Talley, 1991), it is suggested that overturning in the North Pacific has weakened during the past 50 years.

On the other hand, ocean temperature at 40°N in the western North Pacific has significantly decreased in the upper and middle layers during the past 50 years (Levitus *et al.*, 2005). The significant decrease in ocean temperature occurs at isopycnal level (*e.g.*, Wong *et al.*, 1999; Nakanowatari *et al.*, 2007). Thus, it is considered that cooling in the intermediate layer is related to the change in water mass property.

Several studies have shown that the significant decrease in upper ocean temperature in the western North Pacific is related to the change in surface heat flux, Ekman transport, and ocean circulation associated with the Pacific Decadal Oscillation (PDO) (*e.g.*, Miller and Schneider, 2000). However, the effect of atmospheric forcing on the 50-yr scale decrease in ocean temperature at intermediate layers has not been investigated.

In this study we investigate the effect of atmospheric forcing on a 50-yr scale change in intermediate water temperature in the western North Pacific by using observational data and hindcast data of an eddy resolving sea ice coupled Ocean General Circulation Model (OGCM) driven by realistic atmospheric forcing.

Data and Methods

Model description and experiment

The hindcast data used in this study is integrated by the sea ice coupled OGCM developed at the Meteorological Research Institute (MRI.COM: Ishikawa *et al.*, 2005). The ocean model is described by a primitive-equation system with a vertical depth coordinate, free surface, Boussinesq and hydrostatic approximations. The model domain occupies the entire North Pacific from 100°E to 75°W and from 15°S to 65°N. Horizontal resolution is 1/12° (eddy resolving) in the zonal and meridional direction, respectively. Thus, ocean circulation in the Sea of Okhotsk and narrow features in the Oyashio front and Kuroshio–Oyashio confluence can be resolved.

In this model, the sea ice model is coupled to realistically simulate vertical mixing in the Sea of Okhotsk. Thermodynamics is based on Mellor and Kantha (1989), and dynamics is based on elastic-viscous-plastic rheology (Hunke and Ducowicz, 1997). In addition, the tidal mixing process is represented in the form of parameterization of the vertical diffusive coefficient (St. Laurent *et al.*, 2002).

As a boundary condition for the hindcast experiment of the sea ice coupled model, 6-h NCEP-NCAR reanalysis data (Kalnay *et al.*, 1996) are used. Heat

flux is calculated by bulk formula (Kara *et al.*, 2000). Freshwater flux is estimated from E – P + river runoff. Sea surface salinity (SSS) is restored with an 8-day damping timescale to avoid the SSS drifting problem.

Observational data sets

Temperature and salinity are taken mainly from the World Ocean Database 2001 (Conkright *et al.*, 2002). In addition, we used observational data obtained by the Japan–Russia–United States international joint study of the Sea of Okhotsk from 1998 to 2004 and data archived by the Japan Oceanographic Data Center. We also used profiling float data obtained by the international Argo program from 2000 to 2004.

From these observational data, we made new isopycnal grid data for potential temperature in the North Pacific on the method similar to previous studies (Itoh *et al.*, 2003; Nakanowatari *et al.*, 2007). Annual mean climatology was calculated on a 1° × 1° latitude/longitude grid by a weighted averaging with a Gaussian window of 150 km. Then, we calculated annual mean anomalies from 1955 to 2004 based on this climatology. All the calculated anomalies were gridded by using simple averaging in a yearly 2.5° × 2.5° grid box, taking account of the trade-off between spatial and temporal resolution.

Results

50-yr scale change in potential temperature in the North Pacific from model and observations

Figure 1a shows the 1977–2004 minus 1955–1976 difference in annual mean potential temperature at 26.8σ_θ for observational data. The 50-yr scale decrease in potential temperature is observed in the western North Pacific, including the subtropical region. The maximum decrease is found in the subtropical region with 0.6°C. The decrease in potential temperature becomes weak at deeper depth. Such a decrease is successfully simulated in the hindcast data (Fig. 1b), although the most prominent decrease is found in Oyashio region.

Figure 2 shows the time series of potential temperature at 26.8σ_θ averaged over the western North Pacific. The potential temperature is dominated by multi-decadal variation like the Pacific Decadal Oscillation, which is characterized by the regime shift which occurred at the end of the 1970s (Mantua *et al.*, 1997; Minobe, 1997). The model quantitatively simulates the multidecadal variation in the observations. The difference in potential temperature for the model is –0.14, which is similar to that for the observations. The correlation between them is 0.67, which is significant at the 99% confidence level.

From the difference map for observational data, significant warming is found around the western subarctic gyre, including the Sea of Okthosk (Fig. 1a). This warming is prominent in the western part of the Sea of Okhotsk, which is consistent with trend analyses of potential temperature on the isopycnal layer (Nakanowatari *et al.*, 2007). However, the warming is not found in the model data. Although we examine the potential temperature at 27.0σ_θ, in which the most prominent warming trend is observed, the result is basically the same as in Figure 1b. Figure 2b shows the time series of potential temperature at 26.8σ_θ averaged over the Sea of Okhotsk. The significant warming trend is dominant in the observational data, but such a long-term variation is quite weak in this model.

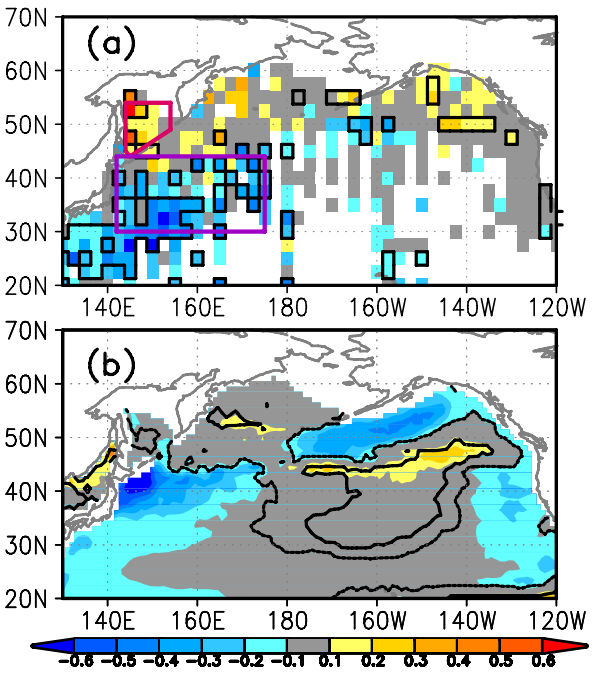

Fig. 1 The 1977–2004 minus 1955–1976 difference (colors) in annual mean potential temperature at 26.8σ_θ for (a) observations and (b) model. The black boundaries indicate the regions where the difference is significant at the 95% confidence level. For calculating the significance of the difference, we assume each year is independent. The boundaries of the western North Pacific region (purple) and the Sea of Okhotsk (magenta), for which area-averaged quantities are displayed in Figure 2, are indicated.

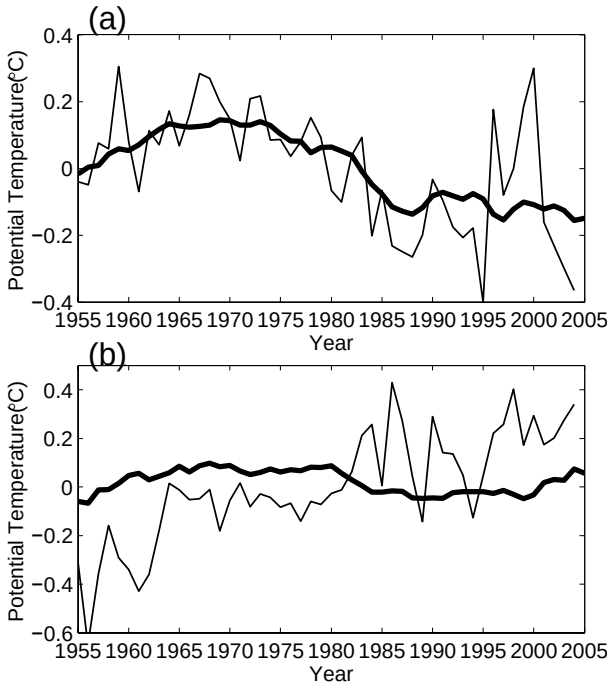

Fig. 2 Time series of annual mean potential temperature for observations (thin line) and model data (thick line) at $26.8\sigma_\theta$ averaged over (a) the western North Pacific and (b) the Sea of Okhotsk. Area averaged region is shown in Figure 1(a).

Effect of Okhotsk Sea Intermediate Water on the 50-yr scale change of intermediate water temperature in the North Pacific

We examine the role of Okhotsk Sea Intermediate Water (OSIW), which is known to be the cooling and freshening source for NPIW, on the 50-yr scale change in intermediate water temperature in the North Pacific by using model data. In order to investigate the water mass property change related to OSIW, we examine potential vorticity, which is defined by $(f + \zeta)\ \rho^{-1}\cdot\partial\rho/\partial z$. Since potential vorticity is minimum in the Sea of Okhotsk at intermediate layer depth, it can be used for a proxy for OSIW (*e.g.*, Mitsudera *et al.*, 2004).

Figure 3 shows the 1977–2004 minus 1955–1976 difference in annual mean potential vorticity at $26.8\sigma_\theta$. A significant decrease in potential vorticity is found in the western North Pacific with a maximum in the Oyashio region. Thus, the spatial pattern of the significant decrease in potential vorticity is very similar to that in potential temperature. On the other hand, the potential vorticity in the Sea of Okhotsk has increased in contrast to the western North Pacific. These results indicate that the cooling in the western North Pacific is not associated with the change in OSIW, but the change in ocean circulation in the North Pacific.

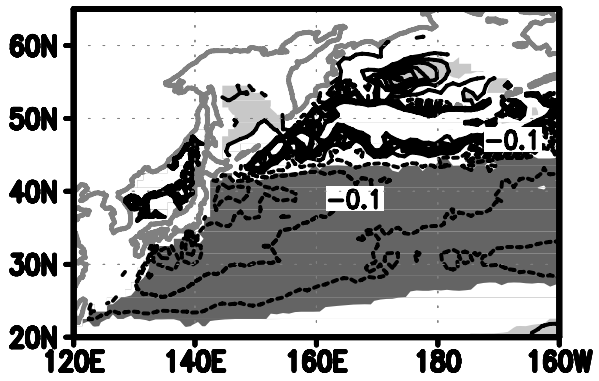

Fig. 3 The 1977–2004 minus 1955–1976 difference in annual mean potential vorticity at $26.8\sigma_\theta$ for the model. The contour interval is 0.05 $m^{-1}s^{-1}$, and the areas with potential vorticity > 0.3 $m^{-1}s^{-1}$ are not contoured. The dense and light shades indicate the region for the negative and positive difference is significant at the 95% confidence level.

Discussion and Summary

In this study, we investigate the influence of atmospheric forcing on the change in the intermediate water temperature in the western North Pacific during the past 50 years by using observational data and the hindcast data of the sea ice ocean coupled model. The model quantitatively represents the 50-yr scale decrease in the western North Pacific. The decrease in the intermediate water temperature is significant at the $26.8\sigma_\theta$ isopycnal surface in the western North Pacific with a maximum in the Oyashio region. The variation is dominated by multi-decadal variation like the Pacific Decadal Oscillation.

The decrease in the intermediate water temperature is accompanied by the decrease in potential vorticity. Since the significant decreases in potential temperature and potential vorticity are found in Oyashio region, it is suggested that the multi-decadal scale change in the intermediate water temperature is due to the variation of the Oyashio. It has been considered that the variation in water temperature in the western North Pacific is related to the change in wind-driven ocean circulation associated with westward Rossby waves (*e.g.*, Deser *et al.*, 1999).

However, the multi-decadal variation in intermediate water originates from the western boundary. Thus, the western boundary current and the associated eddies seems to be important for 50-yr scale cooling in the NPIW.

The coastal region of the western North Pacific is one of the most important fishery regions. It has been reported that consumption of phosphate and chlorophyll-*a* has decreased in the Oyashio region (Ono *et al.*, 2002). Thus, the effect of multi-decadal scale change in the Oyashio on the ecosystem and material circulation in the North Pacific should be examined by using an eddy resolving ecosystem–biogeochemical model.

In this model, the warming trend in the Sea of Okhotsk, reported by Itoh (2007) and Nakanowatari *et al.* (2007), is not simulated. A possible cause for the unrealistic variation in the Sea of Okhotsk is that the amount of sea ice formation is not simulated accurately in the model. A restoring of sea surface salinity may lead to an underestimation of dense shelf water formation associated with sea ice production. Since observational data are very limited in the Sea of Okhotsk, atmospheric forcing data used in this study also may not be satisfactorily realistic.

Recent observational data show that in the northwestern North Pacific, iron, which is an essential micronutrient for phytoplankton, may come from the intermediate water of the Sea of Okhotsk (Nishioka *et al.*, 2007). Thus, realistic simulation for the OSIW and its variability are needed for prediction of the marine environment and ecosystem in the western North Pacific.

References

Conkright, M.E., Garcia, H.E., O'Brien, T.D., Locarnini, R.A., Boyer, T.P., Stephens, C. and Antonov, J.I. 2002. World Ocean Database 2001, Vol. 1, Introduction, NOAA Atlas NESDIS 42 [CD-ROM] *edited by* S. Levitus, 167 pp., U.S. Govt. Print. Office, Washington, D.C.

Deser, C., Alexander, M.A. and Timlin, M.S. 1999. Evidence for a wind-driven intensification of the Kuroshio current extension from the 1970s to the 1980s. *J. Climate* **12**: 1697–1706.

Hunke, E.C. and Dukowicz, J.K. 1997. An elastic-viscous-plastic model for sea ice dynamics, *J. Phys. Oceanogr*. **94**: 1849–1867.

Ishikawa, I., Tsujino, H., Hirabara, M., Nakano, H, Yasuda, T. and Ishizaki, H. 2005. Meteorological Research Institute Community Ocean Model (MRI.COM) Manual. Tech. Rep. Meteorol. Res. Inst., 47, pp. 1–189 (in Japanese).

Itoh, M., Ohsihma, K.I. and Wakatsuchi, M. 2003. Distribution and formation of Okhotsk Sea Intermediate Water: An analysis of isopycnal climatology data. *J. Geophys. Res.* **108**: 3258, doi:10.1029/2002JC001590.

Itoh, M. 2007. Warming of intermediate water in the Sea of Okhotsk since the 1950. *J. Oceanogr*. **63**: 637–641.

Kalnay, E., Kanamitsu, M., Kistler, R., Collins, W., Deaven, D., Gandin, L., Iredell, M., Saha, S., White, G., Wollen, J., Zhu, Y., Leemaa, A., Reynolds, R., Chelliah, M., Ebisuzaki, W., Higgins, W., Janowiak, J., Mo, K.C., Ropelewski, C., Wang, J., Jenne, R. and Joseph, D. 1996. The NCEP/NCAR 40-year reanalysis project. *Bull. Amer. Meteor. Soc.* **77**: 437–472.

Kara, A.B., Rochford, P.A. and Hurlburt, H.E. 2000. Efficient and accurate bulk parameterization of air-sea fluxes for use in general circulation models. *J. Atmos. Ocean. Tech.* **17**: 1421–1438.

Levitus, S., Antonov, J. and Boyer, T., 2005. Warming of the world ocean, 1955–2003. *Geophys. Res. Lett*. **32**: L02604, doi:10.1029/2004GL021592.

Mantua, N.J., Hare, S.R., Zhang, Y., Wallace, J.M. and Francis, R.C. 1997. A Pacific interdecadal climate oscillation with impacts on salmon production. *Bull. Amer. Meteor. Soc.* **78**: 1069–1079.

Mellor, G.L. and Kantha, L. 1989. An ice-ocean coupled model. *J. Geophys. Res.* **94**: 10937–10954.

Miller, A.J. and Schneider N. 2000. Interdecadal climate regime dynamics in the North Pacific Ocean: Theories, observations and ecosystem impacts. *Progr. Oceanogr*. **27**: 257–260.

Minobe, S. 1997. A 50–70-year climatic oscillation over the North Pacific and North America. *Geophys. Res. Lett*. **24**: 683–686.

Mitsudera, H., Taguchi, B., Yoshikawa, Y., Nakamura, H., Waseda, T. and Qu, T. 2004. Numerical study of the Oyashio water pathways in the Kuroshio-Oyashio confluence. *J. Phys. Oceanogr*. **34**: 1174–1196.

Nakanowatari, T., Ohshima, K.I. and Wakatsuchi, M. 2007. Warming and oxygen decrease of intermediate water in the northwestern North Pacific, originating from the Sea of Okhotsk, 1995-2004. *Geophys. Res. Lett.* **34**: L04602, doi:10.1029/2006GL028243.

Nishioka, J., Saito, H., Nakatsuka, T., Takeda, S., Yoshimura, T., Suzuki, K., Kuma, K., Nakabayashi, S., Tsumune, D., Mitsudera, H., Johnson, W.K. and Tsuda, A. 2007. Iron supply to the western subarctic Pacific: Importance of iron export from the Sea of Okhotsk. *Geophys. Res. Lett.* **112**: C10012, doi:10.1029/2006JC004055.

Ono, T., Tadokoro, K., Midorikawa, T., Nishioka, J.

and Saino, T. 2002. Multi-decadal decrease of net community production in western subarctic North Pacific. *Geophys. Res. Lett.* **29**: 1186, doi:10.1029/12001GL014332.

St. Laurent, L.C., Simmons, H.L. and Jayne, S.R. 2002. Estimating tidally driven mixing in the deep ocean. *Geophys. Res. Lett.* **29**: 2106, doi:10.1029/2002GL015633.

Talley, L.D. 1991. An Okhotsk Sea water anomaly: Implications for ventilation in the North Pacific. *Deep-Sea Res. Part A* **38**: S171–S190.

Wong, A.P.S., Bindoff, N.L. and Church, J.A. 1999. Large-scale freshening of intermedia te waters in the Pacific and Indian Oceans. *Nature* **400**: 440–443.

Vertical movement of water masses in the western part of the Sea of Okhotsk

Gennady Kantakov

Far-Eastern Ecological Center Ltd., Yuzhno-Sakhalinsk, Russia
E-mail: deco@sakhalin.ru

Sakhalin Research Institute of Fisheries and Oceanography (SakhNIRO), Yuzhno-Sakhalinsk, Russia (former address)

Abstract

Recent observations of the well studied dichothermal layer (with T < 0 °C) in the Sea of Okhotsk provides an update of its inner structure. In the 1990s, CTD vertical soundings with 1 m resolution found cases of "double" or "triple" dichothermal layers on the continental slope and in the deepest part of the Sea of Okhotsk. The genesis of those phenomena is linked with pre-winter cooling of the water column, following convection and brine rejection under ice floes, and frontal interactions between water masses. Based on new data to explain dichothermal structure, we note an obvious discrepancy between calculated winter convection depth and real descending horizons for subzero temperatures reaching few hundreds meters at the southwestern part of the Sea of Okhotsk. Because of the lack of applied theory to account for vertical movements in the Sea of Okhotsk, an experiment using year-round mooring data was conducted for its study. From August 2006 to October 2007, the N-5 mooring was deployed at the northern tip of Sakhalin Island in the western part of the Sea of Okhotsk at mid-shelf depth around 100 m close to the region where the East Sakhalin Current originates. A year's run of vertical current data showed clear seasonal signals averaged over the whole depth layer current changing from downwelling in the summer to the upwelling during cold period of the year. The vertical structure showed a complex nature with heterogeneous vertical movements occurring at relatively shallow depths on the Sakhalin shelf. Differences in vertical current structure are discussed for the fall, winter, spring, and summer seasons alternately with vertical movements through the year.

Introduction

Despite the well-known Sea of Okhotsk's cold intermediate or dichothermal layer (DTL), discovered in 19th century by Makarov (1894), which is characterized by subzero temperatures, little attention has been paid to its inner structure. The vertical movement of water masses from the surface to the bottom during winter convection after surface cooling, and brine rejection under ice floes, are one of the most obvious processes explaining the presence of negative temperatures at different depths in the Sea of Okhotsk, and especially in the western part, due seasonal ice distribution.

Water, having a negative temperature in winter, located beneath the surface layer and later insulated during summer warming, is called the cold intermediate layer (dichothermal layer). Before the era of CTD measurements, it was difficult to obtain a detailed picture of the water column due to the scarcity of vertical measurements by water bottle sampling. With the introduction of CTD sensors and probes, the internal vertical structure of the water could be observed with meter and submeter vertical resolution (UNESCO-MHI, 1993). From detailed CTD measurements in the western part of Sea of Okhotsk, temperature inversions inside the cold interlayer or "double", sometimes "triple", cold interlayers have been found in mostly stable water stratification during the summer (Kantakov, 1995). Besides the discovery of dual thermal structures inside the dichothermal layers, the residual depth of convection after winter in the western part of the Sea of Okhotsk is often exceeded in calculations, which makes it necessary to explore the role of the mechanisms of vertical motion of water masses here. To explain the oceanic conditions responsible for the appearance of double dichothermal layers and to explain the over-estimation of the convection depths missed with calculations, we have processed a number of CTD data, and the vertical velocity of

water masses in the western part of the Sea of Okhotsk was measured.

This article attempts to present new facts which will allow us to understand the role of the vertical motions of water in the subarctic Sea of Okhotsk from the points of view of physical and biological oceanography, climatic changes and hydrography of the sea.

Data and Methods

The study region of the Sea of Okhotsk, showing the arrangement of standard and additional oceanographic stations with the N-5 mooring site, are given in Figure 1. The physical parameters of the marine environment were measured in the free drift of vessels equipped with different sensors such as the Neil Brown Mk-III, ICTD FSI and Guildline. The N-5 mooring, equipped with an ADP with frequency of 0.500 MHz, was deployed on August 27, 2006 and recovered on October 8, 2007 by SakhNIRO's R/V *Dmitry Peskov*. Most of the CTD data were collected during joint expeditions of SakhNIRO with the Pacific Oceanological Institute (POI, Vladivostok) and the Far-Eastern Hydrometeorological Institute (FEHRI, Vladivostok) during the 1990s.

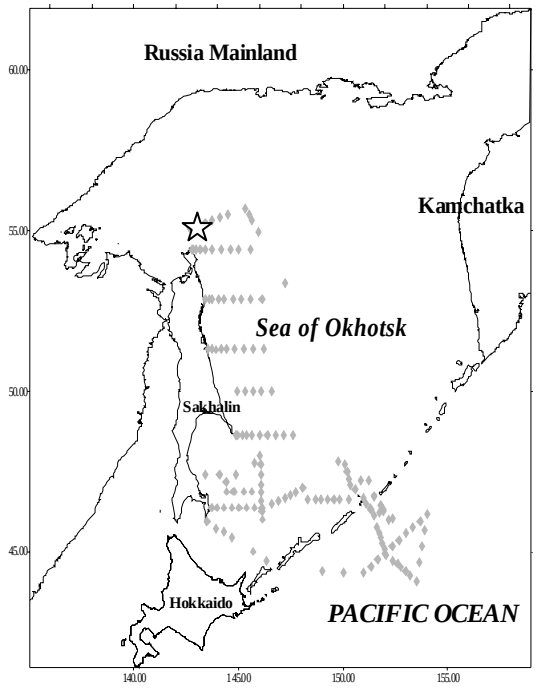

Fig. 1 Location of CTD stations in 1996–2000 during the joint expeditions between SakhNIRO, POI and FEHRI, and the N-5 mooring (star) in 2006–2007.

Convection calculations were carried out according to Arkhipkin (1992). A spatial flow pattern in the western part of Sea of Okhotsk was obtained using the dynamics method from the "zero" surface of 1000 db (Timofeev and Panov, 1962).

Study of the currents, including the vertical component, was conducted using three-component Doppler profilers (Cabrera *et al.*, 1987; Polonichko *et al.*, 2000), which made it possible to investigate both the horizontal and vertical velocities of the flows *in situ*.

Results and Discussion

Figure 2 presents a typical vertical temperature distribution in the western part of Sea of Okhotsk based on the standard horizon measurements and characterizing the northeastern shelf/slope of Sakhalin. Two main features are apparent – the dichothermal layer has a united body, and temporal changes from summer to autumn are insignificant (Fig. 2). However, during the soundings with greater depth resolution, frequent inversions are seen. One such example is shown in the Figure 3.

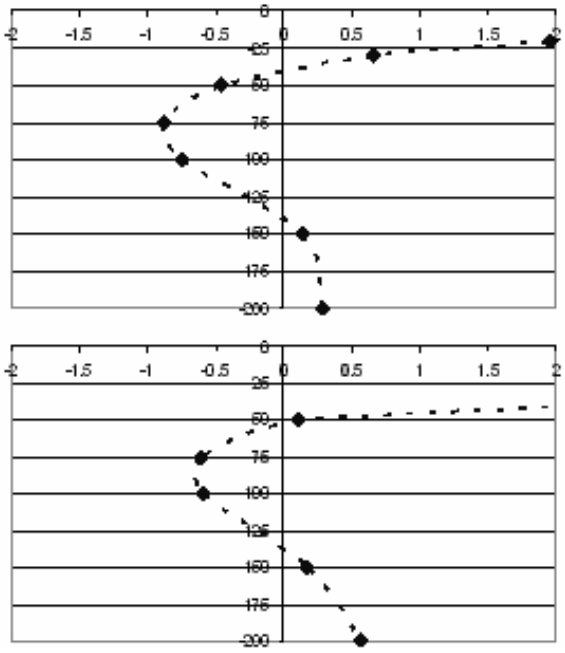

Fig. 2 An example of the vertical temperature distribution (°C) of an average DTL at standard horizons in June (upper), and in October 1994 (bottom) in the western part of the Sea of Okhotsk, Sakhalin NE shelf area (Source: FEHRI–SakhNIRO data).

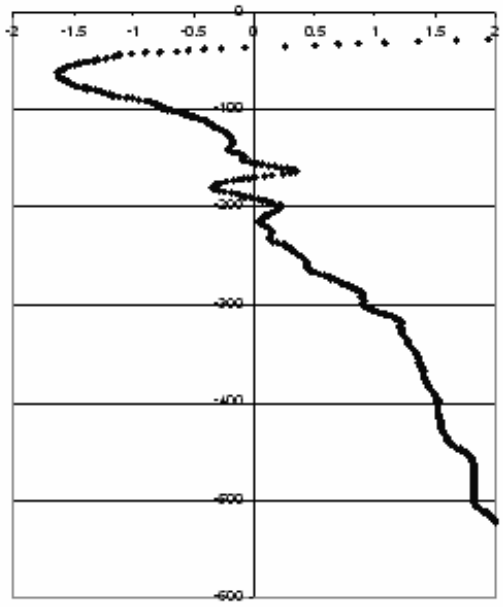

Fig. 3 Vertical temperature distribution (°C) on the slope at the western part of the Sea of Okhotsk, using 1-m resolution sounding, June 17, 2000. (Source: FEHRI–SakhNIRO data, R/V *Pavel Gordienko*).

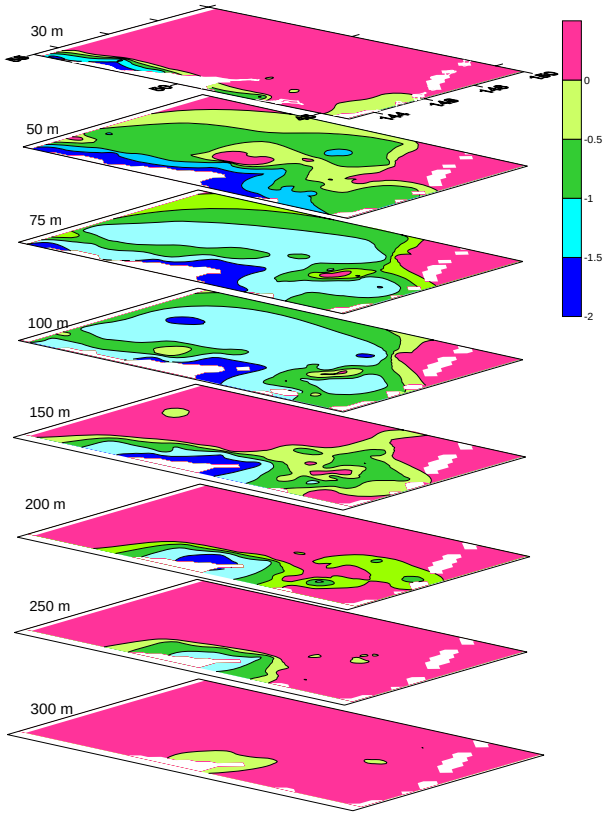

Fig. 4 Subzero temperature distribution (°C) at selected standard horizons, western part of the Sea of Okhotsk, June 1996 based on Figure 1 CTD stations (Source: POI–SakhNIRO 1996 data).

If the vertical distribution has temperature inversions (Fig. 3), how are the inversions arranged spatially, for example, in the western part of Sea of Okhotsk? In order to understand the distribution of inversions inside the DTL, 1996 data have been processed from the joint POI-SakhNIRO expedition. For clarity and ease of presentation, the arrangement of inversions inside the DTL temperature distributions on the standard horizons superimposed on one another from top (30 m) to bottom (300 m) are shown in Figure 4. Such superpositioning of the different horizons shows regions of temperature inversions inside the DTL, but it is obvious, that there is no spatial predominance of inversions inside the layer –this is apparently local phenomena according the 1996 data analysis (Fig. 4). Nevertheless, new facts about the vertical distribution of temperature inversions in the DTL pose a new question – Why do the temperature inversions penetrate more deeply than calculated?

Knowing the characteristics of the ice thickness in the western part of the Sea of Okhotsk, we know that theoretically convection does not penetrate deeper than 250–300 m. But we actually do observe the presence of DTL depths on the order of 500 m. How can we explain such measurements? Are they showing a flow downward or are they the remainders of the past year, or year before last? (What causes the DTL to "think", *i.e.*, have a "dichothermal layer memory", which reflects the convection level of previous year?)

Here, we analyze convection during the cold period of the year. How is it shown for the Sea of Okhotsk? Besides the winter type of classical convection for the cooling and freezing areas, the Sea of Okhotsk possesses convection during the summer period when the flow of salt with the Soya Current inside Sea of Okhotsk leads to the lowering of waters at its southwestern basin near the South Kuril Islands. Here, we can observe an underwater waterfall with a horizontal scale tens of kilometers and hundred meters vertically, which also makes it necessary to think about the reasons for vertical motions in the Sea of Okhotsk.

A similar picture in the winter period is also observed on the Kamchatka shelf and slope (Kashiwai, this report) when more salt water from the Pacific Ocean causes convection, but this exceeds the scope of our article. Therefore, we do not discuss it further, but keep it in mind for future investigations.

This allows us to concentrate on the following issue. If we observe the DTL practically the year round in the western part of the Sea of Okhotsk, then apparently there are conditions for its retention here, some of which we know a little about regarding the vertical components of currents in this region. It is known that the general cyclonic circulation of the surface flows in the Sea of Okhotsk water mass distribution (Leonov, 1960; Moroshkin, 1966; Chernyavsky, 1981) must lead to the rise of waters in the central Sea of Okhotsk basin, with the dichothermal layer disappearing, probably seasonally. However, it exists in the western part Sea of Okhotsk all year-round.

Aiming to measure the vertical component of the current velocities, the N-5 mooring with an ADP was installed at the northern tip of Sakhalin, just inside the zone of the beginning of the Eastern Sakhalin Current. At the same time, temperature was recorded at a depth of 100 m on the layer where the DTL should exist; current profiles at different horizons were also taken. The year-round duration of the velocities and temperature measurements are shown in Figure 5. It can be seen that the motion of the averaged vertical velocity possesses an expressed seasonal signal with positive vertical velocities (upward) for the cold period of year and negative ones (downward) during summer and early fall period.

Analyzing the layer below the seasonally heated upper one, we found that during observation period the vertical component was negative and directed towards the bottom without any seasonally induced changes in the magnitude and sign of the vertical velocities, except for interannual differences between the fall periods of 2006 and 2007, respectively (Fig.6). In addition, bottom temperature was negative all year (Fig.7). A period of about one month, between mid-October and mid-November 2006 had a signal, which indicates some reflection of weak warming near the bottom from subzero temperatures. Temperature was mainly stable between about –1.7° and –1.6°C for the rest of the year at this depth after peaking to –0.65°C in early December (Fig.7).

The year-round subzero temperatures at 100 m depth on the shelf strongly confirm and update previously obtained results (Gladyshev *et al.*, 2000, 2003; Mizuta *et al.*, 2003; Shcherbina *et al.*, 2003). The shelf and slope at the northwestern part of the Sea of Okhotsk is defined as a permanent source of water with subzero temperatures supplying the DTL in the western part of the Sea of Okhotsk.

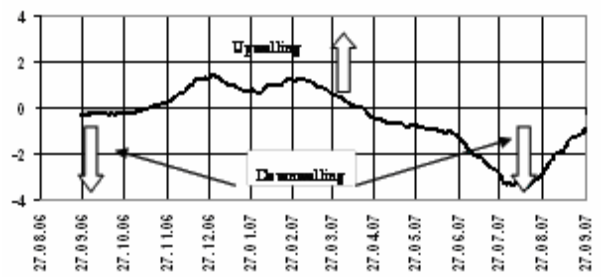

Fig. 5 Vertical (W) component of velocity measured by the N-5 ADP mooring. Note: The whole depth layer, averaging 0–100 m, is smoothed monthly data. Horizontal axis is from August 2006–September, 2007. Vertical axis is in cm s^{-1}.

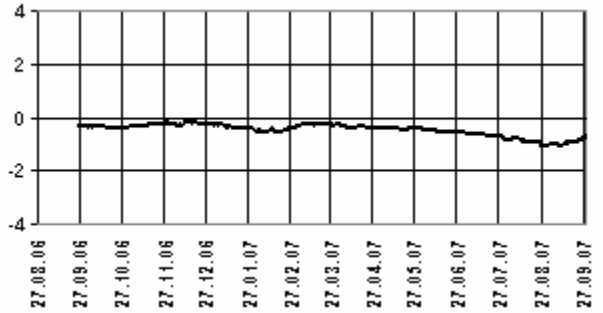

Fig. 6 Vertical (W) component of velocity measured by the N-5 ADP mooring Note: The subsurface layer averaging 30–100 m is smoothed monthly data. Horizontal axis is from August 2006–September, 2007. Vertical axis is in cm s^{-1}.

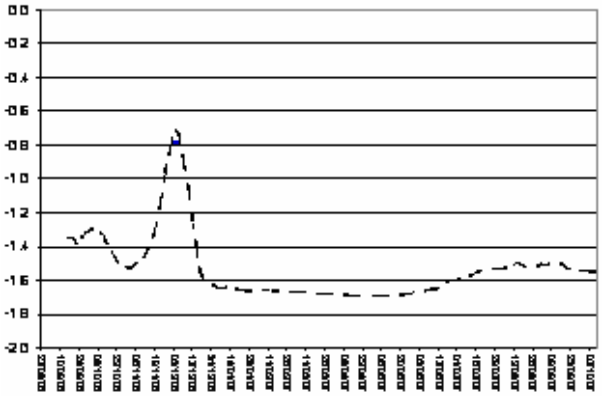

Fig. 7 Temperature dynamics (°C) at 100 m depth at the N-5 mooring site from August 2006 to October 2007.

Meanwhile a relatively strong warming signal inside the DTL coincided in time with the amplification of the East Sakhalin Current in the fall. It is known that in the western, but mostly in the northwestern, part of the Sea of Okhotsk, the current circulation system is a function of the year type (Figurkin, 2000). Cold years are characterized by the alongshore East

Sakhalin Current which is directed to the south (Ohshima *et al.*, 2002); an opposite picture should be obtained for the warm years when northward water flows mostly along the shelf and slope of Sakhalin. Currently, we have no measurements of the vertical components for the East Sakhalin Current directed to the north, or in the period when circulations are undergoing change.

Figure 8 shows locations of the "double" DTL at the shelf and continental slope of Sakhalin which are found in current convergence zones or at eddy borders in deep waters.

Comparing the dynamic topography map with the location of sea surface temperature fronts (Belkin and Cornillon, 2004), we note the agreement of belts of convergence with places of inversions inside the DTL, both in the deepest basin of the southwestern Sea of Okhotsk and in the waters around Terpeniya Peninsula. Examining the more generalized map of the Sea of Okhotsk frontal zones (Belkin and Cornillon, 2004), we conclude that the high temperature intrusions inside the DTL are generated at the frontal borders of water masses in the Sea of Okhotsk.

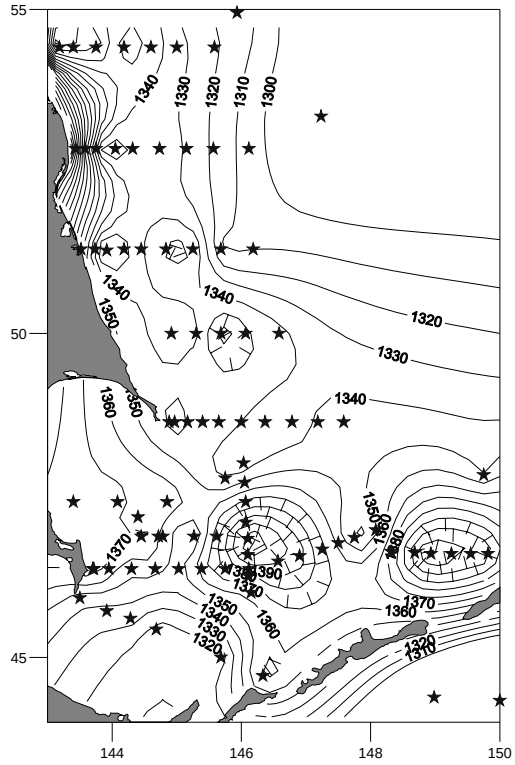

Fig. 8 Dynamic heights distribution (10/1000 db) in the western part of the Sea of Okhotsk, June 1996 (Source: POI–SakhNIRO data, R/V *Gagarinsky*).

Conclusions

Temperature inversions inside the DTL are located in the convergence zone and (or) near the thermal fronts in the Sea of Okhotsk. In the Sea of Okhotsk at least two types of the convections are obtained, linked with the transport of salt water during the warm period by the Soya Current or Pacific waters, and connected with cooling and brine rejection under ice floes during the late autumn and winter.

Observations at the N-5 ADP mooring from 2006–2007 confirmed DTL waters submerging during the whole period of observations. The upper mixed layer had another type of vertical motion, switching from upwelling to downwelling in the cold and the warm period of year, respectively. These data need to be confirmed by other studies, including those of seasonal behavior of the open water levels. The changeability in the vertical motions of water inside the Sea of Okhotsk must be investigated in relation to its obvious influence on sea biota, especially for early ontogenetic stages, and to contemporary trends in climate oscillations and hydrography.

Observed convection depths of the DTL are deeper in the comparison with those calculated by theory for the western part Sea of Okhotsk, and requires separate and detailed studies. It is obvious that organizing a series of ice-breaker expeditions is needed to study the formation of convections under the ice and in polynyas in the Sea of Okhotsk in winter because there are no oceanographical, chemical or biological data during ice formation and seasonal melting.

References

Arkhipkin, V.S. 1992. Algorithms and FORTRAN programs for oceanological data analysis. MSU, Moscow, p. 83 (in Russian).

Belkin, I.M. and Cornillon, P.C. 2004. Surface thermal fronts of the Okhotsk Sea. *Pacific Oceanogr.* **2**: 6–19.

Cabrera, R., Deines, K., Brumley, B. and Terray, E. 1987. Development of practical coherent acoustic Doppler current profiler. Proc. Ocean'87. Halifax, NS, Canada. IEEE Oceanic Engineering Society. pp. 93–97.

Chernyavsky, V.I. 1981. Sea of Okhotsk circulation systems. TINRO Proc. No. 105, pp. 13–19 (in Russian).

Figurkin, A.L. 2000. Okhotsk sea shelf and slope waters circulations in cold seasons of the year. 9th PICES Annual Meeting. Hokkaido, Japan, p. 51 (Abstract).

Gladyshev, S.S., Martin, S., Riser, S. and Figurkin, A. 2000. Dense water production on the northern Okhotsk shelves: Comparison of ship-based spring-summer observations from 1996 and 1997 with satellite observations. *J. Geophys. Res.* **106**: 26,281–26,299.

Gladyshev, S.S., Talley, L., Kantakov, G., Khen, G., and Wakatsuchi, M. 2003. Ditribution, formation, and seasonal variability of Okhotsk Sea Mode Water. *J. Geophys. Res.* **108**: 3186.doi:10.1029/2001JC000877.

Kantakov, G. 1995. Vertical temperature distribution feature in an intermediate cool water layer of the Sea of Okhotsk. Workshop on the Okhotsk Sea and adjacent areas PICES Abstracts. June 19–24, 1995, Vladivostok, Russia, pp. 21–22.

Leonov, A.K. 1960. Regional Oceanography. Gidrometeoizdat, Leningrad, 766 pp. (in Russian).

Makarov, S.O. 1894. Vityaz i Tikhiy Okean, Vol. 1, p. 337; Vol. 2, p. 543 (in Russian).

Kashiwai, M. 2009. The occurrence of winter convection at the open ocean polyna in the eastern part of the Okhotsk Sea indicated by the World Ocean Atlas 2005. This report.

Mizuta, G., Fukamachi, Y., Ohshima, K.I. and Wakatsuchi, M. 2003. Structure and seasonal variability of the East Sakhalin Current. *J. Phys. Oceanogr*. **33**: 2430–2445.

Moroshkin, K.V. 1966. Water masses of the Sea of Okhotsk. Joint. Publ. Res. Serv. 43942, U.S., p. 98.

Ohshima, K.I., Wakatsuchi, M., and Fukamachi, Y. 2002. Near-surface circulation and tidal currents of the Okhotsk Sea observed with satellite-tracked drifters. *J. Geophy. Res.* **107**: 16-1–16-18.

Polonichko, V., Mullison, J. and Cabrera, R. 2000. Pulse-coherent acoustic Doppler profiler. *Sea Technol*. **2**: 76–78.

Shcherbina, A., Talley, L. and Rudnick, D. 2003. Direct observations of North Pacific ventilation: Brine rejection in the Sea of Okhotsk. *Science* **32**: 1952–1955.

Timofeev, V.T. and Panov, V.V. 1962. Indirect Methods for Classification and Analysis of Water Masses. Hydrometeoizdat, Leningrad, 351 pp. (in Russian).

UNESCO-MHI. 1993. Data analysis of the Oceanographic Station. Sebastopol, p. 136 (in Russian).

Current meter observations in the Sea of Okhotsk near Shmidt Peninsula, northern Sakhalin

Georgy Shevchenko[1], Gennady Kantakov[2*] and Valery Chastikov[2]

[1] Institute of Marine Geology and Geophysics FEB RAS, Yuzhno-Sakhalinsk, Russia
E-mail: shevchenko@imgg.ru
[2] Sakhalin Research Institute of Fisheries and Oceanography, Yuzhno-Sakhalinsk, Russia
E-mail: okhotsk@sakhniro.ru
* now at Far-Eastern Ecological Center Ltd., Yuzhno-Sakhalinsk, Russia

Abstract

Current meter measurements from the summer of 2006 at the Kaygano-Vasyukansky (KV), Vostochno-Shmidtovsky (VS) and Zapadno-Shmidtovsky (ZS) oil and gas-bearing blocks are analyzed. Observations revealed the important role of the diurnal tidal currents, which predominated over other types of water motions in the area which adjoins the remote part of northern Sakhalin Island (Shmidt Peninsula). The ellipses of main tidal constituents were highly compressed and changed little with depth. Residual (non-tidal) flows in the intermediate and near-bottom layers had a steadier nature in comparison with the surface, in which the wind effect was shown. The main flow in these layers had orientations on the KV block to the south and south-southwest; on the VS block to the east and south-southeast; in the northern part of the ZS block to the south-southwest and to the east; in the southern part of the ZS block to the north and northeast.

Introduction

In the summer of 2006, the Sakhalin Institute of Fisheries and Oceanography (SakhNIRO) carried out comprehensive studies on potential oil fields in the Sea of Okhotsk, which adjoin Shmidt Peninsula at the northern end of Sakhalin Island. The program included taking flow measurements at the water surface, intermediate and near-bottom layers every 10 minutes at four autonomous stations which were deployed on the Kaygano-Vasyukansky (KV), Vostochno-Shmidtovsky (VS) and Zapadno-Shmidtovsky (ZS) oil and gas-bearing blocks. The moorings positions are represented in Figure 1 and related parameters are given in the Table 1.

Dynamic processes in the waters adjacent to Shmidt Peninsula represent significant interest not only for offshore development, but because our current measurements were the first full-scale experiment in this region. During the period from 1988 to 1997, a large amount of observational data were obtained in the oil and gas-bearing areas of the northeastern shelf of the island, but in the region more to the south. The results of these analyses have been well described (Popudribko *et al.*, 1998; Putov and Shevchenko, 1998; Kochergin *et al.*, 1999; Krasavtsev *et al.*, 2001; Rybalko and Shevchenko, 2003; Shevchenko and Rybalko, 2003; Shevchenko, 2004). These investigations revealed the extraordinarily complex

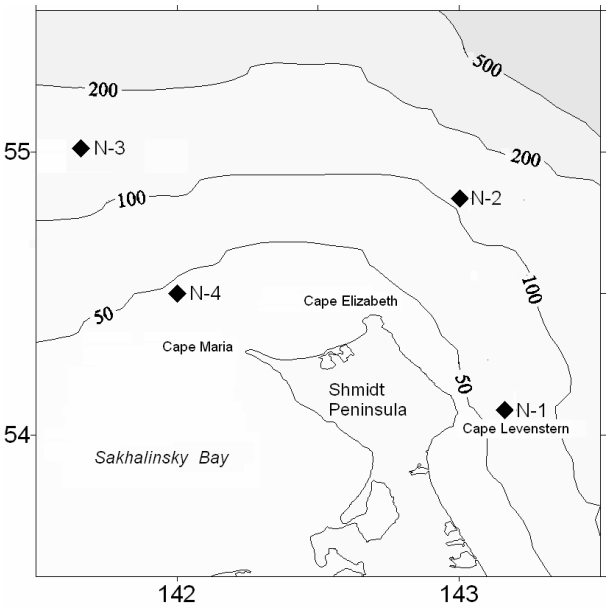

Fig. 1 Bathymetric map of the research area and mooring locations. Mooring station N-1 was deployed at KV, N-2 at VS, and N-3 and N-4 at ZS.

Table 1 Moorings information.

Oil and gas-bearing blocks	Mooring	Latitude (N)	Longitude (E)	Deployment date	Recovery date	Depth (m)
KV	N-1	54°05′	143°10′	July 21, 2006	August 27, 2006	78
VS	N-2	54°50′	143°00′	July 21, 2006	August 26, 2006	97
ZS	N-3	55°00′	141°40′	July 21, 2006	August 26, 2006	130
ZS	N-4	54°30′	142°00′	July 21, 2006	August 26, 2006	45

nature of water dynamics in this region, the main features of which are:

- Strong diurnal tidal currents of 2–3 knots (1–1.5 m/s) in the coastal zone from Cape Elizabeth to Lunsky Bay (approximately 51°25′N);
- Coastal upwelling due to the action of the southern winds during the summer season;
- The sharp strengthening of coastal flow to the south in the fall period as a result of the change in the wind field to winter monsoon conditions, with characteristic winds blowing from the north and northwest directions, which transfer low salinity water caused by the Amur River run-off along the east coast of Sakhalin.

However, only at the KV block it is possible to expect that these dynamic processes will have a similar nature, since topographical conditions in the region to the north of Sakhalin differ significantly from the northeastern shelf of the island. Currents in this area are especially interesting, since it was studied to the much smaller degree. One of a few works (Putov and Shevchenko, 2001) was dedicated to the analysis of current meter measurements in the shelf region near Okhotsk (the Kukhtuyskaya oil and gas-bearing area). Although the measurements were conducted at the significant distance from Shmidt Peninsula, let us examine some results of this work, since it is interesting to compare them with the measurements obtained in the present project.

Near Okhotsk, currents were measured in the surface, intermediate and near-bottom layers for two weeks at the end of May–beginning June 1988 (Putov and Shevchenko, 2001). Records showed that tidal fluctuations prevailed, and they were somewhat weaker in the surface layer compared to the intermediate layer which was influenced by water stratification. In the thin heated upper layer, inertial flows were also noted, but were practically absent at depths below the thermocline.

Residual currents were comparatively small and oriented in a west–southwest direction, and their intensity diminished with the depth. In the middle layer flow was observed in a western direction, while in the upper layer, directions were more irregular, probably due to the variable action of the wind.

KV Block (N-1) Mooring Results

The N-1 mooring, which included the SonTek/YSI Acoustic Doppler Profiler (ADP), was deployed on July 21 near Cape Levenshtern (Fig. 1, Table 1). It was in this area that coastal radar measurements of ice drift were made in 1992–1995 and thus, there was information about the pattern of flows (Tambovsky and Shevchenko, 1999). The ADP was fixed on a special stainless steel frame which was held on the substrate with the aid of two anchors. The depth of the sea at the point of deployment was 78 m. Current measurements were performed in 18 layers with a thickness of 4 m each, except for a "blank zone" approximately about 5 m above the sensor heads where no measurements were taken. The distinctive feature of the Doppler profilers established on the bottom is that the measurements in the near-surface layer are usually contaminated by surface waves. We will have this in mind when we discuss the observations.

For observations, three different layers were selected: the near-bottom (1st layer from the ADP), intermediate (9th layer from the ADP) and upper (surface) layer (18th layer from the ADP). The measured velocity vectors of the currents are represented in Figure 2. The north–south meridional component of the currents clearly predominates for all the horizons. This is due to the orientation of coastline where the KV block is almost parallel to the meridian. Observations show that diurnal tidal currents prevail. Characteristic of them is a two-week changeability where there is a sharp weakening on

August 1–3 and on August 14–16. This is expressed especially in the intermediate and near-bottom layers. At the surface, due to an increase in the role of winds, the contribution of the residual component generally grows with the intensity of total flows. It is possible that, to a certain extent, the high speed of the residual component and the less regular nature of the tidal currents are caused by the distorting influence of the free surface, which was discussed above.

Let us examine the results of the calculated distributions of current velocities at different horizons (Fig. 2). In the surface layer, the highest repetition (34.4%) is obtained in the northern direction where maximum speeds (more than 180 cm/s) are prevalent. The repetition of the flows of the southern direction is somewhat less (21.8%), while maximum speeds are also high (180.9 cm/s); in this direction, the average speed is the highest (75.4 cm/s). In the middle layer the situation is quite different—here the currents are predominantly in the southern direction—their repetition is the highest (42.5%); in this direction speeds attain maximum values (134.7 cm/s), and greatest average values (63.7). The near-bottom layer is also characterized by a separation of currents to the southern direction (30.9%), but the greatest repetition in the flows is in the northwestern direction (37.4%). Here, we note an increase in the portion of the currents in the southeastern direction (14.6%). This indicates that in the near-bottom layer, the currents flow counterclockwise in comparison with the upper layers. The maximum speeds are in the southern (100.3 cm/s), southeastern (95.6 cm/s) and northwestern directions (76.4 cm/s), which are substantially less than in the intermediate and surface layers. The average speeds are 40, 39 and 35 cm/s, respectively.

According to the observational data at each station, the velocity vectors of the currents on the parallel and on the meridian are usually determined from harmonic constant amplitudes and phases of 8 basic tidal constituents: 4 diurnal (Q_1, O_1, P_1, K_1) and 4 semidiurnal (N_2, M_2, S_2, K_2). At the N-1 mooring, in addition to the very fast diurnal tidal currents, two additional diurnal waves ($2Q_1$, HI_1) were determined. For other points in this area, measurements are negligibly small. Tidal currents are traditionally characterized by ellipses, which are designed on the basis of the calculated harmonic constants. Figure 3 shows the current ellipses for the two main tidal constituents: diurnal K_1 and semidiurnal M_2.

Starting from the origin in each panel in Figure 3, the current vector arising from each constituent traces out an ellipse over that constituent's period. The rhombs on each ellipse denote the end positions of the vector at each successive hour for the diurnal constituent and half-hour for the semidiurnal waves. In the surface layer the ellipses of diurnal tidal constituent are compressed and have a bi-meridian orientation. The ellipse of the semidiurnal constituent is less compressed, major semi-axes

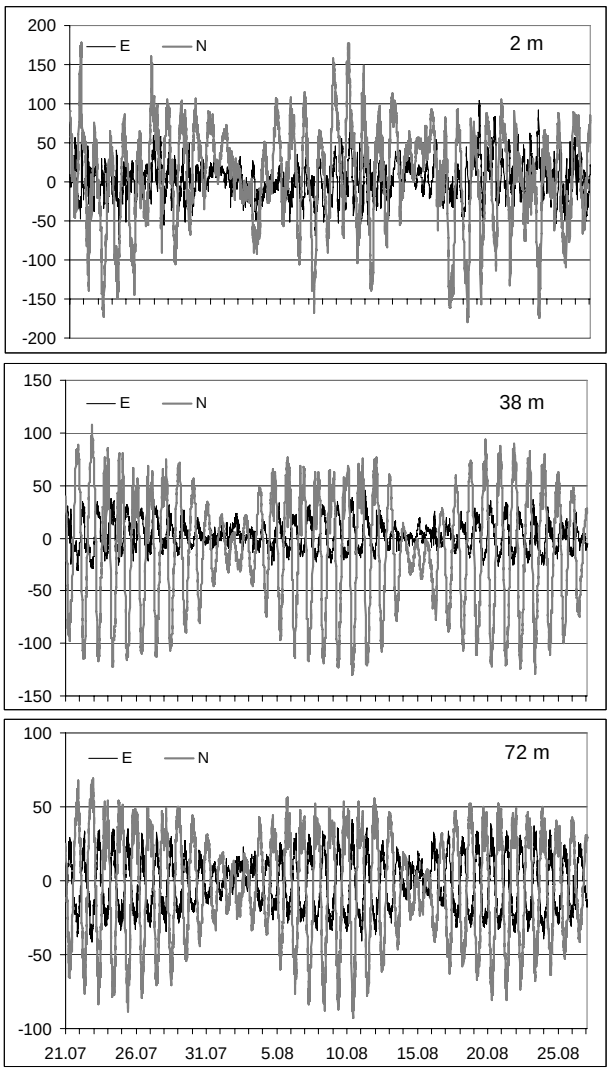

Fig. 2 Meridional (N) and zonal (E) velocity components (cm/s) at depths 2, 38 and 72 m obtained at Mooring N-1, KV block (July 21–August 26, 2006).

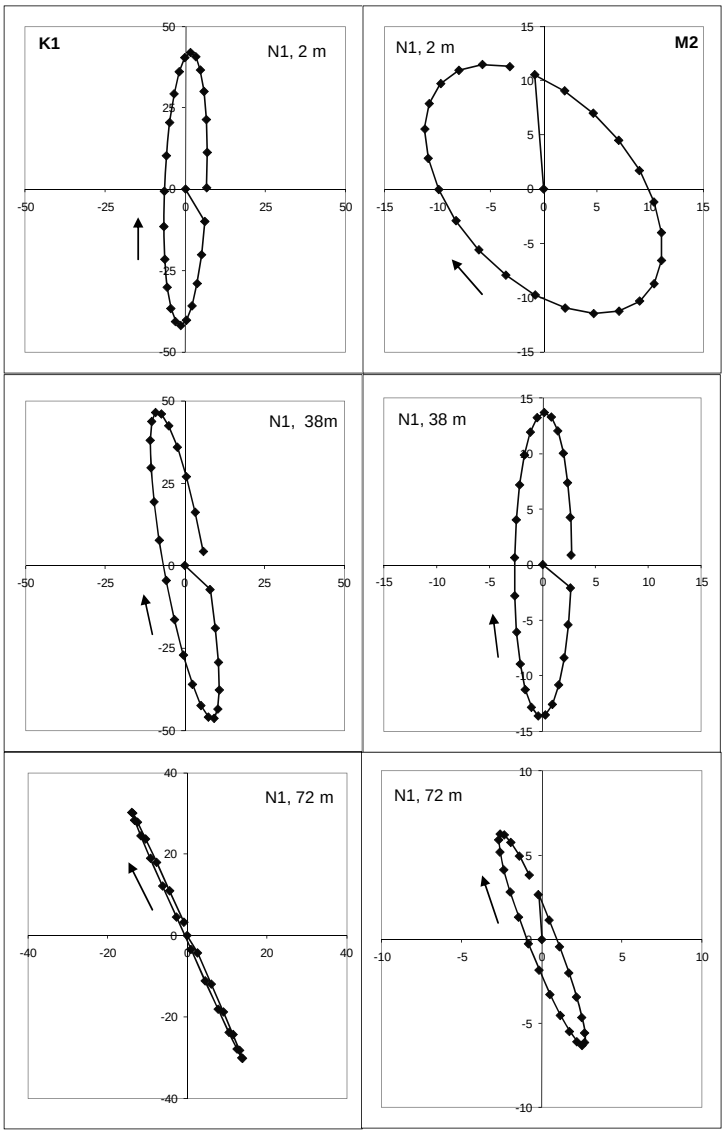

Fig. 3 Current ellipses of the major diurnal K_1 and semidiurnal M_2 tidal constituents at Mooring N-1, KV block at the surface, middle and near-bottom layers, respectively (July 21–August 26, 2006).

are oriented along the axis southeast–northwest. In the middle layer the ellipse of the diurnal harmonics is somewhat turned clockwise, their major semi-axes somewhat more than in the surface layer. The ellipses of semidiurnal currents are highly compressed, their major semi-axes are greater than in the surface layer, and they are elongated along the meridian.

This difference in the characteristics of tidal currents at different depths can be related to the influence of baroclinic effects in the thoroughly heated upper layer (Putov and Shevchenko, 2001), and is more applicable to the semidiurnal constituent whose period is lower than the Coriolis period in this region. In the near-bottom layer the ellipses of all waves are highly compressed, their major semi-axes decrease in comparison to the intermediate layer and are turned clockwise. Such changes are typical when ground friction plays a role, and they agree well with the results for the Piltun–Astokhskaya area, northeast Sakhalin (Popudribko *et al.*, 1998). The obtained estimations of major tidal constituent make it possible to estimate different characteristics of tidal currents, in particular, the maximum speeds, based on astronomical conditions.

It is well known that for this region to account for the inter-annual fluctuations of tide ranges, it is necessary to consider variations with the period of 18.6 years (usually rounded off to 19 years) (Putov and Shevchenko, 1998). To adequately describe the distribution of tidal components, it is necessary to construct distributions in the gradations of speed and the directions, pre-calculated for the 19-year period. In the surface layer intensive fluctuations with periods of 1–2 weeks were observed, which is typical for currents caused by the action of wind. Variations in the meridional component were especially great; their amplitude reached 80 cm/s, which is uncharacteristic for the summer period, when synoptic processes are expressed relatively weakly (Kochergin *et al.*, 1999). In the middle and near-bottom layers the speeds of residual currents noticeably decrease, the meridional components have a similar nature, and the zonal components are distinguished more substantially. The distribution of the residual flows in the gradations of speed and the directions (Fig. 4) reflect these changes. Thus, in the intermediate layer, the main flow is oriented south–southeast (repetition 48.6 and 21.1%, respectively); in the near-bottom layer the greatest repetition is in the southern (27.4%) and southwestern directions (20.1%), followed by increases in the western (13.5%) and northwestern (15.1%) directions.

Similar differences were found in the Piltun–Astokhskaya area (Krasavtsev *et al.*, 2000; Shevchenko, 2004) where an increase in the near-bottom layer of the repetition of flows oriented along the coast was connected to coastal upwelling, which occurs on the northeastern shelf of Sakhalin due to the action of the winds from the south, and characterized the summer season.

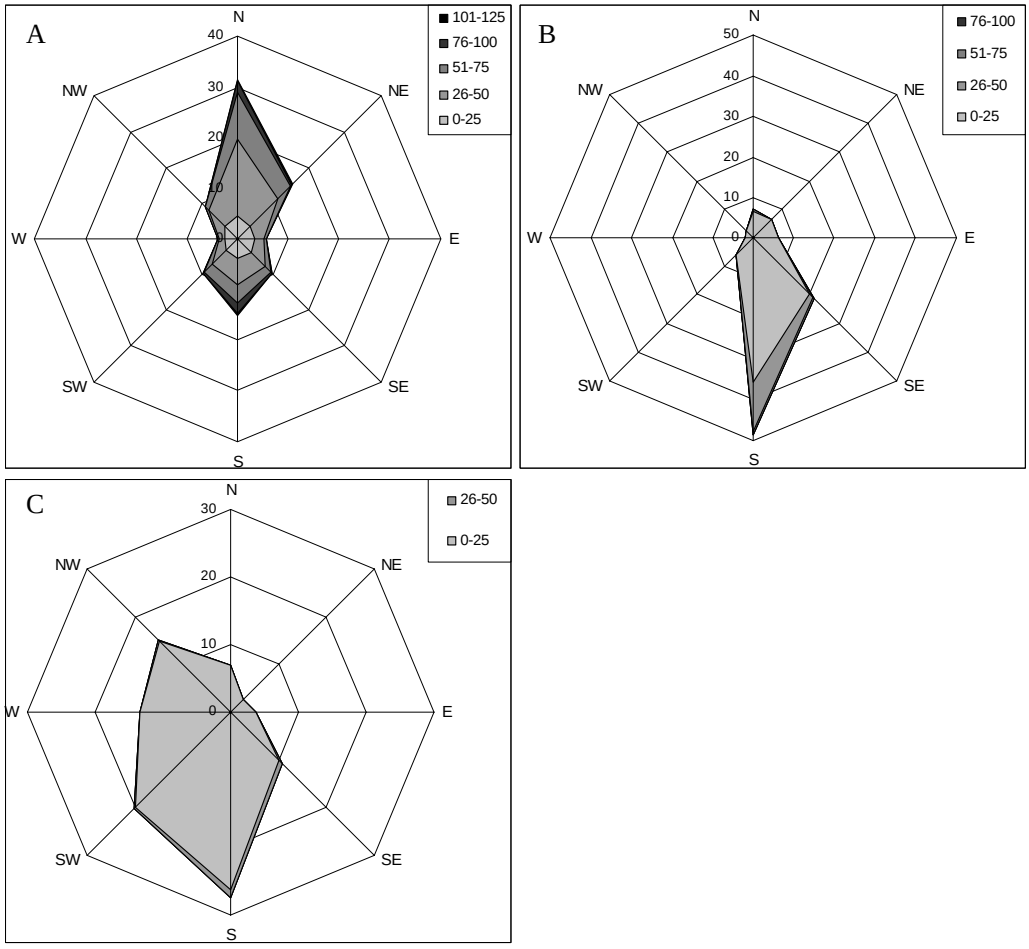

Fig. 4 Distribution of residual currents (%) by speed (cm/s) and direction gradations in (a) surface, (b) middle and (c) near-bottom layers at Mooring N-1, KV block.

VS Block (N-2) Mooring Results

Let us examine the current measurements obtained on the VS block collected by the N-2 mooring. At this mooring, three single-point current meters, SonTek Argonaut-MD, were fixed at horizons of 8, 49 and 94 m. The mooring depth reached 97 m (Fig. 1, Table 1). The vertical tension of the rope was ensured by plastic subsurface buoys, and the mooring was fixed on the bottom by two anchors.

The velocity vectors of the currents at different horizons are presented in Figure 5. Similar to the KV block, diurnal tidal currents prevailed; however, they differed from the KV block in that their intensity was considerably less and there were no essential differences between meridional and zonal components, although the speed of meridian currents were slightly higher, especially in the upper two layers.

Distributions of speed and direction show that in the surface layer, the highest repetition (16–17%) was less for the southern and southeastern directions, and for the northern and northwestern directions. Meanwhile, the highest average speed (30–33 cm/s), with a maximum value (65 cm/s) was noted in the southeastern direction. With depth there was an increase in the proportion of southeastern and northwestern flow directions (particularly in the near-bottom layer, where the repetition of southeastern direction increased to 31.2%). Differences in the distributions in the surface and middle layers were insignificant.

The harmonic constants of 8 major tidal constituents, defined in the same way as for the N-1 mooring, were used for constructing the tidal ellipses for the main diurnal and semidiurnal constituents represented in Figure 6. The harmonic constants of the main diurnal constituents are very similar at different horizons. There is only an insignificant reduction in the amplitude of meridian with an analogous increase in the amplitude of the zonal component, which indicates a certain turn of ellipses in the cyclonic direction with the depth. The vector direction in the tidal cycle was clockwise for both constituents (except for M_2 at 49 m depth). Vertical changes in the ellipses of semidiurnal harmonics are more apparent. Compared to the surface, the middle layer has compressed ellipses with a decrease of the major semi-axis. The direction of rotation of the vectors in the tidal cycle changes to the cyclonic. In the near-bottom layer ellipses are even more compressed; in this case, they turn significantly, and have an almost zonal orientation. The observed differences in the orientation of the axes of diurnal and semidiurnal constituents, even in spite of smaller velocity of the latter, are the reasons for the fairly complicated picture of the distributions of tidal currents in the gradations of speed and the directions.

First of all, in the surface layer the northern (21.9%) and southern (20.3%) directions are separated; in the intermediate layer this is also southern (23.5%) and northwestern (26.9%). In the near-bottom layer these are already southeastern (28.9%) and northwestern (25.5%) directions. Non-tidal currents at the VS block were comparatively small, with fluctuations of periods 1–2 weeks. High-frequency variations

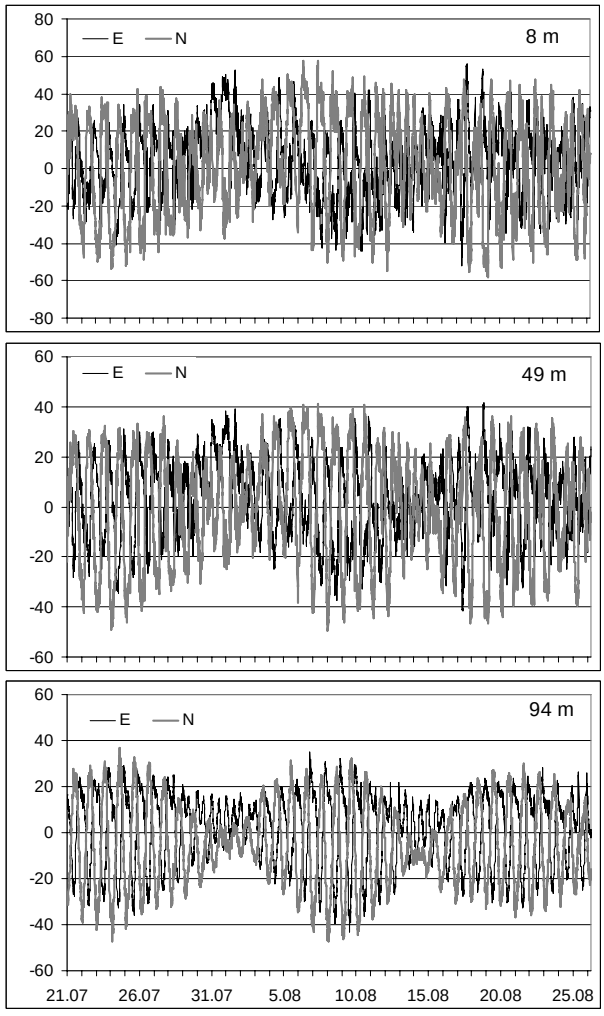

Fig. 5 Meridional (N) and zonal (E) velocity components (cm/s) at depths 8, 49 and 94 m obtained at mooring N-2, VS block (July 21–August 26, 2006).

occurred, which are characteristic of regions with developed turbulence. The pattern of residual flows in the surface and intermediate layers was identical, in the near-bottom layer the rate of flows were noticeably lessened. Moreover, variations in the synoptic time range were manifested more distinctly.

The distributions of residual flows in the gradations of speed and the directions (Fig. 7) reveals a predominance in the surface layer of the flows of northern (15%), northeastern (16.3%) and eastern (16.3%) directions. In the middle layer, the eastern direction (18%) is separated more clearly from the northeastern and southeastern directions which are similar (about 15%). In the near-bottom layer there is a noticeable turn in the main flow, with the greatest share of repetition in the southern (34%) and southeastern (33.5%) directions. The difference between the surface and near-bottom layers is most likely due to the influence of the winds from the south predominating during the summer season. On the surface, therefore, a large proportion is in the northern direction, which is analogous to that already noted above for the KV block. In this case, a compensating current in the opposite direction appears on the bottom layer.

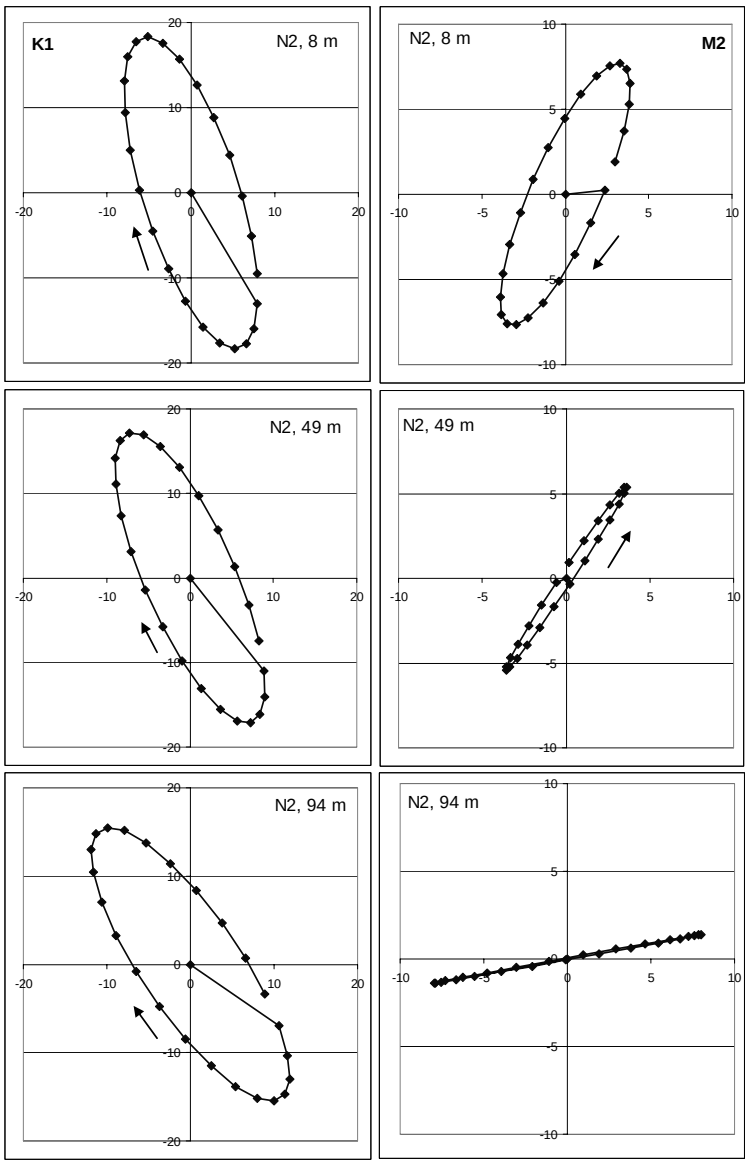

Fig. 6 Current ellipses of the major diurnal K_1 and semidiurnal M_2 tidal constituents at Mooring N-2, VS block at the surface, middle and near-bottom layers, respectively (July 21–August 26, 2006).

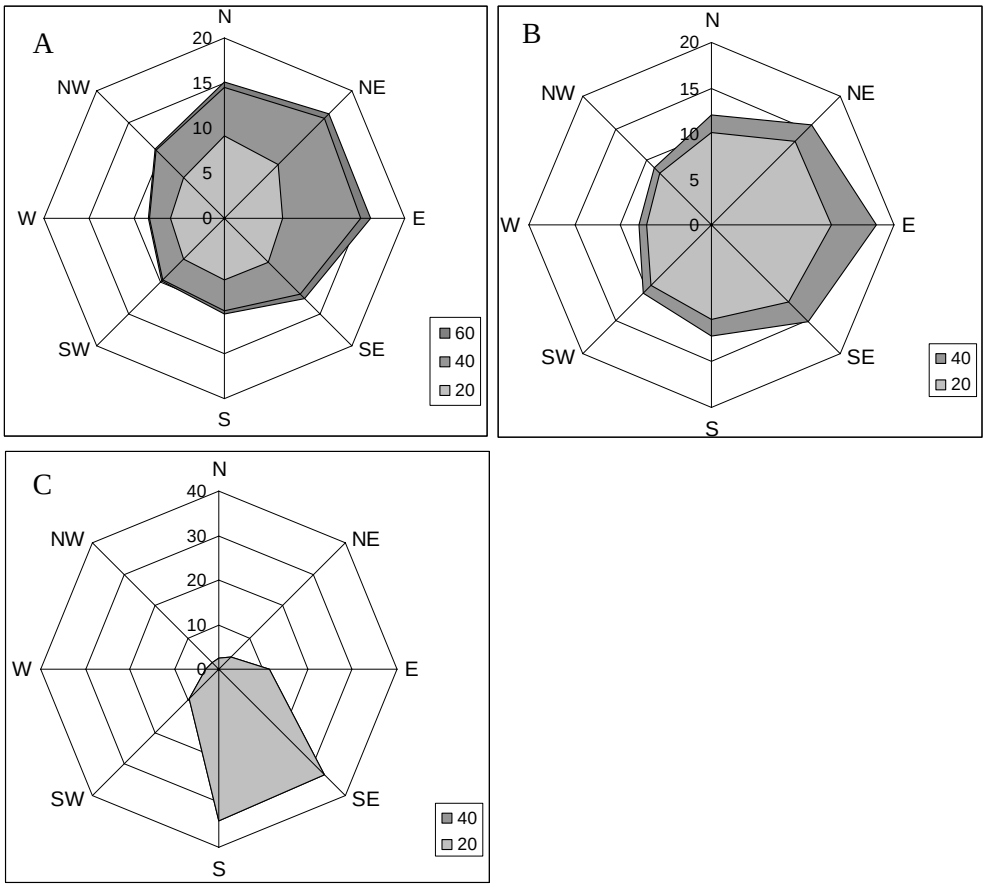

Fig. 7 Distribution of residual currents (%) by speed (cm/s) and direction gradations in (a) surface, (b) middle and (c) near-bottom layers at Mooring N-2, VS block.

ZS Block Mooring Results

Northern (N-3) observations

Here, the N-3 mooring, with the same design as N-2, was deployed. The single-point current meters registered currents at 8, 62 and 127 m horizons. Although the depth on this block is the greatest (130 m) compared to the others, the currents are the smallest. In contrast to cases described above, the zonal component of the currents predominate (Fig. 8), especially in the near-bottom layer. Flow patterns in the gradations of speed and the directions were calculated. In the subsurface layer the highest repetition corresponds to the western (20%), eastern (19.2%) and southeastern directions (16.4%), and maximum speeds are in the western and southwestern directions (about 66 cm/s). The average speeds are approximately the same with respect to all directions. In the intermediate layer the repetition of western and southeastern currents increases somewhat (22.8% and 24.2%, respectively) with a decreasing share in eastern direction (14.1%), but as a whole the nature of distribution does not change. The maximum values of speed also coincide with the western direction, but they decrease more than two times (30.8 cm/s). In the near-bottom layer a change in the nature of distribution is more apparent. Here, the currents in the eastern direction clearly predominate (45.7%), and the share in the western direction sharply decrease (3.5%). The maximum and average values of speed are approximately the same as in the middle layer, with exception of the eastern directions, where they increase somewhat.

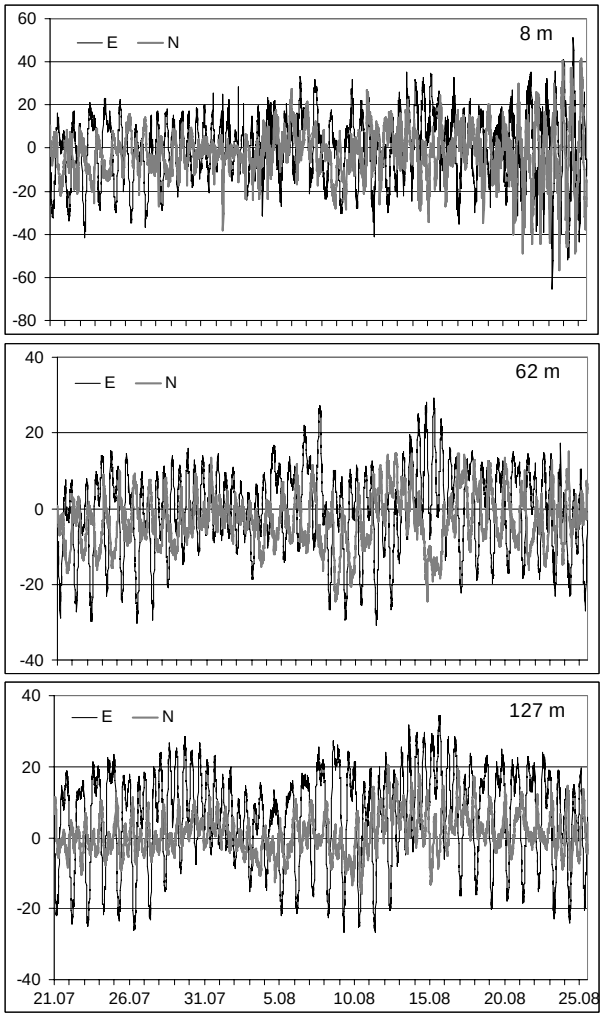

Fig. 8 Meridional (N) and zonal (E) velocity components (cm/s) at depths 8, 62 and 127 m obtained at mooring N-3 ZS block (July 21–August 26, 2006).

Amplitudes and phases of the main tidal constituents were calculated for each horizon, and the ellipses of the main diurnal and semidiurnal constituents are represented in Figure 9. It is most interesting that at 127 m depth the amplitude of the diurnal harmonics increases somewhat in comparison with two upper layers (an analogous phenomenon was observed in the region of Okhotsk port (Sea of Okhotsk northwestern shelf) (Putov and Shevchenko, 2001). Current speeds for the main diurnal and semidiurnal components are approximately the same; in the surface and middle layers the ellipses are compressed and oriented along the axis east–west and northwest directions; and the rotation of vectors in the tidal cycle is counter-clockwise. In the near-bottom layer the ellipses are oriented almost along-latitude, the compression ratio somewhat decreases, and the direction of rotation remains counterclockwise. For the semidiurnal components, in particular S_2, an increase in speed and a decreasing compression ratio of ellipses in the near-bottom layer is also characteristic (not shown).

The intensity of non-tidal flows in the northern part of the ZS block is comparatively small. Against the background flows at all horizons, variations with periods of approximately 1 week are expressed more weakly than on the VS block. A notable strengthening of the flows in the southeastern direction was observed on August 14–16, especially in the middle layer. The most interesting moment was at the end of the observational period when there was a sharp intensification in currents at the surface layer. These currents had a quasi-periodic nature, with a period of approximately 14 hours, which is close to the Coriolis period for deployment at that latitude. This indicates that the inertial flows were the most probable reason for the observed current intensification, with amplitudes reaching 40–45 cm/s. An analogous manifestation of this form of periodic flow, also in the thoroughly heated upper layer, was noted in the region near the port of Okhotsk (Putov and Shevchenko, 2001). Generally, the formation of these flows is connected with strengthening of the wind, which was noted during weather observations taken onboard the R/V *Dmitry Peskov*. At 62 m depth only weak transmissions of these currents are examined, which, as a rule, are most intensive near the thermocline. According to the results of our CTD survey, the thermocline was located at a depth of approximately 20 m, and at depths more than 30 m in this region uniformly cold waters (–1.4ºC) with the sufficiently high salinity (33 psu) were observed.

The flow pattern in the gradations of the speed and the directions (Fig. 10) in the surface layer reveal approximately the same values of repetition in different directions. Flows in the southern (16.7%) and southwestern (17%) directions are weak and separated. In the middle layer, these directions share approximately the same increase (21.2% and 21.4%); in the near-bottom layer the current is well expressed to the east (44.3%).

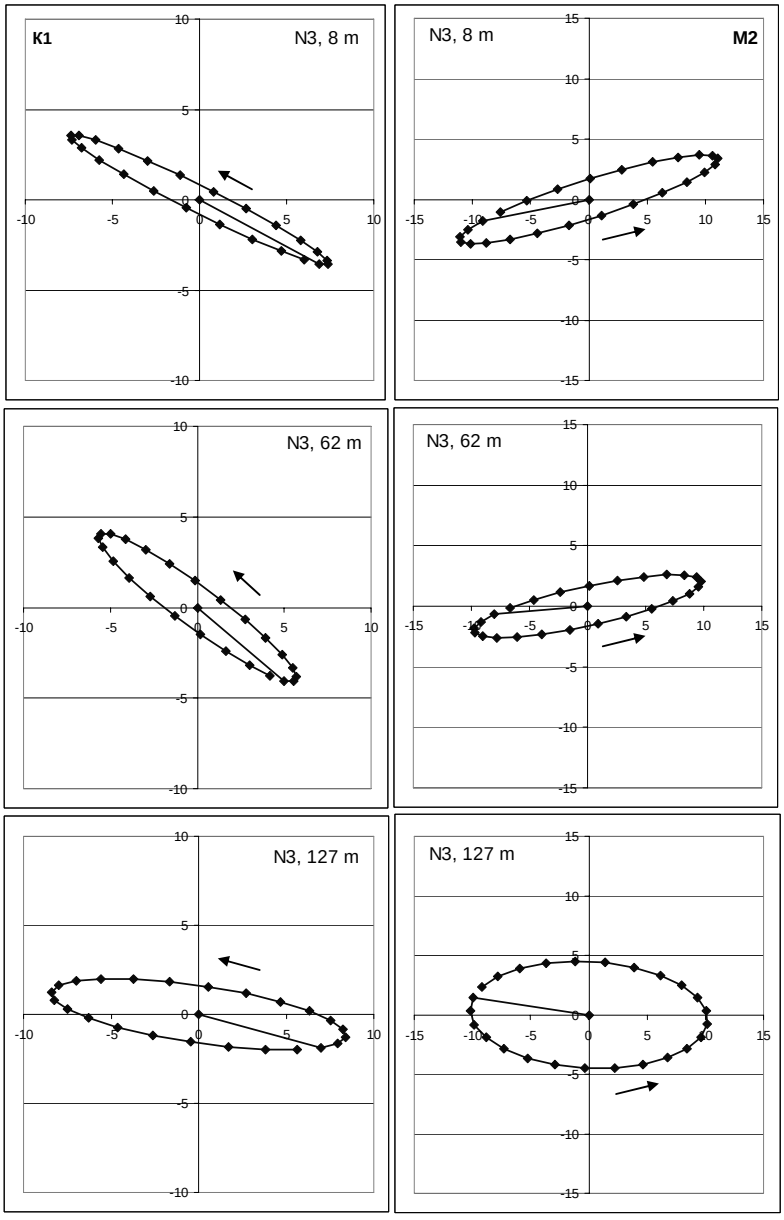

Fig. 9 Current ellipses of the major diurnal K_1 and semidiurnal M_2 tidal constituents at Mooring N-3, northern ZS block at the surface, middle and near-bottom layers, respectively (July 2–August 26, 2006).

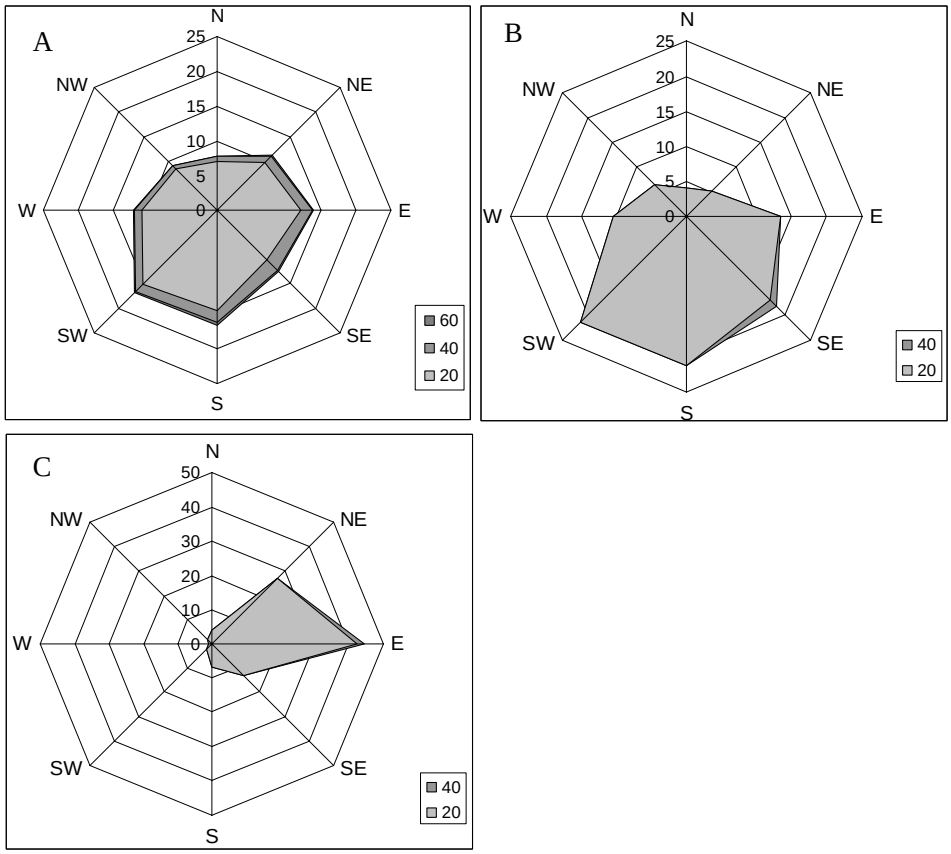

Fig. 10 Distribution of residual currents (%) by speed (cm/s) and direction gradations in (a) surface, (b) middle and (c) near-bottom layers at Mooring N-3, VS block.

Southern (N-4) observations

Mooring N-4 was deployed at a depth of 45 m (Fig. 1, Table 1), and currents measurements were conducted with an ADP in which the water column was divided into the 21 sublayers of 2 m thickness. Deployment conditions were the same as for the N-1 mooring. For observations, the following layers were chosen – the near-bottom (1st layer from the ADP), intermediate (11th layer from the ADP) and surface (21st layer from the ADP). North and east projections are shown in Figure 11.

The role of tides was approximately the same in the N-2 and the N-4 mooring data (in contrast with N-1 and N-3 mooring data). Diurnal tidal currents prevailed, especially in the intermediate and near-bottom layers. To a lesser degree this was characteristic for the surface layer, where the relative role of non-tidal flows is more significant.

The ellipses of the main diurnal harmonic K_1 (Fig. 12) at the surface and intermediate layers are almost identical – they are compressed, elongated along the east–west and south–west axis, and the rotation of vectors in the cycle is clockwise. In the near-bottom layer diurnal flows have a clear reversible nature; their intensity noticeably decreases in comparison with the upper layers. For the O_1 constituent (not shown) the change in rotation is counterclockwise. The ellipses of the main semidiurnal constituent, M_2, are also very similar at the surface and middle layers, with compressed and elongated axes in the northeast–southwest direction. In the near-bottom layer, in contrast to the diurnal flows, the compression ratio of the ellipses decreases, and the direction of vector rotation in all layers is anticyclonic. The contribution to the formation of the tidal currents by another semidiurnal wave, S_2, is insignificant and is not shown.

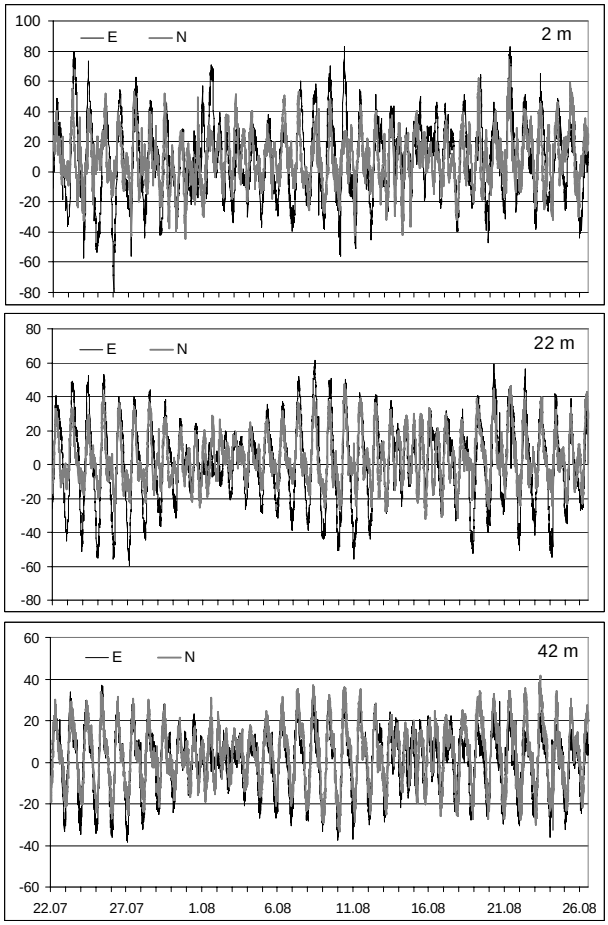

Fig. 11 Meridional (N) and zonal (E) velocity components (cm/s) at depths 2, 22 and 42 m obtained at mooring N-4, ZS block (July 21–August 26, 2006).

Non-tidal flows, similar to other moorings, reveal variations in the synoptic range of periods and high-frequency noise. Their intensity decreases substantially with the depth, with average speeds in the surface layer of about 15 cm/s, in the intermediate layer of approximately 10 cm/s, and in the near-bottom layer of approximately 8 cm/s. The distributions of residual currents in the gradations of speed and direction (Fig. 13) reveal the predominance of flows in the northeastern direction in the upper layer (34.1%). With increasing depth, the flow turns to the north. In the middle layer the portion of northern and northeastern flows is approximately the same (23.7% and 25.2%), and in the near-bottom layer, the flow to the north clearly predominates (31.7%). It is probable that the significant role of the northern component in the distribution of non-tidal currents at the N-4 mooring is connected with the influence of Amur River runoff whose waters, according to the existing knowledge, move as a relatively narrow coastal flow mixing with Sea of Okhotsk waters, and go around the northern part of Sakhalin Island (Shmidt Peninsula).

Conclusions

From current measurements taken in the region adjacent to Shmidt Peninsula, the following conclusions can be drawn.

First, it should be noted that a sufficient amount of high quality data were obtained. This is confirmed by a good agreement in tidal current characteristics at different horizons at each mooring, and are typical according to changes with depth (in particular for the sub-inertia diurnal waves, which are to a lesser degree subjected to baroclinic effects).

Currents on the KV block are different from those located to the north in parameters of higher dynamics. Diurnal tidal currents reach 1 m/s and have characteristics typical at other oil and gas sites of the northeastern shelf of Sakhalin. Non-tidal currents reach 80 cm/s in the surface layer, which exceeds the maximum speeds according to long-term observations in this region in the summer period. The repetition of the flows of southern direction in the middle layer is higher here than over the Piltun–Astokhskaya area for the same season. In the near-bottom layer, the flow is directed to the coast, which should be coordinated with the observations carried out previously.

Diurnal tidal constituents, in spite of their noticeable decrease in comparison with the KV block and at other moorings locations, determine the major role in the formation of currents to the north of Sakhalin. Their influence decreases in proportion to their removal from the coast, and at the deep mooring station at N-3 (ZS block), they are less than semidiurnal currents. In the upper layer at this mooring, intensive quasi-periodic fluctuations (amplitude of approximately 40 cm/s) are also noted.

The oscillatory period is close to the Coriolis period for the measurement sites, which is probably due to the inertial flows. Residual flows, which are caused by the action of variable wind fields, are very intensive in the surface layer. In the lower layers the flow is more consolidated and has a direction predominantly to the southeast in the intermediate layer and south-southeast in the near-bottom layer at the VS block.

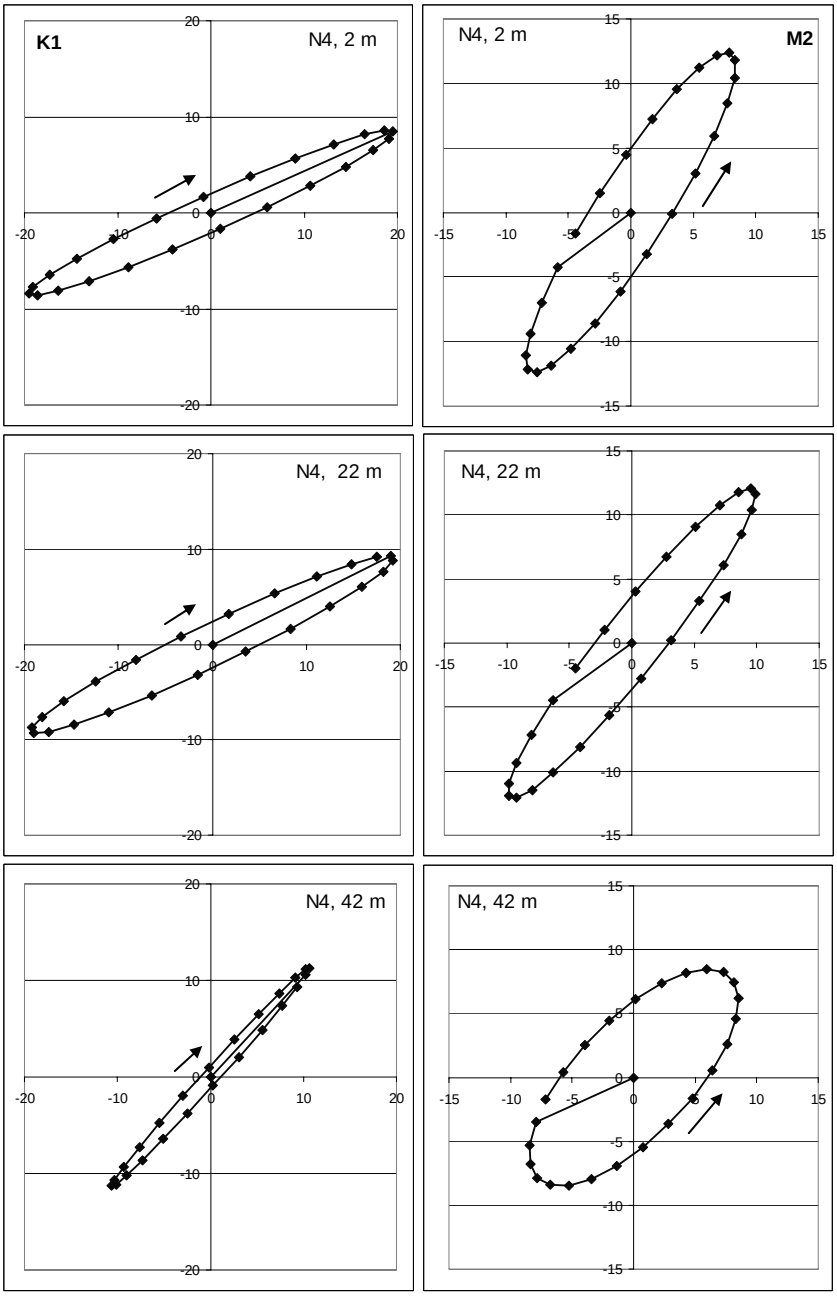

Fig. 12 Current ellipses of the major diurnal K_1 and semidiurnal M_2 tidal constituents at Mooring N-4, southern ZS block at the surface, middle and near-bottom layers, respectively (July 21–August 26, 2006).

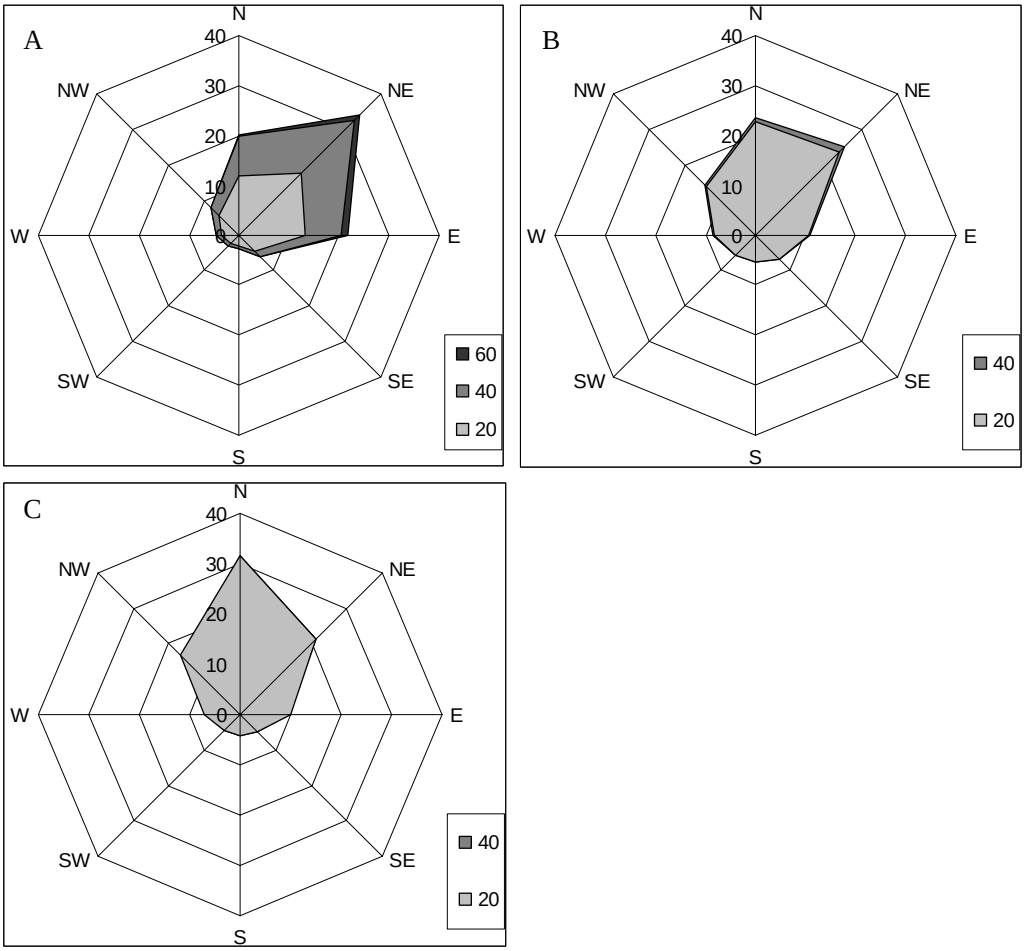

Fig. 13 Distribution of residual currents (%) by speed (cm/s) and direction gradations in (a) surface, (b) middle and (c) near-bottom layers at Mooring N-4.

On the ZS block at mooring N-3, the currents in the southern and southwestern directions are separated in the middle layer, and are oriented to the east in the near-bottom layer. In the southern part of the ZS block (coastal mooring N-4), the currents are oriented to the northeast direction in the intermediate layer and to the north in the near-bottom layer.

The current measurements carried out have made it possible for the first time to collect data on ocean dynamics in the area adjacent to the northern part of Sakhalin, in the place where East Sakhalin Current originates.

There is an additional important practical significance for obtaining these results: for continuing offshore oil and gas development, they will be required for evaluating the possible loads on the offshore constructions and for assessing the most probable direction of propagation of pollutants, which are dangerous for marine and human life.

References

Kochergin, I.E., Rybalko, S.I., Putov, V.F. and Shevchenko, G.V. 1999. Some results of the data analysis by current instrumental measurements of currents on the Piltin-Astokh and Arkutun-Dagi squares at the North-Eastern Sakhalin. pp. 96–113 *in* Hydrometeorological and Ecological Conditions of the Far-Eastern Seas: Impact Assessment to the Marine Environment. Dalnauka, Vladivostok (in Russian).

Krasavtsev, V.B., Puzankov, K.L. and Shevchenko, G.V. 2000. Up-welling wind formation at the North-Eastern shelf of the Sakhalin. pp. 106–120 *in* Hydro-meteorological and Ecological Conditions of the Far-Eastern Seas: Impact Assessment to the Marine Environment. Dalnauka, Vladivostok (in Russian).

Krasavtsev, V.B., Popudribko, K.K. and Shevchenko, G.V. 2001. Spatial structure of the non-tidal currents on the North-Eastern shelf of Sakhalin by 1990 measurements. pp. 48–61 *in* Dynamic Processes at the Sakhalin and Kuril Shelves. Yuzhno-Sakhalinsk: IMGG FEB RAS (in Russian).

Rybalko, S.I. and Shevchenko, G.V. 2003. Seasonal and spatial variability of sea currents on the Sakhalin northeastern shelf. *J. Pac. Oceanogr.* **1**: 168–178.

Popudribko, K.K., Putov, V.F. and Shevchenko, G.V. 1998. Characteristics of marine currents assessment at the Piltun–Astokh area (North-Eastern shelf of Sakhalin). *Meteorol. Hydrol.* **8**: 82–95 (in Russian with English translation).

Putov, V.F. and Shevchenko, G.V. 1998. The features of tidal regime in the northeastern shelf of Sakhalin. pp. 61–82 *in* Hydrometeorological Processes on the Shelf: Impact Assessment to the Marine Environment. Dalnauka, Vladivostok (in Russian).

Putov, V.F. and Shevchenko, G.V. 2001. Current instrumental measurements analysis at the North-Western part of the Sea of Okhotsk. pp. 36–47 *in* Dynamic Processes at the Sakhalin and Kuril's Shelves. Yuzhno-Sakhalinsk, IMGG FEB RAS (in Russian).

Tambovsky, V.S. and Shevchenko, G.V. 1999. Ice drift characteristics under influence of the tides and the wind at the North-Eastern shore of the Sakhalin island. pp. 114–137 *in* Hydrometeorological and Ecological Conditions of the Far-Eastern Seas: Impact Assessment to the Marine Environment. Dalnauka, Vladivostok (in Russian).

Shevchenko G.V. and Rybalko, S.I. 2003. Distribition composition method applying to the extremely currents calculation (on the North-Eastern shelf of Sakhalin island). pp. 34–48 *in* Hydrometeorology and Ecology of the Far-East. Dalnauka, Vladivostok (in Russian).

Shevchenko, G.V. 2004. Extremely currents calculation (on the Piltun-Astokh oil field at the North-Eastern shelf of Sakhalin island). *Meteorol. Hydrol.* **1**: 53–73. (in Russian with English translation).

Current mooring observations in the area of the South Kuril Islands

Georgy Shevchenko[1], Gennady Kantakov[2*] and Valery Chastikov[2]

[1] Institute of Marine Geology and Geophysics FEB RAS, Yuzhno-Sakhalinsk, Russia
E-mail shevchenko@imgg.ru
[2] Sakhalin Research Institute of Fisheries and Oceanography (SakhNIRO), Yuzhno-Sakhalinsk, Russia
E-mail: okhotsk@sakhniro.ru
* now at Far-Eastern Ecological Center Ltd., Yuzhno-Sakhalinsk, Russia

Abstract

Our knowledge of dynamic processes in the area adjacent to the South Kuril Islands is very limited because of a lack of current mooring observations. The information related to currents in this region was obtained from satellite-tracked drifters (Rabinovich and Thomson, 2001; Ohshima *et al.*, 2005). To investigate currents in this region, the Sakhalin Research Institute of Fisheries and Oceanography installed two moorings in the shelf waters of Urup and Kunashir islands in 2003. Experimental studies of dynamic processes were conducted from 2004–2005 in the areas adjacent to Kunashir Island. Diurnal tidal currents strongly dominate on the northern shelf of Urup Island, especially the east-directed component. Tidal currents are almost rectilinear and very steady. Stable east-directed residual currents with an average velocity of 10–12 cm/s were found from April until September which means that there was an outflow of Okhotsk Sea water to the Pacific Ocean through Urup Strait during this period. We found significant amplification of the current in October and November, with the current direction becoming northeast. Autumn typically is a time of atmospheric fields changing to the so-called winter monsoon, with its strong northwesterly winds; however, we did not find this changing in the fall of 2003, from reanalysis data. Another cause of current amplification probably followed, besides the baroclinic effect. However, the noted phenomena are still unclear because there were no salinity sensors at the moorings. A temperature maximum (8–9°C) was found in the second half of October (about two times greater than in August). A similar current amplification was observed near Ekaterina Strait in September–October. We also found tides weakening at this time.

Introduction

Our knowledge of dynamic processes in the area adjacent to the South Kuril Islands is very limited because of the scarcity of current mooring observations. Direct current measurements have been carried out in Ekaterina and Freez straits (Luchin, 1996; Fux, 1997) but they were relatively short period observations (two or three weeks) which were focused on the study of tidal currents. Very strong tidal currents which cause mixing of the Ohkotsk Sea and Pacific Ocean waters were found in the straits. The same information related to currents in this region was also obtained from satellite-tracked drifters (Thomson *et al.*, 1997; Rabinovich, Thomson, 2001; Ohshima *et al.*, 2005). Strong diurnal tidal motions were found on the shelf waters of Urup and Iturup islands. Low-frequency eddy-induced drifter oscillations were observed in the area of the Kuril Trench.

To investigate currents in this region, the Sakhalin Research Institute of Fisheries and Oceanography installed two moorings on the Okhotsk Sea shelf of Urup and Kunashir islands in 2003. Experimental studies of dynamic processes were conducted from 2004–2005 in the areas adjacent to Kunashir Island. Mooring current measurements were mainly directed to the study of seasonal changes in circulation.

Observations

The first mooring “Leya-1” was installed on the shelf of Urup Island on February 28, 2003, at coordinates 46°28′ N and 150°09′ E (Table 1, Fig.1). Total depth in this spot equaled 110 m and a current meter, SonTek Argonaut MD, was fastened at a depth of 30 m. The current meter included a water temperature sensor. The mooring was lifted on board the R/V *Dmitry Peskov* on November 19, 2003. The period of observations amounted to 265 days.

The second mooring "Leya-2" was installed on the shelf of Kunashir Island on June 10, 2003, at coordinates 44º39′ N 146º26′ E, close to Ekaterina Strait. Total depth in this spot equaled 126 m and an acoustic Doppler current profiler, SonTek ADP, was placed on the sea bottom housed in a special stainless frame. The ADP measured currents in 15 layers with each layer 8 m thick. The mooring was lifted onto the R/V *Dmitry Peskov* on October 16, 2003. The period of observations amounted to 127 days.

The experimental study of currents was continued on August 2, 2004. The mooring "Leya-3", with the same equipment used for Leya 2, was installed a small distance east of Leya-2 (Table 1). The depth was 130 m, and the ADP measured current velocities in 15 layers of thickness 8 m each. Unfortunately, one block of ADP memory was damaged which resulted in significant data gaps from August 2 to December 10. Because of the gaps, we did not use these data for analysis. The mooring was lifted onto the R/V *Dmitry Peskov* on June 30, 2005.

Almost simultaneous to the deployment of Leya 2, current mooring measurements were carried out on the Pacific side of Ekaterina Strait (Fig.1, Table 1). The mooring "Olga" was installed on August 3, 2004 (current measurements started at 0:00 Sakhalin summer time, August 4). A three-dimensional acoustic current meter, SonTek Argonaut, was used. Total depth was 210 m, and the depth of the current meter was about 45 m. The mooring was fixed by a 200-kg ballast, and an acoustic breaker, Edge Tech, was fastened 3 m above it. The length of the halyard was 160 m, and the vertical tension of the halyard was provided by several silumin buoys which were fastened above the current meter. The number of buoys was insufficient to hold the current meter in place, so the depth of the current meter was changed under the influence of the currents (mainly tidal currents). This effect was noted from the hydrostatic pressure data (Argonaut was fitted with water temperature and pressure sensors). The mooring was lifted onto the R/V *Dmitry Peskov* on July 3, 2005.

Table 1 Information about SakhNIRO moorings in the area of South Kuril Islands.

Mooring	Current meter	Latitude (N)	Longitude (E)	Total depth (m)	Current meter depth (m)
Leya-1	Argonaut MD	46°28′	150°09′	110	30
Leya-2	ADP	44º39′	146º26′	126	15 layers
Leya-3	ADP	44º41′	146º42′	130	15 layers
Olga	Argonaut MD	44º11′	146º51′	210	45
Shalila	Argonaut MD	43º30′	145º51′	27	25

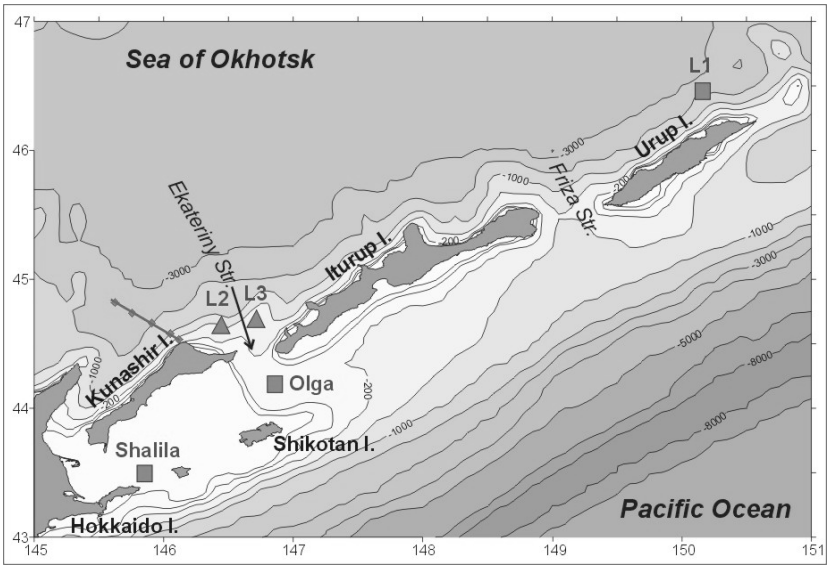

Fig. 1 Mooring locations in the areas adjacent to the South Kuril Islands. Moorings Leya-1, -2, and -3 are marked by L1, L2, and L3, respectively.

About one and half months earlier, on May 14, 2005, the mooring "Shalila" was installed near Tanfilieva Island (Fig. 1, Table 1). A three-dimensional acoustic current meter, SonTek Argonaut, was placed in a crab trap which was set on the sea bottom. Total depth was about 27 m, and currents were measured at 25 m depth. The Argonaut was also fitted with water temperature and pressure sensors. The mooring was lifted onto the R/V *Dmitry Peskov* on October 29, 2005.

Results and Discussion

East- and north-directed current components, which were measured on the shelf waters of Urup Island, are shown in Figure 2. Diurnal tidal currents strongly dominate, especially the east-directed component. Tidal currents are almost rectilinear and very steady. A well-expressed fortnightly modulation of tides was found, which is typical for areas with predominantly diurnal waves. The amplitude of the main diurnal constituent K_1 measured 17 cm/s, and the main semidiurnal M_2 constituent measured 10 cm/s.

Ten-day mean vectors of residual currents (tides were predicted and subtracted) on the shelf of Urup Island and wind vectors (reanalysis data) are shown in Figure 3. We found a stable east-directed residual current with an average velocity of 10–12 cm/s from April until September which means that there was an outflow of Okhotsk Sea water to the Pacific Ocean through Urup Strait during this period. We found significant amplification of the current in October and November, with the current direction becoming northeast.

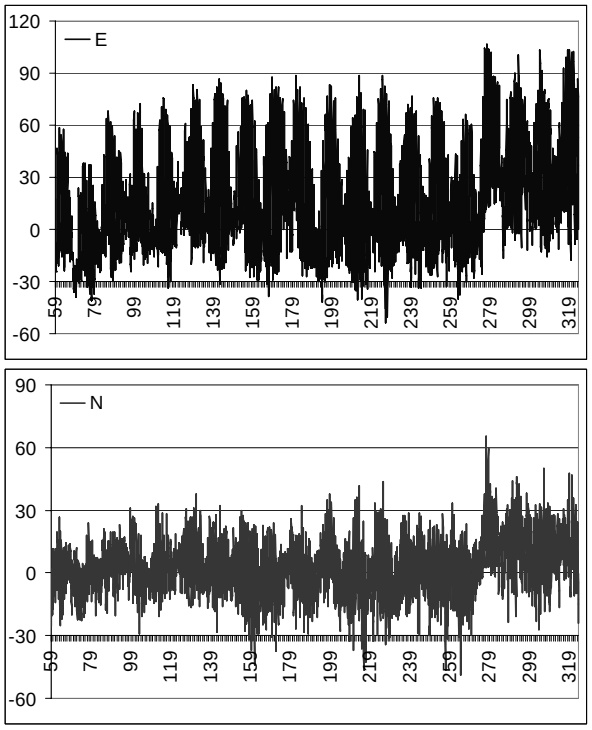

Fig. 2 East-directed and north-directed current components (cm/s), Leya-1 mooring. Bottom axis is time (2003, Julian days).

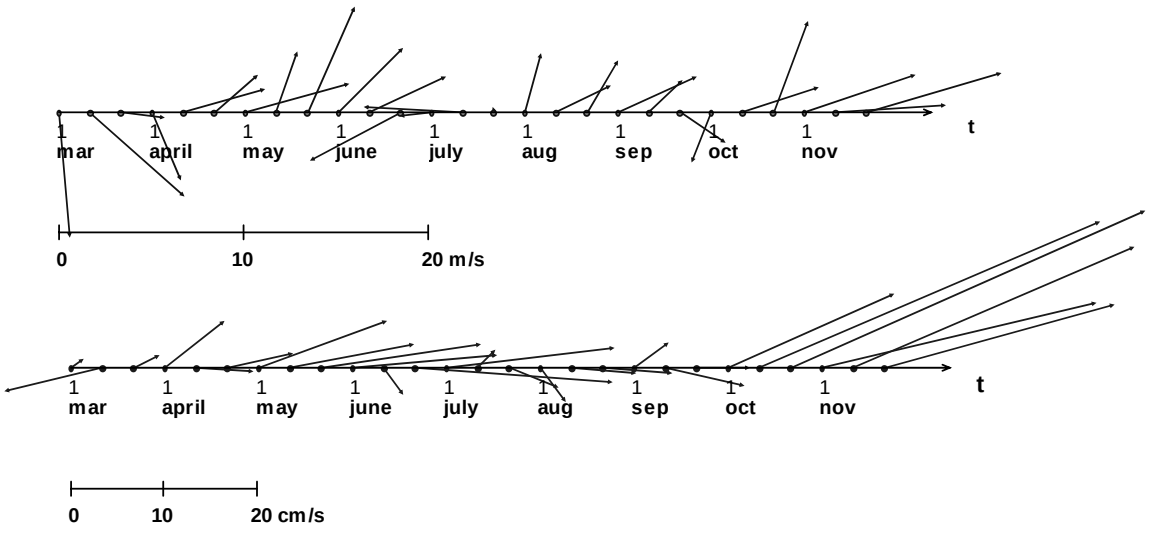

Fig. 3 Ten-day mean vectors of residual currents (Leya-1 mooring, bottom) and wind (reanalysis, top) from March 1 to November 19, 2003.

Autumn typically is a time of atmospheric fields changing to the so-called winter monsoon, with its strong northwesterly winds; however, we did not find this changing in the fall of 2003. Another cause of current amplification may have been due to changes in water temperature and salinity. The current meter had a temperature sensor but no salinity sensor, so we could not study salinity changes. It is very interesting that a temperature maximum (8–9°C) was found in the second half of October, which was about two times greater than in August (Fig. 4). This late temperature increase is probably connected with current amplification.

East and north-directed current components on the shelf of Kunashir Island (Leya-2 mooring) are shown in Figure 5. Diurnal tidal currents strongly dominate, especially in the north-directed component. Tidal currents are almost rectilinear and steady until September. A well-expressed fortnightly modulation of tides was found from June to August. The amplitude of the main diurnal constituent K_1 measured 25 cm/s, and that of the main semidiurnal constituent M_2 was 12 cm/s.

Five-day mean current vectors in the middle and near-bottom layers in the area adjacent to Ekaterina Strait (Leya-2) are shown in Figure 6. Southeasterly currents (which correspond to the outflow to the Pacific Ocean), with an average velocity of 10–15 cm/s were from June until mid-September. Significant current amplification and counter-clockwise vector turning were observed in the fall season. A northeasterly current was found in the middle layer and a northerly current in the near-bottom layer. The amplification was similar to that on the Urup shelf.

A strong northeasterly current was observed from January to mid-February 2005 (Leya-3 mooring, see Fig. 7). From the middle of February, an outflow to the Pacific Ocean was observed, especially in the middle layer.

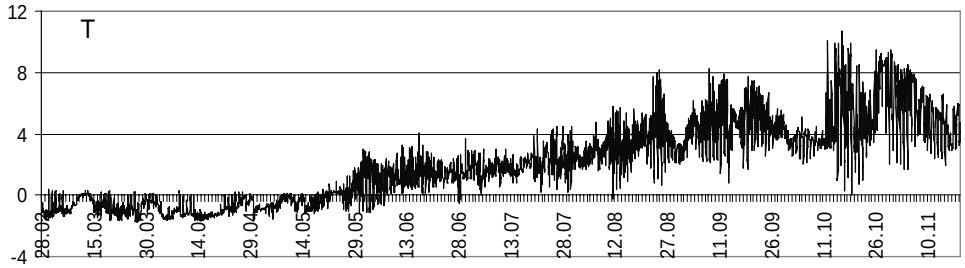

Fig. 4 Water temperature changes (°C) on the shelf of Urup Island at 30 m depth.

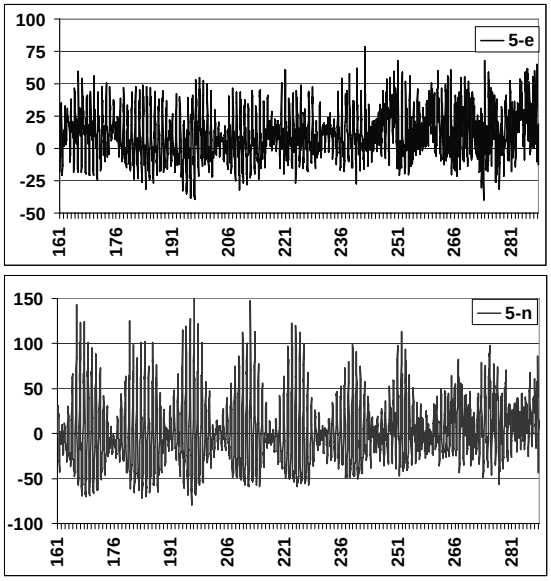

Fig. 5 East-directed and north-directed current components (cm/s), Leya-2 mooring, fifth layer (about 80 m depth). Bottom axis is time (2003, Julian days).

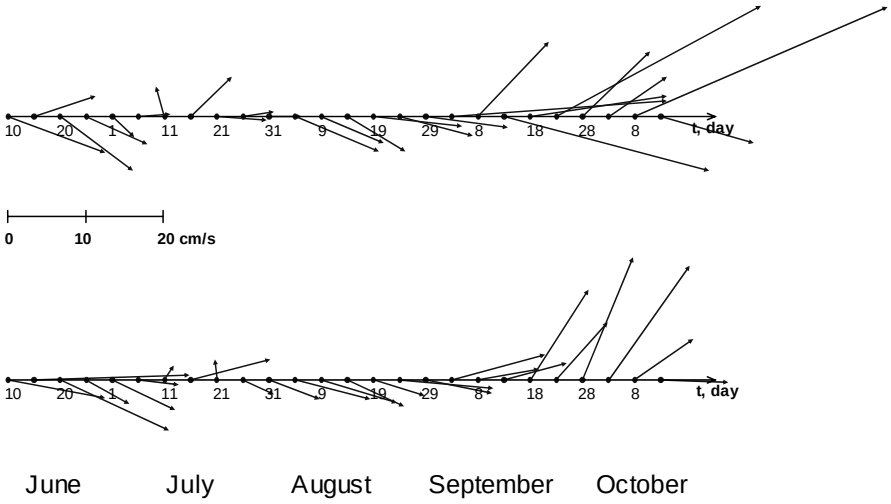

Fig. 6 Five-day mean vectors of residual currents at a depth of 48 m (middle layer) and 120 m (near-bottom layer) on the Kunashir shelf (Leya-2 mooring) from June 10 to October 16, 2003.

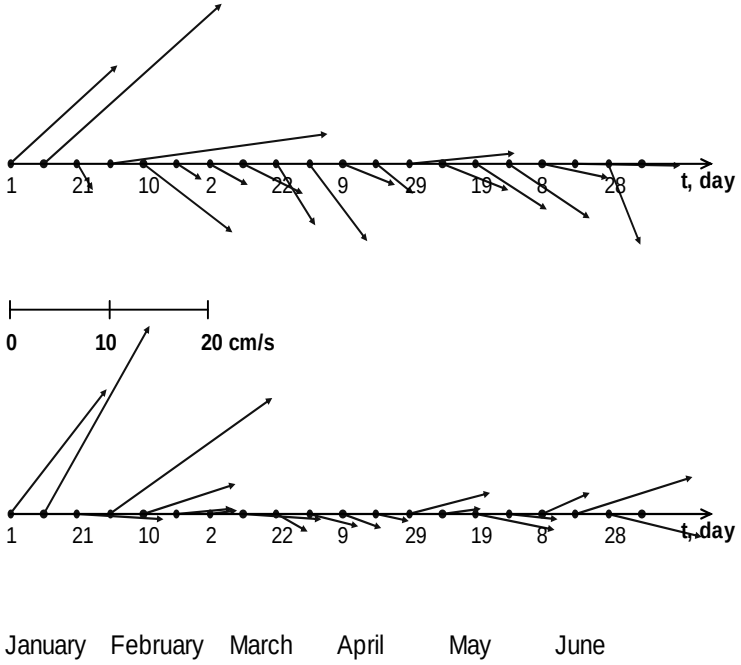

Fig. 7 Ten-day mean vectors of residual currents at a depth 48 m (middle layer and 120 m (near-bottom) on the Kunashir shelf (Leya-3 mooring) from January 1 to June 30, 2005.

East and north-directed current components on the shelf of Tanfilieva Island (Shalila mooring) are shown in Figure 8. Diurnal tidal currents strongly dominate, in both east and north-directed components. Tidal currents are almost rectilinear (the larger axis of tidal ellipses has a southwest–northeast orientation) and steady until August. A well-expressed fortnightly modulation of tides was found from May–July and some instability occurred in August–October. The amplitude of the main diurnal constituent O_1 measured 15 cm/s, and that of the main semidiurnal wave M_2 was 4 cm/s. Small residual currents were found, with an average velocity of about 2–3 cm/s.

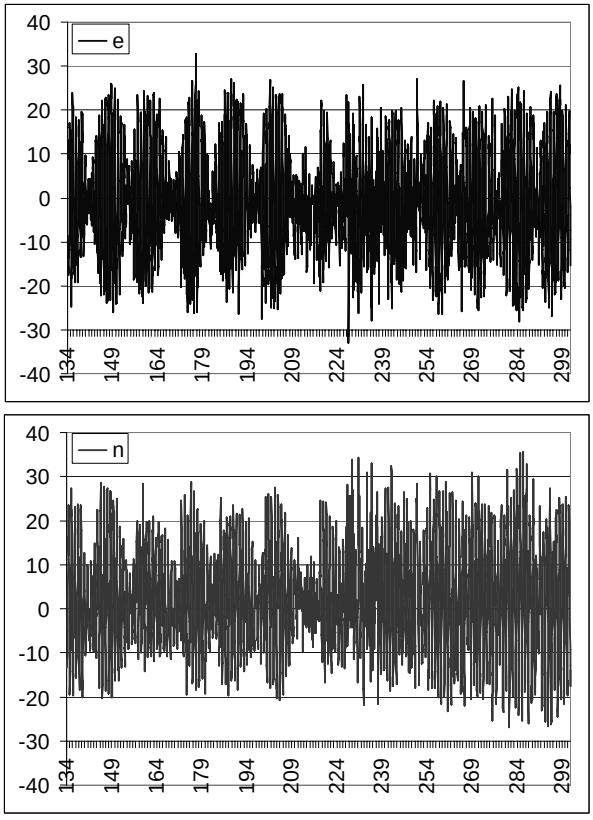

Fig. 8 East-directed and north-directed current components (cm/s), Shalila mooring. Bottom axis is time (2005, Julian days).

Conclusions

- Long-term observations of currents near the South Kuril Islands revealed strong diurnal tidal currents, which significantly dominate all other types of motions in this region;
- Amplification of northeasterly currents on the Okhotsk Sea shelf of the South Kuril Islands was found in October–January. This amplification is probably induced by a baroclinic gradient ;
- Outflow through Urup Strait to the Pacific Ocean was observed from March until September;
- The outflow through Ekaterina Strait to the Pacific Ocean was observed from February to mid-September, especially in the middle layer;
- Small residual currents were found near Tanfilieva Island.

References

Luchin, V.A. 1996. Characteristics of tidal motions in the Kuril Straits. pp. 188-193. *in* Proceedings of the Workshop on the Okhotsk Sea and Adjacent Areas *edited by* Y. Nagata, V.B. Lobanov and L.D. Talley, PICES Sci. Rep. No. 6, Sidney, BC, Canada.

Ohshima, K.I., Wakatsuchi, M. and Saitoh, S. 2005. Velocity field of the Oyashio region observed with satellite-tracked drifters during 1999–2000. *J. Oceanogr.* **61**: 845–855.

Fux, V.R. (*Ed.*) 1997. Oyashio Origin. St. Peterburg State University, 248 pp.

Rabinovich, A.B. and Thomson, R.E. 2001. Evidence of diurnal shelf waves in satellite-tracked drifters trajectories off the Kuril Islands. *J. Phys. Oceanogr.* **31**: 2650–2668.

Thomson, R.E., LeBlond, P.H. and Rabinovich, A.B. 1997. Oceanic odyssey of satellite-tracked drifters: North Pacific variability delineated by a single drifter trajectory. *J. Oceanogr.* **53**: 81–87.

Energy characteristics of tidal and residual level variations in the Okhotsk Sea from satellite altimetry data

Georgy Shevchenko[1] and Alexander Romanov[2]

[1] Institute of Marine Geology and Geophysics FEB RAS, Yuzhno-Sakhalinsk, Russia
E-mail shevchenko@imgg.ru
[2] Federal State Unitary Enterprise Russian Institute of Satellite Device Engineering (FSUE "RISDE"), Moscow, Russia

Abstract

A unified satellite altimetry database, TOPEX/Poseidon (1993–2002) and Jason-1 (2002–2007) containing about 7,000 locations, was created for the Okhotsk Sea and adjacent areas. Amplitudes and phases of main tidal consituents were calculated for each location, and maps of tidal character and height were constructed. It is shown that diurnal waves dominate in the amphidromic areas of semidiurnal waves in Sakhalinsky Bay, near the Yamskie Islands, and the eastern Sakhalin coastline. Tidal energy increases along the axis southwest–northeast and reaches maximal values in Shelikhov Bay. Root mean square amplitudes of residual time series were taken to represent non-tidal sea level variations. Areas with the highest values were considered to be energetic ocean zones. They have been found near the southeastern Kamchatka coast and on the Pacific shelf side of Hokkaido where mesoscale eddies are often observed. To a lesser extent they relate to the whole Kuril-Kamchatka deep trench (especially to its outside edge), as well as to the western Hokkaido shelf and northern Okhotsk Sea shelf where seasonal changes in currents are significant. A map showing the relative portion of tides and residual variations in total sea level energy has been constructed.

Introduction

Satellite altimetry sea level data are used to study dynamic processes, such as tidal motions, seasonal sea level circulation changes and meso-scale eddy formations in different parts of World Ocean. Areas of high intensity sea level variations are interesting for many scientific and practical reasons. The Okhotsk Sea (OS) is one of these areas because of its very strong tides and non-tidal sea level variations. Satellite altimetry data give us very important information related to the dynamic processes in this area, especially in light of the small number of coastal tide gauges relative to the large area of the OS.

To determine areas with high intensity sea level variation (so-called energetic ocean zones) on the continental shelf and in the marginal seas is difficult because the Global Ocean Tide (GOT) model (Ray, 1999) is not exact enough to determine shallow water zones. To solve this problem, a special modification of the least squares method to determine tidal amplitudes and phases in each location of a sub-satellite track was developed (Shevchenko and Romanov, 2004). This method is similar to the algorithm used by Cherniawsky *et al.* (2001). In this way, we estimated the average amplitude of tidal and residual (non-tidal) sea level variations as an index of energy zones in the OS and its adjacent areas.

Data and Methods

TOPEX/Poseidon and Jason-1 satellite altimetry data were used as initial sea level data. These data were obtained from the NASA Physical Oceanography Distributed Active Archive Center at the Jet Propulsion Laboratory, California Institute of Technology.

For sea level calculation relative to a reference ellipsoid (the first-order definition of the non-spherical shape of the Earth as an ellipsoid of revolution with equatorial radius of 6378.1363 km and a flattening coefficient of 1/298.257) by satellite altimeter data, the following equation was applied:

$$H_y = H_c - (H_A + C_{WT} + C_{DT} + C_I + C_{EMB}) - H_{IB}, \quad (1)$$

where H_y is the sea level, H_c is the height of the

satellite's orbit, H_A is the altimetry range, C_{WT} is the wet troposphere correction, C_{DT} is the dry troposphere correction, C_I is the ionosphere correction, C_{EMB} is the electromagnetic bias correction, and H_{IB} is the inverse barometer correction.

All necessary corrections to the altimetry signal (except tidal GOT model corrections) were taken from a TOPEX/Poseidon MGDR-B dataset and were considered according to recommendations in Benada (2003). The standard technique described in Benada (2003) was used to obtain the reliability of altimetry data. A previously created (Shevchenko and Romanov, 2004, 2006) TOPEX/Poseidon sea level database (1993–2002) for the Okhotsk Sea and adjacent areas (northern Japan Sea, northwestern part of Pacific Ocean) was further developed using data of the Jason-1 satellite (2003–2007) which has the same orbits as TOPEX/Poseidon, and in a space 8 degrees southward. The total number of locations was about 7,000. The length of data sets varied significantly in different parts of the OS. Some gaps were due to ice cover, especially in the northwestern OS. For the area adjacent to Shantary Islands, the data sets were too short for the exact determination of tidal amplitudes and phases. Because of this problem, we did not analyse the sea level variations in this area.

Calculations of tidal amplitudes and phases were carried out for each location using the authors' method. The root mean square amplitude of the residual series (*Ar*) was used to estimate the quality of the database. The exact attachment of Jason-1 data demanded additional mean sea level correction. Without this correction, the amplitude of the residual oscillations would have an unrealistically large value. By including the correction, *Ar* values were not more than 20 cm, and in the main part of the study area, not more than 10 cm. Usually residual variations on coastal tide gauges have a similar amplitude. We consider areas with high amplitude as energy production zones.

The average amplitude of 8 main tidal constituents (4 diurnal Q_1, O_1, P_1, K_1 and 4 semidiurnal N_2, M_2, S_2, K_2) is considered as an index of tidal variation intensity:

$$L = (H_{Q1}^2 + H_{O1}^2 + H_{P1}^2 + H_{K1}^2 + H_{N2}^2 + H_{M2}^2 + H_{S2}^2 + H_{K2}^2)^{1/2}. \quad (2)$$

Another index that is the relationship between amplitudes of main diurnal and semidiurnal waves is

$$R = (H_{O1} + H_{K1}) / (H_{M2} + H_{S2}), \quad (3)$$

which indicates zones where diurnal ($R > 2$) and semidiurnal ($R < 0.5$) waves predominate. Spatial distributions of *L*, *R* and *Ar* were constructed for the OS and adjacent areas.

Results and Discussion

The spatial distribution of the average tidal amplitude *L* is shown in Figure 1. This index increases from 25–30 cm in the southwestern part of the OS to 150 cm in the northeastern part. Maximal values (more than 200 cm) were found in Shelikhov Bay, in the northeastern part of the OS. In the 1980s, there was a plan to construct a tidal power station in this area (Bernstein, 1987). Some effects of the proposed station's dam on tidal amplitudes and phases were analysed by Nekrasov and Romanenkov (2003). They found that high tidal amplitudes occurred on the northern OS shelf, on the western shelf of Kamchatka peninsula, and in the northern part of Tatar Strait (Northern Japan Sea). Small amplitudes were detected in the central Japan Sea, in the southwestern OS and in the deep Pacific Ocean far from the Kuril Islands.

The spatial distribution of index *R* (Fig. 2) indicates a dominant role of diurnal tides in the OS that is in good agreement with the results of numerical simulations (Kowalik and Polyakov, 1998; Nekrasov and Romanenkov, 2003). We found areas with *R* values less than 1 near the northern OS coastline and in the part of the Pacific Ocean which is adjacent to Japan. As mentioned above, we did not analyse sea level variations in the area adjacent to the Shantary Islands where semidiurnal tides strongly predominate. *R* is high (greater than 2) in the middle part of the OS and on the northern and northeastern shelves of Sakhalin Island, especially in amphidromic areas in Sakhalinsky Bay and near the eastern Sakhalin coast. The same results were obtained for the semidiurnal tidal amphidrome near the Yamskie Islands. The presence of these amphidromes was first detected by Ogura (1933) as a result of coastal tide gauge data analysis, and is also verified by numerical modeling. An exception occurred for the east coast of Sakhalin, where an amphidrome was not identified by results of calculations at all (Kowalik and Polyakov, 1998). This amphidrome has an unusually large size due to it's instability (Shevchenko and Romanov, 2004), and *R* reaches its highest values (greater than 10) here.

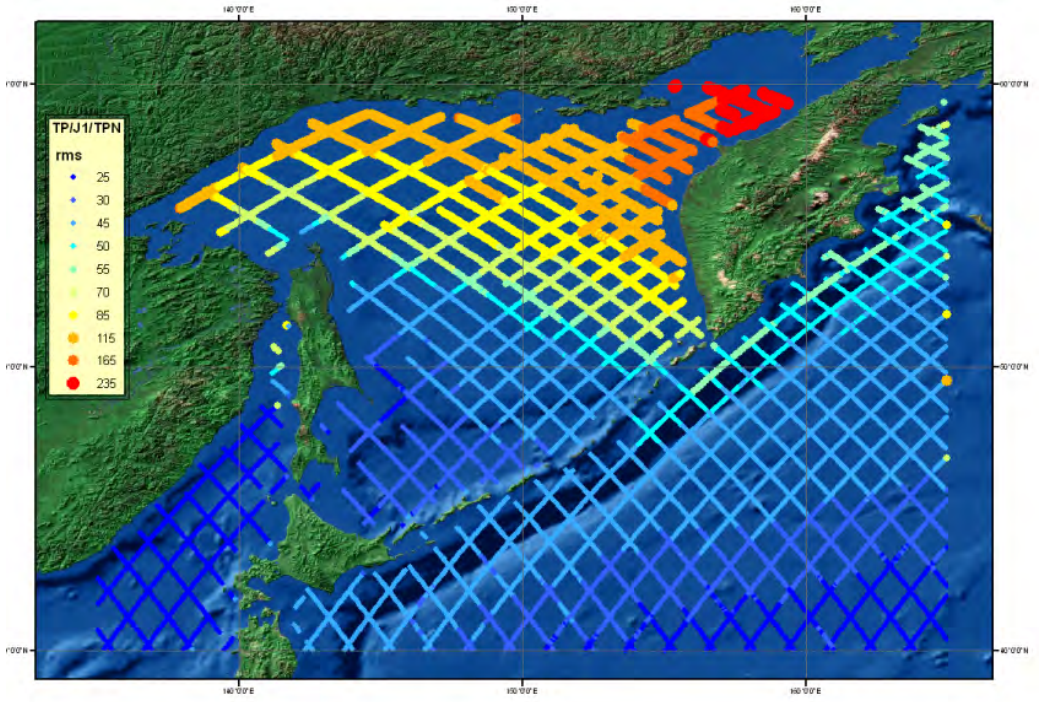

Fig. 1 Spatial distribution of tidal root mean square amplitude *L* in the Okhotsk Sea and adjacent areas. TOPEX/ Poseidon–Jason-1 sub-satellite tracks are shown.

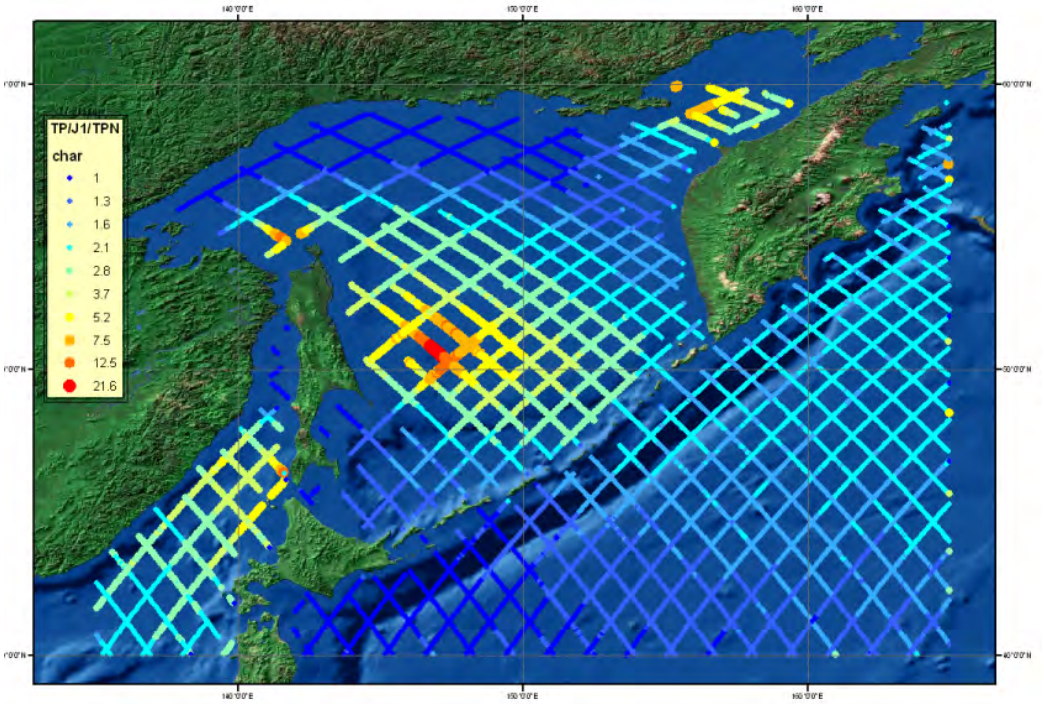

Fig. 2 Spatial distribution of amplitudes of main diurnal and semidiurnal waves (*R*).

The spatial distribution of the root mean square amplitude of residual sea level variations is shown in Figure 3. The Kuril–Kamchatka deep trench, especially in the areas adjacent to Hokkaido–South Kuril Islands and southeastern Kamchatka–North Kuril Islands, are energetic ocean zones. Both these areas are known as areas of intensive meso-scale eddy formation (Bulatov and Lobanov, 1983; Darnitsky and Bulatov, 2005). Another area with high *Ar* values is found in the deep trench (especially to its outside edge) near the middle part of the Kuril Ridge.

We found a zone of intensive eddy formation in the deep Kuril Basin in the southern part of the OS. High values of *Ar* are the result of strong seasonal sea level changes with a maximum in the wintertime and a significant negative surge in the fall (Romanov *et al.*, 2004). This negative surge is produced by strong and stable northerly and northwesterly winds which are typical for autumn (so-called "winter monsoon"). The winter maximum corresponds to winter amplification of the Yamskoe and North Okhotsk Currents. Seasonal sea level changes in the area of the East Sakhalin Current are weaker in comparison to the northern OS shelf, so the eastern shelf of Sakhalin Island is not an area of high *Ar* values, in contrast to Sakhalinsky Bay and Amursky Liman. High seasonal sea level changes in these latter areas are induced by Amur River runoff. We also found some influence of Amur River runoff in the northern part of Tatar Strait, especially in the area adjacent to the mainland coastline. The area of the Tsushima Warm Current is also a region of high *Ar* amplitude. This effect is brought about by strong seasonal changes in the Current, which is weak in the wintertime and reaches maximal intensity in summer. In the central part of the OS, on the shelf of the Kuril Islands and in the area adjacent to western Kamchatka coast, *Ar* values are small, less than 10 cm.

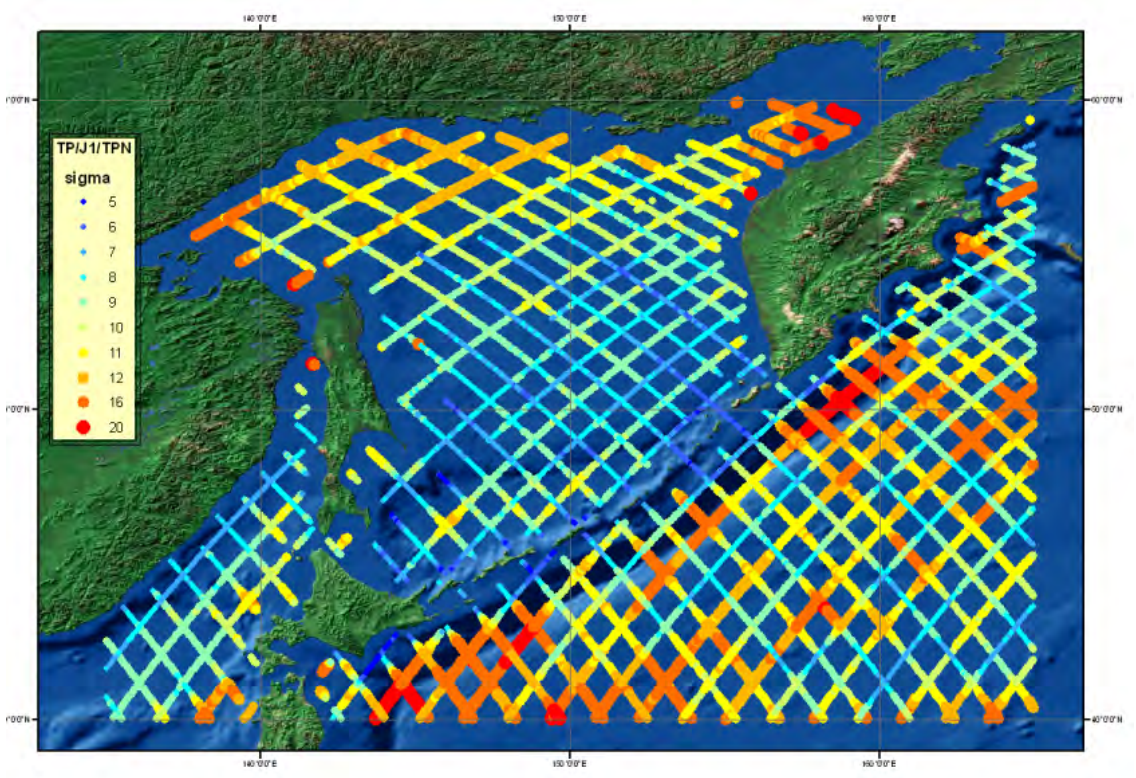

Fig. 3 Spatial distribution of root mean square amplitude *Ar* residual level oscillations in the Okhotsk Sea and adjacent areas.

Figure 4 shows the spatial distribution of residual oscillation rates in total sea level variance (energy) in the study area. This rate is small (about 10–15%) in the northern, eastern, and especially the northwestern part of the OS because of very high tidal amplitudes. As stated above, the mean amplitude of residual oscillations is relatively high on the northern OS shelf. However, it is small in comparison with the tidal amplitude.

The influence of residual oscillations increases in southwestern part of the OS, especially in the deep Kuril Basin, shallow Terpenia Bay and La Perouse Strait. In the Japan Sea, the rate of residual oscillations increases from the northern part of Tatar Strait to the western Hokkaido and northwestern Honshu shelves where it reaches 50–60% of total sea level variance. Similar values were found in the deep ocean area adjacent to Kuril Islands. The dominant role of residual oscillations is caused by both the decrease in tidal amplitude and the influence of Tsushima and Kuroshio currents seasonal changes and their meander formations.

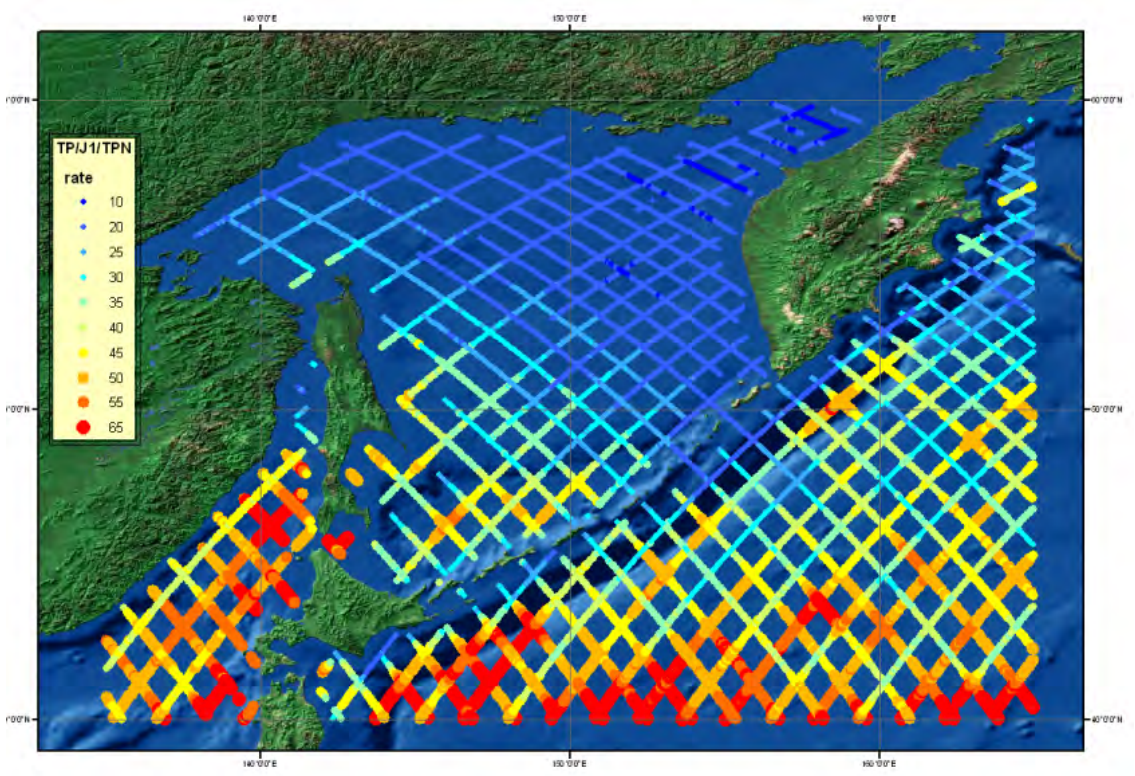

Fig. 4 Spatial distribution of residual oscillation rates in total sea level variance in the OS and adjacent areas (%).

Conclusions

Using a unified satellite altimetry database, TOPEX/Poseidon (1993–2002) and Jason-1 (2002–2007), spatial distributions of root mean square tidal and residual amplitudes were constructed for the OS and adjacent areas.

Diurnal tides were found to predominate over semidiurnal tides in the OS, with the exception of the northern shelf. The relation between amplitudes of main diurnal and semidiurnal tides *R* reaches maximal values in the semidiurnal tide amphidromic areas (Yamskie Islands, Sakhalinsky Bay, eastern Sakhalin shelf). Tidal amplitude reaches maximal values in the northern, eastern, and especially northeastern parts of the OS. It is significantly smaller in the southwestern part of OS, in the central part of Japan Sea, and in the Pacific Ocean far from the Kuril Ridge.

The mean amplitude of residual oscillations indicates zones of intensive eddy formations in the deep Kuril–Kamchatka Trench. Its maximal values are

found in the areas adjacent to Hokkaido–South Kuril Islands and southeastern Kamchatka–North Kuril Islands; smaller values are found in the area of the Middle Kuril Islands. High residual amplitudes on northern OS shelf and western Hokkaido shelf are caused by seasonal changes of sea level and circulation.

Acknowledgement

This work was sponsored by the Russian Foundation of Basic Research (grant 07-05-00637-a).

References

Bernstein, L.B. 1987. Tidal Power Stations. Energoatomizdat, Moscow, 296 pp. (in Russian).

Benada, J.R. 2003. Merged GDR (TOPEX/ POSEIDON) Generation B Handbook Version 2.

Bulatov, N.V. and Lobanov, V.B. 1983. Investigation meso-scale eddies easterly of Kuril Islands from meteorological Earth's satellite data. *J. Earth Res. Space* **3**: 40–47 (in Russian).

Cherniawsky, J.Y., Foreman, M.G.G., Crawford, W.R. and Henry, R.F. 2001. Ocean tides from the TOPEX/POSEIDON sea level data. *J. Atmos. Oceanic Technol.* **18**: 649–664.

Darnitsky, V.B. and Bulatov, N.V. 2005. Structure elements and meso-scale eddy evolution underwater mountains Erimo – Takuie: remote and in-situ observations. *Comm. Fish. Oceanogr.* **2**: 277–302 (in Russian).

Kowalik, Z. and Polyakov, I. 1998. Tides in the Sea of Okhotsk. *J. Phys. Oceanogr.* **28**: 1389–1409.

Nekrasov, A.V. and Romanenkov, D.A. 2003. Prognostic estimation of tidal sea level transformation as result of lager-scale construction in the Beloe and Okhotsk Seas. Level oscillations in seas. Russian State Hydrometeorological University, St. Peterburg, pp. 57–78 (in Russian).

Ogura, S. 1933. The tides in the seas adjacent to Japan. Bull. Hydrographic Dept., Imp. Japan Navy, Vol.7, Tokyo.

Ray, R.D. 1999. A global ocean tide model from Topex/Poseidon altimetry: GOT99.2. – NASA Tech. Memo. 209478.

Romanov, A.A., Sedaeva, O.S. and Shevchenko, G.V. 2004. Seasonal level changes in the Okhotsk Sea from coastal tide gauges and satellite altimetry data. *J. Earth Res. Space* **6**: 59–72 (in Russian).

Shevchenko, G.V. and Romanov, A.A. 2004. Tides characteristics in the Sea of Okhotsk definition from Topex/Poseidon sea level data. *J. Earth Res. Space* **1**: 49–62 (in Russian).

Shevchenko, G.V. and Romanov, A.A. 2006. Seasonal changes of circulation in the upper layer of the Sea of Okhotsk from satellite altimetry data. *Russian Meteorol. Hydrol.* **8**: 59–71 (in Russian with English translation).

Session A2

Sea ice, watermass and freshwater processes/Coastal lagoons

Session Chairs

Yoshihiro Tachibana and Anastasiya Abrosimova

Sea-ice flow from the Okhotsk Sea to the Pacific Ocean through the Nemuro Strait in 2008

Tatsuo Motoi[1], Wing-Le Chan[2], Takuya Miyakawa[3] and Norihisa Usui[1]

[1] Meteorological Research Institute, Japan Meteorological Agency, Tsukuba, Japan. E-mail: tmotoi@mri-jma.go.jp
[2] Frontier Research Center for Global Change, Japan Marine Science and Technology Center
[3] Meteorological Satellite Center, Japan Meteorological Agency

Abstract

Observations from the Multi-functional Transport Satellite (MTSAT)-1R show that Okhotsk sea ice flowed southward in the Nemuro Strait and reached the northern coast of the Nemuro peninsula on February 25, 2008. Wind data from Cape Nossapu and Rausu town indicate that a north-northwesterly to northwesterly winter monsoon wind with speeds of 5 to 10 m/s blew across the sea surface all day long and drove sea surface ice and water southward. Sea-ice drift from the Nemuro Strait through the Goyoumai Pass to the Pacific Ocean was clearly observed on February 28 and 29 by MTSAT-1R. The direction of the sea-ice drift in the Pacific was distinctly southwestward during this period against west-northwesterly to southwesterly wind of speeds 2 to 8 m/s. The Oyashio Current is a possible factor for southwestward drift of sea ice. Sea-ice flow from the Nemuro Strait through the Goyoumai Pass and its drift in the Pacific Ocean were also observed on March 2, 3, 7, 8 and 9 by MTSAT-1R. In these cases, the path of sea-ice drift was near the coast along the Coastal Oyashio Current. Sea ice finally floated off Tokachi District and parts of them reached the shores of the Pacific coast of southeastern Hokkaido around Kushiro city on March 8 due to a westerly to south-southwesterly winds of 3 to 18 m/s which started on March 7 and continued until March 9.

Introduction

Okhotsk sea ice reached the shores of the Pacific coast of southeastern Hokkaido, around Kushiro city on March 8, 2008. During late February to early March, sea ice usually drifts into the Nemuro Strait from the Okhotsk Sea and flows to the Pacific Ocean through the Goyoumai Pass. However, sea ice does not frequently reach the shores of the Pacific coast of Hokkaido.

Uda and Watanabe (1936) reported sea-ice drift off the Pacific coast of southeast Hokkaido. Uda (1943) and Akagawa (1959) studied the melting process of drifting sea ice in this region by the theoretical approach. Akagawa (1964) pointed out the hazard of sea ice to shipping and fisheries, focusing on the drifting of sea ice in the Pacific Ocean.

Sea ice carries freshwater, salt, organic matter, stones and nutrients, which provide a productive environment for creatures, for example, phytoplankton, zooplankton, seaweed, shellfish, fishes and mammals. These include ice algae, krill, tangle, sea urchins, scallops, abalone, crabs, walleye pollock, seals, dolphins and whales. However, sea ice sometimes poses a threat to seaweed, especially tangle, by scraping along on the shores which causes continual damage to the ecosystem.

Floating sea ice can block access to bays, ports and navigation routes, disrupting both the transport of goods and the economic infrastructure. One dangerous aspect of sea ice is its ability to damage ships and cause disasters at sea. On March 17, 1970, sea ice destroyed 8 fishing boats and 30 fishermen went missing as they attempted to make their way to Hitokappu Bay on Etorofu Island while fleeing a severe storm in the Pacific Ocean.

Okhotsk Sea gateways such as the Soya and Nemuro straits play an important role in the environment of the Japan Sea and Pacific Ocean by transporting sea ice through them from the Okhotsk Sea. Sea-ice rafted materials are carried to remote areas through the gateways. Figure 1 shows the land–sea distribution and bottom topography in the study area. Goyoumai Pass, to the south of the Nemuro Strait, is the most important gateway for the Pacific coast of eastern Hokkaido since it faces Cape Nossapu and is closest to the eastern coast of Hokkaido.

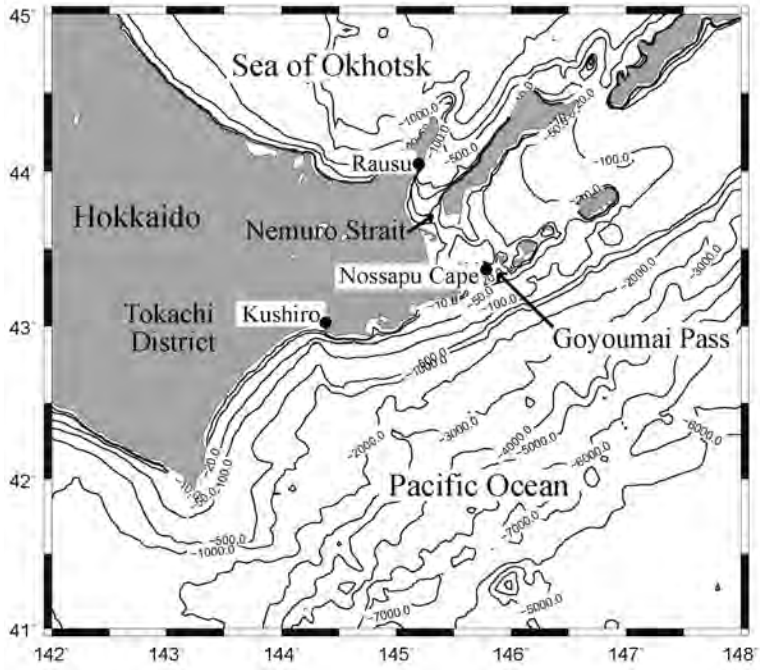

Fig. 1 Land-sea distribution and bottom topography (10, 20, 50, 100, 500, 1000, 2000, 3000, 4000, 5000, 6000, 7000 m) in the study area. Rausu town, Cape Nossapu, and Kushiro city are marked by solid circles.

The purpose of the present study is to investigate the path of sea-ice drift and to detect the dominant forcing factors of the drift, focusing on the drift that reached the shores of the Pacific coast of southeastern Hokkaido around Kushiro on March 8, 2008. In the next section, the dataset used in this study is described. Four observed events of sea-ice drift, which are southward sea-ice drift in the Nemuro Strait, sea-ice drift along the Oyashio Current, sea-ice drift along the Coastal Oyashio Current and sea-ice drift reaching the shores of southeastern Hokkaido around Kushiro in late February and early March, are presented in the next 4 sections after which we discuss the problems of Okhotsk sea-ice drifting to adjacent oceans through the gateways. A summary of the results and our proposal for future work are presented in the final section.

Dataset

The data used in this study are satellite data, atmospheric reanalysis data, meteorological data at observational stations and oceanic reanalysis data. Satellite data are obtained by Multi-functional Transport Satellite (MTSAT)-1R visible sensors for each hour. Atmospheric reanalysis data are daily wind stress from the Japanese 25-year Reanalysis Project (JRA25) (Onogi *et al.*, 2007). Meteorological data are wind data observed at Rausu town, Cape Nossapu and Kushiro city. Oceanic reanalysis data are daily surface currents from MOVE/MRI.COM-WNP, which is the western North Pacific version of the Meteorological Research Institute (MRI) multivariate ocean variational estimation (MOVE) system (Usui *et al.*, 2006) using the MRI community ocean model (MRI.COM) (Ishikawa *et al.*, 2005; Tsujino and Fujii, 2007; Nakano *et al.*, 2008). The model does not represent tidal currents explicitly but tidal mixing is expressed by the estimation of St. Laurent *et al.* (2002).

In order to study sea-ice drift, clear MTSAT-1R images of hourly sea-ice conditions on February 25, 28 to 29, and March 2 to 3 and 7 to 9 were selected. The spatial resolution of the satellite observation was 1 km, which can resolve narrow sea ice bands and streams of about 10 km. The time resolution of the satellite observation was 1 h, which is suitable for studying sea-ice drift with timescales of about 1 to 3 days.

Southward sea-ice drift in the Nemuro Strait

Okhotsk sea ice piled up off Rausu town and flowed southward in the Nemuro Strait in late February

2008. Figure 2 shows sea-ice conditions in the Nemuro Strait at 10 and 16 Japan Standard Time (JST) on February 25, observed by MTSAT-1R. Sea ice moved 8 km southward within 6 h, with an average speed of about 35 cm/s. It reached the northern coast of the Nemuro peninsula at 16 JST.

As shown in Figure 3, a low-pressure field developed in the northern North Pacific. A strong northwesterly wind with a cold surge was induced in the southwestern part of the low-pressure field, and passed over Rausu town and Cape Nossapu on February 25. Clouds of Karman Vortex in the upper right corner of Figure 2, top, clearly reveal the north-northwestern wind over the ocean off eastern Hokkaido at 10 JST, February 25.

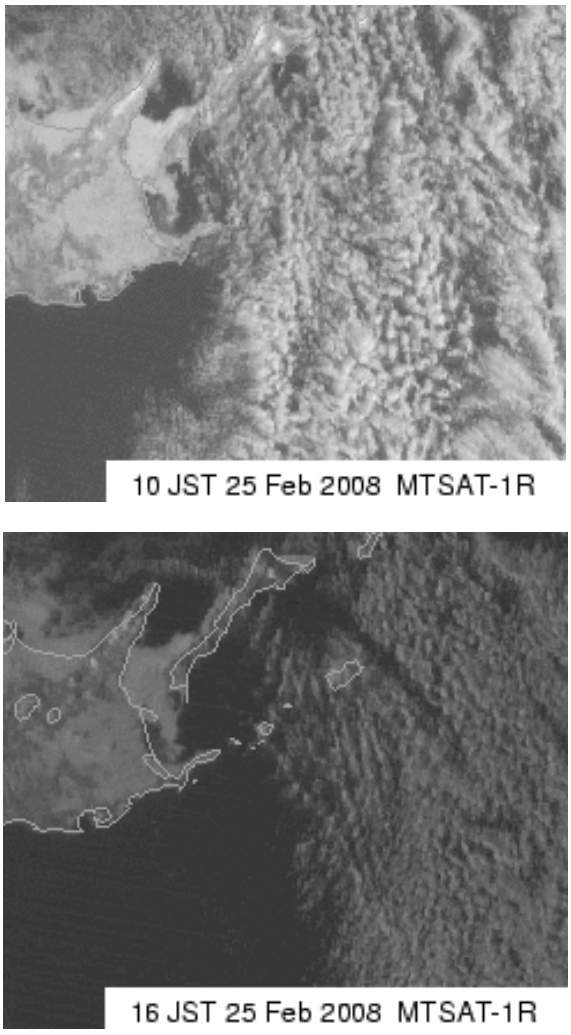

Fig. 2 Sea-ice conditions in the Nemuro Strait at 10 (upper panel) and 16 (lower panel) in Japan Standard Time (JST) on February 25, 2008, observed by Multi-functional Transport Satellite (MTSAT)-1R.

Wind vectors for each hour on February 25 at observational stations in Rausu town, Cape Nossapu and Kushiro city are shown in Figure 4. The data at Rausu town and Cape Nossapu indicate that north-northwesterly to northwesterly winter monsoon winds with speeds of 5 to 10 m/s blew across the sea ice continuously for more than a half day.

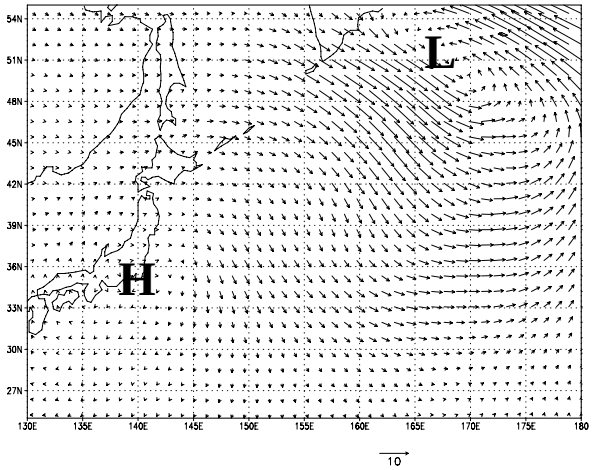

Fig. 3 Daily surface wind stress on February 25, 2008 from JRA-25. Unit is N/m^2.

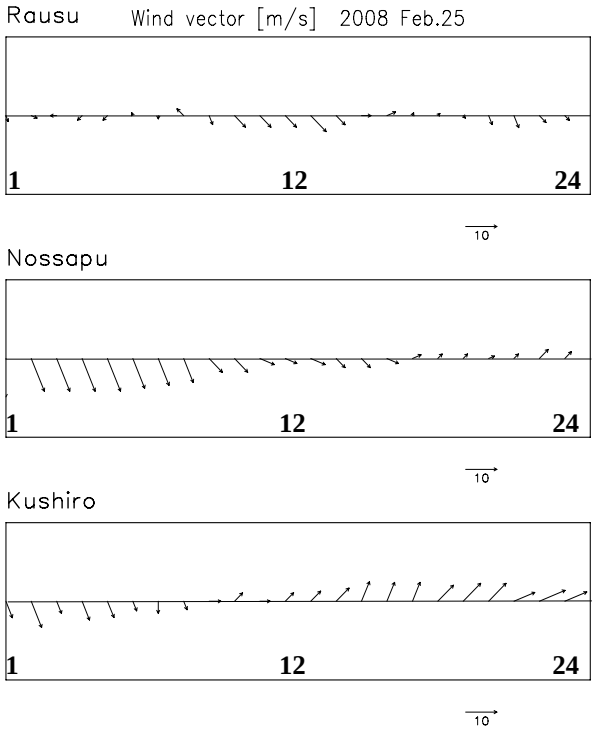

Fig. 4 Wind vectors for each hour on February 25, 2008 at the observational station in Rausu town, Cape Nossapu and Kushiro city. North and east are up and right. Unit is m/s.

Figure 5 shows the surface current around eastern Hokkaido on February 25 from MOVE/MRI.COM-WNP. The Oyashio Current flows southwestward over the continental slope along the contours of 2000 to 5000 m depth (see Fig. 1) with about 80 km width, influenced by an anti-cyclonic eddy of about 160 km in diameter. The speed of the Oyashio Current is estimated to be 60 cm/s in the center of its jet. In the Okhotsk Sea, meandering currents with speeds of of 35 cm/s are represented by a 30 km width along the contours of depths 100 to 1000 m north of Shiretoko Peninsula and Kunashiri Island. Over the continental shelf, at depths shallower than 100 m, a Coastal Oyashio Current of width 20 km develops with a west-southwestward velocity of 30 cm/s along the Pacific coast around the Goyoumai Pass.

A weak southward current of 10 cm/s is produced in the Nemuro Strait, connecting the Okhotsk meandering current with the Coastal Oyashio Current. A southward flow of sea ice and surface water was driven by north-northwesterly to northwesterly winds which blew across the Nemuro Strait all day long.

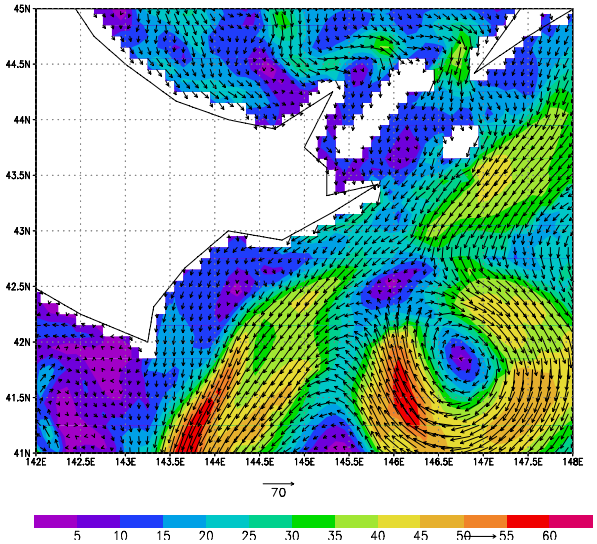

Fig. 5 Daily surface currents around eastern Hokkaido on 25 February 2008 from MOVE/MRI.COM-WNP. Unit is cm/s.

Sea-ice drift along the Oyashio Current

Figure 6 shows sea-ice conditions off the south-eastern coast of Hokkaido at 10 JST on February 28 and 29 by MTSAT-1R. Sea ice flowed east-southeastward from the Nemuro Strait to the Pacific through the Goyoumai Pass. After sea ice flowed out to the Pacific, it turned southwestward as it crossed the Coastal Oyashio Current. The southwestward drift of sea ice continued for 50 km off the southeastern coast of Hokkaido along the Oyashio Current, forming a sea-ice band of about 10 km. The southernmost edge of the sea-ice band moved about 25 km in one day, from February 28 to 29, with an average speed of about 30 cm/s.

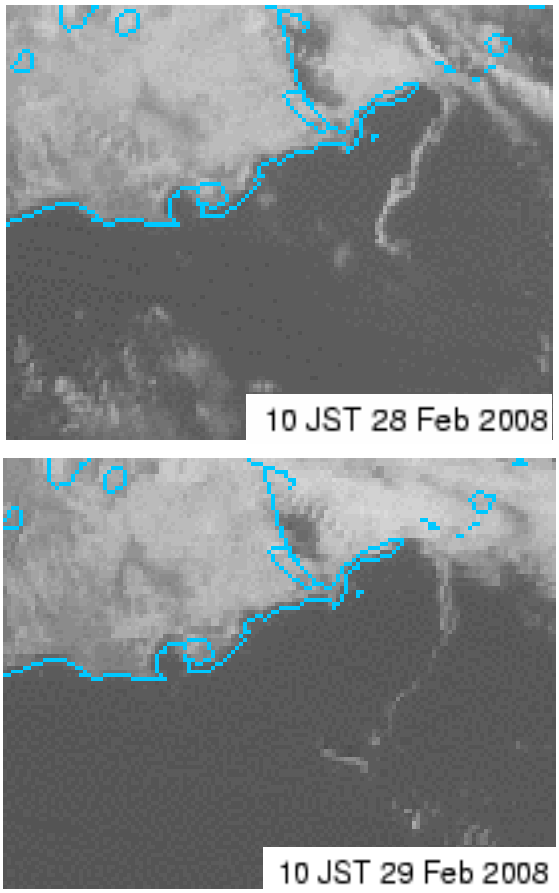

Fig. 6 Sea-ice conditions off the southeastern coast of Hokkaido at 10 in Japan Standard Time (JST) on February 28 (upper panel) and February 29 (lower panel) 2008, observed by Multi-functional Transport Satellite (MTSAT)-1R.

The sea-ice band had a wavy structure with a wavelength of about 10 km. The band usually consists of many sizes, thickness and types of floes such as rotten ice, brash ice, small floes and hummock ice. Sea ice in the southern part of the band melted on February 29, probably due to heating from warmer seawater above freezing point in the warm and saline open ocean region.

Reanalyzed daily surface wind stress fields over the northwestern North Pacific and the adjacent seas on February 28 and 29 are shown in Figure 7. A low-pressure field developed southwest of Kamchatka in

the Okhotsk Sea. Cyclonic winds in a low-pressure field caused west-northwesterly to southwesterly winds in the southern region off the southeastern coast of Hokkaido.

Figure 8 shows wind vectors for each hour at observational stations in Rausu town, Cape Nossapu and Kushiro city on February 28 and 29. West-northwesterly and southwesterly winds were clearly observed as the dominant winds, with a maximum wind speed of 8 m/s. The direction of the wind off the southeastern coast of Hokkaido is west-northwesterly to southwesterly as shown in Figure 7, which is different from that of sea-ice drift toward the southwest as shown in Figure 6.

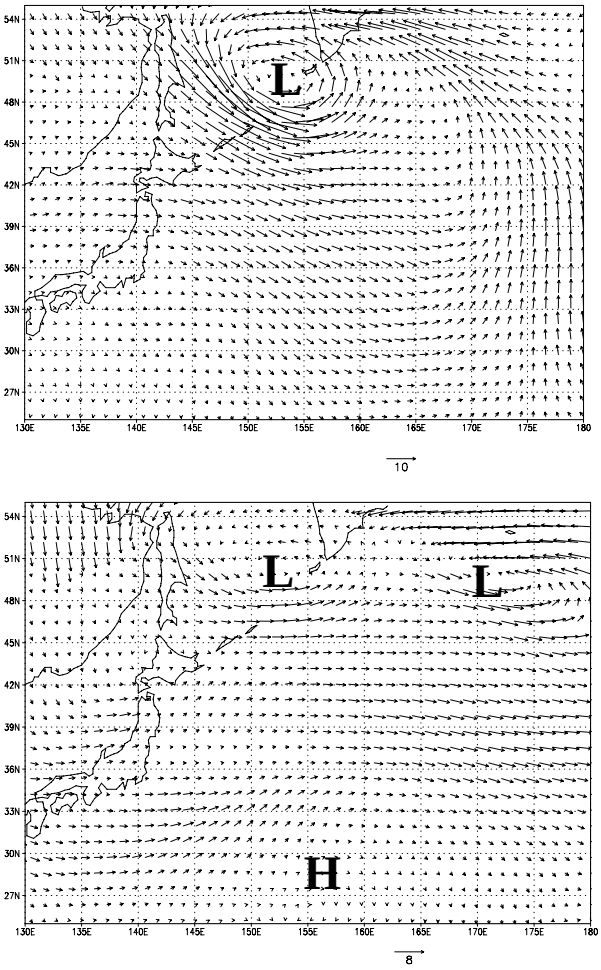

Fig. 7 Daily surface wind stress over the northwestern North Pacific and adjacent seas on February 28 (upper panel) and February 29 (lower panel), 2008 from JRA-25. Unit is N/m^2.

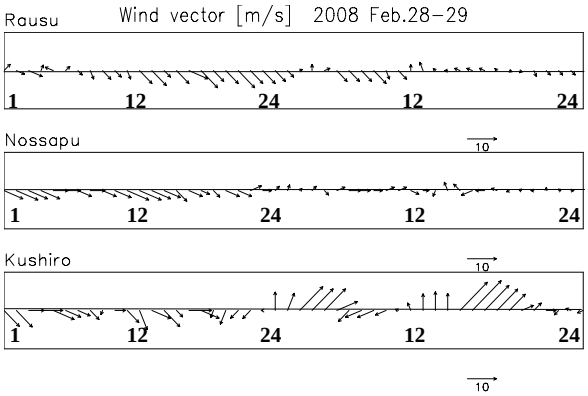

Fig. 8 Wind vectors for each hour at observational stations in Rausu town, Cape Nossapu and Kushiro city on February 28 and 29, 2008. Northerly wind is shown as downward. Unit is m/s.

Figure 9 shows daily surface currents around eastern Hokkaido on February 28 and 29 from MOVE/ MRI.COM-WNP. The Oyashio Current flows mainly southwestward off the southeastern coast of Hokkaido as seen in Figures 5 and 9. The direction and magnitude of the sea-ice drift shown in Figure 6 are the same as those of the Oyashio Current.

From atmospheric and oceanic reanalyzed data, it is seen that sea-ice drifted southwestward along the Oyashio Current against a west-northwesterly to southwesterly wind on February 28 and 29. The southwestward drift of sea ice was probably driven by water stress due to the Oyashio Current.

Sea-ice drift along the Coastal Oyashio Current

MTSAT-1R clearly observed sea-ice drift along the Coastal Oyashio Current from March 2 to 3, 2008. Figure 10 shows sea-ice conditions off the southeastern coast of Hokkaido at 11 JST on March 2 and 3, 2008. Sea ice flowed from the Goyoumai Pass and spread west-southwestward, forming an extended sea-ice band about 20 km off the coast. The southernmost edge of the sea-ice band moved about 35 km in one day, from March 2 to 3, with an average speed of about 40 cm/s.

The sea-ice band had a wavy structure with wavelength of about 10 km, similar to that observed on February 28 and 29. However, it drifted closer to the coast and remained intact for a longer time, probably due to the colder sea water (near freezing point) around it.

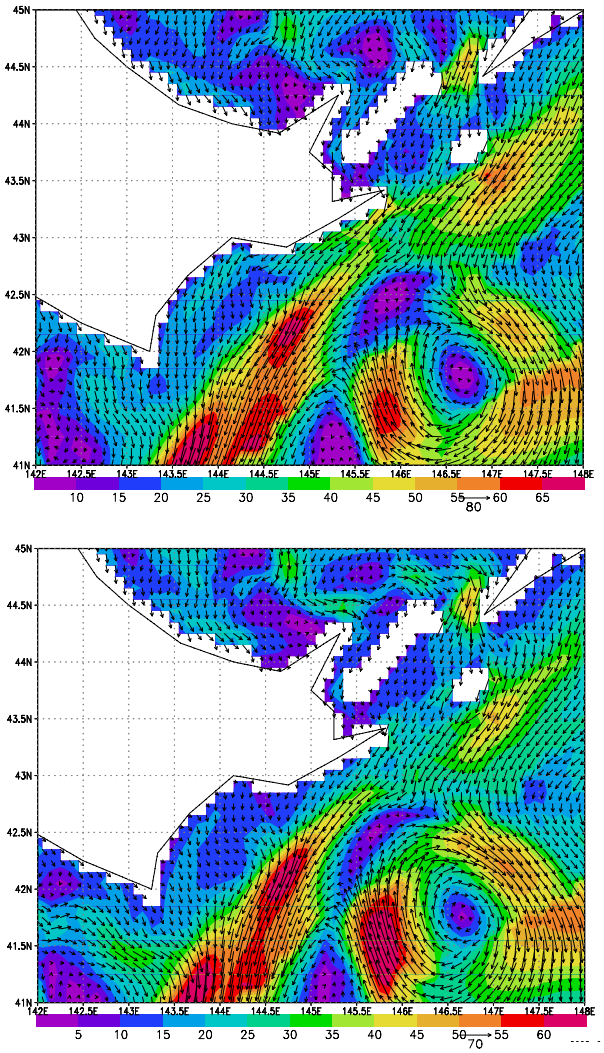

Fig. 9 Daily surface currents around eastern Hokkaido on February 28 (upper panel) and February 29 (lower panel), 2008 from MOVE/MRI.COM-WNP. Unit is cm/s.

Reanalyzed daily surface wind stress fields over the northwestern North Pacific and adjacent seas on March 2 and 3 are shown in Figure 11. A low-pressure field developed south of Kamchatka and cyclonic winds blew around it. The cyclonic wind system induced a northwesterly wind over eastern Hokkaido. The strength of the northwesterly wind stress was less than 1 N/m^2.

Figure 12 shows wind vectors for each hour at observational stations in Rausu town, Cape Nossapu and Kushiro city on March 2 and 3, 2008. Northwesterly winds were observed to be the dominant winds at stations in Rausu town and Cape Nossapu, with a maximum wind speed of 5 m/s.

As revealed in Figure 11, the direction of the wind off the southeastern coast of Hokkaido is north-westerly, different from the southwestward direction of sea-ice drift, as shown in Figure 10.

Figure 13 shows the daily surface current around eastern Hokkaido on March 2 and 3, 2008 from MOVE/MRI.COM-WNP. The west-southwestward Coastal Oyashio Current flowed south of the Goyoumai Pass and developed significantly, with speeds of 30 to 40 cm/s, on March 3. The directions and magnitudes were exactly the same as those for sea-ice drift observed off the southeastern coast of Hokkaido (see Fig. 10).

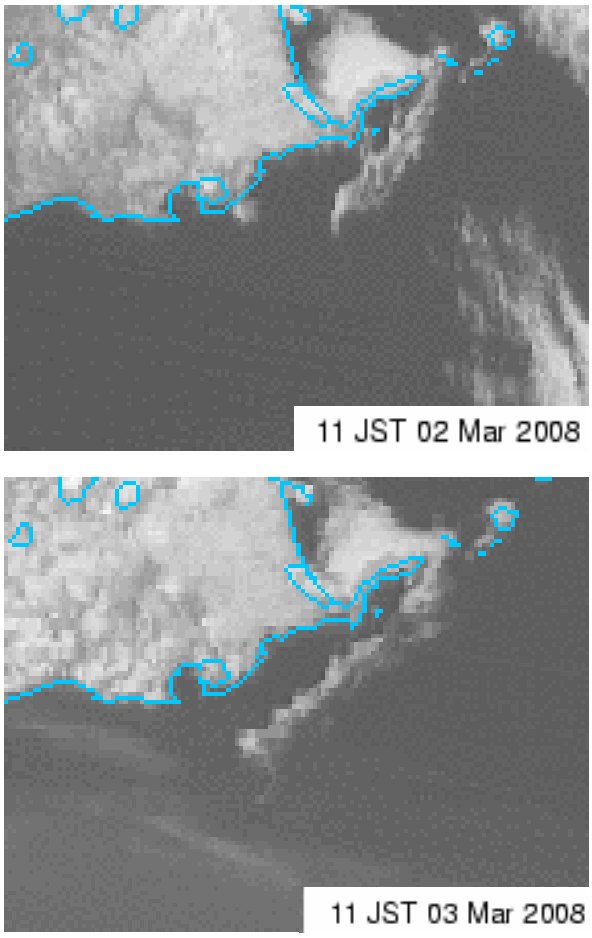

Fig. 10 Sea-ice conditions off the southeastern coast of Hokkaido at 11 in Japan Standard Time (JST) on March 2 (upper panel) and March 3 (lower panel), 2008, observed by Multi-functional Transport Satellite (MTSAT)-1R.

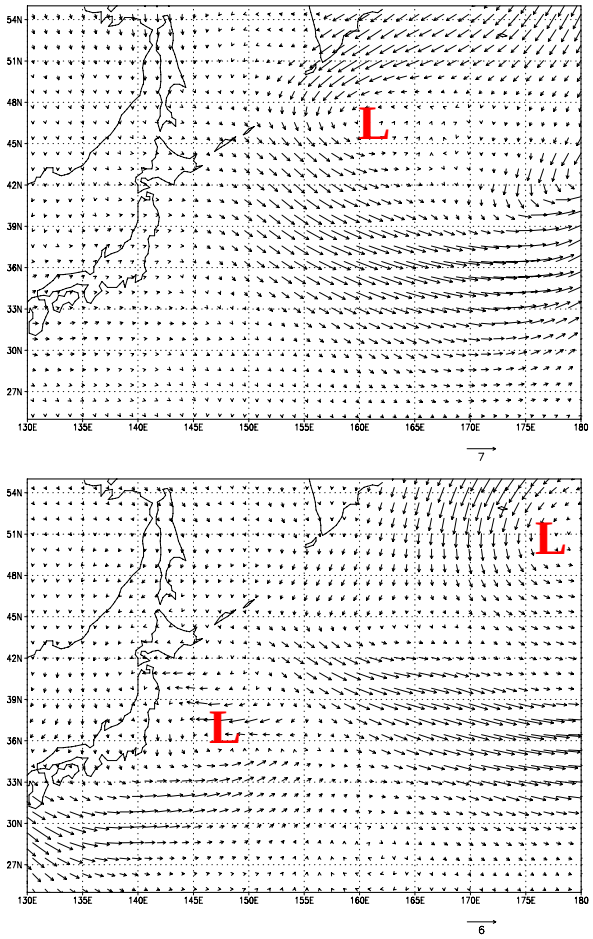

Fig. 11 Daily surface wind stress over the northwestern North Pacific and adjacent seas on March 2 (upper panel) and March 3 (lower panel), 2008 from JRA-25. Unit is N/m^2.

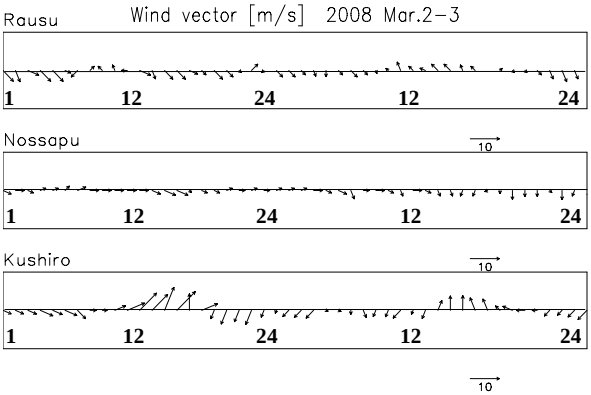

Fig. 12 Wind vectors for each hour at observational stations in Rausu town, Cape Nossapu and Kushiro city on March 2 and 3, 2008. Northerly wind is shown as downward. Unit is m/s.

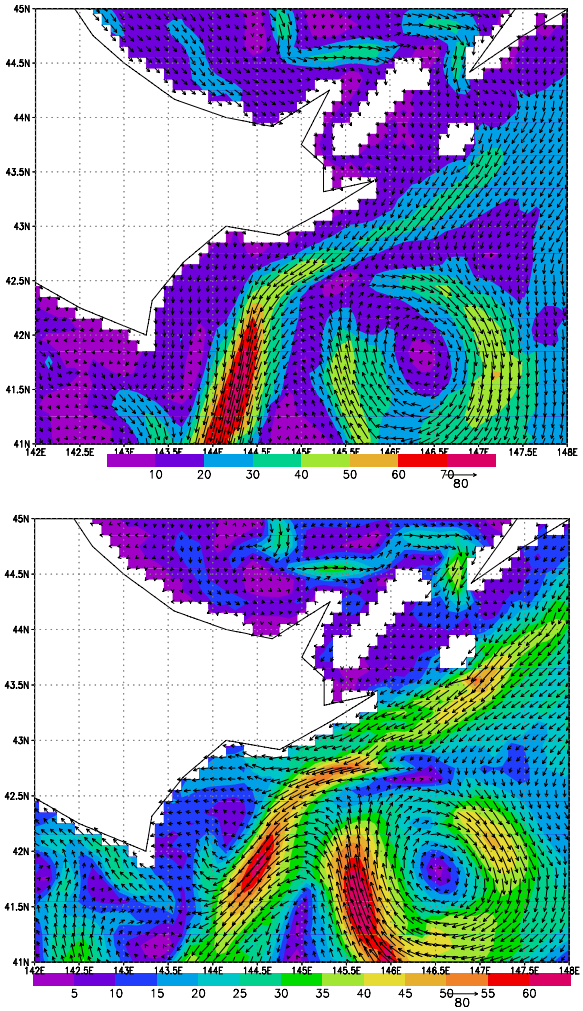

Fig. 13 Daily surface currents around eastern Hokkaido on March 2 (upper panel) and March 3 (lower panel), 2008 from MOVE/MRI.COM-WNP. Unit is cm/s.

These atmospheric and oceanic reanalyzed data suggest that observed west-southwestward sea-ice drift on March 2 and 3 is probably driven mainly by water stress due to the development of the Coastal Oyashio Current. Both the Oyashio Current over the continental slope and the anti-cyclonic eddy in the open ocean are clearly revealed in Figures 5, 9 and 13. However, the Coastal Oyashio Current varied over a shorter time scale (days). Coastal ocean response to the atmospheric cyclone might be a key factor in the variability of the Coastal Oyashio Current and sea-ice drift along it.

Sea-ice drift reaches the shores of southeastern Hokkaido

Sea ice drifted off the southeastern coast of Hokkaido from the Goyoumai Pass to the eastern

coast of Tokachi District on March 7 to 9, 2008. Figure 14 shows sea-ice bands and streams floating in this region, as observed by MTSAT-1R. Parts of the floating sea ice reached the southeastern coast of Hokkaido and the shores around Kushiro on March 8, 2008.

During this period, the atmospheric pressure field featured a low pressure in the central Okhotsk Sea and a high pressure south of Hokkaido, causing westerly to south-southwesterly winds off the southeastern coast of Hokkaido, as shown in Figure 15.

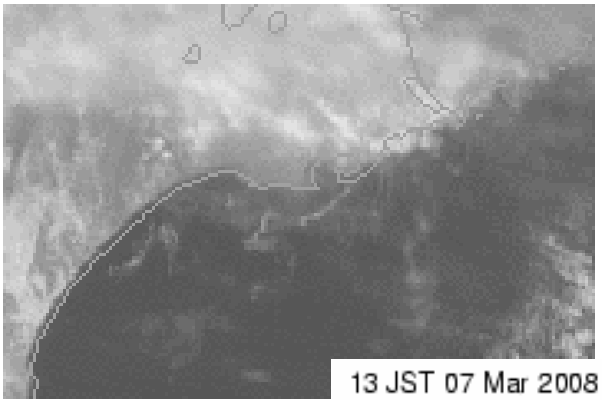

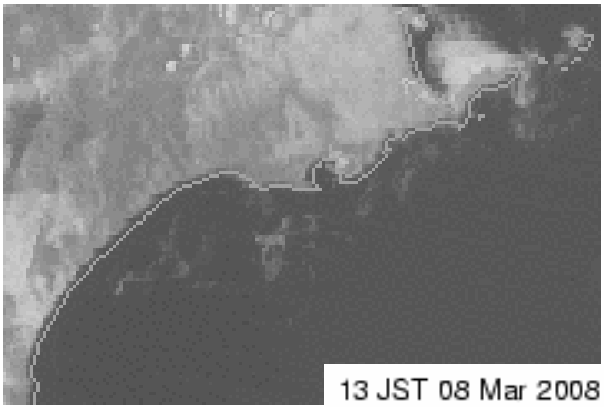

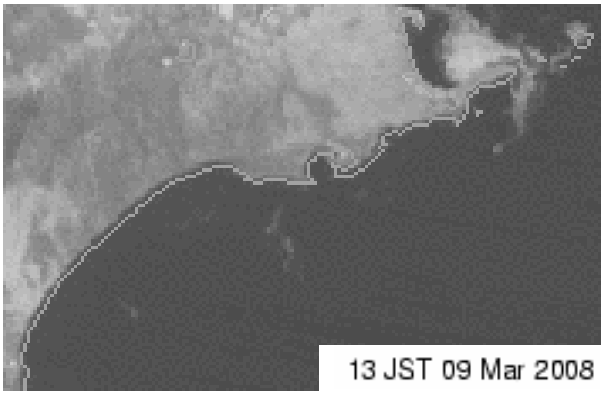

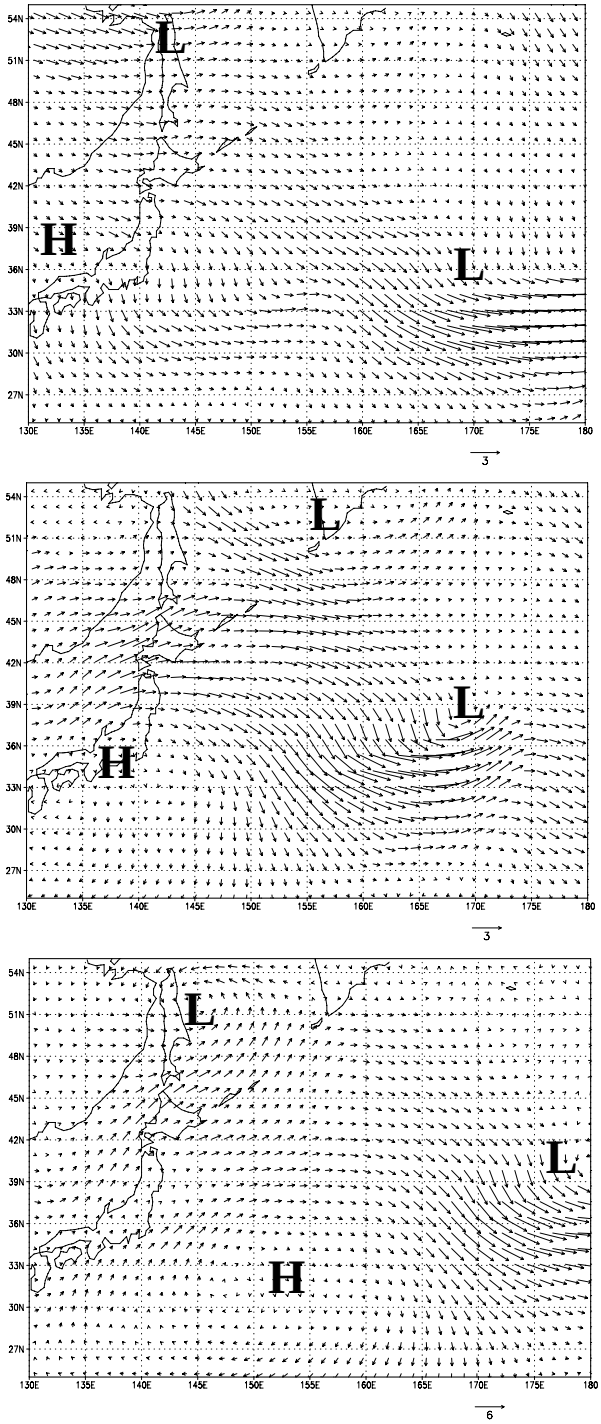

Fig. 15 (above) Daily surface wind stress over the northwestern North Pacific and its adjacent sea on March 7 (top panel), March 8 (middle panel) and March 9 (bottom panel), 2008 from JRA-25. Unit is N/m^2.

Fig. 14 (left) Sea-ice conditions off the southeastern coast of Hokkaido at 13 in Japan Standard Time (JST) on March 7 (top panel), March 8 (middle panel) and March 9 (bottom panel), 2008, observed by Multi-functional Transport Satellite (MTSAT)-1R.

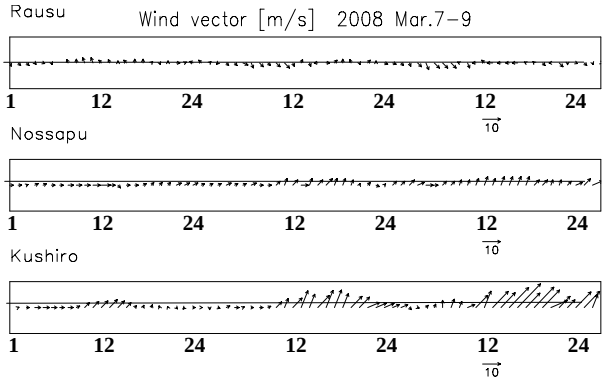

Fig. 16 Wind vectors for each hour at observational stations in Rausu town, Cape Nossapu and Kushiro city on March 7 to 9, 2008. Northerly winds are shown as downward. Unit is m/s.

Figure 16 shows the wind vectors for each hour at observational stations in Rausu town, Cape Nossapu and Kushiro city from March 7 to 9, 2008. Westerly to south-southwesterly winds, with speeds of 3 to 18 cm/s, were observed at stations in Cape Nopssapu and Kushiro city for three days.

The Coastal Oyashio Current is estimated to have weakened to less than 10 cm/s (see Fig. 17), while the Oyashio Current and anti-cyclonic eddy are represented as stronger currents over the continental slope. The direction of the Coastal Oyashio Current was offshore south of Kushiro, which is opposite to that of sea-ice drift toward the shore around Kushiro. Based on atmospheric and oceanic reanalysis data, a possible factor for sea ice reaching the shores of southeastern Hokkaido around Kushiro on March 8, 2008 is a strong westerly to south-southwesterly wind, lasting for several days near the coast.

Discussion

The path of sea-ice drift along the Coastal Oyashio Current is clearly observed by MTSAT-1R. Sea ice melts during the drift and, as Ohtani (1989) mentioned, acts as a freshwater source for the Coastal Oyashio water which is cold and has low salinity. Nakamura *et al.* (2003) and Kono *et al.* (2004) studied the Coastal Oyashio by model simulation and successfully reproduced the Coastal Oyashio Current, consistent with the sea-ice path identified in the present study. Sea-ice drift from the Okhotsk Sea to the Coastal Oyashio region through the Nemuro Strait is direct evidence supporting the mixing process presented by Oguma *et al.* (2008), from isotopic tracers.

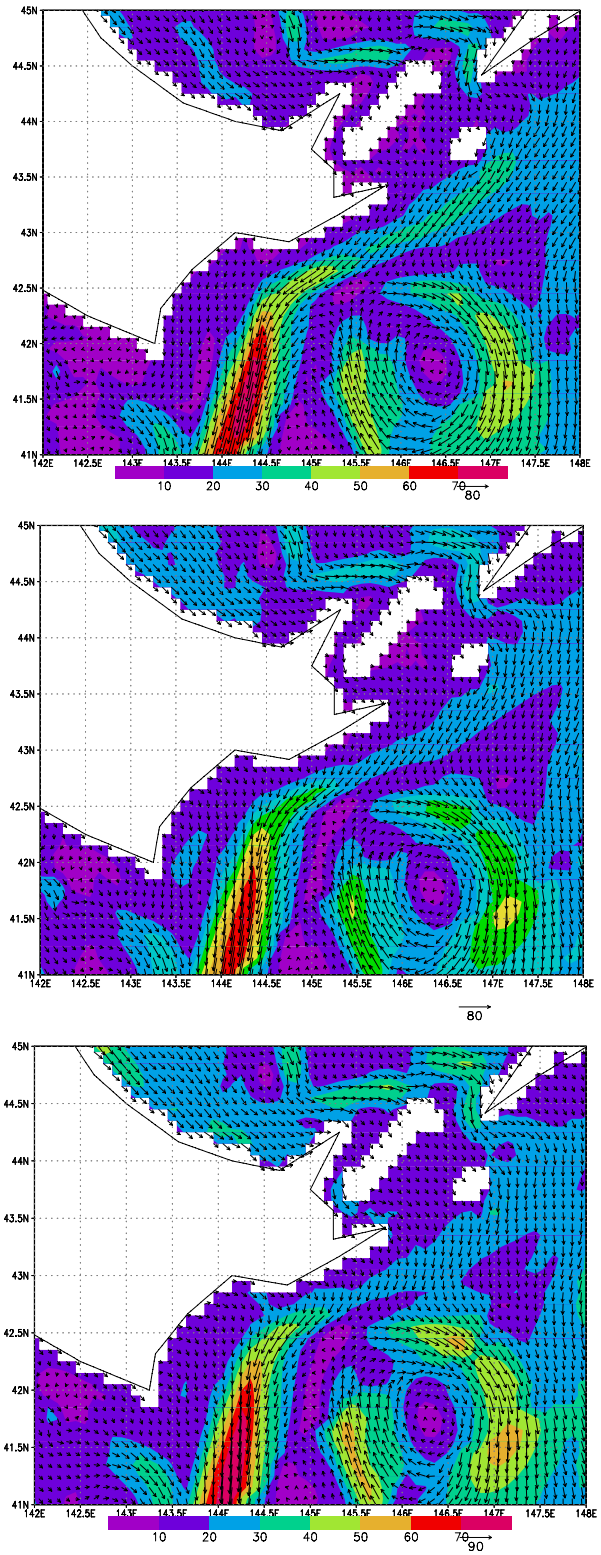

Fig. 17 Daily surface current around eastern Hokkaido on March 7 (top panel), March 8 (middle panel) and March 9 (bottom panel), 2008 from MOVE-MRI.COM-WNP. Unit is cm/s.

Besides present-day sea-ice and Coastal Oyashio water conditions mentioned above, Last Glacial Maximum (LGM) conditions of sea ice and water are also important for the study of the sensitivity of sea ice and water in the environment. Ikehara (2003) and Sakamoto *et al.* (2005) reconstructed the history of sea ice in the Japan Sea and the Okhotsk Sea, respectively. Sea ice might extend to lower latitudes in LGM. Oba (2006) reconstructed sea surface temperatures (SST) in the western North Pacific and estimated them to be about 20 degrees lower in the LGM over the present-day Kuroshio extension region, which suggests that sea ice drifted to lower latitudes along currents with eddies and streamers off the eastern coast of Honshu, the central island of Japan.

In any epoch, whether the present day, the LGM or in a future global warming world, the sea-ice trajectory can be expressed by Newton's second law of motion with the Coriolis force. Wind and current induce air and water drag and work as a driving force for sea-ice drift. The sea-ice trajectory observed in the present study should be expressed by forces from both the wind and currents. By solving the momentum equation of sea ice, its trajectory can be represented and the driving force on it analyzed, as Smith (1993), Bigg *et al.* (1997), Matsumoto (1997) and Gladstone *et al.* (2001) have done for icebergs.

Summary

The path of sea-ice drift from the Okhotsk Sea to the Pacific Ocean during late February to early March, 2008 is investigated and the dominant forcing factors of the drift are detected for four sea-ice drift events, which are (1) southward sea-ice drift in the Nemuro Strait on February 25, (2) sea-ice drift along the Oyashio Current on February 28 to 29, (3) sea-ice drift along the Coastal Oyashio Current on March 2 to 3 and (4) sea-ice drift reaching the shores of southeastern Hokkaido around Kushiro on March 7 to 9.

As summarized in Figure 18, wind data observed at Cape Nossapu and Rausu town reveal that north-northwesterly to northwesterly wind with speeds of 5 to 10 m/s drove sea surface ice and water southward on February 25 all day long. The sea-ice outflow from the Nemuro Strait through the Goyoumai Pass to the Pacific Ocean resulted in a distinct southwestward drift of sea ice against west-northwesterly to southwesterly winds of speeds 2 to 8 m/s, which suggests that the Oyashio Current is a possible factor for the southwestward drift of sea ice on February 28 to 29.

In the case of Okhotsk sea-ice flow into the Pacific Ocean through the Goyoumai Pass on March 2, 3, 7, 8 and 9, the path of sea-ice drift was near the coast along the Coastal Oyashio Current. Sea ice reached Tokachi District and parts of it reached the shores of southeastern Hokkaido around Kushiro city on March 8 due to westerly to south-southwesterly winds with speeds of 3 to 18 m/s. These winds started on March 7 and continued for three days.

It has been shown that the Goyoumai Pass and the Coastal Oyashio Current are key factors in the drift of Okhotsk sea ice in the Pacific. Based on the present research, our proposal for future work is to study the role of Okhotsk sea-ice drift through gateways such as the Soya Strait, the Nemuro Strait and the Goyoumai Pass which link the Okhotsk Sea to the Japan Sea and the Pacific Ocean. We hope to use satellite sea-ice data, ocean and atmosphere reanalysis data and a sea-ice trajectory model for analysis of sea-ice drift driving forces and sea-ice rafted material fluxes.

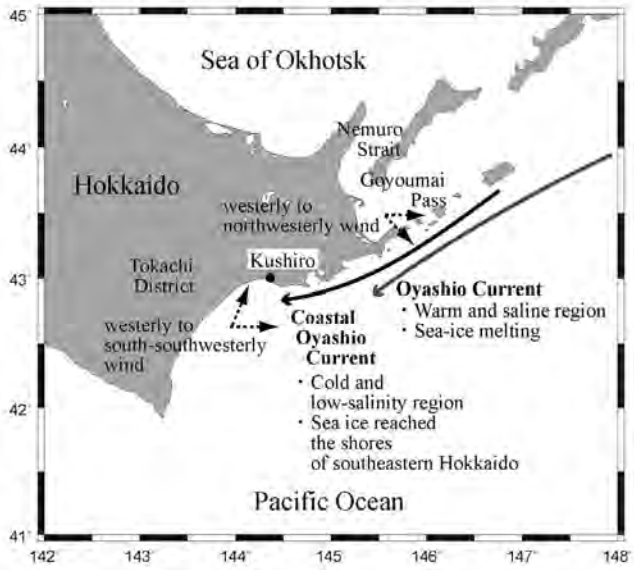

Fig. 18 Schematic view summarizing our findings. Winds in the Goyoumai Pass and off the coast of Kushiro are key factors for sea-ice spreading into the Pacific from the Nemuro Strait and reaching the shores around Kushiro off Tokachi District, respectively. The Coastal Oyashio Current is a key factor for west-southwestward sea-ice drift from the south of Goyoumai Pass to the east of Tokachi District along the southeastern coast of Hokkaido.

Acknowledgements

We wish to thank Dr. Makoto Kashiwai for recommending that we to present our research at the 4th PICES Workshop on the Okhotsk Sea and Adjacent Waters. We also appreciate Mrs. Yukiko Suda's assistance in preparing this paper. The research was partially supported by a grant from the Ministry of Education, Culture, Sports Science and Technology, Grant-in-Aid for Scientific Research No. 20540433.

References

Akagawa, M. 1959. On the melting of pack-ice field. *Kenkyu Jihou.* **11**: 921–932 (in Japanese with English abstract).

Akagawa, M. 1964. On the drifting of pack-ice in the Pacific Ocean off Hokkaido. *Bull. Hakodate Mar. Observ.* **11**: 50–65 (in Japanese with English abstract).

Bigg, G.R., Wadley, M.R., Stevens, D.P. and Johnson, J.A. 1997. Modelling the dynamics and thermodynamics of icebergs. *Cold Regions Sci. Technol.* **26**: 113–135.

Gladstone, R.M., Bigg, G.R. and Nicholls, K.W. 2001. Iceberg trajectory modeling and meltwater injection in the Southern Ocean. *J. Geophys. Res.* **106**: 19,903–19,915.

Ikehara, K. 2003. Late Quaternary seasonal sea-ice history of the north-eastern Japan Sea. *J. Oceanogr.* **59**: 585–593.

Ishikawa, I., Tsujino, H., Hirabara, M., Nakano, H., Yasuda, T. and Ishizaki, H. 2005. Meteorological Research Institute Community Ocean Model (MRI.COM) Manual. Tech. Rep. Meteorol. Res. Inst., No. 47, 189 pp. (in Japanese).

Kono, T., Foreman, M., Chandler, P. and Kashiwai, M. 2004. Coastal Oyashio South of Hokkaido, Japan. *J. Phys. Oceanogr.* **34**: 1477–1494.

Matsumoto, K. 1997. Modeled glacial North Atlantic ice-rafted debris pattern and its sensitivity to various boundary conditions. *Paleoceanogr.* **12**: 271–280.

Nakamura, T., Awaji, T., Toyoda, T. and Ishikawa, Y. 2003. Coastal Oyashio in a North Pacific Simulation Experiment. *Bull. Coast. Oceanogr.* **41**: 13–22 (in Japanese with English abstract).

Nakano, H., Hirabara, M., Tsujino, H. and Motoi, T. 2008. Development of a global ocean model with the resolution of 1˚x1/2˚ and 1/8˚x1/12˚. *CLIVAR Exchanges* **13**: 11–13.

Oba, T. 2006. Paleoenvironmental changes in the Japan Sea and off Kashima over the last 150 kyr based on oxygen and carbon isotopes of foraminiferal tests. *J. Geogr.* **115**: 652–660.

Oguma, S., Ono, T., Kusaka, A., Kasai, H., Kawasaki, Y. and Azumaya, T. 2008. Isotopic tracers for water masses in the coastal region of eastern Hokkaido. *J. Oceanogr.* **64**: 525–539.

Ohtani, K. 1989. The role of the Sea of Okhotsk on the formation of the Oyashio water. *Umi to Sora* **65**: 63–83 (in Japanese with English abstract).

Onogi, K., Tsutsui, J., Koide, H., Sakamoto, M., Kobayashi, S., Hatsushika, H., Matsumoto, T., Yamazaki, N., Kamahori, H., Takahashi, K., Kadokura, S., Wada, K., Kato, K., Oyama, R., Ose, T., Mannoji, N. and Taira, R. 2007. The JRA-25 Reanalysis. *J. Meteor. Soc. Japan* **85**: 369–432.

Sakamoto, T., Ikehara, M., Aoki, K., Iijima, K., Kimura, N., Nakatsuka, T. and Wakatsuchi, M. 2005. Ice-rafted debris (IRD)-based sea-ice expansion events during the past 100 kyrs in the Okhotsk Sea. *Deep-Sea Res. II* **52**: 2275–2301.

Smith, S.D. 1993. Hindcasting iceberg drift using current profiles and winds. *Cold Regions Sci. Technol.* **22**: 33–45.

St. Laurent, L., Simmons, H.L. and Jayne, S.R. 2002. Estimating tidally driven mixing in the deep ocean. *Geophys. Res. Lett.* **29**: 2106, doi:10.1029/2002 GL015633.

Tsujino, H. and Fujii, Y. 2007. Improved representation of currents and water masses in the upper layer of the North Pacific Ocean in eddy-resolving OGCMs. *CLIVAR Exchanges* **12**: 19–21.

Uda, M. and Watanabe, N. 1936. *Kagaku* **6**: 192–193 (in Japanese).

Uda, M. 1943. *Seppyou* **5**: 43–47 (in Japanese).

Usui, N., Ishizaki, S., Fujii, Y., Tsujino, H., Yasuda, T. and Kamachi, M. 2006. Meteorological Research Institute multivariate ocean variational estimation (MOVE) system: Some early results. *Adv. Space Res.* **37**: 806–822.

Outflow of Okhotsk Sea Water and the oceanic condition of the sea east of Hokkaido

Yutaka Nagata

Marine Information Research Center, Japan Hydrographic Association, Tokyo, Japan
E-mail: nagata@kud.biglobe.ne.jp

Introduction

The Okhotsk Sea Water flows into the Pacific Ocean through gaps of the southern Kuril Islands, as discussed in several papers in this workshop. Along the East Coast of Hokkaido, a narrow coastal band of cold and less saline water is usually found in the first half of the year and a narrow band of warm and saline water is found in the second half of the year. The former water type is referred to as the Coastal Oyashio (*e.g.*, Ohtani 1980; Isoda *et al.*, 2003; Kono *et al.*, 2004), and the latter will be called the Coastal Warm Current in this paper. Combining these two currents, Ogasawra (1990) called these currents the East Hokkaido Coastal Current.

The Hokkaido Fisheries Research Institute set a moored current system in the flow region of the East Hokkaido Coastal Current during the period from May 2003 to May 2004. Observations were conducted at four depths ranging from 16 m to 76 m. It was found that the currents exhibit considerable short-period variations. Variation patterns are very similar for all depths, though the magnitude of the current tends to decrease with depth. The current directions are identical for all depths and are southwestward (parallel to the coastline, and stable throughout year; Ohtani, 1980) suggesting that the origin of the Coastal Oyashio Water could be melted sea ice water from the Okhotsk Sea because of its low temperature and low salinity. Also, the origin of the East Hokkaido Warm Current could originate from the Soya Current in the Okhotsk Sea because of its high temperature and high salinity.

However, the flow paths of these waters remain unknown. In this paper, the seasonal variations of the oceanic states in the sea to the east of Hokkaido are analyzed by using the observed data from the Hokkaido Kushiro Fisheries Experimental Stations in order to explore this problem.

Data

The Hokkaido Kushiro Fisheries Experimental Station keeps a routine observation network in the sea to the east of Hokkaido. The distribution of the observation points improved considerably after 1990, with temperature and salinity profiles now taken six times per year (usually in February, April, June, August, October and December). The distribution of the observation points is shown in Figure 1. We analyze mainly the area north of 42°N, and investigate the cross-sectional distributions of temperature and salinity along four north–south observation lines: P1, PK0, P2, PK1, and P3 (from east to west). We used 7 years of data, from 1990 to 1996. The observations were conducted in May instead of June from 1990 through 1993 and in July instead of August in 1992. Otherwise, it is assumed that observations were made in June or August for this analysis.

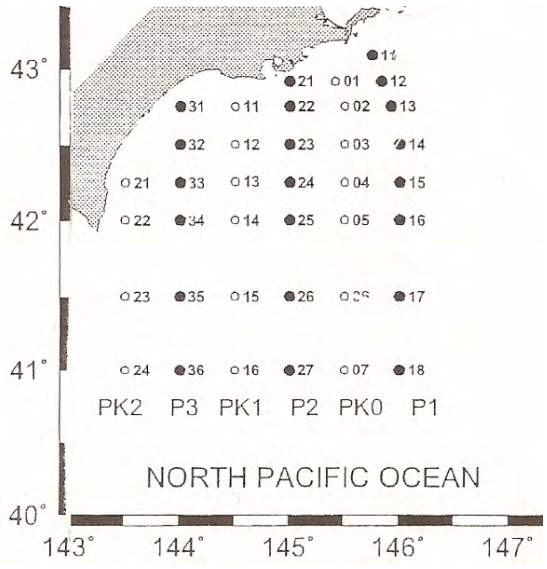

Fig. 1 Distribution of routine observation points east of Hokkaido set by the Hokkaido Kushiro Fisheries Experimental Station after 1990.

Typical examples of the Coastal Oyashio and the East Hokkaido Warm Current

Typical examples of the horizontal distributions (upper column) and cross-sectional distributions (lower column) of temperature (left) and salinity (right) of the Coastal Oyashio are shown in Figure 2. A band structure of cold and less saline water can be found along the coast. It is usually seen more clearly in the salinity field than in the temperature field.

Also, typical examples of the horizontal distributions (upper column) and cross-sectional distributions (lower column) of temperature (left) and salinity (right) of the East Hokkaido Warm Current are shown in Figure 3. Here, the band structure of warm and saline water can be found along the coast, and is usually seen more clearly in the temperature field than in the salinity field.

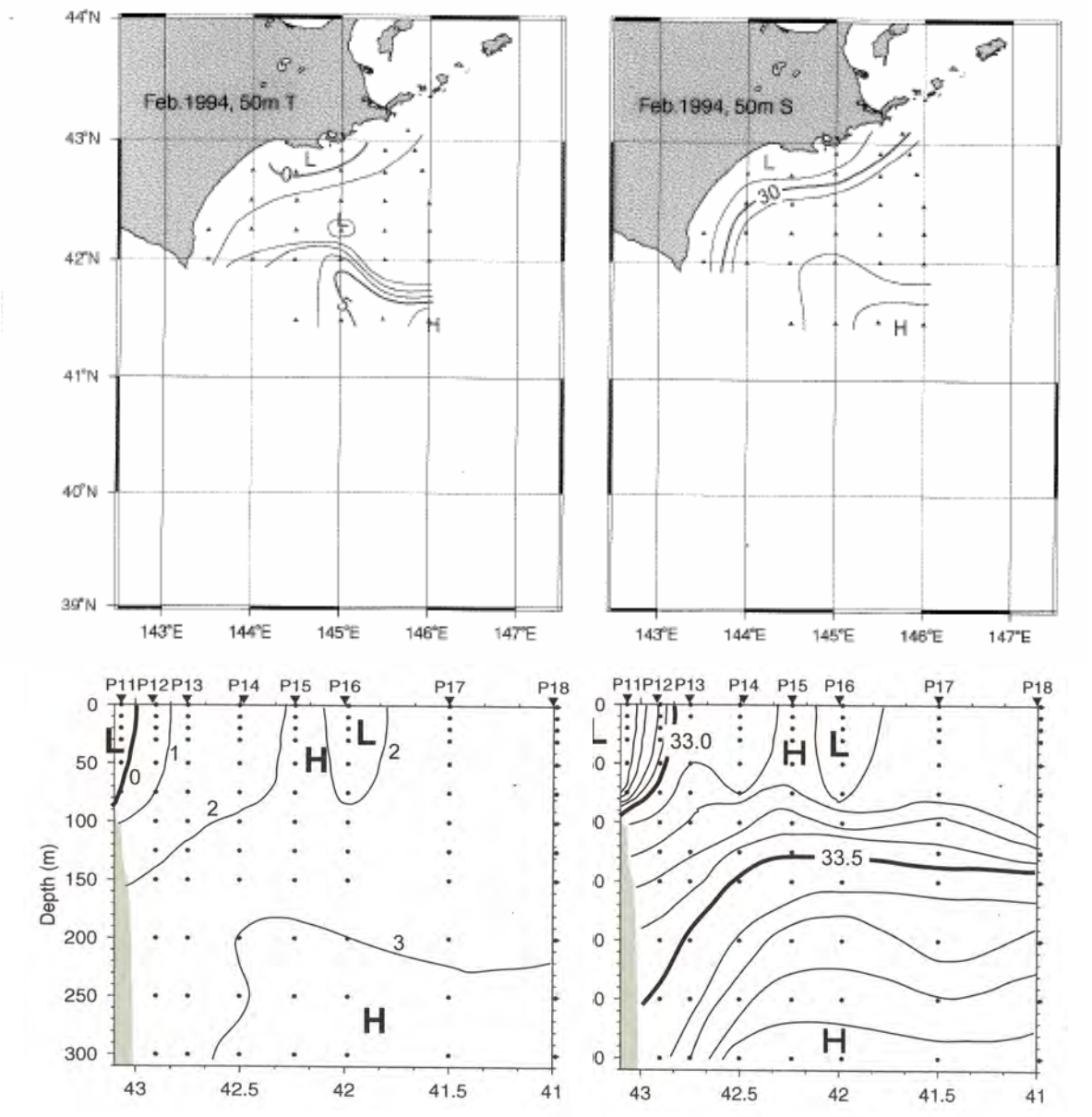

Fig. 2 Examples of the temperature (°C, left column) and salinity (right column) fields of the Coastal Oyashio. Upper panels show horizontal distributions taken at 50 m depth in February 1992, and lower panels indicate cross-sectional distribution along P1 line taken in February, 1996.

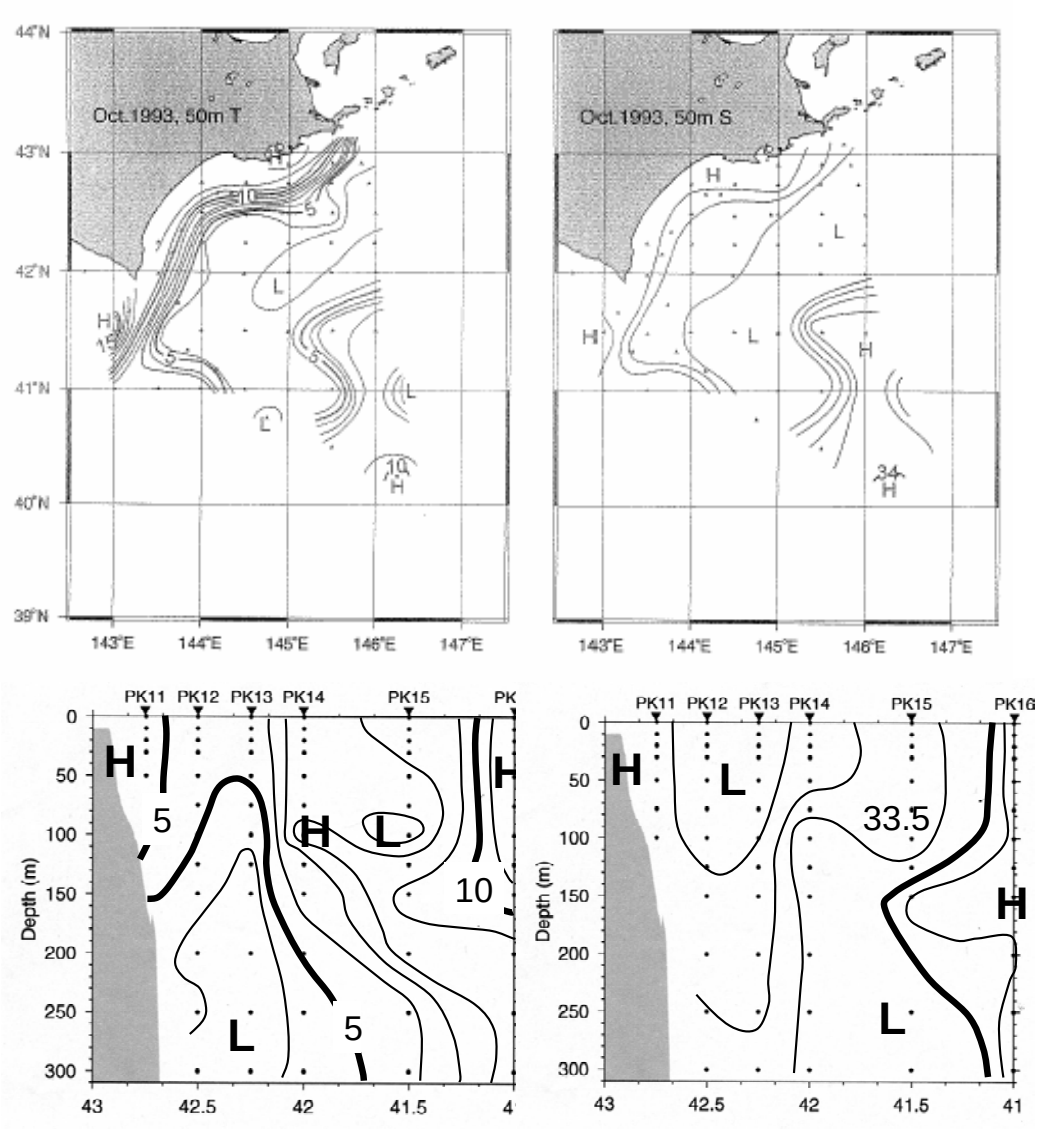

Fig. 3 Examples of the temperature (°C, left column) and salinity (right column) fields of the East Hokkaido Warm Current. Upper panels show horizontal distributions taken at 50 m depth in October 1993.

Temperature and salinity values show considerable seasonal variations, and the temperature and salinity distributions are changeable month by month. Sometimes the horizontal distribution patterns change considerably with selected depths. So, we confine our attention to the configurations of the temperature and salinity contours in the cross-sectional fields only. We examined the temperature and salinity fields independently, and checked whether or not the coastal band of colder or warmer water in the temperature field could be seen just near the coast, and whether or not that of less or more saline water could be found along the coast.

Appearance status of the East Hokkaido Coastal Current

All of the observed temperature and salinity cross-sectional distributions were examined for the period from 1990 to 1996, and the grade of appearance is determined for each observation month, for each observation line and for each standard depth. The results are shown in Figure 4 (Period I: February, April, and June) and in Figure 5 (Period II: August, October, and December). In each column, the left side symbol is for the temperature field and right side symbol is for the salinity field. As shown in the

lower column of Figures 2 and 3, the East Hokkaido Coastal Current (the Coastal Oyashio and the East Hokkaido Warm Current) appears as closed isotherms or isohalines attached to the coastal slope. The grades of appearance are determined as follows. The grade is 5 if the East Hokkaido Warm Current is seen with well closed contours, and is shown in Figures 4 and 5 with open circles. The grade is 3 if the contours are not so well closed, and is shown with open squares. The grade is 1 if warmer or more saline water exists but is doubtful as contours are not closed or have irregular forms, and is shown in figures with open triangles. Similarly, we also determined the grades for the Coastal Oyashio: –5 (closed circles) for very clear cases, –3 (closed squares) for clear cases, and –1 (closed triangles) for ambiguous cases. If no coastal current is seen, the grade is 0, and is shown with an × mark. The values of the grade are used for statistical analysis in the next section.

The difference between Figures 4 and 5 is easily recognized. Figure 4 is much darker than Figure 5 as black symbols are dominant, while Figure 5 shows more white symbols. This indicates that the coastal band of cold and less saline water appears frequently in Period I, while that of the warm and saline water appears frequently in Period II. Period I is the season of the Coastal Oyashio and Period II is the season of the East Hokkaido Warm Current.

In Figure 4 dark shading decreases from February through June, and the grade of appearance is highest in February. Similar monthly changes can also be seen in Figure 5. The grade of appearance is almost identical for August and October, but for December is considerably darker, especially in 1996: the Coastal Oyashio appears to exist sometimes in December.

In both figures the Coastal Oyashio is seen more clearly in the salinity field than in the temperature field, while the East Hokkaido Warm Current is seen more clearly in the temperature field than in the salinity field. To get a better representation, we performed a statistical analysis by replacing the symbols in Figures 4 and 5 with numbers, described in the next section.

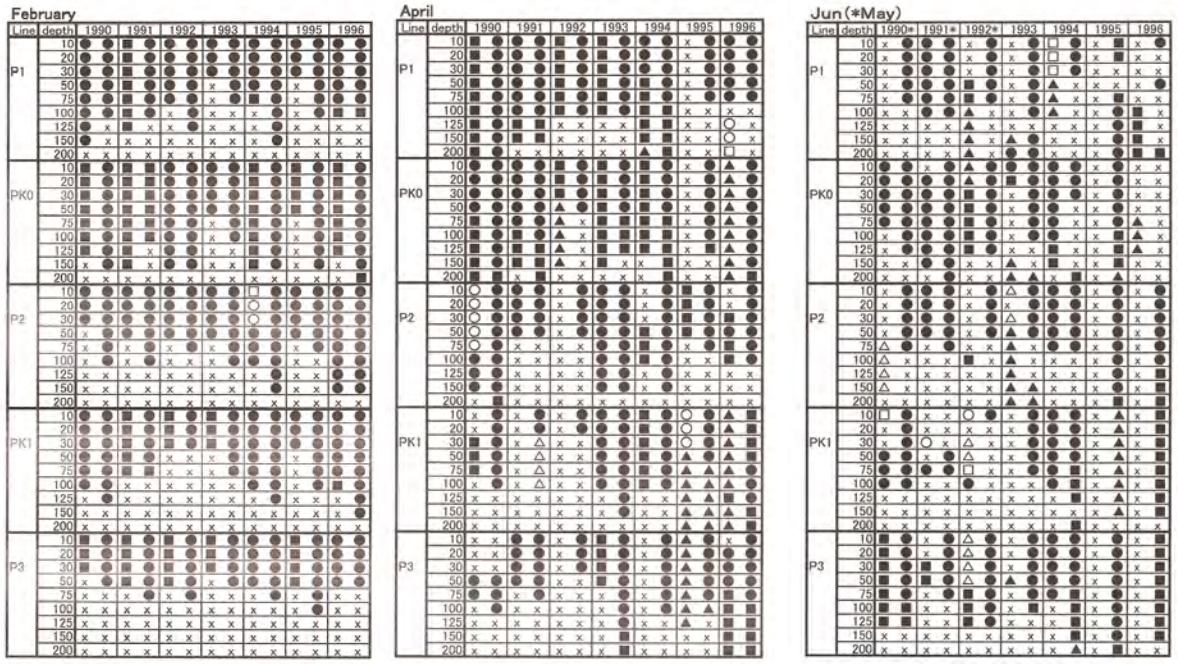

Fig. 4 Appearance state of the East Hokkaido Coastal Current for Period I (February, April and June). Left and right sides in each column show the state of the temperature field and salinity field, respectively. Black symbols indicate that cold or less saline water is observed at the station nearest to the coast. White symbols indicate that warm or saline water is observed at the station nearest to the coast. Circles represent "very clear" cases, squares "clear" cases and triangles "ambiguous" cases. If no isolated water is found or if the observation point is outside of the isolated water, an × mark is shown. The month with an * indicates that data of the former month were used.

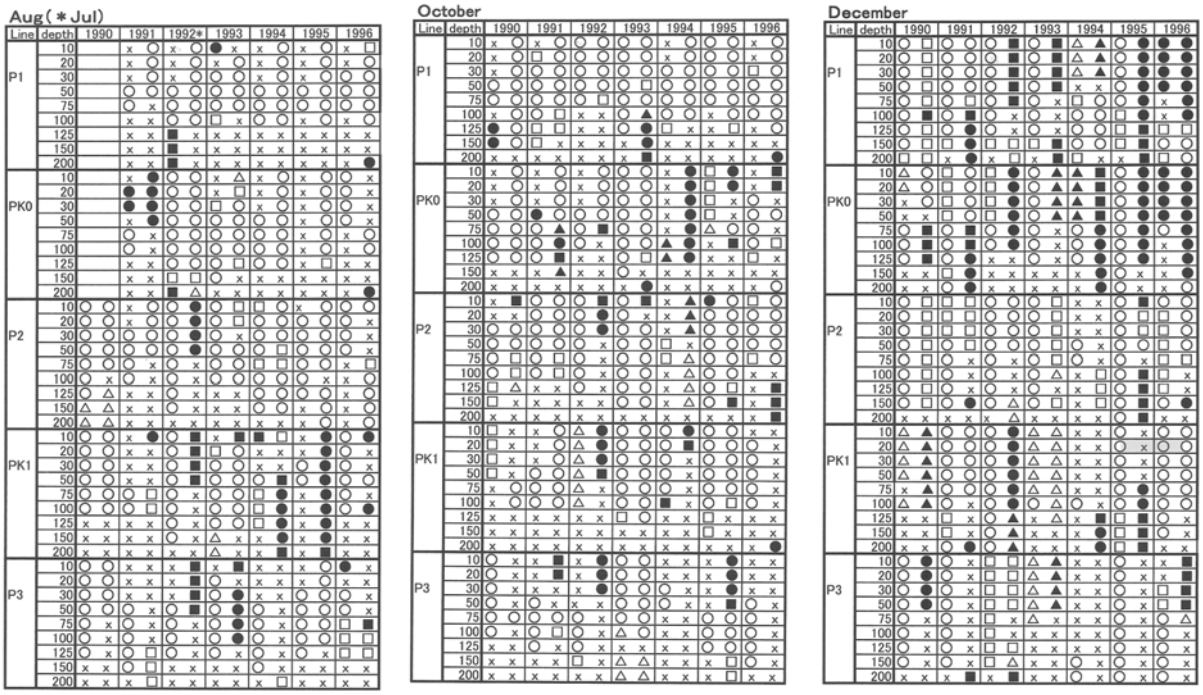

Fig. 5 Same as in Figure 4, except for Period II (August, October and December).

Numerical representation

By using the numerical values of the grade of appearance, we calculated the appearance indices averaged over 7 years (over 6 years for the P1 and PK0 lines) for each observation line, at each depth and for each month. Then, we averaged over the observation lines to find out how the appearance index changes if the observation depth is changed. The results for period I (February, April and June) are shown in upper row in Figure 6, and those for Period II (August, October and December) in lower row in Figure 6. The solid lines indicate the variation of the temperature index, and the dotted lines denote that of the salinity index.

All of the indices for Period I lie only in the negative domain (except for February, near 200 m depth), indicating that Period I is the season of the Coastal Oyashio. The indices for Period II lie in the positive domain (except near 200 m depth, and for salinity in December), indicating that Period II is the season of the East Hokkaido Warm Current. The magnitude of the salinity indices is always larger than that of the temperature indices in Period I, showing that the Coastal Oyashio appears more clearly in the salinity distributions. On the other hand, the magnitude of the temperature indices is larger than that of the salinity indices, except for the near surface layers in August, as indicated by the East Hokkaido Warm Current appearing more clearly in the temperature distributions.

The magnitudes of the salinity indices in Period I decrease monotonically with depth and keep a value less than –4 while the indices (especially temperature indices) in August and October show the maxima near 50–75 m depth. Temperature and salinity cross-sections were averaged over 7 years from 1990 to 1996 and the results obtained along the Pk0 line for August are shown in Figure 7. In the summer season from August through October, along all of the observation lines, the surface layer is characterized by high temperature and less saline waters. This surface layer is generated by sea surface warming and precipitation in summer. The signature of the East Hokkaido Warm Current near surface appears to be hidden by this warm and less saline water. Thus, the East Hokkaido Warm Current is observed most easily in the mid-layers of 50–75 m depth.

The situation in December is very special. The temperature indices show high positive values except at 200 m depth, indicating that December is the season of the East Hokkaido Warm Current. However, the salinity indices show small negative values between 0 and –1. This corresponds to the appearance of black and white symbols with almost the same frequency in Figure 5. The situation differs

year by year, and the condition which is favorable to the Coastal Oyashio already appears in December, at least in some years.

The variations of the temperature and salinity indices against the observation lines were also calculated in a similar way. The results are shown in Figure 8. It should be noted that the magnitudes of the indices in February and in April tend to increase when the observation line moves from east to west, indicating the structure of the Coastal Oyashio is weakened from east to west. The indices of both temperature and salinity in October and that of salinity in August tend to decrease from east to west. The temperature index might be influenced by the surface warm water layers. This appears to indicate that the structure of the East Hokkaido Warm Current is weakened from east to west. The indices in June and December do not show a clear tendency, but this could be because the Coastal Oyashio or the East Hokkaido Current is not clearly defined for these months, as seen in Figures 4 and 5. This would indicate that the waters of the Coastal Oyashio and the East Hokkaido Warm Current are carried from the sea to the northeast, namely to the area near the southern Kuril Islands.

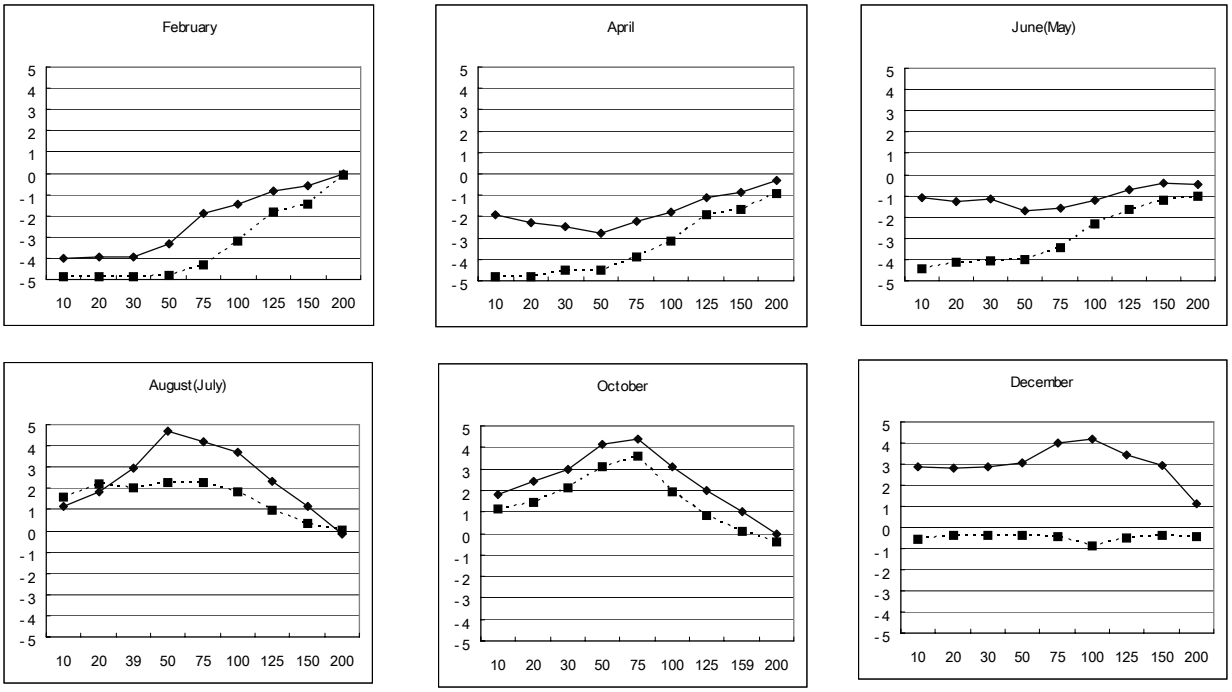

Fig. 6 Changes in the appearance indices for temperature (solid lines) and of salinity (dashed lines) against standard observation depths. Period I (February, April and June) is shown in the upper row, and Period II (August, October and December) is shown in the lower row.

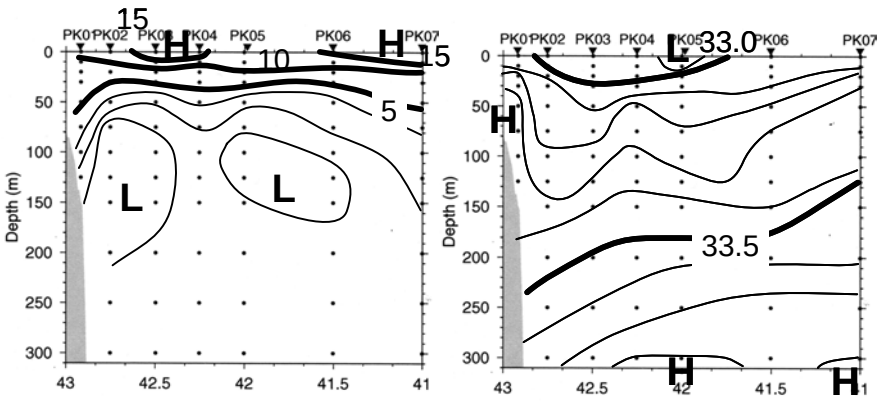

Fig. 7 Temperature (left) and salinity (right) cross-sections in August averaged over 7 years from 1990 to 1996.

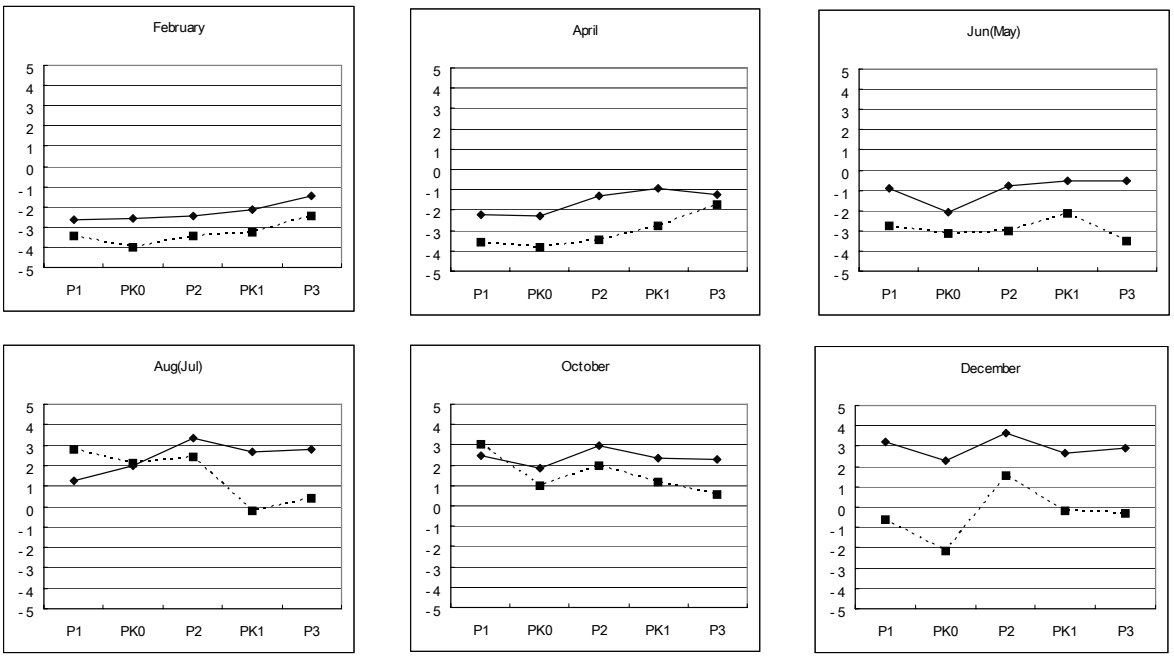

Fig. 8 Same as in Figure 6 except changes against observation lines.

Seasonal changes of the East Hokkaido Coastal Current

Ogasawara (1990) discussed the seasonal changes of water type for the East Hokkaido Coastal Current, and schematically showed its migration on a T-S diagram by analyzing specific one year data. As discussed in the previous section, the appearance indices for the Coastal Oyashio Water decrease below 50 m depth, and those for the East Hokkaido Warm Current have maxima at 50–75 m depth. In order to discuss seasonal changes of water type, we chose two stations nearest to the coast along each observation line, and the temperature and salinity values at the depth of 50 m are used.

We collected the data points which are located inside the coastal band of the Coastal Oyashio or the East Hokkaido Warm Current, and water types were plotted on T-S diagrams for each month (EHCC plot). The results are shown in the first and third rows in Figure 9. All of the water types are plotted as reference in the second and fourth rows (Reference plot). The temperature range in June is much greater in the Reference plot compared to the EHCC plot, indicting that the water could be

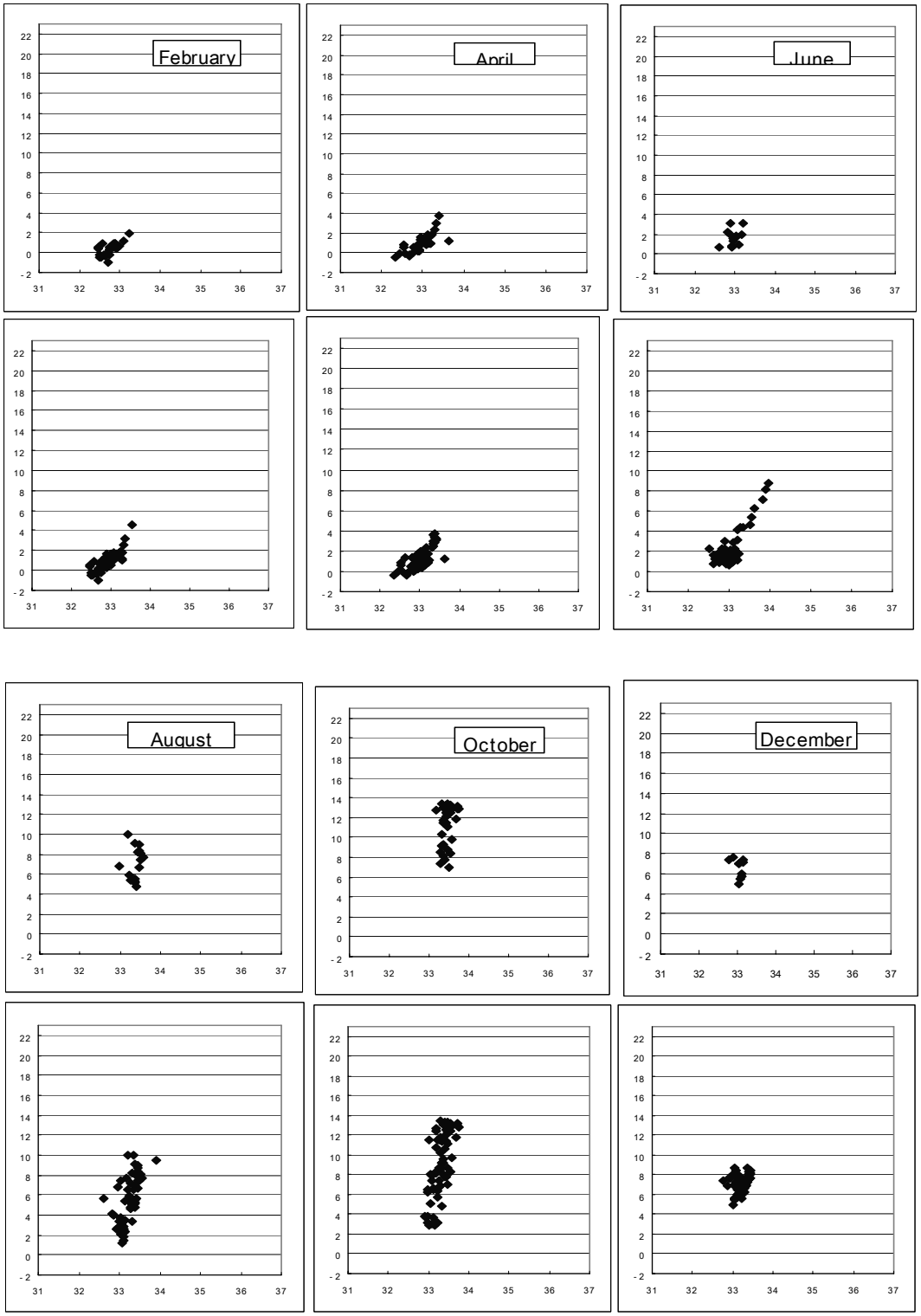

Fig. 9 Scatter diagrams of water type for each month: the upper two rows are for Period I (left: February, middle: April and June: right), and the lower two rows for Period II (left: August, middle: October and December: right). Horizontal axis is salinity and vertical axis is temperature (°C). The data are taken at the observation points nearest the coast and at 50 m depth. To create the plots in the first and third rows, only the data from the observation points located inside of the East Hokkaido Coastal Current were used. Plots in the second and fourth rows were created using all of the data.

influenced by the warm surface layer which prevails in the summer season. Generally, the areas of the Reference plots have a broader temperature range than those of the EHCC plots, but it should be noted that the distribution area for EHCC plots lie well inside of that of the Reference plot for each month. This means that the water type of the East Hokkaido Coastal Current has almost the same characteristics as the surrounding waters for each month and that the East Hokkaido Coastal Current (the Coastal Oyashio and the East Hokkaido Warm Current) could not be identified by its water type.

The water type of the East Hokkaido Coastal Current for each month is plotted altogether on a T-S diagram in Figure 10. The water type distribution of the Coastal Oyashio (in Period I) is confined in the domain below 4°C, while that of the East Hokkaido Current (in Period II) is restricted to the domain above 4°C.

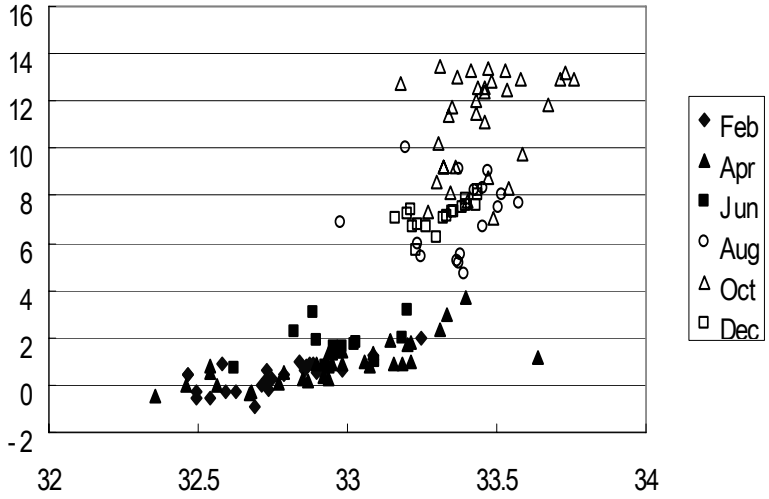

Fig. 10 Seasonal variations of the water type of the East Hokkaido Coastal Current. Horizontal axis is salinity and vertical axis is temperature (°C).

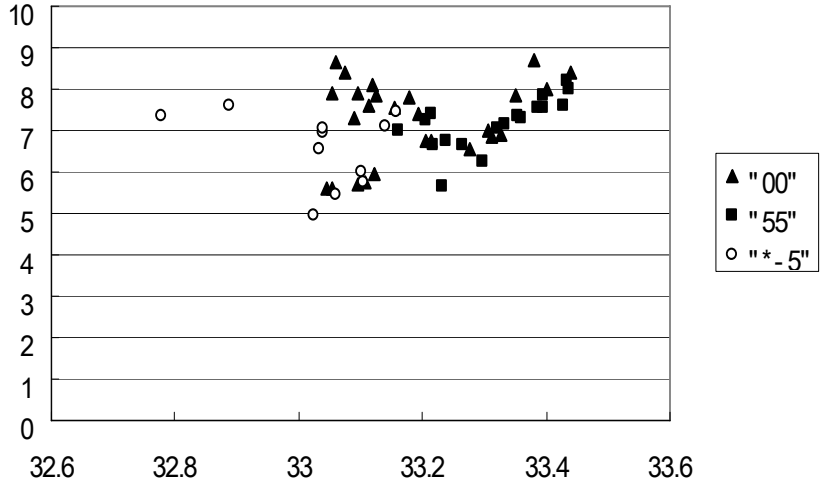

Fig. 11 Scatter diagram of water types at two observation points nearest to the coast at 50 m depth in December: “00” indicates the case in which the East Hokkaido Coastal Current is not seen (case 3), “55” the case in which the structure of the East Hokkaido Warm Current is seen both in temperature and salinity cross-section (case 2), and “* –5” the case that the structure of the Coastal Oyashio is seen at least in the salinity cross-section (case 1). Horizontal axis is salinity and vertical axis is temperature (°C).

As seen in Figure 5, the structure of the Coastal Oyashio may appear in December in some years. The water types in December are plotted in Figure 11 for three typical cases: case (1) in which the structure of the Coastal Oyashio is seen at least in the salinity cross-section, case (2) in which no East Hokkaido Warm Current is seen either in temperature or in salinity cross-sections, and case (3) in which no coastal band is seen along the coast. The domain of these water types are distributed overlapping one another. The water types of case (1) tend to have a lower salinity distribution, but their temperature and salinity values are considerably different from those in February and April when the typical Coastal Oyashio appears. The structure similar to the Coastal Oyashio in December might be called a forerunner of the Coastal Oyashio, but it should be mentioned that the water type is considerably different from the typical Coastal Oyashio.

Conclusions

It has been shown that the first half of the year is the season of the Coastal Oyashio, and the second half is that of the East Hokkaido Warm Current. The Coastal Oyashio shows the clearest appearance in February. A structure like the Coastal Oyashio is seen in December in some years. This means that the source of the Coastal Oyashio cannot be traced to the melt water of the sea ice in the Okhotsk Sea, otherwise, the Coastal Oyashio would be clearest in or after April.

In the summer season, the East Hokkaido Warm Current is hard to recognize because the surface layers of the area under consideration are covered by warm and less saline water. So, the temperature and salinity structures at 50 m depth appear to be the most suitable to analyze the seasonal changes in water type of the East Hokkaido Coastal Current (the Coastal Oyashio and the East Hokkaido Warm Current). The temperature and salinity of the East Hokkaido coastal Current Water show considerable seasonal variation. Typical water types can be determined only for each month. It is surprising that the water type is almost the same for each month whether the East Hokkaido Coastal Current exists or not. The water mass appears to have been modified before it reaches the region under consideration due to warming and precipitation through the sea surface or due to the influence of freshwater supply from land. This means that water mass analysis is not very effective for determining the source of the East Hokkaido Coastal Current Water.

Acknowledgements

The author wishes to express his thanks to Dr. Sachiko Oguma of the Hokkaido National Fisheries Research Institute, Mr. Kimihiro Aikawa and Mr. Keiichi Nagase of the Nemuro City Fisheries Research Institute, Mr. Iori Tanaka and Mr. Akifumi Nakata of the Hokkaido Central Fisheries Experimental Station, and Mr. Masashi Natsume of the Hokkaido Kushiro Fisheries Experimental Station for their co-operation and discussions throughout this study. Materials used here are based on the observations made by the Hokkaido Kushiro Fisheries Experimental Station. The author also thanks the officers and crew of R/V *Hokusei-Maru* for their great efforts in oceanographic observations. The research was conducted as part of the SakhNIRO/Nemuro City Joint Study on the Hanasaki crab.

References

Isoda, Y., Kuroda, H. Meisei, T. and Honda, M. 2003. Hydrographic feature of Coastal Oyashio and the seasonal variation. *Study Coastal Ocean* **41**: 5–12 (in Japanese).

Kono, T., Foreman, M., Chandler, P. and Kashiwai, M. 2004. Coastal Oyashio south of Hokkaido, Japan. *J. Phys. Oceanogr*. **34**: 1477–1494.

Ogasawara, J. 1990. The seas to the east and to the south of Hokkaido II. Physics. pp. 473–482 *in* Coastal Waters around Japan (Second series) (in Japanese).

Ohtani, K. 1980. The role of the Sea of Okhtsk on formation of the Oyashio Water. *Umi to Sora* **65**: 63–83 (in Japanese).

The occurrence of winter convection at the open ocean polynya in the eastern part of the Okhotsk Sea indicated by the World Ocean Atlas 2005

Makoto Kashiwai

Faculty of Bio-Industry, Tokyo University of Agriculture, Abashiri, Japan
E-mail: m3kashiw@bioindustry.nodai.ad.jp

Introduction

The Okhotsk Sea is identified as the principal ventilation site of the intermediate density waters of the North Pacific (Talley, 1991). This ventilation process is driven by an overturn associated with brine concentration from sea ice formation at coastal polynyas on the northeastern shelf. Previous studies on the source of North Pacific Intermediate Water, or on the formation of Kuril Basin Intermediate Water, Okhotsk Sea Intermediate Water, Okhotsk Sea Mode Water or Dense Shelf Water (Watanabe and Wakatsuchi, 1998; Galdyshev *et al*., 2003; Itoh *et al*., 2003; Shcherbina *et al*., 2004a,b; Yamamoto *et al*., 2004) have made no reference to the ventilation or convection process at the open ocean polynya in the eastern part of the Okhotsk Sea. "Winter convection" usually means a deepening of the surface mixed layer by cooling and stirring by cold air temperatures and strong winds, and in the Okhotsk Sea, is reported to occur in the upper 100–150 m layer (Moroshkin, 1966) and is believed to not penetrate below the halocline or the temperature minimum layer (Gladyshev *et al*., 2003).

While turning attention to the interannual variation in the water adjacent to the Okhotsk Sea, the effect of oceanographic processes of the Okhotsk Sea appearing in the Oyashio Water, depicted by monitoring on the 'A-line' by HNFRI/FRA, is the increased magnitude and earlier initiation of spring blooms after the 1998 regime shift (Kasai *et al*., 1997). This enhancement of primary productivity is associated with the increase in the density gradient of the water column within the euphotic layer (Kasai *et al*., 1997) by increased temperature or decreased salinity in the surface layer (Kasai and Ono, 2007). The basis for these changes in oceanographic structure may include the interannual changes in the waters lying over the intermediate density ranges, *i.e*., the water formed by winter convection. Thus, we need to pay attention to winter convection in the Okhotsk Sea.

In visualizing World Ocean Atlas 2005 (WOA05) data (Locarnini *et al*., 2006a,b) using Ocean Data View (ODV; Schlitzer, 2006) to obtain a standard textbook picture of wintertime surface mixed layer convection, we found a pycnostad, *i.e*., vertically dense homogeneous water extending down to *ca.* 500 m deep over the eastern part of the Okhotsk Sea in January. A pycnostad reaching this depth in the Okhotsk Sea has never been reported. Thus, this paper attempts to describe the pycnostad water, the history of its formation or deformation, its contribution in water mass formation processes in the Okhotsk Sea, and to indicate that pycnostad water is nothing more than the evidence of deep winter convection.

Pycnostad Water in the Eastern Part of the Okhotsk Sea

The WOA05 data indicate the existence of water having pycnostads in the eastern part of the Okhotsk Sea, in January (Fig. 1). This pycnostad water extends down to 300~500 m deep. As shown in Figure 2, this pycnostad water is not observed in December or February.

Pycnostad water in σ_0 sections

The left panel of Figure 3 is the January σ_0 section at 57.5°N, which runs on the northern shelf and at the northern end of TINRO Basin. The pycnostad reaching a depth of about 400 m exists on the bottom depression corresponding to the northern end of TINRO Basin. A low density surface layer of a few 10s of meters extends from the western (left) side of the section, but does not lie over the pycnostad water occupying the eastern (right) side of the section. The pycnostad water shows horizontal density variation

ranging from 26.2 to 26.7 σ_0, which corresponds to that of the water just above the Okhotsk Sea Mode Water (26.7 to 27.0 σ_0; Gladychev *et al.*, 2003). At the top of the pycnostad water, there is no surface mixed layer, *i.e.*, the surface 'sky-light' is open to the air and 'ventilation' is available.

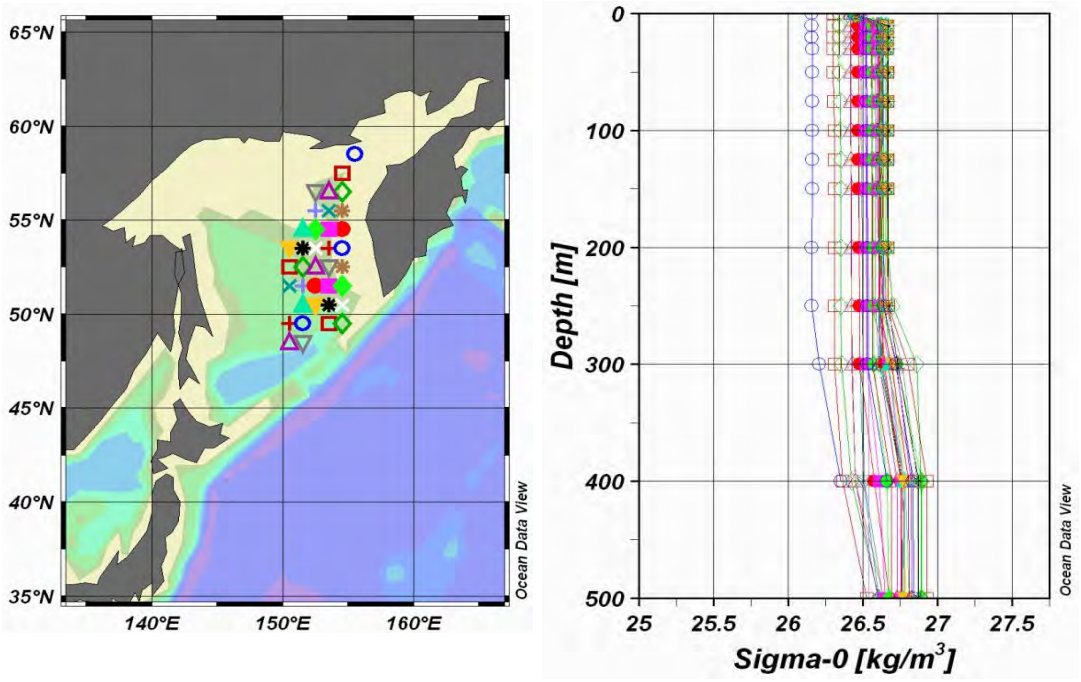

Fig. 1 January σ_0 profiles of the pycnostad water, and the location of the monitoring stations in the eastern part of the Okhotsk Sea.

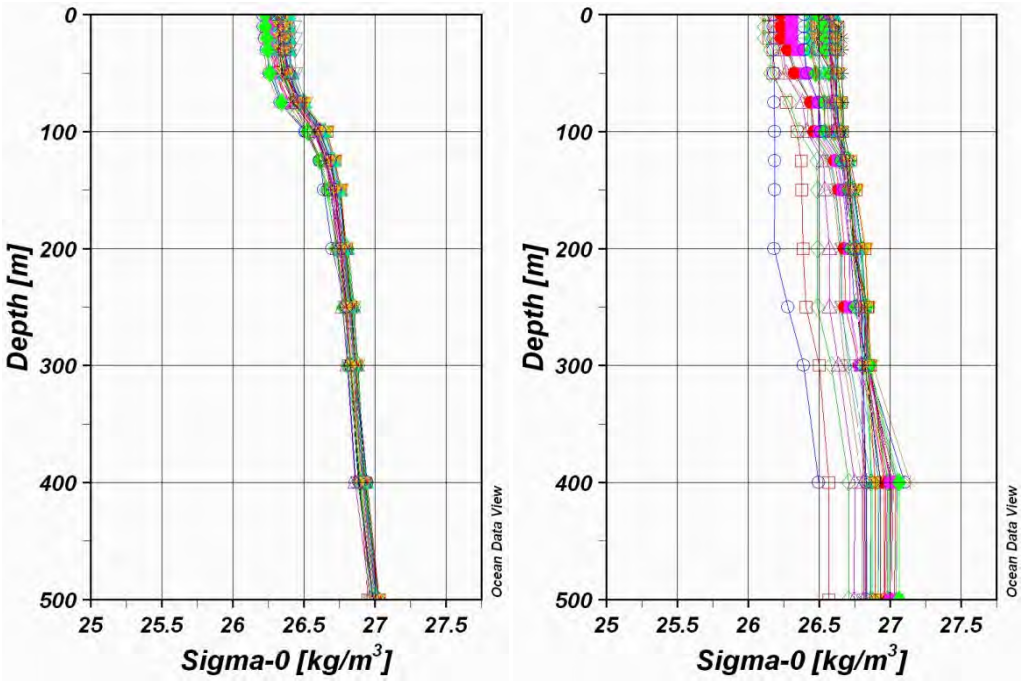

Fig. 2 December (left) and February (right) σ_0 profiles of the stations shown in the map of Figure 1.

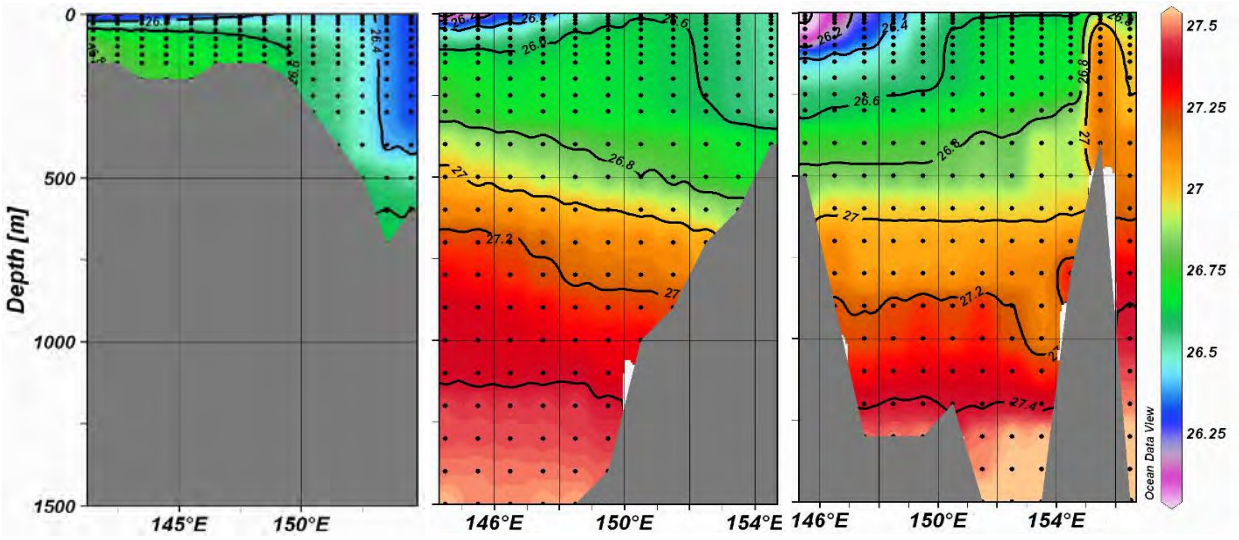

Fig. 3 January distribution of σ_0 (kg m^{-3}) for sections 57.5ºN (left), 53.5ºN (middle) and 49.5ºN (right).

The middle panel of Figure 3 is the 53.5ºN section, which passes through the northern part of Deryugin Basin (deeper than 1500 m in the Central Basin and east off the northern part of Sakhalin Island). In this section, the σ_0 range of the pycnostad water becomes a little denser to 26.5~26.6. The bottom of the pycnostad water extends westward along 350 m depth.

The right panel of Figure 3 is the 49.5ºN section, extending from the north of Cape Terpeniya to Onekotan Island, north of Kruzenshtern Strait. In this section, a higher density water mass of well mixed Kuril Islands Water appears in the eastern part of the section, connects with the pycnostad water interfaced by a sharp density front. This suggests that the tidal mixing and tidal exchange at/through the Kuril Straits have an important roll in the formation of the pycnostad water. The pycnostad water becomes denser to 26.6~26.7σ_0. The detailed structure (doming or depression) of the pycnostad water shown by shape of the isopycnals (*e.g.*, σ_0 = 26.6) can be interpreted as a result of either dynamic balance or local vertical mixing or convection. Thus, we must suspend interpretation here, based on a specific assumption.

As seen from Figure 3, the core density of the pycnostad water becomes less dense towards the north. On top of the dense homogeneous water, there is a very thin surface mixed layer with a pycnocline of moderate density gradient. The vertical gradient of σ_0 in the pycnostad water is as low as an order of 1 kg·m^{-3}·km^{-1} or less. The east–west difference in density structure in the upper layer (<500 m) suggests a geostrophic balance with strong currents, including the East Sakhalin Current, driven by a strong northerly winter monsoon.

The evidence of pycnostad water identified in the density sections can be summarized as follows:

- The T/S vertical profile compensating each other tends to be isopycnic;
- A horizontal density gradient exists;
- Depth reaches 300~400 m;
- The horizontal extent north–south is 1000 km and east–west is 300 km;
- It is observed only in January.

The most important questions to be addressed are "What is the nature of this pycnostad?" and "Is it merely a deepening of the surface mixed layer or the result of simple tidal mixing?" In view of its appearance only in January and disappearance in February, this pycnostad water may not be a simple deepening of the surface mixed layer or the result of tidal mixing.

T/S sections of pycnostad water

Figures 4, 5, and 6 represent the temperature and salinity sections corresponding to Figure 3. The temperature and salinity of the pycnostad water are not vertically homogeneous, but compensate each other so that the density becomes vertically homogeneous, as is clearly shown in the T/S diagram of pycnostad water for January (Fig. 11).

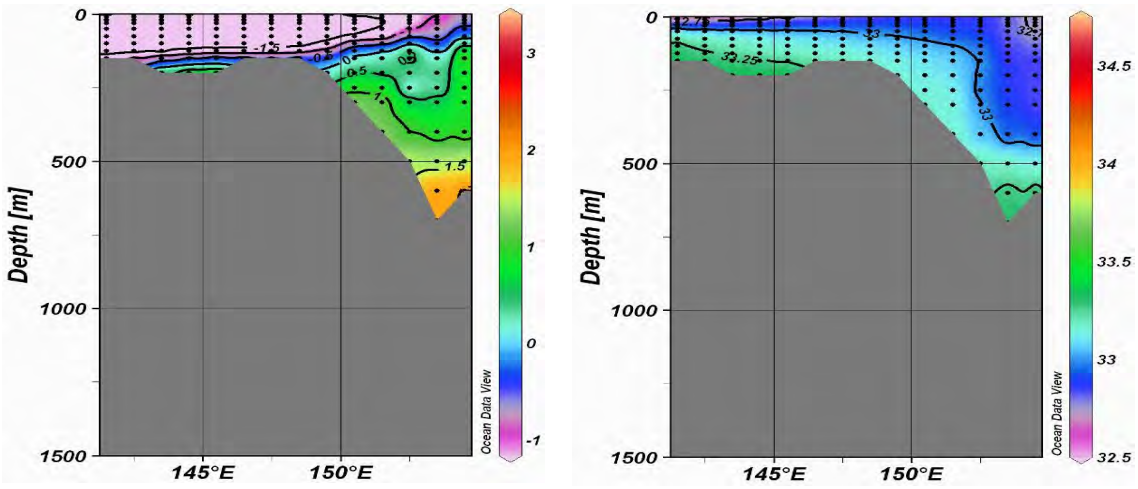

Fig. 4 57.5°N section in January for (left) temperature (°C) and (right) salinity (psu).

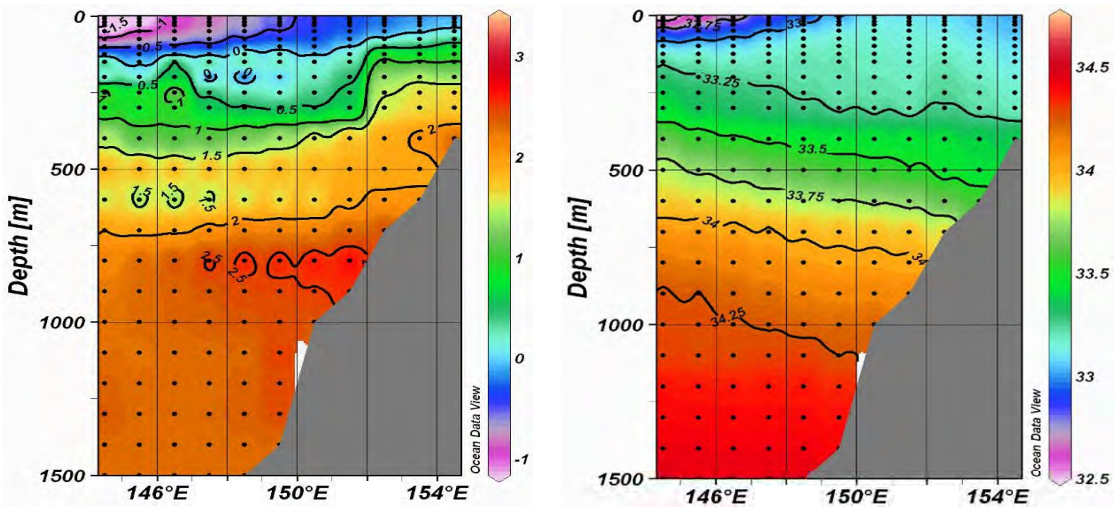

Fig. 5 53.5°N section in January for (left) temperature (°C) and (right) salinity (psu).

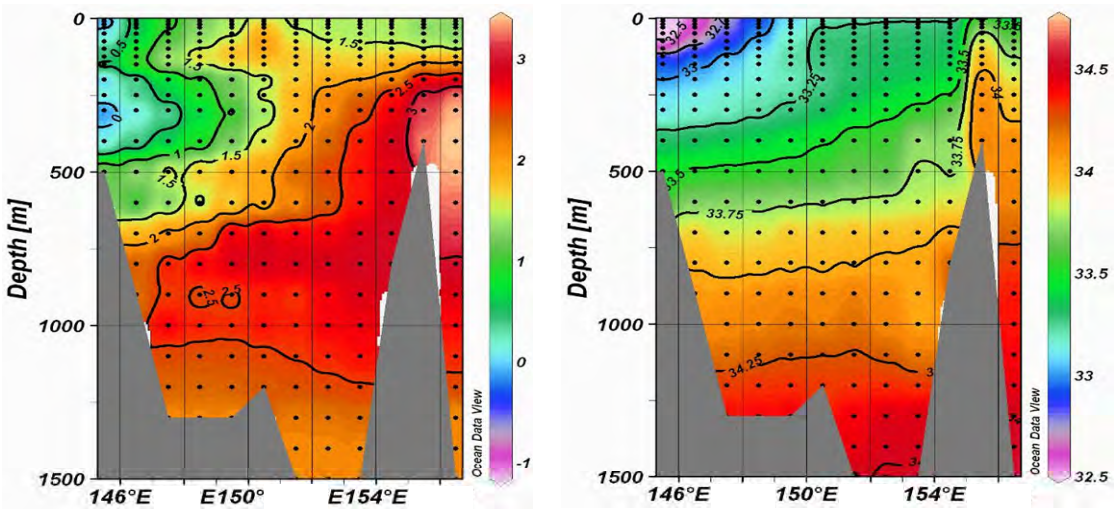

Fig. 6 49.5°N section in January for (left) temperature (°C) and (right) salinity (psu).

The important observations from the above temperature and salinity sections are as follows:

1) Warmer water extending from the North Pacific is dominant only in the middle layer of the southern part of Central Basin (Fig. 6, left). The surface of pycnostad water is covered by water colder and less saline compared to the water occupying the Kuril Straits. This means that the open ocean polynya observed in the eastern half of the Central Basin is not caused by the inflow of warm North Pacific Water.
2) Comparing with density sections, the effect of salinity dominates in determining density structure.
3) The major source of saline water is the inflow of North Pacific Water through the Kuril Straits.
4) The cold and low salinity water is distributed along the western side of the Central Basin, *i.e.*, along the coast of Sakhalin Island, but does not extend eastward beyond 150ºE.

The open ocean polynya and pycnostad water in the eastern part of the Okhotsk Sea had long been considered to be formed by the inflow of warm North Pacific Water, but this assumption is not supported by the temperature and salinity sections of Figures 4–6. Another possible explanation is that the polynya in the eastern part of the Okhotsk Sea can be formed and maintained, not by heat advection from the Pacific Ocean, but by mechanical processes, such as wind and/or currents. Thus, the pycnostad water could be formed by the result of local processes, *e.g.*, upwelling or vertical mixing or convection.

These two explanations bring quite different points of view on the watermass formation and modification process in the Okhotsk Sea. In order to answer the question "What will happen when sea ice of the Okhotsk Sea disappears due to global warming?", the cause and results of the open ocean polynya and pycnostad water in the eastern part of Okhotsk Sea will be very important.

Formation and Deformation of Pycnostad Water

Time evolution from December to January/ January to February

To look for evidence on possible formation mechanisms of the pycnostad water, the difference in time between December and January for the cross-sections of temperature, salinity and σ_0 in each section is shown in Figures 7, 8, 9. The T/S diagrams for December and January are shown in Figures 10 and 11, respectively.

The remarkable changes occurring from December to January are:

1) The density decrease of almost the entire water column of the Central Basin, except for the upper 100 m. The degree of decrease is more intense in the northern part;
2) The density increase of the surface mixed layer shallower than about 100 m in the middle and eastern portions of the sections;
3) The increase of salinity in the middle layer of the central section and decrease of temperature in the middle layer of the southern section. These changes may be the result of freezing.

These changes in temperature and salinity are shown in the general pattern of the T/S profiles between December and January (Figs. 10–11). The December T/S profile (Fig. 10) conserves characteristics similar to those of the Okhotsk Sea in summer time, *i.e.*, a fresh and warm surface layer, temperature minimum layer and deep temperature maximum.

The temperature minimum layer disappears from January T/S profiles (Fig. 11), while those of the surface/middle layer align parallel to isopycnals instead. The positions where the surface or intermediate layer T/S profiles are aligning correspond almost to the position of the temperature minimum layer in December ($26.4 \sim 26.7\sigma_0$), except at the shallow stations on the shelf. The aligned T/S profiles of the pycnostad water are the result of a salinity increase and temperature decrease in the surface water, and a salinity decrease and temperature increase or decrease in the water just below temperature minimum layer in December. This change means that the distribution of T/S plots becomes more compact. In other words, the uniformity of the water mass increases. The deep temperature maximum moves to a lower salinity and higher temperature position in January. Thus, we can see that the pycnostad water is formed by a density increase in the surface mixed layer of thickness *ca.*100 m, and by a density decrease in the rest of the water column.

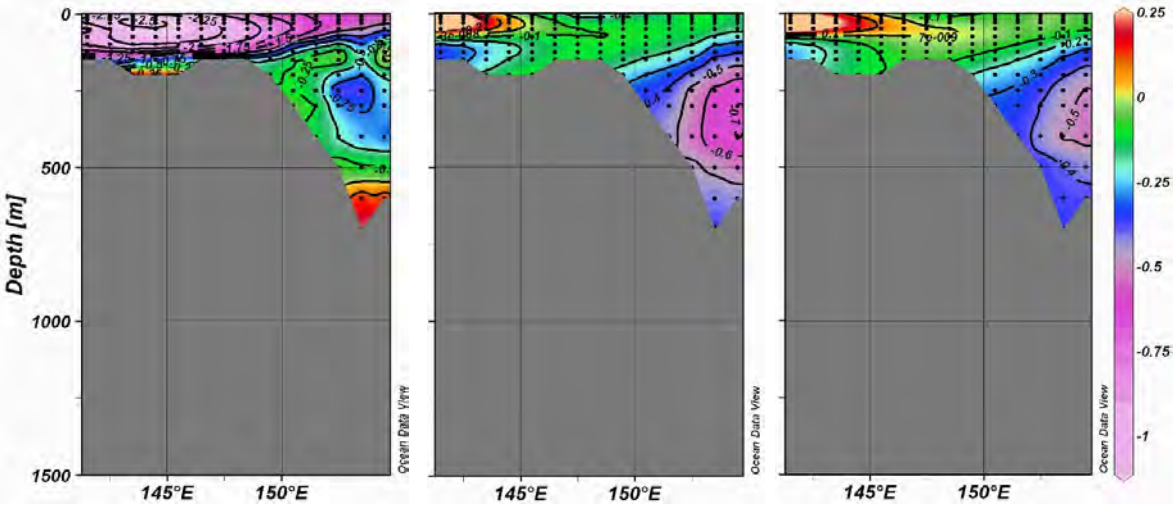

Fig. 7 The differences in (left) temperature, (middle) salinity and (right) σ_0 between December and January for the 57.5°N section.

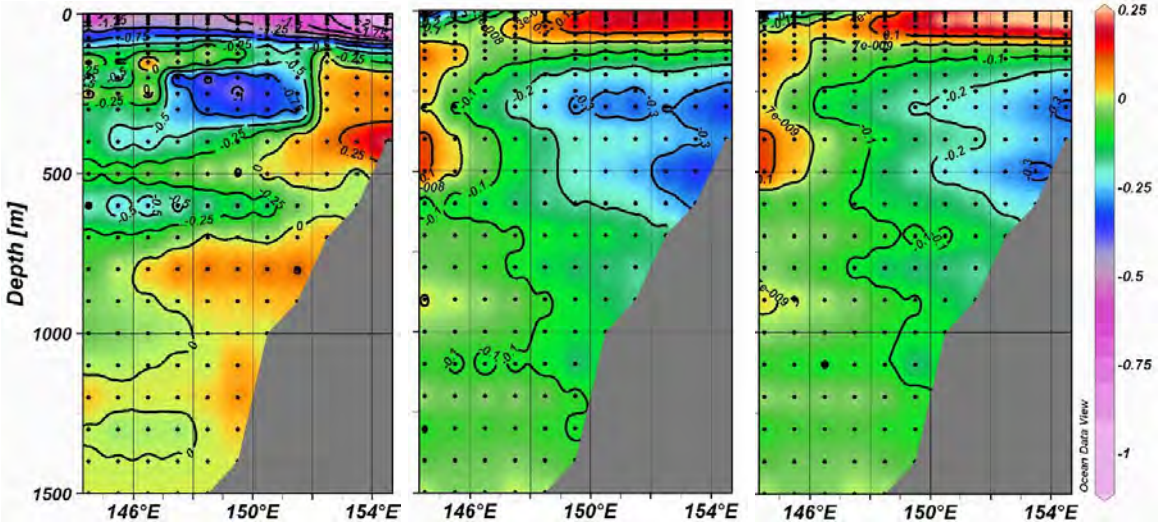

Fig. 8 The same as in Figure 7 but for the 53.5°N section.

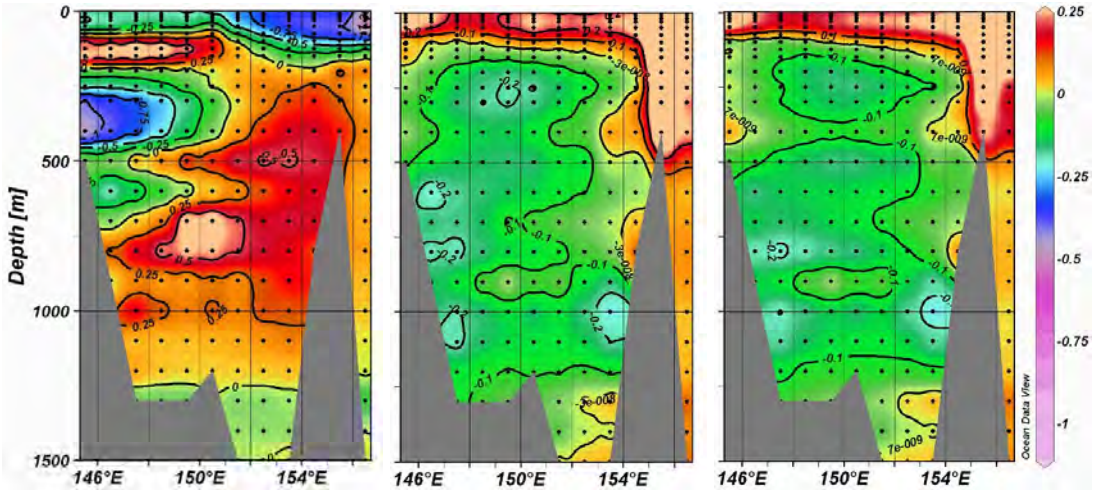

Fig. 9 The same as in Figure 7 but for the 49.5°N section.

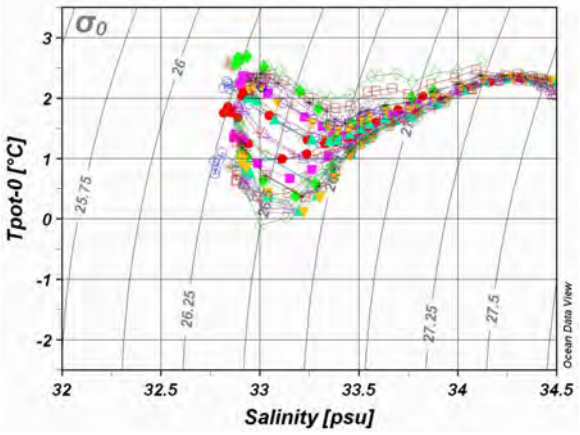

Fig. 10 T/S diagram of the pycnostad region in December.

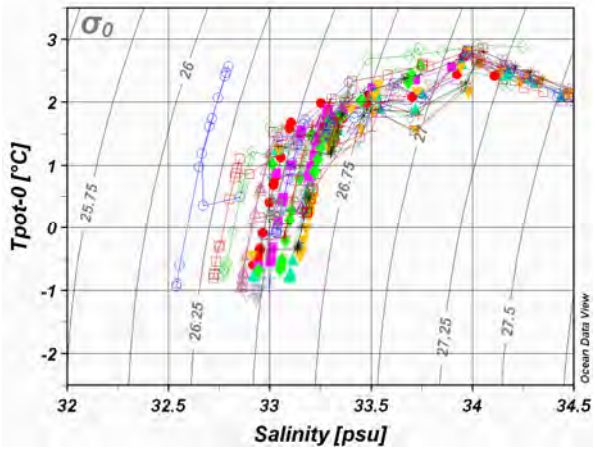

Fig. 11 T/S diagram of the pycnostad region in January.

The density increases of the surface layer in the eastern and central portion of sections are caused by an increase of salinity and decrease of temperature. These changes in T/S could be the result of vertical mixing with the lower layer. However, as shown in Figure 9, the increase of surface mixed layer salinity is most outstanding at the Kuril Straits, where salinity increases over whole water column. The tidal mixing at the Kuril Straits could transport higher salinity water from the deep layer, or from East Kamchatka Current Water. If the West Kamchatka Current, forming the northward flow of counter-clockwise circulation as the eastern side of the Okhotsk Sea circulation dominates, this saline water could be transported north along the western shelf slope of the Kamchatka coast. However, the existence of a sharp front, bounding the tidal mixing zone around the Kuril Islands, makes the explanation by simple advection of a water mass through it difficult, and needs to be explained using transport by tidal currents, *i.e.*, tidal exchange.

The decrease in density in the lower layer of the sections corresponds to the decrease in salinity and partly to the increase in temperature, though the contribution of the latter is not remarkable. However, what is notable is the decrease in salinity of the lower layer in the northern section as shown in the middle panel of Figure 7, and the increase in temperature of middle layer in the southern section as shown in the left panel of Figure 9.

As the changes in temperature and/or salinity from December to January are different in the layers, explaining the mechanisms of changes by isopycnal mixing will be not easy. Possible mechanisms of decreasing density by a decrease in salinity in the lower layer of the northern section can be vertical mixing, convection by surface cooling, and strengthening of the cyclonic gyre. Among these, the only mechanism that can generate a pycnostad with compensating T/S distribution is the sinking of the water parcel by a density increase to the depth with same density, *i.e.*, cooling convection.

In the February T/S diagram (Fig. 12), for the same water for Figures 10 and 11, the vertically dense homogeneous water is not so developed as in January. However, through careful examination of Figure 12, we will find the following features; (1) the pycnostad waters starting from the surface still exist in the lower salinity stations, *i.e.*, in the stations on the shelf; (2) the middle layer pycnostad waters can be indentified in the intermediate density layer (σ_θ = 26.8 ~ 27.1). The possible mechanism forming intermediate pycnostad layer can be diapycnal mixing by tidal currents and bottom topography. This is an important and interesting phenomenon, but in order to focus of this paper on the formation mechanism of the pycnostad layer starting from the surface, here it is sufficient to just point out this phenomenon.

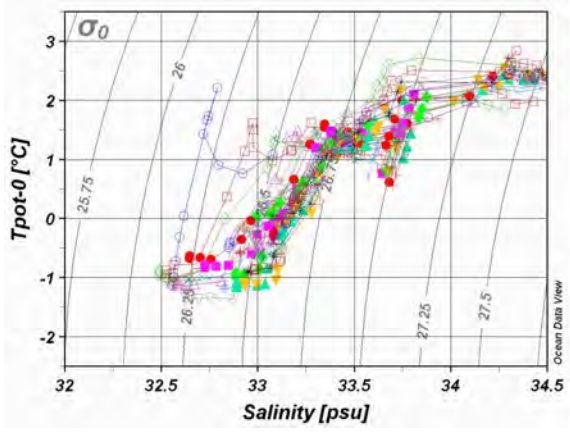

Fig. 12 T/S diagram of pycnostad region in February.

Changes in volume of water for density ranks

The changes in the volume of water for each density rank are clearly shown by comparing the occurrence of σ_0 ranks in each section between January and February (Fig. 13). As the occurrences are counted for data of standard depths, having different spacing from surface to depth, the counts of occurrence are not equally comparable between different σ_0 ranks.

The formation of pycnostad water is clearly shown as dominant peaks in the January histogram (Fig. 13, upper panel) at σ_0 of 26.2~26.7, which corresponds to the density range of the water just above the Okhotsk Sea Mode Water in the Okhotsk Sea, and to the density range of Oyashio Water just above the temperature minimum layer or around the salinity minimum layer. This formation can still be observed among the histogram peaks in February when the pycnostad water is already deformed. However, the volume of water having higher σ of 26.75~27.1 increases between January and February. At the same time, the volume of water having a lower density increases in the northern section. Thus, winter is the season when the water masses of surface, intermediate and deeper layers are formed through typical mechanisms, including that which forms pycnostad water.

Is it Deep Convection?

The most plausible formation process of this pycnostad water, having a signature of aligned T/S profiles, is 'deep convection', because this signature is quite similar and unique to that of deep convection sites, such as the Gulf of Lions, south of France (Schott *et al*., 1996) and/or the Labrador Sea (Lilly *et al*., 1999). The T/S profiles for these deep convection sites produced from WOA05 data also indicate the existence of a pycnostad exhibiting T/S profiles aligning along the isopycnals (Fig. 14).

The semblance of the T/S profiles may not be enough to identify winter convection as the process responsible for the formation of the pycnostad. Thus, we must first present an overview of past studies in order to understand the specific requirements of winter deep convection; then those requirements may be examined for the case of eastern part of Okhotsk Sea.

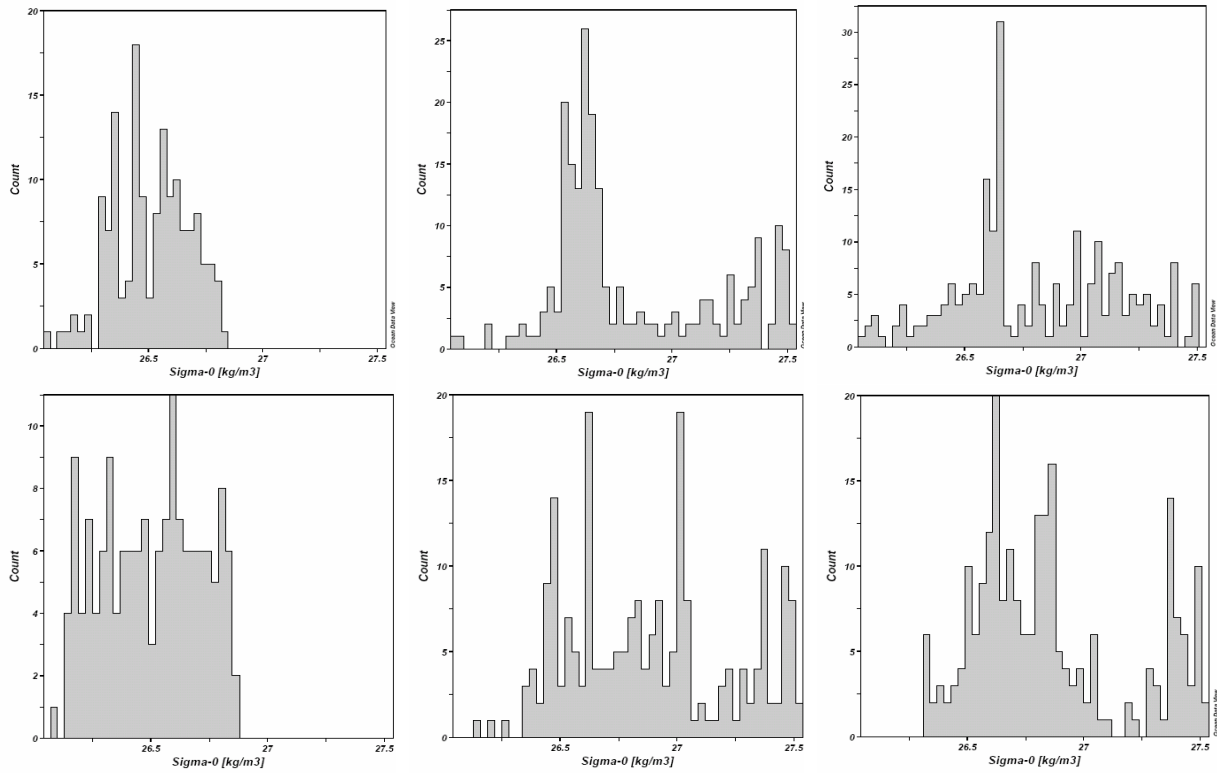

Fig. 13 Comparison between the occurrence of σ_0 ranks in January (upper panel) and February (lower panel); left: 57.5°N section; middle: 53.5°N section; right: 49.5°N section.

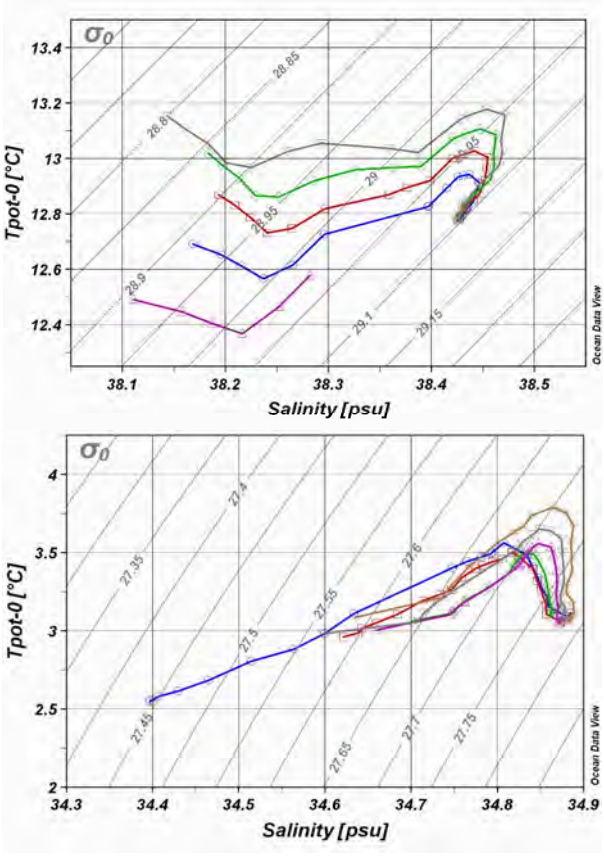

Fig. 14 T/S diagrams in February for (top) Gulf of Lions and (bottom) Labrador Sea.

The development of convective overturn is well illustrated not only through intensive field studies by Schott *et al*. (1996) and Lilly *et al*. (1999), but also through a series of laboratory tank experiments by Maxworthy and Narimousa (1994) and through a series of plume-resolving numerical model experiments by Send and Marshall (1995).

Deep convection in the Gulf of Lions and the Labrador Sea

Based on extensive observations, the development of deep convection in the Gulf of Lions (Send and Marshall, 1995; Schott *et al*., 1996) can be outlined as follows:

1) The situation leading to deep convection is based on a permanently present cyclonic circulation.
2) This cyclonic circulation leads to a doming of the isopycnals with shallowest mixed layer depths.
3) Cold and dry offshore winds blow from the land over the isopycnal dome: the Mistral out of the Rhone Valley and the Tramontane from the Pyrenees.
4) With continued cooling during the early phase of winter, the upper layer continues to be cooler, deeper, and saltier by entraining warm and saline water from below.
5) The stability against the weakly stratified sublayer is reduced enough for deep convection to set in.
6) The downwelling velocities (exceeding 10 cm s^{-1}) of dense water plumes 'raining down' from surface mixed layer are compensated by upwelling velocities in between the 'convection plumes' and thus the integral effects of a patch of convection plumes are mainly to act in mixing the water column vertically and do not act as the mechanism of net vertical mass transfer.
7) These convective plumes comprise a convection region called the 'Convection Chimney' of 50~100 km scale.
8) A 'rim current' is generated around the edge of the convection regime, in thermal wind balance with the density gradient between the interior of the regime and the exterior.
9) The rim current develops meanders and instability eddies. These eddies break up the convection chimney into 'cones'. The heavy water in the cones propagates and slumps down to its neutrally buoyant level, adding extra volume to the deep water.
10) Under weakened forcing, a thin stratified surface layer of warmer water moves in by lateral advection and forms capping over convection water.
11) Immediately following the end of convection, the convection region is a mixture of cold/fresh and warm/salty water, which soon settles down into a more isopycnally homogeneous and vertically stratified state through the sorting and mixing of lateral fine structure.

The Labrador Sea is one of the deepest convection sites in the world ocean. Air temperatures at nearby Iqaluit can average colder than –30ºC during winter months, when northerly and northwesterly winds can average 6 m s^{-1}. The regional ocean circulation is dominated by a cyclonic circulation, the western extremity of the cyclonic subpolar gyre of the North Atlantic. The sea off the continental shelf is held ice free by an inflow of warm, saline waters from the subtropics. This collision of cold air and ice-free ocean leads to large upward heat flux, reaching 700 W m^{-2} or more, with monthly averages in the range 200~300 W m^{-2}. Combined wind and

buoyancy forcing uplifts isopycnals in the central Labrador Sea, reduces the stratification and makes the central waters susceptible to repeated deep convection.

Another important characteristic of winter convection is an essentially instable oceanographic structure, with increasing instability by negative buoyancy flux at the sea surface, sustained by dynamic balance, with increasing cyclonic circulation spun up by increasing wind stress. Thus, winter convection is a transitory phenomenon only observable during a strong and cold wind event. When driving forces of convection weaken or stop, the pycnostad water, forming a 'convection chimney', will collapse down into the oceanographic structure with density stratification in hydrostatic balance.

The process of winter deep convection forces us to revise the ordinary concept of 'ventilation' with an outcropping of isopycnals at the surface. With the exception of deep convection events, there remains a firm stratification with capping by the surface mixed layer. We cannot expect to capture the evidence of winter deep convection by making usual bimonthly or monthly ship observations, as winter deep convection can occur during monitoring breaks.

During deep winter convection, cyclonic circulation and its enhancement by strong, cold, dry winter winds blowing off the surface capping layer, and source of the salinity supply, can be common preconditioning and driving factors for the winter convection, as summarized in Table 1. Thus, in order to identify the mechanism of pycnostad water formation in the eastern part of the Okhotsk Sea to be winter convection, the occurrences of these factors will be examined in the next section, and compared to the Gulf of Lions and Labrador Sea.

Comparison of the Gulf of Lions and Labrador Sea, and with the Okhotsk Sea

We must note that the winter convection in the Gulf of Lions and the Labrador Sea is facilitated by the existence of higher salinity and higher temperature subsurface water, and with temperature maximum and salinity maximum or halostad, these are characteristics of tropical or subtropical waters. On the other hand, in the Okhotsk Sea the density stratification is mainly comprised from salinity stratification. Another difference is in the temperature of convection water, with potential temperature ranging from 12.8~12.95ºC in the Gulf of Lions (Schott *et al*., 1996) and 2.7~2.9ºC in the Labrador Sea (Lilly *et al*., 1999) compared to –1.0~2.0ºC in the Okhotsk Sea.

Surface cooling will bend the head of T/S profiles downward to be aligned to isopycnals. Further cooling will shift them to the right (direction of salinity increase), as vertical mixing associated with convection produces mixed water of less saline and cold water surface water, and saline and warmer intermediate water. Colder air with stronger winds will deepen the convection depth. In the case of the Gulf of Lions or the Labrador Sea, this procedure can take place in a temperature domain far higher than the freezing point while in case of the Okhotsk Sea, as water temperature is ranging near zero, and density is determined mainly by salinity, freezing

Table 1 Comparison of factors preconditioning and driving winter convection in the Gulf of Lions, Labrador Sea and Okhotsk Sea.

Factors preconditioning and driving winter convection	Winter convection sites		
	Gulf of Lions	**Labrador Sea**	**Okhotsk Sea**
Cyclonic circulation	Yes	Yes	Yes
Strong wind	Yes (Mistral)	Yes	Yes
Coldness	Yes	Yes	Yes
Open water	Open water	Open water	Open ocean polynya
Salinity supply	Warmer and saltier (13ºC, 38.47 psu) Levantine Intermediate Water	Warm and high salinity (4ºC, 34.95 psu), Irminger Water	Sea ice formation (North Pacific Water?)

can be easily reached. Therefore, for the winter convection to occur in the Okhotsk Sea, we need to consider the possible contribution of sea ice formation.

Another characteristic of the convection region in the Okhotsk Sea is that it is connected to the pycnostad waters in the Kuril Straits and to shallow water on the shelf, where strong tidal mixing dominates. Therefore, we also need to examine the effects of tidal mixing.

Factors preconditioning and driving winter convection in the eastern part of the Okhotsk Sea

Cyclonic circulation and strong winds

As currents over the Okhotsk Sea are difficult to measure in winter, a map of general circulation is produced only for the warm season, as shown in Figure 15. In this figure, the general cyclonic circulation around the Okhotsk Sea can be recognized, traced by the major currents.

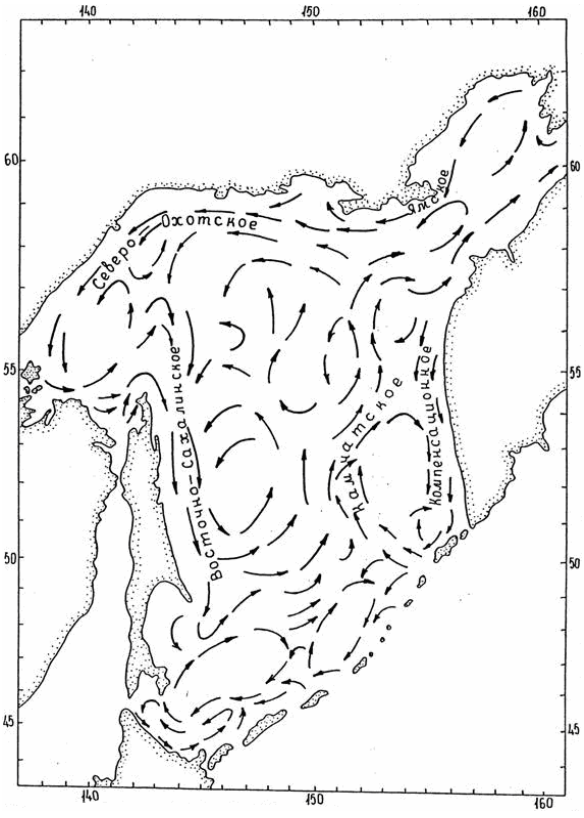

Fig. 15 General surface circulation of the Okhotsk Sea (Luchin, 1998). Clockwise from top right: the Yamskoe Current, the (West) Kamchatka Current and its northern countercurrent branch, the East Sakhalin Current, and the Northern Okhotsk Current.

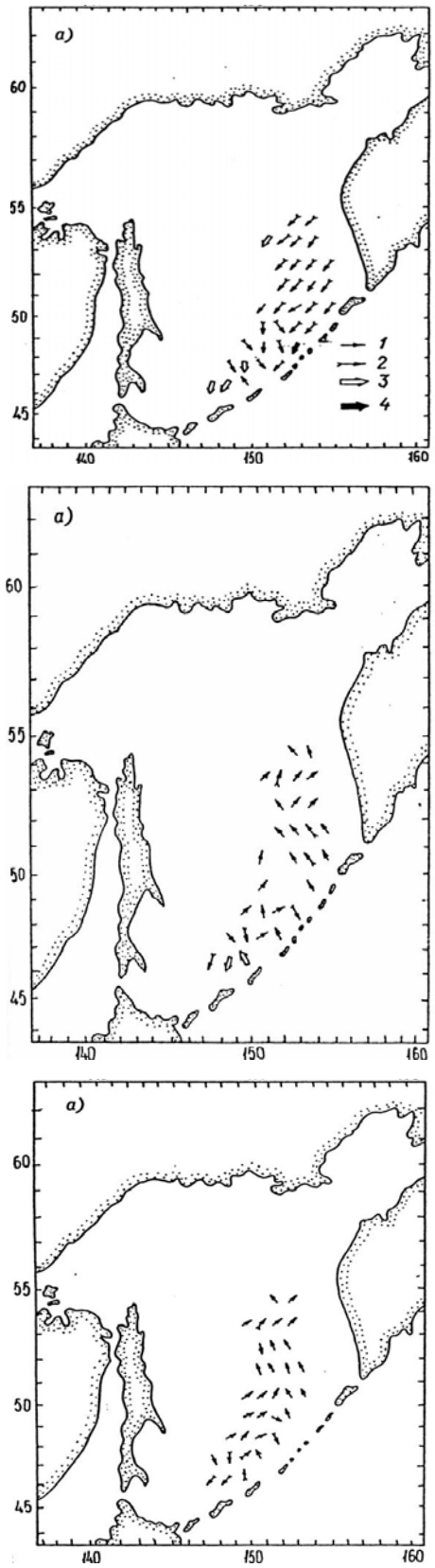

Fig. 16 February currents in the Okhotsk Sea calculated from density distribution and surface wind stress: (top) surface; (middle) 5m; (bottom) 100 m. (Luchin, 1998).

Figure 16 shows the surface, 5 and 100 m current vectors in the open water of the Okhotsk Sea in February (Fig. 16). The surface current vectors are directed southwest, indicating Ekman transport caused by strong northern winter monsoons. However, the current vectors for the 5 and 100 m layers are directed northward. Figure 17 displays the monthly mean transport of the East Sakhalin Current at 53ºN (Mizuta *et al.*, 2003). Therefore, the observed currents in winter are a strong northward current (the West Kamchatka Current) in the eastern part and a strong southward current (the East Sakhalin Current) in the western part of the Okhotsk Sea, indicating the development of a cyclonic circulation by strong winter monsoons. The transport of the East Sakhalin Current has a sharp peak in January–February, indicating that the driving wind is strongest at this time of year (Fig. 17).

Coldness and ice cover

A comparison of net heat flux between four marginal subarctic seas (Wang *et al*., 2007; Fig. 18) shows that the net heat flux from the sea surface greater than 200 $W \cdot m^{-2}$ occurs in the Okhotsk Sea during winter (December and January), and is the greatest among the four marginal subarctic seas.

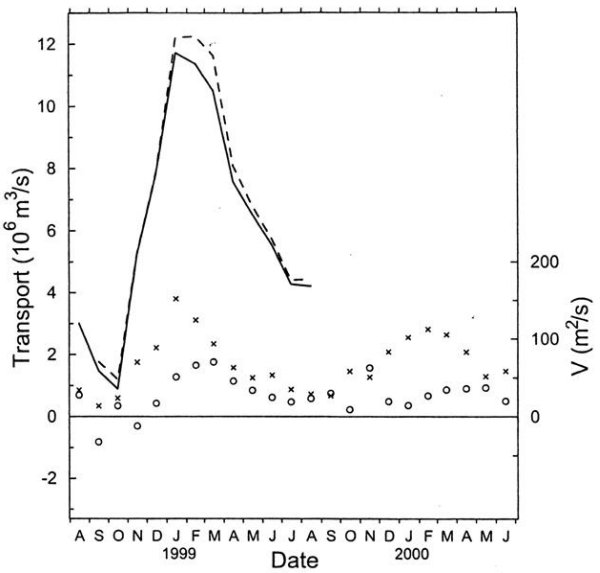

Fig. 17 Time series of the monthly mean transport (10^6 m^3s^{-1}) and vertically integrated velocity obtained from the data of four moorings M1 to M4 on the cross section at 53ºN on the east shelf slope of the Sakhalin Island. Solid and dashed lines denote the transport with and without the extrapolation outside of the mooring sites, respectively. Positive value indicates southward transport. Crosses and open circles indicate vertically integrated velocity at mooring sites M2 and M4, respectively (Mizuta *et al*., 2003).

Ice cover over the Okhotsk Sea exhibits large interannual variation, with a maximum of 150 × 10^4 km^2, minimum of 80 × 10^4 km^2, and average of 115 × 10^4 km^2. The period of annual maximum extent is February~March. Even in this period the open ocean polynya exists in the eastern part of the Okhotsk Sea, except when almost the whole Okhotsk Sea is covered by sea ice at the time of historical sea ice extent.

Ice potential analysis

For winter convection to reach a specific depth penetrating shallow stratification of surface capping, the density of the surface water must become equal to the density of water at that specific depth, through an increase of density by a decrease of temperature through cooling, and/or by an increase of salinity through the entrainment of saltier water laterally or vertically, as shown in the cases of the Gulf of Lions and the Labrador Sea. However, in the case of the subarctic Pacific, as density stratification is mainly determined by salinity stratification, simple cooling cannot cause density inversion and automatically deepen the cooling convection as in the subtropical waters or waters under the influence of subtropical water. Therefore, salinity increase through brine concentration during ice formation is an important driving factor for winter convection to reach deeper depths.

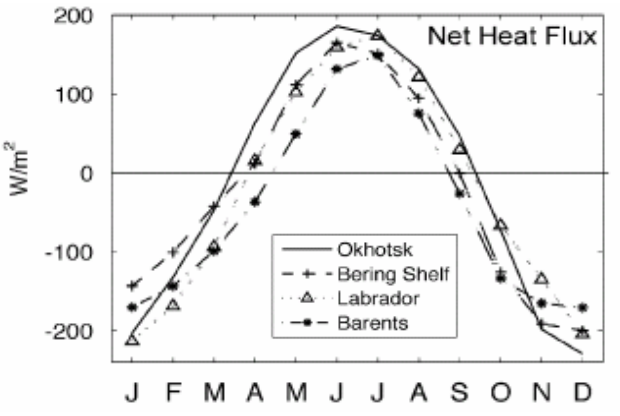

Fig. 18 Comparison of annual cycle of net heat flux among four marginal seas around the North Pacific (Wang *et al*., 2007).

Zubov (1945) coined the term 'ice potential', the amount of heat to be transferred from the water surface to air, necessary for convection to reach a specific depth 'without ice formation' in an effort to answer the questions "When will sea ice be formed?" and "How much heat is needed to be transferred from the water column to air before sea ice can form?" Terms needed to compute the ice potential include thickness of ice to be formed for convection to reach a specific depth, and the heat necessary to be transferred from sea. Thus, the ice potential calculation can be a useful diagnostic tool to determine winter convection in the first order approximation.

For calculation, the density of seawater is assumed equal to 1.00; density of sea ice is assumed equal to 0.90; salinity of sea ice is assumed 0; and latent heat of sea ice is equal to 335 $kJ \cdot kg^{-1}$ (= 80 $cal \cdot g^{-1}$). Results for the January ice potential at 52.5ºN, following the method of Zubov (1945) introduced by Tabata (1977), are shown in Tables 2 and 3. Table 2 shows the thickness of ice to be formed in order for convection to reach different depths for various stations. At the stations east of 149.5ºE, ice does not need to be formed by cooling for convection to reach as far down as 300 m. For stations in the western part of the section, ice some 10s of centimeters thick need to be formed by cooling in order for convection to reach beyond 100 m depth.

Table 2 Ice potential as depth of convection and ice thickness for January at 52.5°N in the Okhotsk Sea. The ranks of ice thickness are indicated by colour of cells: red: 0–10 cm; orange: 10–20 cm; yellow: 20–40 cm; green: 40–60 cm; light blue: 60–80 cm; blue: 80–100 cm; purple: 100–140 cm.

Ice Potential / Ice Thickness (cm) / 52.5°N January / Okhotsk Sea												
Depth	**144.5E**	**145.5E**	**146.5E**	**147.5E**	**148.5E**	**149.5E**	**150.5E**	**151.5E**	**152.5E**	**153.5E**	**154.5E**	**155.5E**
0 (m)												
10												
20	11	7	5	3	3	3	4	0	0	0	0	8
30	27	20	14	10	3	3	4	3	2	2	2	8
50	32	26	14	10	7	6	4	3	3	2	2	8
75	38	27	20	14	10	8	4	3	3	3	4	9
100	50	35	27	20	15	13	4	4	4	5	7	22
125	83	74	38	31	28	22	6	7	8	9	10	45
150	98	83	69	56	43	25	8	9	10	12	10	45
200	151	131	110	86	59	23	8	9	11	12	10	
250		148	120	91	54	21	7	9	12	14	10	
300		178	143	104	58	13	8	13	19	22	19	
400		336	168	127	81	38	27	28	37	55	91	
500		559	477	414	185	151	143	150	152	216		
600		632	544	475	409	354	321	312	289	376		
700		1335	1242	1161	1093	1034	543	506	483			
800		1348	1256	1187	1121	1062	1003	971	945			
900		1702	1585	1518	1453	1400	1354	1345				
1000		1874	1796	1739	1676	1627	1592	1602				
1100		1882	1986	1957	1921	1892	1869					
1200		1965	1995	2037	2058	2045	2035					
1300		2176	2261	2414	2417	2340						
1400		2426	2545	2743	2674							
1500		2628	2668									

Table 3 Ice potential as depth of convection and necessary heat transfer for January at 52.5°N in the Okhotsk Sea. The ranks of necessary heat transfer are indicated by colour of cells: red: 0–500 MJ m^{-2}; orange: 500–1000 MJ m^{-2}; yellow: 1000–1500 MJ m^{-2}; green 1500–2000 MJ m^{-2}; light blue: 2000–2500 MJ m^{-2}; blue: 2500–3000 MJ m^{-2}; purple: 3000–3500 MJ m^{-2}.

Ice Potential / SumQ (MJ m^2) / 52.5°N January / Okhotsk Sea												
Depth	**144.5E**	**145.5E**	**146.5E**	**147.5E**	**148.5E**	**149.5E**	**150.5E**	**151.5E**	**152.5E**	**153.5E**	**154.5E**	**155.5E**
0[m]												
10												
20	44	71	77	81	85	90	95	86	87	89	94	123
30	111	158	166	171	163	173	181	182	182	185	191	219
50	152	228	230	243	254	263	267	269	271	275	285	313
75	235	341	376	399	418	435	439	446	452	464	494	509
100	375	517	569	604	633	666	657	678	697	727	788	805
125	627	816	792	838	880	927	891	928	965	1015	1096	1178
150	900	1061	1110	1134	1159	1177	1134	1188	1243	1311	896	977
200	1361	1481	1505	1487	1465	902	842	872	1514	1597	1705	
250		2021	2001	2010	1893	747	1846	1951	2065	2188	2309	
300		2563	2501	2577	2318	2265	2322	2489	2659	2828	2973	
400		3554	3085	3203	2877	2850	2913	3105	3341	3609	3886	
500		5216	5025	5118	4267	4350	4503	4819	5129	5658		
600		6740	6500	6593	6270	6342	6499	6851	7118	7764		
700		10249	9977	10042	9739	9828	8653	8980	9311			
800		11688	11414	11539	11271	11397	11604	11989	12391			
900		14445	14038	14179	13940	14117	14456	14912				
1000		16709	16376	16563	16351	16564	16996	17497				
1100		15348	18672	18961	18844	19127	19592					
1200		20389	20419	20940	21005	21344	21830					
1300		22707	22919	23786	23808	23964						
1400		25147	25469	26472	26269							
1500		27457	27542									

Important features of Tables 2 and 3 are that a reduction in heat transfer of 3×10^3 MJ·m^{-2} can deepen the pycnostad water down to 400 m, with a total ice production of 30 cm. With the help of wind forcing creating anti-cyclonic circulation in the blowing off of the surface mixed layer, the necessary heat flux from the surface by cooling will be largely reduced. For validation of this possibility, estimates of heat flux at severe cooling events are needed.

Note the fact that although sea ice does not exist on the pycnostad water, it should not be understood as evidence for the disproof of the ice potential calculation. During a deep convection event, newly formed frazil ice and the surface mixed layer are to be blown off from the convection region but denser water produced by ejected brine can form a downwelling plume to drive convection.

Contribution of tidal mixing to winter convection

The unique feature of winter convection in the eastern part of the Okhotsk Sea is that the convection region is connected to the tidally mixed waters on the shallow coastal shelf and in the Kuril Straits. As the strong tidal current prevails in the coastal shelf from the west coast of Kamchatka through Shelikov Bay to the northern coast of the Okhotsk Sea, and in the Kuril Straits, vertically mixed water can be distributed around these areas and be advected along horizontal circulation. However, since the pycnostad water and convection with ice formation can only be observed in January, tidal mixing cannot be the major driving factor in the formation of pycnostad water and winter convection.

Conclusion

Judging from the factors preconditioning and driving deep convection (Table 1), the pycnostad water in the eastern part of the Okhotsk Sea can be seen as evidence of ongoing winter convection. The wind stress of strong northerly winter monsoons over the Okhotsk Sea drives the cyclonic circulation of the sea, including the East Sakhalin Current and the West Kamchatka Current, and accumulates and piles up the surface water and drift ice to the western side of the sea. This may be a possible mechanism for maintaining the open ocean polynya in the eastern half of the Okhotsk Sea.

The volume of water increased as the result of deep convection is the water having a σ_0 range of 26.75~27.1, which corresponds to the density of Okhotsk Sea Mode Water for the inside of the Okhotsk Sea, and to that of intermediate layer of Oyashio Water for the outside of the Okhotsk Sea. Thus, stronger and/or longer winter convection will produce a larger volume of Okhotsk Mode Water or water of the intermediate layer of Oyashio Water, which can make the intermediate layer of Oyashio Water colder and less saline. This suggests that the extent of decreased sea ice accompanied by global warming can bring a colder and less saline intermediate layer of Oyashio Water into the Okhotsk Sea.

In considering the results of winter convection on watermass formation and modification in the eastern part of the Okhotsk Sea, we note that the water mass formed by winter convection:

1) is not a homogeneous water mass that can be represented by single water type, but a group of pycnostad water types with different T/S value pairs for different depths and with different horizontal density trends;
2) has a relatively large spatial extent, with a range of 10ºN × 3ºE (*ca.* 1000 km × 300 km), comparable or larger than that of the Labrador Sea or Gulf of Lions.

Thus, the water mass produced by winter convection at the open ocean polynya of the Okhotsk Sea will cause considerable interannual variability in temperature and salinity of the intermediate layer in response to the interannual variability of the winter climate in the region.

Kasai *et al.*'s (1997, 2007) analysis of the A-line dataset shows the enhancement of primary productivity in the Oyashio region after the 1998 regime shift, and the increased density gradient in the euphotic zone by increased temperature and/or lowered salinity in the surface layer can be the possible environmental conditions causing enhancement of primary production. The present study suggests that winter deep convection can be one of the physical processes causing these changes.

Subjects for future studies

This is a preliminary study, as analyses are limited to winter and at the stations of pycnostad sites. The deep convection resulting from cooling at the sea surface persists only for a period of a few days but occurs over regions of horizontal extent of order of 100 km (Thorpe, 2005). However, depending on its spatial scale, the resultant effect on water mass formation is not negligible, although the temporal nature of the phenomenon makes winter deep convection seem like a trivial transient event and hides its existence from synoptic features. Thus, it is a marvel that the WOA05 contains a fine shot of winter deep convection in the Okhotsk Sea.

Furthermore, as primitive equations used in general circulation models exclude convection with vertical acceleration, diagnosing or interpreting winter convection by ordinary general circulation models based on the premise of a hydrostatic ocean, are basically difficult. Thus, the development of a combined atmosphere–sea ice–ocean model that allows winter deep convection is necessary for assessing the effects of winter deep convection on climate variability associated with global warming.

The following items are subjects for study of the Okhotsk Sea to be performed in near future under international collaboration such as the PICES FUTURE (Forecasting and Understanding Trends, Uncertainty and Responses of North Pacific Marine Ecosystems) program:

1) The necessary preconditioning for winter convection, including possible maximum heat transfer from sea to air during cooling events;
2) The time change in temperature and salinity, including the effect of inflowing East Kamchatka Water;
3) The process of mixing and transport of ejected brine at ice formation sites on the shelf;

4) The freshwater supply to open water by stray drift ice;
5) The effects of tidal mixing and internal tides on the formation of pycnostad water;
6) The response of the convection process to interannual climate variability.

A full elucidation of the winter convection process needs to be addressed in field process studies, including the use of pop-up floats, modeling studies, and historical data analyses.

References

Gladyshev, S., Talley, L., Kantakov, G., Khen, G. and Wakatsuchi, M. 2003. Distribution, formation, and seasonal variability of Okhotsk Sea Mode Water. *J. Geophys. Res.* **108**: 3186, doi: 10.1029/2001JC 000877.

Itoh, M., Ohshima, K.I. and Wakatsuchi, M. 2003. Distribution and formation of Okhotsk Sea Intermediate Water: An analysis of isopycnal climatological data. *J. Geophys. Res.* **108**: 3258, doi: 10.1029/2002JC001590.

Kasai, H., Saito, H., Yoshimori, A. and Taguchi, S. 1997. Variability in timing and magnitude of spring bloom in the Oyashio region, the western subarctic Pacific off Hokkaido. *Japan Fish. Oceanogr.* **6**: 118–129.

Kasai, H. and Ono, T. 2007. Has the 1998 regime shift also occurred in the oceanographic conditions and lower trophic ecosystem of the Oyashio Region? *J. Oceanogr*. **63**: 661–669.

Lilly, J.M., Rhines, P.B., Visbeck, M., Davis, R., Razier, J.R.N., Schott, F. and Farmer, D. 1999. Observing deep convection in the Labrador Sea during winter 1994/95. *J. Phys. Oceanogr*. **29**: 2065–2098

Locarnini, R.A., Mishonov, A.V., Antonov, J.I., Boyer, T.P. and Garcia, H.B. 2006a. World Ocean Atlas 2005, Volume 1: Temperature *edited by* S. Levitus, NOAA Atlas NESDIS 61, U.S. Gov. Printing Office, Washington, DC,182 pp.

Locarnini, R.A., Mishonov, A.V., Antonov, J.I., Boyer, T.P. and Garcia, H.B. 2006b. World Ocean Atlas 2005, Volume 2: Salinity *edited by* S. Levitus, NOAA Atlas NESDIS 62, U.S. Gov. Printing Office, Washington, DC, 182 pp.

Luchin, B.A. 1998. Non-periodic current, *in* Project "SEA", Chapter 7, Hydrometeorology and Hydrochemistry of Sea, Volume IX: Okhotsk Sea, Number 1: Hydrological Conditions. Hydrometeoizdat, St. Petersburg, pp. 233–256.

Maxworthy, T. and Narimousa, S. 1994. Unsteady, turbulent convection into a homogeneous, rotating fluid, with oceanographic applications. *J. Phys. Oceanogr.* **24**: 865–887.

Mizuta, G., Fukamachi, Y., Ohshima, K. and Wakatsuchi, M. 2003. Structure and seasonal variability of the East Sakhalin Current. *J. Phys. Oceanogr.* **33**: 2430–2445.

Moroshkin, K.V. 1966. Water Masses of Okhotsk Sea. Nauka, Moscow, 67 pp.

Send, U. and Marshall, J. 1995. Integral effects of deep convection. *J. Phys. Oceanogr*. **25**: 855–872.

Schlitzer, R. 2006. Ocean Data View. http://odv.awi.de.

Schott, F., Visbeck, M., Send, U., Fischer, J. and Stramma, L. 1996. Observations of deep convection in the Gulf of Lions, northern Mediterranean, during the winter of 1991/92. *J. Phys. Oceanogr*. **26**: 505–524.

Shcherbina, A.Y., Talley, L.D. and Rudmick, D.L. 2004a. Dense water formation on the northwestern shelf of the Okhotsk Sea: 1. Direct observations of brine rejection. *J. Geophys. Res.* **109**: C09S08, doi: 10.1029/2003JC002196.

Shcherbina, A.Y., Talley, L.D. and Rudmick, D.L. 2004b. Dense water formation on the northwestern shelf of the Okhotsk Sea: 2. Quantifying the transports. *J. Geophys. Res.* **109**: C09S09, doi: 10.1029/2003JC002197.

Tabata, T. 1977. Sea ice *in* Physical Oceanography IV, Tokai University Press (in Japanese).

Talley, L.D. 1991. An Okhotsk water anomaly: Implications for ventilation in the North Pacific. *Deep-Sea Res. I* 38: S171-S190.

Thorpe, S.A. 2005. Deep convection. pp. 128–131 *in* The Turbulent Ocean *edited by* S.A. Thorpe, Cambridge University Press, Cambridge.

Wang, M., Bond, N.A. and Overland, J.E. 2007. Comparison of atmospheric forcing in four sub-arctic seas. *Deep-Sea Res. II* doi: 10.1016/j.dsr2.2007.08. 014.

Watanabe, T. and Wakatsuchi, M. 1998. Formation of 26.8–26.9σ_θ water in the Kuril Basin of the Okhotsk Sea as a possible origin of North Pacific Intermediate Water. *J. Geophys. Res.* **103**: 2849–2865.

Yamamoto-Kawai, M., Watanabe, S., Tsunogai, S. and Wakatsuchi, M. 2004. Chlorofluorocarbons in the Sea of Okhotsk: Ventilation of the intermediate water. *J. Geophys. Res.* **109**: C09S11, doi: 10. 1029/2003JC 001919.

Zubov, N. 1945. Arctic Ice. Moscow, 360 pp. (referred from Tabata, T. 1977).

Influence of Amur River discharge on hydrological conditions of the Amurskiy Liman and Sakhalin Bay of the Sea of Okhotsk during a spring–summer flood

Anastasiya Abrosimova, Igor Zhabin and Vyacheslav Dubina

V.I. Il'ichev Pacific Oceanological Institute, FEB RAS, Vladivostok, Russia. E-mail: amber@poi.dvo.ru

Introduction

The Amur River is one of the largest rivers of the world. Its length is 4350 km and its total discharge is about 390 km^3 from a river basin of 1,855,000 km^2. The regime of the Amur River is distinguished by the spring–summer flood, summer low water, summer–fall flood, and winter low water. The spring flood is caused by melting snow and the summer–fall flood is caused by monsoon rains in the river basin. About 87% of the annual discharge falls during the warm part of year (May–October).

The Amur River flows into the Amurskiy Liman which is a narrow and shallow strait connecting the Sea of Japan and the Sea of Okhotsk. The Amurskiy Liman can also be considered as an estuary of the Amur River within which are several navigation channels. The Sakhalin and the Southern navigation channels connect the Sea of Okhotsk and the Sea of Japan, and from the Amur River mouth the Nevelskoy (Northern), the Southern and the East navigation channels (Petrov, 1959) exit. The Nevelskoy Strait connects the Amurskiy Liman to the Tatar Strait (Sea of Japan).

The dynamic conditions of the Amurskiy Liman are formed under the influence of the Amur River discharge, the ratio of background sea levels between the Sea of Japan and the Sea of Okhotsk, strong tidal currents and mixing. As a result of the monsoon character of the atmospheric circulation, southern winds prevail over the Amurskiy Liman in the summer and northern ones in the winter.

On the northern border of the Amurskiy Liman in the summer, the background level of water falls, and in the winter it rises; on the southern border of the Liman the sea level fluctuations occur in the opposite manner. Thus, during the warm period of the year (May–October), the difference in background levels between the Sea of Japan and the Sea of Okhotsk is positive (northward inclination). Due to this difference in sea levels, estuarine circulation is formed, and in the summer, the mean current is directed to the north. The data on sea level changes during the winter period are inconsistent. Some researchers (Lobanova, 1987) state that the difference in the levels during the winter period becomes negative (southward inclination) and the current is directed mainly to the south (into the Sea of Japan). Other data (Chao and Boicourt, 1986) suggest that the difference of the background levels is close to zero in the winter which should lead to the uniform distribution of the Amur River discharge between the Sea of Japan and the Sea of Okhotsk. Considering the available data on seasonal changes of the difference in the background sea levels and the variability of the Amur River discharge (Glukhovskiy *et al.*, 1998), it is possible to roughly estimate the volume of freshwater inflow into the Okhotsk Sea and the Sea of Japan during a year under average conditions. During the period from May till October, all river discharge is directed towards the Sea of Okhotsk. During this period the average discharge is equal to 331 km^3. If, during the cold period of the year (November–April), the discharge is uniformly distributed between the seas, about 6.5% of the Amur River annual discharge (31.5 km^3) is directed towards the Sea of Japan. Thus, on average, the Sea of Okhotsk receives 362.5 km^3 of fresh water within a year.

In the Amurskiy Liman two structural zones divided by a front have been determined (Lobanova, 1987; Zhabin *et al.*, 2007). The northern zone is associated with the mouth of the Amur River, the Sakhalin channel and the Nevelskoy channel, and the southern zone with the Southern channel and the Nevelskoy Strait. The northern part of the estuary is stratified under the influence of the river discharge. The southern zone is characterized by a homogeneous vertical distribution of oceanographic parameters. In the warm part of the year the waters of low salinity flow from the Amurskiy Liman to the Sakhalin Bay (the Sea of Okhotsk) and form the Amur River plume

(Rostov and Zhabin, 1991; Zhabin *et al.*, 2005; Zhabin *et al.*, 2007).

A study of the Amur River mouth ecosystem was carried out during a cruise of the R/V *Professor Gagarinskiy* in June, 2007. Oceanographic measurements were conducted with the CTD-probe SBE 19plus. The location of hydrological stations for this study is shown in Figure 1.

The data obtained during the cruise and from remote sensing (Terra and Aqua satellites, radiometer MODIS) allow us to investigate the structure and dynamics of the waters near the Amur River mouth during the spring–summer flood.

Oceanographic structure near the Amur River mouth

At the mouth of the Amur River, the mixing of seawater and river water occurs. The area around the mouth includes the Amurskiy Liman and the adjoining parts of Sakhalin Bay and the Tatar Strait.

Looking at the section through the Amurskiy Liman (Fig. 2), bounded by the Southern and the Sakhalin channels, there are two distinguished structural zones – a mixed zone and a stratified one. The southern zone has a typical homogeneous vertical distribution of hydrographical characteristics with high salinity; the northern one has a two-layered structure with water of very low salinity in the surface layer. The stratification in the northern part of the estuary is supported both by the flow into the near-bottom layer of the Sea of Okhotsk (a salt wedge on the northern outlet of the Liman), and by the near-bottom advection of saltier waters from the Sea of Japan (the stratified regime near the river mouth). The stratification in the northern part of the estuary is essentially weakened in the zone that is under direct influence of the river discharge.

The southern part of the Amurskiy Liman is filled by the waters flowing from the Sea of Japan. Intensive tidal and wind mixing in this zone leads to a homogeneous vertical distribution of oceanographical characteristics. The influence of the river discharge on this part of the Amurskiy Liman is insignificant. The salinity in the mixed zone increases in the direction to the southern outlet from the estuary. The distribution of temperature and salinity in the section across the Amur River plume in Sakhalin Bay is shown in Figure 3.

Low salinity and warm waters flow from the Amurskiy Liman to Sakhalin Bay through the northern outlet of the Liman. The plume is about 7 m thick, the salinity in the plume ranges from 7 to 15 psu, and temperature ranges from 7 to 12°C. A sharp pycnocline separates the plume from very cold (< –1.5°C) and salty (> 32 psu) bottom shelf waters of the Sea of Okhotsk. Higher values of temperature and smaller values of salinity are observed in the discharge current.

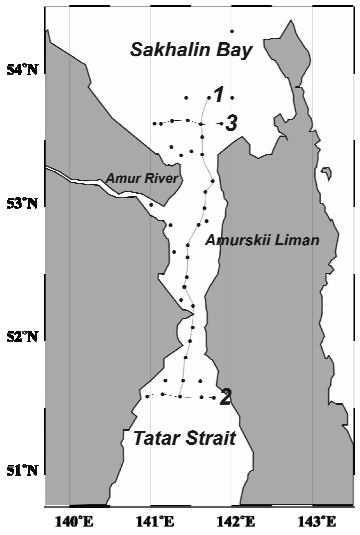

Fig. 1 Hydrographic sections occupied during the cruise of the R/V *Prof. Gagarinskiy* in June 2007. Closed circles show the station locations.

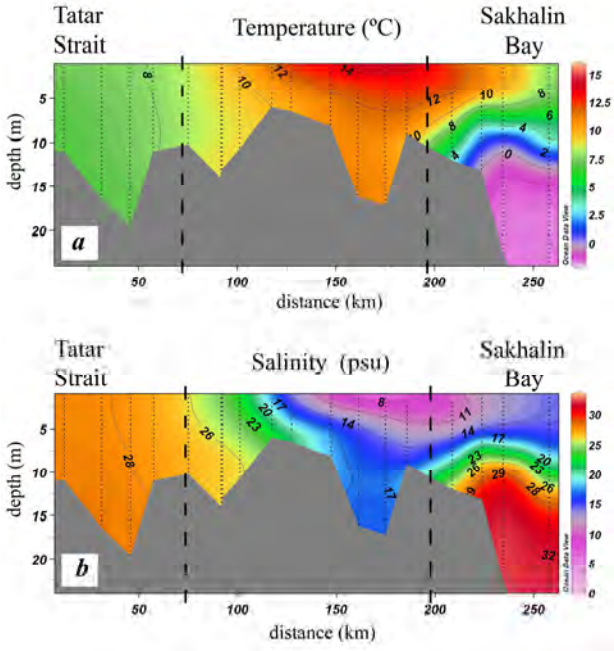

Fig. 2 Vertical distributions of (a) temperature and (b) salinity along section 1, June 2007.

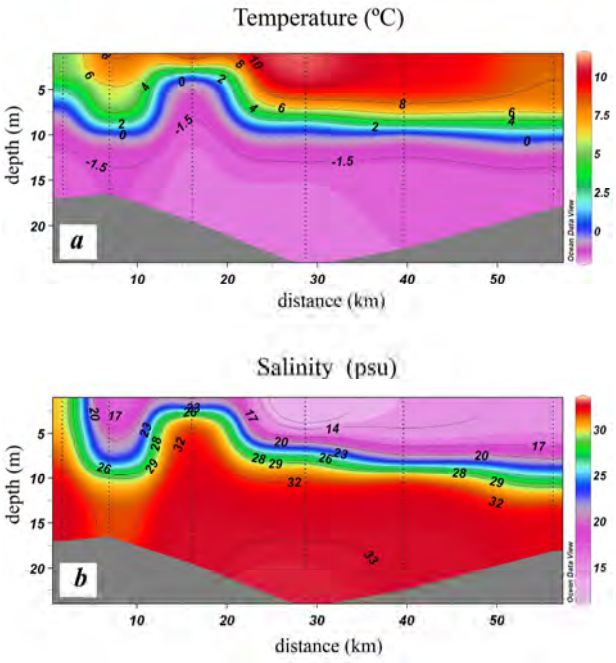

Fig. 3 Vertical distributions of (a) temperature and (b) salinity along section 3, June 2007.

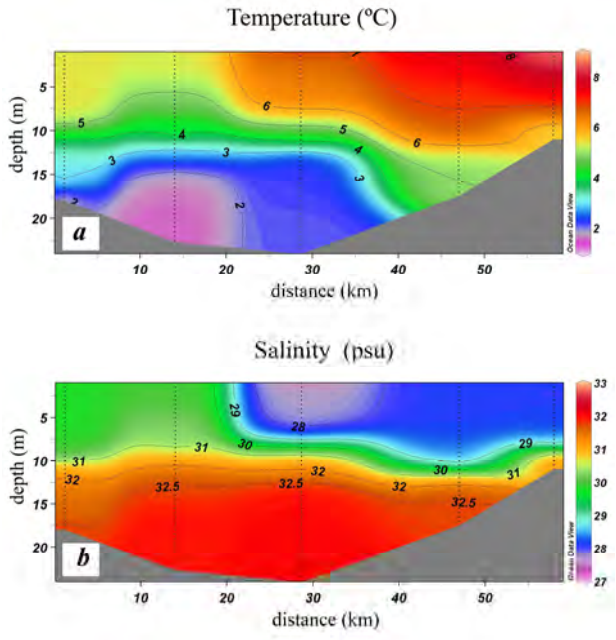

Fig. 4 Vertical distributions of (a) temperature and (b) salinity along section 2, June 2007.

Two cross-sections were obtained for the Tatar Strait. On the southern section a two-layer vertical structure of waters was observed (Fig. 4).

The upper layer was about 10 m thick and was separated from the bottom water layers by a sharp thermohalocline. The surface layer near the coast of the continent was characterized by low values of temperature (about 5°C) and high values of salinity (> 30). In the middle part of the Tatar Strait and near Sakhalin Island, waters with lower salinity (< 28.5) and higher surface temperatures (6–8°C) were observed. The origin of this zone of low salinity could have been caused by the discharge of the waters from the southern part of the Amurskiy Liman through the Nevelskoy Strait in the period preceding the observation.

A second cross-section of the observation (Fig. 1) was executed near the southern inlet of the Nevelskoy Strait. The vertical thermohaline structure in this section differed from the structure of waters of the northern part of the Tatar Strait. At the inlet to the strait a more homogeneous vertical distribution of hydrological characteristics was observed. The temperature monotonically decreased and the salinity increased with depth. The waters in the central part of the section were completely mixed from the surface to the bottom. The salinity of the surface layer did not exceed 28.5 and the temperature changed within the range of 7–9°C. The waters of low salinity at the outlet from the Amurskiy Liman demonstrate the influence of the Amur discharge in the northern part of the Tatar Strait during the spring–summer flood.

The Amur River discharge from satellite observations

The Amur River discharge contains a significant amount of sediments. This allows us to see contrasts in turbidity from remote sensing in order to study the Amur River discharge distribution in the shelf zone of the Sea of Okhotsk. Figure 5 shows a visible satellite image of Sakhalin Bay, acquired during the survey period (June 7, 2007). It can be seen that turbid waters fill the northern part of the Amurskiy Liman and through the northern outlet outflow to Sakhalin Bay. Two structural elements are distinguished: a discharge lens with a jet current (bulge) and the coastal Amur current. The discharge lens is filled by the inflow of more turbidity (warm and low salinity) waters. The coastal Amur current is observed near the Sakhalin coast of Sakhalin Bay.

A map of current vector speeds, calculated by the displacement of markers (drifting ice floes and other characteristic points), is superimposed on a pair of images taken from the Aqua and Terra satellites on June, 7, 2007 with a 100-min time difference (Fig. 5).

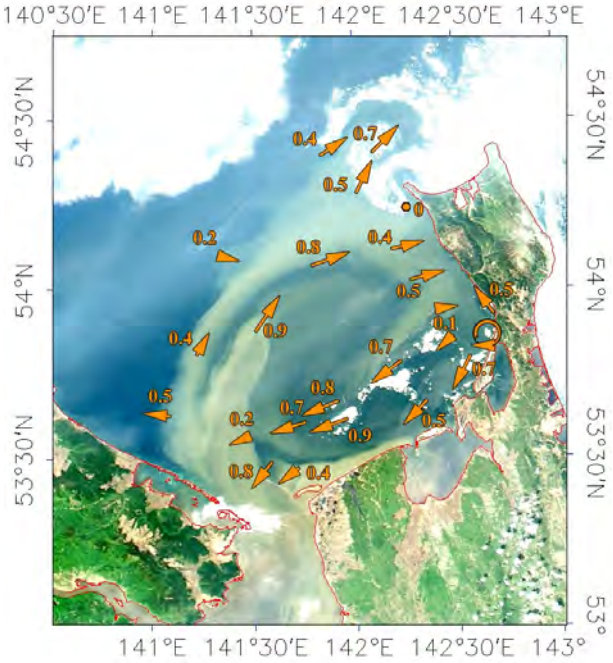

Fig. 5 Color image from the Aqua satellite, (June 7, 2007) illustrating the plume bulge formation as the Amur River plume exits the estuary. The overlaid current vectors identify the recirculation zone within the bulge.

The images show that the Amur River discharge, while leaving the estuary, forms an anticyclonic circulation on the periphery of the plume. The recirculation provides the inflow of low salinity waters to the internal field of the plume. The current speeds in the discharge current leaving the estuary reach 1 km/s. The speed ranges between 0.4 to 1.5 km/s in the jet current passing along the periphery of the lens.

Dynamics of the Amur River discharge

The river discharge in the shelf zone forms bulge and coastal density currents. Garvin (1995) offers a dynamical system for classifying buoyant discharges. The key parameter of this classification is the Kelvin number which is defined as the relation of the coastal current scale L to the baroclinic Rossby deformation radius L_D. The deformation radius is $L_D = c/f = (g'h)$ $0.5/f$, where f is the Coriolis parameter, c is the phase velocity of long interfacial waves, h is the plume thickness, $g' = g(\rho_2 - \rho_1)/\rho_2$, is the reduced gravity (g is gravitational acceleration, ρ_1 and ρ_2 are densities of the upper and the lower layers, respectively). One more important parameter used in this classification is the non-dimensional densimetric Froude number $F = U/c$, where U is a characteristic velocity within the coastal current. It is known that at $F > 1$ the current will be "rough" (supercritical regime), and at $F < 1$ it will be quiet (a subcritical regime). At the transition from a supercritical movement regime to a subcritical one ($F = 1$, critical Froude number) an internal hydraulic jump is observed which is accompanied by energy dissipation and mixing.

The Kelvin number can be used to compare the contributions of inertial and rotary effects in the dynamics of the discharge current near the outlet from the Liman. In the limiting case when $K << 1$, the influence of the Coriolis effect on the distribution of river discharge waters is insignificant. In this case the dynamic regime near the mouth or the outlet from the Liman is determined by the advection of low salinity waters. At greater Kelvin numbers (>> 1) the dynamics of the current outflow from the Liman (mouth) is defined by rotation of the Earth.

The dynamic classification is diagnostic and requires preliminary data on the parameters and scales of the phenomenon, such as stratification, characteristic speed of the stream and the scale of current. Estimations of these parameters for the discharge of the Amur River to the Sea of Okhotsk are received through oceanographic and satellite observations. The discharge current is characterized by the difference in density of $\rho_2 - \rho_1 = 20$ kg/m^3, and the average thickness of the plume is 7 m. The scale of the current according to satellite data is equal to approximately 20 km. The scale of the current coincides with the width of the northern outlet from the Liman. The Coriolis parameter at the latitude of Sakhalin Bay is equal to 1.15×10^{-4} s^{-1}. At the observed values of the parameters, the baroclinic radius of deformation is 10 km which gives $K = 2$. This estimation shows that the dynamics of the Amur River discharge depends on the effects of rotation.

The estimation of the speed the outflow of low salinity waters from the Liman to the Sea of Okhotsk (the area of the section at the outlet is 105 m^2) can be determined by the average value of the Amur River discharge in June (166,000 m^3/s) (Glukhovskiy *et al.*, 1998). The salinity at the outlet from the Liman was 10 psu. Therefore, when making the calculations, it is supposed that the Amurskiy Liman river waters (salinity ~0) mix with the waters of the Sea of Japan (salinity 30 psu) in the ratio of 1:2. In this case, the average speed equals 0.5 km/s which gives $F = 0.4$. The estimation of the discharge current speed during the study can be determined with the help of satellite observations, using the method of sea markers. For

this purpose, the displacement of characteristic points on consecutive images (time interval is 100 minutes), received on June 5, 7, 8 and 15, 2007 from the satellites Terra and Aqua were calculated. According to the satellite data, the average current speed at the outlet from the Liman is 0.85 km/s which gives F = 0.7. At such values of Froude numbers the regime of movement will be subcritical and the river discharge should extend as a superficial current above the layer of denser surrounding waters.

Thus, the calculation of nondimensional parameters shows that the contribution of the effect of the Earth's rotation to the dynamics of the discharge current of the Amur River exceeds the contribution of inertial effects. The numerical models of coastal circulation (James, 1997) show that at $K \sim 1$ near the river mouth two zones with various dynamics are formed – a bulge with an anticyclonic circulation and a density coastal current. The scale of this current is equal to the baroclinic Rossby deformation radius. A more complex dynamic regime with a steady anticyclonic circulation in the lens is formed in the bay which is under the influence of intensive river discharge.

Conclusion

In the estuary of the Amur River occurs mixing of river and sea waters which flow into the Amurskiy Liman from the Sea of Japan. The waters of low salinity flow into the Sea of Okhotsk in the form of a discharge current. Under the influence of the Earth's rotation the discharge current deviates to the right and forms an anticyclonic circulation in Sakhalin Bay. The mesoscale Amur River plume is formed and filled during a spring–summer flood. Further research on the dynamics, conditions of formation, and evolution of the plume is necessary.

References

Lobanova, N.I. 1987. Basic characteristic of mixing area in estuary of Amur River. *FERHRI Works* **130**: 33–44 (in Russian).

Garvin, R.W. 1995. A dynamic system of classifying buoyant coastal discharges. *Cont. Shelf Res.* **15**: 1585–1596.

James, I.D. 1997. A numerical model of the development of anticyclonic circulation in a gulf-type region of freshwater influence. *Cont. Shelf Res.* **17**: 1803–1816.

Petrov, V.S. (*Ed.*). 1959. Sailing Directions of the Sea of Japan. The Tatar Strait and the Amurskiy Liman and the La Perouse Strait. 296 pp. (in Russian).

Chao, S.-Y. and Boicourt, W.C. 1986. Onset of estuarine plumes. *J. Phys. Oceanogr*. **16**: 2137–2149.

Rostov, I.D. and Zhabin, I.A. 1991. Hydrological conditions of the Amur River near mouth area. *Meteorol. Hydrol.* **7**: 94–99 (in Russian).

Glukhovskiy, B.Kh., Goptarev, I.P. and Terziev, F.C. (*Eds*). 1998. Sea Hydrometeorology and Hydrochemistry. The Okhotsk Sea. Volume 9. Hydrometeorological Conditions. 343 pp. (in Russian).

Zhabin, I.A., Propp, L.N. Volkova, T.I. and Tishchenko, P.Ya. 2005. Variability of hydrochemical and hydrological parameters near Amur River Mouth. *Oceanology* **45**: 703–709 (in Russian).

Zhabin, I.A., Dubina, V.A., Nekrasov, D.A. and Dudarev, O.V. 2007. Structural features of the mixing zone between river and sea waters near the Amur River mouth as detected by satellite and hydrological observations. *Res. Earth Space* **5**: 61–70 (in Russian).

Seasonal and interannual variations of Amur River discharge and their relationships to large-scale atmospheric patterns and moisture fluxes

Yoshihiro Tachibana[1,2], Kazuhiro Oshima[3] and Masayo Ogi[4,5]

[1] Institute of Observational Research for Global Change, Japan Agency for Marine-Earth Science and Technology, Yokosuka, Japan. E-mail: tachi@bio.mie-u.ac.jp
[2] Faculty of Bioresources, Mie University, Tsu, Japan
[3] Faculty of Environmental Earth Science, Hokkaido University, Sapporo, Japan
[4] The Joint Institute for the Study of the Atmosphere and Ocean, University of Washington, Seattle, WA, USA
[5] Frontier Research Center for Global Change, Japan Agency for Marine-Earth Science and Technology, Yokohama, Japan

Abstract

Using reanalysis data, we investigate the relationship of Amur River discharge and vertically integrated atmospheric horizontal moisture flux. The discharge has two peaks, one in spring and the other in autumn. A northward flux associated with storms in the previous autumn and winter contributes to the spring discharge. The autumn discharge is supplied by a northward flux associated with the Asian summer monsoon and by an eastward flux originating from evaporation in Eurasia. Interannual variation is also investigated. The strong summer monsoon strengthens the summer flux convergence, resulting in anomalously large discharge in autumn. The strong winter monsoon wind with a dry air mass activates evaporation. The anomalously large spring discharge is related to the warm phase of the Arctic Oscillation. These results indicate that the monsoon plays an important role in the freshening of the Okhotsk Sea.

This work is partially based on a paper by Tachibana, Oshima and Ogi (2008) in the *Journal of Geophysical Research.* See this paper for details.

Introduction

The Amur River, with a basin area of 1.86×10^6 km^2, is the fourth largest river in northern Eurasia and supplies much of the fresh water to the Okhotsk Sea, one of the southernmost ice-covered seas in the Northern Hemisphere. Freshwater discharge from the Amur River, which causes large stratification that suppresses deep convection and promotes freezing, is an important factor controlling the formation of sea ice in the Okhotsk Sea.

According to Ogi *et al.* (2001), the annual amount of discharge from the Amur River is 333 km^3/year (10,929 m^3/s). A distinctive characteristic of the seasonal cycle of the Amur River is its two discharge peaks, one in June and the other in September (Fig. 1a). The Amur River is the only river in northern Eurasia to have double discharge peaks (Masuda, 2007, pers. comm.). Ogi *et al.* (2001) speculated that the first peak occurs due to melting snowpack and frozen soil, whereas the second peak is caused by summertime monsoon precipitation.

Past studies have commonly applied vertically integrated horizontal moisture flux analysis, using reanalysis and river discharge data, to rivers flowing toward the Arctic. This method might indicate the origins of the moisture that becomes river discharge. According to a tagged water experiment using an atmospheric general circulation model simulation by Numaguti (1999), the summer precipitation in northern Eurasia originates partially from water vapor that evaporates from inland areas of the Eurasian continent. However, because of the lack of detailed study of the moisture flux associated with the Amur River, the moisture source remains unclear.

Few papers have described the interannual variability of the Amur River. Ogi and Tachibana (2006) found that the interannual variation in the Amur River discharge is related to the annual mean Northern Hemisphere Annular Mode/Arctic Oscillation (NAM/AO). However, because there are two peaks in the discharge, the large-scale atmospheric patterns and local-scale storm tracks governing the spring

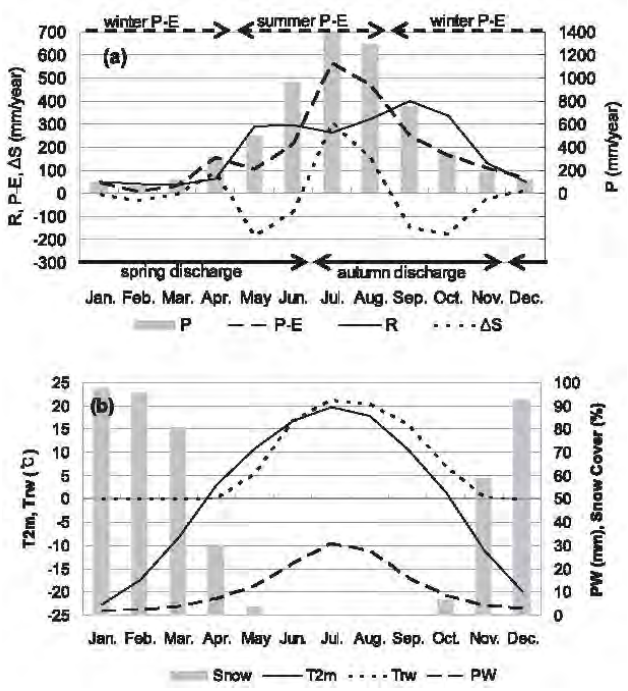

Fig. 1 (a) Seasonal cycle of the Amur River discharge (solid line), net precipitation (dashed line), precipitation from APHRODITE (www.chikyu.ac.jp/precip/; gray bars) and $\partial S/\partial t$ (dotted line) over the Amur River basin. (b) Other climatological conditions over the basin; temperature at 2 m (solid line), river water temperature (dotted line), snow cover (gray bars) and PW (precipitable water; dashed line).

discharge peak must differ from those governing the autumn peak. However, no previous studies have clarified the large-scale atmospheric patterns and local-scale storm tracks that determine individual discharge peaks.

The purpose of this study is to determine which atmospheric patterns govern the spring and autumn discharge peaks. We will illustrate the origin of the moisture. Moreover, we will determine the interannual variations in the atmospheric patterns that influence the two discharge peaks.

Data and Methods

Monthly mean Amur River discharge data from 1980 through 2001 are used for the analysis. These data were recorded at Bogorodskoe, the lowest-reach hydrological station of the Amur River at which discharge has been routinely measured by the Far Eastern branch of the Russian Federal Service for Hydrometeorology and Environmental Monitoring (FERFSHEM).

Data from the European Centre for Medium-Range Weather Forecasting is used to perform a 40-year reanalysis (ERA40) (Uppala *et al.*, 2005). The time resolution of the data is 6 hourly. The horizontal resolution is 2.5° latitude × 2.5° longitude. The analysis period is from 1979 through 2001.

We estimated the net precipitation (precipitation minus evaporation, $P - E$) over the Amur River basin from moisture flux. $P - E$ is estimated using the atmospheric moisture budget equation as follows:

$$\frac{\partial PW}{\partial t} = -\nabla \langle q\mathbf{v} \rangle + E - P, \qquad (1)$$

where PW is precipitable water, q is the specific humidity, $\mathbf{v}$ is the wind vector, and $\langle q\mathbf{v} \rangle$ represents the vertically integrated horizontal moisture flux. $P - E$ is estimated from the area-weighted average values of PW and the horizontal convergence of $\langle q\mathbf{v} \rangle$ over the area of the Amur River basin (Fig. 2).

Water vapor in the mid-latitudes is transported by both atmospheric stationary waves and moving transient eddies. Because the temporal scales of these two transports are quite different, dividing the moisture flux into these two categories provides useful information on the atmospheric causes of the discharge (Oshima and Yamazaki, 2006). We divide the monthly mean total moisture flux into stationary flux and transient flux as follows:

$$\langle \overline{q\mathbf{v}} \rangle = \langle \overline{q}\,\overline{\mathbf{v}} \rangle + \langle \overline{q'\mathbf{v}'} \rangle, \qquad (2)$$

where the overbars represent the monthly average, and the primes represent the deviation from the monthly average. The stationary flux is calculated from the monthly mean fields of wind, moisture, and surface pressure. The transient flux is obtained by subtracting the stationary flux from the total flux.

The connectivity of the $P - E$ and the river discharge R is described using the terrestrial water budget equation. The time rate of change in land water storage S is written as:

$$\frac{\partial S}{\partial t} = P - E - R, \qquad (3)$$

where R is the river runoff. Thus, R is determined by $\partial S/\partial t$ and $P - E$.

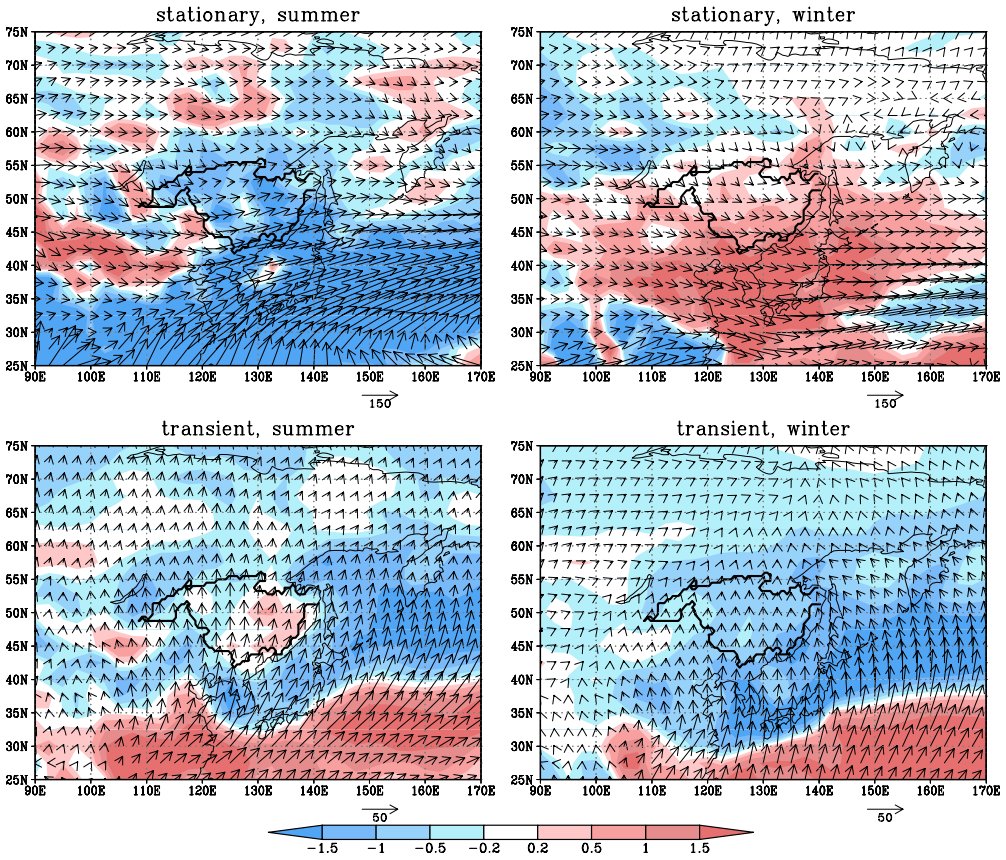

Fig. 2 Moisture flux and its divergence fields for the stationary (upper panels) component and transient (bottom panels) component in association with the summer $P - E$ (left panels) and winter $P - E$ (right panels).

Comparison of Discharge with Net Precipitation

Seasonal cycle of discharge and net precipitation

We compared the Amur River discharge with the $P - E$ estimated by the ERA40. The annual mean $P - E$ (182 mm/year) is close to the observed annual discharge (190 mm/year). The seasonal means and the interannual variation of $P - E$ are also close to those of the discharge, as will be shown later.

As discussed earlier, the river discharge has two discharge peaks, in June and September, while a single peak in $P - E$ occurs in July that is approximately 2 months later than discharge in autumn. This time lag of the autumn discharge peak behind the $P - E$ peak is related to the fact that runoff takes approximately 2 months to reach the outlet of the basin, given the massive size of the Amur River basin. Figure 1b shows several climatological conditions over the Amur River basin. The temperature at 2 m height changes from negative to positive in April and back to negative in October. This indicates that precipitation accumulates as snow from October to March and that the accumulated snow and frozen soil start to melt in April. The river water temperature has a seasonal cycle similar to that of temperature at 2 m height. The river water temperature becomes positive in May, indicating that frozen river water begins to melt in this month. The river water temperature falls to zero in November, and the river starts to freeze. Satellite observations indicate maximum snow coverage in January, a large decline beginning in April, and accumulation starting again in October. This suggests that snowmelt starts in April and that the discharge peaks in May to June with the decrease in storage.

To compare the discharge with moisture flux and atmospheric patterns in association with the two discharge peaks, we first confirm the months of $P - E$ that cause the respective spring and autumn discharge. Based on the two clear discharge peaks, we define December through June as the months of

spring discharge and July through November as the months of autumn discharge (Fig. 1a). We determined the periods of summer $P - E$ and winter $P - E$ that correspond to the spring and autumn discharge, respectively. From a procedure for the definition of the period in Tachibana *et al.* (2008), the time averaged $P - E$ from May through August (summer $P - E$) corresponds to the autumn discharge, and that from September through April (winter $P - E$) corresponds to the spring discharge (Fig. 1a). The summer $P - E$ (113) and winter $P - E$ (69) closely agree with the spring discharge (121 mm/year) and autumn discharge (69 mm/year), respectively.

Moisture flux patterns in association with summer $P - E$ and winter $P - E$

We compare the seasonal cycles of the moisture flux convergence and the $P - E$ over the Amur basin (Figure not shown). The seasonal $P - E$ cycle is similar to that of the moisture flux convergence, except in spring and autumn due to the large changes of PW (Fig. 1b). The stationary component of the moisture flux convergence is dominant in summer. Therefore, the moisture is transported mainly by stationary waves. In the winter, the transient component of the moisture flux convergence is positive and plays a principal role in supplying the water vapor in the Amur basin, while the stationary component is negative.

These characteristics are shown in the moisture flux fields associated with the summer $P - E$ and winter $P - E$ (Fig. 2). In summer, the northeastward flux of the stationary component mainly determines the total flux convergence. The flux from the East China Sea to Japan indicates the rain belt that coincides with the Baiu/Meiyu stationary front, in association with the Asian summer monsoon. Therefore, the summer flux is partially influenced by the Asian summer monsoon. The eastward flux from the west of the basin, which can be caused by mid-latitude westerlies, also contributes to the precipitation. Divergent areas are located in the far western inland area of the continent. Because the divergent area indicates that surface evaporation exceeds precipitation, the figure implies that water vapor which evaporates from inland areas also supplies precipitation to the Amur basin. This is consistent with a model study by Numaguti (1999).

In winter, the flux by the transient component converges over the Amur basin, whereas the flux by the stationary component diverges. The flux convergence of the transient component can be caused by storm activity in this season and region, where wintertime cyclones are known to begin and develop. The fluxes of the transient component suggest that the river water in the spring discharge originates from the Pacific, although these arrows are not the same as the material trajectories. In contrast, the fluxes of the stationary component around the Amur basin point southeastward. This direction is associated with the winter monsoon that blows from the cold, dry Eurasian continent toward the warm Pacific Ocean. Evaporation due to the stationary component associated with the dry monsoon wind over the Amur basin can cause the moisture flux divergence. Overall, the total flux in winter slightly converges over the Amur basin because of a larger moisture flux from the south by the transient component rather than by the stationary component.

Interannual Variation of Discharge

Interannual variation and its relationship to horizontal moisture flux patterns

Next, we investigate the causes of interannual variation in Amur River discharge. We compared the time series of spring and autumn discharge and their associated winter and summer $P - E$, respectively. Correlation coefficients are 0.84 for autumn discharge and summer $P - E$, and 0.57 for spring discharge and winter $P - E$. The large correlation for autumn discharge indicates that summer atmospheric processes principally govern autumn discharge. On the other hand, spring discharge is influenced not only by atmospheric processes related to the $P - E$, but also by other hydrological processes that are affected by variation in water storage S.

The variations in the total moisture flux convergence correlate well with the stationary components in both seasons. Thus, the stationary components are the prime determinant for the interannual variation in discharge. Now, we examine the stationary moisture flux in association with the interannual variation in spring and autumn discharge (winter and summer $P - E$). Figure 3 shows the composite maps of the stationary moisture fluxes in years of large (top 5) and small (bottom 5) summer $P - E$. Moisture flux fields in the top 5 years show counterclockwise circulation centered in the west of the basin. This indicates that the moisture tends to come from the Pacific to the southeastern Amur basin. In contrast, the flux in the bottom 5 years is more zonal than in

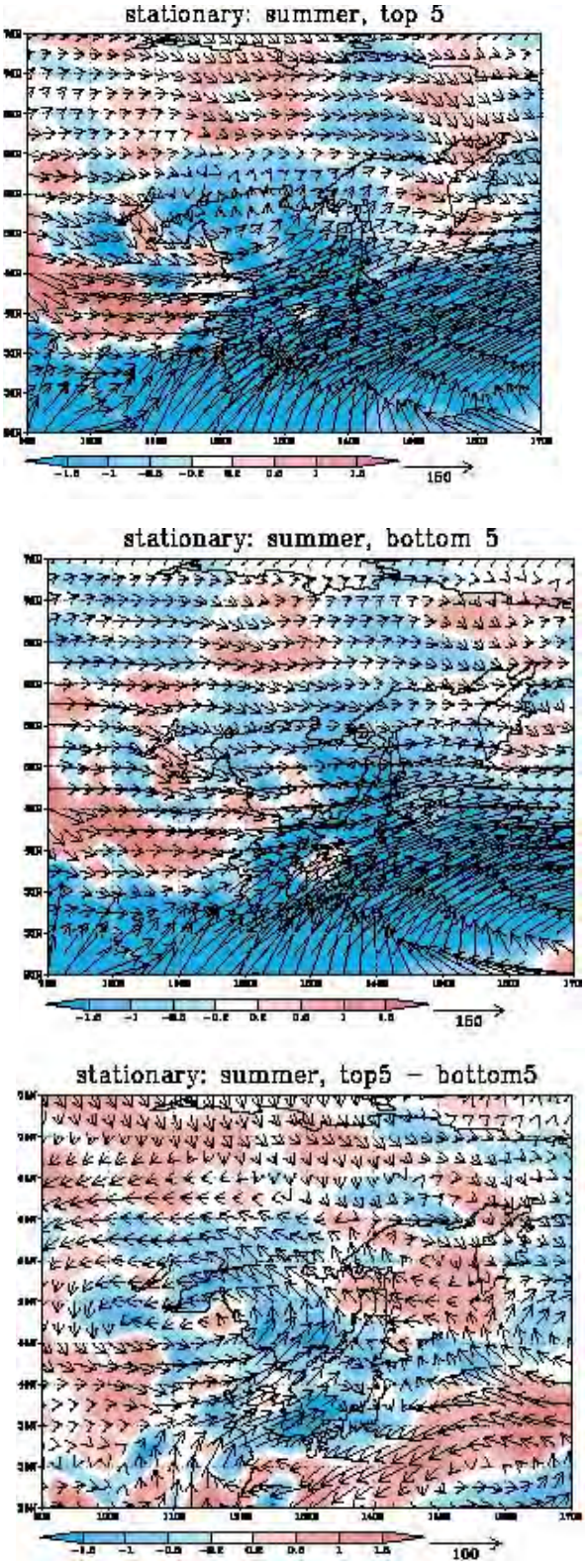

Fig. 3 Composite maps of the stationary moisture flux and its divergence in (top) the top 5 summer *P*– *E* years and (middle) bottom 5 years; (bottom) difference between the top 5 and bottom 5 years.

the top 5 years. The source region of the water in the bottom 5 years is thus mainly in inland continental areas. Figure 3 also shows the flux difference between the top 5 and bottom 5 years. A counterclockwise anomalous moisture flux pattern is obvious, suggesting that anomalous moisture flux from Southeast Asia also promotes anomalous *P* – *E* in the Amur basin, which then leads to anomalous autumn discharge.

In winter, on the other hand, the differences in the flux fields between the top 5 and bottom 5 years exhibit a counterclockwise circulation pattern centered to the west of the Amur basin (Figure not shown). The counterclockwise pattern and the overall northward orientation in the Amur basin suggest the weakness of the Asian winter monsoon.

Interannual variation and its relationship to large-scale atmospheric patterns

Large-scale atmospheric fields linearly regressed onto the interannual variation in the stationary component of the moisture flux convergence show that a notable feature in the circum-Amur basin area in summer is the presence of negative anomalies over the west of the basin (near Lake Baikal) in the sea level pressure (SLP), 500-hPa, and 200-hPa height fields, signifying a barotropic structure. Cold anomalies can be also seen around Lake Baikal (Figure not shown). The location of the cyclonic circulation anomaly in association with the cold anomalies is located just to the west of the Amur basin. This cyclonic circulation agrees with the counterclockwise moisture flux pattern of the stationary component in the years of large summer *P* – *E* (Fig. 3). Also, positive anomalies over the Okhotsk Sea can be seen in the SLP field. These anomalies are related to the appearance of the Okhotsk High. The contrast between the anomalous low pressure over land and the anomalous high pressure over the Okhotsk Sea brings about a northward moisture flux in association with northward wind anomalies in the lower troposphere over the Amur basin. This northward wind can then supply the Amur basin with moisture in association with the strengthened Asian summer monsoon. A west-to-east wavy pattern crossing the Eurasian continent at approximately 40° N, along the core of a subtropical westerly jet, is clearly visible at 200-hPa height. This wave train is possibly a stationary Rossby wave that originated over western Europe. The cyclonic circulation around Lake Baikal, which

directly influences the discharge, is thus related to this hemispheric mid-latitude circulation.

Winter atmospheric patterns associated with the winter flux of the stationary component have a continent-to-ocean contrast in the SLP field similar to that in summer. Significant positive SLP anomalies widely cover the Okhotsk and Bering seas, signifying the weakness of the Aleutian Low. Also, over Lake Baikal, significant negative anomalies appear in the SLP field. This feature implies a weakness of the winter Siberian High. Weakness of both the Siberian High and Aleutian Low causes weakening of the Asian winter monsoon, which usually blows from the continent to the Pacific. This atmospheric pattern is consistent with the moisture flux pattern in winter. The weak winter monsoon wind over the Amur basin can suppress the evaporation there. For this reason, the moisture flux divergence over the basin in the top 5 years can be weaker than in the bottom 5 years.

In addition, a hemispheric-scale pattern shows negative anomalies in the Arctic and positive anomalies in mid-latitudes from the surface to the upper troposphere at 200-hPa height, although statistical significance is low. These anomaly patterns are similar to the pattern of the positive phase of NAM/AO. This indicates that the NAM/AO pattern tends to be positive in winter with the large moisture flux. The positive phase of the NAM/AO is related to the weakened eastern Asian winter monsoon. Therefore, the relationship between this large moisture flux and the positive phase of NAM/AO is consistent with previous studies.

Summary

Using long-term discharge data to analyze horizontal moisture flux, we have uncovered processes that determine Amur River discharge and their seasonal and interannual variations. Comparison of the moisture flux with the discharge showed that the spring discharge, which peaks in June, is supplied by the moisture flux in the previous autumn and winter. The spring discharge is supplied mainly by short-lived storm activity from the previous autumn and winter. On the other hand, the autumn discharge peak is supplied by the summertime moisture flux. The autumn discharge is supplied mainly by stationary atmospheric patterns in association with the Asian summer monsoon and mid-latitude westerlies.

Interannual variation in the summer moisture flux is related to the strength of the Asian summer monsoon and a stationary anticyclone, the Okhotsk High. The Asian summer monsoon, in association with anomalous cyclonic circulation over Eurasia, strengthens the anomalously large summer moisture flux from the south, resulting in anomalously large discharge in autumn. The Asian winter monsoon, in association with the anomalously strong Siberian High and Aleutian Low, strengthens the moisture flux divergence (*i.e*., activated evaporation in the Amur basin, resulting in anomalously small discharge in spring). The hemispheric atmospheric pattern relates to the moisture flux convergence and, to some extent, resembles the NAM/AO. Anomalously large spring discharge is also related to the warm phase of the NAM/AO, which prompts the melting of snow and frozen soil and thus contributes to the anomalously large spring discharge. Therefore, the NAM/AO pattern influences both the moisture flux and the change in land water storage.

References

Numaguti, A. 1999. Origin and recycling processes of precipitating water over the Eurasian continent: Experiments using an atmospheric general circulation model. *J. Geophys. Res.* **104**: 1957–1972, doi:10.1251029/1998JD200026.

Ogi, M. and Tachibana, Y. 2006. Influence of the annual Arctic Oscillation on the negative correlation between Okhotsk Sea ice and Amur River discharge. *Geophys. Res. Lett.* **33**: L08709, doi:10.1029/2006GL025838.

Ogi, M., Tachibana, Y., Nishio, F. and Danchenkov, M. A. 2001. Does the fresh water supply from the Amur river flowing into the Sea of Okhotsk affect sea ice formation? *J. Meteor. Soc. Japan* **79**: 123–129.

Oshima, K. and Yamazaki, K. 2006. Difference in seasonal variation of net precipitation between the Arctic and Antarctic regions. *Geophys. Res. Lett.* **33**: L18501, doi:10.1029/2006GL027389.

Tachibana, Y., Oshima, K. and Ogi, M. 2008. Seasonal and interannual variations of Amur River discharge and their relationships to large-scale atmospheric patterns and moisture fluxes. *J. Geophys. Res.* **113**: D16102, doi:10.1029/2007JD009555.

Uppala, S.M. *et al.* 2005. The ERA-40 reanalysis. *Quart. J. Roy. Meteorol. Soc.* **131**: 2961–3012, doi:10.1256/QJ.04.176.

The Okhotsk Sea coastal lagoons: Types, evolution and use of resources

Peter F. Brovko

Far East National University, Vladivostok, Russia. E-mail: brovko@meteo.dvgu.ru

Abstract

As part of the Okhotsk Sea, but separated from it by a depositional feature, lagoons have a particular hydrology and specific conditions for bottom sediment accumulation. Marine organisms in lagoons can be exposed to water temperature and salinity fluctuations of significant range. The Okhotsk Sea lagoons are grouped by size into large (100–500 km^2), medium (10–100 km^2), small (1–10 km^2) and very small (less than 1 km^2) ones. The largest lagoons in terms of area are Baikal, Schastya, Piltun, and Perevolochnaya. Many small lagoons are linked to river estuaries. In terms of water depth, lagoons are grouped into shallow (less than 1 m deep), medium-depth (1–5 m), deep (5–20 m) and very deep (more than 20 m) ones. The evolution of Okhotsk Sea lagoons is associated with the Holocene transgression, during which time they came into existence. As evidenced by well-studied coastal-marine depositions, large sea water bodies, separated by sand banks and morphologically close to modern lagoons, started to form at a higher level in the sub-boreal period. During subsequent sea level fluctuations above the present-day level, the inner shoreline contour of lagoons was reshaping. Today, some lagoons are separated from the sea, partly filled with alluvial-marine, eolian, and biogenic depositions and have turned into lakes. Lagoons are used as harbors for sheltering small fishing and transport vessels. Some lagoons are used for aquaculture farms where fish, seaweeds, and scallops are cultivated. Lagoons are also a convenient recreational resource for developing sports, tourism, health cures and recreation. The best-studied lagoons of the Okhotsk Sea are Nabil, Chayvo, Busse, and Saroma.

A lagoon is part of the sea, separated from it by a bar or spit. It is characterized by a lower salinity and by specific relief formation and sedimentation conditions. Lagoons are a component of many coastline geomorphologic types: fiords, rias, corals, abrasive accumulative and accumulative flattened coasts. Most lagoons are located along low seacoasts, forming a separate lagoon type of coast (Leontyev, 1961; Leatherman, 1981; Safyanov, 1996). Lagoon development has been addressed in detail in all major scholarly writings on seacoasts, with main emphasis placed on the formation of sand and pebble barriers separating lagoons from the sea (Zenkovich, 1962; Bird and Schwartz, 1985; Horikawa, 1988, and others).

The following specific trend was identified upon a review of relevant literature from the last decades of the past century. Researchers have been showing the greatest interest in relatively small water bodies. Thus, of the 97 explored lagoons, with their area varying from 1 to 8,000 km^2 (average value is 78 km^2), the great majority of studies have focused on water bodies with an area of 30–40 km^2 (Nixon, 1982). The average area of 240 lagoons studied in the Far East of Russia (1–500 km^2) is 31.3 km^2, and the best studied lagoons, Busse on Sakhalin Island and Novgorodskaya in Primorsky Krai, have an area of 43 and 30.7 km^2, respectively. One possible explanation for this phenomenon is that medium-size lagoons are the most interesting for analysis of their ecosystems and commercial use. On the other hand, small water bodies do not show individual features of lagoon characteristics due to high impacts of alluvial or eolian input. As for large lagoons, the high wave impact on shores and marine facilities make them less favorable for transportation possibilities and commercial activities.

Due to the development of oil and gas offshore resources on the continental shelf of Northeast Sakhalin, a significant range of research in lithology–geomorphology and aquatic biology was carried out in recent years in larger lagoons such as Piltun, Niyvo, Chayvo (121 km^2), and Nabil (181 km^2) (Brovko, 2000; Kafanov *et al.*, 2003).

The Okhotsk Sea lagoons are grouped by size into large (100–500 km^2), medium (10–100 km^2), small (1–10 km^2) and very small (less than 1 km^2) ones. The largest of the large lagoons are Baikal, Piltun, and Perevolochnaya. In terms of water depth, lagoons are grouped into shallow (less than 1 m

deep), medium-depth (1–5 m), deep (5–20 m) and very deep (more than 20 m) ones. Lagoon distribution in terms of their shape is also of interest. The shoreline contour of a water body may be linearly stretched, elongate, rounded, segmental, triangular or rectangular (Brovko, 1990; Brovko *et al.*, 2002) as a result of the evolution of coastal processes. Thus, segmental lagoons are found on the abrasive bay/coast in the northwestern part of the Okhotsk Sea (Ikit Lagoon) and rectangular ones are located on a fiord-type coast (Severnaya Lagoon, Bering Sea). Spit-blocked estuaries are often triangular (Starka Lagoon, Sea of Japan).

According to the degree of isolation from the sea, and to what degree they are influenced by hydrodynamic conditions, and by biological, chemical and other processes taking place inside lagoons, lagoons can be grouped into open lagoons (Tyk), semi-open (Baikal), semi-closed (Nabil), and closed (Ainskaya). There is also a separate group of dismembered lagoons composing lagoon lakes (Rybachye) that have no connection with the sea.

Two lagoon types predominate in the Okhotsk Sea. The first type includes large and medium lagoons located along the edge of seacoast flatlands (Pomr, Piltun, Busse, Saroma, *etc.*). This is a "classical" lagoon type. They have a contour stretched along the coast and are connected with the sea by one of two channels. The second type is associated with seacoast segments of river valleys (Bolshoye, Nabil, Niyvo, Ptichya, *etc.*). These lagoons are often stretched perpendicular or at an angle to the coastline general direction. Their development is dominated by alluvial processes. Small water bodies in straits between islands, typical of low elongate peninsulas, make up a separate lagoon type (Terpeniya).

There is complex differentiation of sediment material taking place in lagoons, governed by the direction and velocities of runoff and tidal currents. Bottom sediment is dominated by silts and fine-grain sands. Gravel, pebble material and shell fragments also occur frequently.

The evolution of Okhotsk Sea lagoons is associated with the Holocene transgression, during which time they came into existence (Brovko *et al.*, 2002; Brovko and Kaplin, 1997). As evidenced by well-studied coastal-marine depositions, large seawater bodies, separated by sand banks and morphologically close to modern lagoons, started to form at higher sea level in the sub-boreal period. During subsequent sea level fluctuations above the modern level, the inner shoreline contour of lagoons was reshaping. Some water bodies are already at the post-lagoon stage, being partly or fully filled with alluvial-marine, eolian, or biogenic depositions.

The Okhotsk Sea lagoons have great commercial importance in terms of marine civil and transport construction, development of mineral deposits, production of building materials, fishing and aquaculture, and recreation. Many lagoons are convenient harbors protected against storms. This makes them suitable for the organization of transport facilities and cargo reloading bases, for the construction of sheltered ports for small vessel, and for the erection of wharves and other civil structures, particularly in oil and gas production areas.

Analysis of the interaction of 17 main production and other activities showed that conflicts could arise in lagoons in 72 cases, 8 of which could have serious environmental consequences. Human-induced impacts on the coast of Sakhalin Island are of a local nature; however, their zone of influence is gradually expanding.

Busse Lagoon, granted an important wild area status in 1977, is the scene of aquaculture operations being conducted by "Sakhalinsky Rybak-2" and "Sakhkor" companies which cultivate sea cucumbers and scallops. Important wild area status was earlier given to other lagoons on Sakhalin Island: Tunaicha, Vavayskiye, Izmenchivoye, and Lunsky.

Other uses of lagoons and lagoon coasts that are coming to the fore are recreational activities. Annual sporting and cultural events in the vicinity of Saroma Lagoon (Hokkaido) have become widely known. Izmenchivoye, Dagi, and Ekhabi lagoons on Sakhalin Island have unique reserves of therapeutic muds. Scientists of the Far East National University and Primorye Branch of Russian Geographic Society have launched a proposal to establish the Tunaichinsky National Park in the Sakhalin southeast, including Tunaicha, Busse, Izmenchivoye and other lagoons. This project could greatly benefit from Japan's experience in establishing their national parks, where beautiful coast, spa resorts and cultured pearl farms can all be found within a relatively small territory of the park (Sutherland and Britton, 1980).

There is a gray whale habitat area extending from Lunskaya Lagoon to Piltun Lagoon in the Okhotsk Sea, which coincides with the offshore oil platform deployment area. Currently, the Korean/Okhotsk Sea whale population slightly exceeds 100 individuals, and there are proposals to organize a federal-level wildlife preserve for their protection. This would contribute to bird protection as well: there are 10,000–12,000 swans and 60,000–80,000 ducks staying in lagoons during autumn and spring migrations. This would also be beneficial for the habitat of Steller's sea eagle, this area's permanent resident listed on the Red Book of protected species.

Chayvo Lagoon in Northeast Sakhalin, which has been a site for semi-stationary observations by the Coast Research Center of Far East National University since 1982, is exposed to heavy human impact. The greatest changes occurred on Chayvo Spit, separating the lagoon from the Okhotsk Sea, during construction of *Yastreb*, an onshore directional drilling rig for the Sakhalin-I Project. It is the industry's largest rig, intended for operations in a highly seismic area. During construction, the spit surface, representing three beach ridge generations, was graded so that all the vegetation cover was removed, which resulted in a higher intensity of eolian processes.

For the lagoon's outer, seaward side facing the Okhotsk Sea, a coastal dynamic forecast was made and stable and retreating coast segments were identified, based on multi-year data (Brovko and Mikishin, 1999). It was in one of those "problem" segments that a basin for small vessels supporting the platform was "cut" into the spit mound and a barge was deployed several times as a temporary berthing facility (as intended by project design), which resulted in a shore-perpendicular "spur dike". Due to highly active lithodynamic processes on the open seacoast, sediment accumulation on one side has resulted in scour on the other side, at a rate of more than 20 m a year. The American method used for shore protection is sand bags placed on the beach in close rows. Unfortunately, this environmentally sound method has proved to be ineffective on the Okhotsk Sea coast.

Keywords: The Okhotsk Sea**,** Sakhalin Island, coastal lagoons, barrier-lagoon sedimentary system, marine culture, national park

References

Brovko, P.F., Mikishin, Yu.A. *et al*. 2002. Atlas of Sakhalin Seacoasts. Far East National University, Vladivostok, 56 pp. (in Russian).

Brovko, P.F. 1990. Coastal lagoons development. Far East National University, Vladivostok, 148 pp. (in Russian).

Brovko, P.F. 2000. Morphology and evolution of the lagoon type lakes. pp. 45–49 *in* International Conference on "Lakes of the Northern Regions", Yakutsk State University, Yakutsk (in Russian).

Brovko, P.F. and Kaplin, P.A., 1997. Lagoon coasts of the Northern and Eastern Sakhalin. pp. 243–258 *in* Russian Sea Coasts Evolution. Moscow State University, Moscow (in Russian).

Brovko, P.F. and Mikishin, Yu.A. 1999. Development of the Northern-East Sakhalin coasts. pp. 193–203 *in* Hydrometeorological and Ecological Conditions of the Far-eastern Seas, Issue 2, Publishing House of Academy of Science, Vladivostok (in Russian).

Bird, E.C.F. and Schwartz, M.L. 1985. The World's Coastline. Van Nostrand Reinhold Co., NY, 1071 pp.

Horikawa, K. 1988. Nearshore Dynamics and Coastal Processes, University of Tokyo Press, Tokyo, 522 pp.

Kafanov, A.I., Labay, V.S. and Pecheneva, N.V. 2003. Biota and macrobenthic communities of the Northeast Sakhalin lagoons. Sakhalin Research Institute of Fisheries and Oceanography, Yuzhno-Sakhalinsk, 176 pp. (in Russian).

Leatherman, S.P. 1981. Barrier beach development. A perspective of the problem. *Shore & Beach* **49**: 3–9.

Leontyev, O.K. 1961. Basics of the sea coasts geomorphology. Moscow State University, Moscow, 418 pp. (in Russian).

Nixon, S.W. 1982. Nutrient dynamics, primary production and fisheries fields of lagoons. *Oceanol. Acta.* **4**: 357–371.

Safyanov, G.A. 1996. Sea coasts geomorphology. Moscow State University, Moscow, 400 pp. (in Russian).

Sutherland, M. and Britton, D. 1980. National Parks of Japan. Kodanka International Ltd., 17-14 Otowa 1-chome, Bunkyoku, Tokyo 112, 148 pp.

Zenkovich, V.P. 1962. Principles of the Science of the Sea-shore Development. Publishing House of the USSR Academy of Sciences, Moscow, 710 pp. (in Russian).

Session A3

New technology

Session Chairs

Alexey Romanov and Naoto Ebuchi

HF radar technology in the Sea of Okhotsk

Naoto Ebuchi, Yasushi Fukamachi, Kay-Ichiro Ohshima and Masaaki Wakatsuchi

Institute of Low Temperature Science, Hokkaido University, Sapporo, Japan
E-mail: ebuchi@lowtem.hokudai.ac.jp

Abstract

In order to monitor variations in the Soya Warm Current (SWC), three high frequency (HF) radar stations were installed around the Soya Strait in August 2003. The radar covers a range of approximately 70 km from the coast. Comparisons of the observed current velocity with drifting buoy and shipboard ADCP data showed good agreement with root-mean-square differences of 20 cm/s. It is shown that the HF radars clearly capture seasonal variations of the SWC. The velocity of the SWC reaches its maximum, approximately 1 m/s, in summer, and weakens in winter. The velocity core is located 20 to 30 km from the coast, and its width is approximately 50 km. The almost same seasonal cycle was repeated in each of these five years from 2003 to 2008. Surface transport by the SWC shows a significant correlation with the sea level difference along the strait, as derived from coastal tide gauge records. The cross-current sea level difference, which is estimated from the sea level anomalies observed by the Jason-1 altimeter and a coastal tide gauge, also exhibits variation in concert with the surface transport and along-current sea level difference. In addition to the annual variation, the SWC exhibits subinertial variations with a period of 5–20 days.

Introduction

The Sea of Okhotsk (Fig. 1), a marginal sea adjacent to the North Pacific, is one of the southernmost seasonal sea ice zones in the Northern Hemisphere and it has been conjectured that it is a region in which the North Pacific Intermediate Water is ventilated to the atmosphere. The Sea of Okhotsk is connected with the Sea of Japan through the Soya/La Perouse Strait, which is located between Hokkaido, Japan, and Sakhalin, Russia. The Soya Warm Current (SWC) enters the Sea of Okhotsk from the Sea of Japan through the Soya Strait and flows along the coast of Hokkaido as a coastal boundary current. It supplies warm, saline water in the Sea of Japan to the Sea of Okhotsk. The current is roughly barotropic and shows a clear seasonal variation (Aota, 1984; Matsuyama *et al.*, 1999). However, the SWC has never been continuously monitored due to the difficulties involved in field observations related to various reasons, such as severe weather conditions in winter, political issues at the border strait, and conflicts with fishing activities in the strait. Detailed features of the SWC and its variations have not been clarified. Information concerning the variations of the SWC and the water exchange between the Sea of Japan and the Sea of Okhotsk is important for the study of both of these seas.

In this report, observation of the SWC using the HF radars is briefly introduced together with variations of the SWC revealed by a combination of the observed surface current fields with the sea level observations from coastal tide gauges and satellite altimetry. A detailed description of the HF radar system and validation of the observed surface current

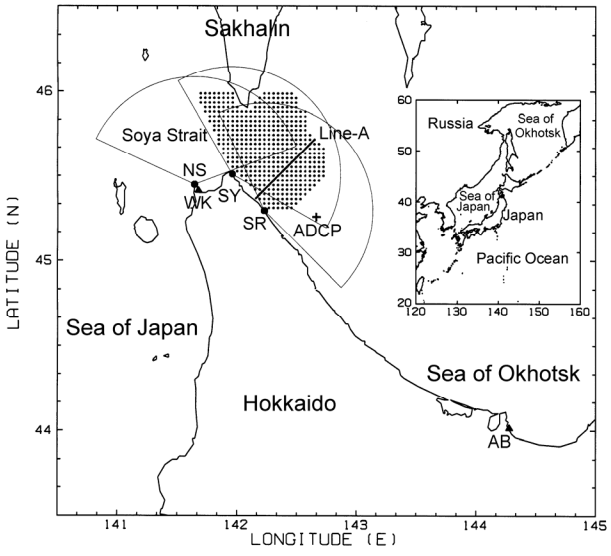

Fig. 1 Map of the Soya/La Perouse Strait, and location and coverage of the HF radar stations.

data were reported by Ebuchi *et al.* (2006). Fukamachi *et al.* (2008) estimated volume transport of the SWC using the surface current fields together with current velocity profiles observed by a bottom-mounted acoustic Doppler current profiler (ADCP). Ebuchi *et al.* (2008) investigated seasonal and subinertial variations in the SWC using data from HF radar, coastal tide gauges and bottom-mounted ADCP.

Observation of the SWC using the HF radar system

In order to continuously monitor the SWC, three HF radars (CODAR Ocean Sensors, SeaSonde) (Barrick *et al.*, 1977) were installed around the Soya Strait (Fig. 1). The frequency of the HF radar is 13.9 MHz, and the range and azimuth resolutions are 3 km and 5°, respectively. The HF radar covers a range of approximately 70 km from the coast. The observations were made at one-hourly intervals. We measured the beam pattern of the receiving antenna and corrected for distortion of the antenna pattern to derive accurate radial velocities. Surface current vectors were composed in grid cells of 3 × 3 km using the radial velocity components observed by the radars according to a least squares method.

An example of the observed surface current vector field is shown in Figure 2. Figure 3 is an example of the monthly-averaged surface current field. In these figures, the SWC, which flows from west to east across the Soya Strait and turns toward the southeast along the coast, is captured very clearly. They also show southward currents along the west coast of Sakhalin, as predicted by numerical experiments (Ohshima and Wakatsuchi, 1990; Ohshima, 1994).

The surface current velocity observed hourly by the HF radars was compared with *in-situ* data from drifting buoys and shipboard ADCPs (Ebuchi *et al.*, 2006). The current velocity derived from the HF radars showed good agreement with that observed using drifting buoys (Fig. 4). The root-mean-square differences were found to be less than 25 cm/s for the zonal and meridional components. The observed current velocity was also found to exhibit reasonable agreement with the shipboard ADCP data (Fig. 5).

Structure and seasonal variation of the Soya Warm Current

Using the surface current vector fields observed by the HF radars, we discuss seasonal variations of the SWC. In order to remove the tidal constituents, a 25-h running average was applied to the time series of the hourly surface current vectors in each grid cell, and then daily and monthly mean current fields were calculated. To remove the tidal variations, we examined a 25-h running average, harmonic analysis, and 48-h tide killer filter, and confirmed that the residual of the tidal components are negligibly small. An example of the monthly-averaged field is shown in Figure 3.

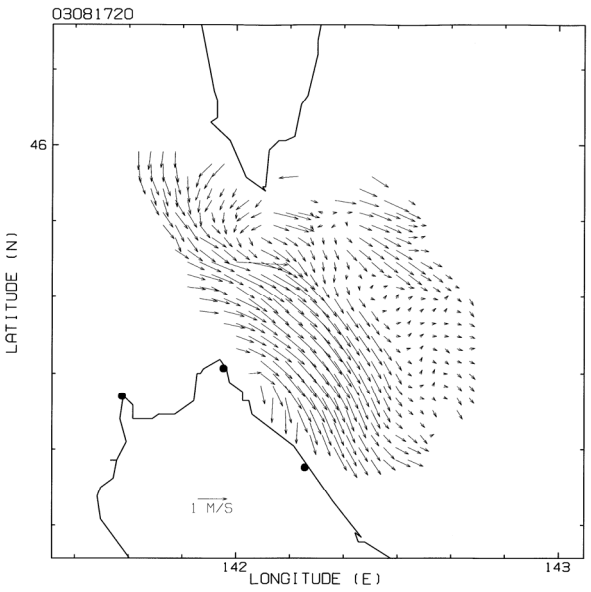

Fig. 2 An example of an hourly surface current vector field (1100 UTC, August 17, 2003).

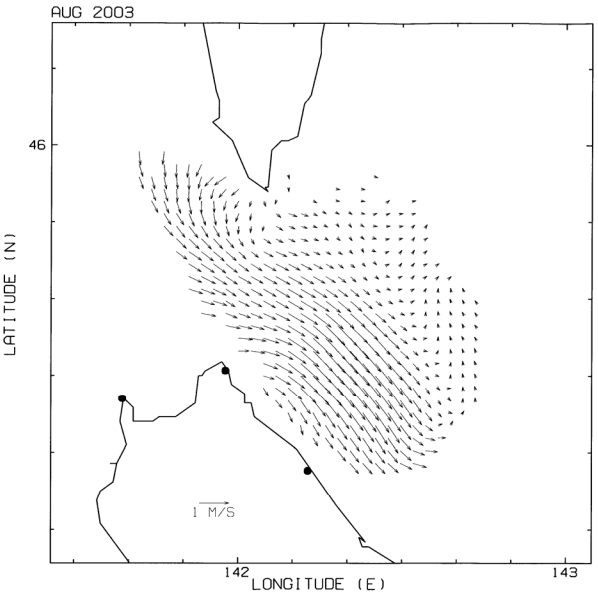

Fig. 3 An example of a monthly-averaged surface current field (August 2003).

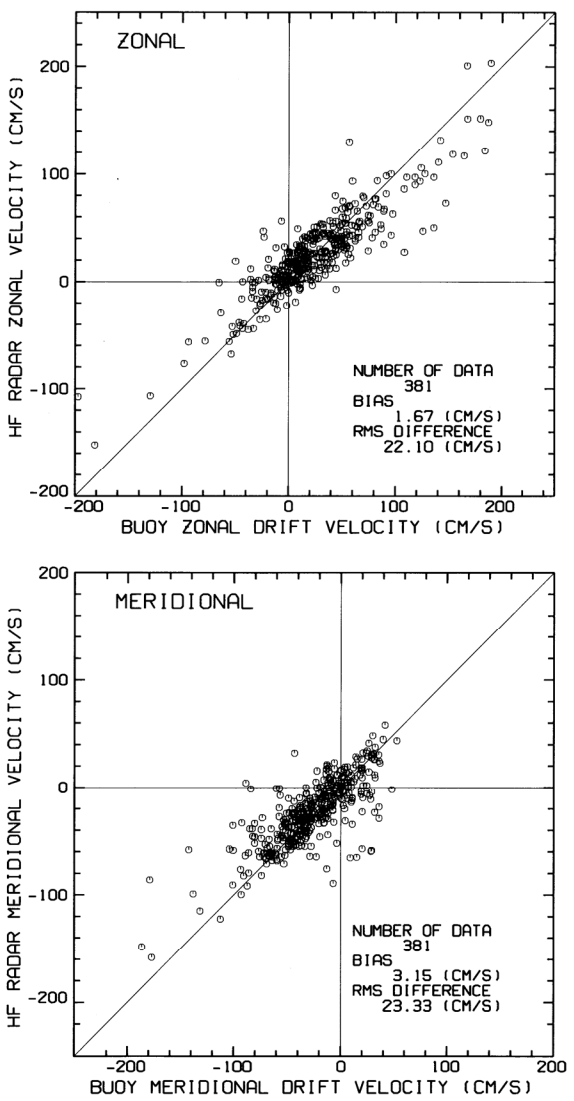

Fig. 4 Comparison of HF radar with drifting buoy observations for zonal (upper) and meridional (lower) velocity components.

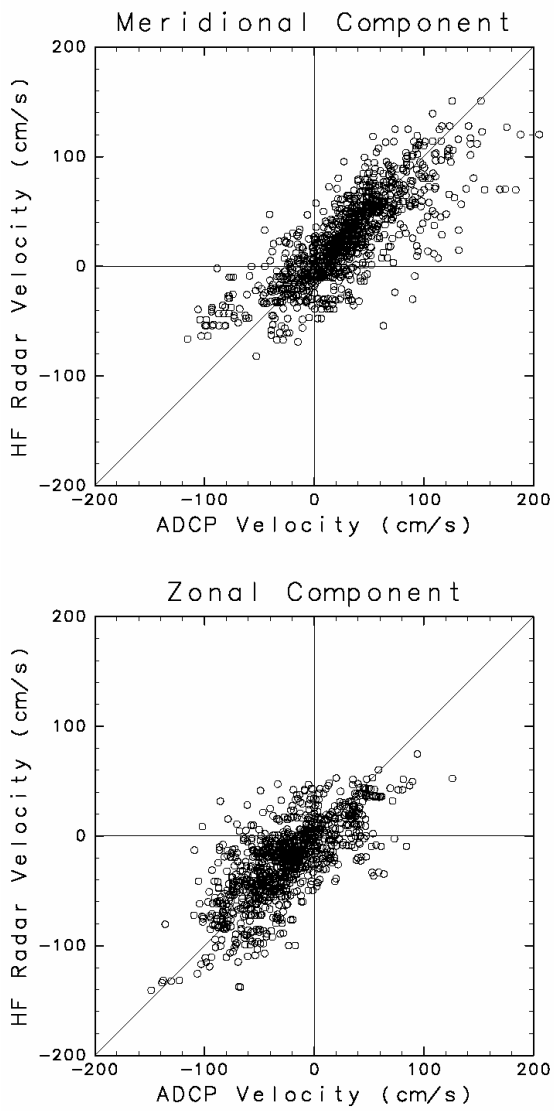

Fig. 5 Comparison of HF radar with shipboard ADCP observations for zonal (upper) and meridional (lower) velocity components.

Daily southeastward current components across Line-A (Fig. 1) were averaged monthly and are shown with standard deviations in Figure 6 for the period from August 2003 to July 2004. Figure 7 shows year-to-year variations of the monthly mean profiles within the five years from 2003 to 2008. The monthly-mean profiles show a clear seasonal variation. The velocity of the SWC reaches its maximum of approximately 1 m/s in summer (August and September) and becomes weak in winter (January and February). The current axis is located 20 to 30 km from the coast in this region, and the typical width of the SWC is approximately 50 km. These features of the SWC are consistent with the results of short-term or point-wise observations reported in previous studies (Aota, 1984; Matsuyama *et al.*, 1999). In Figure 7 it is shown that the almost same seasonal cycle has been repeated in these five years.

Variations of the surface transport and their relationship with sea level differences

Daily surface transport across Line-A was defined by the integration of the daily southeastward current component along the line from the coast to a point at which the component becomes negative. Figure 8 shows the time series of the surface transport (thick

line). Note that the unit of surface transport is not volume/time but area/time because the HF radars provide only the surface current velocity. In winter (from January to March), there is often a lack of data because the observation region is covered by sea ice.

The driving force of the SWC is ascribed to the sea level difference between the Sea of Japan and the Sea of Okhotsk (Aota, 1984; Ohshima, 1994). The surface velocity of the SWC has been reported to be closely related to the sea level difference (Aota, 1984; Matsuyama *et al.*, 1999). For comparison with the surface transport, as observed by the HF radars, we calculated the sea level difference between two tide gauge stations, Wakkanai (labeled as WK in Fig. 1) and Abashiri (AB in Fig. 1), which represents the sea level difference between the Sea of Japan and the Sea of Okhotsk. A 48-hour tide-killer filter was applied to the hourly tide gauge records at these stations. The daily-mean sea levels were then calculated, and atmospheric pressure correction was performed using the daily-mean sea level pressure observed at weather stations in the cities of Wakkanai and Abashiri. The time series is shown by a thin line in Figure 8. The surface transport of the SWC and the sea level difference along the current show a good correlation with a correlation coefficient of 0.702. Both time series exhibit not only the seasonal variation but also variations with time scales of approximately 10 to 15 days. The generation mechanism of this subinertial variation in the SWC was discussed by Ebuchi *et al.* (2008) in relation with wind-generated coastally trapped waves propagating along the east coast of Sakhalin and west coast of Hokkaido. The results shown in Figure 8 confirm the correlation at various time scales between the SWC and the along-current sea level difference.

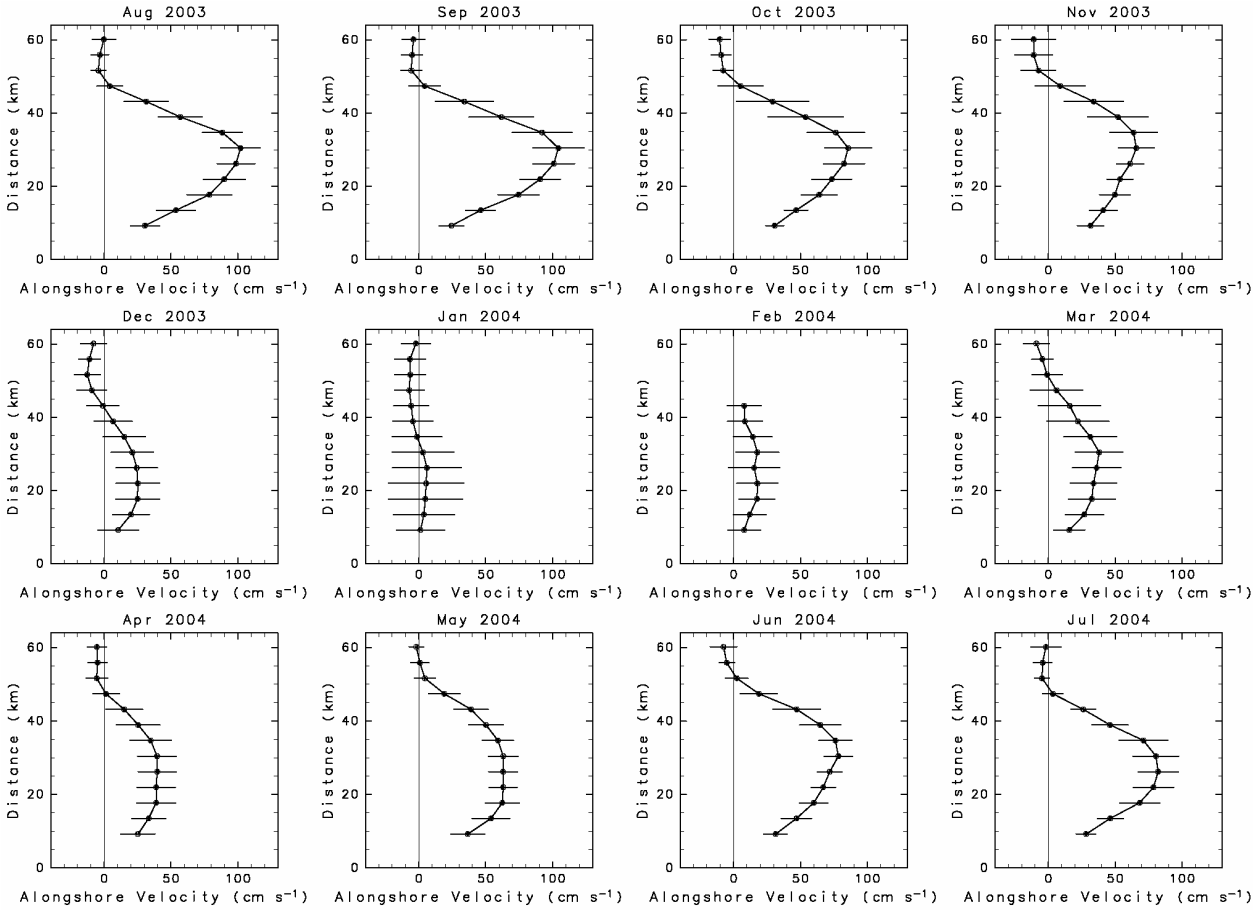

Fig. 6 Monthly-averaged profiles of the southeastward current velocity component across Line-A (Fig. 1) with respect to the distance from the coastline for the period from August 2003 to July 2004.

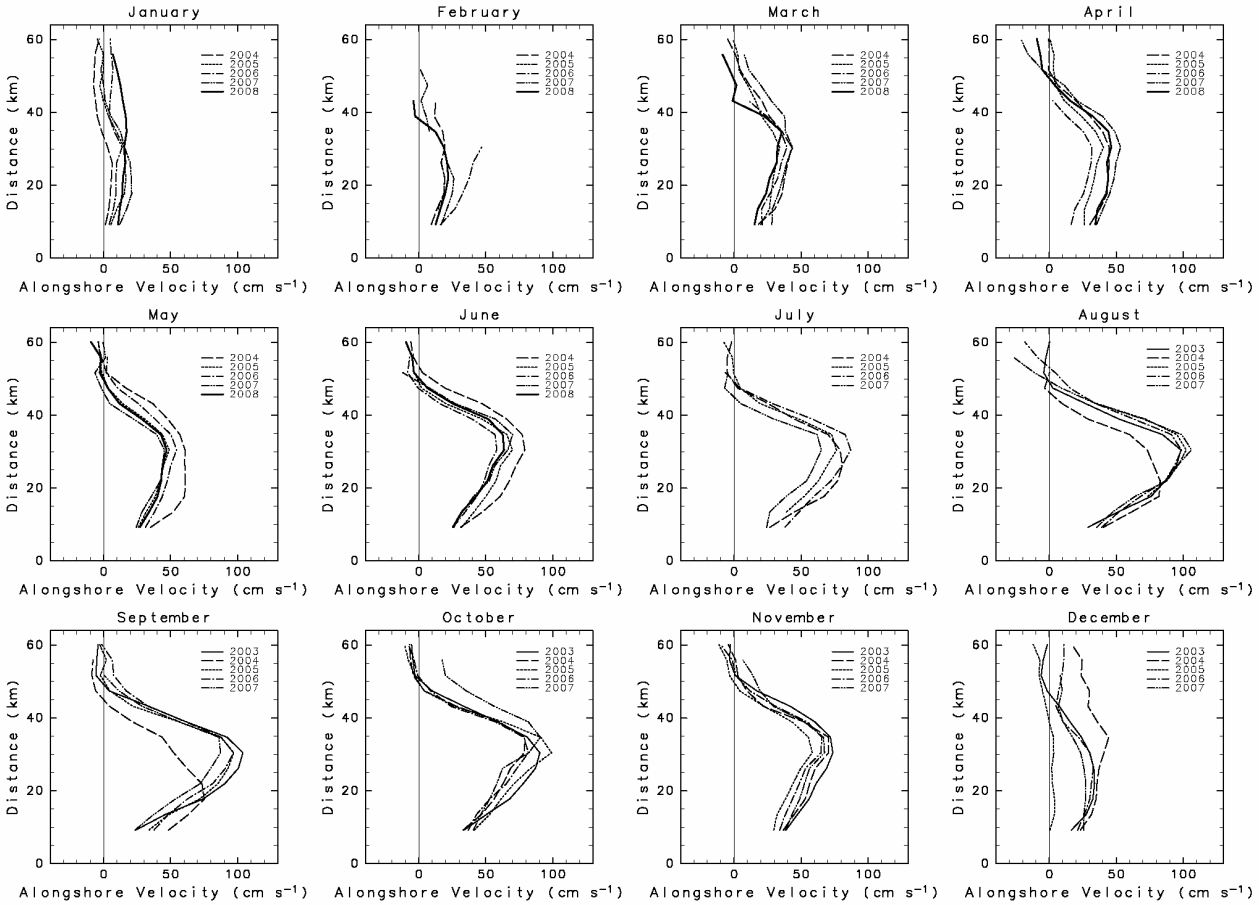

Fig. 7 Year-to-year variations of the monthly-averaged profiles of the southeastward current velocity component across Line-A (Fig. 1).

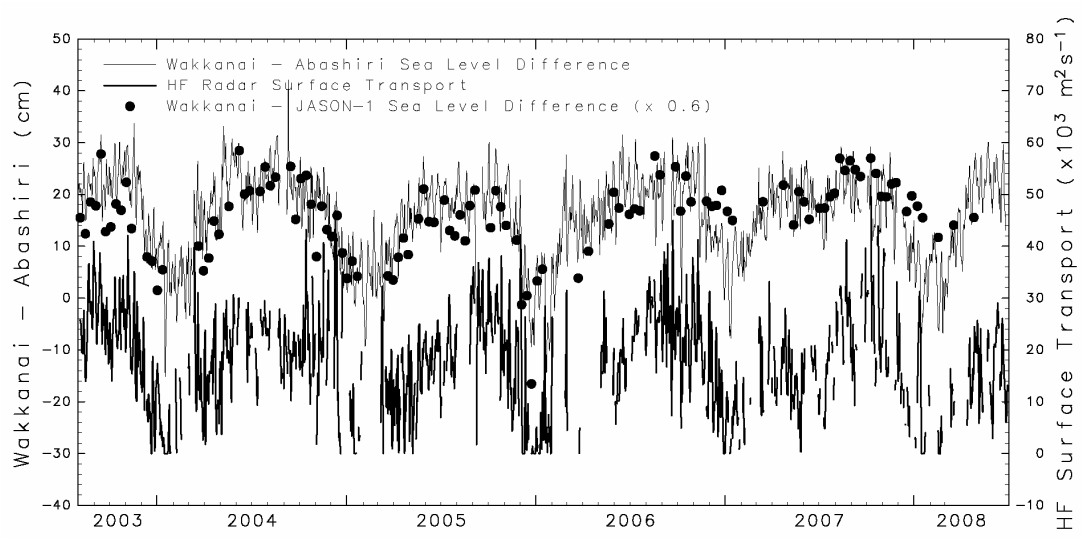

Fig. 8 Time series of the surface transport of the Soya Warm Current (SWC, thick line), the sea level difference between Wakkanai and Abashiri (thin line), and anomaly of the sea level difference between Wakkanai and the ground track B (Fig. 9) of the Jason-1 altimeter (solid circles).

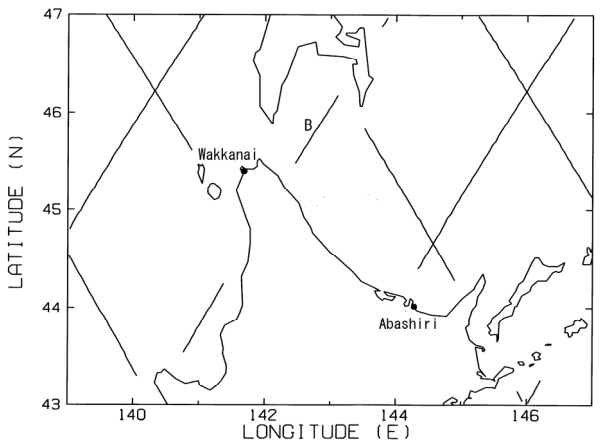

Fig. 9 Locations of ground tracks of the Jason-1 altimeter and tide gauge stations of Wakkainai and Abashiri.

In order to assess variations of the sea level difference in the cross-current direction, we utilized the sea level anomalies observed by the Jason-1 satellite altimeter. Figure 9 shows locations of ground tracks of Jason-1 in the Sea of Okhotsk. Since the spaceborne radar altimeter is not able to observe the sea surface height accurately in the region close to the coastline, we cannot obtain the cross-current sea surface height profiles associated with the SWC directly from the altimeter data. Therefore, the difference of the sea level anomalies between the offshore observations by the altimeter (indicated by B in Fig. 9) and the coastal tide gauge records at the Wakkanai station is utilized to represent the sea level variations across the SWC.

In Figure 8, the variation of sea level difference across the SWC is indicated by solid circles. The amplitude of the cross-current sea level difference is multiplied by 0.6 and is shifted vertically to match with the along-current sea level difference (thin line) in Figure 8. The temporal interval of the Jason-1 observation is 9.91 days. It is shown that the cross-current sea level difference is well correlated with the along-current sea level difference and also with the surface transport of the SWC. These results support evidence that the SWC is in geostrophic balance in the cross-current direction, and is driven by the sea level difference between the Sea of Japan and the Sea of Okhotsk (Aota, 1984). The same relationship between the cross- and along-current sea level differences were discernible in the 10-year record of the sea level anomaly obtained by the TOPEX/Poseidon altimeter combined with the coastal tide gauge records (not shown here).

Concluding Remarks

In this report, we briefly introduced the HF radar system deployed in the Soya/La Perouse Strait region and analyses of the observed surface velocity fields. The HF radars clearly captured seasonal and subinertial variations in the SWC. It is demonstrated that HF radar system is a powerful tool to monitor surface current fields in coastal regions.

References

Aota, M. 1984. Oceanographic structure of the Soya Warm Current. *Bull. Coast. Oceanogr.* **22**: 30–39 (in Japanese).

Barrick, D.E., Evans, M.W. and Weber, B.L. 1977. Ocean surface currents mapped by radar. *Science* **198**: 138–144.

Ebuchi, N., Fukamachi, Y., Ohshima, K.I., Shirasawa, K., Ishikawa, M., Takatsuka, T., Daibo, T. and Wakatsuchi, M. 2006. Observation of the Soya Warm Current using HF radar. *J. Oceanogr.* **62**: 47–61.

Ebuchi, N., Fukamachi, Y., Ohshima, K.I. and Wakatsuchi, M. 2009. Subinertial and seasonal and variations in the Soya Warm Current revealed by HF ocean radars, coastal tide gauges and a bottom-mounted ADCP. *J. Oceanogr.* **65**: 31–43.

Fukamachi, Y., Tanaka, I., Ohshima, K.I., Ebuchi, N., Mizuta, G., Yoshida, H., Takayanagi, S. and Wakatsuchi, M. 2008. Volume transport of the Soya Warm Current revealed by bottom-mounted ADCP and ocean-radar measurement. *J. Oceanogr.* **64**: 385–392.

Matsuyama, M., Aota, M., Ogasawara, I. and Matsuyama, S. 1999. Seasonal variation of Soya Current. *Umi no Kenkyu* **8**: 333–338 (in Japanese with English abstract and captions).

Ohshima, K.I. and Wakatsuchi, M. 1990. A numerical study of barotropic instability associated with the Soya Warm Current in the Sea of Okhotsk. *J. Phys. Oceanogr.* **20**: 570–584.

Ohshima, K.I. 1994. The flow system in the Sea of Japan caused by a sea level difference through shallow straits. *J. Geophys. Res.* **99**: 9925–9940.

Automated information technology for ionosphere monitoring of low-orbit navigation satellite signals

Alexander Romanov, Sergey Trusov and Alexey Romanov

Federal State Unitary Enterprise Russian Institute of Space Device Engineering (FSUE "RISDE"), Moscow, Russia
E-mail: romanov@rniikp.ru

Introduction

In the last couple of decades ionospheric radio tomography by navigation low earth orbit satellite signal methods has been intensively evaluated. This kind of tomography consists of the synchronous registration of one satellite signal by a number of receiving stations and is followed by an ionosphere electron content distribution reconstruction based on a set of integral values (signal phase delay). Setting receivers along a satellite pass allows us to obtain height–latitude ionosphere cross-sections. The horizontal size of such sections is commonly a few thousand kilometres, and the vertical size is about 1000 km. The first radio tomography experiments were processed about 20 years ago (Kunitsyn and Tereshchenko, 2001) and the theoretical part has been well investigated, but the approaches to data acquisition and processing have been less well studied.

Usually the time gap between satellite signal registration at the receiving stations and the end of thematic data processing is weeks, or even months. The main reason for such a time delay in most modern tomography systems is because manual procedures are used in the process of acquiring and processing data which constrains the speed of the information being transmitted to the receiver. Consequently, data processing requiring visual analysis or qualitative assessment for decision making needs to be modified to reduce output time. At the same time, it is necessary to organize the high-speed data acquisition.

The process of tomography data acquisition and processing consists of several stages: (1) data acquisition from the receiving stations, (2) analysis of data characteristics, (3) different transformations necessitating decision making, and (4) reconstruction of problem solving quality assessments. Thus, it is necessary to develop an automated system of the tomography data acquisition and processing in order to increase the capability of the data receiving operation.

The automated ionospheric tomography data processing technique, the processing center and data acquisition receiving station interaction algorithm and the special software for information acquisition, processing, storing and representing are needed to develop such a system.

The automated ionospheric tomography data processing technique

The technique is based on the phase-difference tomography method (Kunitsyn and Tereshchenko, 2001). The technique parameters were obtained as a result of numeric modeling carried out for the geometry of the receiving stations' network, located on Sakhalin Island. The network consists of three receiving stations spaced about 250 km apart.

The technique consists of three stages:

1. Useful signals allocated from data are received from the stations on the basis of empirically obtained boundary conditions (dispersion of the differential phase values in running average window $N = 10$ is less than 1 and the length of the signal part is longer than 60 s).
2. The systematization of the existing data is realized by radio sounding sessions. The data belonging to one session are characterized by a common satellite identifier and the time difference between registering data on the receiving stations of the chain is less than 35 min.
3. The high-frequency signal component (greater than 0.1 Hz) is eliminated and then the phase derivative with respect to time is calculated. The data are decimated and only every eighth measurement is used for further research.
4. The orbit satellite location row is calculated using the SGP4 orbit model (Kelso, 1996) for the satellite communication session according to the procedure of signal decimation. Thus, the satellite

location is calculated for every conformed measurement from the data files.

5. The redundant data for tomography task solving are rejected as soon as the locations of the radio signals in the area of interest are defined. For example, it is necessary to discard part of the received initial data from the southern station if the smallest satellite latitudes, fixed for it, are the smallest for all the tomography chain stations. It is also necessary to reject the data of the southern station if the satellite latitudes characterizing this information are also less than the minimum latitudes for the northern stations. The analogous but opposite conditions are used for culling data of the northern stations.
6. The projecting operator matrix is formed on the basis of the signals' path locations and piece-planar approximation function for the grid dimensions 50 × 25 km and 1000 km height. The vertical grid size is defined by the current session geometry.
7. An optimal initial guess is picked up by forming the finite set of the model electron concentration distributions and by correspondence analysis of the integral measurements calculated on their (model distribution sets) basis to experimental data.
8. The linear equation system (SLE) is formed using the created projecting operator matrix, the initial guess and measurement vectors $Ax = b$. The SLE solving procedure is realized by the algebraic reconstruction technique (ART) with the relaxation iteration algorithm. The iteration procedure ends if the velocity of the SLE right part of the reconstruction error change becomes less than 0.001, otherwise, it will end after 50 iterations. Thus, the electron concentration reconstruction is completed as soon as the values in regular grid nodes are calculated.

Consequently, the numerical parameters of every stage of the proposed technique were formalized and defined as a result of our research. The special software for automated ionospheric tomography operative data processing was developed.

Remote receiving station network administration

The task of operative data transfer is solved by means of receiving stations connected to the Internet. The transfer time of the data from one satellite communication session (220 Kb) is 14 s, with a typical connection speed of 128 Kb/s to a local Internet provider.

It is necessary to provide the receiving station with an actual schedule of satellite radio visibility sessions used. The proposed decision is based on the satellite orbit parameters, and the radio visibility zone calculation on the basis of the SGP4 model. If the communication session is invisible even for one receiving station in the tomography chain, the records of satellite communication sessions need to be culled after the communication schedule is formed. Thus, the files with the communication schedule are formed in the way represented above to transmit to the receiving station.

The remote control problem is solved by checking the accessibility of the receiver stations via the Internet and analyzing the retrieved log files periodically.

The proposed approaches were realized in the algorithm consisting of three procedures: the calculation of the satellite radio visibility zone, schedules, new data receiving, and receiving station administration. The execution of the procedure is determined by the task manager in accordance with pre-defined rules. The task manager works permanently and checks the schedule periodically. If the current time corresponds to the time of some procedural execution, the special process in charge for this procedure is initiated.

Special software for ionospheric tomography data acquisition and processing

To automate tomography data processing, it is necessary to solve a number of supplementary tasks such as ballistic data acquisition and managing the studies of the data processing. Special software was developed to solve the whole spectrum of the ionospheric tomography system data processing problems revealed above.

The special software structure consists of functional segments in charge of acquiring, processing, storing and representing information, and management and administration of the acquisition and processing information processes (Fig. 1). The basic functionality of each segment is provided with the execution of one, or more often, several program modules. A user web-interface allows the user to access data processing results and manage the acquisition and processing data procedures interactively using any computer with an Internet connection (Fig. 2).

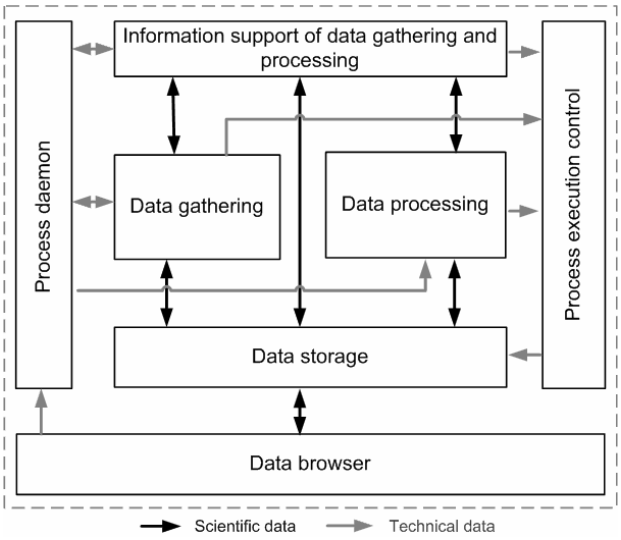

Fig. 1 Flowchart of special software developed for ionospheric tomography data acquisition and processing.

Information storage in the system consists of managing information acquisition and processing from a set of tomography chains realized with the provision for further possible enlargement of the receiving system segment.

This approach is based on special metadata structure usage where each receiving station is characterized by the set of the hierarchical and geographical characteristics, and allows the system to work with a single tomography chain as a set element.

Numerical Modeling Results

The reconstruction of the ionosphere electron concentration model distribution was carried out by developing special software according to conditions identical to real experiment geometry described in Romanov *et al.* (2008) for thematic processing quality assessment. The reconstruction errors were obtained by calculating the discrepancy between initial and reconstructed functions, and defined by the following relations (Kunitsyn and Tereshchenko, 2001):

$$\delta_2 = \frac{\sqrt{\sum_i (F_i - \tilde{F}_i)^2}}{\sqrt{\sum_i F_i^2}};$$

$$\delta_m = \frac{\max_i |F_i - \tilde{F}_i|}{\max_i |F_i|},$$

where F is the initial value and $\tilde{F}$ is the reconstructed one.

Results showed that the errors of the model distribution reconstruction, describing the disturbed ionosphere state (the existence of the irregularities and the horizontal gradient of electron concentration), are characterized by $\delta_2 = 0.08$ and $\delta_m = 0.10$ and become less with the regulating of the ionosphere structure.

Experiment Results

Experimental research on the quality of the developed system of ionospheric tomography data acquisition and processing was carried out using real ionospheric tomography data from stations located on Sakhalin Island.

The system of ionospheric tomography data acquisition and processing working results are the height–latitude distribution of electron concentration (Fig. 3). Figure 4 represents the results of the comparison between the data from the ionosonde in Wakkanai city (Hokkaido Island, Japan), located approximately in 150 km to the south of Yuzhno-Sakhalinsk city (Sakhalin Island, Russia) and the information reconstructed with the aid of the specially developed software. The ionosonde data were provided by "WDC for Ionosphere, Tokyo, National Institute of Information and Communications Technology". Data from the reconstruction of 90 ionosphere states were used: 50 were received in summer period of 2007 (July–August) and 40 in January 2008.

The maximum values of ionosphere electron concentration in the region of the ionosonde location were recalculated to the critical frequency foF2 terms for the further comparison. Good agreement was shown, with a mean discrepancy of 15% and $\delta_2 = 0.13$. Maximum discrepancies of 41% and 46% were obtained for two reconstructions.

The correlation ration for two data rows was 84% ($R = 0.84$). These results are in good accordance with quality assessments of the ionosphere tomography reconstructions represented in independent research ($\delta_2 = 0.9$–0.11) (Kunitsyn *et al.*, 2007). However, it is necessary to note that independent assessments were obtained using the phase difference tomography approach, but without any automation technique.

The correspondence of these results shows that the new technique proposed in this research allows us to automatically reconstruct the electron concentration distribution in the ionosphere with typical accuracy as for the phase difference tomography approach.

The operational speed of the ionospheric tomography reconstruction using this system is 5–15 min. The speed of this automated data acquisition and processing has no analogue in Russia, and has not yielded the best foreign samples.

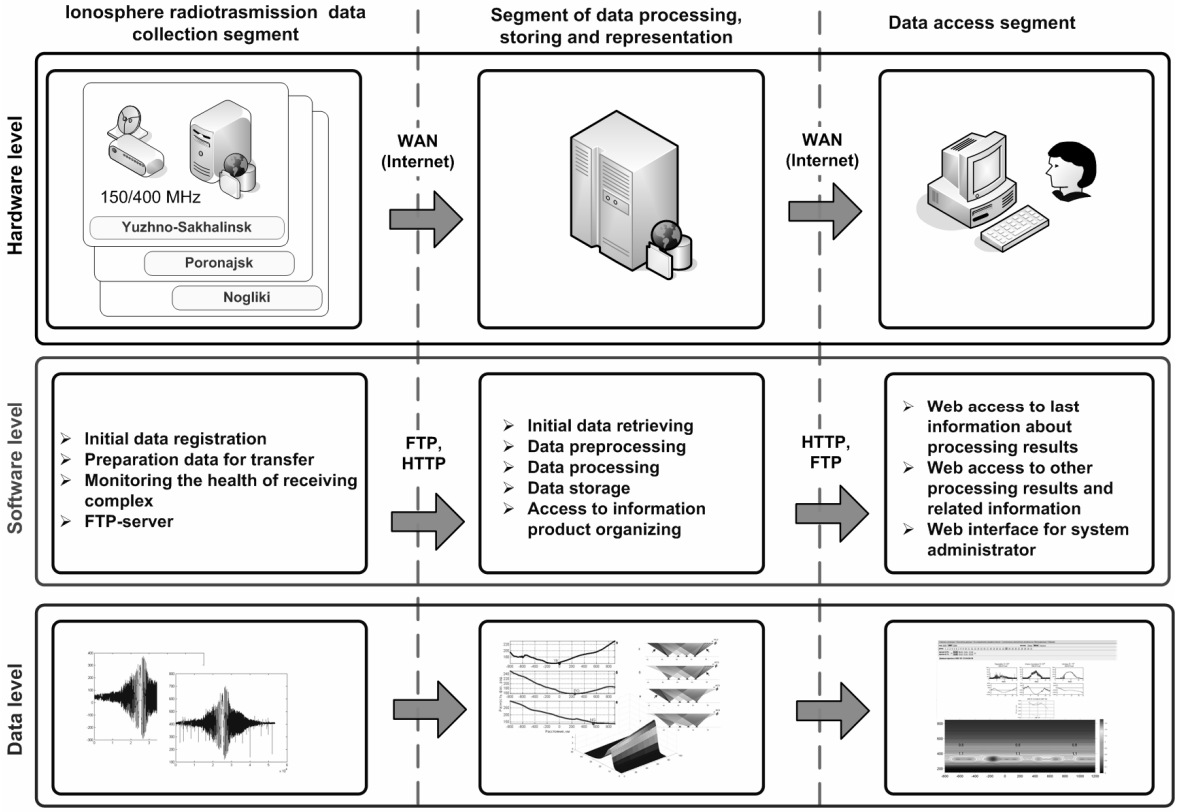

Fig. 2 The structure of ionospheric tomography data acquisition and processing automated system.

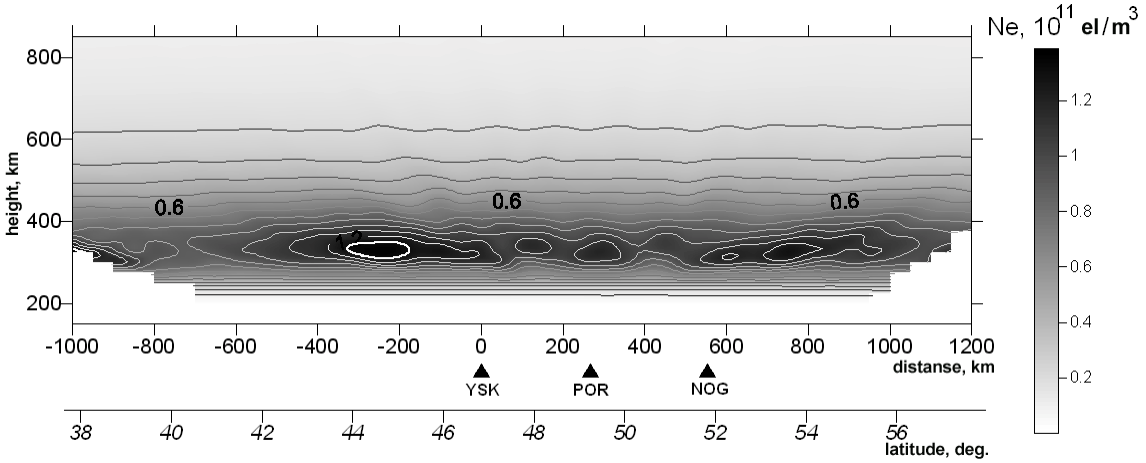

Fig. 3 Electron concentration distribution on July 29, 2007, 0:30 (local time) on Sakhalin Island.

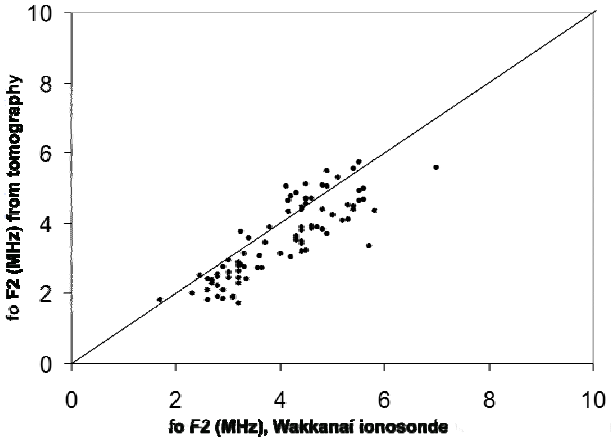

Fig. 4 The scatter plot of the values of critical frequency (foF2 calculated from tomography reconstruction and measured by ionosonde in Wakkanai (Hokkaido Island, Japan).

Conclusions

In the current research, the following results were achieved. The technique of automated ionospheric tomography data processing was developed. The automated ionosphere reconstruction has an accuracy about 15%.

A remote network management algorithm was developed which allows tasks to be solved automatically for ionospheric tomography data acquisition, dataware and workability administration of the receiving stations.

The special software for automated ionospheric phase difference tomography data acquisition and processing was developed. It allows the reconstruction of the ionosphere vertical electron concentration distribution in 5–15 min after the satellite communication session ends.

References

Kelso, T.S. 1996. Real-world benchmarking. *Satellite Times* **3** (November/December): 80–82.

Kunitsyn, V.E. and Tereshchenko, E.D. 2001. Ionosphere Tomography. Springer, Berlin.

Kunitsyn, V.E., Tereshchenko, E.D. and Anreeva E.S. 2007. Ionosphere Radiotomography. 336 pp. (in Russian).

Romanov, A.A., Trusov, S.V., Romanov, A.A. *et al.*, 2008. Researching of ionosphere disturbances on phase-difference tomography method at Russian Far East region. *Earth Remote Sensing* **2**: 14–20 (in Russian).

A pilot project on the comphrensive diagnosis of earthquake precursors on Sakhalin Island: Experiment results from 2007

Alexey Romanov, Youry Urlichich, Sergey Pulinets, Alexander Romanov and Victor Selin

Federal State Unitary Enterprise Russian Institute of Space Device Engineering (FSUE "RISDE"), Moscow, Russia
E-mail: romanov@rniikp.ru

Introduction

Last year's research clearly revealed the existence of specific variations in the atmosphere and ionosphere parameters during the buildup, or preparation, period leading to an earthquake (M > 5) in the area where it was about to take place. The characteristic dimensions of the earthquake preparation area are defined by $R = 10^{0.43M}$, where R is the radius of a preparation area and M is the magnitude of an earthquake (Pulinets and Boyarchuk, 2004).

The appearance, major morphology characteristics, and correlation of the atmosphere and ionosphere anomalies are explained in terms of a lithosphere-atmosphere-ionosphere (LAI) coupling (LAIC) model which has been developed recently (Pulinets and Boyarchuk, 2004; Pulinets *et al.*, 2006a; Pulinets, 2007).

The most active seismic region in Russia is the Far East where more than 500 earthquakes of varying intensity have taken place in the last 10 years (Fig. 1).

In 2007 the decision to conduct a comprehensive experiment using different types of experimental data was realized by the completion of the first stage of a pilot project to test navigation equipment with the signals of Russian and foreign space navigation systems to diagnose the precursors of strong earthquakes.

The main goal of the experiment was the verification and validation of methods and algorithms of data acquisition, processing and distribution based on existing Russian and foreign navigation, meteorological and resource satellites, and helio-geophysical *in-situ* information in seismic active region of the Russian Far East using the scientific principals of Pulinets and Boyarchuk (2004), Pulinets *et al.* (2006a) and Pulinets (2007).

It was first necessary to carry out a registration of the different atmosphere and ionosphere (Fig. 2) parameters described by the LAIC model for the pilot project. A comprehensive approach can lead to a new reliable earthquake short-term forecast prediction method using even a single parameter of atmosphere or ionosphere registration.

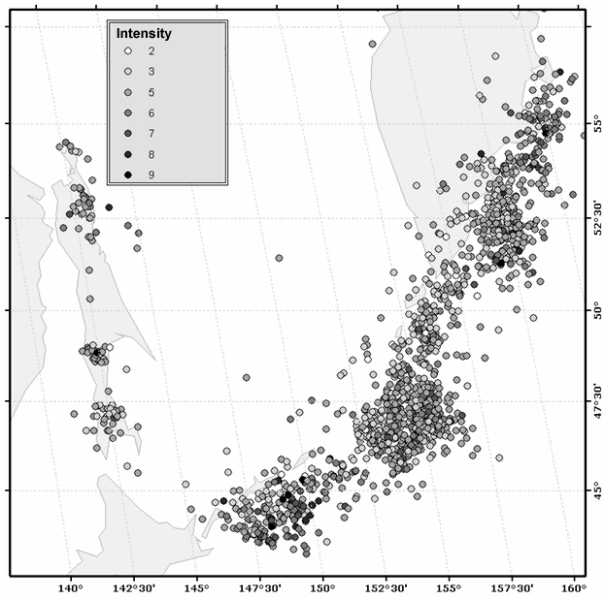

Fig. 1 Earthquake distributions on Sakhalin Island, Kamtchatka and the Kuril Islands region in 1994–2004 (data taken from the Russian Geophysical Survey).

During the experiment on August 2, 2007 at 02:59 UTC, an earthquake took place, with epicenter coordinates 46.55°, 141.81° and M = 6.3 near Nevelsk city, Sakhalin Island. Thus the current research is directed to the study of anomaly phenomena in different media prior to this seismic event.

Experimental Data and Joint Analysis

Comprehensive analysis of meteorology data for a series of recent strong earthquakes (Pulinets *et al.*, 2006a,b) that have taken place in the world reveals the temporal dynamics of surface air temperature and humidity. The most sensitive parameter is the daily temperature range (the difference between minimum

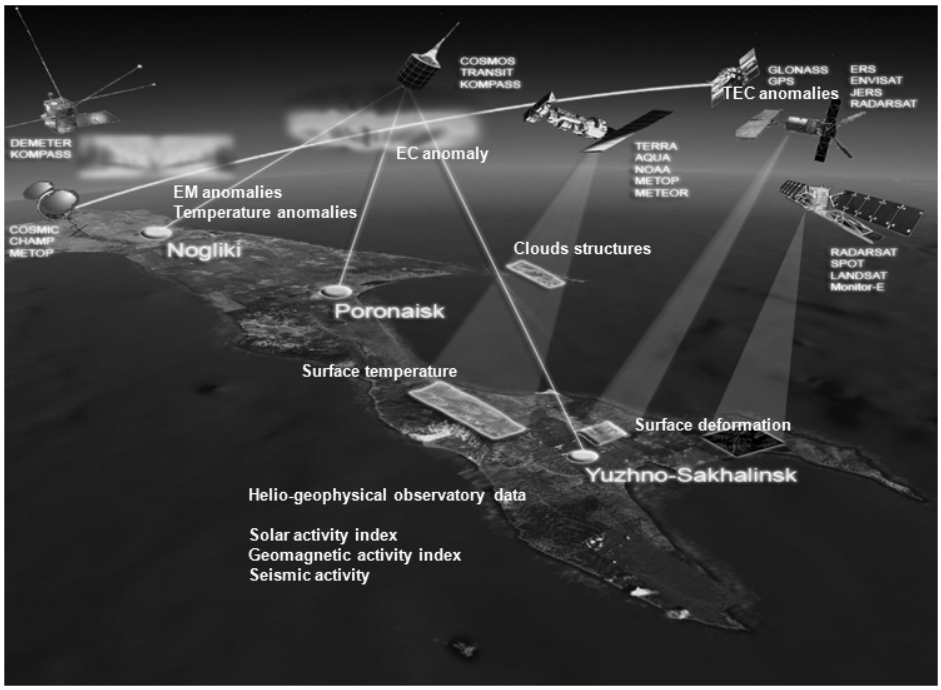

Fig. 2 The scheme of a comprehensive monitoring system of earthquake precursors in different media from space.

and maximum values). Approximately 5–7 days before an earthquake, this parameter usually reaches the local maximum and then decreases to the event moment. The maximum of the daily temperature range coincides with the minimum of the air humidity at the same time.

The temperature and humidity variations from standard meteorology observations were analyzed for the period of July–August in 2007. It can be seen (Fig. 3) that neither surface air temperature nor humidity demonstrate anomalous values. These parameters are within the limits of monthly variations but the variation corresponds to a typical form (simultaneous but opposite variations of the temperature and humidity expressed by the ellipse in Figure 3) for different earthquakes and the time range of the temperature maximum and humidity minimum is 4 days before the earthquake. It can be seen that the maximum daily temperature range occurred on July 29–30 whereas the humidity minimum was on July 30.

Anomalous cloud structures formed over the area of earthquake preparation were also analyzed. The linear cloud structures, corresponding with the fault system and tectonic plate borders, were distinguished in meteorological data by American satellites. The inset in the left hand panel of Figure 4 represents the structure of tectonic plates in the Sakhalin and Japan areas, and the rest of the panel is the image taken on July 30, 2007 by the TERRA satellite. It can be seen that the cloud cover is cut along the tectonic border, across Sakhalin Island (marked with an ellipsis). The right hand panel shows an image taken by AQUA on July 31. Inside the area marked with an ellipse one can clearly distinguish the thread-like cloud lying almost over the epicenter of the future earthquake. The dimensions of the cloud structures and their locations show the scale of tectonic activity before the earthquake and confirm the conclusion of Pulinets and Dunajecka (2007) that tectonic activity increases not only near the epicenter of a future earthquake but also on the tectonic borders. This example shows another important factor: the gases emanating into the atmosphere from tectonically active structures takes place both in the earth and in the ocean and the short-term precursors of earthquake activity can be successfully registered over the ocean surface too. The results of the analysis for the outgoing infrared radiation (OLR) from satellite radiometers, of 10–12 μm (Ouzounov *et al.*, 2007; Fig. 5), support the evidence discussed above. Because of the existence of the atmospheric transparency window in these wavelength ranges, the radiance is not absorbed by clouds and special data processing technology allows us to measure OLR under the clouds to approximately 12 km height.

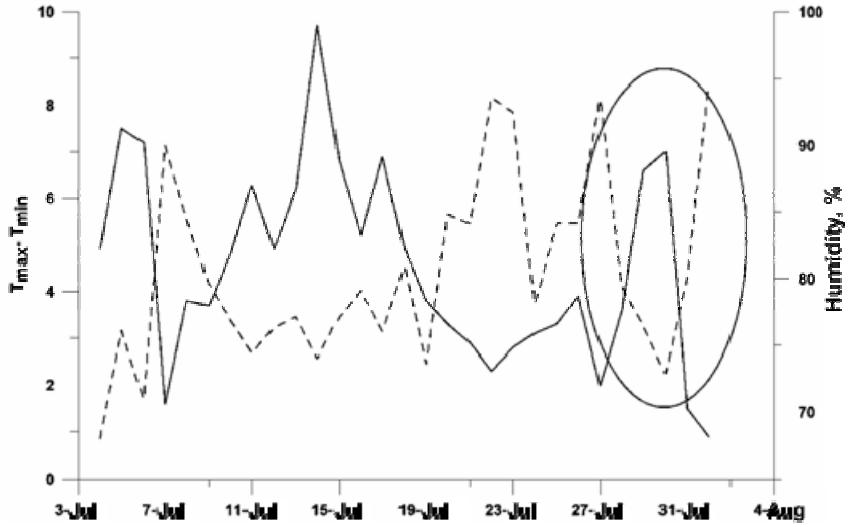

Fig. 3 The daily temperature (solid line) and humidity (dashed line) range change in Nevelsk city (Sakhalin Island) before the M6.3 earthquake of August 2, 2007. Simultaneous but opposite variations in temperature and humidity are shown by an ellipse.

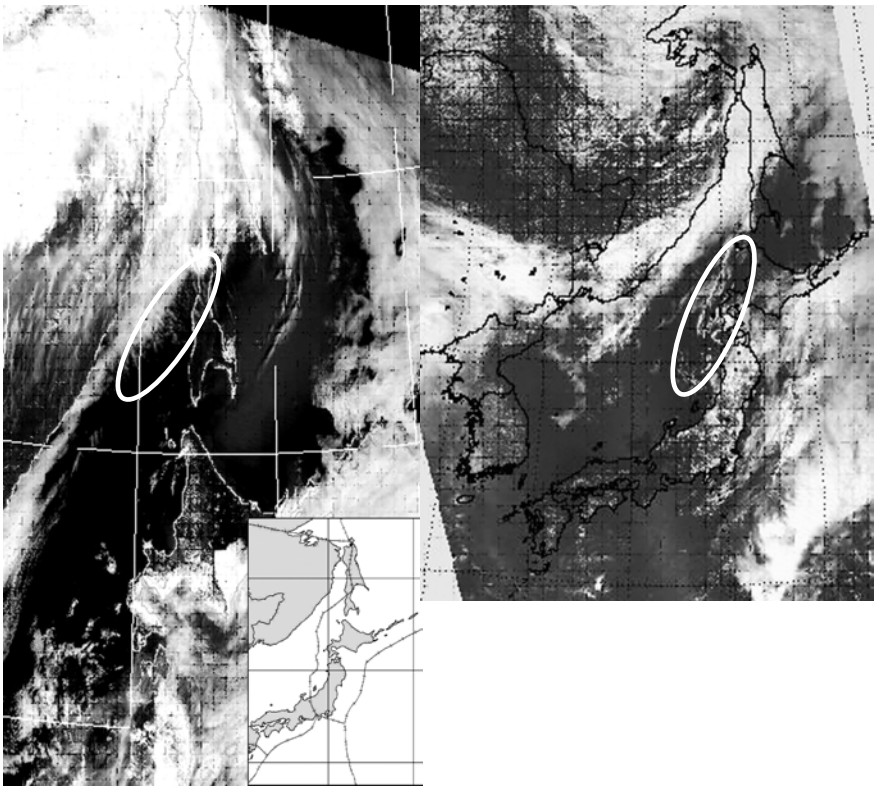

Fig. 4 Anomalous cloud structures marked by an ellipse (left panel) July 30, 2007 from TERRA data and (right panel) July 31, 2007 from AQUA data. The satellite data were taken from Institute of Industrial Science, University of Tokyo, Japan.

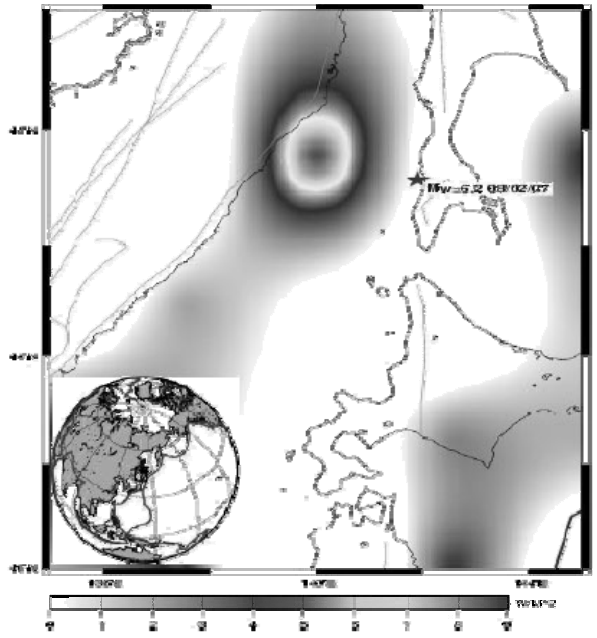

Fig. 5 OLR distribution (W m^{-2}) off Sakhalin Island using AIRS data from the AQUA satellite (Granted by D. Ouzounov).

The variations of total electron content (TEC) for three different GPS stations in the study region were calculated for July–August 2007. The geomagnetic disturbance analysis (Dst index, bottom panel in Figure 6) shows almost quiet geomagnetic conditions in the region. On July 12 and 14 there were small geomagnetic disturbances of less than 50 nT. Nevertheless, the regional ionosphere variability calculation method of Pulinets *et al.* (2007) is used to distinguish the possible seismology caused by ionosphere variations. This method allows us to reveal ionosphere variations in difficult geomagnetic conditions. The result is represented in the upper panel of Figure 6. A week before the earthquake (from July 24 to 31, marked by arrows), an increase of the seismic activity was observed. The second maximum after the earthquake is caused by after-shocks observed during the longer time period.

The regional ionosphere variability index running average curve has three local maxima in the period before the seismic event: July 24, 28 and 30. Tomography reconstructions of the vertical electron concentration distribution in the ionosphere showed the anomalies just in these days. These anomalies are represented in Figure 7. The figures were reconstructed by the phase-different method (Kunitsyn and Tereshchenko, 2001) during night satellite communication sessions (Fig. 7a, b, and c, respectively). Tomography reconstruction for the undisturbed ionosphere conditions is represented in Figure 7d.

The reconstructions for July 24 and 28 can be interpreted as a spreading horizontal wave disturbance with wavelength about 200 km. This could be an acoustic-gravity wave induced by an electric field anomaly according to Hegai *et al.* (1997). The reconstruction on July 30 can be interpreted as a ring-like structure with a minimum over the epicenter of the future earthquake.

In addition to the parameters discussed above, lithosphere plate dynamics were analyzed as a result of an experiment conducted in the Far East region using GPS data of the International Ground Station (IGS) network, located in Yuzhno-Sakhalinsk (Russia) and Shintotsukawa (Japan) (Fig. 8).

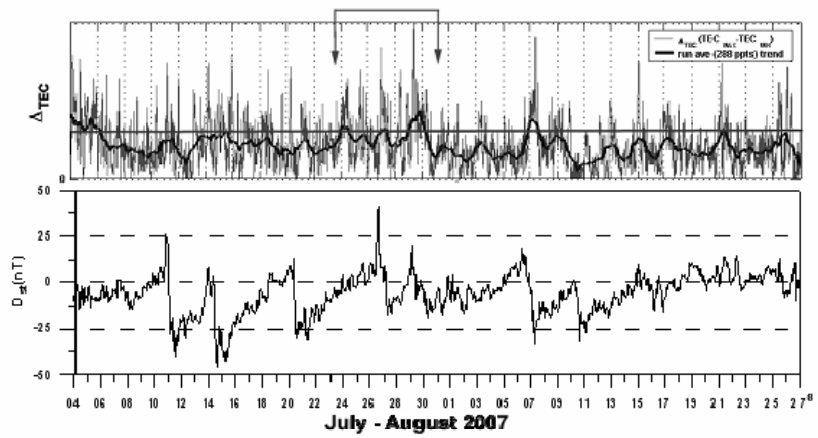

Fig. 6 The regional ionosphere variability index (upper panel), by GPS data (July–August 2007). Bottom panel is the Dst index for the same time period in July and August 2007.

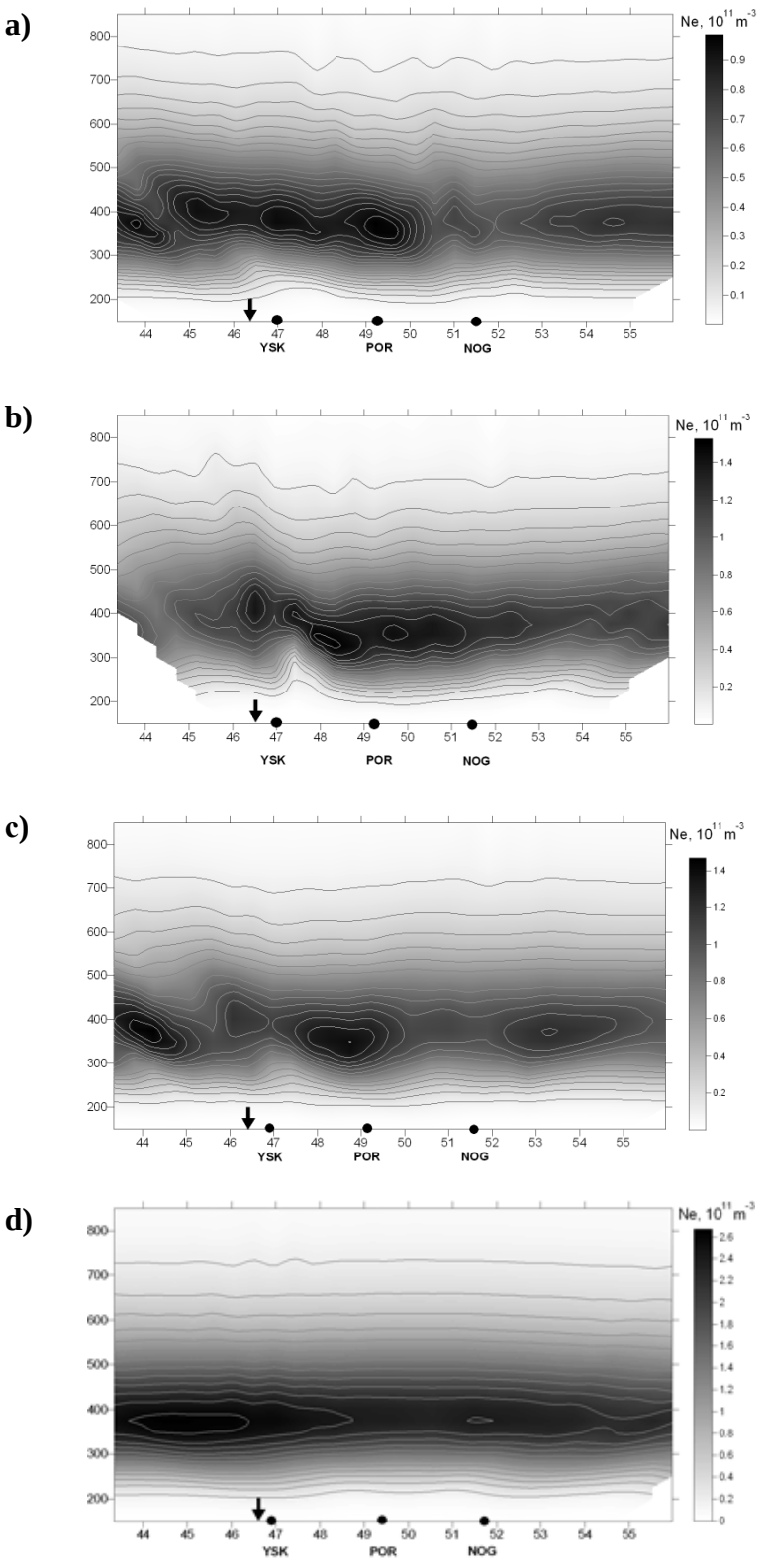

Fig. 7 Vertical distribution of ionosphere electron concentrations reconstructed from the signals of Russian low-orbit navigation satellites. (a) July 24, 2007, (b) July 28, 2007, (c) July 30, 2007, and (d) July 27, 2007. Panel d, having undisturbed ionospheric conditions, is shown for comparison.

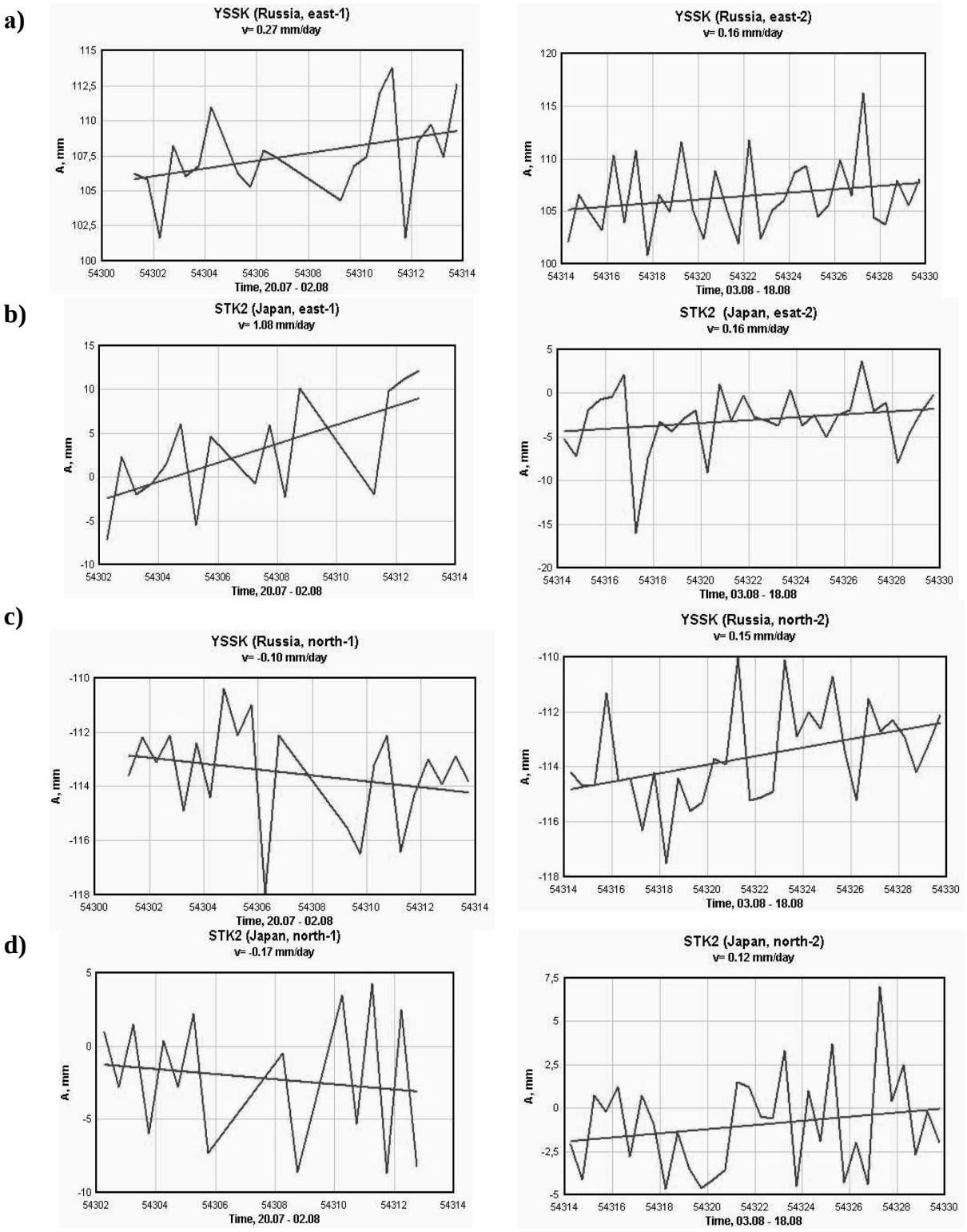

Fig. 8 IGS GPS station displacement (in mm) calculated for stations located in Yuzhno-Sakhalinsk (Russia) and Shintotsukawa (Japan) before (left column) and after (right column) the earthquake. Panels a and b show the horizontal component of displacement in Yuzhno-Sakhalinsk (YSSK) and Shintotsukawa (STK2), respectively. Panels c and d show the vertical component of displacement in Yuzhno-Sakhalinsk and Shintotsukawa, respectively.

As can be seen, the patterns in IGS station displacement velocity changes cannot be considered good earthquake precursors. However, the displacement velocity is almost the only directly measured parameter characterizing the processes taking place in the Earth's crust.

Preliminary analysis of the IGS stations' coordinates shows that the sign for the vertical component of velocity displacement changed to the opposite sign after the earthquake (Fig. 8c and d). Similar behavior is typical both for the Yuzhno-Sakhalinsk and Shintotsukawa stations. For the horizontal component, (Fig. 8a and b) there is a significant decrease in velocity in the lithosphere plate after the earthquake, similar to the results of Carlson and Langer (1989).

Conclusions

The major portion of the scientific program of a comprehensive experiment carried out in a pilot project is mostly completed. Information describing the atmosphere and ionosphere state was collected and analyzed. The anomalies of the parameters characterizing the LAI system were revealed, confirming the LAIC model represented in Pulinets and Boyarchuk (2004), Pulinets *et al.* (2006a) and Pulinets (2007). It is necessary to note that there was a time coherency in the appearance of all anomalies registered during the week from July 24 to 31 before the earthquake took place on August 2.

From gathered information and from the analysis of retrospective earthquake supplementary data, it can be concluded that the morphology of the registered variations of atmosphere and ionosphere parameters before the earthquake of August 2007 on Sakhalin Island completely corresponds to the indications that were revealed before for strong earthquakes around the world. Nevertheless, the successful realization of the experiment only expresses the necessity to intensify international efforts in the framework of the current research. Because of the transboundary nature of the phenomena being studied – the signatures of the earthquake precursors in different media measured on the territory of just one country (Russia or Japan), cannot provide the whole picture, but must be a collaborative effort between the two countries. In the case of Russian tomography chain prolongation to the Japanese territory (Mombetsu and Obihiro cities), the accuracy of the vertical distribution of the ionosphere electron concentration reconstruction will significantly increase due to the amount of data sources increasing. Thus, at the same time, the reliability of ionosphere earthquake precursor diagnostics will increase.

Acknowledgement

The research is carried out under the financial support of Russian Fund of Fundamental Researches, grant #08-07-12014-ofi.

References

Carlson, J.M. and Langer, J.S. 1989. Properties of earthquake generated by fault dynamics. *Phys. Rev. Lett.* **22**: 123–128.

Hegai, V.V., Kim, V.P. and Nikiforova, L.I. 1997. A possible generation mechanism of acoustic-gravity waves in the ionosphere before strong earthquakes. *J. Earthquake Predict. Res.* **6**: 584–589.

Kunitsyn, V.E. and Tereshchenko, E.D. 2001. Ionosphere Tomography. Springer, Berlin.

Ouzounov, D., Liu, D., Chunli, K., Cervone, G., Kafatos, M. and Taylor, P. 2007. Outgoing long wave radiation variability from IR satellite data prior to major earthquakes. *Tectonophysics* **431**: 211–220.

Pulinets, S.A. 2007. Natural radioactivity, earthquakes and the ionosphere. *Eos* **88**: 217–218.

Pulinets, S.A. and Boyarchuk, K.A. 2004. Ionospheric Precursors of Earthquakes. Springer, Berlin.

Pulinets, S.A. and Dunajecka, M.A. 2007. Specific variations of air temperature and relative humidity around the time of Michoacan earthquake M8.1 Sept. 19, 1985 as a possible indicator of interaction between tectonic plates. *Tectonophysics* **431**: 221–230.

Pulinets, S.A., Kotsarenko, A.N., Ciraolo, L. and Pulinets, I.A. 2007. Special case of ionospheric day-to-day variability associated with earthquake preparation. *Adv. Space Res.* **39**: 970–977.

Pulinets, S.A., Ouzounov, D., Karelin, A.V., Boyarchuk, K.A. and Pokhmelnykh, L.A. 2006a. The physical nature of the thermal anomalies observed before strong earthquakes. *Physics Chem. Earth* **31**: 143–153.

Pulinets, S.A., Ouzounov, D., Ciraolo, L., Singh, R., Cervone, G., Leyva, A., Dunajecka, M., Karelin, A.V., Boyarchuk, K.A. and Kotsarenko, A. 2006b. Thermal, atmospheric and ionospheric anomalies around the time of the Colima M7.8 earthquake of 21 January 2003. *Ann. Geophys*. **24**: 835–849.

An adaptive spectroellipsometric technology for ccological monitoring of sea water

Ferdenant A. Mkrtchyan, Vladimir F. Krapivin, Vitaly I. Kovalev and Vladimir V. Klimov

Institute of Radio Engineering and Electronics, Russian Academy of Sciences, Moscow, Russia
E-mail: ferd@ms.ire.rssi.ru, ferd47@mail.ru

Abstract

Spectroellipsometry is the peak of polarization optics. The creation of multichannel polarization optical instrumentation and use of spectroellipsometric technology are very important for the real-time ecological monitoring of the aquatic environment. Spectroellipsometric devices give us high precision of measurements. Spectroellipsometric and their multichannel measurements in an aquatic environment provide the basis for the application of modern algorithms for the recognition and identification of pollutants (Klimov *et al.*, 2002). New original elements (coaxial polarization switchers and achromatic compensators), developed at the Institute of Radio Engineering and Electronics of the Russian Academy of Sciences, allow the design of inexpensive polarization systems, such as spectroscopic ellipsometers, polarization spectrometers, polarimeters, dichrometers, polarization microscopes and interferometers, sensitive photometers, and differential reflectometers without expensive standard polarization elements.

Introduction

The creation of multichannel polarization optical instrumentation and the use of spectroellipsometric technology are very important for the real-time ecological monitoring of aquatic environment. The ability to handle multiparametric problems in monitoring efficiently greatly depends on the precision and simplicity of ellipsometric devices.

This report aims to describe:

- A technology that combines the use of spectroellipsometry and algorithms of identification and recognition which allows the creation of a standard integral complex of instrumental, algorithmic, modular and software tools for the collection and processing of data on aquatic environment quality, and has forecasting and decision-making functions;
- A compact measuring–information multichannel spectroellipsometric system for monitoring the quality of the aquatic environment that is based on the combined use of spectroellipsometry and training, classification, and identification of algorithms.

This spectroellipsometric system will differ from modern foreign analogues by the use of a new and very promising method of ellipsometric measurements, an original element base of polarization optics and a complex mathematical approach to estimating the quality of a water body subjected to anthropogenic influence.

Unlike foreign analogues, the system has no rotating polarization elements. This allows one to increase the signal-to-noise ratio and the long-term stability of measurements to simplify and reduce the price of multichannel spectroellipsometers. The system will be trained to recognize pollutants in the aquatic environment.

Methodology

Methodology consists of:

- A new approach in ellipsometry, based on binary polarization modulation,
- New low cost-effective polarization elements,
- No rotating polarization elements,
- Excellent signal-to-noise ratio and the long-term stability of measurements that makes it possible to simplify and reduce the price of multichannel spectroellipsometers,
- One of the key elements of the systems being a polarization switch which transforms unpolarized light from a source into highly linear polarized light with alternate (up to KHz or more) and orthogonal polarizations,
- Sets of silicon photodiodes with arbitrary access to them,

- Flexibility, simple design, low cost, high precision, long-term stability.

Specifications

a) Portable 128-channel spectroellipsometer:
   - Spectral range 280–600 nm,
   - Minimal measurement time 0.5 s,
   - Precision and stability to 0.01 and 0.02 degrees in Psi and Delta, respectively, and polarization rotation angle 0.001 degree,
   - Sources: miniature pulsed xenon lamp PX-2 with high resource and laser diode,
   - Micro-spot focus 300 μm with PX-2 and 30 μm with laser diode,
   - Acromatic compensator,
   - User-friendly software,
   - Weight of measuring device about 4 kg.

b) Compact 128-channel spectroellipsometer with halogen lamp:
   - Spectral ranges 380–740 nm and 650–930 nm,
   - Minimal measurement time 0.6 s,
   - Precision to 0.003 and 0.01 degrees in Psi and Delta, respectively, polarization rotation angle 0.001 degree,
   - Sources: halogen lamp KGM-9-70,
   - Long-term stability 0.01 degree,
   - Use of an acromatic compensator on the basis of Fresnel rhomb made of fused quartz that enhances the precision of measurements,
   - Weight of measuring device about 4 kg,
   - Polarization block 2 kg; analyzer block 2 kg.

This is the first time the combined use of real-time spectroellipsometry measurements and data processing methods have been realized in an Adaptive Identifier (Fig. 1).

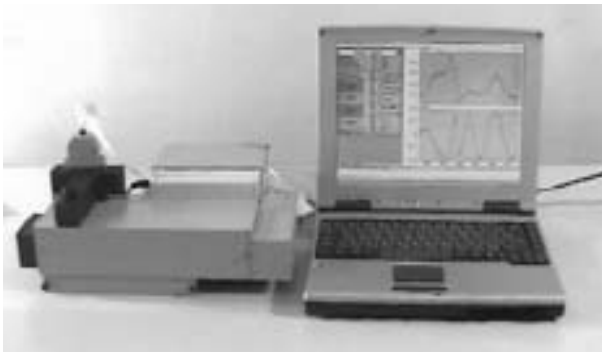

Fig. 1 High precision real-time multi-wavelengths spectroscopic ellipsometer with binary polarization modulation.

Adaptive Identifier device composition

- Polarizer block,
- Analyzer block,
- Power supply unit,
- Illuminator,
- Fiber-optic cable,
- Notebook with interface unit,
- Wide-band filters.

The algorithmic support of the Adaptive Identifier is based on a complex application of recognition and classification algorithms using 128 spectra images registered during a fixed period of time (Mkrtchyan *et al.*, 2004; Mkrtchyan *et al.*, 2005).

A time interval of 1 second is usually established and provides about 30 values of brightness for each of the 128 optical channels. The spectra obtained are sources for a set of statistical parameters and different characteristics united into vector spaces to be used for comparison with the standard samples of common pollutants stored on the computer.

The technology of this comparison depends on the diversity of identification methods. The system is trained to recognize the pollutants of an aquatic environment.

The Adaptive Identifier is designed to learn from the measurements of spectral characteristics and the simultaneous independent measurement of chemical element contents in the aquatic environment. As a result, a standard data bank is created in the knowledge base so that identifications and comparisons can be made. The software of the Adaptive Identifier provides different algorithms for the solution for identification problems, and cluster analysis is among of them.

Using spectroellipsometric technology:

1. Measurements of natural and waste water quality may be performed using:
   a) A **transmission scheme** when quality of the sample is measured by inserting the fused quartz cuvette containing analyzed water into the spectroellipsometer device.
   b) A **reflection scheme** when the quality of water is measured by inserting the spectro-ellipsometer sensor into water media being examined.
2. Because of the high accuracy of measurements with the spectroellipsometer, it is not possible to

use a whole method potential for remote measurements of natural and waste water quality. (Even small waves, ripples, foam can influence the quality of measurements.)

Results

The Adaptive Identifier can be used in different fields where the quality of water should be estimated or the presence of a particular set of chemical elements should be revealed. The Adaptive Identifier solves these problems by real-time monitoring of the aquatic environment. In the stationary version it allows the tracking of the dynamics of water quality in a stream, and when placed on a ship, it allows the measurement of water parameters along the route.

The functionality of the Adaptive Identifier can be extended by increasing the volume of standards in the knowledge base. The use of a natural light source allows the examination of soils, the indication of oil products on a water surface, the determination of the degree of pollution in the atmosphere and the estimation of the conditions of other elements in the environment whose spectral images may change.

An adaptive spectroellipsometric technology may be applied to the following areas for:

- Estimation of natural and wastewater quality,
- Analysis of liquids in medicine, biochemistry, food industry,
- Measurement of the mineralization level and chemical pollution of reservoirs, depending on the pollution type,
- Estimation of water salinity variations,
- Ellipsometrically based biosensor and gas sensor systems,
- Testing organic pollution clots in the water environment.

Experience

The Adaptive Identifier was tested under expeditionary conditions on board the R/V *Dmitry Mendeleev* in the Japan Sea, in the central areas of the Pacific Ocean, and during the investigation of aqueous systems of South Vietnam and Siberia (Lake Baikal, Angara and Yenisey rivers) within the framework of Russian–American and Russian–Vietnamese ecological expeditions.

A Russian–Vietnamese scientific and engineering laboratory has been built to create a standards base and to prepare the Adaptive Identifier for full-scale production.

Conclusions

The main objective of this work is to create compact information systems for monitoring the quality of the aquatic environment and to investigate their potential efficiency. These systems are based on the combined application of methods of the spectroellipsometry, and algorithms of training, classification, and identification. The realization of this objective will require the combined use of engineering and the algorithmic tools providing real-time measurements and data processing.

The technology, using a combination of spectroellipsometry and the algorithms of detection and classification will allow the creation of an original system of instrumental, algorithmic, modular and software tools for the collection and processing of data on the aquatic environment, and has forecasting and decision-making functions.

The **theoretical part** of the work will include the use of methods of polarization optics, mathematical statistics, the theory of pattern recognition and mathematical modeling for:

- Creation of a new element base for polarization optics with simple and efficient switches of the polarization state (SPS) that will successfully substitute for the conventional expensive polarizer–modulators of polarization state with rotating polarization elements;
- Optimization of the ellipsometric method regarding the change of amplitudes and phases of mutually orthogonal components of electro-magnetic radiation used to measure the thickness of thin films on a water surface, and the determination of sensitivity and precision limits of adaptive spectroellipsometers in different operating regimes;
- Creation of methods for investigating the water surface, and the determination of statistical characteristics of “spottiness” as informative signs for solving detection, classification and identification problems;
- Elaboration and optimization of algorithms for the detection, classification and identification of the characteristics of the aquatic environment for adaptive spectroellipsometers;
- Creation of a bank of standards used for the measurement of pollution levels in the aquatic

environment to be employed for training the adaptive spectroellipsometer.

The **experimental part** of the work described in report will include a description of the laboratory and on-site measurements of absorption, scattering, and reflection of electromagnetic waves from different aquatic objects.

The results given in this paper illustrate how the combined use of spectroellipsometric measurements and recognition algorithms give a possibility to economize material resources. It is obvious that the strategy of the modeling technology is in the interplay of model calculations and on-site experiments.

References

Klimov, V.V., Kovalev, V.I., Krapivin, V.F., Mkrtchyan, F.A. 2002. New informational technologies for problems of ecological monitoring of the aquatic environment. pp. 29–32 *in* Fifth International Symposium on Ecoinformatics Problems, Moscow, December 3–5, 2002.

Mkrtchyan, F.A., Krapivin, V.F., Kovalev, V.I., Klimov, V.V., Rukovishnikov, A.I., Golovachev, S.P. 2004. An adaptive spectroellipsometric technology for the ecological monitoring of the aquatic environment. pp. 7–13 *in* 25th Asian Conference on Remote Sensing, Chiang-Mai, Thailand, November 24–28, 2004.

Mkrtchyan, F.A., Krapivin, V.F., Kovalev, V.I., Klimov, V.V., Rukovishnikov, A.I. and Golovachev, S.P. 2005. An adaptive spectroellipsometric technology for the precise real-time monitoring of the quality of natural and waste waters. p. 87 *in* 10th International Symposium on Microwave and Optical Technology (ISMOT-2005), Fukuoka, Japan, August 22–25, 2005.

Remote sensing radiometry technology for the Okhotsk Sea ecosystem biocomplexity assessment

Vladimir F. Krapivin and Ferdenant A. Mkrtchyan

Institute of Radio Engineering and Electronics, Russian Academy of Sciences, Moscow, Russia
E-mail: ferd@ms.ire.rssi.ru, ferd47@mail.ru

Abstract

Biocomplexity of the Okhotsk Sea ecosystem (OSE) and its synthesis using a simulation model of the OSE, allowing us to assess conditions in the ecosystem, depending on global and regional changes in an environment, poses a difficult problem. By using this model it may be possible to establish some laws of dynamics of a trophic pyramid of the sea, and also to understand the mechanisms regulating the community of the sea due to external influences. This paper is oriented to the development of biocomplexity indices based on remotely measured environmental characteristics. Microwave radiometry is used as an effective technique to assess sea water parameters. Other ranges help to provide input information for the Okhotsk Sea Biocomplexity Model that will be developed in the framework of this work.

Introduction

Biocomplexity refers to phenomena that result from dynamic interactions between the physical, biological and social components of the *Nature/ Society System* (NSS). The investigations of the processes of interaction between the *Society* and *Biosphere* are, as a rule, targeted at understanding and estimating the consequences of such interactions. The reliability and precision of these estimations depend on criteria founded on conclusions, expertise and recommendations. At present, there is no unified methodology for selecting criteria due to the absence of a common science-based approach to the ecological standardization of anthropogenic impacts on the natural environment. After all, the precision of ecological expertise for the planning and functioning of anthropogenic systems, as well as the quality of the global geoinformation monitoring data, depend on these criteria.

The processes that have their origin in the environment can be presented as a combination of interactions between its subsystems. The human subsystem is a part of the environment and it is impossible to divide the environment into separate subsystems such as Biosphere and Society. The task is to search for methodologies to describe existing feedbacks between Nature and Humanity and to simulate reliably the dynamic tendencies in the NSS. Unfortunately, the part of the NSS that is responsible for the quality of modeling the climatic processes introduces instability in the modeling results. That is why it is supposed that the NSS climatic component is replaced by a scenario describing stable climatic trends during the time interval of investigation. What is actually studied is the NSS.

We introduce a scale of biocomplexity ranging from the state where all interactions between the environmental subsystems are broken down to the state level where they correspond to natural evolution. In this case, we have an integrated indicator of the environmental state including bioavailability, biodiversity and survivability. It reflects the level of all types of interactions among the environmental subsystems. In reality, specific conditions exist where these interactions are changed and transformed. For example, under the biological interaction of the *consumer/producer* or *competition-for-energy-resources* type there exists some minimal level of food concentration where contacts between interacting components cease. In the common case, physical, chemical and other types of interactions in the environment depend upon specific critical parameters. Environmental dynamics is regulated by these parameters and the main task is in the parametrical description of it. Biocomplexity reflects these dynamics.

Biocomplexity Model

The NSS consists of subsystems $B_i (i = 1,\ldots, m)$, the interactions of which are formed during time as functions of many factors. The NSS biocomplexity reflects the structural and dynamic complexity of its components. In other words, the NSS biocomplexiry is formed under the interaction of its subsystems $\{B_i\}$. In due course the subsystems B_i can change their state and, consequently, change the topology of the relations between them. The evolutionary mechanism of adaptation of the subsystem B_i to the environment allows the hypothesis that each subsystem B_I, independent from its type, has the structure $B_{i,S}$, behaviour $B_{i,B}$ and goal $B_{i,G}$, so that $B_i = \{B_{i,S}, B_{i,B}, B_{i,G}\}$. The strivings of subsystem B_i to achieve certain preferable conditions are represented by its goal $\hat{A}_{i,G}$. The expedience of the structure $B_{i,S}$ and the purposefulness of the behaviour $B_{i,B}$ for subsystem B_i are estimated by the effectiveness with which the goal $B_{i,G}$ is achieved.

As an example, we consider the process of fish migration. The investigations of many authors revealed that this process is accompanied by an external appearance of purposeful behaviour. From these investigations it follows that fish migrations are subbordinated to the principle of complex maximization of effective nutritive ration, given the preservation of favourable environmental conditions (temperature, salinity, dissolved oxygen, pollution level, depth). In other words, the travel of migrating species takes place at characteristic velocities in the direction of the maximum gradient of effective food, given adherence to ecological restrictions. That is why we can formulate that the goal $B_{i,G}$ of the fish subsystem is toward the increase of their ration, and the behaviour $B_{i,B}$ consists in the definition of the moving trajectory securing the attainability of the goal $B_{i,G}$.

Since the interactions of the subsystems B_i (i = 1, …, m) are connected with chemical and energetic cycles, it is natural to suppose that each subsystem B_i realizes the geochemical and geophysical transformation of matter and energy to remain in a stable state. The formalism of approach to this process consists in the supposition that the interactions between the NSS subsystems are represented as a process whereby the systems exchange a certain quantity V of resources spent in exchange for a certain quantity W of resources consumed. We represent this process by the name (V,W)-exchange.

The goal of the subsystem is the most advantageous (V,W)-exchange, *i.e.*, it tries to get maximum W in exchange for minimum V. The quantity W is a complex function of the structure and behaviour of interacting subsystems, $W = W(V,B_i,\{B_k,\ k\in K\})$, where K is the space of subsystem numbers interacting with the subsystem B_i .

We designate $B_K = \{B_k, k \in K\}$. Then the following (V,W)-exchange is the result of interactions between the subsystem B_i and its environment B_K:

$$W_{i,0} = \max_{B_{ii}} \min_{B_K} W_i\left(V_i, B_{i,opt}, B_{K,opt}\right);$$

$$W_{K,0} = \max_{B_K} \min_{B_i} W_k\left(V_K, B_{i,opt}, B_{K,opt}\right).$$

Figure 1 represents a block-scheme for the global model of the NSS (GMNSS). The synthesis of the GMNSS is based on its consideration as a self-organizing and self-structuring system, in which the elements are coordinated in time and space by the process of natural evolution. The anthropogenic constituent in this process breaks this integrity. Attempts to parameterize, on a formal level, the process of co-evolution of nature and humans, as elements of the biosphere, are connected with the search of a single description of all processes in the NSS, which would combine all spheres of knowledge in perceiving the laws of the environment. Such a synergetic approach forms the basis of numerous studies in the field of global modeling (Kondratyev *et al.*, 2002; Kondratyev *et al.*, 2004).

All of this corroborates the fact that biocomplexity is related to categories which are difficult to measure empirically and to express by quantitative values. However, we will try to transfer the truly verbal tautological reasoning to formalized quantitative definitions. For the transition to gradations of the scale Ξ with quantitative positions it is necessary to postulate that relationships between two values of Ξ are of the type $\Xi_1 < \Xi_2$, $\Xi_1 > \Xi_2$ or $\Xi_1 \equiv \Xi_2$. In other words, there always exists a value of the scale ρ that defines a biocomplexity level $\Xi \rightarrow \rho = f(\Xi)$, where f is a certain transformation of the bio-complexity concept to a number. Let us attempt to search for a satisfactory model with which to reflect the verbal

biocomplexity image onto the field of conceptions and signs, subordinating to the formal description and transformation. With this purpose *m* subsystems of the NSS are selected. The correlations between these subsystems are defined by the binary matrix function: $X = ||\, x_{ij} \,||$, where $x_{ij} = 0$, if subsystems B_i and B_j do not interact and $x_{ij} = 1$, if subsystems B_i and B_j are interacting. Then any one point $\xi \in \Xi$ is defined as the sum

$$\xi = \sum_{i=1}^{m} \sum_{j>i}^{m} x_{ij}.$$

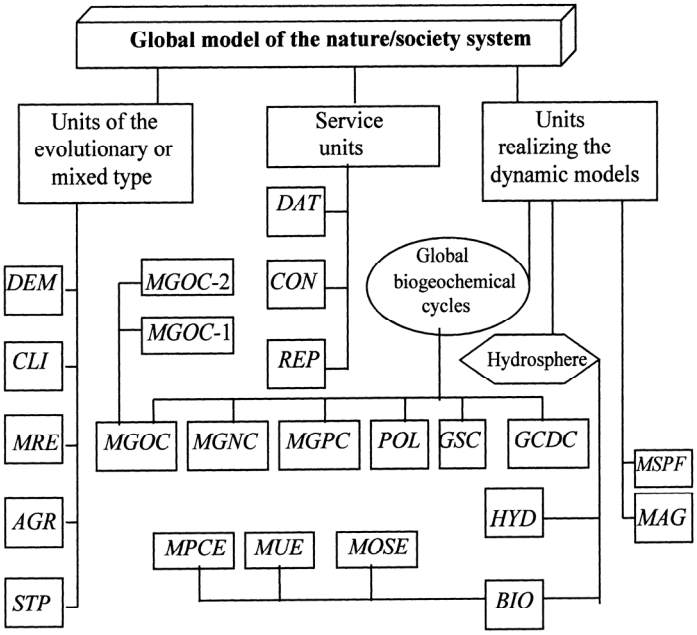

Fig. 1 Structure and items of the GMNSS. List of items is given in Table 1.

Table 1 A description of the items used in Figure 1.

Item	Item description
DEM	A set of demographic models that parameterize the population dynamics with the consideration of age structure
CLI	A set of climate models with various spatial resolutions
MRE	Model for the control of mineral resources
AGR	Model of agriculture production
STP	Model of science-technical progress
DAT	Controlling procedure of interface between the MGNSS items and database
REP	Reporting and visualization procedure
GSC	Model of global sulphur cycle
POL	A set of models parameterizing the pollutant kinetics within different medias
BIO	A set of models parameterizing the aquatic ecosystems in different climatic zones
HYD	Model of global hydrodynamic processes and the biosphere water balance
MAG	Model of the magnetosphere processes related to the global biogeochemical cycles
MUE	Typical model of the upwelling ecosystem of the World Ocean
MOSE	Model of the Okhotsk Sea Ecosystem

Certainly there arises the need to overcome uncertainty for which it is necessary to complicate the scale Ξ, for example, to introduce weight coefficients for all NSS subsystems. The origin of these coefficients depends on the type of subsystem. That is why three basic subsystem types are selected: living and nonliving subsystems and vegetation. Living subsystems are characterized by their density, estimated by numbers of elements or by biomass value per unit area or volume. Vegetation is characterized by the type and portion of occupied territory. Nonliving subsystems are measured by their concentration per unit square or volume of the environment. In the common case, certain characteristics $\{k_i\}$, corresponding to the significance of the subsystems $\{B_i\}$, are assigned to every subsystem B_i (i = 1,..., m). As a result, we obtain more closely the definition of the formula to move from the biocomplexity concept to the scale Ξ of its indicator:

$$\xi = \sum_{i=1}^{m} \sum_{j>i}^{m} k_j x_{ij}.$$

It is clear that $\xi = \xi(\varphi,\lambda,t)$, where φ and λ are geographical latitude and longitude, respectively, and t is the current time. For the territory Ω, the biocomplexity indicator is defined as mean value

$$\xi_\Omega(t) = (1/\sigma) \int_{(\varphi,\lambda)\in\Omega} \xi(\varphi,\lambda,t)\, d\varphi\, d\lambda,$$

where σ is the area of Ω. Thus the indicator $\xi_\Omega(t)$ is the integrated NSS complexity characterization reflecting the individuality of its structure and the behaviour at each time t in the space Ω. According to natural evolution laws, a decrease (increase) in ξ_Ω will correspond to an increase (decrease) of biocomplexity and the survivability of the nature–anthropogenic systems. Since a decrease of biocomplexity disturbs the exclusiveness of the biogeochemical cycles and leads to a decrease in stress on nonrenewable resources, then the binary structure of the matrix X is changed in the direction to intensify the resource-improverishment technologies.

Biocomplexity of the Okhotsk Sea

A trophical pyramid of the Okhotsk Sea ecosystem is described by the matrix $X = \|x_{i\,j}\|$, where $x_{i\,j}$ is a binary value equal to «1» or «0» under the existence or absence of the nutritive correlation between the ith and jth components, respectively. Biocomplexity is defined as

$$\xi(\varphi,\lambda, z, t) = \sum_{i=1}^{20} \sum_{j=1}^{19} x_{i\,j} C_{i\,j};$$

$$x_{ij} = \begin{cases} 1, \text{ if } B_m \geq B_{m,\min}; \\ 0, \text{ if } B_m < B_{m,\min}; \end{cases}$$

where φ and λ are geographical latitude and longitude, t is current time, z is the depth, $B_{m,\min}$ is the minimal biomass of the mth component consumed by other trophic levels, $C_{i\,j} = k_{j\,i} B_{i,*} / \Sigma_{j+}$ is the nutritive pressure of the jth component upon the ith component, $\Sigma_{i+} = \sum_{m\in S_i} k_{im} B_m$ is real food storage which is available to the ith component, $B_{m,*} = \max\{0, B_m - B_{m,\min}\}$, $k_{i\,m} = k_{i\,m}(t, T_W, S_W)$ (i = 1, …, 17) is the index of the satisfaction of nutritive requirements of the ith component at the expense of the mth component of biomass; $k_{i\,m}$ (i = 18,19) is the transformation coefficient from the mth component to the ith component, k_{i20} is the characteristic of anthropogenic influence on the ith component; $S_i = \{i : x_{i\,j} = 1\ j = 1, \ldots, 19\}$ is the food spectrum of the ith component, T_W is water temperature, and S_W is water salinity.

A maximal value of $\xi = \xi_{\max}$ (≈ 20) is reached during spring–summer time when nutritive relations into the Okhotsk Sea ecosystem are extended, the intensity of energetic exchanges is increased, horizontal and vertical migration processes are stimulated. In the wintertime, the value of ξ is changed near $\xi_{\min}$ (≈ 8). The spatial distribution of ξ reflects a local variability of the food spectrum for the components. Calculations show that basic variability into the $\xi^* = \xi/\xi_{\max}$ is caused by migration processes. Under these processes the quick redistribution of the interior structure of matrices X and $\|C_{ij}\|$ occurred. Many fishes migrate to the shelf zone during springtime, and during winter they move to the central aquatories of the Okhotsk Sea. Therefore, $\xi^* \to 1$ during spring and $\xi^* \to 0.6$ during winter for the shelf zone. This means that the biocomplexity of the Okhotsk Sea ecosystem on the shelf decreases by 40% in winter in comparison with spring. For the central aquatories, ξ^* is changed to near 0.7 during the year. Such stability of a biocomplexity indicator is explained by the balance between nutritive correlations and productivity during spring, summer and winter.

It can be to establish that variability in ξ^* reflects the changes of fish congestions which are controlled by environmental conditions. Specifically, during springtime. Pacific herring *Clupea pallasi escapes* occupy the area with $T_W < 5$°C. Other fishes choose different depths for their feeding and spawning. All these processes have an influence on the variability of ξ^*. A more detailed investigation of correlations between ξ^* and the structural and behavioral dynamics of the Okhotsk Sea ecosystem demand additional studies.

Spatial distribution of the biocomplexity indicator in the Okhotsk Sea in the spring and summer period, designed by a technique described in the previous section is shown Figure 2. It reflects the level of complexity of the sea ecosystem. The basic variability in ξ is caused by the migration process.

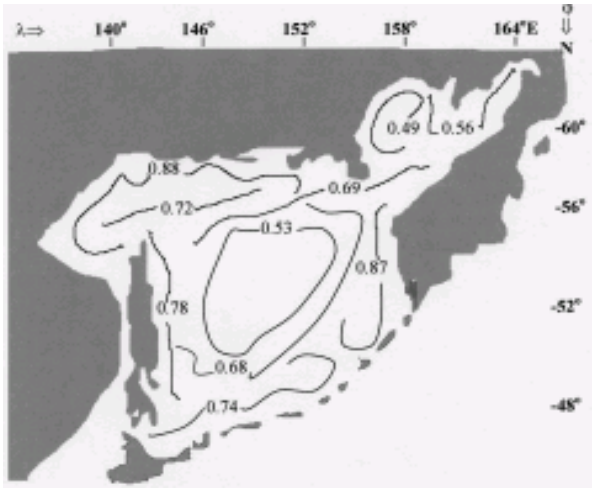

Fig. 2 Spatial distribution of the biocomplexity indicator in the Okhotsk See during spring and summer.

Conclusion

Biocomplexity is clearly an important characteristic of the NSS dynamics. It has importance for the complex study of interactions between living and non-living elements of environment and, more significantly, it can be used to make valuable contributions to the understanding and solution of key socio-economic and environmental problems. It is reasonable to expect that over the near future the biocompexity will be able to be used as an indicator analogous to such indicators as the normalized difference vegetation index (NDVI) and leaf area index (LAI) (Krapivin *et al.*, 2006). It appears that the only satisfactory way to develop an appropriate definition of a biocomplexity indicator is to summarize the many structural ideas of a series of global biospheric models. The synthesis of these models requires not only their compatibility with global databases, but also the interconnections between different sources of data.

The Okhotsk Sea ecosystem maintains a significant position in the global natural system. At the present time it has a low level of pollution, with fishing being the main anthropogenic influence. A correlation between the OSE state and global changes is one of problems which is discussed both in the framework of regional investigations and in global studies of the environment. The OSE interacts with biosphere processes via the influence of the global climate, and on the Pacific Ocean. This influence is reciprocal.

This paper proposes a global model and biocomplexity indicator for only one category in which biospheric processes are considered to predominate. Further study will be oriented to the expansion of information, taking into account the global model, and it will be necessary to correlate the dependencies between socio-economic and biospheric components.

References

Kondratyev, K.Ya., Krapivin, V.F. and Phillips, G.W. 2002. Global environnmental change: Modelling and Monitoring. Springer, Berlin.

Kondratyev, K.Ya., Krapivin, V.F., Savinikh, V.P. and Varotsos, C.A. 2004. Global Ecodynamics: A Multidimensional Analysis. Springer/PRAXIS, Chichester U.K.

Krapivin, V.F., Shutko, A.M., Chukhlantsev, A.A., Golovachev, S.P. and Phillips, G.W. 2006. GIMS-based method vegetation microwave monitoring. *Environ. Model. Software* **21**: 330–345.

The use of airplane-lidar for registration of fish schools and plankton

Vladimir Chernook[1], Yurij Goldin[2], Alexander Lisovski[1] and Alexander Vasilev[1]

[1] Research Institute for Fishing Fleet "GIPRORYBFLOT", St. Petersburg, Russia. E-mail: chernook@grf.spb.ru
[2] P.P. Shirshov Institute of Oceanology RAS, Moscow, Russia

Abstract

The main advantage of the remote sensing lidar method is the potential to acquire data from oceanic subsurface layers, including the recording of phytoplankton and zooplankton layers, pelagic fish schools and transparency of water. The maximum depth for registering fish schools and plankton by airplane-lidar is equal to 30–40 m for the Barents Sea and Sea of Okhotsk.

The development of identification methods for recording schools of organisms (pelagic fishes, medusae, phytoplankton, zooplankton) is the main task in the practical use of airborne lidar surveys. The analysis of lidar data shows that each organism object has a specific combination of parameters and types of correlation with each other. So, a system of signatures for object identification is being designed.

A set of criteria is developing in several directions:

- The analysis of full-scale research results applying aerial and vessel lidars supplied with the data from accompanying observations;
- the conducting of full-scale nature and laboratory experiments with certain objects, first with fish and plankton to determine their characteristics of reflection, scattering and depolarization of light;
- The development of specific software for the visualization of laser sounding data and calculation of light scattering layer parameters and single signals.

The algorithms for efficient object identification in real-time surveying of the marine area are under development.

Session B1

Biological processes/Disturbances by oil and gas development

Session Chairs

Atsushi Yamaguchi and Vyacheslav S. Labay

Spatial distribution of the toxic dinoflagellate, *Alexandrium tamarense*, in summer in the Okhotsk Sea off Hokkaido, Japan

Hiroshi Shimada[1], Mayumi Sawada[1], Takanori Kuribayashi[1], Akifumi Nakata[1], Akira Miyazono[1] and Hiroki Asami[2]

[1] Hokkaido Central Fisheries Experiment Station, Yoichi, Hokkaido, Japan
E-mail: shimadah@fishexp.pref.hokkaido.jp
[2] Hokkaido Wakkanai Fisheries Experiment Station, Wakkanai, Hokkaido, Japan

Abstract

Spatial distributions of the toxic dinoflagellate, *Alexandrium tamarense*, were examined in the Okhotsk Sea off Hokkaido in summer to clarify the relationship between its distribution and water mass structure. Surveys were conducted at 37 stations in late July in 2002–2007. Water samples for cell counts of *A. tamarense* were collected from each layer of 0, 10, 20, 30 and 40 m depth at each station. Nutrient concentrations of each water sample in 2004–2007 were analyzed. Results show that *A. tamarense* appeared every year although its abundance fluctuated year by year, and it rarely appeared in 2005. A high abundance of *A. tamarense* tended to be found frequently in the oceanic area of surface low-salinity water (LSW, salinity $\leqq$ 32.5) and in mixed water (MW) among the water masses, while a low abundance was found along the coastal area of the Soya Warm Current (SWC, salinity $\geqq$ 33.6) and in the dichothermal water (DTW, water temperature $\leqq$ 2°C) layer depth > 30 m. PO_4-P concentrations in each water mass were in the order DTW > LSW > SWC. The lowest PO_4-P concentration in the SWC might be limiting factor for growth of *A. tamarense*. On the other hand, the reason for low *A. tamarense* abundance in the DTW might be due to the low water temperature. The results suggest that the LSW is the optimum water mass for growth of *A. tamarense*.

Introduction

Paralytic shellfish poisoning caused by the toxic dinoflagellate, *Alexandrium tamarense*, accounts for much economic damage to the scallop culturing fishery along the coast of Hokkaido in the Okhotsk Sea once every few years (Nishihama, 1994; Shimada and Miyazono, 2005). Prediction of the poisoning is very important for fishing and shipping plans for scallops.

The Okhotsk Sea off Hokkaido is known for its very characteristic oceanographic structures, such as sea ice in winter (Aota, 1975). The following four water masses generally distribute in the area in summer (Aota, 1975).

1. Soya Warm Current (SWC, salinity $\geqq$ 33.6): Warm current flowing along the coast of Hokkaido in the direction from Wakkanai to Abashiri, originating the Tsushima Warm Current;
2. Surface low-salinity water (LSW, water temperature > 2°C, salinity $\leqq$ 32.5): Low salinity water mass in the surface layer of the oceanic area;
3. Dichothermal water (DTW, water temperature $\leqq$ 2°C): Cold water mass under the LSW of the oceanic area;
4. Mixed water (MW): Water mass existing among the above, but not belonging to the above.

Nishihama (1994) reported that *A. tamarense* appeared in the surface waters of the oceanic area in July 1989 at the same stations as in the present study. However, the sampling was conducted only in the surface layer so that the spatial distribution of *A. tamarense* in the four water masses had not been revealed. The present study was carried out to clearly detail the relationship between spatial distribution and water mass structure and to get fundamental information for the prediction of shellfish poisoning.

Materials and Methods

A map of sampling stations and survey periods are shown in Figure 1 and Table 1, respectively. Water

samples were collected from each layer of 0, 10, 20, 30 and 40 m depth using Nansen bottles (1 liter) at each station. The 500-ml water samples were fixed with 2% formalin and concentrated to 1 ml by sedimentation for 6 h. The 0.1 ml subsamples stained with one drop of fluorescent brightener 28 (Sigma) saturated solution were used for cell counting of *A. tamarense* under an epi-fluorescence microscope (Nikon, XF-EFD2) with UV excitation. Water temperature and salinity were measured using CTD instruments (Seabird, SBE-911plus). The 230-ml surface water samples were filtered with Whatman GF/F. The filters were frozen at –20°C *in situ*, and chlorophyll-*a* concentrations were measured using a fluorometer (Turner Design, 10-AU) after 6 h extracting with 90% acetone in the laboratory. Nutrient concentrations (NO_3-N and PO_4-P) of all the 30-ml water samples in 2004–2007 were analyzed using an autoanalyzer (Bran + Luebee, Autoanalyzer II).

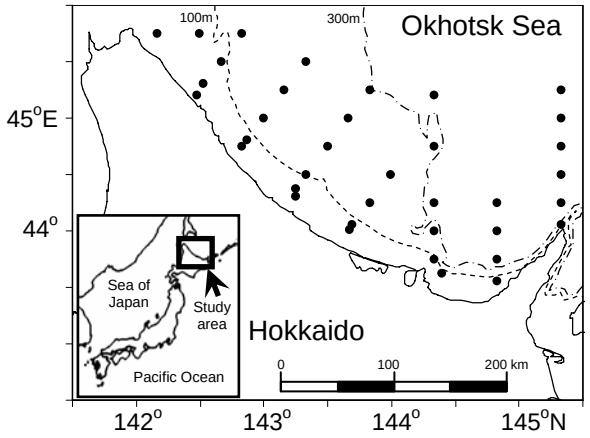

Fig. 1 Map showing 37 sampling stations in the Okhotsk Sea off Hokkaido.

Table 1 Periods of surveys, number of sampling stations and research vessels.

Period of survey	No. stations	Research vessel*
July 22–25, 2002	37	*Hokuyou Maru*, *Oyashio Maru*
July 24–26, 2003	37	*Oyashio Maru*
July 23–25, 2004	35	*Oyashio Maru*
July 21–23, 2005	37	*Oyashio Maru*
July 25–27, 2006	34	*Oyashio Maru*
July 25–27, 2007	35	*Oyashio Maru*

* *Hokuyou Maru*: 214 ton, R/V of Hokkaido Wakkanai Fisheries Experiment Station.
Oyashio Maru: 178 ton, R/V of Hokkaido Central Fisheries Experiment Station.

Results

The spatial distribution of water temperature, water masses, and cell density of *A. tamarense* are shown in Figures 2a and b. The SWC flowed along the coast of Hokkaido, the LSW was found in the surface shallower than 10 m deep, the DTW was observed in the layer lower than 30 m deep, and the MW was found among the water masses every year from 2002–2007. *Alexandrium tamarense* was widely found in the oceanic area outside the SWC, fluctuating annually both quantitatively and spatially although it was rarely found in 2005. Blooms of *A. tamarense* ($\geq 10^3$ cells l^{-1}) appeared near the front area outside the SWC in 2004 and 2006.

Cell density of *A. tamarense* superimposed on a temperature–salinity diagram is shown in Figure 3. Cell density of *A. tamarense* in each water mass is shown in Table 2 and water temperature and salinity in each range of *A. tamarense* cell density is shown in Table 3. Table 2 shows that the highest cell densities were found in the LSW followed by the MW. However, cell densities were low in the SWC and the DTW. As to the vertical distribution, *A.tamarense* was frequently found in the surface layer shallower than 20 m deep occupied by the LSW and the MW, but rarely found in the layer deeper than 30 m, occupied by the DTW (Fig. 2). Blooms of *A. tamarense* ($\geq 10^3$ cells l^{-1}) appeared at a water temperature of 5.9–14.4°C with a salinity of 31.9–32.5 (Table 3).

Nutrient concentrations in each water mass are shown in Table 4. Higher cell densities did not tend to be found in water with higher nutrients. Especially, the lowest densities were found in the DTW with highest nutrients, but lowest water temperature. On the other hand, in water of the lower nutrients, such as the LSW and the SWC, *A.tamarense* was frequently found in the LSW and rarely found in the SWC. Comparing nutrient concentrations of the LSW and the SWC, mean NO_3-N concentration was lower in the LSW, and mean PO_4-P concentration was lower in the SWC, respectively (t-test, $p < 0.01$).

Discussion

A schematic diagram of the spatial distribution of water masses and *A. tamarense* from the results of present study is shown in Figure 4. It is seen that *A. tamarense* appear frequently in the surface layer

of the LSW and the MW in the oceanic area while they rarely appear in the SWC along the coastal area and in the DTW under the LSW and the MW. The present study reveals the detailed spatial distribution of *A. tamarense* in all the water masses in addition to the report on the distribution only in the surface layer by Nishihama (1994). Studies have shown that the optimum water temperature for *A. tamarense* is 8–12°C (Nishihama, 1982) or 5–10°C (Shimada *et al.*, 1996) in Funka Bay, southern Hokkaido. In the present study the water temperature for *A. tamarense* blooms, 5.9–14.4°C, was almost same as that reported for Funka Bay.

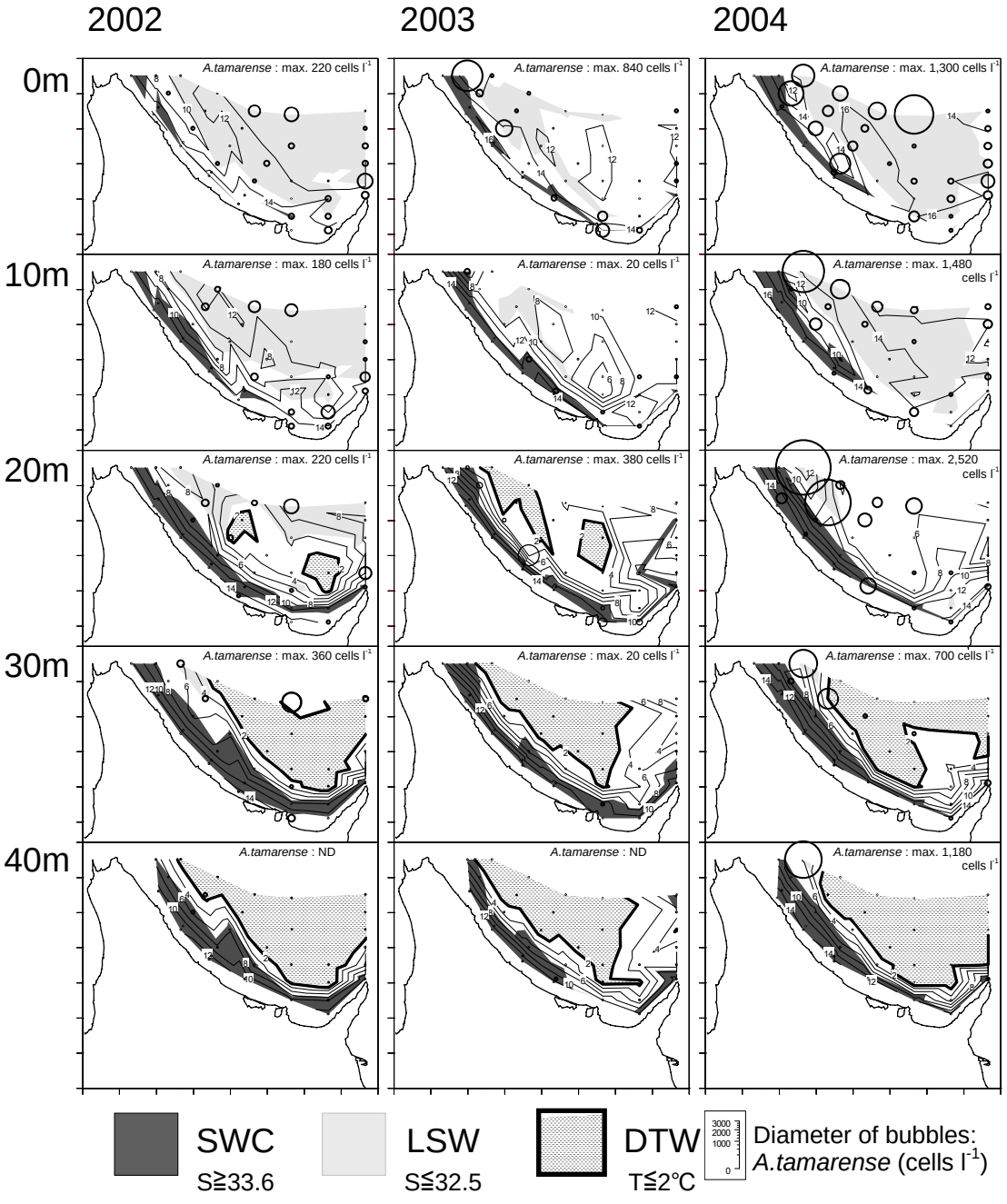

Fig. 2a Spatial distribution of water temperature (contour), water masses (screentone) and cell density of *A. tamarense* (bubbles) from 2002–2004. SWC = Soya Warm Current, LSW = Low Salinity Water, DTW = Dichothermal Water, ND = No detection.

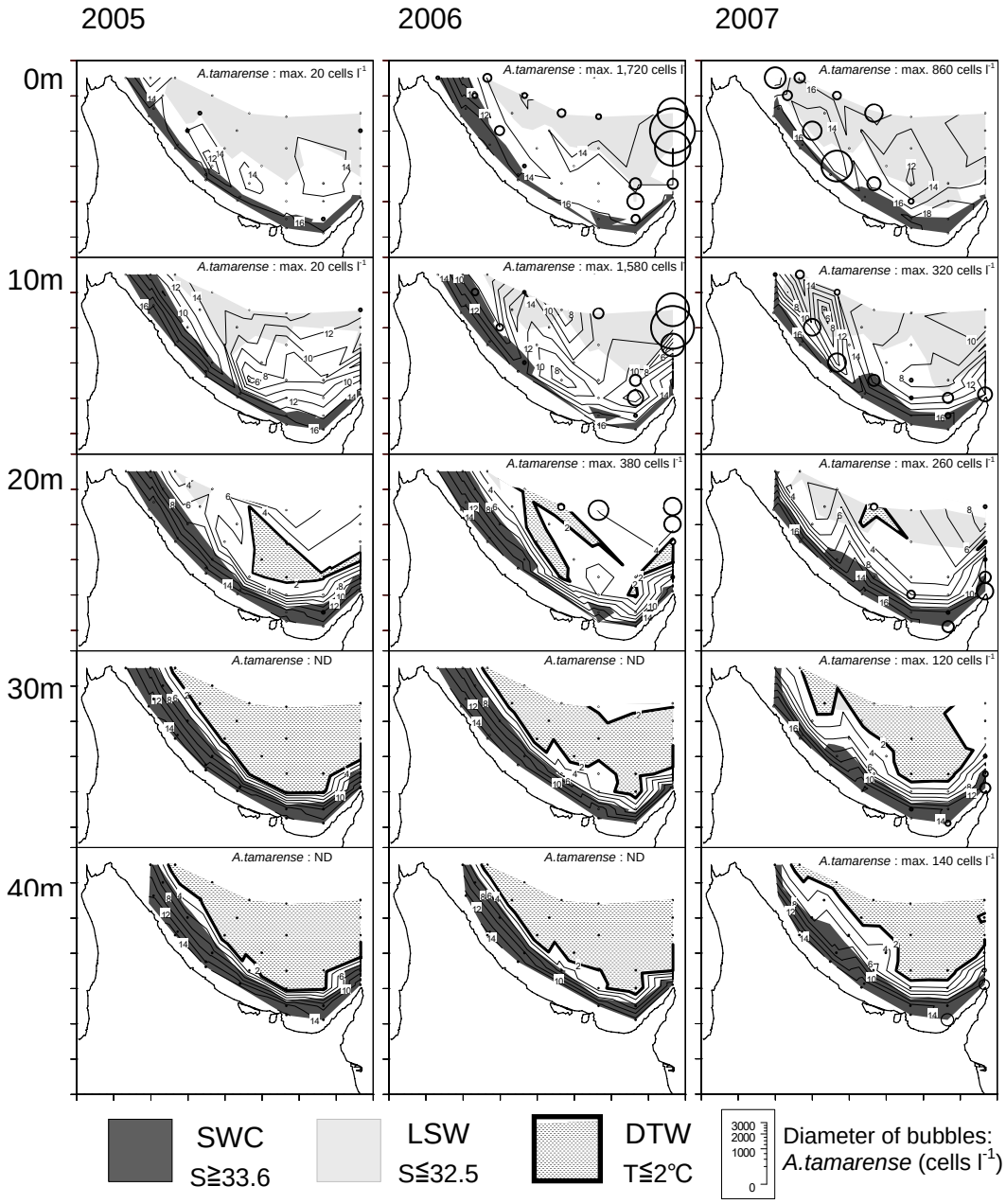

Fig. 2b Spatial distribution of water temperature (contour), water masses (screentone) and cell density of *A.tamarense* (bubbles) from 2005–2007. SWC = Soya Warm Current, LSW = Low Salinity Water, DTW = Dichothermal Water, ND = No detection.

Fukuyo (1982) noted that germinated cells of *A. tamarense* could not grow at low water temperatures less than 5°C. Tarutani (1999) and Yamamoto and Tarutani (1999) suggested that *A. tamarense* was difficult to increase to dominant species because of their larger half-saturation constant compared to that of dominant diatom species for PO_4-P uptake. Shinada (2005) suggested that PO_4-P concentration of the SWC was too low for growth of *A. tamarense*. From these reports, and the present study, it is suggested that *A. tamarense* cannot increase in the DTW having low water temperature and cannot increase in the SWC having low PO_4-P concentrations.

MacIntire *et al.* (1997) suggested that *A. tamarense* could sustain growth through nocturnal migrations to a nutrient-rich deeper layer for nitrogen uptake. In the present study, it is suggested that *A. tamarense* could increase in the LSW of low NO_3-N concentration through the nocturnal migrations to the MW mixed with the DTW for NO_3-N uptake. Ogata *et al.* (1996) reported that *A. tamarense* could increase through utilization of organic nitrogen. It is also supposed that *A. tamarense* might utilize organic nitrogen in the LSW in the present study.

Therefore, it can be concluded that LSW is the optimum water mass for growth of *A. tamarense*. Annual fluctuations of relative frequency of each water mass of samples on the same layers at common stations are shown in Figure 5. It can be found in the fluctuations that for the sum of the LSW and the MW, the frequency of preferable water for *A. tamarense* was lowest in 2005. The result suggests that the frequency, that is, the volume of each water mass is one of the important factors to control the abundance of *A. tamarense* in the area.

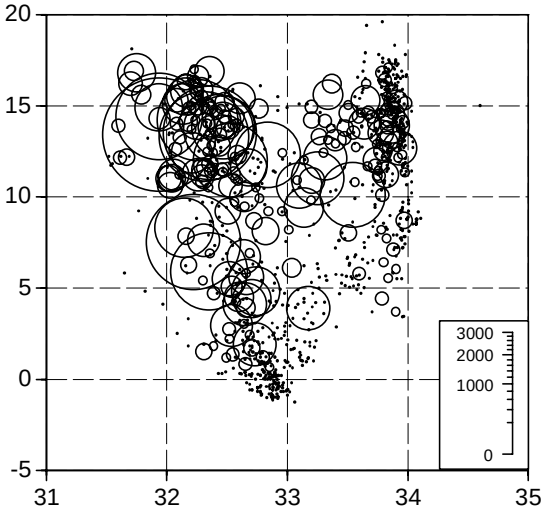

Fig. 3 Cell density of *A. tamarense* (bubbles) on a temperature–salinity diagram in 2002–2007.

Table 2 Cell density of *A. tamarense* in each water mass in 2002–2007.

Water mass	Number of samples	Cell density of *A. tamarense* (cells l^{-1}, mean ± SD)
SWC	312	7.4 ± 27.7
LSW	182	114.0 ± 342.1
MW	262	40.8 ± 127.5
DTW	183	3.7 ± 29.2

SWC = Soya Warm Current, LSW = Low Salinity Water, MW = Mixed Water, DTW = Dichothermal Water

Table 3 Water temperature and salinity in each range of *A. tamarense* cell density in 2002–2007.

Range of *A. tamarense* cell density (cells l^{-1})	Number of samples	Water temperature (°C, mean ± SD, [min – max])	Salinity (mean ± SD, [min – max])
0	730	8.1 ± 5.8 [–1.3 – 19.6]	33.2 ± 0.8 [31.5 – 34.1]
20–80	137	11.1 ± 4.3 [0.7 – 17.0]	32.9 ± 0.7 [31.6 – 34.0]
100–980	64	11.4 ± 3.9 [1.9 – 16.9]	32.7 ± 0.6 [31.7 – 33.9]
1000≤	8	11.8 ± 3.2 [5.9 – 14.4]	32.2 ± 0.2 [31.9 – 32.5]

Table 4 Nutrient concentrations in each water mass in 2004–2007.

		Nutrient concentration	
Water mass	Number of samples	NO_3-N (μM l^{-1}, mean ± SD)	PO_4-P (μM l^{-1}, mean ± SD)
SWC	225	1.52 ± 2.41	0.26 ± 0.22
LSW	120	0.21 ± 0.86	0.35 ± 0.15
MW	156	3.51 ± 4.55	0.59 ± 0.37
DTW	125	15.79 ± 4.53	1.55 ± 0.29

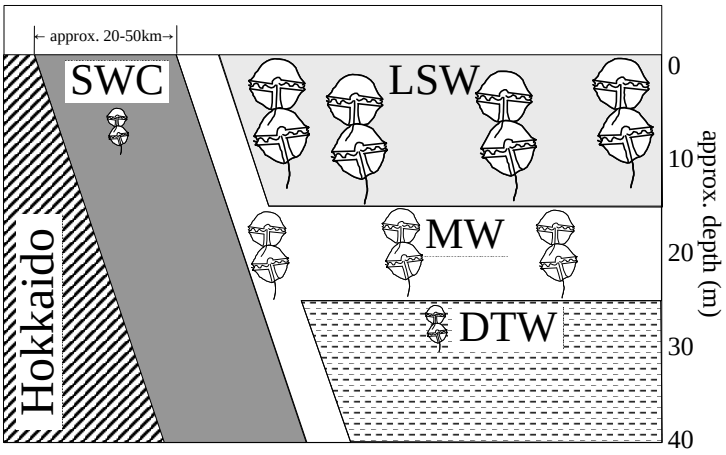

Fig. 4 Schematic diagram of spatial distribution of water masses and *A. tamarense* in vertical section.

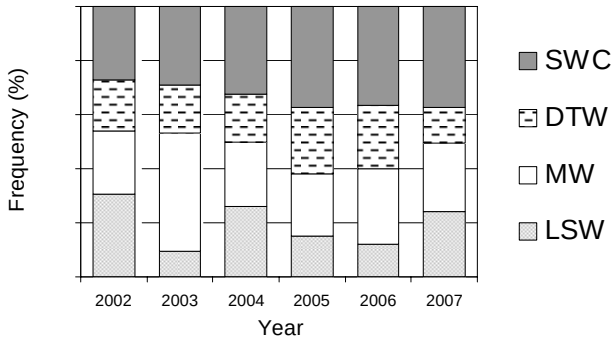

Fig. 5 Relative frequency of each water mass of samples on the same layers at 34 common stations in 2002–2007.

Acknowledgement

We are grateful to the captains and crews of R/Vs *Hokuyo Maru* and *Oyashio Maru* for kindly helping with sampling *in situ*. We also thank colleagues at the Hokkaido Fishery Experiment Station for helpful comments.

References

Aota, M. 1975. Studies on the Soya Warm Current. *Low Temp. Sci.* **A33**: 151–172 (in Japanese with English summary).

Fukuyo, Y. 1982. Taxonomical and ecological studies on *Protogonyaulax* occurring in Japanese coastal waters. Ph.D. thesis, University of Tokyo, Tokyo (in Japanese).

MacIntire, J.G., Cullen, J.J. and Cembella, A.D. 1997. Vertical migration, nutrition and toxicity in the dinoflagellate *Alexandrium tamarense*. *Mar. Ecol. Prog. Ser.* **148**: 201–216.

Nishihama, Y. 1982. Seasonal abundance of *Protogonyaulax* sp. causing paralytic shellfish poisoning in Funka Bay. pp. 319–327. *In* Proceedings of North Pacific Aquaculture Symposium, Anchorage, AK.

Nishihama, Y. 1994. Paralytic shellfish poisoning. *In* Scallop Fishery in the Okhotsk Sea Coast of Hokkaido. Hokkaido University Press, Sapporo, pp. 170–180 (in Japanese).

Ogata, T., Koike, K., Nomura, S. and Kodama, S. 1996. Utilization of organic substances for growth and toxin production by *Alexandrium tamarense*. pp. 343–346 *in* Harmful and Toxic Algal Blooms *edited by* T. Yasumoto, Y. Oshima and Y. Fukuyo, UNESCO, Sendai.

Shimada, H., Hayashi, T. and Mizushima, T. 1996. Spatial distribution of *Alexandrium tamarense* in Funka Bay, Southwestern Hokkaido, Japan. pp. 219–221 *in* Harmful and Toxic Algal Blooms *edited by* T. Yasumoto, Y. Oshima and Y. Fukuyo, UNESCO, Sendai.

Shimada, H. and Miyazono, A. 2005. Horizontal distribution of toxic *Alexandrium* spp. (Dinophyceae) resting cysts around Hokkaido, Japan. *Plankton Biol. Ecol.* **52**: 76–84.

Shinada, A. 2005. Limiting factor for growth of *Alexandrium tamarense* in the coastal water, northeastern part of Hokkaido, Japan in summer. *Sci. Rep. Hokkaido Fish. Exp. Stn.* **69**: 117–121 (in Japanese with English abstract).

Tarutani, K. 1999. Ecophysiological studies on the population dynamics of toxic dinoflagellate *Alexandrium tamarense*. *Bull. Fish. Environ. Inland Sea* **1**: 63–96 (in Japanese with English abstract).

Yamamoto, T. and Tarutani, K. 1999. Growth and phosphate uptake kinetics of the toxic dinoflagellate *Alexandrium tamarense* from Hiroshima Bay in the Seto Inland Sea. *Japan. Phycol. Res.* **47**: 27–3.

Spatial and seasonal distributions of copepods from spring to summer in the Okhotsk Sea off eastern Hokkaido, Japan

Hiroki Asami[1], Hiroshi Shimada[2], Mayumi Sawada[2], Yasuyuki Miyakoshi[3], Daise Ando[3], Makoto Fujiwara[3] and Mitsuhiro Nagata[3]

[1] Hokkaido Wakkanai Fisheries Experiment Station,[1] Wakkanai, Hokkaido, Japan
E-mail: asamih@fishexp.pref.hokkaido.jp
[2] Hokkaido Central Fisheries Experiment Station, Yoichi, Hokkaido Japan
[3] Hokkaido Fish Hatchery, Kitakashiwagi-3, Eniwa, Hokkaido Japan

Abstract

Spatial and seasonal distributions of copepods were investigated in the Okhotsk Sea off eastern Hokkaido, in relation to the hydrography from spring to summer in 2002. Several cold water species such as *Neocalanus* spp. other than *Neocalanus cristatus*, *Pseudocalanus minutus*, *Pseudocalanus newmani*, *Metridia pacifica*, *Metridia okhotensis*, *Acartia longiremis*, and *Oithona similis* were predominant. Three groups of coastal, pelagic, and mixtures of coastal and pelagic copepod assemblages were identified during the investigations. These assemblages might be affected by the Soya Warm Current (SWC) and the extension of the front of Cold Intermediate Water (CIW).

Introduction

Copepods are the most numerous taxonomic group in the zooplankton community and are important as links between primary production and many species of fishes in the ecosystems (Mauchline, 1998). The Okhotsk Sea along the coast of Hokkaido supports many fishery resources such as salmon, herring, walleye pollock, arabesque greenling, *etc*. Copepods are one of the most important prey for these fishes (Motoda and Sato, 1949; Kamba, 1977; Blaxter and Hunter, 1982; Pearcy, 1992). We studied the spatial and temporal variability of zooplankton, including copepods, in near the coasts of the Okhotsk Sea off eastern Hokkaido, as part of an ecological study of juvenile chum salmon (Asami *et al.*, 2007), and suggested that the Soya Warm Current (SWC) along the coast of the Okhotsk Sea of Hokkaido might be one of the key factors affecting zooplankton variability. Irie (1990) also studied the seasonal biomass of zooplankton in waters further off-shore of the Okhotsk Sea of eastern Hokkaido from spring to summer. However, there is little information on the zooplankton community at the species level. This study was conducted in order to describe the copepod assemblages and to understand the factors affecting copepod variability from spring to summer in the Okhotsk Sea off eastern Hokkaido.

Materials and Methods

Study sites were located along O3 line (44°02.1′N ~45°08.1′N, 144°19.8′E), established as a monitoring line by the Hokkaido Fisheries Experiment Station (Fig. 1). Six stations were on this line. Since this line transverses along the Kitami-Yamato Rise, the depth between Stn. O34 and St. O36 varied greatly. Investigations were conducted in mid-April (April 16 and 17), early June (June 3 and 4) and late July (July 22 and 24) in 2002. Water temperature and salinity were measured by using a CTD. Surface water temperature was measured with a thermometer from a surface bucket sample. Surface salinity was also sampled by bucket and determined by salinometer in the laboratory.

Zooplankton samples were collected with a Norpac net (45-cm mouth and 0.33 mm mesh size) equipped with flowmeter from 150 m at Stn. O33, O34, O35 and O36 or near bottom at Stn. O31, and O32 from the surface. The net was towed vertically at a speed of 1.0 m/s. All samplings were done at night. After zooplankton collections, samples were immediately preserved in 5% buffered formalin. At a laboratory, a plankton splitter was used to divide samples into subsamples (Motoda, 1959), depending on abundance, and a dissecting microscope was used to

count the number of zooplankton in each taxonomic group. Copepods were identified to species level as far as possible.

Dominant species of copepods were determined as follows (Hosokawa *et al.*, 1968):

$$\text{Dominant species } Ni > (1/S)\ \Sigma\ Ni$$

where Ni indicates the number of *i*th species, and S means total number of species. Similarity indices among each station were calculated to access the copepod assemblages. Then a Percent Similarity Index (PSI) was adopted as follows (Schoener, 1970):

$$PSI = 1.0 - 0.5\Sigma\ |\ Pij - Phj\ |$$

where Pij and Phj mean the ratio of species j at station i and h, respectively. Based on the PSI, cluster analysis was done by a single linkage clustering method.

Results

Hydrography

In mid-April, water shallower than 20 m depth was occupied by less saline Okhotsk Surface Water (OSW) indicated by salinity of < 32.5 (Fig. 2). Cold Intermediate Water (CIW) underlying the OSW was recognized in which water temperature was less than 2°C and salinity was around 33.0 at stations beyond O33. Water temperature at Stns. O31 and O32 reached 8–10°C in early June, coinciding with high saline water, the Soya Warm Current (SWC), having a salinity of >33.6. CIW was found at stations beyond O34. Water temperature in coastal areas increased 10 to 14°C in late July. The SWC was found below 10 m depth at Stn. O32. CIW occupied the layer below about 40 m depth at stations beyond O33. Throughout the investigations, the fronts of the CIW were observed between Stns. O32 and O33 in mid-April and late July, and between Stns. O33 and O34 in early June.

Total zooplankton abundance and copepod dominance

The maximum of total zooplankton abundances (1,864 inds. m^{-3}) was found at Stn. O31 in early June, and the minimum (43 inds. m^{-3}) was observed at Stn. O35 also in early June (Fig. 3). Average abundances decreased toward July. Throughout the investigations, copepods occupied more than 90% of the composition, except for at Stn. O31 in early June and late July when Cladocera or Appendiculata were predominant at the coastal stations. Twenty genera and twenty five species could be identified, except for one calaniod species (Table 1). Copepods were composed of mostly cold water species. In these species, seven species such as *Neocalanus* spp. other than *Neocalanus cristatus*, *Pseudocalanus minutus*, *Pseudocalanus newmani*, *Metridia pacifica*, *M. okhotensis*, *Acartia longiremis* and *Oithona similis* were determined as dominant species throughout investigations.

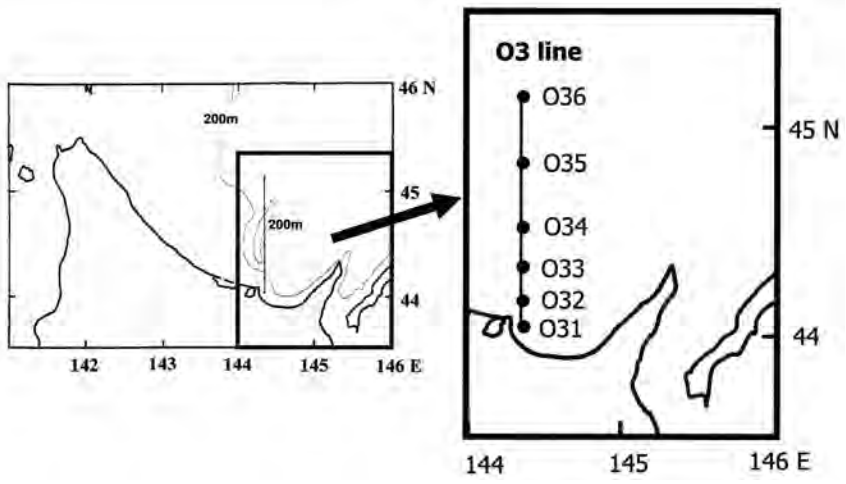

Fig. 1 Study sites and zooplankton sampling stations during mid-April to late July 2002 in the Okhotsk Sea off eastern Hokkaido.

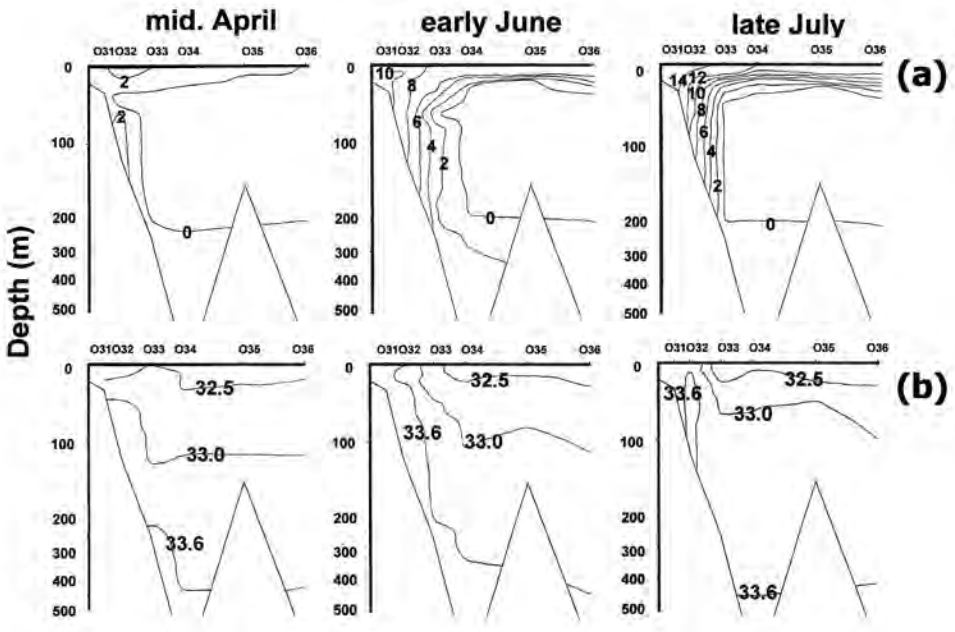

Fig. 2 Transcript profiles of (a) water temperature and (b) salinity at O3 line in 2002.

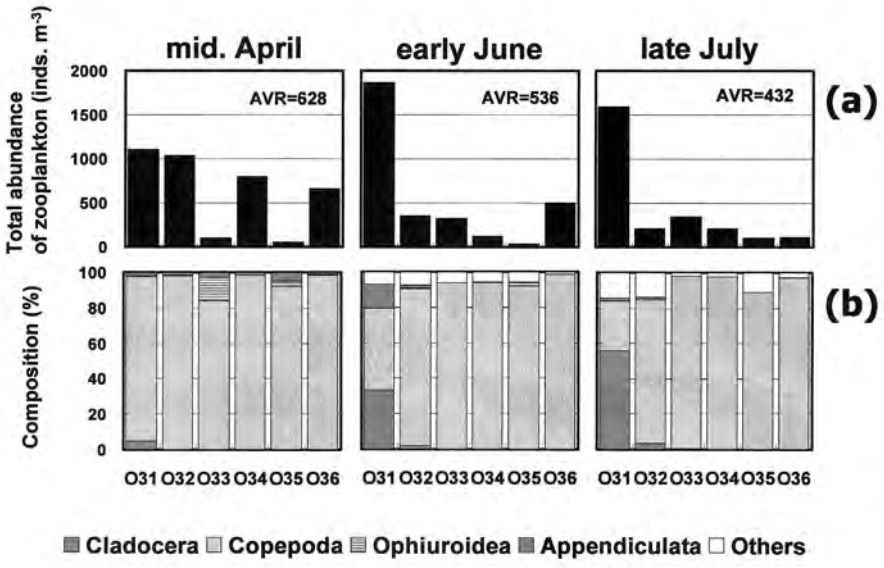

Fig. 3 (a) Total zooplankton abundances and (b) their dominant taxonomic compositions, at O3 line in 2002.

Table 1 List of copepod species observed during the investigations.

Calanoida	
●	*Calanus glacialis* Jaschenov
○	*Calanus pacificus* Brodsky
●	*Neocalanus cristatus* (Kroyer)
●	*Neocalanus* spp.
○	*Mesocalanus tenuicornis* (Dana)
□	Calanidae
●	*Eucalanus bungii* Giesbrecht
○	*Paracalanus parvus* (Claus)
●	*Pseudocalanus minutus* (Kroyer)
●	*Pseudocalanus newmani* Frost
●	*Microcalanus pygmaeus* (Saras)
○	*Clausocalanus pergens* Farran
△	*Aetideopsis* sp.
○	*Gaetanus armiger* Giesbrecht
●	*Paraeuchaeta elongate* (Easterly)
●	*Scolecithricella minor* Brady
●	*Eurytemora herdmani* Thompson & Scott
●	*Metridia pacifica* Brodsky
●	*Metridia okhotskensis* Brodsky
●	*Centropages abdominalis* Sato
●	*Acartia longiremis* (Lilljeborg)
●	*Tortanus discaudatus* Thompson & A. Scott
Cyclopoida	
●	*Oithona atlantica* Farran
●	*Oithona similes* Claus
Harpacticoida	
△	*Microsetella norvegica* (Boeck)

● Cold water species; ○ Warm water species; △ Eurythermic species; □ Not clear

Species composition and assemblages of copepods in relation to hydrography

Average abundances of copepods were the highest in mid-April, in spite of extremely low abundances at Stns. O33 and O35 (Fig. 4a). *P. newmani* made up 80–87% at Stns. O31 and O32 in mid-April (Fig. 4b). *M. pacifica*, *M. okhotensis* and *Neocalanus* spp. were the main components at stations beyond O33. *M. pacifica* made up 46% at Stn. O33 and 68% at Stn. O36, respectively. *M. okhotensis* occupied 67% at Stn. O34 and 30% at Stn. O36, respectively. *P. newmani* dominated from Stns. O31 to O33 in early June, and it made up 62–91% of total copepod abundances. *M. pacifica* and *M. okhotensis* were predominant in addition to *P. newmani* at Stns. O34 and O35. The composition of *M. okhotensis* reached 94% at Stn. O36. *A. longiremis* made up 93% at Stn. O31 in late July. *P. newmani* was predominant in addition to *A. longiremis* at Stn. O32. At stations beyond O33, *M. okhotensis* dominated, making up 30–70% of total copepod abundances.

As a result of cluster analysis based on PSI, three assemblages were recognized by fitting a 0.5 PSI in each month (Fig. 5). At the boundary front of CIW, one assemblage (assemblage 1) in mid-April and early June, and two assemblages (assemblages 1 and 2) in late July were observed in the coastal stations. These groups were composed of *P. newmani* or *A. longiremis* (*cf.*, Fig. 4b). Two assemblages (assemblages 2 and 3) were observed in mid-April and early June (Fig. 5). In these assemblages, at stations far from the front (assemblage 3), the main components were *M. okhotensis* or *M. pacifica* (*cf.*, Fig. 4b). Dominant species in assemblage 2 consisted of mixtures with assemblages 1 and 3 (*cf.*, Fig. 4b). Although *M. okhotensis* was one of the dominant species in assemblage 3 in late July, *P. newmani* was also an important component in this group (*cf.*, Fig. 4b). Because *P. newmani* was predominant in assemblage 2 in late July, the species composition of assemblage 3 might be mixed with assemblage 2.

Figure 6 shows the abundances of dominant species in each month. At the boundary of the CIW, the distributional characteristics are divided into three types. The coastal type composed of *P. newmani* and *A. longiremis* tended to distribute clearly in coastal areas. Four species, such as *Neocalanus* spp., *P. minutus*, *M. pacifica* and *O. similis* distributed in both coastal and pelagic stations, although two species of *Neocalanus* spp. and *P. minutus* were abundant in coastal stations in middle April. Distributions of *M. okhotensis* were limited beyond the front, and contributed to pelagic type.

Discussion

Different water properties, such as the Soya Warm Current (SWC), less saline Okhotsk Surface Water (OSW) and the Cold Intermediate Water (CIW) are known in the Okhotsk Sea (Takizawa, 1982). The dynamics of the SWC from spring to summer affected zooplankton variability along nearshore waters of the Okhotsk Sea, eastern Hokkaido (Asami

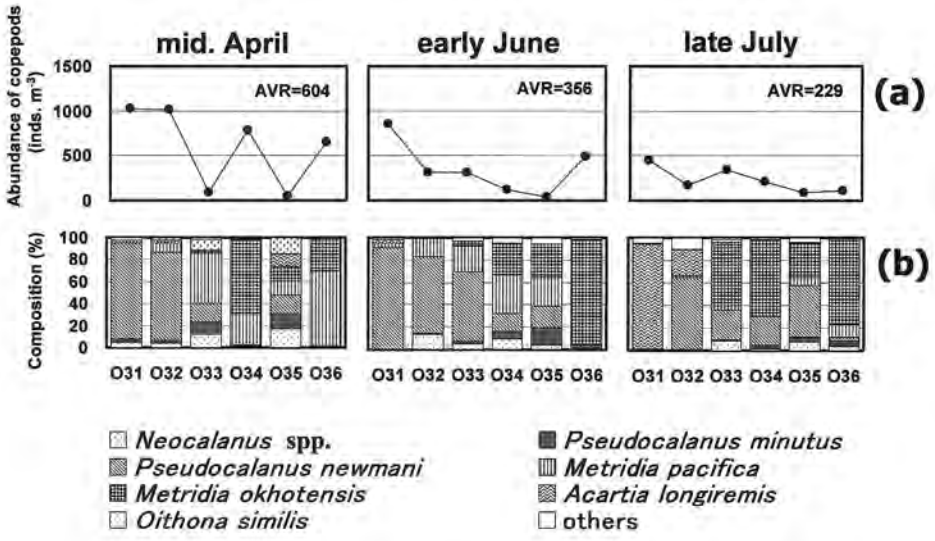

Fig. 4 Total abundance of (a) copepods and (b) their dominant species composition at O3 line in 2002.

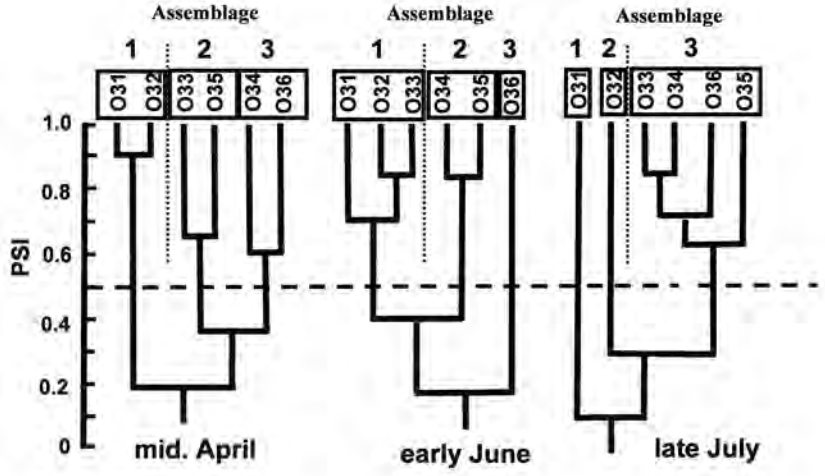

Fig. 5 Cluster analysis of copepod assemblages based on the PSI index. Dotted line indicates the front of the CIW.

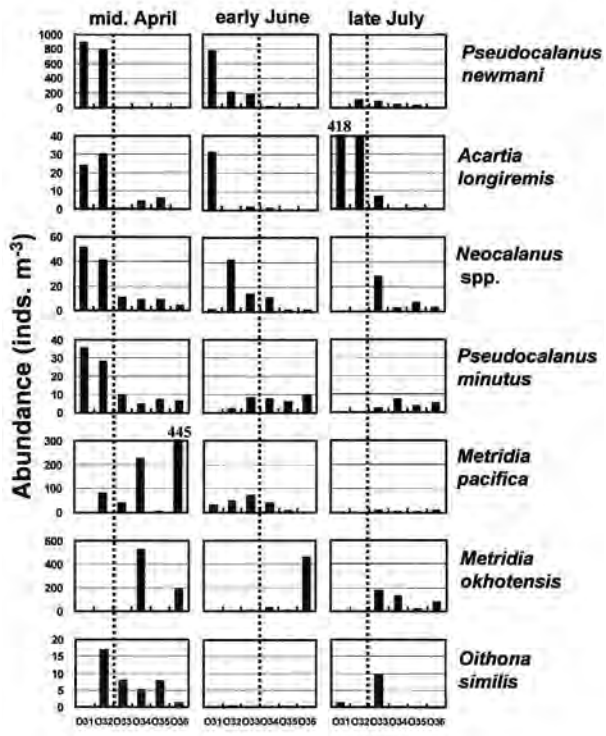

Fig. 6 Abundances of dominant copepod species related to the front of the CIW at O3 line in 2002. Dotted lines indicate the front of the CIW.

et al., 2007). Although some studies have dealt with the vertical and horizontal distributions of zooplankton in the Okhotsk Sea (Vinogradov, 1954; Takeuchi, 1972), there is little information for the horizontal distributions of zooplankton related to the CIW. The present study suggests that spatial distributions of copepods in offshore areas relate to the extension of the CIW. At the boundary of the front of the CIW, *P. newmani* was the most abundant copepod in coastal areas. In the Oyashio region of southwestern Hokkaido, *P. newmani* peaked in abundances after the spring blooms emerged and abundances decreased when water temperature reached 15°C (Yamaguchi and Shiga, 1997). Since the abundances of *P. newmani* decreased when coastal water temperature reached >14°C in this study, seasonal distributions of *P. newmani* might strongly depend on water temperature. *Neocalanus* spp., *P. minutus*, *M. pacifica* and *O. similis* were dominant species in assemblages mixed with coastal and pelagic assemblages. Among these species, the seasonal distributions of *Neocalanus* spp. and *P. minutus* seemed to relate to the movements of the SWC because these species tended to be abundant in coastal areas in mid-April when the SWC did not appear. However their distributions shifted toward pelagic areas when the SWC was found in the coastal areas in early June and late July. *Neocalanus* spp. are known as the important prey organisms of juvenile chum salmon (Simenstad and Salo, 1982; Nagata *et al.*, 2007). Spatial distributions of *Neocalanus* spp. may be important factors in taking account of the offshore migrations of juvenile chum salmon.

M. okhotensis was the most dominant species and appeared in pelagic areas affected by the CIW during the investigations. According to the reviews by Pinchuk and Paul (2000), *M. okhotensis* distributed in the depth below thermocline where water temperature decreased from 10 to 0°C sharply in northern Okhotsk Sea in summer. The fine vertical distribution related to the CIW must be also studied in southern Okhotsk Sea along Hokkaido. Biomass of *M. okhotensis* occupied more than 30 to 80% during spring to summer (Asami *et al.*, unpublished data). Since *M. okhotensis* also makes active diel vertical migrations (Vinogradov, 1954; Hattori, 1989), it is thought that *M. okhotensis* plays an important role in carbon dynamics of ecosystems, and more detailed research efforts are required in the Okhotsk Sea.

Acknowledgements

We thank the efforts in samplings given by officers and crew of the R/V *Hokuyo Maru*. We also thank Mr. M. Iwabuchi of Econixe Co., Ltd. for his support of species identifications.

References

Asami, H., Shimada, H., Sawada, M., Sato, H., Miyakoshi, Y., Ando, D., Fujiwara, M. and Nagata, M. 2007. Influence of physical parameters on zooplankton variability during early ocean life of juvenile chum salmon in the coastal waters of eastern Hokkaido, Okhotsk Sea. *N. Pac. Anadr. Fish Comm. Bull*. **4**: 211–221.

Blaxter, J.H.S. and Hunter, J.R. 1982. The biology of the clupeoid fishes. *Adv. Mar. Biol*. **20**: 1–323.

Hattori, H. 1989. Bimodal vertical distribution and diel migration of the copepods *Metridia pacifica*, *M. okhotensis* and *Pleuromamma scutullata* in the western North Pacific Ocean. *Mar. Biol*. **103**: 39–50.

Hosokawa, T., Kato, M., Kitazawa, Y., Nomura, K., Taguchi, R., Torii, Y. and Yagi, S. 1968. An Introduction to Ecology. Yokendo, Tokyo (in Japanese).

Irie, T. 1990. Ecological studies on the migration of juvenile chum salmon, *Oncorhynchus keta*, during

early life. *Bull. Seikai Natl. Fish. Res. Inst*. **68**: 1–142 (in Japanese with English abstract).

Kamba, M. 1977. Feeding habits and vertical distribution of walleye pollock, *Theragma chalcogramma* (Pallas), in early life stage in Uchiura Bay, Hokkaido. *Res. Inst. N. Pac. Fish.*, Hokkaido Univ. Spec. Vol., pp. 175–197.

Mauchline, J. 1998. The biology of calanoid copepods. *Adv. Mar. Biol*., **33**: 1–170.

Motoda, S. 1959. Devices of simple plankton apparatus. *Mem. Fac. Fish. Hokkaido Univ*. **7**: 73–94.

Motoda, S. and Sato, S. 1949. The food of the spring Atka-fish (*Pleurogrammus azonus*) with its hydrographic bearing. *Nipponsuisangakkaishi* **15**: 343–353 (in Japanese with English abstract).

Nagata, M., Miyakoshi, Y., Ando, D., Fujiwara, M., Sawada, M., Shimada, H. and Asami, H. 2007. Influence of coastal seawater temperature on the distribution and growth of juvenile chum salmon, with recommendations for altered release strategies. *N. Pac. Anadr. Fish Comm. Bull*. **4**: 223–235.

Pearcy, W.G. 1992. Ocean Ecology of North Pacific Salmonids. Washington Sea Grant Program, University of Washington Press, Seattle, WA.

Pinchuk, A.I. and Paul, A.J. 2000. Zooplankton of the Okhotsk Sea: a review of Russian studies. University of Alaska Sea Grant College Program, Fairbanks, AK.

Schoener, T.W. 1970. Nonsynchronous spatial overlap of lizards in patchy habitats. *Ecology* **51**: 408–418.

Simenstad, C.A. and Salo, O. 1982. Foraging success as a determinant of estuarine and nearshore carrying capacity of juvenile chum salmon (*Oncorhynchus keta*) in Hood Canal, Washington. pp. 21–37, Proceedings of the North Pacific Aquaculture Symposium, Anchorage, AK.

Takeuchi, I. 1972. Food animals collected from the stomachs of three salmonid fishes (*Oncorhynchus*) and their distribution in the natural environments in the northern North Pacific. *Bull. Hokkaido Reg. Res. Lab*. **38**: 1–118 (in Japanese with English abstract).

Takizawa, T. 1982. Characteristics of the Soya Warm Current in the Okhotsk Sea. *J. Oceanogr. Soc. Japan* **38**: 281–292.

Vinogradov, M.E. 1954. Diurnal vertical migrations of zooplankton in the far-eastern seas. *Tr. IOAN* **8** (quoted from Vinogradov, M.E. 1972).

Yamaguchi, A. and Shiga, N. 1997. Vertical distributions and life cycles of *Pseudocalanus minutus* and *P. newmani* (Copepoda; Calanoida) off Cape Esan, southwestern Hokkaido. *Bull. Plankton Soc. Japan* **44**: 11–20 (in Japanese with English abstract).

Characteristics of the zooplankton community in the Okhotsk Sea in autumn: A comparison with the Oyashio region

Atsushi Yamaguchi

Graduate School of Fisheries Sciences, Hokkaido University, Hakodate, Hokkaido, Japan
E-mail: a-yama@fish.hokudai.ac.jp

Abstract

Based on the vertical stratified zooplankton samples collected during the autumns (September–December) of 1996 to 1998, vertical distribution, biomass, and community structure of zooplankton and calanoid copepods in the southern Okhotsk Sea were evaluated and compared with those of the same period in the Oyashio region. In terms of fauna, zooplankton in the Okhotsk Sea are similar to that in the Oyashio region. However, their biomass, community structure and vertical distribution patterns are quite different between these two regions. Zooplankton biomass near the surface layer (0 m to thermocline) in the Okhotsk Sea was less than that of the Oyashio region. To understand the reason for this, we look at the distribution of large copepods in the mesopelagic layer in the Okhotsk Sea (this is epipelagic in the Oyashio region). Standing stocks of most zooplankton taxa were smaller in the Okhotsk Sea, while only the copepod *Metridia okhotensis* showed an opposite pattern. The abundance of *M. okhotensis* in the Okhotsk Sea was 30 times greater than that in Oyashio region, and they predominated (60% of the total copepod number) in the Okhotsk Sea. The development of a strong pycnocline in the Okhotsk Sea may be a key feature responsible for these regional differences in the zooplankton community in the Okhotsk Sea and Oyashio region.

Introduction

The Okhotsk Sea is known to be the lowest latitude sea to be ice covered in winter. Two factors contribute to the special characteristics of the Okhotsk Sea. The first one is in physical oceanography. There is the development of a strong pycnocline below which near-zero temperature cold intermediate water is present (Kitani, 1973). The second factor is related to biological oceanography. Juveniles of Japanese salmon born in a given year are known to migrate to the Okhotsk Sea for feeding in summer (Ueno and Ishida, 1996). Both these factors are considered to affect the abundance and distribution of zooplankton.

To clarify the characteristics of the zooplankton community in the Okhotsk Sea, we studied the vertical distribution of biomass, copepod community structure, population structure and body sizes and compared the results with those in the adjacent Pacific (Oyashio region).

Methods

In the present study, two types of samplings were made. The first one was stratified sampling between 0 and 2000 m depth using a closing net (Fig. 1, open circles). The second one was stratified sampling between 0 to 500 m depth using the IONESS system, which is a version of MOCNESS (solid circles). Stratified sampling at the IONESS stations was made four times per day to evaluate diel changes in vertical distribution.

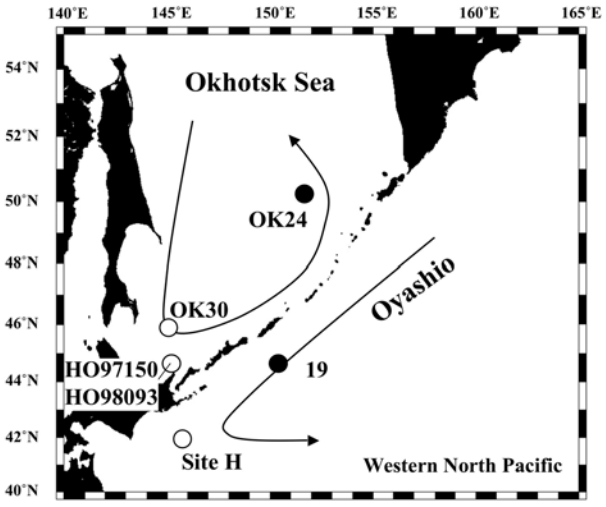

Fig. 1 Sampling stations in the Okhotsk Sea and the Oyashio region. Open circles indicate where samplings were done with a closing net and solid circles indicate samplings taken with the IONESS.

All of the samplings were conducted between September and December from 1996–1998. Results were compared assuming that inter-annual changes were minimum. To estimate biomass, the settling volume was measured for closing net samples. To determine the community structure, major zooplankton taxa and species, and stages of calanoid copepods were identified and quantified. Results were tested to find out whether inter-oceanic differences were present or not.

Hydrography

Temperature data are shown in Figure 2 for the closing net and IONESS stations. In the Okhotsk Sea, cold intermediate water is observed below the pycnocline. One station reached below 0°C. Since this study was conducted in autumn, this negative temperature was considered to be formed in the winter of the previous year. In the Oyashio region, there was no cold intermediate water. No station registered below 2°C in the Oyshio region (Fig. 2).

Biomass

The vertical distribution of zooplankton biovolume is shown in Table 1. In the Oyashio region, the highest biomass was commonly observed in the surface layer (0 m to thermocline) while in the Okhotsk Sea, it was commonly observed in the 250–500 m depth strata. Significant differences were noted only in the surface layer, where the zooplankton biomass in the surface layer of the Okhotsk Sea was lower than that in the Oyashio region by a factor of 1/4. Since there was no variation in the rest of the water column (Tc–2000 m depth), the biomass also did not vary (Table 1).

Taxonomic content

Thirteen taxa and 34 calanoid copepods were identified from the samples collected by IONESS. Of these, 6 taxa and 7 calanoid copepod species showed significant differences in abundance between the regions. Six taxa: Amphipoda, Appendicularia,

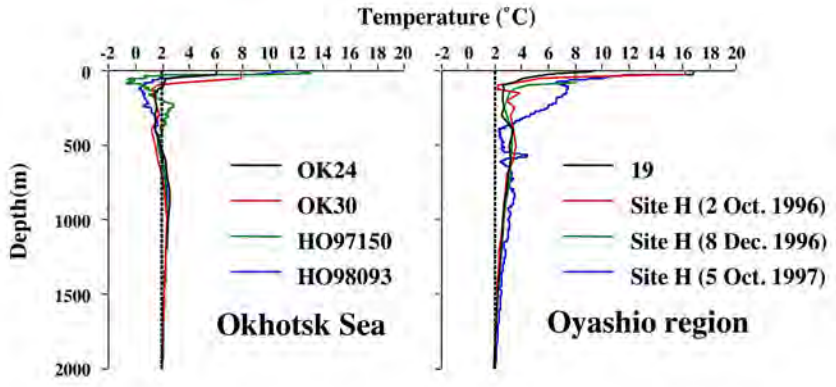

Fig. 2 Vertical distribution of temperature at stations in (left) the Okhotsk Sea and (right) Oyashio region. For comparison, position of 2°C is indicated by dotted lines.

Table 1 Inter-oceanic comparison of zooplankton biovolume (mL m^{-3}).

Depth strata (m)	Okhotsk Sea (*n*=5)	Oyashio region (*n*=6)	Mann-Whitney *U*-test
0–Tc	0.88 ± 0.11	3.59 ± 1.81	*
Tc–250	0.53 ± 0.43	0.65 ± 0.36	ns
250–500	1.14 ± 0.20	0.90 ± 0.32	ns
500–1000	0.37 ± 0.29	0.47 ± 0.12	ns
1000–2000	0.35 ± 0.24	0.24 ± 0.12	ns
0–2000	0.39 ± 0.23	0.53 ± 0.17	ns

Tc: thermocline, *: $p < 0.01$, ns: not significant

Chaetognatha, Poecilostomatoida, Polychaeta, Mollusca, and 6 calanoid copepods: *Eucalanus bungii, Metridia pacifica, Neocalanus cristatus, Pleuromamma scutullata, Pseudocalanus minutus* and *P. newmani* were more abundant in the Oyashio region. Only one calanoid copepod, *Metridia okhotensis*, showed greater abundance in the Okhotsk Sea, by a factor of 30 times (9369 inds. m^{-2} in the Okhotsk Sea vs. 367 inds. m^{-2} in the Oyashio region).

Since calanoid copepods were the predominant component of the zooplankton community (>80%) in both regions, the species compositions of calanoid copepods were further analyzed (Fig. 3). In the Oyashio region, the most dominant copepods were *Metridia pacifica*, followed by *Eucalanus bungii, Pseudocalanus mintus, P. newmani, Neocalanus plumchrus* and *M. okhotensis*, which was similar to the patterns of the both the western and eastern subarctic Pacific (*cf.*, Goldblatt *et al.*, 1999; Ikeda *et al.*, 2008). In the Okhotsk Sea, *M. okhotensis* was the predominant component and accounted for 66% of the total copepod abundance. Since the composition of *M. okhotensis* was only 0.9% of the total copepod abundance in the Oyashio region, the anomalously high abundance of *M. okhotensis* in the Okhotsk Sea is considered to be a special characteristic of copepod communities in the Okhotsk Sea.

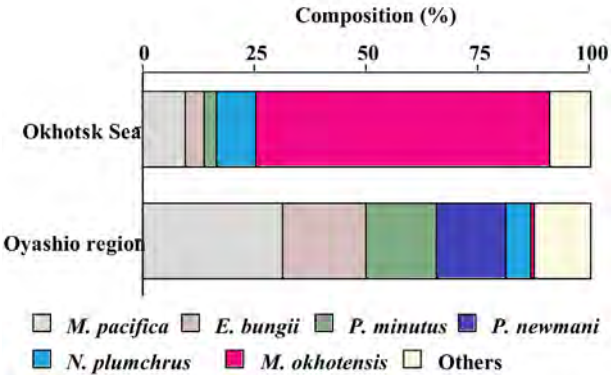

Fig. 3 Species composition of the calanoid copepod communities in the Okhotsk Sea (upper) and Oyashio region (lower).

Summary

Low zooplankton biomass in the epipelagic layer of the Okhotsk Sea was evident when comparing the Okhotsk Sea and adjacent Oyashio region. This was partly because of the low abundance of the most of zooplankton taxa and calanoid copepod species. Only the calanoid copepod *Metridia okhotensis* was the predominant component of the open area of the Okhotsk Sea. The *Metridia* species is known to be a strong diel vertical migrant (Hays, 1995). Both the low zooplankton biomass in the epipelagic layer and strong migrant capabilities of the *Metridia* species suggests that the development of a strong pycnocline and the presence of cold intermediate water play a key role in the distribution of the zooplankton community in the Okhotsk Sea. Since development of a pycnocline is greater in the Okhotsk Sea, it may prevent diel vertical migration of most zooplankton taxa (= low biomass in the epipelagic layer). The dominance of the strong migrant species *Metridia* suggests that *M. okhotensis* can cross the strong pycnocline and cold intermediate layer in the Okhotsk Sea.

Future Prospects

Since *Metridia okhotensis* is the predominant component of the open area of the Okhotsk Sea, future study should focus on the ecology of this species. A time-series of zooplankton samples collected at Rausu (face towards the Okhotsk Sea) located on Shiretoko Peninsula, Japan, at 350 m depth (Shiretoko Rausu Deep-Seawater) is being examined. Here, *M. okhotensis* also dominates (ca. 50% of calanoid copepod abundance; Yamaguchi, unpublished data). From this analysis, we are planning to reveal the life cycle of *M. okhotensis* in the open area of the Okhotsk Sea.

References

Goldblatt, R.H., Mackas, D.L. and Lewis, A.G. 1999. Mesozooplankton community characteristics in the NE subarctic Pacific. *Deep-Sea Res. II* **46**: 2619–2644.

Hays, G.C. 1995. Ontogenetic and seasonal variation in the diel vertical migration of the copepods *Metridia lucens* and *Metridia longa*. *Limnol. Oceanogr*. **40**: 1461–1465.

Ikeda, T., Shiga, N. and Yamaguchi, A. 2008. Structure, biomass distribution and trophodynamics of the pelagic ecosystem in the Oyashio region, western subarctic Pacific. *J. Oceanogr*. **64**: 339–354.

Kitani, K. 1973. An oceanographic study of the Okhotsk Sea. Particularly in regard to cold waters. *Bull. Far Seas Fish. Res. Lab.* **9**: 45–77.

Ueno, Y. and Ishida, Y. 1996. Summer distribution and migration routes of juvenile chum salmon (*Oncorhynchus keta*) originating from rivers in Japan. *Bull. Natl. Res. Inst. Far Seas Fish*. **33**: 139–147.

Determinants of fish species composition in Abashiri River

Minoru Kanaiwa, Takuya Inoue and Atsuya Yamamoto

Faculty of Bio-Industry, Tokyo University of Agriculture, Abashiri, Japan
E-mail: m3kanaiw@bioindustry.nodai.ac.jp

Introduction

Because natural organisms are a part of the factors constituting the ecosystem for each organism, it is important to clarify both physical and biological exploitable factors to determine species compositions which exist in that ecosystem. The variation in factors which constitute an ecosystem makes up the variation in species composition. At the same time, each species will interact and will make a dynamic ecosystem.

The Abashiri River is one of the longest rivers in eastern Hokkaido and flows into the Okhotsk Sea. Its drainage area is over 1380 km^2 and various types of environment are found along the river; *i.e.*, intact natural vegetation upriver, lots of farmland in the middle section and residential areas downriver. Such variations in the environment around the river affect the ecosystem in the river.

In the Abashiri River basin, rainbow trout were introduced after World War II. Some individuals settled in certain places of the river basin but were not able to settle in other parts of it. Alien species are one of the big interests in conservation biology. It is important to understand the difference in habitat requirements between alien and indigenous species in order to help control the number of alien species. In previous studies, analyses were independent of each species and there was a lack of analyses to determine the interaction among them.

Generalized Linear Models (GLM: Nelder and Wedderburn, 1972) allow for the variation of error distribution that includes multinomial distribution. GLMs are useful for finding out what factors will present the composition of fish species by a model selection method using information criteria. In this study, we evaluate a preliminary method to clarify the composition of fish species using a GLM with multinomial error distribution.

Materials and Method

Fish species and environmental data were gathered between June and November in 2007, at least once per each month for a total of 7 times. We set 5 survey areas (A1, A2, A3, H and K) in the upper reaches of Abashiri River (Fig. 1). Each survey area measured 100 m in length. We caught fishes using an electric fisher (Smith-Root Co., Model 12-b, DC100-1, 100V, Max 60A). We recorded pH, water temperature and water depth at 6 points (3 points upstream and 3 points downstream) in each survey location.

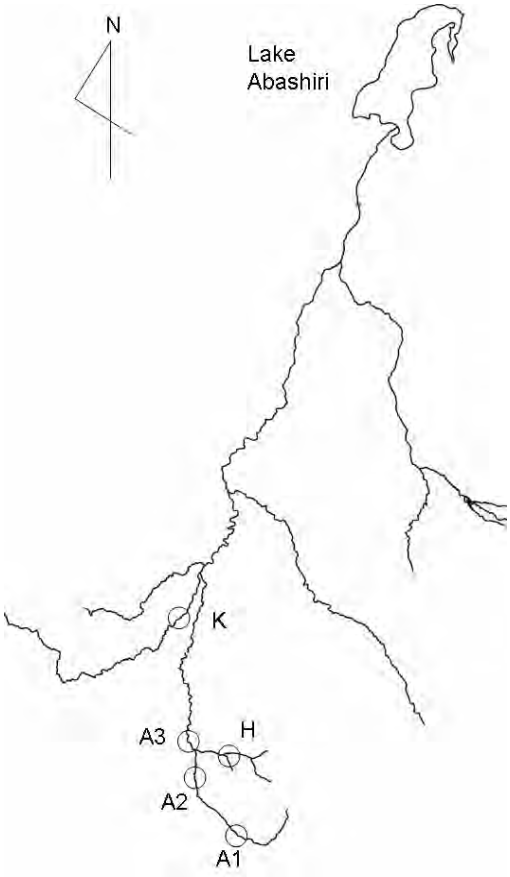

Fig. 1 Survey locations along the Abashiri River, from June to November 2007.

To clarify the explaining factors determining the composition of fish species, we used a GLM with multinomial error distribution (Araki, 2007). We used an average of 6 data points recorded in each survey location as environmental factors. Location name and month were the other explaining factors. So the initial model becomes

$$\text{composition of fish species} = a_1 p + a_2 t + a_3 d + a_4 m + a_5 l + \varepsilon.$$

Here, a_i, p, t, d, m and l are the coefficients of each explaining variable, pH, water temperature, water depth, month and survey location, respectively, and ε is an error variable followed by a multinomial distribution. We used a step-wise procedure with both directions (Burnham and Anderson, 2002) setting a Bayesian Information Criteria (BIC) as the estimating value to evaluate an optimal model and to find out which factors affect the composition of fish species. After getting the optimal model, if categorical explaining variables (*i.e.*, month and survey location) were selected, we clustered categorical explaining variables by using BIC as estimating values.

We then evaluated how the model would predict fish species composition. Two criteria provided by Sato (2002) were applied for this evaluation. The first criterion was the proportion that when a species 'A' is observed and predicted one is correct. This means the predicted performance for an occurrence ratio. The second criterion was the proportion when an observed species is not A and predicted one is not A either. This means the predicted performance for a non-occurrence ratio. If these criteria are high, it means this model can figure out a real situation well. We calculated these criteria for three main species, masu-salmon (*Oncorhynchus masou*), white spotted char (*Salvelinus leucomaenis*) and a kind of loach (*Noemacheilus barbatulus toni*).

Results and Discussion

Catch

There were 5 fish families containing 7 species in the catch. The catch for each species is shown in Table 1.

Optimal model

For the optimal model, variables of water temperature (*t*) and survey location (*l*) were selected. Survey locations grouped into 3 clusters, *i.e.*, A1 + H, A2 + A3 and K. The estimated values of each species were compared to *Salvelinus leucomaenis* (A) which was given the value 0. The coefficients and standard errors of the survey locations were compared to that of A2 + A3. Each estimated coefficient and standard error are shown in Table 2 and 3, respectively.

Looking at Table 2, we see that if the estimated value for various species is positive, it means the variable tested is more favorable for an individual of that species compared to white spotted char. If the value increases, the number of fish increases. So, sculpin prefer A1 + H more than other species and Japanese dace prefer K. Japanese dace prefer the lowest temperatures compared to other species. However, if the standard error is higher, the confidence interval will become larger.

Table 1 Catch for each species.

Japanese name	English name	Scientific name	Abbrev.	Catch (No. of individuals)
Yamame	Masu salmon*	*Oncorhynchus masou*	Y	822
Niji-Masu	Rainbow trout	*Oncorhynchus mykiss*	N	32
Ame-Masu	White spotted char*	*Salvelinus leucomaenis*	A	346
Ugui	Japanese dace	*Tribolodon hakonensis*	U	86
Fuku-Dojo	type of loach	*Noemacheilus barbatulus toni*	F	227
Hana-Kajika	Sculpin	*Cottus nozawae*	J	8
Siberia Yatsume Unagi	Siberian lamprey	*Lethenteron kessleri*	S	3

***** Salmonids included landlocked individuals because there were few smolts in our survey areas.

Table 2 Estimated coefficient compared to white spotted char *Salvelinus leucomaenis* (A).

		Cluster		
Sp.	**Intercept**	**A1 + H**	**K**	**water temp., *t* (°C)**
Y	0.74	– 0.69	0.21	0.06
N	– 9.37	– 0.81	9.93	0.08
U	– 9.55	– 0.08	12.00	– 0.02
F	– 2.12	– 3.30	3.75	0.13
J	– 9.56	5.37	1.11	0.07
S	– 15.10	– 0.74	– 5.26	1.01

Survey location variables are compared to A2 + A3. The criteria for model evaluation are shown in Table 4.

Table 3 Estimated standard errors.

		Cluster		
Sp.	**Intercept**	**A1 + H**	**K**	**water temp., *t* (°C)**
Y	0.22	0.15	0.37	0.02
N	8.71	11.06	8.71	0.03
U	15.43	17.20	15.43	0.03
F	0.33	0.55	0.39	0.03
J	10.07	10.00	17.60	0.12
S	6.01	1.41	3.78	0.47

Table 4 Model evaluation criteria.

Sp.	**1st criterion**	**2nd criterion**
Y	0.9396	0.5039
A	0.0000	1.0000
F	0.8048	0.8954

Water temperature was the only environmental variable, except survey location, used to explain fish species composition. The survey location variable may represent all other factors which we did not set in the initial model. So we cannot say that fish species composition depends on only water temperature. However, we found it is one of the most important habitat requirements. White spotted char especially favor a habitat of lower temperature compared to the other species. This fits to the results of a former study (Nakamura, 2007). Rainbow trout favor warmer locations compared to other salmonids. The cluster of survey locations was found to be appropriate because the clusters shared similar physical relationships, *i.e.*, upriver cluster (A1 + H), middle river cluster (A2 + A3) and tributary river (K).

The model performed well for masu-salmon and a kind of loach, but not for white spotted char (Table 4). This could be because we used a simple model without any interacting terms among the variables. In addition, the niches of masu-salmon and white spotted char overlapped in many situations and the number of white spotted char was less than for masu salmon. This may make it hard to distinguish the habitat preference of white spotted char. Our study shows such a possibility, and modification of the initial model is required in a future study.

The methodology used to predict habitat requirements was provided, and the selected model is appropriate. Except for white spotted char, the optimal model can predict fish species fairly well.

This is still a preliminary study and we need to improve our selection of explaining variables to be included in the initial model. However, we believe this type of approach will provide an objective model to explain habitat requirements of fish species. For the analysis of ecosystems, we recommend adopting this type of strategy because if there are various factors constituting an ecosystem, this type of analysis is the only way to get appropriate results.

References

Araki, K. 2007. The Multiple Classification Analysis with R and R Commander. Nikka Giren Press, Japan (in Japanese).

Burnham, K.P. and Anderson, D.R. 2002. Model Selection and Multimodel Inference. Springer, New York.

Nakamura, T. 2007. I want to increase the amount of Iwana mountain trout more. Furai No Zasshi Sha, Japan (in Japanese).

Nelder, J.A. and Wedderburn, R.W.M. 1972. Generalized linear models. *J. Roy. Stat. Soc., Ser. A* **135**: 370–384.

Sato, Y. 2002. Prediction model of occurrence/non-occurrence of stream fishes in the Katsuura River, *Gyoruigakuzasshi* **49**: 41–52 (in Japanese).

Scientific evidence and questions identified by the Hanasaki Program

Makoto Kashiwai[1] and Gennady Kantakov[2]

[1] Tokyo University of Agriculture, Abashiri, Japan. E-mail: m3kashiw@bioindustry.nodai.ac.jp
[2] Far-Eastern Ecological Center Ltd., Yuzhno-Sakhalinsk, Russia. E-mail: deco@sakhalin.ru

Introduction

A joint research project, the Hanasaki Program, conducted by Nemuro City and Sakhalin Research Institute of Fisheries and Oceanography (SakhNIRO), is in its fifth year. Although the program is small, it has a large scientific scope and has identified several important pieces of scientific evidence and posed new scientific questions. Thus, we would like to present them as potential items for the Okhotsk Sea component of the new PICES integrative science program on Forecasting and Understanding Trends, Uncertainty and Responses of North Pacific Ecosystems (FUTURE).

What is the Hanasaki Program?

The Hanasaki Program is a program dedicated to the study of Hanasaki crab, *Paralithodes brevipes*, which is distributed mainly around the Nemuro Peninsula, once called the Hanasaki Peninsula, in the waters around Hokkaido, Japan. Hanasaki crab is the symbolic sea food of Nemuro City because of its brilliant red color when boiled, and its vivid taste. However, the catch of this crab has been very low in spite of stock management and enhancement efforts. Moreover, the Nemuro market, among other Hokkaido fisheries markets in recent years, has been supplied with Hanasaki crab landings as well as by illegal catches from the Okhotsk Sea and nearby waters.

The Hanasaki Program is addressing the following questions which have a broad scientific scope covering biology, ecology, oceanography, ecosystem modeling, fisheries management, culturing technology, and taste quality.

Why does stock not recover in spite of stock management efforts? Is it due to:

– Illegal catch?
  Action: identify the unit of stock management.
– Overestimation of abundance resulting in too large of an allowable catch?
  Action: review the stock assessment method and develop a tagging method.
– Abundance of settling larvae?
  Action: conduct a joint larval survey.

2) How can the culturing method be improved?
   – How can the mass mortality in seed production be avoided?
     Action: conduct a comparative parallel test on possible alternative measures.

3) How can the value of stock in the market be realized and enhanced?
   – When is the best taste season and where is the best place to find the best tasting crab?
     Action: monitor the changes in taste through the seasons and between sites by conducting organoleptic tests.
   – Is the molting phase linked to taste?
     Action: examine changes in the umami relating chemical components through the molting process.

The five following themes were developed to address these questions, and four years after the program was implemented, the following results have been obtained by the Nemuro and SakhNIRO teams.

Major Achievements of Research

Theme 1. Study on the dynamics of the *P. brevipes* fishery and population

Objectives and research items

- To identify hidden problems in stock management practice through an overview of fishery operations and catch dynamics;
- To review if the appropriate level of allowable catch has been set or not;
- To develop tags to be retained through multiple moltings for the estimation of stock abundance, mortality and emigration/immigration;
- To elucidate the effects of the environment on stock dynamics through investigation of seasonal changes in water temperature of the fishing grounds;

- To know the status of local populations of *P. brevipes* distributed in the Okhotsk Sea and adjacent waters by looking at:
  1) *Features of the fishery and catch efficiency of crab pots*;
  2) *Improvement of stock assessment and development of tagging methods*;
  3) *Oceanographic conditions and structures*;
  4) *Status of local populations*.

Results

1) *Features of the fishery and catch efficiency of crab pots*

Catch efficiency of crab pots

Nemuro

Results of past surveys showed that:

- The attracting range of crab pots was estimated to be between 9 and 12 m; the maximum number of crabs in a pot was estimated to be around 5 individuals; and the duration of pot immersion to maximize crab catch was about 3 days;
- Selectivity of pot cover nets by crabs indicated no significant difference in carapace size composition for meshes of 30, 60, and 120 mm (Fig. 1).

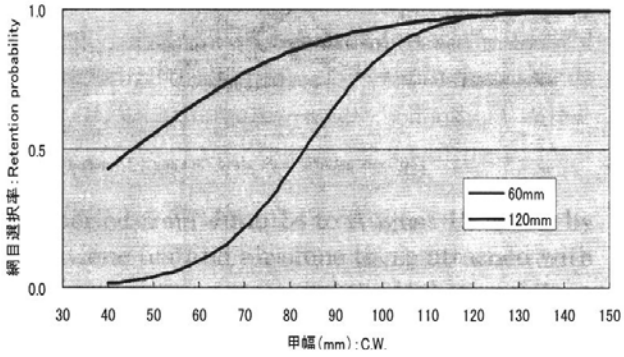

Fig. 1 Mesh selectivity curve of Hanasaki crab pots of 60 and 120 mm mesh using 30 mm mesh catch as reference. Horizontal axis is carapace width.

SakhNIRO

Diving results showed that:

- *P. brevipes* in crab pots stuck to the inside of the side net, or at the outside of the crab pots, attached to the bottom of the pot, or stuck outside or close to the net wall, crowding together in two or three tight rows, as if waiting in the turn to enter the pot;
- Within a distance of 10 m from the pots, groups of 2 to 3 individuals hid under brown algae, at the bottom of protruding rocks, or in the cracks of rocks;
- At a distance of 15 to 20 m, crabs were distributed as single individuals;
- Beyond 20 m from the pots, no crabs were observed;
- Just after molting, *P. brevipes* showed high feeding activity at the crab pots and, at night, moved actively to form local swarms; the pot catch in the survey area showed sudden jumps at various points.

2) *Improvement of stock assessment and development of tagging methods*

Improvement of stock assessment methods

Nemuro

- A review of the present method for *P. brevipes* stock assessment indicated a large uncertainty resulting from peculiarities in catch efficiency of the crab pots. The major source of uncertainty causing an overestimation of stock was the individual number-based catch–density relation. In other words, stock estimation by the CPUE–density relation at around a saturation level of gear capacity can cause a larger uncertainty and possible overestimation of stock density, especially when the size dependency of the gear saturation level is ignored in the CPUE–density relation.

Development of tagging methods

Nemuro

- Tagging was one of the most efficient methods for field surveys of population dynamics. However, in the case of crustaceans, tags had a tendency to drop off with the old carapace at the time of molting, and the duration of the tagging survey was limited to a short interval between molting. The straight-type anchor tag (Photo 1) and marking by making an excision on the side of the carapace (Photo 2) were tested, and confirmed that tag retention after the fifth molting was a highly practicable method for *P. brevipes*.

Photo 1 Straight anchor tag: (top to bottom) putting on the tag, just after tagging, after second molting, and after fourth molting.

Photo 2 Excision of the side of the carapace: (top to bottom) side of carapace before excision, just after excision, after first molting, and after fourth molting.

- The inner membrane taken from a chip excised from the side of the carapace for marking has proven to be useful for DNA analysis, and the possibility of a tag mark with DNA information for individual identification is being developed.

3) *Oceanographic conditions and structures*

Nemuro

- Water temperature of fishing grounds near the bottom was monitored for 3 years. The very special nature of seasonal changes of oceanic conditions there (not changes in vertical structure but changes in horizontal shore–offshore structures) was clarified. These changes appear to continue to offshore oceanic conditions such as the Coastal Oyashio and the East Hokkaido Warm Current;
- Seasonal variations of the East Hokkaido Coastal Current were investigated. Results showed that the outflow of Okhotsk Sea Water does not influence the East Hokkaido Coastal Current Water. The water would have been greatly modified before it reached the sea to the east off Hokkaido. The results support the conclusion of DNA analysis on the genetic difference between the Sakhalin-Shiretoko populaton and the Kuril-Nemuro-Erimo population.

(For details, please refer to the paper by Nagata in these proceedings.)

SakhNIRO

- Downwelling was observed and measured in the aggregation areas of *P.brevipes* larvae and adults;
- From the spatial distribution of temperature and salinity, a pair of cyclonic and anti-cyclonic eddies were identified in the South Kuril Strait which showed that the current field is favorable for retention of planktonic larvae;
- The Princeton Oceanographic Model (POM) approach applied to *P. brevipes* larval distribution in the study area was confirmed by field surveys, except in shallow waters around Nemuro Strait and its vicinities.

4) *Status of local populations*

SakhNIRO

- Aggregations of *P. brevipes* in the coastal waters of the South Kuril Islands were in a good state. Survey results on planktonic larvae indicated a high level of reproduction in the region;
- However, in the 2005 and 2006 surveys, many females with unfertilized eggs were sampled;
- Diving surveys in 2004 determined the habitat of *P. brevipes* and population densities in the embayments around the islands of Shikotan, Yuriy, Zeleniy, and Polonskiy;
- A survey on the distribution of *P. brevipes* in the coastal area from Cape Odyan to the eastern boundary of the northern Okhotsk Sea was performed. Results showed that the spatial distribution of *P. brevipes* is uneven. The crab is confined specifically to the shoal area, and along the broken coastline there are several isolated spots with dense congregations of *P. brevipes* where high catches of commercial individuals have been obtained (MagadanNIRO);
- A survey of *P. brevipes* on the eastern Kamchatka shelf was performed. As there is no demand for *P. brevipes* on the domestic market, this stock is not exploited by commercial fisheries. In some areas, small-sized crabs are dominant (KamchatNIRO);
- Surveys of the *P. brevipes* population along the eastern coast of Terpeniya Peninsula, on Sakhalin Island, identified stable abundant colonies of this crab. Molting was observed mainly from the last 10 days of July to the first 10 days of August. Fecundity averaged 40,000 eggs for crabs with average carapace width of 104 mm (SakhNIRO);

Future study

1) *Features of the fishery and catch efficiency of crab pots*

Catch efficiency of crab pots

- Determine the saturation point of crab pots under different carapace size composition, and the relation between the pot escapement rate and size of crab.

2) *Improvement of stock assessment and development of tagging methods*

Improvement of stock assessment

- Improve methods of obtaining fishery data, especially on fishing locations and size composition of catch.

Development of tagging methods

- Implement field tests and practical applications.

3) *Oceanographic conditions and structures*

Nemuro

- Determine the relationship between seasonal changes in bottom temperature of fishing grounds and catches;
- Increase efforts to obtain direct current measurement data;
- Develop CTD and hydro-chemical data archives.

SakhNIRO

- Understand the possible causes of downwelling (by examining the possibility of a secondary flow by residual currents in the vertical section), and the current structure;
- Understand the formation mechanism of eddies in the South Kuril Strait (including the possibility of tidal residual currents) and their seasonal variability;
- Perform seasonal and interannual water property monitoring by remote sensing and *in situ* measurements.

4) *Status of local populations*

- Understand the genetic relationship between the Sakhalin population and the population at the northern coast of the Okhotsk Sea; the relationship between the distribution area and the area of circulation formed by the East Sakhalin Current and offshore countercurrent during the warm period of the year; the spatial difference in size composition within the distribution area and distribution of recruitment;
- Understand the genetic relationship between the eastern Kamchatka and Sakhalin populations; the relationship between the distribution area and the area of circulation formed by the Northern Okhotsk Current and its countercurrent; the spatial difference in size composition within the distribution area and distribution of recruitment.

Theme 2. Study of ecology and population structure of *P. brevipes*

Objectives and research items

- To elucidate the independency and mutual interchange among local populations, through DNA analyses, for identifying a strategy for stock management and stock recovery;
- To elucidate the ecology of crab;
- To develop an ecosystem model on larval transport and survival processes by looking at:
  1) *Genetic diversity and population structure*;
  2) *Transport and dispersion of planktonic larvae*;
  3) *Field survey of planktonic larvae*;
  4) *Ecological study*.

Results

1) *Genetic diversity and population structure*

Nemuro

- Novel DNA markers (eight microsatellite DNA and mtDNA AT-rich regions) were used to assess the genetic variability and population structure of *P. brevipes* (Fig. 2);
- Both microsatellite DNA and mtDNA analyses suggested that the populations of Sakhalin-Shiretoko, Kamchatka, and South Kuril-Nemuro-Erimo are genetically different;

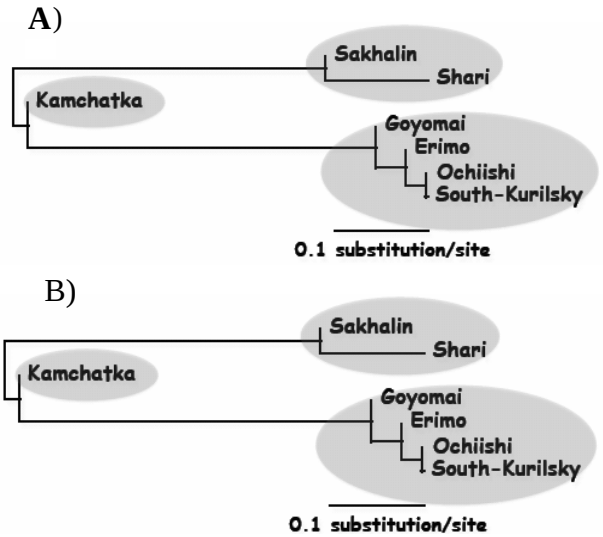

Fig. 2 Genetic relationships among Hanasaki crab (*P. brevipes*) populations inferred from (A) micro-satellite and (B) mitochondrial DNA data.

- The population on the coast of Nemuro Peninsula had high genetic variability and is clearing the critical level of effective population size (Ne) of 500 for keeping genetic variability of the population and preventing extinction;
- Artificial seeds produced by Nemuro City had relatively high genetic variability compared to the natural population;
- A new DNA typing method for future tag-and-release surveys was established without harming the individual and commercial value of the crab;
- Groups of *P. brevipes* in the Nemuro Peninsula–east of Cape Erimo area and in the South Kuril waters had minimum genetic differences and probably belong to the same population. Greater differences were obtained between the Sakhalin and northwest coast of Shiretoko Peninsula populations and Kamchatka populations (Fig. 3).

2) *Transport and dispersion of planktonic larvae*

Nemuro

Results of numerical simulations (POM) clarify the following:

- Planktonic larvae of Sakhalin origin reach the coast of Hokkaido Island to at least north of the Shiretoko Peninsula;
- Seasonal variability of the East Sakhalin Current and Soya Current plays an important role in the settlement of planktonic Sakhalin-originating larvae;
- The recruitment of crab must be influenced by interannual variability of oceanic conditions, especially surface currents and sea surface temperature around the Nemuro coast and Okhotsk Sea coast of Japan;
- The South Kuril waters around Malaya Kurilskaya Gryada and Nemuro Bay were identified as the most possible settling sites for larvae;
- An anti-cyclonic eddy in the South Kuril Strait may play an important role in the retention and accumulation of larvae.

3) *Field survey of planktonic larvae*

Nemuro

- Stations where planktonic larvae were sampled were mainly on the south side of the Nemuro Peninsula (Fig. 4, Table 1); the number of larvae sampled were considerably fewer than those sampled in the waters of the South Kuril Strait by SakhNIRO;
- In the 2007 and 2008 surveys, no *P. brevipes* larvae were sampled from Nemuro Strait;
- *P. brevipes* larvae appeared early, suggesting early shifting of the hatch-out time due to the effects of regional warming (Fig. 5).

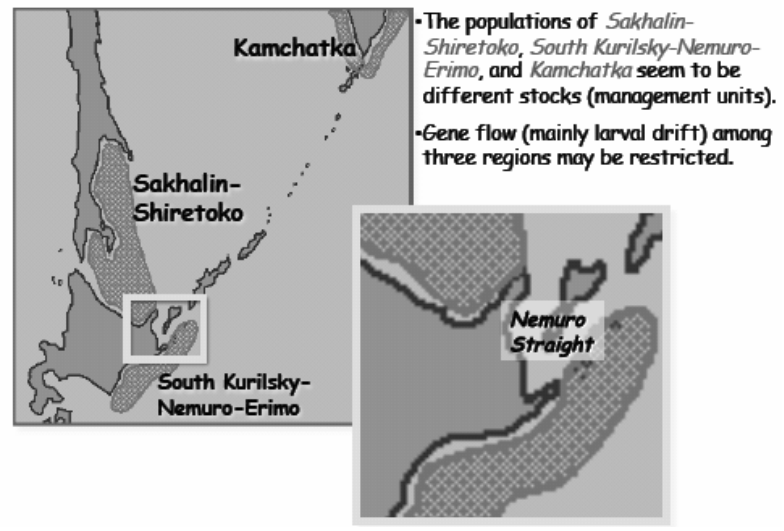

Fig. 3 Genetic population structure of Hanasaki crab (*P. brevipes*; cross-hatched areas) estimated by DNA analyses.

Table 1 Results of field surveys of planktonic larvae in 1984, 1985, 2006 and 2007 for stations off Nemuro Peninsula (total number of individuals sampled).

	1984				1985				2006				2007			
	Z1	Z2	Z3	G	Z1	Z2	Z3	G	Z1	Z2	Z3	G	Z1	Z2	Z3	G
May 1–10	–	–	–	–	35	–	–	–	16	36	–	–	–	1	1	–
May 10–20	10	–	–	–	2	6	–	–	–	–	–	–	–	–	–	–
May 20–31	–	–	–	–	–	37	86	–	–	–	–	–	–	–	52	–
June 1–10	–	–	–	–	–	–	15	–	–	–	4	1	–	–	–	1
June 10–20	–	1	4	–	–	–	–	4	–	–	–	–	–	–	–	–
June 20–30	–	–	1	–	–	–	–	–	–	–	–	–	–	–	–	–
July 1–10	–	–	–	–	–	–	–	–	–	–	–	–	–	–	–	–
July 10–20	–	–	–	–	–	–	–	–	–	–	–	–	–	–	–	–
Subtotal	10	1	5	–	37	43	101	4	16	36	4	1	–	1	53	1
Total	16				185				57				55			

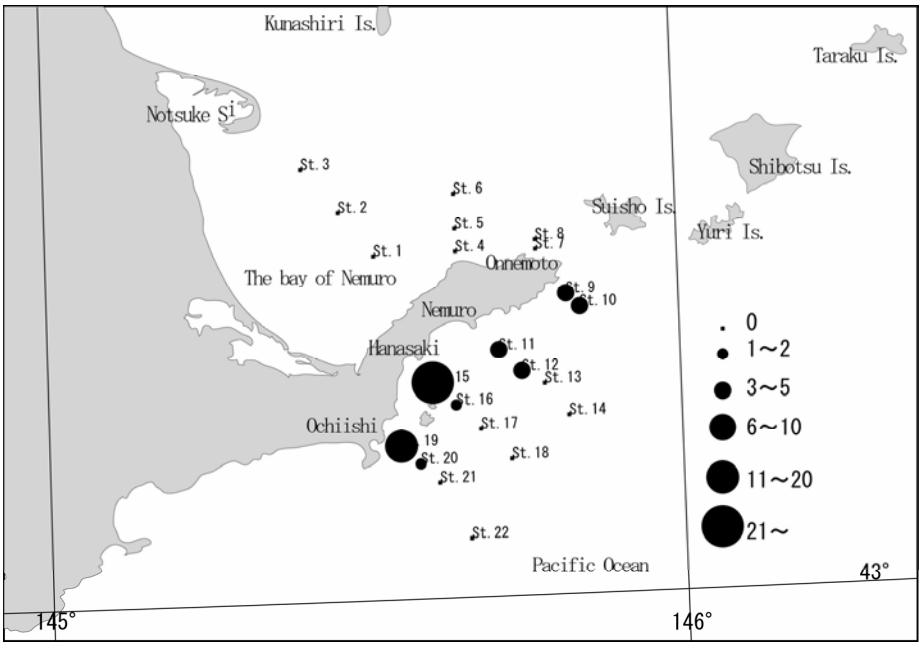

Fig. 4 Geographical distribution of sampled *P. brevipes* larvae in the last 10 days of May 2007 off Nemuro Peninsula.

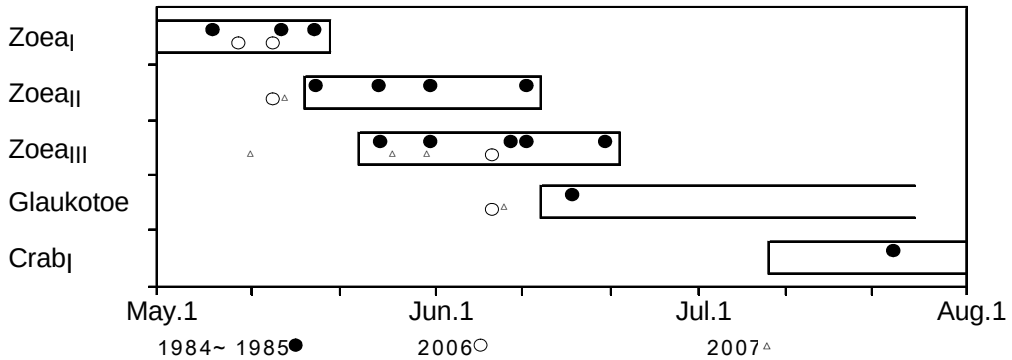

Fig. 5 Comparison of appearance times of *P. brevipes* larvae at different developmental stages, for surveys conducted in 1984, 1985, 2006 and 2007.

SakhNIRO

- May–June distribution density of planktonic larvae of *P. brevipes* in the waters around the South Kuril Islands was high and varied from 10s to 100s of individuals/m^2.

4) *Ecological study*

Nemuro

- From previous research conducted by Torisawa *et al.* (1999), the growth curve was re-examined to overcome the difference between early growth obtained through rearing individuals (Kittaka and Onoda, 2002) and that obtained through examination of wild samples (Abe and Koike, 1982; Sasaki and Yoshida, 1999). By synthesizing past results, a new age–carapace width–length relation was proposed (Torisawa, 2005);
- Molting of *P. brevipes* was observed during culturing studies;
- Results of laboratory measurements on the phototaxis swimming speed of larvae were introduced as an important parameter for larval transport model experiments.

SakhNIRO

- The diet of male king crab (*Paralithodes camtschaticus*), Hanasaki crab (also known as red spiny crab) (*Paralithodes brevipes*) and golden king crab (*Liathodes aequispinus*) near the South Kuril Islands were compared; Sea urchins of genus *Strongylocentrotus* prevailed in the diet of these three crabs; 90.8% for *L. aequispinus*, 84.1% for *P. brevipes*, and 53.8% for *P. camtschaticus*; High stomach fullness of *P. brevipes* was recorded only near the Malaya Kurilskaya Gryada between 19 and 48 m depth.

Future study

1) *Genetic diversity and population structure*
   - Study the genetic diversity and population structure of *P. brevipes* in the waters of northern and eastern parts of the Okhotsk Sea, Kuril Islands, Kamchatka and Bering Sea (Fig. 6).

2) *Transport and dispersion of planktonic larvae*

   - Using the POM approach to validate the model and examine the factors controlling distribution of the larvae, a biological oceanographic database on the habitat of *P. brevipes* larvae is needed (Fig. 7):
     – A GIS-oriented approach should be used;
     – Because of a lack of initial data in the region, including a deficiency of chemical materials, new specific and task-oriented field/database/model studies will be needed in the coming 1–2 years;
     – Intergovernmental efforts would be productive and helpful for the joint development of a biological oceanographic database, its implementation and scientific publication;
   - Problems to resolve:
     – Obtain Russian and Japanese governmental approvals for joint research;
     – Establish a task team;
     – Look for funding;

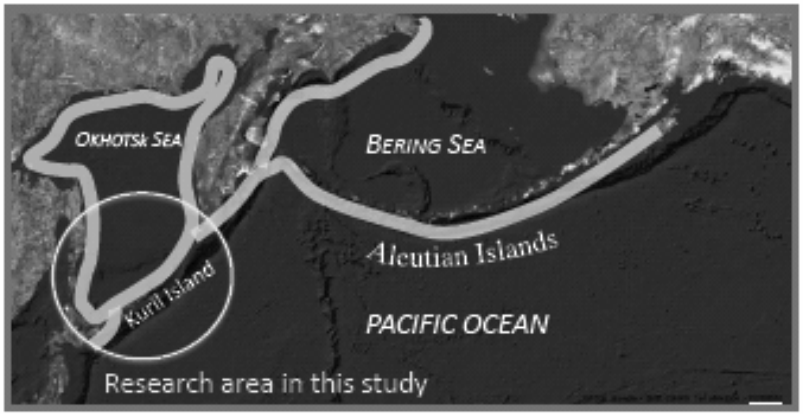

Fig. 6 Area of this study (circled) and possible distribution (thick grey lines) of *P. brevipes*.

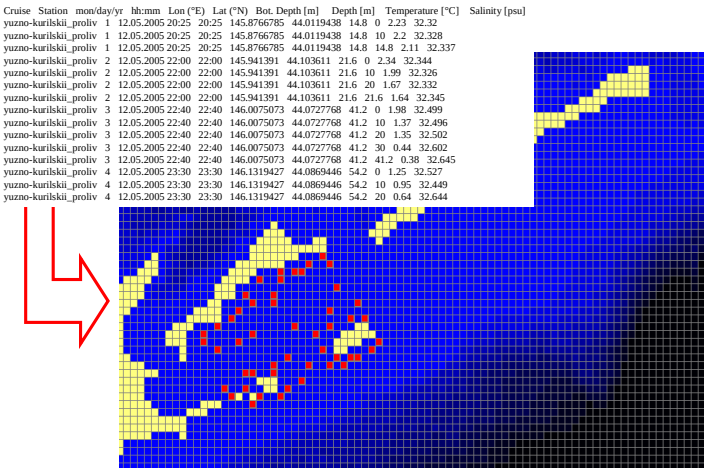

Cruise	Station	mon/day/yr	hh:mm	Lon (°E)	Lat (°N)	Bot. Depth [m]	Depth [m]	Temperature [°C]	Salinity [psu]
yuzno-kurilskii_proliv	1	12.05.2005	20:25	20:25	145.8766785	44.0119438	14.8	0	2.23	32.32
yuzno-kurilskii_proliv	1	12.05.2005	20:25	20:25	145.8766785	44.0119438	14.8	10	2.2	32.328
yuzno-kurilskii_proliv	1	12.05.2005	20:25	20:25	145.8766785	44.0119438	14.8	14.8	2.11	32.337
yuzno-kurilskii_proliv	2	12.05.2005	22:00	22:00	145.941391	44.103611	21.6	0	2.34	32.344
yuzno-kurilskii_proliv	2	12.05.2005	22:00	22:00	145.941391	44.103611	21.6	10	1.99	32.326
yuzno-kurilskii_proliv	2	12.05.2005	22:00	22:00	145.941391	44.103611	21.6	20	1.67	32.332
yuzno-kurilskii_proliv	2	12.05.2005	22:00	22:00	145.941391	44.103611	21.6	21.6	1.64	32.345
yuzno-kurilskii_proliv	3	12.05.2005	22:40	22:40	146.0075073	44.0727768	41.2	0	1.98	32.499
yuzno-kurilskii_proliv	3	12.05.2005	22:40	22:40	146.0075073	44.0727768	41.2	10	1.37	32.496
yuzno-kurilskii_proliv	3	12.05.2005	22:40	22:40	146.0075073	44.0727768	41.2	20	1.35	32.502
yuzno-kurilskii_proliv	3	12.05.2005	22:40	22:40	146.0075073	44.0727768	41.2	30	0.44	32.602
yuzno-kurilskii_proliv	3	12.05.2005	22:40	22:40	146.0075073	44.0727768	41.2	41.2	0.38	32.645
yuzno-kurilskii_proliv	4	12.05.2005	23:30	23:30	146.1319427	44.0869446	54.2	0	1.25	32.527
yuzno-kurilskii_proliv	4	12.05.2005	23:30	23:30	146.1319427	44.0869446	54.2	10	0.95	32.449
yuzno-kurilskii_proliv	4	12.05.2005	23:30	23:30	146.1319427	44.0869446	54.2	20	0.64	32.644

Fig. 7 Example page of a biological oceanographic database.

- In order to identify the hatching-out sites and settling sites of *P. brevipes* larvae from the results of field larval surveys, a modeling study on larval transport in the South Kuril waters has been implemented by a local physical oceanography model. An example of output bottom concentration of *P. brevipes* larvae (without other zooplankton) is shown in Figure 8;
- In this example, *P. brevipes* larvae are settling in the southern part of Nemuro Strait, while no individuals were sampled during field surveys by the Nemuro team. Further improvements need to be made to the model and field survey.

3) *Field survey of planktonic larvae*
   - Propose a joint international Japan–Russia expedition for a larval survey in the southern Okhotsk Sea and its vicinities to be executed by one or two research vessels in May–June, 2008, or later. The proposed sampling plan is shown below (Fig. 9).

4) *Ecological study*
   - Conduct ecological and muscle physiology studies on molting;
   - Perform rearing tests on recovery from molting.

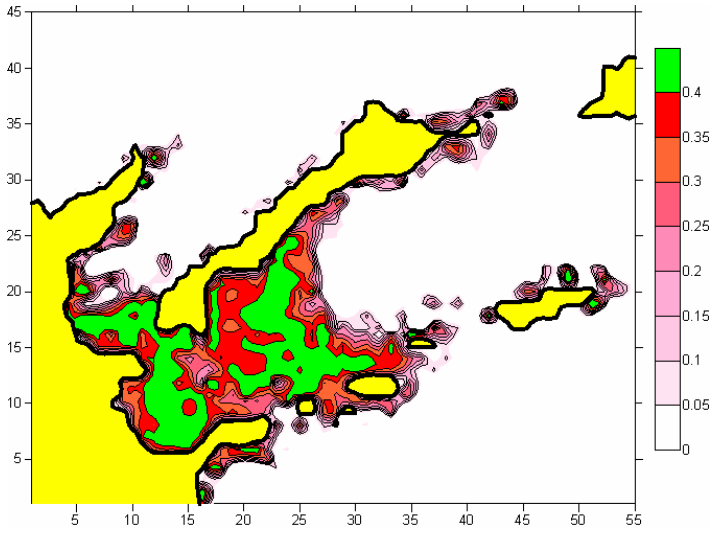

Fig. 8 Example of output on larvae distribution; *x* and *y* axes are model coordinates and the color pattern is larval density of the water column (individuals per m^2).

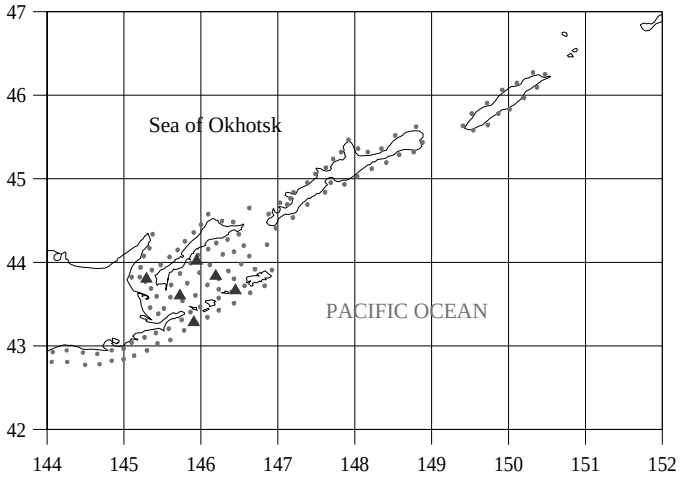

Fig. 9 Proposed larvae sampling plan. Grey dots represent net sampling stations and triangles denote mooring stations for current, temperature, salinity and sea-level measurements, with larval collectors.

Theme 3. Improvement of culturing technology for *P. brevipes*

Objectives and research items

- To improve the practicability of culturing technology by improving survival rate and economical efficiency through:
  1) *Improvement of seeding technology*;
  2) *Improvement of intermediate culturing technology*;
  3) *Development of a stock enhancement technology system*.

Results

1) *Improvement of seeding technology*
   - The cause of mass mortality of *P. brevipes* larvae at the glaukotoe stage was examined.

2) *Improvement of intermediate culturing technology*
   - A test of two batches of seeds using females with eggs at early hatch-out dates and females with late hatch-out dates, reared under different water temperatures, was implemented successfully.

3) *Development of a stock enhancement technology system*
   - A "Manual for seed production and seed release" was compiled as summary results.

Future study

1) *Improvement of P. brevipes seeding technology*
   - Develop seed releasing technology.

2) *Improvement of intermediate culturing technology*
   - Develop an artificial settlement base.

3) *Development of a stock enhancement technology system*
   - Develop stock assessment capabilities for identifying a strategy for stock enhancement.

Theme 4. Study on preservation and improvement of taste quality of *P. brevipes*

Objectives and research items

- To develop technology to preserve and improve taste quality of *P. brevipes* through analysis of chemical components governing the quality of taste, and to develop an index to make objective grading possible by:
  1) *Developing indices of freshness/liveliness*;
  2) *Investigating the geographical/seasonal change of taste components*;
  3) *Studying methods to improve taste quality*.

Results

1) *Development of indices of freshness/liveliness*
   - Energy Charge was an effective index for determining the liveliness of *P. brevipes*.

2) *Geographical/seasonal change of taste components*
   - Taste differences were found between male and females, but no systematic geographic differences in taste were detected.

3) *Methods to improve taste quality*
   - Rearing in higher salinity water increased the taurine level in *P. brevipes*, which suggests a possible method for improving taste;
   - The recovery process after molting indicated that the increased water content ratio and taste composition were dramatically recovered in accordance with hardening of the carapace;
   - Panelists composed from staff of the fishermen's cooperative evaluated the taste quality of *P. brevipes* during different stages of recovery from molting by organoleptic tests. Crab at one stage before complete recovery were graded relatively higher than at other stages;
   - The best cooking method and best time for flavour was boiled crab when it was still warm;
   - Results from chemical analyses of taste components indicated a degradation in part of the taste components by freezing or boiling;
   - A "Manual for preservation and improvement of taste quality of *P. brevipes*" was compiled as summary results.

Future study/activity

To publish a best procedure for cooking and tasting P. brevipes *for consumers*.

Theme 5. Study on the design of the *P. brevipes* fishery system for recovering and sustaining its resources

Objectives and research items

- To compare cost/performance of stock recovery measures;
- To identify a most suitable stock management method;
- To design a fishery system for establishment of a sustainable *P. brevipes* fishery.

Results

A "Manual for selecting stock recovery measures" was compiled as summary results.

Future study

- To improve stock assessments in selecting stock recovery measures;
- To arrange *P. brevipes* total catch information and exchange.

Final Remarks and Acknowledgements

The authors expect that the FUTURE Program of PICES will provide an opportunity to extend our small scientific collaboration into an international one. The scientific results reached in the Hanasaki Program are planned for publication in SakhNIRO proceedings in 2009.

The authors would like to express thanks to the scientists who contributed their efforts and results in the Hanasaki Program, obtaining new information on the ecology, biology, and habitat of *P. brevipes*, the Promoting Committee for the Nemuro City Hanasaki Program and SakhNIRO. We recognize the importance of widening scientific collaboration on *P. brevipes* issues around the Okhotsk Sea and its vicinities in the near future.

References

Abe, K. and Koike, M. 1982. The growth of the Hanasaki crab, *Paralithodes brevipes*. Sci. Rep. Hokkaido Fish. Exp. Stn., No. 24, pp. 1–14.

Kittaka, J. and Onoda, S. 2002. Effect of temperature on growth and maturity of the king crabs, *Paralithodes brevipes* and *P. camtschaticus* in the laboratory. Proceedings of International Commemorative Symposium, 70th Anniversary of the Japanese Society of Fisheries Science, Nov. 2002, *Fish. Sci.* **68**(Suppl. 1): 921–924.

Nagata, Y. 2009. Outflow of Okhotsk Sea Water and the oceanic condition of the sea east of Hokkaido. This report.

Sasaki, J. and Yoshida, H. 1999. Growth of juvenile Hanasaki crabs, *Paralithodes brevipes* in the littoral zone, north western North Pacific off Hokkaido. Sci. Rep. Hokkaido Fish. Exp. Stn., No. 55, pp. 155–160.

Torisawa, M., Kohno, S., Sakamoto, K. and Hakata, I. 1999. Growth in the early life stage of the spiny king crab, *Paralithodes brevipes* in the Pacific Ocean off the coast of eastern Hokkaido. Sci. Rep. Hokkaido Fish. Exp. Stn., No. 55, pp. 161–167.

Torisawa, M. 2005 Re-Examination on age-growth relation of Hanasaki crab. Proceedings of the 3rd Hanasaki Program Workshop, pp. 56–59.

Benthos community of a dumping area during liquid natural gas plant construction: Effects of technical impacts or natural changes?

Andrey D. Samatov and Vyacheslav S. Labay

Sakhalin Research Institute of Fisheries and Oceanography, Yuzhno-Sakhalinsk, Russia. E-mail: labay@sakhniro.ru

Introduction

According to the technical-economic substantiation (TES) of the Project "Sakhalin-II. Phase 2", two marine exploration platforms were constructed in the Lunskoye and Piltun-Astohskoe oil-gas fields, and were connected by pipelines to an oil terminal in Aniva Bay (south coast of Sakhalin island) for year-round exploration. Another aspect of the Project involved a liquefied natural gas (LNG) terminal and material operations facilities (MOF) to be added to the LNG plant that was built in 2003–2006 on the Aniva Bay shore near the settlement of Prigorodnoye.

A dredging operation needed to be carried out in the area of the LNG terminal and MOF beforehand in order to provide safe entry and mooring for ships. The dumping of dredged ground was approved in Aniva Bay outside of the 12-mile zone where water depth was 60–65 m. The Project also included comprehensive environmental monitoring.

The purpose of this research was to observe marine biota and the environment in the dredging and dumping areas in Aniva Bay. One of the main monitoring tasks was to estimate the impact of dumping on the benthos community and to forecast the time needed to restore its original abundance and structure in the affected area.

The Sakhalin Research Institute of Fisheries and Oceanography conducted research based on the Agreement with CTSD Ltd. Company. The schedule of observations included the following phases: before dredging, during the dumping, and after the work was completed.

Materials and Methods

Benthos was sampled in August 2003 – before any ground dumping; in October and December 2004, in May and August 2005 – during the operations; in August 2006 and August 2007 – after all the work had been completed. Sampling stations were located at 300, 800 and 2000 m off the central dumping point (coordinates 46°24.5′ N latitude and 142°55.0′ E longitude) to the north, east, south and west. Benthos was sampled from the R/V *Dmitry Peskov* using a Van-Veen grab (0.2 m^2).

The following structure indices and coefficient were used for the assessment of state and comparison of benthos communities:

1. Index of diversity (Shennon),
2. Index of cenotic similarity (Shoener),
3. Species similarity coefficient (Serensen),
4. Community succession index (ABC-method).

Results

Dredging and dumping operations were carried out from March until the middle of May and from mid-September until December to lessen the impact on the environment and biological resources.

In August 2003, before the dumping operation began in the described area, the bottom community was surveyed and a dominance of sipunculids (*Golfingia margaritacea*) and a significant number of polychaetes (*Axiothella catenata*, *Praxillella* spp., *Prionospio* sp.) were observed. There was also a high abundance of amphipods and cumaceans. Average benthos biomass was 53.7 g/m^2 (Table 1).

In December 2004, after the first phase of dumping, the number of species and their abundance was the same as in 2003 and high due to small crustaceans, but mean biomass was about half as much (Table 1). The bivalve *Nuculana pernula pernula* dominated in most of the area. Therefore, this type of community could be considered an indicator of dumping.

In August 2005, the mean benthos biomass was high, reaching 48.6 g/m^2 (Table 1); most of the biomass (71%) was formed by sipunculids. Almost all of sipunculid biomass (413 g/m^2) was accumulated at the station located 2000 m west of the central

dumping point (figure not shown). The benthos community here can be characterized as refugial, that is, recovering to the pre-dumping state. At the rest of the stations, the sipunculid biomass was close to zero, and the total benthic biomass did not exceed 36 g/m^2. In August, benthos biomass (6.5 g/m^2) in the dumping zone (within the 300 m radius), as in May (5.3 g/m^2), was very low; this may be due to the impact of the second dumping phase on the bottom community.

At the station located 300 m north of the dumping point, a high biomass of bivalves (3.5 g/m^2) which was being formed by the common shallow mollusks *Callista brevisiphonata* and *Turtonia minuta*, was observed (figure not shown). Finding these and some other shallow water species, such as green algae and the isopod *Arcturus crassispinis* allows us to suppose that they were discharged here with the extracted nearshore ground.

In August 2006 the mean benthos biomass was 18.2 g/m^2; the major portion of the biomass (69%) was formed by bivalves. Distribution regularities were observed in benthic group's biomass. Figure 1 shows that bivalves (*Nuculana pernula pernula*) prevailed at stations located near the dumping point (0–800 m to the west, east and north), and also 2,000 m to the north of it. Correspondingly, the post-dumping community was observed in this area.

Table 1 Comparison of benthic quantitative indices on the dumping area at different time periods.

Time period	Length of species list	N (ind./m^2)	B (g/m^2)	B (g/m^2) (radius 300 m)
August 2003	36	200	53.7	53.7
October 2004	7	13	26	26
December 2004	35	205	26.3	24.5
May 2005	15	74	5.3	5.3
August 2005	39	120	48.6	6.5
August 2006	35	68	18.2	17.5
August 2007	71	142	12	1.4

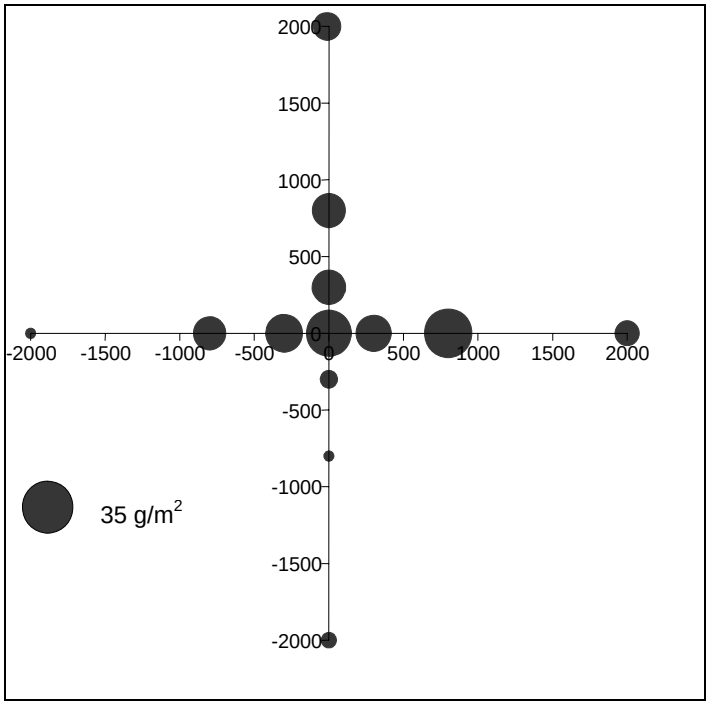

Fig. 1 Bivalve biomass distribution in August 2006 (circle scale is from absence 0 to maximum 35 g/m^2).

Maximum polychaete biomass was observed at a distance 2,000 and 800 m to the west, and 2,000 m to the east and north of the dumping point (Fig. 2); sipunculid biomass was observed 800 m to the west and east of the dumping point) (Fig. 3). Therefore, the bottom community at these stations could be characterized as refugial. In general, high biomasses (from 13 to 30 g/m^2) were observed within a radius of 300 m from the dumping point to the west, north and east. This could be considered a result of the gradual restoration of bottom biota after dumping. The mean biomass within the radius of 300 m of the dumping point was 17.5 g/m^2 which is higher than the indices of May and August 2005.

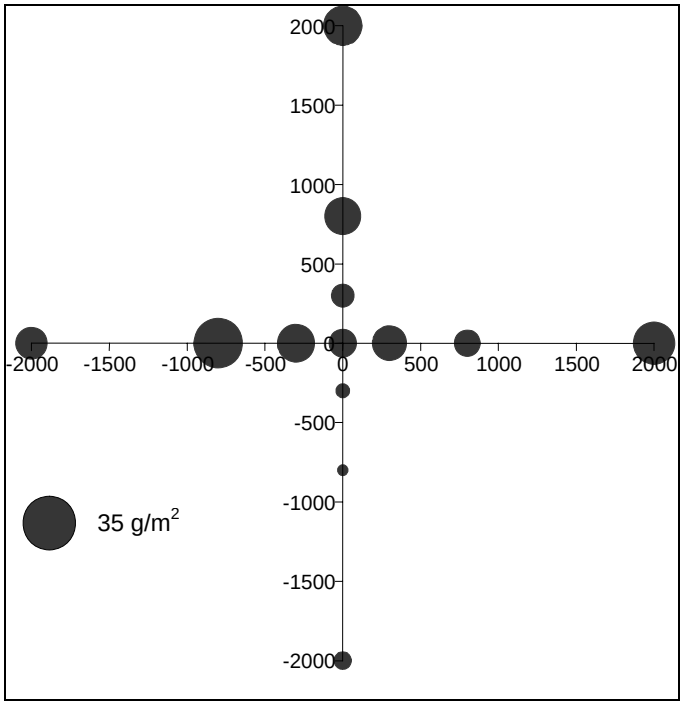

Fig. 2 Polychaete biomass distribution in August 2006 (circle scale is from absence 0 to maximum 10 g/m^2).

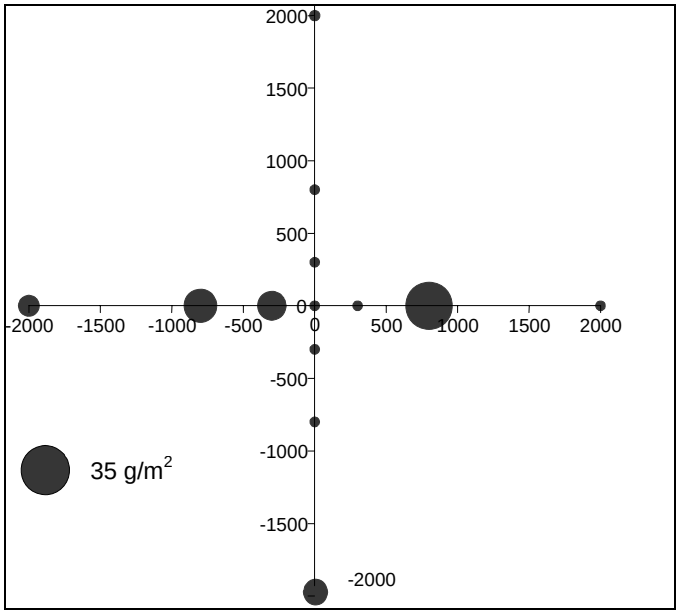

Fig. 3 Sipunculid biomass distribution in August 2006 (circle scale is from absence 0 to maximum 15 g/m^2).

Next, we compare benthos structure characteristics on the dumping area by the study periods (Table 2). In August 2005 the community structure was also close to that of the background (pre-dumping) phase (August 2003); this is supported by Shennon's index and the ABC-index. The level of cenotic and species similarity (Serensen's coefficient) with the background community was also high; this shows that there was a gradual recovery of the post-dumping benthic community similar to the background one, although the predominance of bivalves was significant. Thus, in August 2005, the negative impact of dumping on the bottom community was generally less significant than expected, and a process of recovery up to the initial pre-dumping state was progressing rapidly. However, 2007 data showed an unexpected significant change in the structure and quantitative characteristics of the benthos community.

Table 2 Comparison of benthic structural characteristics on the dumping area (radius 300 m) by different time periods.

Time period	Shennon's index		ABC-index	Cenotic similarity (2003-other) (%)	Serensen's coefficient (2003-other) (%)
	Abundance	Biomass			
August 2003	1.34	0.79	35.6	–	–
October 2004	0.71	0.11	26.4	77	12
December 2004	0.81	0.67	17	30.5	39.4
May 2005	0.94	0.25	22.5	2.9	31
August 2005	1.25	0.45	30.7	74.6	39
August 2006	0.7	0.56	5.8	12.1	53.8
August 2007	0.99	0.67	45.4	2.4	33.3

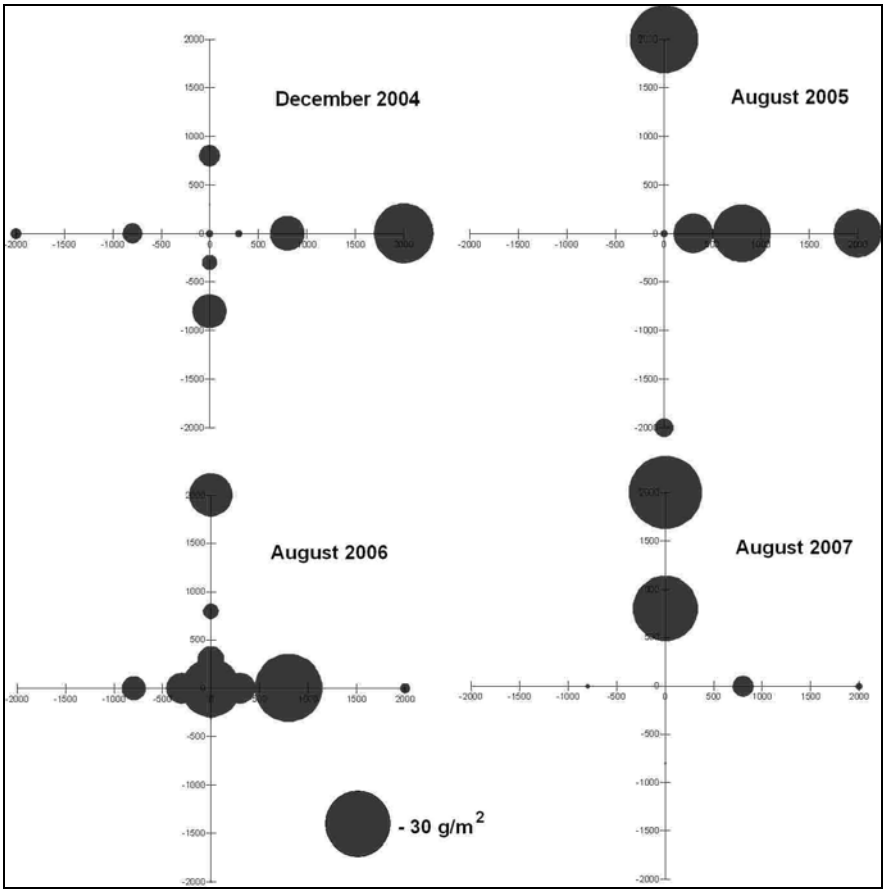

Fig. 4 Bivalve biomass distribution around the dumping site during liquid natural gas plant construction from December 2004 to August 2007 (circle scale is from absence 0 to maximum 30 g/m^2).

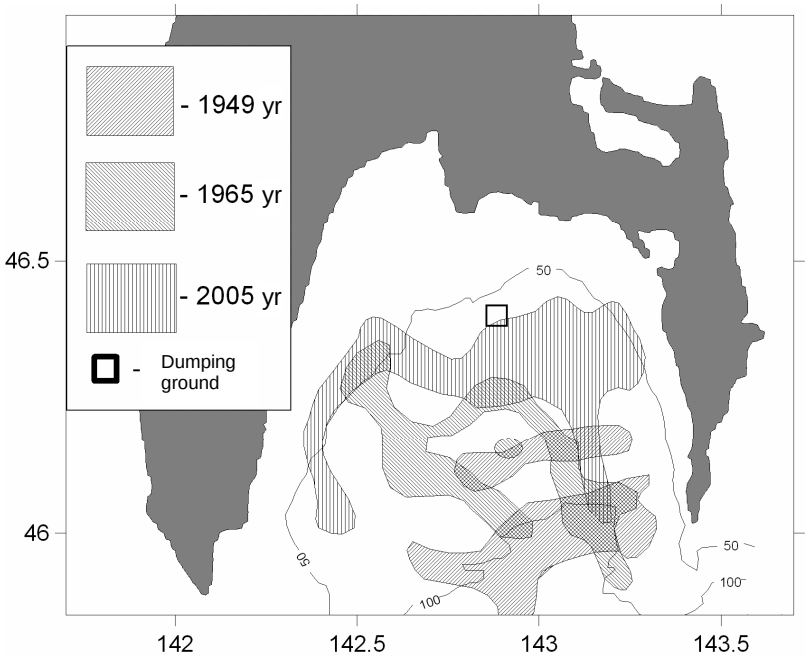

Fig. 5 *Nuculana pernula* community distribution during 1949–2005 in Aniva Bay.

In the radius of 300 m from the dumping point, low values of biomass (from 0.1 to 4 g/m^2) were observed. Such a decline in biomass was connected to the disappearance of bivalve mollusks from the dumping zone. Polychaetes became the dominant group. Structural characteristics show that the benthos community characterizes a high index of diversity and significant stability. Hence, the bottom community passes to the next level of succession. We do not know whether this reorganization was influenced by the construction. After 2005 no more dumping took place.

We next consider the distribution of the basic benthic group (Bivalvia) for different periods. Displacement of *Nuculana* sp. from the south and east to the north of the dumping ground from December 2004 to August 2007 is observed in Figure 4.

We then retrospectively analyse the distribution of the *Nuculana pernula* community in Aniva Bay. Figure 5 is a compilation of scientific, archival and our own survey data which shows the long migration of the *Nuculana pernula* community from deeper waters near the end of Aniva Bay at the middle of last century to shallower waters by 2005. The migration is accompanied by the breakup of a united area into two smaller ones (in 1949 and 1965), a change in community structure to a level of mass species and decrease of its biomass. The migration and changes of the *Nuculana pernula* community is accompanied by a simultaneous decrease in the total benthic biomass. The figure also shows that the dumping area is located on the border of a modern community. Hence, observed changes in the dumping area are connected to natural changes in the benthos.

Conclusion

The influence of ground dumping is traced only directly after impact. Later on it is masked by natural benthos changes.

Conservation of aquatic living resources under conditions of large-scale development of oil and gas resources on the Pacific continental shelf (the Sea of Okhotsk)

Julia Zaitseva

Russian Federal Research Institute of Fisheries and Oceanography (VNIRO), Moscow, Russia
E-mail: yuz@vniro.ru

According to Food and Agriculture Organization projections, high growth rates of the global human population may result in an increase in food shortages, especially in protein food products in the near future. Non-renewable energy sources are dwindling and will tend to rise in price on the world market. The use of living resources is also approaching the maximum sustainable limit. Fierce competition for securing access to biological and hydrocarbon resources is increasing among nations. Often, only the economic benefits are sought, and the conservation of natural resources and environment for future generations is relegated to environmental movements. However, effective and rational use of natural resources is the only guarantee for the well-being of humankind. It should be based on the complex estimation of natural resources and socioeconomic conditions, including regional specific features.

All over the world modernization of economies related to natural resource use, with a simultaneous increase in withdrawal of natural raw material, occurs. It is unlikely that there will be a nation that does not face problems arising from the contradicting interests of ministries and agencies, regions and economic entities whereby each side tries to gain its own benefits while ignoring the interests of society at large.

The fishing industry is, in its own way, unique. Its whole activity is based on exploitation of renewable aquatic bioresources. Thus, their sustainable existence and reproduction of bioresources in all natural water basins is a basic necessary condition without which the stable operation and development of the fisheries are impossible. The state of aquatic bioresources is directly related to the ecological situation which is formed under the influence of numerous natural and anthropogenic factors, such as climate variations, fisheries, hydro construction, engineering, navigation, mining operations, and pollution. Year by year, the anthropogenic impact becomes more and more substantial. With these conditions in mind, regular access to reliable information on the ecological status of water basins and their aquatic bioresources becomes necessary. The data on the types and scale of impacts on aquatic biota should be the basis for decision making and regulatory, legal, organizational and economical measures aimed at minimization or elimination of environmental damage caused by the anthropogenic activities.

In 1972 UNESCO formulated preliminary proposals on the establishment of the Global Environment Monitoring System. However, this system has not been created until now because of disagreements regarding the methods of monitoring, allocation of responsibilities among the existing academic and sector observational systems. The absence of progress in the organization of a system of ecological monitoring is an international problem.

The establishment of a comprehensive ecological monitoring system has become especially necessary because the extraction rate of natural resources has approached an unsustainable level. Recently, coastal regions have faced a conflict of interests between oil and gas development and fisheries on the continental shelf.

When considering the mutual influence of the oil and gas industry and fishery on the environment, the competitive aspects of this interaction are considered. The fact that hydrocarbon resource development at all stages, and even after its completion, may negatively affect aquatic resources and their habitats, is considered foremost. However, besides the direct antagonistic relationships between the oil and fishery industries, there is their indirect interaction occurring in the socioeconomic sphere.

In many coastal regions the oil and fishery industries are the most significant, and often the only components, of the economy that form the basis regional development and employment. However, both industries are based on the use of natural resources and have a number of similar economic features that should be considered when developing a long-term strategy of coastal region development.

The oil industry uses a non-renewable natural resource. To ensure the stable development of oil-producing regions in the long-term, some benefit from hydrocarbon resource extraction should be invested in the development of infrastructure, industries and agriculture in these regions to ensure the dynamic development of the region after hydrocarbon resources are depleted.

Bioresource sustainability is an erroneous notion when thinking of the possibility of stable development and maintenance of socioeconomic infrastructure of coastal regions in the long-term. However, an overview of coastal regions around the world, whose economies are based on fisheries (mainly coastal fisheries) provides evidence on the increase of socioeconomic crises. Employment in fisheries and related industries is continuously decreasing, and governments of many countries are forced to take measures to support the fishermen while making serious efforts to reduce of the number of fishing vessels.

The decrease in the abundance of commercial bioresource species due to overfishing, bycatch, illegal fisheries, disturbance of habitats, and expansion of large-tonnage expedition fleets, is considered to be one of the main reasons leading to this situation. There is no doubt that all these events exist. However, even their complete elimination, and recovery of stocks to optimal levels, do not guarantee the stable development of fishery-dependent regions.

The fishery industry is different from other industries, in which the increase in labor productivity is reached due to the introduction of innovative technologies, high-productive equipment, use of improved materials, *etc*. The increase in production for the fishery industry means only the increase in catch per fisherman. However, the volume and cost of the natural bioresource base, even renewable and maintained at an optimal level, are limited.

In most coastal regions of most developed countries, the fishery industry has failed to provide the financial benefits necessary to fully develop the regional economy and proper resource-saving production. This is because the fisheries on most abundant species are not super-profitable, and the most in-demand and high-value species of aquatic resources are now utilized to the full extent.

The development of the richest shelf oil and gas fields that make large profits should provide the source of investment necessary to ensure the future development of coastal areas. For this to happen, it is necessary to develop a mechanism for withholding some part of the profit by governments in the form of natural rent, to be saved in specialized funds for regional development. It may also be possible to exempt part of the profit from taxation on condition that it be invested in the development of regional economy.

Reasonable planning of oil and fishery industry development should be based on the principle of a balanced management of coastal zones, providing for common interests of users of different resources in both economic and environment protection areas. Making a profit should not be a top priority. For example, in the case of hydrocarbon development on the West Kamchatka shelf, it is necessary to take into account the natural uniqueness of this region and to ban, by law, the exploration and development of resources in the area.

In a balanced approach to natural resource exploitation, the oil and gas industry damage done to the fishery may ironically favor its conservation by creation of alternative employment sources for populations living in coastal regions through the gradual decrease in fishing pressure on aquatic bioresources, and by investing revenue received from the oil and gas industry into environment-oriented projects, including monitoring and protection of aquatic bioresources.

Regarding the organization of efficient ecologic–fishery monitoring, an absence of basic ecological data prevents the reliable identification of anthropogenic components, among other factors, that cause changes in the environment and degradation of aquatic ecosystems. As a result, instead of the harmonious development of natural resources, inter-sectoral disputes emerge resulting in economical and social crises and unavoidable losses for all competing sides.

Debates regarding the causes and amount of damage to living resources determine that the causal relationship between committed actions and the following adverse consequences, or appearance of substantial damage to the environment and human health, is of great importance. It is necessary to find out if these adverse consequences are caused by other factors, including natural factors, and if they occur independently of industrial operations and states of crisis.

Planned sustainable use of natural resources should be made in a stepwise manner. It should include a definition of the purpose of living and non-living resource exploitation, taking into account local specific ecological features, and provide a selection of optimal alternatives and suggest the possibility of planned improvement. The need becomes obvious for developed ecological management within oil and gas producing companies not only during exploratory surveys, planning and designing of industrial complexes, but for the lifetime of the operations until resource depletion.

The initiative and activities of industry, rather than a system of strict governmental management, control and supervision, are the most effective conditions for mutually profitable non-crisis development of the oil and gas producing industry, and fisheries. Fishery companies aiming at long-term development and promotion of urban development should also be interested in maintaining their good reputation by allowing them to obtain cheap credit at banks, *i.e.*, strengthen their positions under the fierce competition. Thus, the participation in a system of ecological monitoring should become necessary for both oil workers and fishermen.

Figure 1 shows the organization of ecologic and fishery monitoring. To obtain reliable information about the status of aquatic bioresources and their habitats, and industrial processes affecting the environment, the free exchange of information, extensive discussions of emerging issues and joint managerial decision making are necessary.

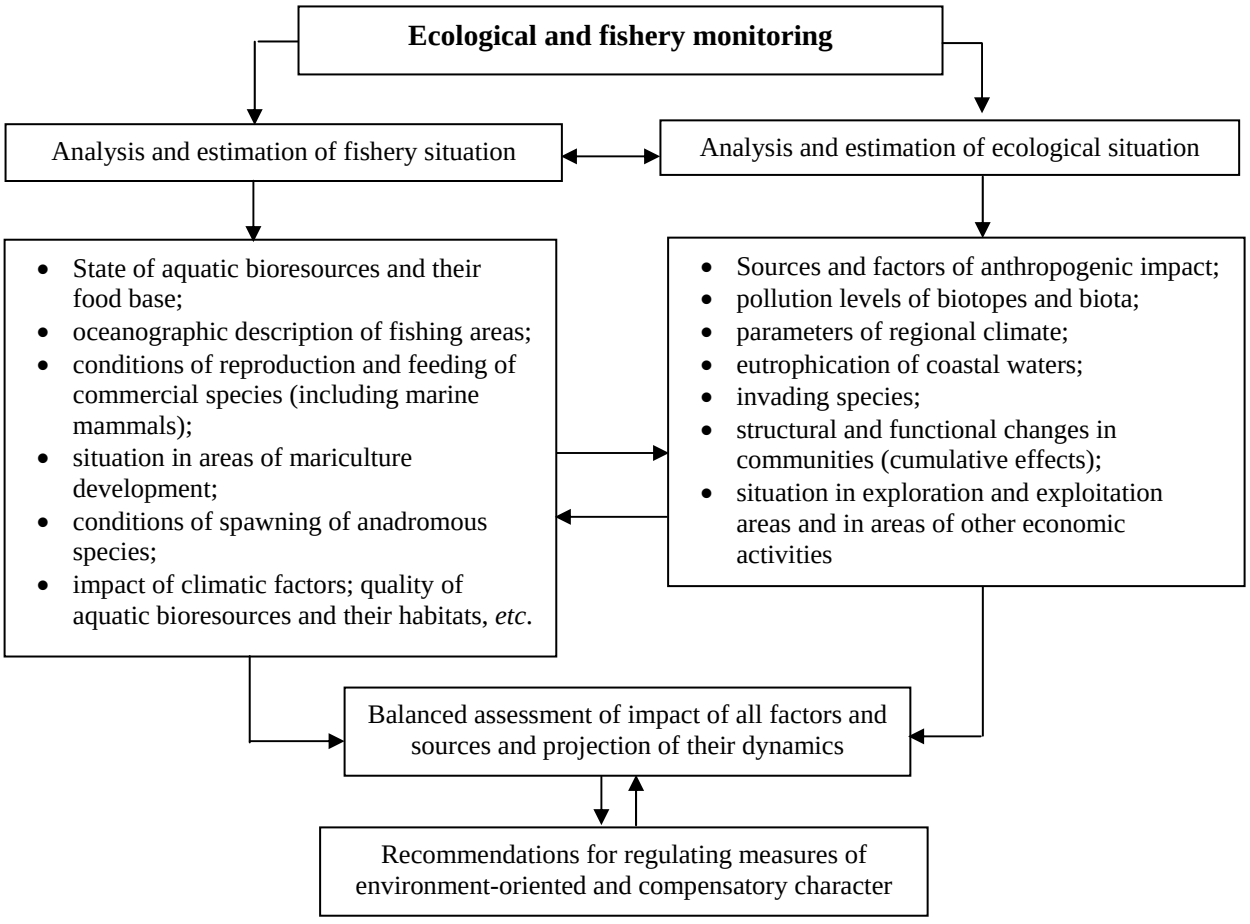

Fig. 1 Scheme of organization of ecological and fishery monitoring.

A stable environment and successful development of the fishery industry as a specific sector of the national economy plays an important role in guaranteeing a secure food supply, and the development and maintenance of a socioeconomic infrastructure in coastal regions. Hence, the strategy of effective resource-conserving natural management is needed, taking into account the conservation of aquatic biological resources and their habitats. Minimization of the growing anthropogenic impact to the marine ecosystem is actual recently and should be managed at the governmental level. For this to happen, it would be expedient to establish consultative bodies which would include representatives of legislative and executive powers, industrial companies, and scientific organizations to ensure the operation of the specific sectors of economy and environment-oriented organizations.

Understanding the danger of taking an antagonistic approach to resource development by nature-oriented structures results from the fact that the stability of environment, natural-resource potential and guaranteed right of future generations to clean environment would otherwise be jeopardized.

Only by the formulation of a common purpose and through the consolidation of efforts by the whole world community are we able to guarantee the diminishing negative anthropogenic impact on marine ecosystems and bioresources, and development of effective exploitation of natural resources.

Session B2

Walleye pollock

Session Chairs

Yasunori Sakurai, Alexander Varkentin and Vladimir Kulik

Walleye pollock (*Theragra chalcogramma*) spawning in the Okhotsk Sea waters off the north Kuril Islands and south-western Kamchatka

Alexander V. Buslov and Alexander I. Varkentin

Kamchatka Research Institute of Fisheries and Oceanography (KamchatNIRO) and Marine Commercial Fishes Laboratory, Petropavlovsk-Kamchatsky, Russia
E-mail: buslov@kamniro.ru, varkentin@kamniro.ru

Abstract

Long-term analysis of ichtyoplankton surveys and growth data indicates that the Okhotsk Sea waters off the north Kuril Islands and south-western Kamchatka is the traditional spawning region of walleye pollock of east Kamchatka origin. In this area the spawning "peak" occurs later than in western Kamchatka waters from the end of April to the beginning of May. So, it is necessary to conduct an additional ichtyoplankton survey at the end of April in order not to underestimate part of the walleye pollock stock.

Introduction

Walleye pollock is one of the most numerous fish species in the North Pacific and is a very important fishery resource. The Okhotsk Sea is a main pollock fishery region. In 1992 the total catch was about 2.7 million metric tons. In the last 5 years it has averaged 0.6 million metric tons.

A great deal of attention is always given to studying walleye pollock biology, stock dynamics, and especially reproduction because:

- Spawning conditions define the efficiency of reproduction leading to generation abundance;
- The walleye pollock fishery in the Okhotsk Sea occurs during the prespawning and spawning periods when the pollock form dense aggregations accessible for fishing;
- Stock estimations and total allowable catch forecasts are based on egg survey data obtained in the period near the spawning peak.

In the eastern part of the Okhotsk Sea ichtyoplankton surveys have been conducted annually by KamchatNIRO since 1972, and from TINRO-Center since 1982. Standard stations grids are used.

The spawning grounds in the Okhotsk Sea have been known for a long time (Fadeev, 1987; Shuntov *et al.*, 1993; Zverkova, 2003) and are located (Fig. 1, counterclockwise from bottom) in the waters of the south Kuril Islands and Hokkaido island; in the waters adjacent to western Kamchatka, including Shelikhov Gulf; in the northwestern part of the Okhotsk Sea; and nearby north-east Sakhalin island.

In the northern part the Okhotsk Sea the center of walleye pollock reproduction is located on the west Kamchatka shelf. In this area, time and location of spawning vary from year to year depending on the temperature conditions (Fadeev and Ovsyannikov, 2001; Varkentin *et al.*, 2001). Reproduction continues from January till July. The average peak of spawning in this region is from the end of March to the beginning of April (Fadeev, 1987).

It is interesting to note that in the beginning of April in the area to the south of 52°N, walleye pollock egg catches are minimal (2–3 eggs/m^2) despite the high concentrations of mature fish there. Is it probable that in this area spawning proceeds later than in the western Kamchatka waters? Some researchers (Fadeev and Ovsyannikov, 2001) have noticed that in the south-western Kamchatka waters usually two spawning peaks, so-called "spawning waves", occur: in the beginning and at the end of April.

Could it be that walleye pollock spawn in the Okhotsk Sea waters off the north Kuril Islands too? Having analyzed archival materials from 1961 to the present, we found that ichtyoplankton surveys have been made here only in the end of March, or in July. These and other questions are the subject of our research.

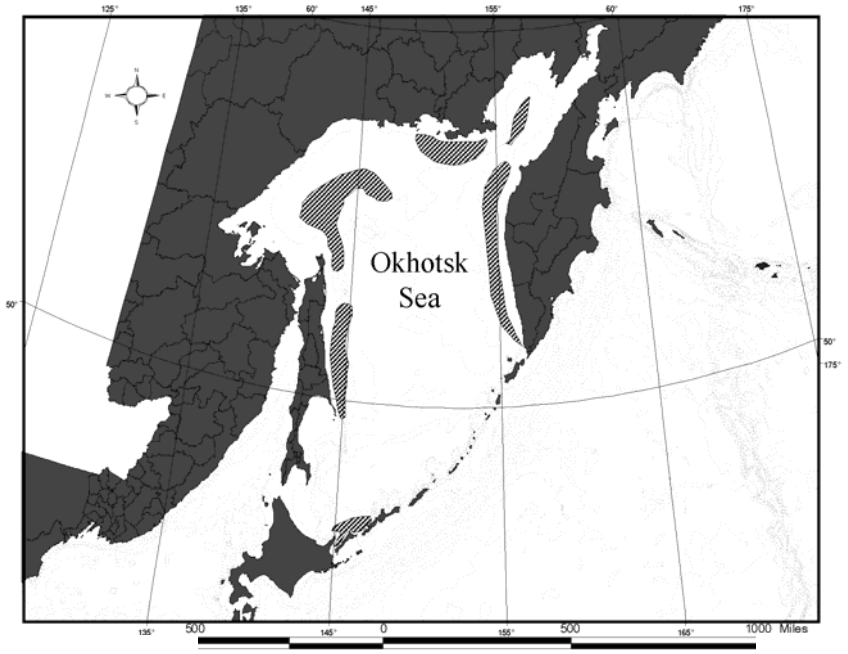

Fig. 1 Walleye pollock spawning grounds (hatched pattern) in the Okhotsk Sea.

Data and Methods

This work is based on ichtyoplankton surveys conducted in 2007–2008 in the Okhotsk Sea waters off the north Kuril Islands and near western Kamchatka (Table 1, Fig. 2).

An ichtyoplankton Conic Net (ICN-80) was used. Egg collections were obtained from 300 m depth to the surface or from bottom to the surface, if depth was less than 300 m. The net was lifted at a speed 0.5–0.6 m/s.

Stages of development of walleye pollock eggs were defined by the Rass scale (Rass and Kasanova, 1966). Total embryogenesis duration was calculated using the equation of Zolotov *et al.* (1987):

$$T = 38.9e(-0.156\ t).$$

Stage I was 20% of embryogenesis duration (Gorbunova, 1954). Total egg production for the entire spawning season was counted by the Gauss curve (Buslov *et al.*, 2004). In addition, we analyzed data from ichtyoplankton surveys made in western Kamchatka waters later than April 20 between 51° and 58°N latitudes (Table 2).

Table 1 Period and number of stations where ichtyoplankton surveys were conducted in the Okhotsk Sea waters off the north Kuril Islands and near western Kamchatka in 2007–2008.

Region	Period	Number of stations
Western Kamchatka	April 12–18, 2007	72
	April 26–28, 2008	38
Okhotsk Sea waters off north Kuril Islands	April 29–30, 2007	17
	April 26–28, 2008	38

Table 2 Period and number of stations where the ichtyoplankton surveys were conducted in western Kamchatka waters later than April 20.

Year	Period	Number of stations
1978	April 24–30	68
1983	April 24–May 3	89
1984	April 24–May 9	125
1985	May 16–25	111
1986	May 26–June 6	109
1992	May 12–23	99
2001	April 25–30	80
2001	July 2–30	56
2002	April 23–May 9	105

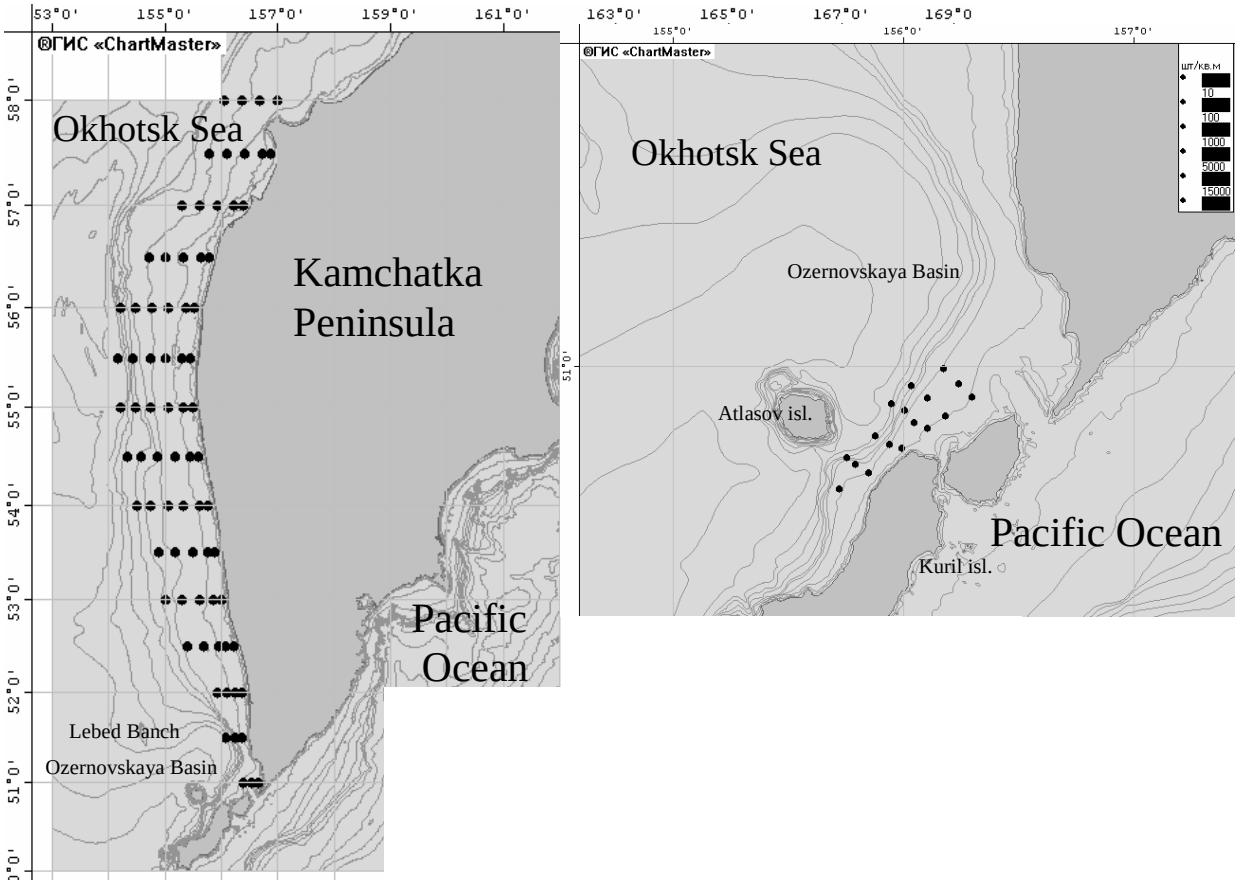

Fig. 2 Standard ichtyoplankton station grid (left) in western Kamchatka waters (from 1972) and additional stations (right) in Okhotsk Sea waters off the north Kuril Islands (from 2007).

Results and Discussion

Relative centers of spawning were determined by the concentrations of stage I eggs. In the western Kamchatka waters, the duration of stage I eggs varies from 7 to 10 days, depending on temperature (Zolotov *et al.*, 1987). Most of the walleye pollock eggs and larvae develop within a quasi-stationary current circulation system created by the West Kamchatka and Compensate Currents (Karmanov, 1982; Vasilkov and Glebova, 1984; Zolotov, 1991; Varkentin *et al.*, 2001).

In the middle of April 2007, egg distribution in the western Kamchatka waters appeared typical. The main concentrations of stage I eggs were found between 53° and 56°N latitudes. The relative center of spawning was at 53°N latitude at a depth of 90 m (Fig. 3). We consider that had the survey been made after the spawning peak, more than 30% of all eggs would be at stage II (Table 3). It is worth noting that south of the research area, egg collections were minimal: about 10 eggs/m^2 despite the high concentrations of mature fish.

An additional survey conducted in the north Kuril Islands area at the end of April shows that there was intensive spawning in this region (Fig. 4; Table 3). Concentrations of stage I eggs reached 12,000 eggs/m^2 at a depth of 80 m. It is the first time that such high egg concentrations have been found in this area.

In 2008 walleye pollock spawning in the Okhotsk Sea waters off the north Kuril Islands and south-western Kamchatka waters also occurred at the end of April, but the area of highest egg concentrations was situated further to the north compared to 2007 (Fig. 5, Table 3).

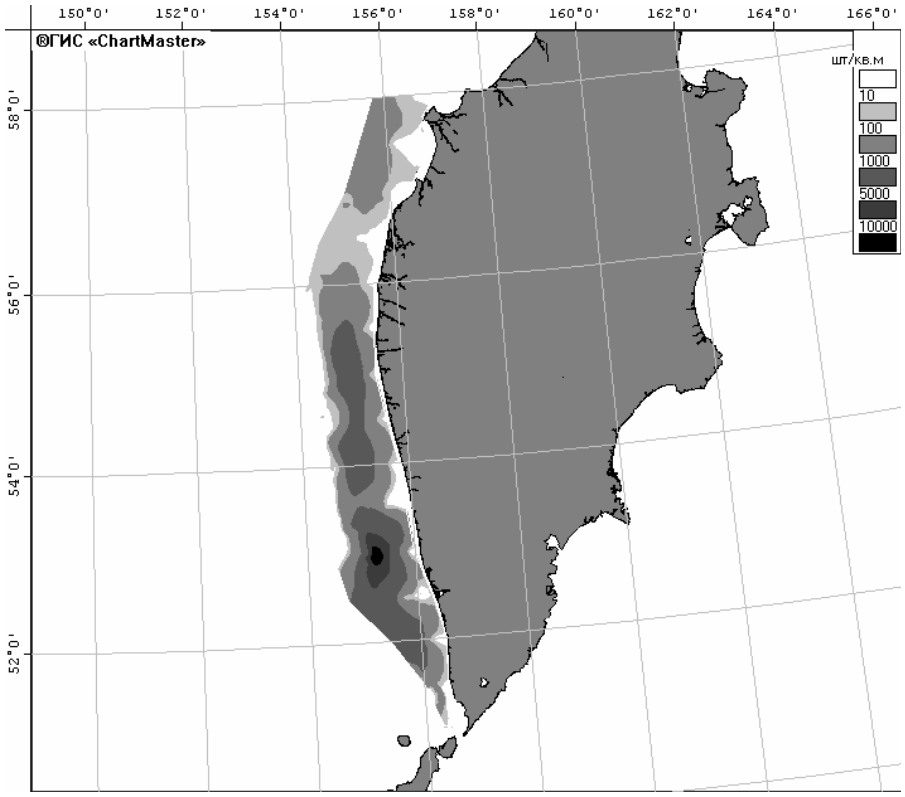

Fig. 3 Walleye pollock eggs on I stage distribution (eggs/m^2) in the west Kamchatka waters during the period April 12–18, 2007.

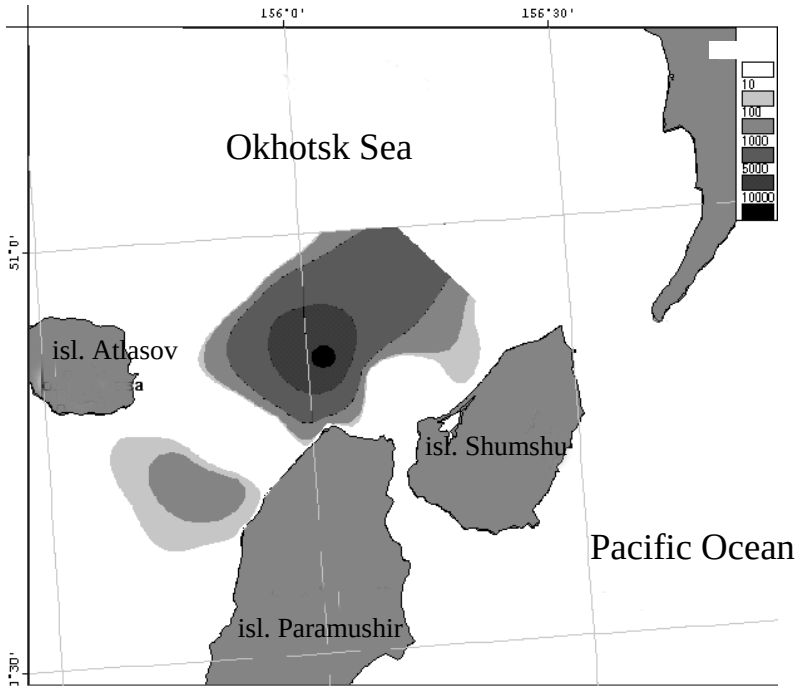

Fig. 4 Stage I walleye pollock egg distribution (eggs/m^2) in the Okhotsk Sea waters off the north Kuril Islands during the period April 29–30, 2007.

Table 3 Walleye pollock eggs composition (%) in 2007–2008.

Region	Average survey date	Stage I	Stage II	Stage III	Stage IV
	2007				
Western Kamchatka	April 15	56.6	31.2	11.4	0.8
Okhotsk Sea waters off the north Kuril Islands	April 30	87.7	12.2	0.1	+
	2008				
Okhotsk Sea waters off the north Kuril Islands and south-western Kamchatka waters	April 27–28	18.8	72.3	8.3	0.7

Note: + indicates less than 0.01%

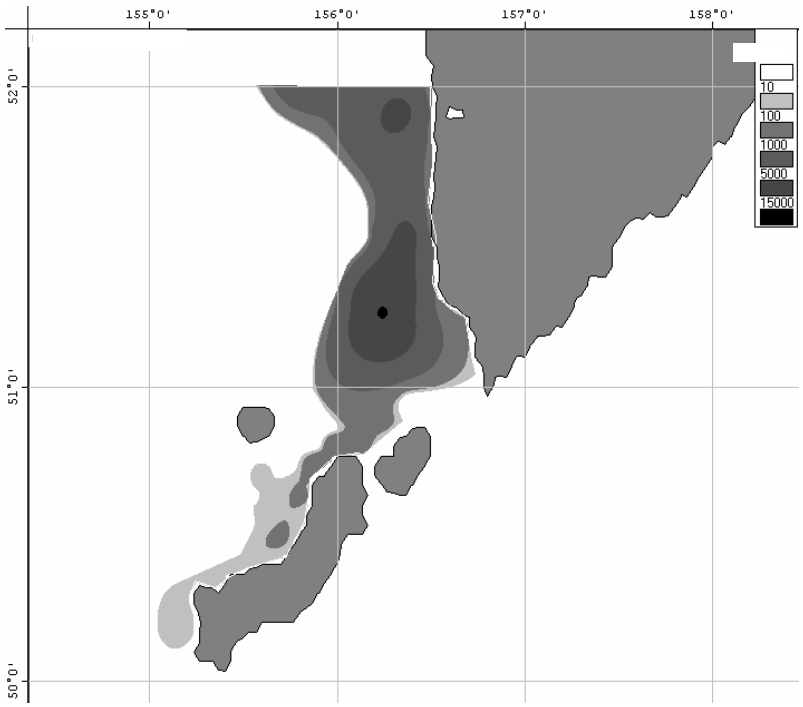

Fig. 5 Stage I walleye pollock egg distribution (eggs/m^2) in the Okhotsk Sea waters off the north Kuril Islands and in the south-western Kamchatka waters during the period April 26–28, 2008.

How much spawning occurs regularly in nearby south-western Kamchatka? We analyzed data of ichtyoplankton surveys made in the western Kamchatka waters later than April 20 for the period 1978 to 2002. Figure 6 clearly shows that in all years there was intensive walleye pollock spawning here. Considering their high migratory activity, it is quite probable that pollock from elsewhere spawn in this region.

The nearest walleye pollock spawning grounds are situated in the south-eastern Kamchatka and north Kuril Islands waters (Fig. 7) which are inhabited by the East-Kamchatka population (Buslov and Tepnin, 2007). Intensive spawning occurs at the end of April to the beginning of May, which is approximately at the same time as at south-western Kamchatka. There appear to be no geographical barriers to walleye pollock migrations from this region to the Okhotsk Sea. They can migrate into the Okhotsk Sea through the north Kuril Islands straits with the East Kamchatka Current (Fig. 8).

For proof of this hypothesis, we made a size-at-age analysis because it is known that the rate of pollock growth in the eastern part of the Okhotsk Sea is lower than in the east Kamchatka area (Buslov, 2003). A selection was made of 6-, 7-, 8-year-old

mature fishes caught in three different regions in the period from February until April:

1) To the north from 53°N in the western Kamchatka waters;
2) To the south from 53°N in Okhotsk Sea waters off the north Kuril Islands and in the south-western Kamchatka waters;
3) To the south from 52°N in Pacific Ocean waters off the north Kuril Islands and in the south-eastern Kamchatka waters.

As noted in Figure 9, the size structure of pollock is different by regions, and is connected with distinct rates of growth. The southeast region (3) has the largest average length-at-age pollock, the western Kamchatka region (1) has the smallest average size, and south-western Kamchatka (2) is intermediate (Table 4). Differences were statistically significant among all regions within age class, except between regions 2 and 3 for 8-year olds (Table 5).

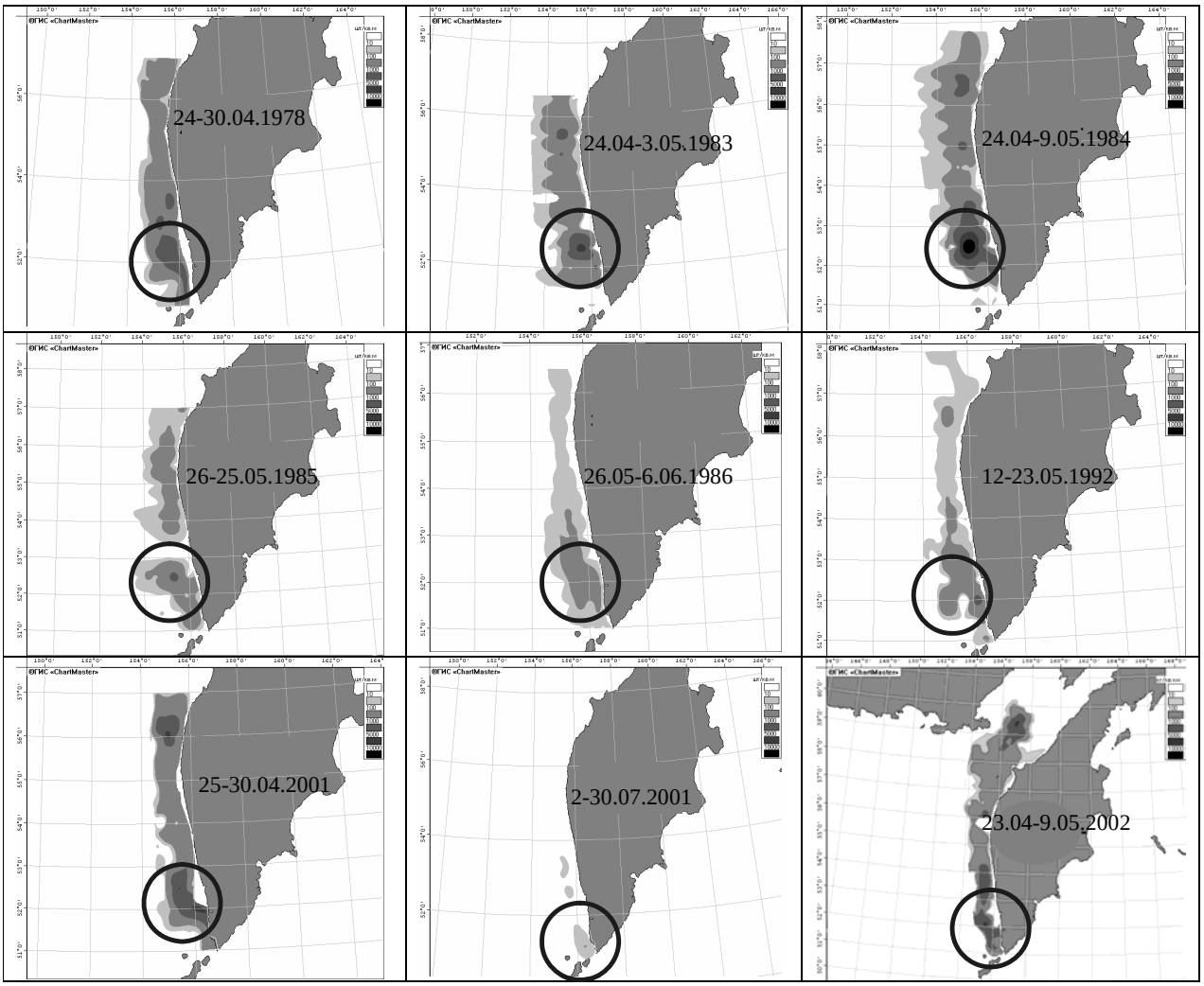

Fig. 6 Interannual stage I walleye pollock egg distribution (eggs/m^2), indicated by the circles, in the south-western Kamchatka waters later April 20 for the period from 1978– 2002.

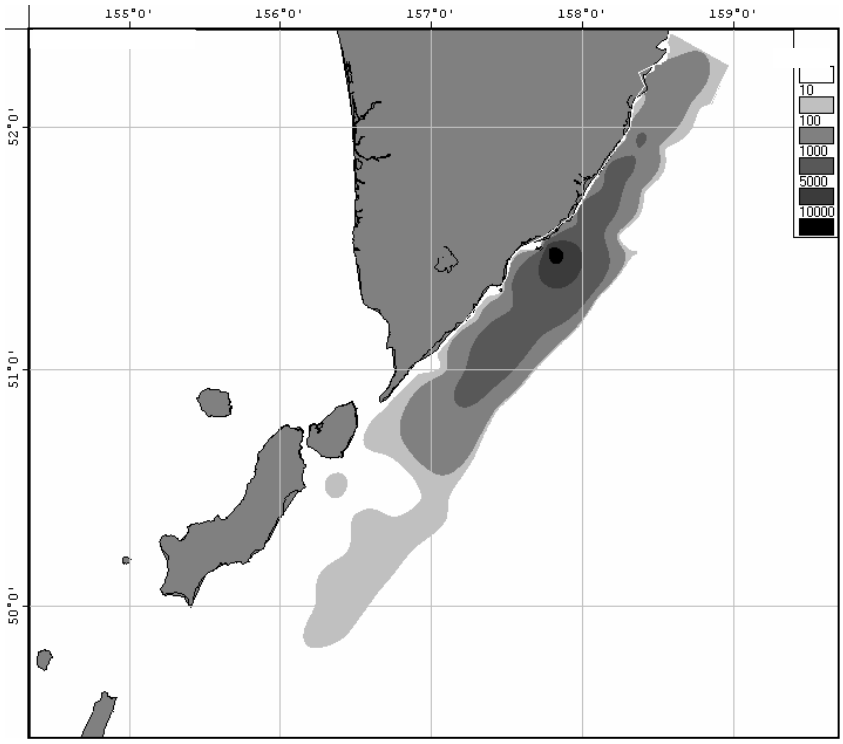

Fig. 7 Stage I walleye pollock egg distribution (eggs/m^2) in the waters adjacent to south-eastern Kamchatka and north Kuril Islands April 25–27, 2007.

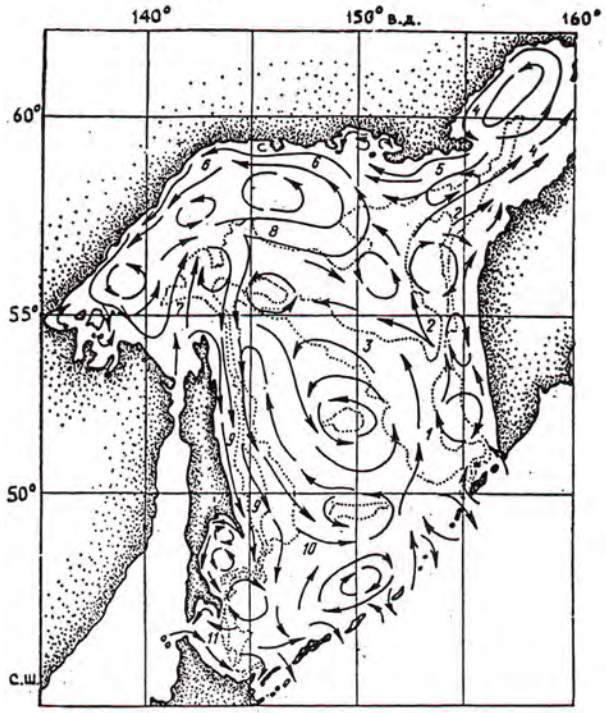

Fig. 8 General currents scheme in the Okhotsk Sea and Kuril Islands area (Chernyavsky *et al.*, 1993). 1 – West Kamchatkan Current, 2 – Northern Branch, 3 – Median Current, 4 – Penzhin Current, 5 – Yamskoye Current, 6 – Northern Okhotsk Current, 7 – Amursky Current, 8 – Northern Okhotsk Counterflow, 9 – East Sakhalin Current, 10 – Northeastern Current, 11 – Soya Current, 12 – East Sakhalin Counterflow.

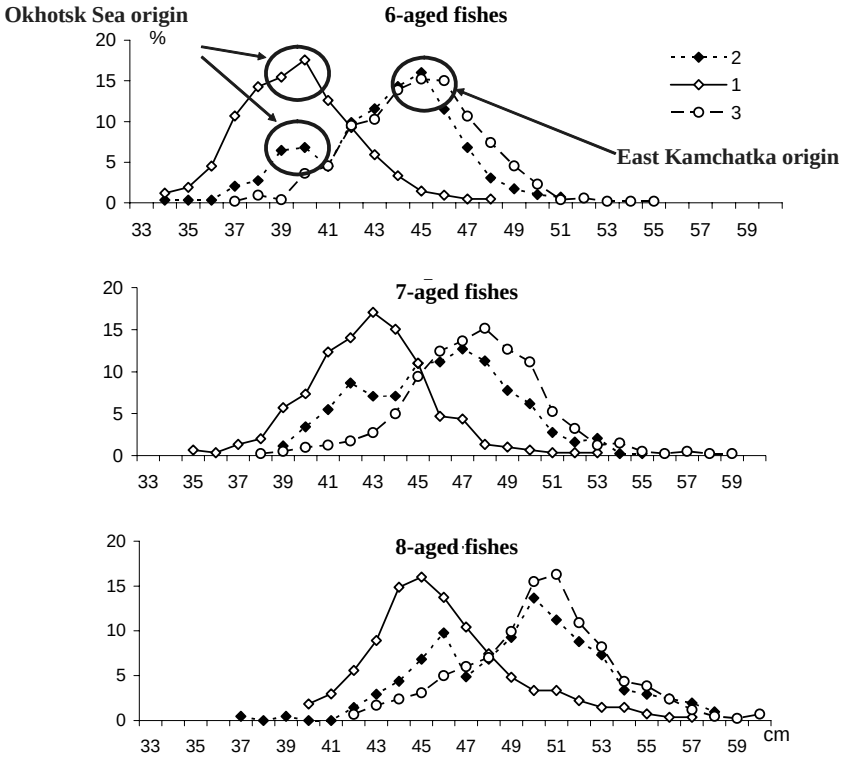

Fig. 9 Walleye pollock size composition at ages 6 to 8 years by statistical region from 2005–2007.

Table 4 Average walleye pollock length (cm) at ages 6 to 8 in February–April for the period 2005–2007, by statistical regions.

	Region								
	1			**2**			**3**		
	Age (year)			**Age (year)**			**Age (year)**		
	6	7	8	6	7	8	6	7	8
N	421	299	269	294	438	205	526	614	414
M	39.21	42.36	45.49	42.75	45.29	48.84	44.40	46.56	49.20
δ	2.51	2.75	3.20	3.03	3.25	3.77	2.73	3.09	3.65

Notes: 1 – western Kamchatka, 2 – south-western Kamchatka, 3 – south-eastern Kamchatka
N – sample size, *M* – average length (cm) , δ – standard deviation

Table 5 Values of Student *t*-criterion in comparison analysis.

	6-year olds			**7-year olds**			**8-year olds**		
	Region			**Region**			**Region**		
Region	1	2	3	1	2	3	1	2	3
1	–	17.02	30.53	–	12.79	20.00	–	10.47	13.59
2	–	–	7.86	–	–	6.41	–	–	1.15

Notes: 1 – western Kamchatka, 2 – south-western Kamchatka, 3 – south-eastern Kamchatka
Correlation is significant at $p < 0.05$ for underlined values.

Despite the long period of walleye pollock study in the Okhotsk Sea, we are just now learning something new about its biology. It is necessary to improve the ichtyoplankton survey method in view of this new knowledge by conducting a second survey in the Okhotsk Sea waters off the north Kuril Islands and in south-western Kamchatka (to the south of 53°N) at the end of April. Otherwise, part of the walleye pollock stock spawning in this area later than in the west Kamchatka waters will be underestimated.

By our assessment, the spawning stock biomass in 2007 in the Okhotsk Sea waters off the north Kuril Islands was about 45,000 metric tons. This allows us to recommend about an additional 9,000 metric tons for a coastal fishery by Danish seine vessels. It is very important for coastal fishery development in this region.

Conclusions

Okhotsk Sea waters off the north Kuril Islands and south-western Kamchatka area is the traditional spawning region of walleye pollock of east Kamchatka origin. In this area a pollock spawning "peak" occurs later than in the western Kamchatka waters at the end of April–beginning of May.

It is necessary to conduct a second ichtyoplankton survey in Okhotsk Sea waters off the north Kuril Islands and in the south-western Kamchatka waters at the end of April. New data will give us the means to develop the walleye pollock fishery in the south-western Kamchatka waters.

References

Buslov, A.V. 2003. Walleye pollock growth and size-age composition of its populations. Dissertation abstract, Candidate of Biol. Science, TINRO, Vladivostok, 24 p.

Buslov, A.V. and Tepnin, O.B. 2007. Walleye pollock spawning in the north Kuril Islands area and south-eastern Kamchatka waters. Investigations of the marine resources nearby Kamchatka peninsula and in the North Pacific area. KamchatNIRO Publishers. Petropavlovsk-Kamchatsky I. 8.

Buslov, A.V., Tepnin, O.B. and Dubinina, A.Y. 2004. Some peculiarities of walleye pollock spawning and embryogenesis in the east Kamchatka waters. *TINRO News* **138**: 282–298.

Chernyavsky, V.I., Zhigalov, I.A. and Matveev, V.I. 1993. Oceanographic bases for the high productivity zones in the Sea of Okhotsk. Seas hydrometeorology and hydrochemistry. "Seas" project. V. IX. Sea of Okhotsk. I. 2. Hydrochemical Conditions and Oceanographic Basis of Biology Productivity. Hydrometeo Press, St. Peterburg, pp. 157–160.

Fadeev, N.S. 1987. Walleye pollock spawning time and location in the northern part Sea of Okhotsk. Walleye Pollock Population Structure, Stock Dynamics and Ecology. TINRO, Vladivostok:, pp. 5–22.

Fadeev, N.S. and Ovsyannikov, E.E. 2001. Walleye pollock distribution and spawning dynamics in the northern part Sea of Okhotsk in winter-spring period. *TINRO News* **128**: 103–124.

Gorbunova, N.N. 1954. Walleye pollock spawning and development. Institute of Oceanography Issues, Vol. 11, pp. 132–195.

Karmanov, G.E. 1982. Some peculiarities of current dynamics during walleye pollock spawning in the west Kamchatka waters. Ecology and spawning conditions of fishes and invertebrates in the Far-Eastern Seas. TINRO, Vladivostok, pp. 3–10.

Lisovenko, L.A. 2000. Reproduction of fishes with interrupt embrioginesys and portion spawning for Walleye pollock nearby west Kamchatka. VNIRO, Moscow, 112 pp.

Rass, T.S. and Kasanova, I.I. 1966. Methodical Guide on Eggs, Larvae and Fry Gathering. Food Industry, Moscow, 42 pp.

Shuntov, V.P., Volkov, A.F., Temnykh, O.S. and Dulepova, E.P. 1993. Walleye pollock in the ecosystems of Far-Eastern Seas. TINRO, Vladivostok, 426 pp.

Varkentin, A.I., Buslov, A.V. and Tepnin, O.B. 2001. Some peculiarities of Walleye pollock spawning and eggs distribution in the west Kamchatka waters. *TINRO News* **128**: 177–187.

Vasilkov, V.P. and Glebova, S.Y. 1984. Factors defined Walleye pollock generations abundance in the west Kamchatka waters. *Ichthyol. Issues* **24**: 561–570.

Zolotov, O.G. 1991. Walleye pollock eggs distribution and drift in the west Kamchatka waters. Investigations and Stock Dynamics of Marine Commercial Fishes in the West Kamchatka Shelf. I. 1. Part 1, Petropavlovsk-Kamchatski, pp. 167–182.

Zolotov, O.G., Kachina, T.F. and Sergeeva, N.P. 1987. Walleye pollock stock estimation in the eastern part Sea of Okhotsk. Walleye Pollock Population Structure, Stock Dynamics and Ecology. TINRO, Vladivostok, pp. 65–73.

Zverkova, 2003. Walleye pollock. Biology, Stock Abundance. TINRO, Vladivostok, 248 pp.

Responses of relative abundance of dominants in fish communities to the Sea of Okhotsk climate variability

Vladimir Kulik

Pacific Fisheries Research Centre (TINRO-Centre), Vladivostok, Russia. E-mail: vladicon82@gmail.com

Summary

The dynamics of the relative abundance of dominant species and the dynamics of the factor scores of all the rest of the species of nekton in the upper and entire epipelagic layers is studied by years, according to the data of the summer and autumnal comprehensive ecosystem studies of the Sea of Okhotsk (1984–2006). Time-spatial differences in the discovered agreements of the fluctuations of relative abundance of species, abstractly have been the factors of multivariate analysis, with the dynamics of the number of sun spots. Climate Indices of the Northern Pacific, hydro- and atmospheric principal components and EOFs of the Sea of Okhotsk are discussed. Perceptible deviation of biotic factor scores noted in 1990, 1991 and 1997, 1998. Strong ($|R| \geq 0.8$) and statistically significant ($p < 0.05$) correlations between changes of relative abundance of species and abiotic factors of environment with a time-lag up to 6 years are extremely rare and most of them appeared as a result of analyzing data samples with a big proportion of common null values. A great role of casual variations is assumed. Attempts to use moving average and autocorrelation functions during time series analysis in most cases fail because there are a lot of gaps in the short time series (less than 25 years) we have. Even the successful one is useless yet because of a big confidence interval which is greater than the observed variability.

Introduction

Shuntov (1986) made a successful forecast for the long-term fluctuation in abundance of the main species in the Far Eastern Seas. Shuntov and his adherents considered that environmental changes were influenced by cosmic and climatic cyclicity. Some TINRO-Centre scientists believe that, in general, the higher trophic levels have sufficient resources for the consumers in the Sea of Okhotsk (Shuntov *et al.*, 1990; Temnykh *et al* 2003), despite the fact that in some regions during certain years there was a high demand for the resources (Kuznetsova, 2005; Chuchukalo, 2006). The study of Far Eastern Seas ecosystems has been based on independent data from commercial fishery scientific surveys, conducted in the late 1970s. Scientists from the Laboratory of Applied Biocenology, TINRO-Centre, processed millions of these records to filter out and normalize the most valuable data to build a new Geo Informatic System and Biological DataBase (BioDB) with datasets of acceptable quality for year-to-year comparisons, independent of the instruments and methods used. The first results of BioDB data processing and analysis, with a 5-year smoothing of selected datasets, were presented in the series of atlases and collection of tables edited by Shuntov and Bocharov (2003a, b). The Laboratory of Applied Biocenology is also trying to determine how the interannual variability of values in our BioDB can be used to forecast short time series. This work describes the use of the correlation method for time series analyses.

Biological patterns

Because of the lack of data for some years, we had to combine some time series from 7 biostatistical regions of the Sea of Okhotsk (Fig. 1); some data were also excluded. The number of sampling stations grouped by region from 1984 to 2006 is shown in Table 1.

The next task was to choose an abstraction method for presenting more then 300 registered marine species. It is almost impossible to describe all selected data records; therefore a principal components analysis (PCA) was used to extract the main factors in biomass fluctuation of communities. Main fish species were not associated with any such factor. Therefore, dominant fish communities were analyzed separately. All biological data sets were normalized by a logarithmic function ($\lg(m + 1)$, where m is kg km^2).

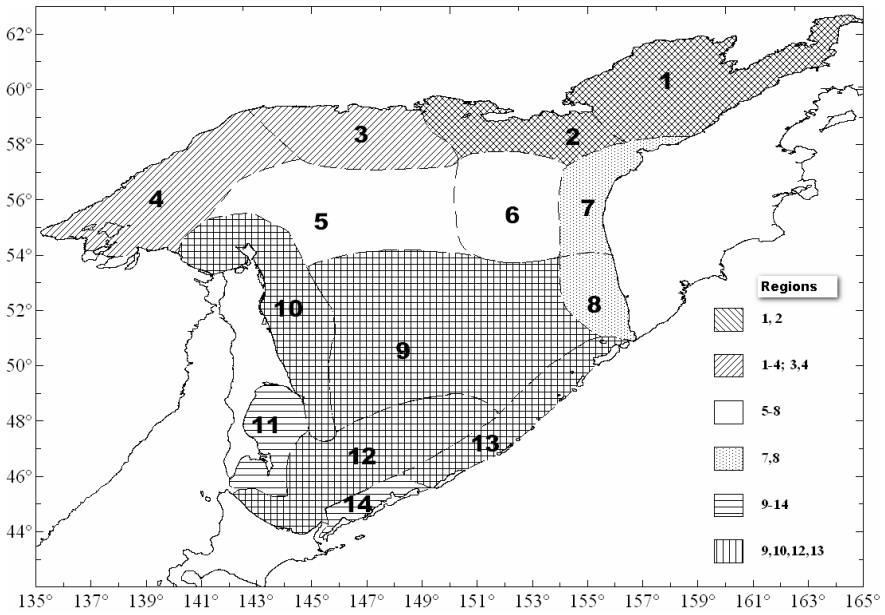

Fig. 1 Grouping of biostatistical regions in the Sea of Okhotsk.

Table 1 Number of samples (the number of stations) in each of seven observational series.

Year	Summer				Fall		
	Upper pelagic layer			Pelagic layer	Upper pelagic layer	Pelagic layer	
	Regions* 1–2	Regions 5–8	Regions 9–14	Regions 3–4	Regions 9, 10, 12, 13	Regions 1–4	Regions 7–8
1984	–**	–	–	–	3	28	10
1985	–	–	–	–	17	42	21
1986	4	15	20	24	–	–	–
1987	–	–	–	–	5	35	–
1988	18	22	26	9	–	–	–
1989	–	–	–	–	–	–	–
1990	–	–	–	–	–	9	14
1991	–	33	79	–	23	–	6
1992	4	64	50	–	–	–	–
1993	–	–	147	–	–	22	–
1994	13	54	86	–	19	11	–
1995	26	36	207	–	19	–	–
1996	–	45	84	–	–	–	–
1997	12	35	27	8	–	–	–
1998	–	–	24	20	36	26	21
1999	–	–	30	14	38	19	14
2000	–	–	32	19	44	23	22
2001	–	–	41	21	47	36	14
2002	–	–	37	10	27	13	–
2003	–	–	–	–	–	–	–
2004	–	–	–	–	44	35	–
2005	–	–	–	–	–	–	–
2006	–	–	–	–	46	13	–

* Scheme of combining biostatistical regions used here is taken from Figure 1.
** No data available, or the number of stations is less then 3.

Regime shifts in total abundance of nekton in the Sea of Okhotsk

It is known that there were some significant regime shifts of the Principal Component (2) SST index in the North Pacific region in 1990 and 1998 (Rodionov *et al.*, 2006). Figure 2 shows that even those species that migrate from mesopelagic depths to the upper pelagic layer also shifted their abundance in 1990–1991 and 1997–1998.

Thus we were motivated to measure the power of correlation between changes in the world with known climatic indices of the Northern Pacific and relative biomass fluctuation of nekton species.

Correlations between abiotic and biotic factors in the Sea of Okhotsk

We first used AOI, NPI.CPC, PDOw, PDOs, PDOa, SI, WPw, WPsp, NPI climatic indices (http://www.beringclimate.noaa.gov) for canonical analysis and relative species abundance. Results showed only one strong and significant (*Canonical R = 0.82585, Chi(70) = 104.22, p* << 0.01) correlation between changes in the WPw index and fluctuation of relative abundance of jelly fish and juvenile chum salmon in the upper pelagic layer during autumn, with a 5-year time lag, which was biologically unrealistic. Other significant correlations were not as strong between the WPw and pink salmon and rock trout juveniles in summer in the upper pelagic layer after a 4- and 6-year time lag (*Canonical R = 0.62690, Chi(54) = 121.58, p << 0.01*) and between the PDOw, SI and walleye pollock and herring juveniles in the epipelagic layer after a 1-year time lag (*Canonical R = 0.55328, Chi(48) = 84.184, p << 0.01*). Only one pair (PDOw, SI and walleye pollock) looks close to normal (Fig. 3) and could be explained, but it is not our main goal. All other 3D graphs showed very bad surface interpolations with negative abundance values in possible integers, and deviations from surfaces were also too big.

We found that the Siberian Index had the most frequent significant correlations with species. Also referred to as the Siberian Center, it reflects the strength of the Siberian High, and thus, the advection of cold Siberian air into the Sea of Okhotsk.

We next checked the strength of statistical correlations of changes in relative abundance of species with different local types of atmospheric and hydrospheric circulations, and compared them with sun spot activity. We chose the types of atmospheric processes over the Sea of Okhotsk classified by Glebova (2002, 2009) and empirical orthogonal functions (EOFs) of Sea of Okhotsk hydrodynamics extracted by Luchin (Luchin and Zhigalov, 2006; Luchin, 2008). Relative species abundance was presented as the principal components obtained from the groups with the longest time series. We had to use a rank type (Spearman) correlation analysis because the dimensions of different variables were not comparable.

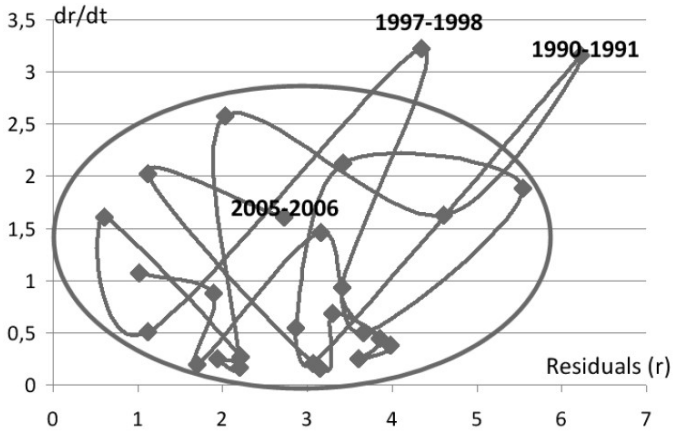

Fig. 2 The velocity of changes (dr/dt) vs residuals (r) of average subtraction from total normalized nekton biomass fluctuation in the Sea of Okhotsk.

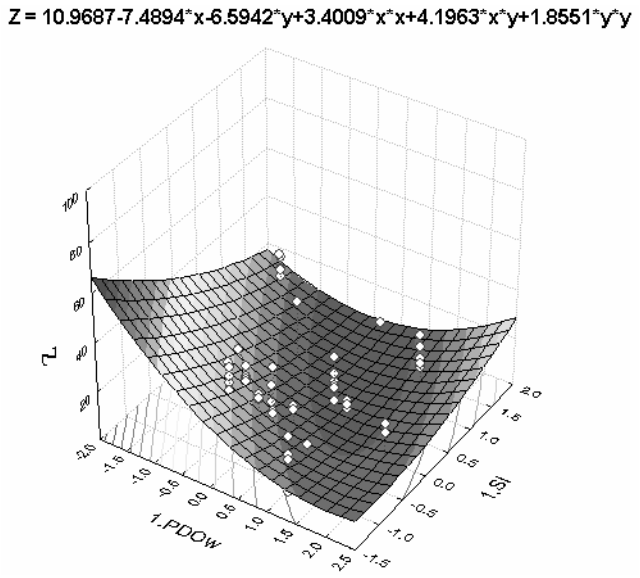

Fig. 3 Surface interpolation to the observed abundance of walleye pollock (Z), X and Y (horizontal) axes represent the values of climatic indices (PDOw and SI) with a 1-year time lag.

Before conducting further analysis, we wanted to know if there were any differences in the influential power on biological factors between sun spot activity, atmospheric and hydrospheric components. Therefore, nonparametric comparison analyses such as the Wald-Wolfowitz runs test, the Mann-Whitney U test, and the Kolmogorov-Smirnov two-sample test were chosen. The results were surprising because they were all different from each other. We obtained from non-significant differences to the next sequence: Hydro ->Atmo -> Sun or Hydro = Atmo > Sun due to the low frequency of strong and significant correlation occurrence. For example, only 6.5% of strong and significant correlation coefficients out of 1320 possible interactions in summer (Table 2) and 5.7% of 1122 possible interactions in autumn (Table 3) were found.

A little hope for stochastic modeling

Bernoulli first described the random walk in the 18th century. Later, Laplas, Brown, Einstein, and Viner advanced the techniques of analyzing stochastic processes (which are widely distributed in natural and technical events). However, population biologists often prefer to use deterministic models which require precise parameters that cannot be obtained experimentally in most cases. Why do they choose to estimate unknown parameters and make a lot of runs instead of using stochastic models so popular among physicists and economists?

The first problem to be solved is: How to fulfill the gaps in a time series where the quantity of real data values is sometimes less than the quantity of absent observations? The second question is: What should we do if the time period is not long enough to determine a model type?

Our answers do not pretend to be the best. At first, we did not use a time series with a big portion of zero values, and then we tried all possible types of moving average and autocorrelation models provided by the program “Statistica”. As a result, we could not find an adequate stochastic model. Instead, we got white noise over covering (even on the rows with determined interventions) after the first trend subtracted run. Unfortunately, we do not have a long uninterrupted time series; therefore, we had to interpolate values for some years from the adjacent points even on the longest time series. In all cases, the models did not have acceptable confidence intervals because all of them were as wide as the observed variability.

Table 2 Significant Spearman correlation coefficients of species group factor scores in the Sea of Okhotsk in summer with types of atmospheric and hydrospheric processes and sun spot activity.

Types of circulation and sun spot activity	Upper epipelagic layer													Epipelagic layer						
	Regions 1–2			Regions 5–8							Regions 9–14			Regions 3–4						
	Bio factors			Bio factors							Bio factors			Bio factors						
	1	2	3	1	2	3	4	5	6	7	1	2	3	1	2	3	4	5	6	7
I-0*	–**	–	–	–	–	–	–	–	–	–	0.7	0.8	–	–	–	0.9	–	–	–	–
I-1	–	–0.8	–	–	–	–	–	–	–	–	–	0.6	–	–	–	–	–	–	–	–
I-2	–	–	–	–	–	–	–	0.8	–	–	–	–	–	–	–	–	–	–	–	–
I-3	–	–	–	–	–	0.8	–	–	–	–	–	–	–	–0.8	–	–	–	–	–	–
I-4	–1	–	–	–	–	–	–	0.7	–0.7	–	–	–	–	–	–	–	–	–	–	–
II-1	0.8	–	–	–	–	–0.8	–	–0.7	–	–	–	–	0.6	–	–	–	–	–	–	–
II-2	0.9	–	–	–	–	–0.8	–	–0.8	0.8	–	–	–	–	–	–	–	–	–	–	–
II-3	–	–	–	–	–	–0.9	–	–0.8	0.7	–	–	–	–	–	–	–	–	–	–	–
II-4	–	–	–	–	–	–0.7	–	–	–	–0.8	–	–	–	–	–	–	–	–	–	–
II-5	–	–	–	–	–	–	–	–	–	–	–	0.6	–	–	–	–	–	–	–	–
III-0	–	–	–	–	–	–	–	–	–	–	–	–0.8	–	–	–	–	–	–	–	–
III-1	–	–	–	–	–	–	–	–	–	–	–	–	–	0.9	–	–	–	–	–0.7	–
III-2	–	–	–0.8	–	–	–	–	–	–	–	–	–	–	–	–	–	–	–	–	–
III-3	–	–	–1	–	–	–0.7	–	–	–	–	–	–	–	–	–	–	–	–	–	–
III-5	–	–	1	–	–	–	–	–	–	–	–	–	–	–	0.9	–	–	–	–	0.7
IV-0	–	–	–0.9	–	–	–	–	–	–	–	–	–	–	–	–	–	–	–	–	–
IV-1	–	–	–	–	–	–	–	–	–	–	–	–	–	–	–	–	–	0.8	–	–
IV-2	–	–0.9	–	–	–	–	–	–	–	–	–	–	–	–	0.9	–	–	–	–	–
IV-3	–	–0.8	–	–	–	–	–	–	–	–	–	–	–	–	–	–	–	–	–	–
IV-4	–	–	0.9	–	–	–	–0.8	–	–	–	–	–	–	–	–	–	–	–	–0.8	–
IV-5	–	–	–	–	–	–	–	–	0.8	–	–	–	–	–0.9	–	–	–	–	–	–
V-3	–	–	–	–	–	–	–	–	0.8	–	–	–	–	–	–	–	–	–	–	–
VI-1	–	–	–	–	–	–	–	–	–	–	–	–0.7	–	–	–	–	–	–	–	–
VI-2	–	0.9	–	–	–	–	–	–	–	–	–	–	0.6	–	–	–	–	–	–	–
VI-3	–	–	–	–	–	–	–	–	–	–	–	–	0.6	–	–	–	–	–	–	–
VI-4	–	–	–0.8	–	–	–0.8	–	–	–	–	–	–	–	0.7	–	–	–	–	–	–
VI-5	–	–	–	–	–	–	–	–	–	–	–	–	–	–	–	–	–	0.7	–	–

Table 2 Continued.

Types of circulation and sun spot activity	Upper epipelagic layer													Epipelagic layer							
	Regions 1–2			Regions 5–8							Regions 9–14			Regions 3–4							
	Bio factors			Bio factors							Bio factors			Bio factors							
	1	2	3	1	2	3	4	5	6	7	1	2	3	1	2	3	4	5	6	7
VII-1	–	–	–	–	–	–	0.8	–	–	–	–	–	–	–	–	–	–	–	–	–
VII-2	–	–	–	–	–	–	–	–	–0.8	–	–	–	–	–	–	–	–	–	–	–
VII-3	–	–	–	–	–	0.7	–	0.9	–	–	–	–	–	0.7	–	–	–	–	–	–
VII-4	–	–	–	–	–	0.7	–	–	–	–	–	–	–	–	0.8	–	–	–	–	–
VII-5	–	–	–	–	–	–	–	–	–	0.7	–	–	–	–	–	–	–	–	–	–
SS -1	–	–	–	–	–	0.8	–	–	–	–	–	–	–0.7	–	0.8	–	–	–	–	–
SS -2	–	–	–	–	–	0.7	–	0.8	–0.8	–	–	–	–0.6	–	–	–	–	–	–	–
SS -3	–	–	–	–	–	0.7	–	0.8	–0.7	–	–	–	–	–	–	–	–	–	–	–
SS -4	–	–	–	–	–	–	–	–	–	–	–	–	–	–0.7	–	–	–	–	–	–
SS -5	0.8	–	–	–	–	–	–	–	–	–	–	–	–	–	–	–	–	–	–	–
v1-1	–	–	–	–	–	0.7	–	–	–	–	–	–	–	–	–0.7	–	–	–	–	–
v1-2	–	–	–	–	–	–	–	–	–	0.8	–	–	–	–	–	–	–	–	–	–
v1-3	–	–	–	–	–	–	–	–	–	–	–	–	–	–	–	–	–	–	–0.7	–
v1-5	–	–	–	–	–	–	–	–	–	0.8	–	–	–	–	–	–	–	–	–	–
v2-0	–	–	0.9	–	–	–	–	–	–	–	–	–0.5	–	–	–	–	–	–	–	–
v2-2	–	–	–	–	–	–	–	–	–	–	–	–0.5	–	–	–	–	–	–	–	–
v2-3	–	0.8	–	–	–	–	–	–	–	–	–	–	–	–	–	–	–	–	–	–
v2-5	–	–	–	–	0.7	–	–	0.7	–	–	–	–	–	–	–	–	–	–	–0.7	–
v3-0	–	–	–	–	–	–	–	–	–	–	–	–	–	–	–	–	–	–0.9	–	–
v3-2	–	–	–	–	–	–	–	–	–0.8	–	–	–	–	–	–	–	–	–	–	–
v3-5	–	–	–	–	–	–	–	–	–	–	–0.6	–0.7	–	–	–	–	–	–	–	–

* Roman numerals represent the type of atmospheric circulations described by Glebova (2002, 2009), SS – sun spot activity, v1, v2 and v3 – EOFs by Luchin and Zhnigalog (2006) and Luchin (2008). Arabic numbers after first signs present a time lag in years.

** Significance of correlation was low ($p > 0.05$).

Table 3 Significant Spearman correlation coefficients of species group factor scores in the Sea of Okhotsk in autumn with types of atmospheric and hydrospheric processes and sun spot activity.

Types of circulation and sun spot activity	Upper epipelagic layer					Epipelagic layer											
	Regions 9, 10, 12, 13					Regions 1–4						Regions 7–8					
	Bio factors					Bio factors						Bio factors					
	1	2	3	4	5	1	2	3	4	5	6	1	2	3	4	5	6
I-0	–	–	–0.6	–	–0.6	–	–	–	–	–	–	–	–	–	–	–0.7	–
I-1	0.7	–	–0.7	–	–0.7	–	–	–	–	–	–	–	–	–	–	–	–
I-2	–	–	–0.8	–	–	–	–	–	–	–	–	–	–	–	–	–	–
I-4	0.8	–	–	–	–	–	–	–	–	–	–	–	–	–	–	–	–
II-0	–0.6	–	–	–	–	–	–	–	–	–	–	–	–	–	–	–	–
II-1	–	–	–	–0.7	–	–	–	–	–	–	–	–	–	–	–	–	–
II-2	–	–	–	–0.6	–	–	–	–	–	–	–	–	–	–	–	–	–
II-4	–	–	–	–	–	–0.6	–	–	–	–	–	–	–	–	–	–	–
III-0	–	–	0.6	–	–	–	–	–	–	–	–	–	–	–	–	–	0.7
III-1	–	–	–	–	–	–	–	–	–	–	0.8	–	–	–	–	–	–
III-2	–	–	–	–	–	–	–	–	–	–	–	–	–	–	–	0.7	–
III-4	–	–	0.6	–	–	0.7	–	–	–	–	–	0.7	–	–	–	0.7	–
IV-5	–	–	–	–	–	–	–	0.7	–	–	–0.7	–0.9	–	–	–	–	–
V-2	–	–	–	–0.6	–	–	–	–	–	–	–	–	–0.7	–	–	–	–
V-4	–	–	–	–	–	–	–	–	–	–	–	–	–	–	–	–0.8	–
V-5	–	–	–	–	–	–0.6	–	–	–	–	–	–	–	–	–	–0.8	–
VI-0	–	–	–	–	–	0.6	–	–	–	–	–	–	–	–	–	–	–
VI-1	–	–	–	–	–	–	–	0.6	–	–	–	–	–	–	–	–	–
VI-2	–	–	–	–	–	–	–	–	–	–	–	–	0.8	–	–	–	–
VI-4	–	–	–	–	–	–	–	–	–	–	–	0.7	–	–	–	–	–
VII-0	–	–	–	–	–	–	–	–	–	–	–	–	–	–	–	–	–0.8
VII-1	–0.6	–	–	–	–	–	–	–	–0.6	–	–	–	–	–	–	–	–
VII-2	–	–	–	0.8	–	–	–	–	–	–	–	–	–	–	–	–	–
VII-3	–	–	–	–	–	–	–	–	–	–	–	–	–	–	–0.7	–	–
VII-4	–	–	–	–	–	–	–	–	–	0.6	–	–	–	–	–	–	–
VII-5	–	–	–	–	–	0.6	–	–	–0.6	–	–	–	–	–	–	–	–

Table 3 Continued.

Types of circulation and sun spot activity	Upper epipelagic layer					Epipelagic layer											
	Regions 9, 10, 12, 13					Regions 1–4						Regions 7–8					
	Bio factors					Bio factors						Bio factors					
	1	2	3	4	5	1	2	3	4	5	6	1	2	3	4	5	6
SS -0	–	–	–	–	–	–	–	–0.8	–	–	–	–	–	–	–	–	–
SS -1	–	–	–	–	–	–	–	–0.7	–	–	–	–	–	–	–	–	–
SS -3	–	–	–	–	–0.6	–	–	–	–	–	–	–0.9	–	–	–	–	–
SS -4	–	–	–	–	–	–	–	0.6	–	–	–	–	–	0.8	–	–	–
SS -5	–	–	–	–	–	–	–	0.8	0.6	–	–	–	–	–	–	–	–
v1-0	0.6	–	–0.7	–	–0.7	–	–	–	–	–	–0.8	–	–	–	–	–	–
v1-3	–	–	–	–	–	–	–0.6	–	0.6	–	–	–	–	–	–	–	–
v1-4	–	–	–	0.6	–	–	–	–	–	–	–	–	–	–	–	–	–
v1-5	–	–	–	–	0.6	–	–	–	–	–	–	0.9	–	–	–	–	–
v2-2	–	0.7	–	–	–	–	–	–	–	–	–	–	–	–	–	–	–
v2-3	–	–	–	–	–	–	0.7	–	–	–	–	–	–	–	–	–	–
v2-5	–	–	–	–	–	–	–	–	–	–	0.6	0.9	–	–	–	–	–
v3-0	–	–	–	–	–	–	–	–	–	–0.8	–	–	–	–	–	–	–
v3-2	–	–	–	–	–	–	–	–	–	–	–	–	0.8	–	–	–	–
v3-4	–	–	–	–	–	0.7	–	–	–	–	–	–	–	–	–	–	–

* Roman numerals represent the type of atmospheric circulations by described by Glebova (2002, 2009), SS – sun spot activity, v1, v2 and v3 – EOFs by Luchin and Zhigalov (2006) and Luchin (2008). Arabic numbers after first signs present a time lag in years.

** Significance of correlation was low ($p > 0.05$).

Conclusions

In spite of the large number of indices and indicators used operationally all over the Northern Pacific to quantify the state of the climate and its variability, almost none of them can be used to predict interannual changes in biological parameters, or dominant nekton species of the epi- and upper epipelagic layer of the Sea of Okhotsk. With all the power of statistics, why are we still unable to make precise predictions on the state of species abundance of nekton in the Sea of Okhotsk ecosystem when we have access to fast and powerful computers, remote sensing, and other facilities?

This work shows the complexity of making even simple (at a first glance) correlations between nekton species of the epipelagic layer and their environment by the use of some sort of abstraction – factors of PCA. A detailed discussion would take a lot of space, and some parts have already been published (Kulik, 2007, 2008). In conclusion, we will not find uninterrupted time series of fish abundance surveys if we chose them only according to the biostatistical regions of the Sea of Okhotsk, studied layers of the water column, and survey season. This limitation forces us to fill the times series with some hypothetical data (interpolated data) for statistical analyses. Therefore, we get wide confidence intervals of approximations, which do not let us even know where the similarities and real differences are. On the other hand, insignificant changes in communities (at a first glance) may lead to unpredictable states in the future (the well known "butterfly effect").

If we want to get precise data, then we need to conduct ecosystem studies of the Sea of Okhotsk every year during the same time periods and in the same regions. Until then, statistical analysis of strong and significant multivariate, canonical and other analyses may lead to unacceptable biologically nonsensical results. Nevertheless, we can make some conclusions:

1. The interrelationship between groups of species are more complex in the southern part of the Sea of Okhotsk in summer, and in the northern part of the Sea in autumn;
2. The changes in abundance correlate both with the regional climate conditions and heliophysical factors (sun spots), but are very rare;
3. Most of the species do not have alternating variability of abundance, although it is usual for dominant species;
4. Perceptible deviation of biotic factor scores were noticed for the periods 1990–1991 and 1997–1998;
5. Strong ($|R| \geq 0.8$) and statistically significant ($p < 0.05$) correlations between changes of relative abundance of species and abiotic factors of the environment, with a time-lag up to 6 years, are extremely rare;
6. Attempts to use moving average and autocorrelation functions during time series analysis failed because there are a lot of gaps in a short time series (less than 25 years).

References

Chuchukalo, V.I. 2006. Feeding and trophic relationship of nekton and nektobenthos in the Far Eastern Seas. TINRO-Centre, Vladivostok, 511 pp.

Glebova, S.Yu. 2009. Long-term changes of atmospheric centers and climate regime of the Okhotsk Sea in the last three decades. This PICES report.

Glebova, S. Yu. 2002. Classification of atmospheric processes over the Far-Eastern Seas. *Meteorol. Hydrol*. **7**: 5–15.

Kulik, V.V. 2007. Long dynamics of nekton and macroplankton relative abundance in the upper layer of the Okhotsk Sea. *Izv. TINRO* **150**: 56–85.

Kulik, V.V. 2008. Stochastic and deterministic processes in the dynamics of domination of nekton species in the pelagic layer of the Far Eastern Seas since 1980s. Conference on "The Current State of Water Bioresources", Vladivostok, pp. 143–147.

Kuznetsova, N.A. 2005. Feeding and trophic relationship of nekton in the upper pelagic layer of the Northern Okhotsk Sea. TINRO-Centre, Vladivostok, 236 pp.

Luchin, V.A. 2008. Thermal regime of the Russian Far Eastern Seas (the Japan (East) Sea, the Sea of Okhotsk, the Bering Sea). Abstract of D.Sc. dissertation, POI, Vladivostok, 47 pp.

Luchin, V.A. and Zhigalov, I.A. 2006. Types of water temperature distribution in active layer of the Okhotsk Sea and possibility of its prediction. *Izv. TINRO* **147**: 183–204.

Rodionov, S., Overland, J. and Bond, N. 2006. Pacific Climate Overview – 2006. North Pacific Climate Overview,http://www.beringclimate.noaa.gov/reports/np_06.pdf.

Shuntov, V.P. 1986. State of many years research in cyclic changes of fish quantity in the Far Eastern Seas. *Biol. Morya* **3**: 3–15.

Shuntov, V.P. and Bocharov, L.N. (*Eds.*). 2003a. Nekton of the Okhotsk Sea. Abundance, biomass and species ratio. TINRO-Centre, Vladivostok, 643 pp.

Shuntov, V.P. and Bocharov, L.N. (*Eds.*). 2003b. Atlas of quantitative distribution of nekton species in the Okhotsk Sea. FGUP "National Fish Resources" Publishing, Moscow, 1040 pp.

Shuntov, V.P., Boretsc, L.A. and Dulepova, E.P. 1990. Ecosystems of the Far Eastern Seas, state and problems of research. Session report XIII. All Russian conference on Fisheries Oceanography. VNIRO, Moscow, pp. 66–78.

Temnykh, O.S., Starovoytov, A.N., Glebov, I.I., Merzlyakov, A.Yu. and Sviridiv, V.V. 2003. Pacific salmons in the pelagic communities of the Southern part of the Okhotsk Sea. *Izv. TINRO* **132**: 112–153.

Walleye pollock research in the open waters of the Okhotsk Sea

Evgeny E. Ovsyannikov, Anatoly V. Smirnov and Gennady V. Avdeev

Pacific Research Fisheries Centre (TINRO-Centre), Vladivostok, Russia. E-mail: eeovsyannikov@tinro.ru

Abstract

Research was carried out in the central part of the Okhotsk Sea on the R/V *Professor Kaganovsky* in the spring of 2007. A total of 22 pelagic trawls were performed across a network of stations on 8 acoustic boards and 23 ichtyoplankton and hydrological stations.

The results of numerous studies done throughout the 1980s and 1990s suggest that there is no pollock spawning in the open waters of the Okhotsk Sea. The maximum catch of pollock eggs was 7 eggs per catch. Pollock of 32–43 cm in length (4- to 6-year olds) dominated the catches. Among the mature females, the dominant group were females with after-spawning gonad maturity – 95%. There were no spawning females.

Depsite sightings of walleye pollock at all the trawl stations, there were no dense concentrations in the observed area. Pollock catches per trawl hour accounted for an average of only 162 kg, or 711 individuals. The maximal pollock catches per trawl hour (695 kg, or 7,623 individuals) was in the northern part of the observation are near the economic zone of Russia. This can be explained by pollock migration from the northern shelf of the Okhotsk Sea. Thus, walleye pollock migrating to feed were caught during the serveys. They spawned in the shelf of the northern part of the Sea.

Does the extent of ice cover affect the fate of walleye pollock?

Jun Yamamoto, Mio Osato and Yasunori Sakurai

Graduate School of Fisheries Sciences, Hokkaido University, Hakodate, Hokkaido, Japan
E-mail: sakurai@fish.hokudai.ac.jp

Introduction

In the late winter and early spring, walleye pollock, *Theragra chalcogramma*, spawn pelagic, individual eggs at mid-water depths. Some of the spawning grounds occur below sea ice, such as in the Sea of Okhotsk, but the effect of cold, low-saline water derived from melting sea ice on eggs is not well known. The present study examined the effect of cold, low-saline water on the survival and hatching success of walleye pollock eggs.

Materials and Methods

Live adult pollock were collected by rod fishing in late January 2007 and 2008 at the mouth of Funka Bay, southwestern Hokkaido Japan, which is known as the main spawning grounds of the Pacific Stocks occurring around Japan. The fishes were moved to, and reared at, 5°C and two different salinities (29.1 in 2007 and 33.0 in 2008) in a 10-ton circular tank. The naturally spawned eggs were collected and maintained under 35 different temperature and salinity conditions (seven temperatures; –1.0, 0.0, 2.0, 5.0, 7.0, 9.0, 11.0°C: five salinities; 24.0, 27.0, 30.0, 33.0, 35.0) to examine the optimal temperature and salinity range for normal hatching, and the developmental time for the each condition. This study used the egg developmental stage model of Kendall and Kim (1989). To clearly understand the movement of eggs in the spawning grounds, the change in their buoyancy during development was examined by liner density column (Coombs, 1981). A summary of the density gradient columns is shown in Table 1.

Table 1 Summary of the density gradient columns.

Temperature (^{o}C), top/bottom	5.0/5.0
Salinity, top/bottom	18.0/42.0
Density (σt)	14.0/33.0

The density of the eggs in the column was determined by density cubes of 14.8, 20.0, 24.9, 30.0σt (Martin Instrument Company). The vertical velocities of the eggs in the spawning grounds of Funka Bay, and Nemuro Strait, eastern Hokkaido, which is known as the spawning ground of the Nemuro Strait Stock, were estimated using the Stokes law (Sundby, 1983).

Results and Discussion

The hatching rate of normal larvae ranged from a low of less than 2°C to a high of 9°C, but showed no significant differences over the salinity range examined (Fig.1). This indicates that temperature < 2.0°C is not favorable for hatching and the success of normal hatching is controlled by temperature rather than by salinities. Additionally, there were no differences in the hatching days after the fertilizations and the developmental stages among the salinities, suggesting that developmental time was also controlled by temperature.

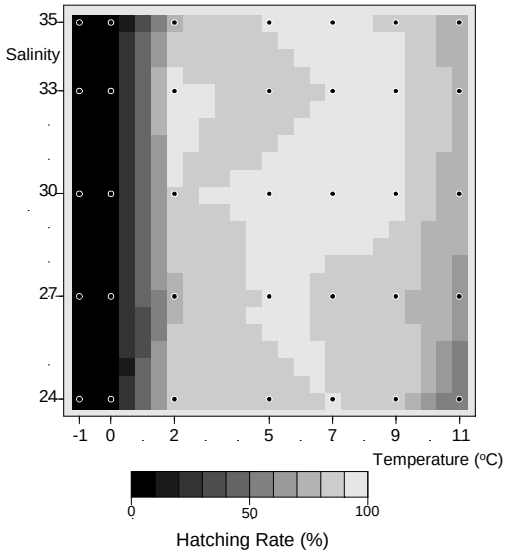

Fig. 1 Hatching rate (%) at 35 different temperature and salinity conditions.

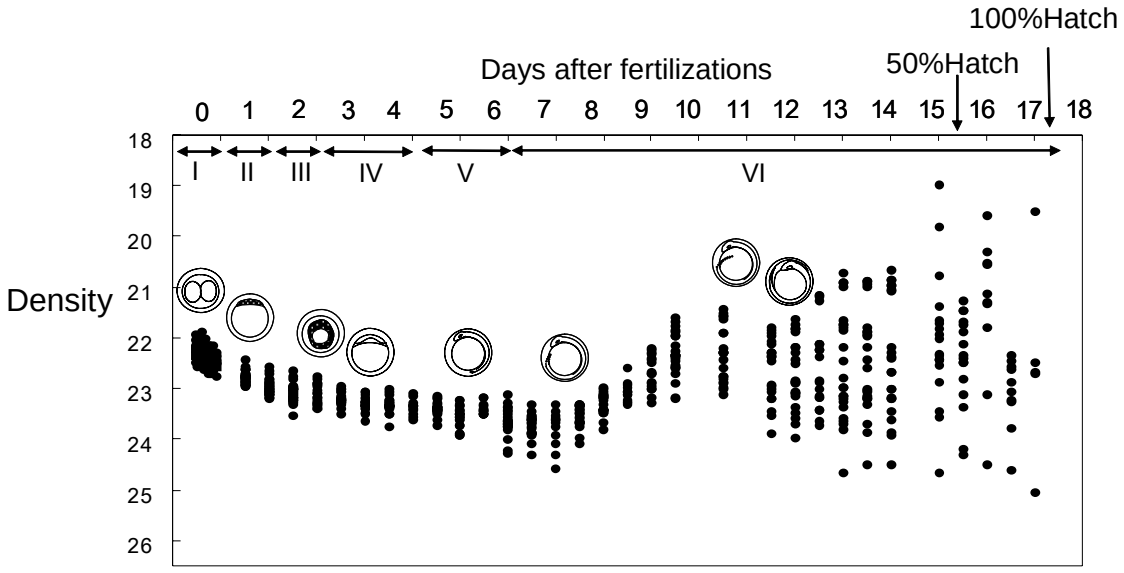

Fig. 2 The change in the density (σt) of the egg during development. Note the inverted *y* axis.

Although, the eggs were spawned in different water properties in 2007 (temperature 5°C, salinity 29.1, density 23.0σt) and in 2008 (temperature 5°C, salinity 33.0, density 23.8σt), the buoyancy of the eggs soon after fertilization showed no difference. Coombs *et al.* (2004) showed that the buoyancy of eggs is affected by the ratio of the volume of the vitelline mass, with almost the same osmotic pressure to the adult, and the volume of the peri-vitelline space, in which the osmotic pressure is almost equal to the sea water. The pollock eggs have a much larger volume of the vitelline mass than that of vitelline space. Thus, the primary buoyancy of the egg is probably determined by the adult. The change in the density of the egg during development is shown in Figure 2. The density ranged from 19.0–25.1(σt), and gradually increased by stage VI (late stage), after which the change in densities varied. The estimated vertical velocities of eggs were 10.8 m/s in Funka Bay and 9.6 m/s in the Nemuro Strait, which indicates that the eggs reach the surface in approximately 7 h in Funka Bay and 21 h in the Nemuro Strait after spawning. It suggests that eggs are exposed to the surface cold water in the early developmental stage. Nakatani and Maeda (1984) suggested that eggs are able to resist cold temperatures after the morula stage. The stage of developmental upon reaching the cold water is probably one of the key factors determining the success of hatching.

References

Coombs, S.H. 1981. A density-gradient column for determining the specific gravity of fish eggs, with particular reference to eggs of the mackerel *Scomber scombrus*. *Mar. Biol.* **63**: 101–106.

Coombs, S.H., Boyra, G., Rueda, L.D., Uriate, A., Santos, M., Conway, D.V.P. and Halliday, N.C. 2004. Buoyancy measurements and vertical distribution of eggs of sardine (*Sardina pilchardus*) and anchovy (*Engraulis encrasicolus*). *Mar. Biol.* **145**: 959–970.

Kendall, A.W. and Kim, S. 1989. Buoyancy of walleye pollock (*Theragra chalcogramma*) eggs in relation to water properties and movement in Sherikof Strait, Gulf of Alaska. *Can. Spec. Publ. Fish. Aquat. Sci.* **108**: 169–180.

Sundby, S. 1983. A one-dimension model for the vertical distribution of pelagic fish eggs in the mixed layer. *Deep-Sea Res.* **30**: 645–661.

Nakatani, T. and Maeda, T. 1984. Thermal effect on the development of walleye pollock eggs and their upward speed to the surface. *Bull. Japan Soc. Sci. Fish.* **50**: 937–942.

Dynamics of the walleye pollock biomass in the Sea of Okhotsk

Boris N. Kotenev and Oleg A. Bulatov

Russian Federal Research Institute of Fisheries and Oceanography (VNIRO), Moscow, Russia
E-mail: obulatov@vniro.ru

Walleye pollock (*Theragra chalcogramma)* is the most valuable fish species in the Sea of Okhotsk. The Russian pollock fishery started in the 1960s and the first considerable landings (35,000 t) occurred in 1962 (Fadeev and Vespestad, 2001). The epoch of large-scale exploitation of pollock resources began in 1965, when the landings totaled 293,000 t. Since then landings had been increasing and in 1968 attained an impressive total of 675,000 t. The first historical maximum was marked in 1975 when 1,300,000 t of pollock were landed. In those years the fishery was exclusively concentrated in the eastern part of the sea, off western Kamchatka. Then landings started to decrease, reaching a low of 482,000 t in 1981. The second period of large catches >1,500,000 t (Fig. 1) occurred in 1985–1997. Discovery of a new fishing ground in the northern part of the Sea of Okhotsk contributed to the outgrowth of catches. These successful years in the fishery were followed by another period of low landings with a minimum (394,000 t) in 2004. The following years saw a significant increase in landings (up to 680,000 t).

The pollock fishery in the open part of the Sea of Okhotsk (*peanut hole*) is much younger than in the other fishing grounds. The first information about the pollock catches taken by foreign fishing vessels in this area appeared in the late 1980s, when there was large-scale unregulated fishing for pollock in the open part of the Bering Sea (*donut hole*). The pollock fishery continued in the peanut hole from 1991–1994 and produced a maximum yield totaling 698,000 t. Considering that this fishery was based on the pollock stocks of Russian origin, Russia suffered a severe amount of economic damage. The presented history of the pollock fishery in the Sea of Okhotsk shows that a considerable interannual variability in the yield introduces large uncertainty in planning and managing this fishery.

However, landings do not show the actual dynamics of the stocks, as they are mostly dependent on the fishing intensity, *i.e.*, on the fishing effort. There are many Russian scientific publications devoted to the pollock stock dynamics in the Sea of Okhotsk (Fadeev, 1980; Kachina, Sergeeva, 1981; Vasil'kov and Glebova, 1984; Shuntov, 1986; Shuntov *et al.*, 1993; Avdeev *et al.*, 2001; Fadeev, 2001; Varkentin and Sergeeva, 2004). Our goal is to identify cyclicity in various levels of the pollock stock and attempt to give a medium-term forecast.

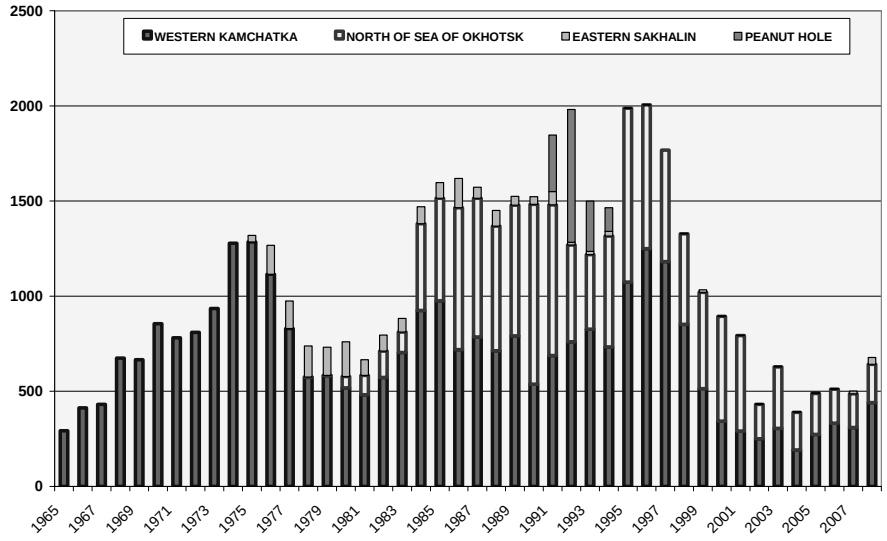

Fig. 1 Walleye pollock catch (thousands of t) by region in the Sea of Okhotsk.

Research conducted in VNIRO (Babayan *et al.*, 2006), based on fishing statistics and the Instantaneous Separable Virtual Population Analysis (ISVPA) modeling, showed that in 1974–2003 the spawning and the fishable biomass of walleye pollock in the eastern part of the Sea of Okhotsk were changing concurrently (Fig. 2). According to our data, there was a high correlation coefficient of 0.94. Over three decades there were four maxima of the fishing and spawning stocks (1974, 1984, 1994, and 2003) and three periods of low stock abundance (1978–1979, 1990, and 2000). During the entire period of observations, the stocks restored from the minimum level to an average one fairly rapidly (3–4 years), thus demonstrating their stability. It is noteworthy that the decrease in stocks from maximum levels to minimum ones occurred with a 5- to 6-year lag after the curve bend.

The TINRO-Center studies (1983–2008) were based on assessment of eggs spawned by pollock females. Surveys took place in spring and were made with an IKS-80 ichthyoplankton net. Results of these observations (Avdeev *et al.*, 2001, TINRO-Center data) showed that values of the spawning biomass of pollock in the eastern part of the Okhotsk Sea and in the entire Sea of Okhotsk changed concurrently (Fig. 3). During the entire period of observations, there were three maxima of stocks (1984–1987, 1994–1995, and 2007–2008) and two minima (1991 and 2000–2001). According to our data, the correlation coefficient was high, having a value of 0.90. Thus, despite different techniques of the biomass assessment used in VNIRO and TINRO-Center, the results of assessment were very close: there is a 10–12 year periodicity in occurrence of the maximum and minimum stocks.

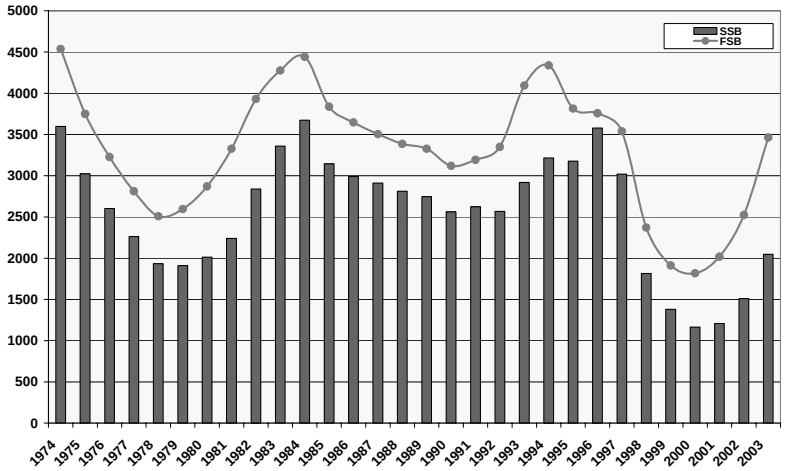

Fig. 2 Spawning stock biomass (SSB) and fishable stock biomass (FSB) of walleye pollock (thousands of t) off western Kamchatka according to the analytical approach (Babayan *et al.*, 2006).

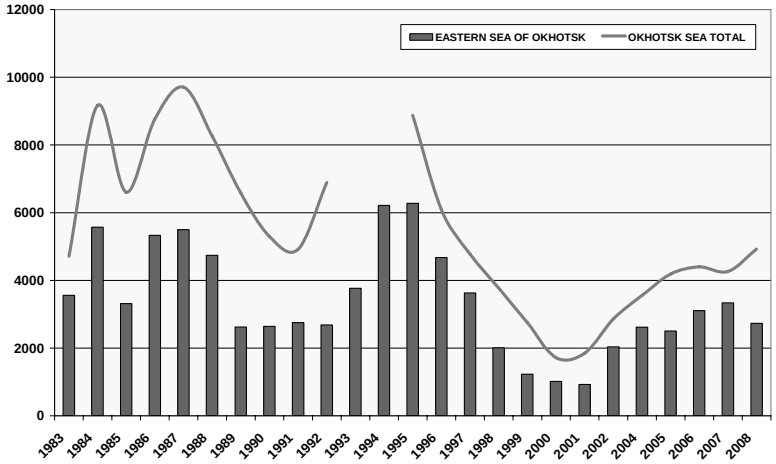

Fig. 3 The spawning stock biomass of walleye pollock in the eastern Sea of Okhotsk and in the entire Sea of Okhotsk, thousands of t (TINRO-Center data).

Water temperature has a significant impact on the generation success in the first year of the pollock life history. As a rule, weak generations appear in cold years, while abundant generations occur in warm years. This phenomenon could be associated with several facts: there is better food availability in warm years; young fish have a higher initial growth rate; metabolism accelerates and increases the fish viability. Abundance of recruitment influences the growth or decrease of the fishing and spawning stocks. Among the most important global climatic events which influence the sea temperature is the Pacific Decadal Oscillation (PDO). We analyzed the variability in the pollock fishable and spawning stocks in connection with the PDO anomalies and found that periods of high pollock biomass occurred during years of PDO positive anomalies. Minimum values of biomass were generally observed in periods of PDO negative anomalies. (Figs. 4 and 5). A sharp drop in the PDO in 2008 suggests that the years of positive anomalies ended and another period of negative anomalies will begin which will likely to lead to a decrease in pollock biomass.

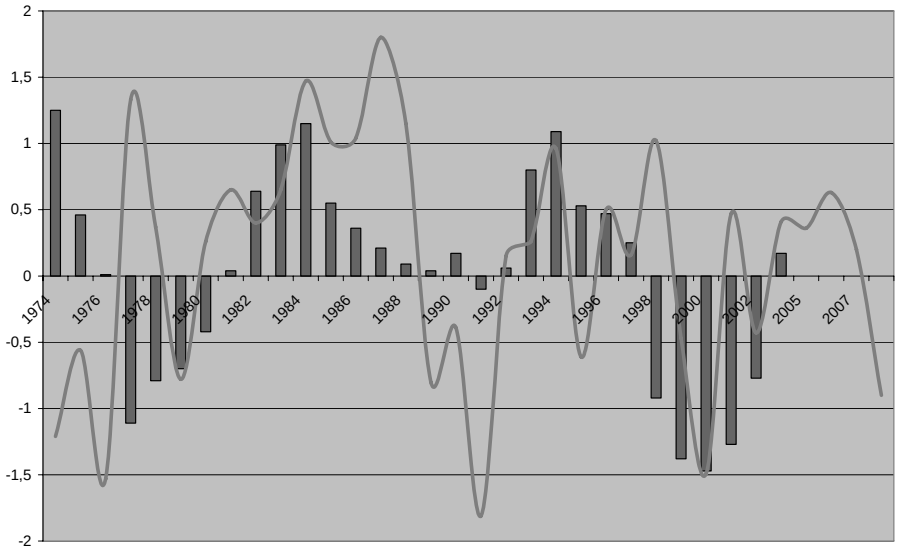

Fig. 4 Fishable biomass of pollock (millions of t, bars) in the eastern Sea of Okhotsk and PDO anomalies (line).

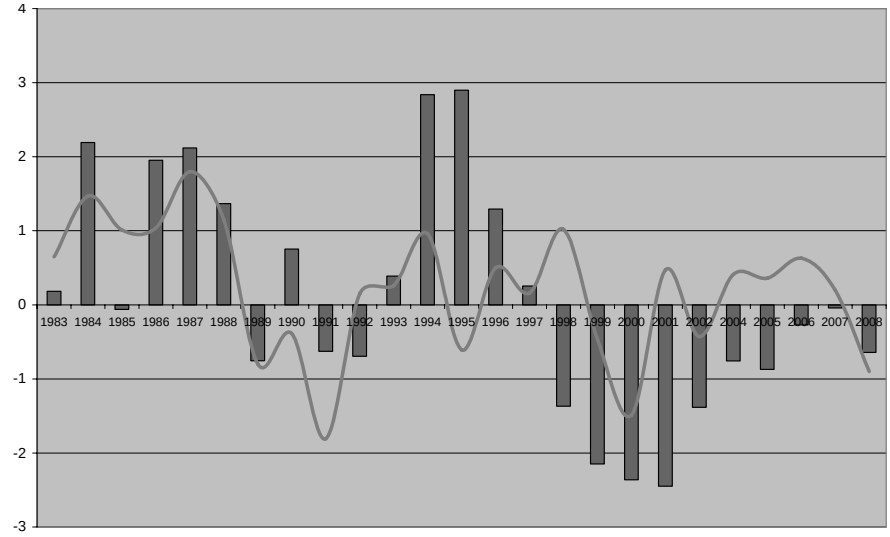

Fig. 5 Spawning biomass of pollock (millions of t, bars) in the eastern Sea of Okhotsk and PDO anomalies (line).

Studies show that the stock dynamics is characterized by a 10-year interval. Tables 1 and 2 summarize data on the pollock stock assessment grouped by decades. Thus, in the first column of Table 1 the value of 4,538,000 t corresponds to 1974, while in the first column of Table 2 the value of 3,560,000 t corresponds to 1983, *etc*. The last column gives averages for the entire period of observations. These data are also presented graphically (Fig. 6). These figures show that the minimum averaged values of spawning and fishing stocks correspond to points 9 and 0 (see Tables 1 and 2), *i.e.*, occur at the end of the decade.

The obtained results allow us to already forecast a considerable decrease in pollock stocks in 2009–2010. The 10-year minimum is likely to be attained in 2011–2012, and the stock will probably restore in 2014–2015 with further growth reaching a maximum in 2016–2017.

Table 1 Assessment of the walleye pollock spawning stock in the eastern Sea of Okhotsk (Avdeev *et al.*, 2001, TINRO-Center data, ichthyoplankton surveys), 1000 t.

	1983–1989	**1990–1999**	**2000–2008**	**Average**
0	no data	2642	1015	1828
1	no data	2750	927	1838
2	no data	2683	2039	2361
3	3560	3766	no data	3663
4	5570	6215	2620	4802
5	3313	6275	2506	4031
6	5330	4671	3105	4368
7	5495	3631	3335	4152
8	4743	2009	2734	3162
9	2623	1230	no data	1926

Table 2 Assessment of the walleye pollock fishable biomass in the eastern Sea of Okhotsk (Babayan *et al.*, 2006, ISVPA), 1000 t.

	1974–1979	**1980–1989**	**1990–1999**	**2000–2003**	**Average**
0	no data	2870	3120	1817	2602
1	no data	3327	3192	2019	2846
2	no data	3930	3349	2525	3268
3	no data	4276	4094	3464	3945
4	4538	4442	4338	no data	4439
5	3750	3837	3815	no data	3801
6	3228	3647	3757	no data	3544
7	2812	3504	3539	no data	3285
8	2508	3386	2371	no data	2755
9	2596	3327	1912	no data	2611

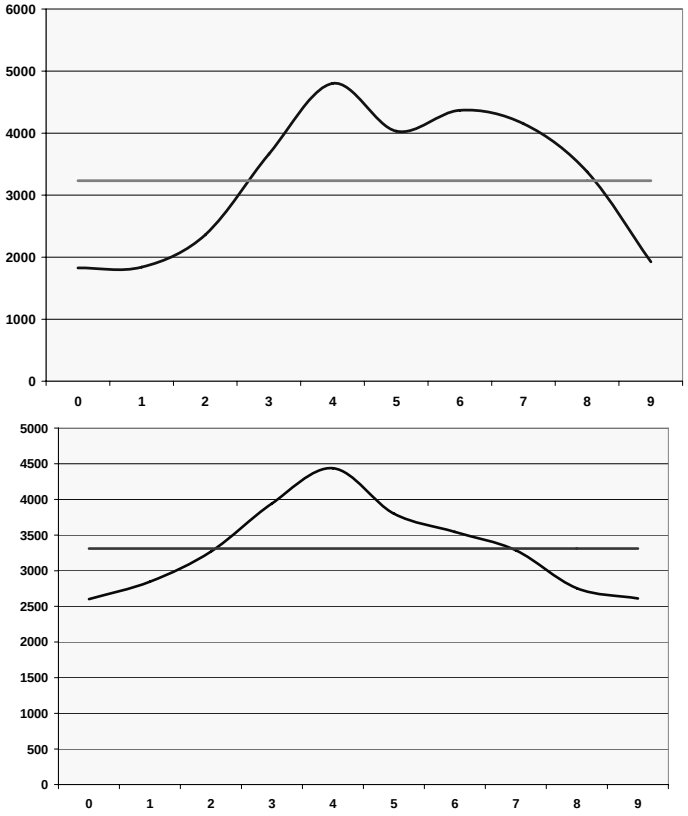

Fig. 6 Average spawning (top) and fishable biomass (bottom) in the eastern Sea of Okhotsk according to ichthyoplankton data from TINRO-Center and the analytical approach by VNIRO (thousands of t). Grey horizontal line represents the average for all the decades.

References

Avdeev G.V., Smirnov, A.V. and Fronek, S.L. 2001. Osnovnie cherty dinamiki chislennosti mintaya severnoi chasti Ohotskogo morya v 90-e gody (General trends in the pollock stock dynamics in the northern part of the Sea of Okhotsk). *Izv. TINRO* **128**: 207–221 (in Russian).

Babayan, V.K., Vasil'ev, D.A., Varkentin, A.I. and Sergeeva, N.P. 2006. Metodicheskie osobennosti obosnovaniya ODU mintaya v usloviyah neopredelennosti (Methodological peculiarities of the pollock TAC estimation under uncertainty). Trudy VNIRO, Vol.146, pp. 13–37 (in Russian).

Kachina, T.F. and Sergeeva, N.P. 1981. Dinamika chislennosti vostochnoohotomorskogo mintaya: Ekologiya, zapasy i promysel mintaya (Dynamics of the pollock stock abundance in the eastern Okhotsk Sea). TINRO, Vladivostok, pp. 19–27 (in Russian).

Fadeev, N.S. 1980. Byla li "vspyshka" chislennosti mintaya v severnoi chasti Tihogo okeana? (Was there an outburst in the pollock abundance in the Northern Pacific?) *Biol. Morya* **5**: 66–71 (in Russian).

Fadeev, N.S. 2001. Urozhainost' pokolenij severoohotomorskogo mintaya (Pollock generation success in the northern part of the Sea of Okhotsk). *Voprosy Rybolovstva* **2**: 299–318 (in Russian).

Fadeev, N.S. and Vespestad, V. 2001. Obzor promysla mintaya (Review of the pollock fishery). *Izv. TINRO* **128**: 75–91 (in Russian).

Shuntov, V.P. 1986. Sostoyanie izuchennosti mnogoletnih tsiklicheskih izmenenij chislennosti ryb dal'nevostochnyh morei (State-of-art in studies of long-term cyclic variations in abundance of fish species in the Far East seas). *Biol. Morya* **3**: 3–14 (in Russian).

Shuntov, V.P., Volkov, A.F., Temnyh, O.S. and Dulepova, E.P. 1993. Mintai v ekosystemah dal'nevostochnyh morei (Pollock in ecosystems of the Far East seas). TINRO, Vladivostok:, 426 p. (in Russian).

Varkentin, A.I. and Sergeeva, N.P. 2004. The fisheries and current state of walleye pollock (*Theragra chalcogramma*) stock abundance in the eastern Sea of Okhotsk. PICES Sci. Rep. No. 26, pp. 251–253.

Vasil'kov, V.P. and Glebova, S.Yu. 1984. Faktory, opredelyayuschie urozhainost' pokolenij mintaya zapadnoi Kamchatki (Factors influencing the pollock generation success off the western Kamchatka). *Voprosy ihtiologii.* **24**: 561–570 (in Russian).

Appendix 1

List of Corresponding Authors

ABROSIMOVA Anastasiya
V.I. Il'ichev Pacific Oceanological Institute (POI)
Far Eastern Branch, Russian Academy of Sciences
43 Baltiyskaya St., Vladivostok
Russia 690041
E-mail: amber@poi.dvo.ru

ANDREEV Andrey
V.I. Il'ichev Pacific Oceanological Institute (POI)
Far Eastern Branch, Russian Academy of Sciences
43 Baltiyskaya Street., Vladivostok
Russia 690041
E-mail: andreev@poi.dvo.ru

ASAMI Hiroki
Hokkaido Wakkanai Fisheries Experiment Station
Suehiro 4-5-15, Wakkanai
Hokkaido, Japan 097-0001
E-mail: asamih@fishexp.pref.hokkaido.jp

BROVKO Peter
Far East State University
8 Sukhanova St., Vladivostok
Russia 690600
E-mail: brovko@meteo.dvgu.ru

CHERNOOK Vladimir
Research Institute "GIPRORYBFLOT"
Malaya Morskaya, 18-20, St. Petersburg
Russia 190000
E-mail: chernook@grf.spb.ru

EBUCHI Naoto
Institute of Low Temperature Science
Hokkaido University
N-19 W-8, Kita-ku, Sapporo
Japan 060-0819
E-mail: ebuchi@lowtem.hokudai.ac.jp

GLEBOVA Svetlana
Pacific Research Institute of Fisheries and Oceanography (TINRO-Center)
4 Shevchenko Alley, Vladivostok
Russia 690950
E-mail: glebova@tinro.ru

HIWATARI Takehiko
National Institute for Environmental Studies
16-2 Onogawa, Tsukuba
Ibaraki, Japan 305-8506
E-mail: hiwatari.takehiko@nies.go.jp

ISADA Tomonori
Graduate School of Environmental Science
Faculty of Environmental Earth Science
Hokkaido University
N10 W5, Kitaku, Sapporo
Hokkaido, Japan 060-0810
E-mail: t-isada@ees.hokudai.ac.jp

KANAIWA Minoru
Faculty of Bio-Industry
Tokyo University of Agriculture
196 Yasaka, Abashiri
Japan 099-2493
E-mail: m3kanaiw@bioindustry.nodai.ac.jp

KANTAKOV Gennady
Sakhalin Research Institute of Fisheries and Oceanography (SakhNIRO)
196 Komsomol'skaya St., Yuzhno-Sakhalinsk
Russian 693023
E-mail: okhotsk@sakhniro.ru

(present address)
Far-Eastern Ecological Center Ltd.
Office 404
426 Mira Ave., Yuzhno-Sakhalinsk
Russia 693004
E-mail: deco@sakhalin.ru

KASAI Hiromi
Hokkaido National Fisheries Research Institute
Fisheries Research Agency
116 Katsurakoi, Kushiro-shi
Hokkaido, Japan 085-0802
E-mail: kasaih@fra.affrc.go.jp

KASHIWAI Makoto
Department of Aqua-Bioscience and Industry
Faculty of Bio-Industry
Tokyo University of Agriculture
196 Yasaka, Abashiri
Japan 099-2493
E-mail: m3kashiw@bioindustry.nodai.ad.jp

KOBAYASHI Mari
Laboratory of Aquatic Management
Department of Aqua-Bioscience and Industry
Faculty of Bioindustry
Tokyo University of Agriculture
196 Yasaka, Abashiri
Japan 099-2493
E-mail: m3kobaya@bioindustry.nodai.ac.jp

KULIK Vladimir
Pacific Research Institute of Fisheries and
Oceanography (TINRO-Center)
4 Shevchenko Alley, Vladivostok
Russia 690950
E-mail: vladicon82@gmail.com

LABAY Vyacheslav
Sakhalin Research Institute of Fisheries and
Oceanography (SakhNIRO)
196 Komsomolskaya St., Yuzhno-Sakhalinsk
Russia 693023
E-mail: labay@sakhniro.ru

LOBANOV Vyacheslav
V.I. Il'ichev Pacific Oceanological Institute (POI)
FEB RAS
43 Baltiyskaya Street, Vladivostok
Russia 690041
E-mail: lobanov@poi.dvo.ru

MKRTCHYAN Ferdenant
Institute of Radio Engineering and Electronics
Russian Academy of Sciences
1 Vvedensky Sq., Fryazino, Moscow
Russia 141190
E-mail: ferd47@mail.ru

MOTOI Tatsuo
Meteorological Research Institute, JMA
Nagamine-1-1, Tsukuba
Ibaragi Pref., Japan 305-0052
E-mail: tmotoi@mri-jma.go.jp

MUKTEPAVEL Larisa
Pacific Research Institute of Fisheries and
Oceanography (TINRO-Center)
4 Shevchenko Alley, Vladivostok
Russia 690950
E-mail: Larisamk@tinro.ru

NAGATA Yutaka
Marine Information Research Center
Japan Hydrographic Association
Daiichi Sogo Bldg. 6F
1-6-6, Haneda-Kuko, Ota-ku
Tokyo, Japan 144-0041
E-mail: nagata@kud.biglobe.ne.jp

NAKANOWATARI Takuya
Institute of Low Temperature Science
Hokkaido University
N-19 W-8, Kita-ku, Sapporo
Japan 060-0819
E-mail: nakano@lowtem.hokudai.ac.jp

NAKATSUKA Takeshi
Institute of Low Temperature Science
Hokkaido University
N-19 W-8, Kita-ku, Sapporo
Japan 060-0819
E-mail: nakatuka@lowtem.hokudai.ac.jp

(**present address**)
Graduate School of Environmental Studies
Hydrospheric Atmospheric Research Center
Nagoya University
Furo-cho, Chikusa-ku, Nagoya, Japan 464-8601
E-mail: nakatsuka.takeshi@f.mbox.nagoya-u.ac.jp
(moved from Hokkaido University on Oct.1, 2008)

NOMURA Daiki
Institute of Low Temperature Science
Hokkaido University
N-19 W-8, Kita-ku, Sapporo
Japan 060-0819
E-mail: daiki@lowtem.hokudai.ac.jp (D. Nomura)

OHSHIMA Kay-Ichiro
Institute of Low Temperature Science
Hokkaido University
Kita-19, Nishi-8, Sapporo
Japan 060-0819
E-mail: ohshima@lowtem.hokudai.ac.jp

OVSYANNNIKOV Evgeny
Pacific Research Institute of Fisheries nd
Oceanography (TINRO-Centre)
4 Shevchenko Alley, Vladivostok
Russia 690950
E-mail: eeovsyannikov@tinro.ru

PEÑA Angelica
Fisheries and Oceans Canada
Institute of Ocean Sciences
P.O. Box 6000, Sidney
BC, Canada V8L 4B2
E-mail: Angelica.Pena@dfo-mpo.gc.ca

ROMANOV Alexander
FSUE "RISDE"
53 Aviamotomaya St., Moscow
Russia 111024
E-mail: romanov@rniikp.ru

ROMANOV Alexey
FSUE "RISDE"
53, Aviamotomaya St., Moscow
Russia 111024

SAKURAI Yasunori
Graduate School of Fisheries Sciences
Hokkaido University
3-1-1 Minato-cho, Hakodate
Hokkaido, Japan 041-8611
E-mail: sakurai@fish.hokudai.ac.jp

SASAJIMA You-ichiro
Center for Climate System Research
University of Tokyo
5-1-5, Kashiwanoha, Kashiwa-shi
Chiba, Japan 277-8568
E-mail: sasajima@ccsr.u-tokyo.ac.jp

SAITOH Sei-Ichi
Graduate School of Fisheries Sciences
Hokkaido University
3-1-1 Minato-cho, Hakodate
Hokkaido, Japan 041-8611
E-mail: sakurai@fish.hokudai.ac.jp

SHEVCHENKO George
Institute of Marine Geology and Geophysics
FEB RAS
1-B Nauki St., Yuzhno-Sakhalinsk
Russia 693022
E-mail: shevchenko@imgg.ru

SHIMADA Hiroshi
Hokkaido Central Fisheries Experiment Station
Hamanaka-cho 238, Yoichi
Hokkaido Japan 046-8555
E-mail: shimadah@fishexp.pref.hokkaido.jp

TACHIBANA Yoshihiro
Faculty of Bio-resources
Mie University
1577 Kurima-machiya-cho, Tsu
Mie, Japan 514-8507
E-mail: tachi@bio.mie-u.ac.jp

TAGUCHI Mioko
Graduate School of Fisheries Sciences
Hokkaido University
3-1-1 Minato-cho, Hakodate
Hokkaido, Japan 041-8611
E-mail: taguchi@fish.hokudai.ac.jp

TRUKHIN Alexey
V.I. Il'ichev Pacific Oceanological Institute (POI)
FEB RAS
43 Baltiyskaya St., Vladivostok
Russia 690041
E-mail: trukhin@poi.dvo.ru

UCHIMOTO Keisuke
Institute of Low Temperature Science
Hokkaido University
Kita 19, Nishi 8, Sapporo
Japan 060-0819
E-mail: uchimoto@lowtem.hokudai.ac.jp

VARKENTIN Alexander
Kamchatka Research Institute of Fisheries and Oceanography (KamchatNIRO)
18 Naberezhnaya St.,
Petropavlovsk-Kamchatsky
Russia, 683000
E-mail: varkentin@kamniro.ru

YAMAGUCHI Atsushi
Graduate School of Fisheries Sciences
Hokkaido University
3-1-1 Minatomachi, Hakodate
Hokkaido, Japan 041-8611
E-mail: a-yama@fish.hokudai.ac.jp

ZAITSEVA Julia
Russian Federal Research Institute of Fisheries and Oceanography (VNIRO)
17 V. Krasnoselskaya, Moscow
Russia 107140
E-mail: yuz@vniro.ru

Appendix 2

List of Participants

[Scientists]

ABROSIMOVA, A. A.	V.I. Il'ichev Pacific Oceanological Institute (POI)	Russia
ANDREEV, A. G.	V.I. Il'ichev Pacific Oceanological Institute (POI)	Russia
ASAKUMA, K.	Tokyo University of Agriculture	Japan
ASAMI, H.	Hokkaido Wakkanai Fisheries Experiment Station	Japan
BROVKO, P.	Far East National University	Russia
CHERNOOK, V.	Research Institute "GIPRORYBFLOT"	Russia
CHIBA, S.	Tokyo University of Agriculture	Japan
EBUCHI, N.	Hokkaido University	Japan
GLEBOVA, S. Y.	Pacific Research Institute of Fisheries and Oceanography (TINRO-Centre)	Russia
HIWATARI, T.	National Institute for Environmental Studies	Japan
ISADA, T.	Hokkaido University	Japan
ISHINAZAKA, T.	Shiretoko Nature Foundation	Japan
ITO, M.	Tokyo University of Agriculture	Japan
JOH, M.	Abashiri Fisheries Experimental Station	Japan
KANAIWA, M.	Tokyo University of Agriculture	Japan
KANTAKOV, G.	Sakhalin Research Institute of Fisheries and Oceanography SakhNIRO	Russia
KASAI, H.	Hokkaido National Fisheries Research Institute	Japan
KASHIWAI, M.	Tokyo University of Agriculture	Japan
KISHI, M. J.	Hokkaido University	Japan
KOBAYASHI, M.	Tokyo University of Agriculture	Japan
KULIK, V. V.	Pacific Research Institute of Fisheries and Oceanography (TINRO-Centre)	Russia
KUROTAKI, H.	Tokyo University of Agriculture	Japan
LABAY, V. S.	Sakhalin Research Institute of Fisheries and Oceanography (SakhNIRO)	Russia
LOBANOV, V.	V.I. Il'ichev Pacific Oceanological Institute (POI)	Russia
MATSUBARA, H.	Tokyo University of Agriculture	Japan
McKINNELL, S.	North Pacific Marine Science Ogranization (PICES)	Canada
MIZUNO, M.	Tokyo University of Agriculture	Japan
MKRTCHYAN, F. A.	Institute of Radioengineering & Electronics	Russia
MOTOI, T.	Meteorological Research Institute	Japan
MUKTEPAVEL, L. S.	Pacific Research Institute of Fisheries and Oceanography (TINRO-Centre)	Russia
NAGATA, Y.	Marine Information Research Center	Japan
NAKANOWATARI, T.	Hokkaido University	Japan
NAKATSUKA, T.	Hokkaido University	Japan
NISHINO, Y.	Tokyo University of Agriculture	Japan
NOBETSU, T.	Shiretoko Nature Foundation	Japan
NOMURA, D.	Hokkaido University	Japan
OHSHIMA, K.-I.	Hokkaido University	Japan

OSHIMA, K.	Hokkaido University	Japan
OVSYANNIKOV, E.	Pacific Research Institute of Fisheries and Oceanography (TINRO-Centre)	Russia
PEÑA, M.A.	Institute of Ocean Sciences (IOS), DFO	Canada
ROMANOV, A. A.	Federal State Unitary Enterprise Russian Institute of Satellite Device Engineering (FSUE "RISDE")	Russia
ROMANOV, A. A.	Federal State Unitary Enterprise Russian Institute of Satellite Device Engineering (FSUE "RISDE")	Russia
SAITOH, S.	Hokkaido University	Japan
SAKAI, K.	Tokyo University of Agriculture	Japan
SAKURAI, Y.	Hokkaido University	Japan
SASAJIMA, Y.	University of Tokyo	Japan
SHEVCHENKO, G.	Institute of Marine Geology and Geophysics	Russia
SHIMADA, H.	Hokkaido Central Fisheries Experiment Station	Japan
SHIMAZAKI, O.	Fisheries Agency of Japan	Japan
SHINADA, A.	Abashiri Fisheries Experimental Station	Japan
SHIOMOTO, A.	Tokyo University of Agriculture	Japan
SONODA, T.	Tokyo University of Agriculture	Japan
TACHIBANA, Y.	Mie University	Japan
TAGUCHI, M.	Hokkaido University	Japan
TANIGUCHI, A.	Tokyo University of Agriculture	Japan
TRUKHIN, A. M.	V.I. Il'ichev Pacific Oceanological Institute (POI)	Russia
UCHIMOTO, K.	Hokkaido University	Japan
UNI, Y.	Tokyo University of Agriculture	Japan
VARKENTIN, A. I.	Kamchatka Research Institute of Fisheries and Oceanography (KamchatNIRO)	Russia
YAMADA, H.	Fisheries Agency of Japan	Japan
YAMAGUCHI, A.	Hokkaido University	Japan
YAMAMURA, O.	Hokkaido National Fisheries Research Institute	Japan
YAMBE, H.	Tokyo University of Agriculture	Japan

[Journalist]

NAKAYAMA, Y.	Abashiri Times	Japan

[Students]

AKIBA, T.	Tokyo University of Agriculture	Japan
ENDO, Y.	Tokyo University of Agriculture	Japan
HIROI, M.	Tokyo University of Agriculture	Japan
ICHINO, A.	Tokyo University of Agriculture	Japan
IIDA, Y.	Tokyo University of Agriculture	Japan
ISHII, M.	Tokyo University of Agriculture	Japan
KAIZU, N.	Tokyo University of Agriculture	Japan
KASHAI, H.	Tokyo University of Agriculture	Japan
OZAKI, M.	Tokyo University of Agriculture	Japan
SUZUKI, T.	Tokyo University of Agriculture	Japan
YOSHIDA, S.	Tokyo University of Agriculture	Japan

Appendix 3

Workshop Schedule

Plenary Session (PS1): *Climate / Ocean dynamics* Session Chairs: **Andreev/Ohshima**

PS1-1 GLEBOVA Svetlana, USTINOVA E.I. and SOROKIN Y.D.
Long-term changes atmosphere center and climatic regime of the Okhotsk Sea in the last three decades.

PS1-2 TACHIBANA Yoshihiro and OGI Masayo
Influence of the annual Arctic Oscillation on the negative correlation between Okhotsk sea ice and Amur River discharge.

PS1-3 OHSHIMA Kay-Ichiro, NAKANOWATARI Takuya, NAKATSUKA Takeshi, NISHIOKA Jun, and WAKATSUCHI Masaaki
Changes in the Sea of Okhotsk due to global warming. - Weakening pump function to the North Pacific.

PS1-4 ANDREEV Andrey G.
Interannual variations of the East-Kamchatka and East-Sakhalin Currents volume transport and its impact on the temperature and chemical parameters in the Okhotsk Sea.

PS1-5 MUKTEPAVEL Larisa and SHATILINA T.A.
Some regularities of formations of extremely low-ice winter seasons in the Okhotsk Sea.

PS1-6 SASAJIMA You-ichiro, HASUMI Hiroyasu and NAKAMURA Tomohiro
A sensitivity study on the dense shelf water formation in the Okhotsk Sea.

Plenary Session (PS2): *Amur River / Geochemical cycle* Session Chairs: **Peña/Kishi**

PS2-1 LOBANOV Vyacheslav, DUDAREV O., TISHCHENKO P., ZHABIN I., ZVALINSKY V., CHARKIN A., KOLTUNOV A., SAGALAEV A. and SHVETSOVA M.
Review of the POI program on the Amur River Estuary and adjacent marine areas.

PS2-2 NAKATSUKA Takeshi, NISHIOKA Jun, SHIRAIWA Takayuki and All members of the "Amur-Okhotsk" Project
Biogeochemical linkage between Amur River basin and western subarctic Pacific by iron transport through Okhotsk Sea Intermediate Water: A new paradigm to explain changes in ocean primary productivity.

PS2-3 PEÑA Angelica
Modelling of biogeochemical cycles and climate change on the Continental Shelf: An example from the Pacific coast of Canada.

PS2-4 NOMURA Daiki, TOYOTA Takenobu, MATOBA Sumito, NISHIOKA Jun and NAGATA R.
Nutrient status of snow cover and sea-ice in the southern Sea of Okhotsk.

PS2-5 HIWATARI Takehiko, KOSHIKAWA Hiroshi, KOHATA Kunio, FUKAMACHI Yasushi and SHIRASAWA Kunio
Interannual variation of material flux under seasonal sea ice in the Okhotsk Sea north of Hokkaido, Japan.

Plenary Session (PS3): *Primary production / Zooplankton / Marine mammals*

Session Chairs: **Saitoh/Trukhin**

PS3-1 MUZZNEENA Ahmad Mustapha and SAITOH Sei-Ichi
Satellite measured seasonal and interannual variability of primary production at the scallop farming area in the Okhotsk Sea.

PS3-2 KASAI Hiromi, ONO T. and HIRAKAWA K.
Seasonal variability of primary production off Abashiri, the southern Okhotsk Sea.

PS3-3 ISADA Tomonori, SUZUKI Koji, LIU Hongbin, NISHIOKA Jun and KATSUKA Takeshi:
Primary productivity and photosynthetic features of phytoplankton in the Sea of Okhotsk during late summer.

PS3-4 KOBAYASHI Mari, KOUNO Y., NISHINA M., FUJIMOTO Y., and KATO K.
Seasonal change in number and movement pattern of spotted seals (*Phoca largha*) migration around the Sea of Japan.

PS3-5 TRUKHIN Alexey M.
Current status of pinnipeds in the Sea of Okhotsk.

PS3-6 TAGUCHI Mioko , ABE S. and MATSUISHI T.
Mitochondrial DNA variation in Japanese Harbor Porpoise.

Session A (SA1): *Current dynamics* Session Chair: **Nakanowatari**

SA1-1 UCHIMOTO Keisuke, NAKAMURA Tomohiro, NISHIOKA Jun and MITSUDERA Humio
Modeling the circulation of the intermediate layer in the Sea of Okhotsk.

SA1-2 NAKANOWATARI Takuya, MITSUDERA Humio, MOTOI Tatsuo and OHSHIMA Kay I., and Ishikawa I.
50-yr scale change in the intermediate water temperature in the western North Pacific simulated by an eddy resolving sea ice coupled OGCM.

SA1-3 KANTAKOV Gennady
Vertical movements of water masses in the western part of Sea of Okhotsk.

SA1-4 SHEVCHENKO George, KANTAKOV Gennady and CHASTIKOV Valery
Mooring current observations in the areas adjacent to Shmidt Peninsula (Northern Sakhalin).

SA1-5 SHEVCHENKO George, KANTAKOV Gennady and CHASTIKOV Valery
Mooring current observations on the Sea of Okhotsk's shelf of Urup and Kunashir Island (Kuril Ridge).

SA1-6 SHEVCHENKO George and ROMANOV Alexander
Energetic characteristics of tidal and residual level oscillations in the Okhotsk Sea from satellite altimetry data.

Session A (SA2): *Sea ice, watermass and freshwater procesess / Coastal lagoons*

Session Chairs: **Tachibana/Abrosimova**

SA2-1 MOTOI Tatsuo, CHAN Wing-Le and MIYAKAWA Takuya
Sea-ice flow from the Okhotsk Sea to the Pacific Ocean through the Nemuro Strait in 2008.

SA2-2 NAGATA Yutaka
Outflow of the Okhotsk Sea Water and the Oceanic condition of the sea to the east of Hokkaido.

SA2-3 KASHIWAI Makoto
World Ocean Atlas 2005 indicates occurrence of winter convection at open ocean polynya in the eastern part of Okhotsk Sea.

SA2-4 ABROSIMOVA Anastasiya, ZHABIN Igor and DUBINA Vyacheslav
Influence of the Amur River discharge on hydrological conditions of the Amurskiy Liman and Sakhalin Bay of the Sea of Okhotsk during a spring-summer flood.

SA2-5 OSHIMA Kazuhiro, TACHIBANA Yoshihiro and OGI Masayo
Seasonal and interannual variations of Amur River discharge and their relationships to large-scale atmospheric patterns and moisture fluxes.

SA2-6 BROVKO Peter F.
The Okhotsk Sea coastal lagoons: types, evolution and use of resources.

Session A (SA3): *New Technology* Session Chairs: **Romanov/Ebuchi**

SA3-1 EBUCHI Naoto, FUKAMACHI Yasushi, OHSHIMA Kay-I., and WAKATUCHI Masaaki
HF-Radar technology in the Sea of Okhotsk.

SA3-2 ROMANOV A.A., TRUSOV S.V. and ROMANOV A.A.
Automated information technology for ionosphere monitoring on the low orbit navigation satellite signals.

SA3-3 ROMANOV A.A., URLICHICH U.M., PULINETS S.A. and ROMANOV, A.A.
The pilot project on complex diagnosis for earthquake precursors in Sakhalin Island: the experiment results in 2007.

SA3-4 MKRTCHYAN Ferdenant A., KRAPIVIN V.F., KOVALEV V.I. and KLIMOV V.V.
An adaptive spectroellipsometric technology for ecological monitoring of the sea water.

SA3-5 KRAPIVIN V.F. and MKRTCHYAN Ferdenant A.
Remote sensing radiometry technology for the Okhotsk Sea ecosystem biocomplexity assessment.

SA3-6 CHERNOOK Vladimir, GOLDIN Yurij, LISOVSKI Alexander and VASILEV Alexander
The using of airplane-lidar for registration of fish schools and plankton.

Session B (SB1): *Biological processes / Disturbance by oil and gas development*
Session Chairs: **Yamaguchi/Labay**

SB1-1 SHIMADA Hiroshi, SAWADA Mayumi, KURIBAYASHI Takanori, NAKATA Akifumi, MIYAZONO, Akira and ASAMI Hiroki
Spatial distribution of toxic dinoflagellate, *Alexandrium tamarense* in summer in the Okhotsk Sea off Hokkaido, Japan.

SB1-2 ASAMI Hiroki, SHIMADA Hiroshi, SAWADA Mayumi, MIYAKOSHI Yasuyuki, ANDO Daisei, FUJIWARA Makoto and NAGATA Mitsuhiro
Spatial and seasonal distributions of copepods during spring to summer in the Okhotsk Sea off Eastern Hokkaido, Japan.

SB1-3 YAMAGUCHI Atsushi, UENO Yasuhiro, SEKI Jiro and IKEDA Tsutomu
Characteristics of zooplankton community of the Okhotsk Sea in Autumn: a comparison with Oyashio region.

SB1-4 KANAIWA Minoru, INOUE Takuya and YAMAMOTO Atsuya
Determinants of fish species composition in Abashiri River.

SB1-5 KASHIWAI Makoto and KANTAKOV Gennady
Scientific evidences and questions identified by Hanasaki Program.

SB1-6 SAMATOV Andrey D. and LABAY Vyacheslav S.
Benthos community of the dumping area during liquid natural gas plant construction: effects of technical impacts or natural changes?

* ZAITSEVA Julia
Conservation of aquatic living resources under conditions of large-scale development of oil and gas resources on the Pacific continental shelf (the Sea of Okhotsk).

Session B (SB2): *Walleye pollock* Session Chairs: **Sakurai/Varkentin**

SB2-1 BUSLOV A.V. and VARKENTIN Alexander I.
Walleye pollock (*Theragra chalcogramma*) spawning in the Okhotsk Sea waters off the north Kuril Islands and south-western Kamchatka.

SB2-2 KULIK Vladimir
Responses of relative abundance of dominants in fish communities to the Sea of Okhotsk climate variability.

SB2-3 OVSYANNNIKOV Evgeny E., SMIRNOV A.V. and AVDEEV G.V.
Walleye pollock researches in the open waters of the Okhotsk Sea.
SB2-4 YAMAMOTO J., OOSATO M. and SAKURAI Yasunori
Does the extent of ice cover affect the fate of walleye pollock?
** KOTENEV B.N. and BULATOV O.A.
Dynamics of the walleye pollock biomass in the Sea of Okhotsk.

_____

*, ** Papers were submitted for the workshop but were unable to be presented at the meeting. They are included in the proceedings.